

Gunter Erhard

Designing with Plastics

HANSER

Hanser Publishers, Munich • Hanser Gardner Publications, Cincinnati

The Author:

Dr.-Ing. Gunter Erhard, Leipziger Straße 1, 68782 Brühl, Germany

Translated by:

Dr. Martin Thompson, 15 Spalding Avenue, Garstang, Preston PR3 1TN, United Kingdom

Distributed in the USA and in Canada by

Hanser Gardner Publications, Inc.

6915 Valley Avenue, Cincinnati, Ohio 45244-3029, USA

Fax: (513) 527-8801

Phone: (513) 527-8977 or 1-800-950-8977

www.hansergardner.com

Distributed in all other countries by

Carl Hanser Verlag

Postfach 86 04 20, 81631 München, Germany

Fax: +49 (89) 98 48 09

www.hanser.de

The use of general descriptive names, trademarks, etc., in this publication, even if the former are not especially identified, is not to be taken as a sign that such names, as understood by the Trade Marks and Merchandise Marks Act, may accordingly be used freely by anyone.

While the advice and information in this book are believed to be true and accurate at the date of going to press, neither the authors nor the editors nor the publisher can accept any legal responsibility for any errors or omissions that may be made. The publisher makes no warranty, express or implied, with respect to the material contained herein.

Library of Congress Cataloging-in-Publication Data:

Erhard, G.

[Konstruieren mit Kunststoffen. English]

Designing with plastics / Gunter Erhard.

p. cm.

ISBN-10: 1-56990-386-7 (hardcover)

ISBN-13: 978-1-56990-386-5 (hardcover)

1. Plastics. 2. Engineering design. I. Title.

TP1122.E7413 2006

620.1'923--dc22

2005029061

Bibliografische Information Der Deutschen Bibliothek

Die Deutsche Bibliothek verzeichnet diese Publikation in der Deutschen Nationalbibliografie;
detaillierte bibliografische Daten sind im Internet über <<http://dnb.ddb.de>> abrufbar.

ISBN-10: 3-446-22590-0

ISBN-13: 978-3-446-22590-9

All rights reserved. No part of this book may be reproduced or transmitted in any form or by any means, electronic or mechanical, including photocopying or by any information storage and retrieval system, without permission in writing from the publisher.

© Carl Hanser Verlag, Munich 2006

Production Management: Oswald Immel

Typeset by Manuela Treindl, Laaber, Germany

Coverconcept: Marc Müller-Bremer, Rebranding, München, Germany

Coverdesign: MCP • Susanne Kraus GbR, Holzkirchen, Germany

Printed and bound by Druckhaus "Thomas Müntzer" GmbH, Bad Langensalza, Germany

Contents

1 Market Overview	1
1.1 Examples of Applications from Various Industry Sectors	4
1.1.1 Aerospace	4
1.1.2 Precision Engineering	7
1.1.3 Automotive Engineering	9
1.1.4 General Mechanical Engineering	14
1.1.5 Design of Technical Equipment	15
1.1.6 Construction Industry	18
1.2 Forecast	22
2 Structure and Properties	31
2.1 Chemical Structure (Constitution)	31
2.1.1 Degree of Polymerization – Relative Molecular Weight	34
2.1.2 Homopolymerization and Copolymerization	38
2.2 Intermolecular Binding Energies (Secondary Valence Bonds)	40
2.2.1 Absorption of Water by Polyamides	41
2.3 Spatial Arrangement of Atoms and Groups of Atoms in Molecules (Configuration)	47
2.3.1 Tacticity	48
2.3.2 Branching	48
2.3.3 Cross-Linking	49
2.4 Architecture of Polymer Systems	50
2.4.1 Homogeneous and Heterogeneous Polymer Mixtures	50
2.4.2 Plasticization	51
2.4.3 Fillers and Reinforcement	51
2.5 Morphology (Supermolecular Structures)	54
2.5.1 Amorphous Microstructure	54
2.5.2 Crystalline Microstructure	55
2.5.3 Anisotropy	60
2.5.3.1 Molecular Alignments	60
2.5.3.2 Filler or Fiber Alignment	62
2.6 Thermomechanical Ranges	64
2.6.1 Thermoplastics with Amorphous Structure	64
2.6.2 Thermoplastics with Semicrystalline Structure	66
2.6.3 Elastomers	67
2.6.4 Thermosets	67
3 Brief Description of the Properties of Generic Polymeric Materials	71
3.1 Thermoplastics	71
3.1.1 Polymer Blends	80
3.1.2 Functional Polymers	83
3.2 Elastomers	88

3.3	Thermosets	90
3.4	Fibrous Reinforcements	94
3.4.1	Glass Fibers	95
3.4.1.1	Production and Reinforcing Forms of Glass Fiber Material ..	95
3.4.1.2	Types of Glass and Fiber Properties	96
3.4.2	Carbon Fibers	97
3.4.3	Aramid Fibers	97
3.4.4	Metal Fibers, Whiskers, and Ceramic Fibers	97
4	Physical Properties – Characteristic Values – Test Methods and Procedures	101
4.1	Deformation Behavior under Uniaxial Dynamic Tensile Stress (Stress-Strain Experiments)	101
4.1.1	Molecular Deformation and Fracture Mechanisms	101
4.1.2	Characteristic Stress-Strain Curves	103
4.1.3	Determination of Stress-Strain Diagrams and Characteristic Properties of Materials	104
4.1.4	Effects of Temperature, Time, and Humidity on Stress-Strain Curves	107
4.1.5	Mathematical Description of Stress-Strain Curves	109
4.2	Deformation Behavior under Uniaxial, Long-Term, Static Tensile Loads (Tensile Creep Testing)	111
4.2.1	Mathematical Description of Creep Curves	113
4.3	Toughness and Impact Resistance	115
4.3.1	Determination of Tensile Stress-Strain Toughness	116
4.3.2	Determination of Toughness by Flexural Impact Test	116
4.3.3	Penetration or Dart Drop Impact Test	119
4.4	Behavior under Cyclic Loads	120
4.4.1	Determination of Characteristic Features of Fatigue	122
4.5	Poisson's Ratio	125
4.6	Thermal Properties	127
4.6.1	Thermal Expansion	127
4.6.2	Dimensional Stability	129
4.6.2.1	Modulus of Elasticity and Modulus of Rigidity as a Function of Temperature	129
4.6.2.2	Deflection Temperature	130
4.6.2.3	Softening Point	131
4.6.3	Heat Aging	132
4.6.3.1	Safety Considerations and Standards	135
4.6.4	Summary Analysis of the Effects of Temperature	136
4.7	Tribological Properties	136
4.7.1	Fundamentals	138
4.7.1.1	Adhesion and Surface Energy of Solids	139
4.7.1.2	Deformation and Hysteresis Loss	144
4.7.1.3	Boundary Conditions for Adhesive and Deformative Sliding	145
4.7.2	Friction and Wear in Mated Polymer and Steel Surfaces	145
4.7.2.1	Effect of Steel Surface Roughness on Steel/Polymer Combinations	147

4.7.2.2	Effect of Relative Molecular Weight on Friction and Wear ..	150
4.7.2.3	Effect of the Moisture Content of Polyamides on Friction and Wear	151
4.7.2.4	Effect of High-Energy Radiation	153
4.7.2.5	Effect of Form and Sequence of Motion on Friction and Wear	155
4.7.3	Friction and Wear in Mated Pairs of Polymeric Materials	156
4.7.3.1	Sliding Friction	156
4.7.3.2	Wear Due to Sliding Friction for Mated Polymeric Material Pairs	157
4.7.4.2	The Effects of Physical Properties on Friction and Wear System Properties	158
4.7.5	Effect of Additives on Friction and Wear Properties	158
4.7.5.1	Effect of Fibers on Wear	159
4.7.5.2	Effect of Other Inorganic Additives	163
4.7.5.3	Effect of Polymeric Additives	163
4.7.6	Stick-Slip	165
4.7.6.1	Changing Stick-Slip Behavior by Modifying the Parameters of the Sliding System	166
4.7.7	Jet Erosion	168
5	Calculations for Structures under Mechanical Load – Examples of Geometrically Simple Structural Parts under Static Loads	175
5.1	Specific Materials and Processing Problems	175
5.1.1	Deformation Behavior under Uniaxial Dynamic Tensile Stress	175
5.2	Determination of Strength	177
5.2.1	Basic Procedure for Structural Part Design	177
5.2.1.1	Characteristic Strength	178
5.2.1.2	Safety Factors	180
5.2.1.3	Reducing Factors	181
5.2.2	Uniaxial State of Stress	182
5.2.2.1	Example of a Thin-Walled Pipe under Internal Pressure ..	183
5.2.3	Multiaxial State of Stress	184
5.2.3.1	Failure Criteria	184
5.2.3.2	Examples of Shear Loads	187
5.3	Calculation of Strains and Deformations	190
5.3.1	Linear Elastic Behavior	190
5.3.2	Nonlinear Elastic Behavior	191
5.4	Analysis of Stress and Deformation in Structures under Flexural Loads with the Aid of a Simple FE Approach	196
5.5	Calculation of Structural Parts Subjected to Impact Loads	198
5.6	Structural Design of Fiber-Composite Structures	199
5.6.1	Mechanical Properties of Laminates	200
5.6.1.1	Deformation Behavior under Uniaxial Tensile Load, Damage Limit	200
5.6.1.2	Fundamental Elasticity Variables in a UD Layer	200

5.6.1.3	Averaged Characteristic Values for Mat Laminates	202
5.6.2	Methods of Calculation	205
5.6.2.1	Calculation of Averaged Values	205
5.6.2.2	Continuum Theory	205
5.6.2.3	Network Theory	205
5.7	Computer-Aided Development	207
5.7.1	Computer-Aided Design (CAD)	207
5.7.2	Rapid Prototyping	208
5.7.3	Rapid Tooling	210
6	Design and Material Considerations for Parts Subjected to Mechanical Loads	213
6.1	Flexible Structures	213
6.1.1	Modulus of Elasticity	213
6.1.2	Design Geometry – Moment of Inertia	214
6.1.3	Load–Geometry Interactions	215
6.2	Flexurally Rigid Structures	218
6.3	Flexurally Flexible, Torsionally Rigid Structures	220
6.4	Flexurally Rigid, Torsionally Flexible Structures	221
6.5	Torsion-Resistant, Torsionally Rigid Structures	221
6.6	Flexurally and Torsionally Rigid Structures	224
6.7	Torsionally Flexible Structures	225
6.8	Tension-Proof, Tensionally Rigid and Torsionally Flexible Structures	225
6.9	High Shear-Strength, Shear-Resistant Structures	226
6.10	Pressure-Yielding and Compression-Resistant Structures	227
6.11	Multifunctional Structures	229
6.12	Thermal Expansion and Thermal Stress	230
6.13	Universal Joints	235
7	Designing for Production	239
7.1	Mold Filling	239
7.1.1	Simulation of the Filling Operation	241
7.1.2	Causes of Orientation in Moldings	243
7.1.2.1	Effects of Orientation	246
7.1.2.2	Controlling Orientation	248
7.1.3	Causes for Formation of Weld Lines and Air Pockets	252
7.1.3.1	Effects of Weld Lines and Air Pockets	254
7.1.3.2	Controlling Weld Lines and Air Pockets	255
7.2	Cooling and Solidification	261
7.2.1	Cooling Rate	261
7.2.1.1	Effects of Cooling Rate	261
7.2.1.2	Controlling the Cooling Rate	261
7.2.2	Changes in Dimensions and Tolerances	264
7.2.2.1	Shrinkage	264
7.2.2.2	Post Molding Shrinkage	267
7.2.2.3	Tolerances	267
7.2.3	Warpage	271

7.2.3.1	Causes of Warpage	271
7.2.3.2	Controlling Warpage	274
7.3	Demolding	277
7.3.1	Draft	280
7.3.2	Demolding of Undercuts	280
7.3.2.1	Forced Demolding	281
7.3.2.2	Mold-Making Measures	281
7.3.2.3	Fusible Cores	283
7.3.3	Avoidance of Undercuts	285
7.3.3.1	Modifying the Design	285
7.3.3.2	Piercing Cores (Blocking or Shutoffs)	285
7.3.3.3	Multipart Designs	287
7.4	Sandwich Molding (Co-Injection Molding)	289
7.4.1	Two-Color Injection Molding	289
7.4.2	Rigid-Flexible Combinations	293
7.4.3	Gas Injection Technology (GIT)	299
7.4.5	External Gas Pressure Technology	303
8	Flexing Elements	311
8.1	Snap-Fit Joints	311
8.1.1	Snap-Fit Beams	317
8.1.1.1	Types of Snap-Fit Beams	317
8.1.1.2	Snap-Fit Beam Calculations	321
8.1.1.3	Additional Functions	322
8.1.2	Torsional Snap-Fit Joints	325
8.1.2.1	Types of Torsional Snap-Fit Joints	325
8.1.2.2	Torsion Snap-Fit Joint Calculations	326
8.1.3	Annular Snap-Fit Joints	327
8.1.3.1	Types of Annular Snap-Fit Joints	327
8.1.3.2	Annular Snap-Fit Joint Calculations	328
8.1.3.3	Additional Functions	330
8.1.4	Segmented Annular Snap-Fit Joints	331
8.1.4.1	Segmented Annular Snap-Fits	332
8.1.4.2	Slotted Annular Snap-Fit Joint Calculations	332
8.1.4.3	Additional Functions	334
8.2	Elastic Elements	335
8.2.1	Elastic Thermoplastic Materials	335
8.2.1.1	Flexing Springs	335
8.2.1.2	Tension Springs	337
8.2.1.3	Compression Springs	337
8.2.1.4	Torsion Springs	341
8.2.2	Springs Made of Fiber-Plastic Composites (Glass-Fiber and Carbon-Fiber Reinforced Plastic)	342
8.2.2.1	Leaf Springs	342
8.3	Integral Hinges and Integral Joints	345
8.3.1	Manufacture of Integral Hinges and Integral Joints	346

8.3.1.1	Injection Molding	346
8.3.1.2	Blow Molding	347
8.3.1.3	Embossing	349
8.3.2	Design	349
8.3.3	Materials	350
8.3.4	Integral Hinge Design Calculations	350
8.3.4.1	Calculation of the Length and Thickness of an Integral Hinge	352
8.3.5	Applications with Integral Hinges	355
8.3.5.1	Lid/Container Hinge Joints	355
8.3.5.2	Bi-Stable Hinge Joints	355
8.3.5.3	Simplified Production	357
8.3.5.4	Dynamically Loaded Integral Hinge Joints	361
8.3.5.5	Assembly Aid and Captive Binding Using Integral Hinges ..	361
9	Mechanical Fasteners	365
9.1	Molded Threads and Threads Produced by Machining	366
9.1.1	Screws and Bolts Made of Polymeric Material	366
9.1.2	Injection-Molded, Blow-Molded, and Machined Threads	368
9.2	Threaded Inserts	368
9.2.1	Encapsulated Threaded Inserts	368
9.2.2	Threaded Inserts Embedded by Ultrasound	368
9.2.3	Press-In Threaded Inserts	369
9.2.4	Expansion Inserts	370
9.2.5	Screw-In Inserts	370
9.2.6	Inserts Made of Polymeric Materials	371
9.2.7	Comparative Evaluation of the Various Inserts	371
9.2.8	Behavior under Dynamic Loads	374
9.3	Self-Threading Screws	374
9.3.1	Screw Shapes and Geometries	375
9.3.1.1	Included Thread Angle	377
9.3.1.2	Self-Locking Screw Threads	377
9.3.2	Design of the Screw Boss	377
9.3.2.1	Screw Engagement Depth	378
9.3.3.2	Boss Pilot Hole Diameter	378
9.3.2.3	Boss Relief Bore	379
9.3.2.4	Boss Outer Diameter	379
9.3.3	Calculation of Key Variables in a Self-Threading Screw Joint	381
9.3.3.1	Screw Drive Torque	381
9.3.3.2	Destruction Torque	383
9.3.3.3	Screw Extraction (Pull-Out) Force	383
9.3.3.4	Tightening Moment and Tensioning Force	384
9.3.3.5	Assembly Conditions	385
10	Ribbed Structures	387
10.1	Comparison with Other Methods of Reinforcement	387

10.1.1	Increasing the Modulus of Elasticity	387
10.1.2	Increasing Wall Thickness	388
10.1.3	Crimps and Corrugations	389
10.2	General Considerations in Ribbed Structures	390
10.2.1	Rib Height	390
10.2.2	Rib Position	391
10.2.3	Number of Ribs (Consumption of Material)	393
10.2.4	Support	395
10.3	Design Rules for Injection-Molded Ribs	396
10.3.1	Rib Thickness	396
10.3.2	Cooling Time	397
10.3.3	Injection Direction	398
10.3.4	Rib Intersection Points (Nodes)	400
10.4	Design Rules for Ribs Produced by Gas-Assist Molding Methods	401
10.5	Design Rules for Blow-Molded Ribs and Corrugations	403
10.5.1	Blow-Molded Corrugations	403
10.5.2	Blow-Molded Ribs	405
10.6	Design Rules for Compression-Molded Ribs	406
10.6.1	Manual Processing (Hand Lay-Up Process)	406
10.6.2	Compression Molding	407
11	Gear Wheels	411
11.1	Calculation of the Tooth and Tooth Face Temperatures in Spur Gears	413
11.1.1	Blok's Flash Temperature Hypothesis	414
11.1.2	Takanashi Method for Calculating Temperature	414
11.1.3	Hachmann and Strickle Method for Calculating Temperature	416
11.1.4	Comparison of Methods of Calculating Temperature	418
11.1.5	Optimized Temperature Calculation	419
11.1.5.1	Speed of Rotation	420
11.1.5.2	Flank Temperature	420
11.1.5.3	Relative Contact Time	422
11.1.5.4	Optimized Numerical Value Equation	423
11.2	Calculation of Load-Bearing Capacity	424
11.2.1	Tooth Damage	425
11.2.2	General Parameters	426
11.2.3	Calculation of the Load-Bearing Capacity of the Tooth Base	427
11.2.4	Calculation of the Load-Bearing Capacity of the Tooth Flank	434
11.2.5	Calculation of Tooth Deformation	440
11.3	Design	442
11.3.1	Injection Molding	442
11.3.2	Production of Gears by Machining	446
11.3.3	Shaft-Hub Joints	447
11.3.3.1	Press-Fit Joints	447
11.3.3.2	Form-Grip Joints	450
11.3.3.3	Pretensioned Form-Grip Joints	452

12	Friction Bearings	459
12.1	Friction Bearing Damage	461
12.2	Calculation of Load-Bearing Capacity for Bearings	463
12.2.1	Calculation of Mean Bearing Temperature	463
12.2.2	Calculation of Temperature of Sliding Surface	466
12.2.3	Static Load-Bearing Capacity	466
12.2.3.1	Load on the Bearing Material	467
12.2.3.2	Deformation of the Bearing Bushing	471
12.2.4	Dynamic Load-Bearing Capacity	475
12.2.4.1	Continuous Operation	475
12.2.4.2	Intermittent Operation	476
12.2.4.3	Wear	477
12.3	Bearing Design	478
12.3.1	Bearing Clearance	478
12.3.2	Bearing Wall Thickness	480
12.3.3	Bearing Production	481
12.3.4	Design Examples of Bearings	481
13	Wheels and Rollers	485
13.1	Roller Damage	486
13.2	Calculation of Load-Bearing Capacity	488
13.2.1	Pressure Parameter as an Approximate Design Limit	488
13.2.2	Deformation of Rollers under Static Load	492
13.2.3	Rollers under Dynamic Load	498
13.2.3.1	Free-Wheeling Rollers (without Drive)	498
13.2.3.2	Driven Rollers	504
Index		509

1 Market Overview

Synthetic polymeric materials form a key branch of production in the chemical industry. In the period from 1950 to 1973, these materials, which are usually also referred to as plastics*, underwent an upswing which could scarcely be matched by any other sector of the chemical industry. Some of the reasons for this were the drop in the prices of raw materials during this period, the lowering of production costs due to increased plant capacity, and the development of new, more efficient technologies for producing and processing these materials and, not least, the properties of the materials. However, the growth of the polymeric materials industry is due in large part to the versatility of these materials (*i.e.*, their wide range of properties).

In 1973, the price of crude oil – the basic raw material for polymeric materials – rose dramatically for the first time. This initially had direct consequences for the further development of this group of materials (see Figure 1.1), even though the production of polymeric materials accounts for only a small proportion of oil consumption, running to approx. 6% [1.1].

As the illustration shows, this oil crisis, as it came to be known, which affected almost all sectors of industry, also resulted in a significant reduction in steel production from which there has not been any significant recovery since. In contrast with this, a further rise in polymeric material production followed relatively quickly and in the 1978–1979 timeframe, the volume production curve for polymeric materials even surpassed that of steel.

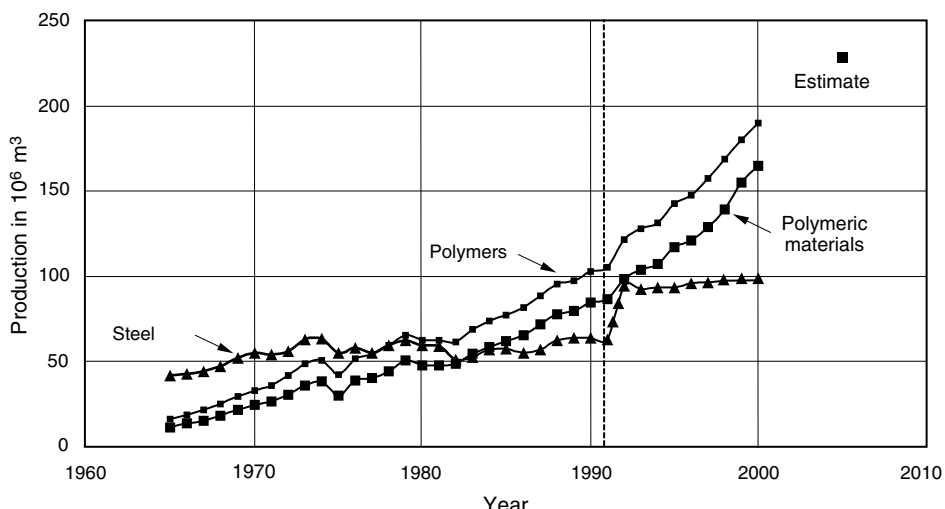


Figure 1.1 Production of raw steel and synthetic polymers in the West and, from 1991, in the world.
Further growth of approx. 5.3% pa is expected.

* In what follows the term plastics will be replaced by the designation “polymeric materials”, as is customary in the field of designing with polymeric materials.

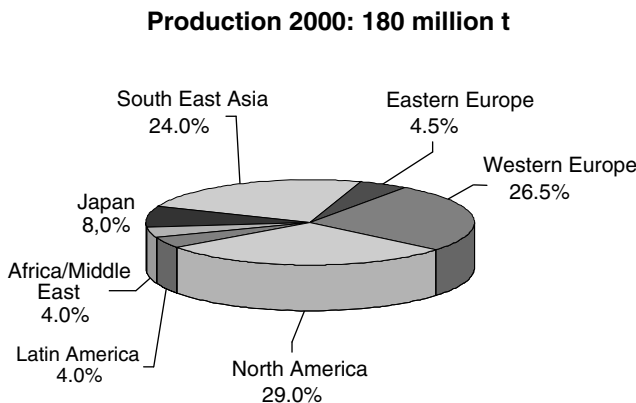


Figure 1.2 World production of polymers (including dispersions, paints, adhesives, etc.) in 2000 broken down by region

The unabating rise in the demand for and consumption of polymeric materials is fueled by an efficient industry. The latter includes producers of plastics, processing companies, and manufacturers of processing machinery. In the Federal Republic of Germany, for example, a production value of \$50 billion was achieved in 1997. Of this, plastics producers contributed approx. 31%, processors approx. 62%, and manufacturers of plastics processing machines approx. 7%. Figure 1.2 shows how polymer production is distributed over the regions of the world.

In the next few years, however, with the spread of globalization, it is projected that there will be a marked shift in the location of production sites and jobs, in particular to Asia as may be seen in Figure 1.3.

Polymeric materials have ushered in an era of very marked technical progress extending over many fields. They have made a quite substantial contribution to improving standards of living for great masses of population that no one would now want to give up. The issues associated with this concerning recycling of materials and recovery of energy in used articles can be solved technically, but in economic terms, material recycling is not always profitable.

The recycling of thermoplastic polymeric materials makes the most sense when:

- High-grade materials are involved; and
- The materials can be recovered sorted according to type

In the case of household waste, the situation is completely different. In Germany, approx. 100 million tons of household wastes have to be disposed of every year. Of this, polymeric materials account for only about 8%. The vast bulk consists of compostable organic waste. The separation of this fraction takes priority and this is already being done in some regions. Composting 1 t of household waste costs between \$100 and \$400. By comparison, mechanical recycling or feedstock recycling of the same quantity costs several times more. Mixed polymeric material recycling is an option when the costs of segregation are not economical; however, these technologies are still evolving. Biodegradable polymeric materials (see Section 3.1.2) could provide an approach to a solution for many packaging purposes [1.38].

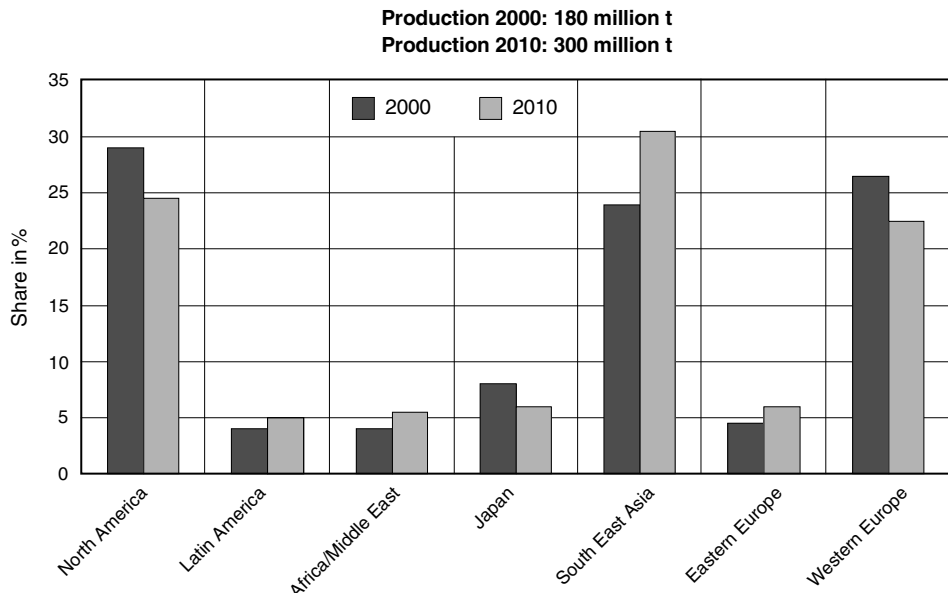


Figure 1.3 Relocation of production sites for polymers by the end of the decade

Statistics on industry-related consumption provide pointers for quantifying the fields of application of polymeric materials. According to these, in Western Europe the packaging sector accounts for the largest proportion of consumption of polymeric materials (see Figure 1.4).

The comparison with steel production presented in Figure 1.1 must not, however, give rise to the false conclusion that the fields of application for the two groups of material are the same. In reality, only a very small proportion of polymeric materials production is employed in functional elements and load-bearing structures. Such structurally demanding applications are found in the transportation sector, including aviation, in the construction industry, in electrical engineering, and of course in mechanical engineering. The latter is difficult to pinpoint in the statistics and at 4 to 8% is subsumed in ‘Other’.

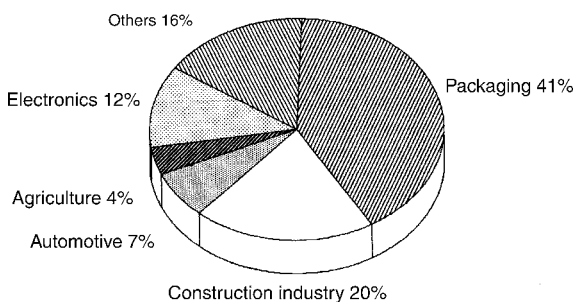


Figure 1.4 Consumption of polymeric materials in Western Europe broken down by industry sector

1.1 Examples of Applications from Various Industry Sectors

Some examples drawn from the numerous tried and tested designs in industry are presented in the following to provide some insight into the state of design engineering today.

1.1.1 Aerospace

The first pointers to the utility of a controlled degree of anisotropy in materials for lightweight construction emerged from work by Hertel in connection with plywood. In the case of polymeric materials, the first practical uses emerged with the introduction of fiber reinforcement, *e.g.*, the reinforcement of polyester resins with glass fibers in the military field after World War II.

Decisive factors were the recognition that the desired reinforcing effects in the longitudinal direction of the fibers simultaneously resulted in a weakening perpendicular to the longitudinal orientation of the fibers and, in addition, that the strength of fiber resin composites had been rendered calculable. The techniques for producing elements having a defined degree of anisotropy, however, are still relatively costly [1.2]. Accordingly, the systematic exploitation of these design advantages has so far largely remained restricted to sectors such as aviation and space technology. First approaches elsewhere may be seen in the development of lightweight construction in automotive engineering. The concept of fiber composites has been further advanced since glass fibers were supplemented by other high-strength and high-rigidity reinforcing materials such as carbon fibers and aramid fibers.

Use of the latter yields high-performance composite materials, a combination affording highest strength and lowest weight.

Commercial aircraft, such as those produced by Airbus Industries, represent an impressive example of the use of carbon fiber composites [1.3]. The rudder unit of the Airbus A 310 (see Figure 1.5) has been manufactured from carbon-fiber reinforced plastic since as early as 1985.



Figure 1.5 Airbus rudder unit composed of carbon fiber/polymeric material composite

Table 1.1 Priorities for the Use of Polymeric Materials in Automotive Engineering

	1980s	1990s
Priority 1	Weight savings	Component costs
Priority 2	Component costs	Operating costs
Priority 3	Operating costs	Weight savings

It was possible to make the tail unit approximately 25% lighter by comparison with the conventional structure made of aluminum. The operating costs of an airplane are reduced over twenty years by \$1,000 per each kilogram of weight saved in the structure. There were even advantages in production engineering, because the 8.3-meter high and 5-meter wide rudder unit could now be produced from only 96 individual parts, whereas 2,072 single parts were needed for the earlier aluminum version. Today, Airbus aircraft have rudder, elevator units, and the landing flaps on the wings made from carbon-fiber reinforced plastic. Seven metric tons of fiber composites are built into the Airbus A 340 [1.4].

Of course in automotive engineering also, fuel consumption can be lowered by savings in weight, although this is only one motivation for the utilization of polymeric materials (see Table 1.1).

The combustion chamber in a lightweight meteorological rocket serves as an example of a component having anisotropic strength characteristics. This rocket developed by Dynamit Nobel is constructed from glass-fiber reinforced plastic. It is in principle a cylindrical pressure vessel, which is manufactured in the form of a polyester resin rolled tube, reinforced with low-alkali glass fibers. Taking into account the principal sources of stress:

- Internal pressure due to combustion of the propellant charge and
- Bending moments in flight

the combustion chamber is built as a three-layered laminate having a 90° annular winding, a 0° axial layer, and a second 90° annular winding (see Figure 1.6). In this manner the strength of the structural part can be ideally matched to the directionally dependent stresses in a tube under internal pressure in which $\sigma_t : \sigma_a = 2 : 1$.

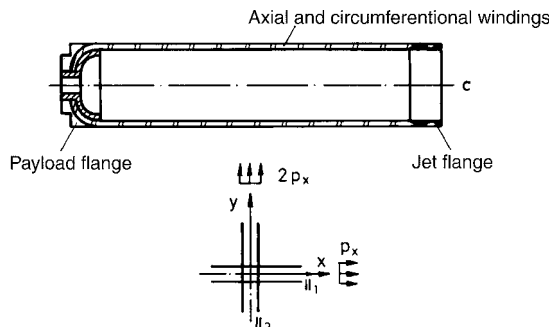


Figure 1.6 Glass-fiber reinforced plastic combustion chamber in the form of a rolled cylinder having a 90°/0°/90° laminate structure [1.5]

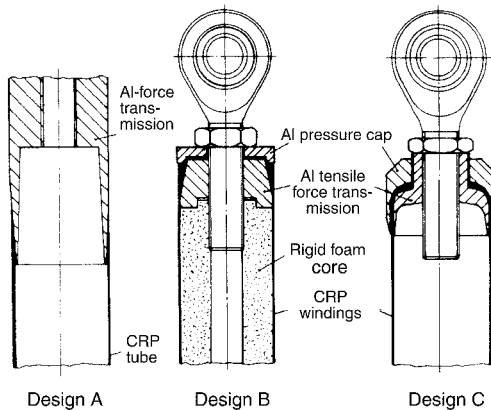


Figure 1.7 Principles of directed transmission of force in compression-tension struts according to [1.6]

Attached at the open end is the jet flange and at the other end the payload flange in such a way that the axially laid glass fibers are led around ribs on the nozzle flange and are laid in slits on the payload flange.

The following application serves as an example of the structural design of force transmission systems.

In a specific wide-body passenger aircraft, the interior of the fuselage is divided into the passenger compartment and the cargo hold by an intervening floor. This flooring is supported on struts which, while having the lowest possible weight, must absorb mechanical loads in the form of high tensile and compressive forces. The struts are composed of a high-strength Al alloy and weigh approx. 1,400 g. A strut having the same load-bearing capacity made of carbon-fiber reinforced epoxide resin weighs about half as much [1.6]. However, the principal problem with such composite structures has less to do with the design and production of the composite than with the directed transmission of force. Three design variants of the directed transmission of force are compared in Figure 1.7.

Design A

When cylindrical tube and flange elements (Design A, right) are bonded, there is only frictional linkage on application of tensile and compressive loads, while in the case of conical joining (Design A, left) there is low positive locking, at least on application of compressive loads. The advantages of this version are the relatively easy production of both the flange as a one-piece turned part and of the tube as a continuous tube. However, control of bonding causes considerable problems. In loading tests, bonding always proved to be the weak point in this design. Quality control in adhesive bonding operations can be difficult but is critical.

Design B

Design B represents two turned parts provided as flange parts. In this case, the carbon-fiber reinforced plastic tube must be rolled over a rigid foam core in a single-piece production operation. Under tensile loads, the force is introduced into the tube in a positive locking

manner via the cone of the flange, while in the case of compressive loading, the tube is supported against the pressure cap.

Design C

Design C represents the most convenient principle of construction. The carbon fibers laid in the longitudinal axis of the tube are laid in loops about the tensile force transmission flange so that optimum positive locking is obtained. The pressure cap placed on top absorbs compressive forces. Although the metal parts require higher production costs, this is compensated because the need for high accuracy in fitting the connecting surfaces is eliminated as is the control of bonding. In loading tests, failures occur predominantly outside the force transmission region; the laminate strength determined in tensile strength tests over the entire cross section of the tube amounting to 548 MPa [1.6].

1.1.2 Precision Engineering

Integrated design methods employing polymeric materials emerged as a main development direction for the European precision engineering industry, which is subject to enormous cost pressures. Companies were striving to cut out as many manufacturing and assembly steps as possible and to systematically exploit the opportunities afforded by thermoplastic processing, such as injection molding, in order to produce multifunctional and readily assembled parts in a single pass. This principle still holds today; it occupies a very important place in the design process in all fields.

Figure 1.8 shows a simple example of an integrated method of construction in comparison with the classical configuration. In order to mount a typical shaft, fix it axially and lubricate it, nine individual parts are required, which can be combined into one or two parts using polymeric materials. Considerations such as the elimination of vendor parts (screws, washers, etc.) and simplification of assembly reveal other advantages of design using polymeric materials [1.7].

Modern construction practices further include the integration of individual functional elements such as springs, anchoring clips, and bearings into base plates or in housing parts (see Figure 1.9).

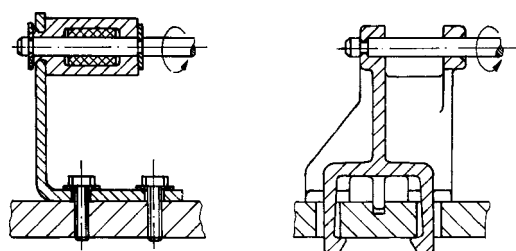


Figure 1.8 Shaft mounting by the classical method (left) and using a multifunctional part composed of polymeric material (right) as described in [1.7]

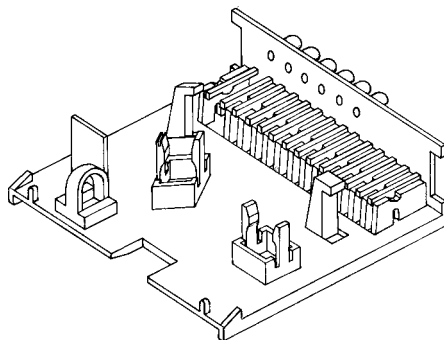


Figure 1.9 Time recorder board with integrated components such as springs, snap-fits, brackets, and so forth

Another example of how subassemblies – usually base plates – with multifunctional tasks can be produced in one working operation is provided by what is known as “outsert” technology. In this case, the principle of task division of functions becomes clear. The support function, rigidity and dimensional stability of the base plate are assumed by a punched blank made from electrolytic or galvanized steel strip, while the tasks of the structural elements such as locating pins, spring elements, snap-fits, axles, bearing points, etc. are fulfilled by appropriate parts made from polymeric material (see Figure 1.10). The latter are injected via a sprue gate in one shot directly onto the blank placed in the parting surface of the injection mold. Closely colocated elements are connected to one another by means of ancillary runners. Most polymeric materials have coefficients of thermal expansion, usually greater than that of steel. This can lead to problems of warpage for thin sheet metal/polymeric material structures. In order to control the problem of differential thermal expansion, expansion joints are provided for elements with large dimensions (see detail in Fig.1.10).

Special problems also arise in precision engineering when trying to produce durable connections between smaller size shafts and hubs. Because of their small dimensions, a positive locking method is often not possible. On the other hand, a merely frictional connection (*i.e.*,

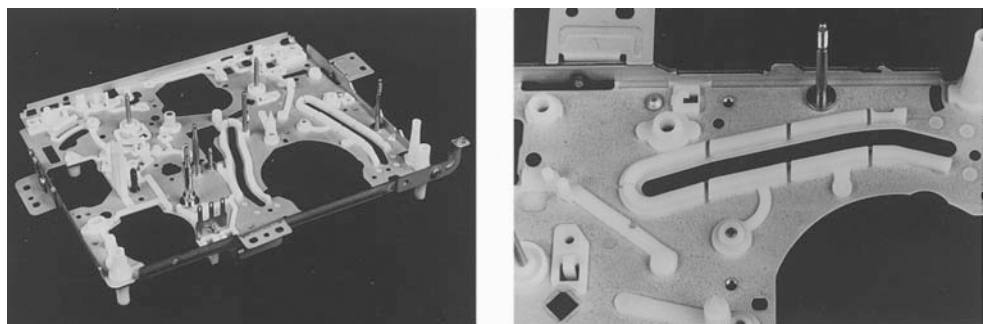


Figure 1.10 Punched blank for a drive with components made from POM injected into position by the outsert technique

(Photo courtesy: Öchsler, Ansbach)

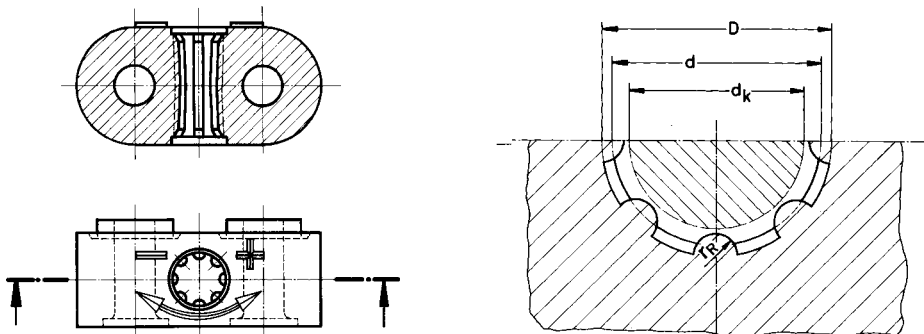


Figure 1.11 Block for accommodating a regulating screw with eight round ribs in the opening according to [1.8]

press fit) may be easy to assemble but from the outset may not be reliable because of stress relaxation in the polymeric material hub that can be expected. In the case of a particularly ductile polyamide (PA 11) it was demonstrated experimentally that a frictional connection to a shaft 0.6 mm in diameter can be produced using a 10% undersized bore which satisfies the requirements for a small press-fit gear wheel in an electricity meter. According to the rules for agency approval, an appliance service life of 20 years must be guaranteed [1.8]. Although, given the unusual degree of undersizing, the polymeric material is deformed at the jointing point beyond the apparent limit of elasticity, the supporting action of the adjacent sections of material is evidently sufficient to maintain the connection. Further support is provided in that the coefficient of friction increases in direct proportion to the service life.

The design of a precise and reliable regulating mechanism, e.g., for the mechanical adjustment of metering equipment, creates problems of a similar nature. If adjustments are to be made by a fine-thread screw passing through a part made of a polymeric material, it must be ensured that adjustment ensues with low force, but that unwanted adjustment (rotation) due to the action of any vibrations does not occur. This performance does need to be retained for years. A design proven to fulfill these requirements very effectively is comprised of eight semicircular ribs arranged around the circumference of the hole for the adjustment screw. This concept works when the area of the semi-circular ribs overlapping with the thread cross section amounts to between 33 and 43% of the cross-sectional area of the threads. In this design, the yield stress of the polymeric material is deliberately (partially) exceeded and the supporting action of the base of the ribs is utilized to maintain a degree of pretensioning.

1.1.3 Automotive Engineering

In modern automobiles, interior fittings account for the major portion, approximately half, of the consumption of polymeric materials. Exterior applications (spoilers, bumpers, lights, etc.) are in second place, accounting for about one quarter of consumption.

Examples of applications, which are not immediately obvious, are found under the hood in the engine compartment (see Figure 1.12).

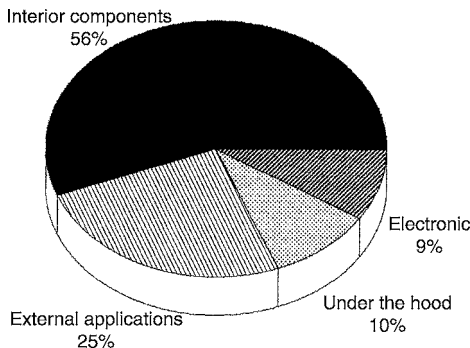


Figure 1.12 Breakdown of use of polymeric materials in a mid-range automobile

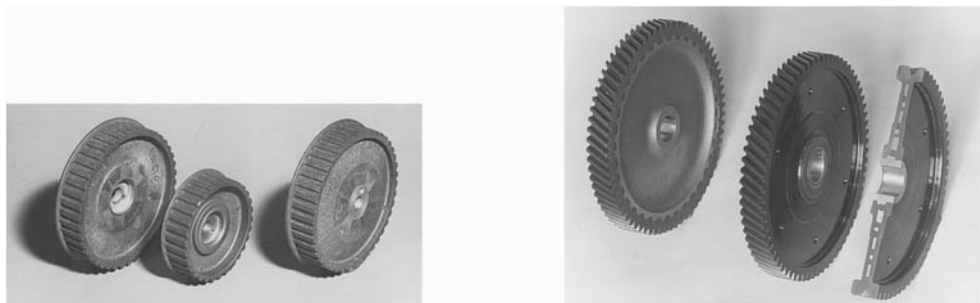


Figure 1.13 Various types of valve timing gear wheels made from polymeric material

Structural elements made from heat-stabilized polyamides have been used for years in the engine compartments of automobiles. Figure 1.13 shows a variety of valve timing gear wheels, some for helical gear drives and some for synchronous belt drives. These are examples of one of the first versions of such wheels from the 1960s. In operation, valve timing gear wheels are acted on by alternating torques with superimposed rotary oscillations. In the examples shown, the actual wheel part with the gearing is overmolded around a punched metal disk, which for its part is welded to a steel hub. This composite structure provides the wheel with high rigidity in the radial direction. In the axial direction, however, the wheel disk is flexible so that load peaks acting in the radial direction due to the helical gearing are dissipated by reversible axial deformations of the wheel disk. In doing so, the tooth faces slide distances up to 1 mm against one another. Although such wheels have proved to be effective, they are no longer used in this expensive configuration. Nevertheless, this principle still remains as an example of how peak loads can be dissipated by deformation.

The savings in weight and costs by the use of polymeric materials in applications under the hood are considerable as shown in Table 1.2.

Very complex polymeric material parts can be injection molded using the “fusible core” injection molding process. The internal dimensions of each part are formed by a low melting temperature metal core that is “melted out” after molding. One of the largest single applications is for automobile engine intake manifolds made from glass fiber-reinforced PA 66 (see

Table 1.2 Cost and Weight Savings Due to the Use of Polymeric Materials

Engine component	Cost saving [%]	Weight saving [%]
Air intake systems	40	50
Valve covers	20	10
Acoustic parts	50	30
Oil pans	20	15
Styling parts	25	20

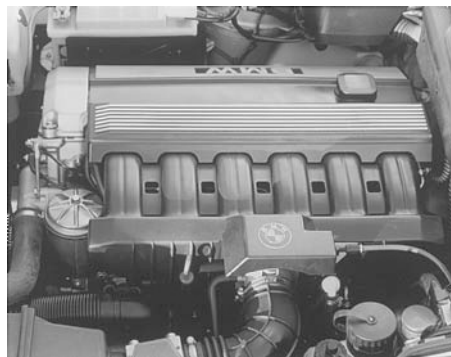


Figure 1.14 Air intake system made from reinforced PA 66 for a BMW 6-cylinder engine (manufacturer: Mann & Hummel, Ludwigsburg)

Figure 1.14). By comparison with conventional pressure diecast aluminum manifolds, the polymeric material counterparts exhibit a series of notable advantages [1.27], including:

- Weight reduction of 30 to 60%;
- Better surface quality and hence lower drag, *i.e.*, enhanced performance; and
- More freedom in contour forming and the possibility of integrated design and hence the potential of lowering of component costs (although process costs may offset this).

Today, due to the relatively high cost of fusible core injection molding, intake manifolds are predominantly injection-molded in two parts and joined by welding, or more recently, by means of snap-fit connections. For snap-fit assemblies, an additional seal is needed between the two halves.

Gas and clutch pedals are mainly manufactured from bent metal profiles or punched metal sheet and supplemented with additional parts, such as foot plates and bearing points, by welding. Injection-molded pedals made from thermoplastic polymeric materials (see Figure 1.15) have already been used in volume production, in some cases for years. These pedals are now no longer installed as single parts but rather prefabricated as a full set of polymeric material pedals in a single unit. The improved manufacturability and suitable performance of early polymeric pedal assemblies may result in a general substitution of metal parts by polymeric materials. Glass-reinforced PA 66, which can be specially impact-modified, has proved to be a material affording high margins of safety for this critical application [1.30].



Figure 1.15 Various types of pedals made from glass-reinforced PA; in some of them, the material is also impact-modified

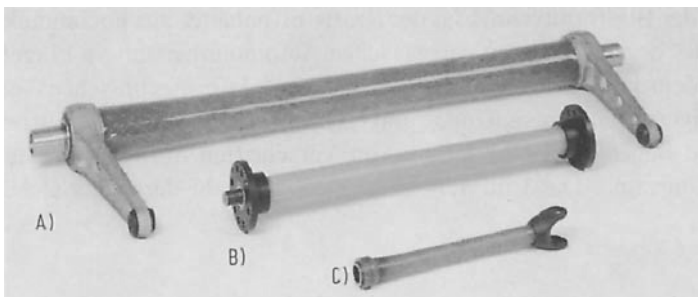


Figure 1.16 Types of glass-fiber reinforced plastic tubular torsion springs [1.9]

- A: Rear axle stabilizer constructed of glass-fiber reinforced plastic and steel for a truck (Thyssen-Henschel, Kassel)
- B: 500 mm long GRP tubular torsion spring for a passenger vehicle
- C: Torsionally elastic Cardan shaft for a motorcycle

Springs of various types provide examples of heavy-duty fiber composite structures for automotive engineering. Figure 1.16 shows a selection of torsion springs, which were developed for a variety of different applications [1.9].

The *lightweight stabilizer* (A) was developed for the rear axle of a truck with a total weight of 9.2 t. Cost considerations led to a combination of a rolled glass-fiber reinforced plastic tube with metal levers. In initial tests, the stabilizer was subjected to a single-stage alternating-load test involving torsional deformation of $\pm 5^\circ$. After $2 \cdot 10^4$ load changes, microcracking and delamination were observed. However, in subsequent driving tests on dirt tracks and normal roadways the stabilizers proved themselves reliable.

The glass-fiber reinforced plastic *tubular torsion spring* (B) was developed as a support spring for a passenger vehicle rear axle [1.28]. A torsion angle of 30° for a length of 440 mm and a limiting torque of 1,700 Nm were required. The nominal shear stress was approx. 250 MPa. Such components can be manufactured on an industrial scale using suitable production equipment to withstand up to a minimum of $2 \cdot 10^5$ vibrations to failure. The somewhat abrupt fracture characteristics, however, are regarded as a problem but can be improved.

The glass-fiber reinforced plastic *cardan shaft* for a motorcycle (C) is a rotating tubular torsion spring. During driving, the Cardan shaft is under a relatively high asymmetric stress distribution in both directions of rotation. Here, a major advantage of glass-fiber reinforced plastic structures comes into play: in the case of such asymmetric stresses, the fiber distribution can be adjusted in line with the stress. Of course such developments should no longer be pursued without computer modeling support (see [1.9]).

Fuel tanks blow molded from high molecular weight HDPE are applications worthy of note. They have now been introduced by many automobile manufacturers. Compared with conventional sheet metal tanks, they offer advantages not only in production engineering but also in much better utilization of space (*i.e.*, design flexibility), weight savings, corrosion resistance, and safety. Figure 1.17 shows a selection of such tanks.

Certain problems arise in meeting the ever tighter regulations concerning the permissible fuel diffusion rate*.

Polymeric additives provide one possible solution. As an example, the DuPont Selar process affords another possibility. This involves mixing 6 to 8% of Selar (polyamide 6 and bonding agent) with the HDPE prior to processing. During plasticization the pellets of granulated polyamide begin to melt, softening only to an extent that they are deformed by shear forces into thin platelets and in this way form a barrier layer on the walls of the tank.



Figure 1.17 Various blow molded fuel tanks made from high molecular weight HDPE

* Measurements have shown that during the service life of a passenger vehicle approx. 27 l of fuel evaporate as a result of diffusion, whereas during refueling approximately 150 l are lost. Attempts are being made to reduce refueling losses by means of pump nozzle design. Some processes for reducing the permeation rate have been successfully applied [1.10]. For example, by means of fluorination, *i.e.*, treating the tank's walls – preferably the inner walls – with gas containing fluorine, a barrier effect is achieved by substituting hydrogen atoms in the HDPE by fluorine atoms.

Of course, extremely good barrier layers can also be obtained by coextrusion blow molding of polyamide or ethylene-vinyl alcohol (EVOH) and HDPE. The thin barrier layers are located near the center and must be linked to the HDPE by films of bonding agent. The impact resistance of such composites can be a problem, especially at poorly produced pinch-off welds. However, this technology is effective.

Another possibility for producing effective barrier layers is provided by the plasma polymerization process [1.31].

1.1.4 General Mechanical Engineering

In sectors of general mechanical engineering, polymeric materials have already taken up a strong position as materials for classic machine elements such as gear wheels, slide members, rollers, and other mechanical components. Here materials handling technology is listed among the sectors which have made the greatest progress in the use of such structural elements made from polymeric materials. The state of the art today includes running wheels for cranes, cable reels, gearwheel and chain wheel drives, and slideways made from low coefficient of friction semi-crystalline polymers such as polyamides as well as wear-resistant cladding and damping elements made from polyurethane.

In the case of crane running wheels, lateral guidance is not effected by wheel flanges but rather by pressure rollers arranged at the side (see Figure 1.18), thus overcoming the problems of strength and wear of wheel flanges.

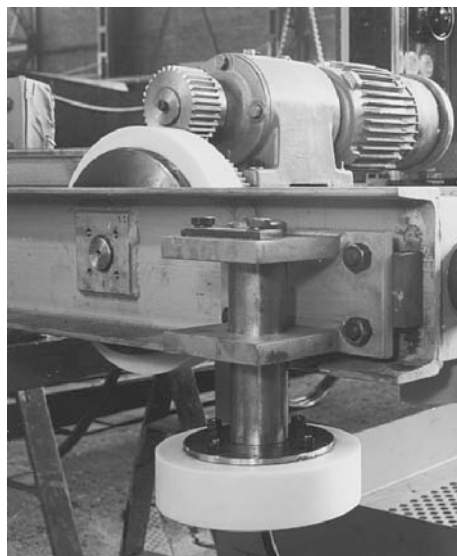


Figure 1.18 Crane running wheels without wheel flanges composed of cast PA.
Lateral guidance of the 3 Mt gantry crane is carried out by separate pressure rollers.
Free span of crane 11.5 m, tare weight of crane approx. 4 t, max. speed of travel 60 m/min.

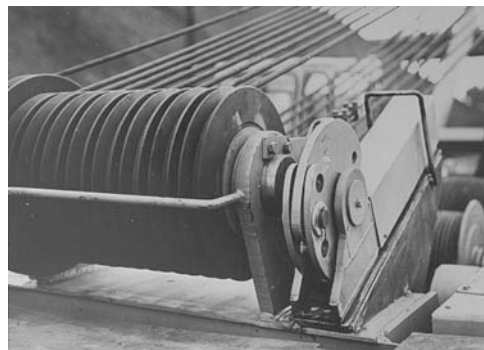


Figure 1.19 Battery of cable reels made from cast PA in a mobile crane.
In the case of 18 reels, the axle load can be reduced by almost 1 t.

Cable reels made from polymeric materials are of interest in materials handling technology for two reasons. Wherever low weight is important, e.g., in mobile cranes (see Figure 1.19) or crane jibs, they contribute to increasing the useful load (and to making assembly easier). In addition, they subject the cable in the groove to less stress, which has been shown to lead to an extension of the service life of the cable by a factor of two to four.

Because of their low weight and high strength, components made from carbon-fiber reinforced polymeric materials are predestined for applications subject to high accelerations, such as in textile machinery design.

1.1.5 Design of Technical Equipment

The origins of the use of polymeric materials in the design of technical equipment date back to the period 1935–1942 [1.11]. Work centered on thermoplastic semi-finished materials which were tested and then employed predominantly as substitute materials in applications requiring good corrosion resistance.

Today, the following key applications may be identified in this sector [1.12]:

- High-volume parts (compression molding, injection molding, extrusion), e.g., filter plates and frames (PE, PP), filter nozzles (PE, SB), small parts (PE, PP, PVC), and heat exchanger plates (PP, SB, PPO, PES);
- Short-run parts and single parts (manual production, compression molding, winding), e.g., containers (glass-fiber reinforced plastic, glass-fiber reinforced plastic/thermoplastic liner), cladding (PE, PP, PIB, fluoropolymers, PVC), pumps and fans (PE, PP, PVC, PU, GRP).
- Piping (extrusion, winding), e.g., pipes, fittings and flanges (PE, PP, PVC, GRP).

Figures 1.20 to 1.23 provide some insight into the state of the art after the technical objective of corrosion protection has been achieved [1.13] and design experience and principles of engineering calculation are further developed [1.14 to 1.17].

**Figure 1.20**

Self-supporting chimney made from glass-fiber reinforced UP for corrosive waste gases during erection. The height above ground is 45.3 m; the internal diameter of the cylindrical part is 2.5 m and at the top end 3.5 m. The chimney is supported at a height of 12 m so that it is freestanding over a length of approximately 33 m. The static calculation is based on wind speeds of up to 150 km/h and a waste gas temperature of 60 °C for a permissible deflection of 300 mm.

**Figure 1.21**

With a capacity of 1,000 m³ this tank for the temporary storage of 70% sulfuric acid is the largest glass-fiber reinforced plastic tank manufactured so far by the winding method. The inside of the tank is provided with a lining of 4 mm thick PVC panels. Calculations for the tank were based on a safety factor of 1.75 for failure due to fracture. Together with the material-specific reduction coefficient, overall safety factors of 5.0 for strength and 4.5 for bulges were taken into account [1.18].

Problems in the use of polymeric materials in technical equipment, which have so far not been solved, relate to the high manual effort in one-off production and the less mature technologies compared to processes such as injection molding and extrusion. This often applies to joining techniques, in particular welding [1.12].

Fiber composites are attractive materials for large fans and rotor blades. Fans made from glass-fiber reinforced UP resins with diameters of several meters are employed, for example, in cooling towers. The marked improvement of performance in gliders and powered aircraft due to the use of glass-fiber reinforced plastic and carbon fiber reinforced plastic has also stimulated the development of rotor blades for wind turbines. In these parts, structural problems occur repeatedly at junction points where high bending moments and transverse forces must be transmitted to a steel hub. Typical solutions for this problem are sketched in Figure 1.22. The loads are transmitted from the circular glass-fiber reinforced plastic ring to an outer and an inner steel jacket via toggle bolts (see Figure 1.22, top). The blade holder is

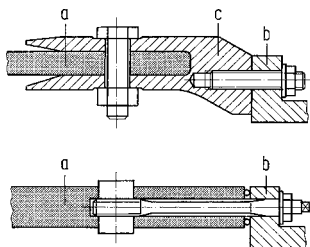


Figure 1.22 Principles of load transmission from glass-fiber reinforced turbine blades to steel hubs [1.29]
top: connection of the blade
(a) with the steel hub (b) via a blade holder (c) and toggle bolts
bottom: connection via pretensioned bolts

tapered at the end and does not fit against the glass-fiber reinforced plastic so that stress peaks due to an abrupt change in rigidity are prevented. The variant in the lower part of the figure avoids the double diversion of the force flux [1.29]

The heat exchanger in Figure 1.23 is said to be the largest single application of polytetrafluoroethylene (PTFE) in the last 10 years. Materials for such applications must be resistant to the corrosive acids (HF, HCl) formed when the temperature falls below the dew point. A further advantage of PTFE is its extremely low surface energy so that no deposits of soot, ash, etc. will form.

Other applications of PTFE in technical equipment include all types of claddings, pipes, fixtures, and fittings exposed to corrosive media and fibers in filtration plants [1.26].

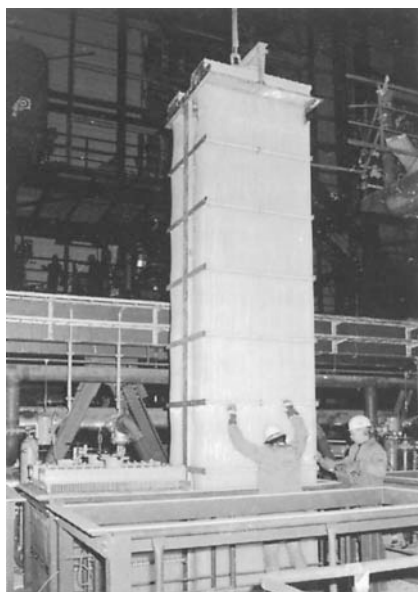


Figure 1.23 Heat exchanger for a flue gas desulfurization plant
(Photo: Bayernwerke AG)

1.1.6 Construction Industry

Window frames, siding, roof members, floor coverings, and drain pipes are established applications of thermoplastic materials such as PVC, ABS, and PP in the construction industry. Containers of all kinds made from glass fiber-reinforced UP resins are also state of the art.

The following examples of applications are not obvious at first sight.

ABS and PP are often used for hot water drainage components. Cross-linked HDPE has achieved acceptance alongside PP and polybutene (PB) as pipe material for underfloor heating systems. Apart from its use in buildings, cross-linked HDPE piping is also used in a modified technology for underground heating in sports grounds (Figure 1.24), airport runways, highways, and bridges in order to keep them clear of snow and ice.

Perhaps the first load-bearing structural part made from a thermoplastic polymeric material to receive general building approval in Germany was the plug made of PA 6 for fastening siding panels in place (see Figure 1.25). The principle of the expansion anchor in this case requires a polymeric material which, on the one hand, is sufficiently ductile when the screw is being driven home and, on the other hand, does not creep under constant tensile load to such an extent that the fastening would become insecure.

The first requirement would indicate that an unreinforced, unfilled thermoplastic should be used. The space to be filled by the plug and the screw are matched in such a way that when the screw is tight in place, the polymeric material is in a state of hydrostatic tension and stress relaxation is minimized. The creep along the outer surface of the screw was investigated in appropriate long term tests.

Today, there is such tight control of manufacturing tolerances in the construction of profile sections that installation-ready structural elements can be manufactured. An example of this is provided by thermal insulation barriers for aluminum window profile sections. Such barriers made from glass fiber-reinforced PA 66 impede the heat flow between the inner and outer parts of the aluminum window profile while conforming with thermal insulation regulations



Figure 1.24 Laying of pipes made from cross-linked HDPE for underground heating in the Munich Olympic stadium

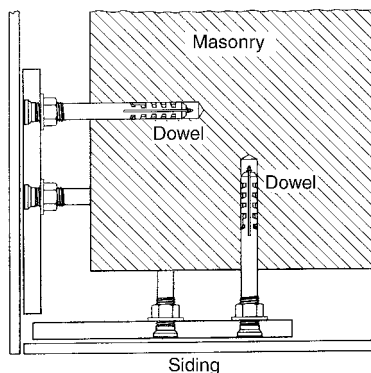
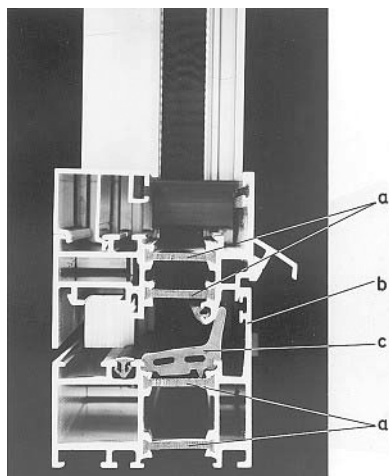


Figure 1.25 Expansion anchor made from PA 6 for fastening siding panels
(Photo: Fischer, Tumlingen)



- a) Insulating barriers made of glass fiber reinforced PA66
- b) Aluminium profile
- c) Seal profile

Figure 1.26 Section through an aluminum-polymer composite window frame fitted with glass fiber-reinforced PA 66 insulating barriers, System Wieland-Werke, Ulm
(Photograph: TKG Ensinger, Nufringen)

(see Figure 1.26). They are wedged into aluminum profiles, the fitting points being profiled or scored to achieve an additional form-fitting connection and to ensure uniform transmission of force along the length of the part [1.19].

In railroad construction, by the end of the 1960s, “anchors” made from HDPE had already replaced the earlier standard version made of hardwood. In the case of concrete sleepers these anchors are inserted into the sleeper mold during manufacture. Rail bearing plates composed of ethylene-vinyl acetate copolymer (EVA) provide an elastic interlayer for distributing loads uniformly and reducing edge pressure from the concrete sleepers.

The rails are usually fastened by tension springs above what are known as angular guide plates. The guide plates manufactured earlier from rolled steel profile sections are now produced

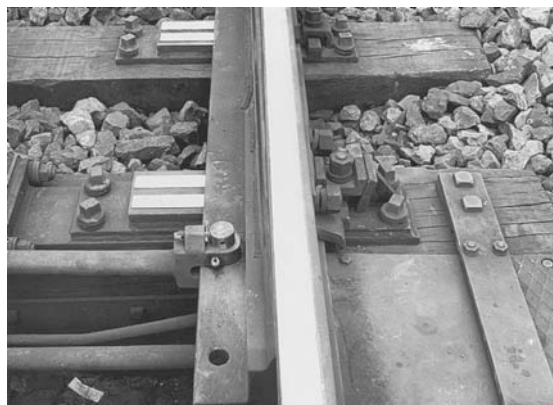


Figure 1.27 Switch slide chair covered by PBT slide plates

from PBT or PA by injection molding at much lower capital and production costs. The polymeric plates also help dampen vibration.

The lubrication of switch slide chairs represents an environmental pollution problem and is, in addition, a constant hazard for maintenance staff. Tests conducted in the 1970s on slide plates made from polymeric material (see Figure 1.27) had a positive outcome and resulted in switch slide chairs in various private railroads, subways, and industrial sidings being covered by maintenance-free or low-maintenance slide plates based on PBT or PA.

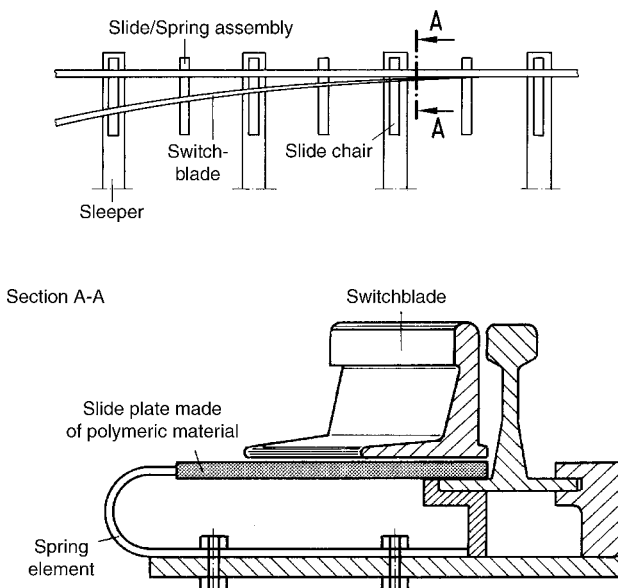


Figure 1.28 Sketch of the underlying principle of a switch setting mechanism having an elastically mounted slide plate affording relief of stress as the train passes over [1.20]

The principal load on these covers arises when a train passes over the switch in that a high, repeated compressive stress with an occasionally superimposed tangential relative movement acts through the adjoining switch blade. In a costly structural variant, this stress should be counteracted in that, after the switch has been set, the slide plate is pushed down by the weight of the vehicles and the switch blade then lies directly on top of the metal switch chair so that the slide plate is relieved of pressure while the train passes over (see Figure 1.28) [1.20]. Although this design was never used, the design principle is of fundamental importance.

As traffic becomes more frequent, measures for noise and vibration insulation are assuming greater importance. Accordingly, subway tracks and new railroad routes under construction by the Deutsche Bundesbahn are being laid on 20 mm thick PU mats foamed to densities of approx. 500 kg/m^3 . In addition, in highway construction, noise insulation walls made from PVC are being built as illustrated in Figures 1.29 and 1.30.



Figure 1.29 Noise insulation wall on a freeway close to residential areas

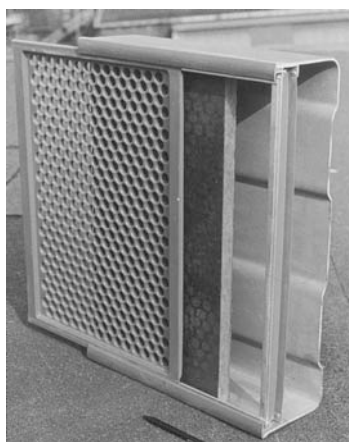


Figure 1.30 Structure of noise insulation panels composed of a PVC frame, glass mat, and perforated PVC wall. These perforated panels are provided initially with thermoformed depressions whose bases are subsequently sawn off.

1.2 Forecast

The future prospects for a material depend on various parameters the most important of which are included in the following relationship [1.21]:

$$FP = f(A_R, E_C, C_p, M_A) \quad (1.1)$$

The independent variables of which FP (future prospects) is a function are defined as follows:

- A_R is the availability of the raw material (e.g., iron ore, crude oil). Shrinking reserves of raw materials are less of a barrier to the production of adequate volumes of polymeric materials (a situation which is more applicable to wood) than political and economic events.
- E_C is the energy consumed for refining and producing the raw material (reduction of iron ore, polymerization of the monomer). Figure 1.31 shows the relative energy consumption for producing some selected materials.
- C_p is the cost of further processing. Statements about this with regard to energy consumption have already been made earlier. Machining is a method of further processing for both metals and polymeric materials and, therefore, allows direct comparisons, although most high volume plastics are molded via some means.
- Polymeric materials generally exhibit higher machining performance, in particular for high machining volumes (e.g., gear wheels with a high modulus). When polymeric materials are handled, cost savings can be significant (see Figure 1.32).
- M_A is the acceptance of the material in the marketplace. Given that the market actually exists, the conditions for this are that the characteristics of the material, in particular the price-performance ratio and increasingly the recyclability and/or the ecological audit of the material*, conform to market expectations.

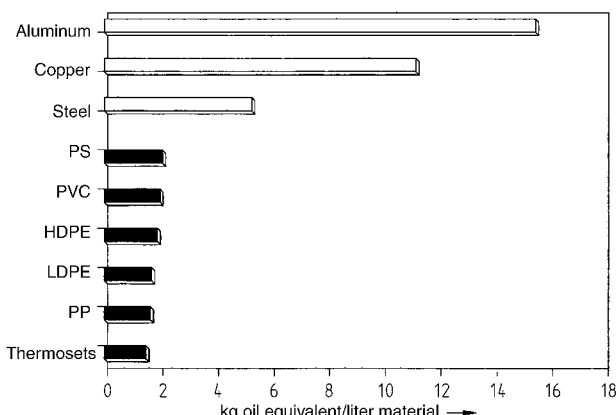


Figure 1.31 Energy consumption for producing various materials

* The true recyclability of a material must not be evaluated in isolation without holistic consideration of its environmental impact starting from the production of the material through any environmental benefits of the parts made from it.

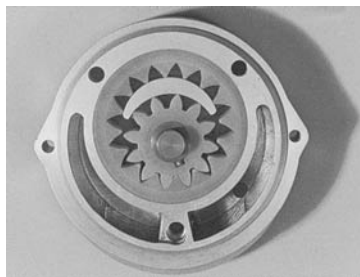


Figure 1.32 Damping element in hydraulic elevator equipment for ski lifts. The wheels in the gear-type pump illustrated are produced from POM and PBT in compliance with IT 7 tolerance quality. When produced by machining, cost savings of 40% are achieved compared with the machining of metal.

(Photograph: TKG Ensinger, Nufringen)

Combining the individual factors, it may be concluded that the market for polymeric materials will likely continue to grow. Commodity polymeric materials (e.g., PP, PE, PS, etc.) based on known monomers will experience higher volume as selective polymer architecture and new catalyst systems evolve. They will push forward into the spheres of application of engineering materials (e.g., PA, POM, PC), which will also continue to grow. These, and particularly high-performance thermoplastics (PEEK, PES, LCP), will likely increase in volume to a lesser degree. Accordingly, there is no great expectation of seeing a plethora of new polymers made from new monomers although “some” will be introduced. Monomers that can be efficiently and easily polymerized have very largely been studied in the past. In addition, launching new polymeric materials is clearly becoming more difficult as the market becomes saturated.

For example, materials such as poly(aryl)ether ketones (PAEK, PEEK and the like) and liquid crystal polymers (LCP) have been on the market for some years. They have remarkable properties. Many notable plastics manufacturers make these polymers available. Unfortunately, it has become clear that the market is not as receptive as originally thought. Most suppliers have now dropped these products although they are available commercially and are used in many applications. The high price necessitated by low production volumes certainly played a major role in this.

A vision for the future might be the production of more polymers whose backbone is not made up primarily of C atoms, but rather of Si-O groups (*i.e.*, silicones).

New Production Processes for Known Polymeric Materials

Modifications and selective improvements of properties clearly offer better market prospects. The most important possibilities worthy of note here are those afforded by *metallocene catalysts*. The structure of the molecule, *e.g.*, its tacticity, or a co-monomer placement can be controlled using these catalysts so that variables such as crystallinity can be altered and, as a result, those properties depending on the degree of crystallinity can be modified. This may be seen in Table 1.3 in the example of the melting characteristics of polystyrene.

PP is also produced using metallocene catalysts. The crystallinity of isotactic polypropylene can be further increased by these catalysts so that a degree of rigidity is attained, which can be

Table 1.3 Alteration of Tacticity, Morphology, and Melting Behavior of Polystyrene

Tacticity	Production	Morphology	Glass transition temperature and melting point
Atactic	Free-radical	Amorphous	$T_g = 100 \text{ }^\circ\text{C}$ $T_m = \text{NA (amorphous)}$
Isotactic	Ziegler-Natta catalysis	Semi-crystalline	$T_g = 100 \text{ }^\circ\text{C}$ $T_m = 210 \text{ }^\circ\text{C}$
Syndiotactic	Metallocene catalysis	Semi-crystalline	$T_g = 100 \text{ }^\circ\text{C}$ $T_m = 270 \text{ }^\circ\text{C}$

Table 1.4 Comparison of Talc-Reinforced PP and Highly Crystalline PP

Property	PP talc-reinforced (20%)	PP highly crystalline
Elastic modulus MPa	2600	2400
Density g/cm ³	1.04	0.905
Heat distortion temperature HDT/B 4.5 MPa °C	118	120

matched by conventional PP only when it is reinforced, e.g., by talc (see Table 1.4). A particular advantage of this very highly crystalline PP by comparison with talc-reinforced PP is its better scratch resistance and lower specific gravity [1.34].

Another important development related to metallocene catalysts is the commercial introduction of cycloolefin copolymer (COC). Metallocene catalysts made the commercial production of this polymer possible. Like PE, COC is a polymeric material composed only of carbon and hydrogen and therefore it has a low density. It also has a glass transition temperature of more than 150 °C, making it suitable for relatively high temperature applications. It is highly transparent and because of its aliphatic structure (without double bonds) is optically isotropic with extremely low optical birefringence. It has been used for applications, such as optical media and other applications where polycarbonate might be used, particularly as additional chemical resistance is required [1.33].

There is also still some potential – less for large volumes than for technically interesting applications – in continuous strand-reinforced thermoplastics or glass mat thermoplastics. Thermoplastics having continuous or long strand reinforcement have strength and simultaneously impact resistance, even at lower temperatures (see Figure 1.33). At present, PP is the most frequently used matrix material. There is, however, special interest in the use of high temperature thermoplastics such as PEEK as a matrix material in order to achieve higher heat resistance. In contrast with laminating and prepreg processes involving thermosetting resins, glass mat thermoplastic compression molding processes can be run with relatively shorter cycle times.

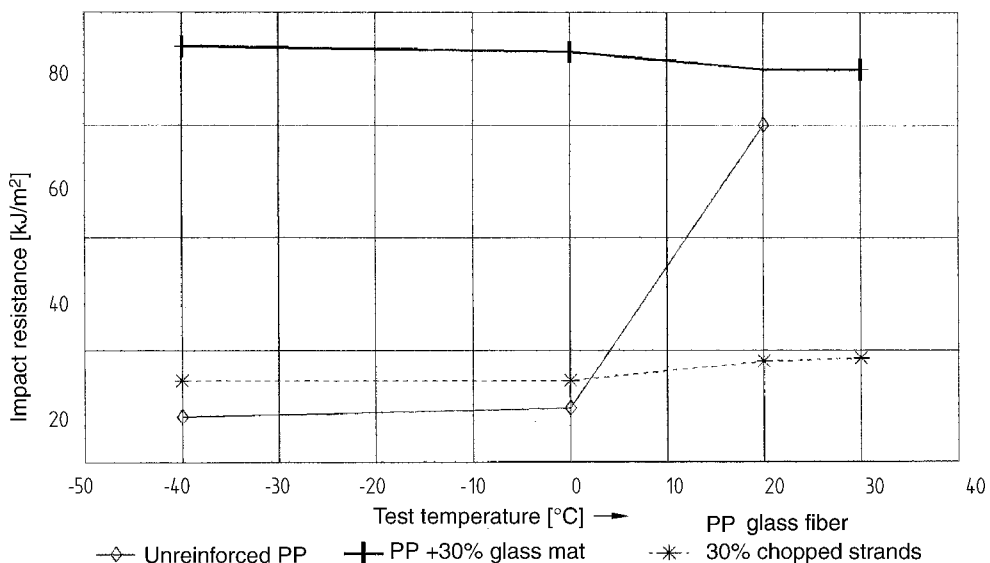


Figure 1.33 Impact resistance of different polypropylene grades

New Applications

Forecasts of specific new applications are always encumbered with a high degree of uncertainty. In *automotive engineering*, further applications in the engine area can be expected. Developments of load-bearing structures in running gear (tie rods, springs, etc.) made from glass-fiber reinforced polymeric materials and high-strength fiber composites have already largely been introduced but have not yet gone into mass production.

Body parts having large surface areas such as fenders, tailgates, or hoods made of SMC are already in use in some high-volume products. Whole bodies made from glass-fiber reinforced resins (usually SMC) are already state of the art for smaller production series.

Exterior body applications using thermoplastics for parts such as bumpers, fenders, doors, spoilers, ram guard strips, mirror housings, and lights, have long been known.

Whole bodies or at least body parts made from *thermoplastics* for high volume vehicles are under development. The use of colored thermoplastic polymeric materials for auto body panels (using either internal pigments or in-mold paint films) are being developed aggressively. For example the Smart car has a complete outer skin made from a PBT/PC blend, which is coated only with a clear coat of lacquer. The Mercedes A class is one of the first mass-produced vehicles having a tailgate made from a thermoplastic PPE + PA blend [1.37]. The thermoplastic part is bonded to a reinforcing framework made of glass mat thermoplastics (see Figure 1.34) and painted off-line*. The fenders of this vehicle are also made from PPE + PA, but are painted in-line.

* An ASA/PC blend has also been used recently and colored polymeric films have also been back-injected (*i.e.*, in-mold paint film).



Figure 1.34 Load-bearing glass mat thermoplastic part for the tailgate of the Mercedes A class

Designers are already talking about easily interchangeable body parts so that the automobile owner can alter the color of his/her vehicle at will or even make it multicolored following fashion dictates [1.36].

Windows – starting with the rear and side windows – have also become a development target for the medium term. Polycarbonates with scratch-resistant silicate coatings together with their lower weight offer good prospects for this development [1.35].

An innovative development in *streetcar and railcar construction* has been launched in Switzerland. The whole car body is produced as a wound part using glass-fiber reinforced resin. Some vehicles manufactured by this method are already doing well in testing (see Figure 1.35). There are still problems with the rigidity of the body, which is not always satisfactory, and with the potential risk to passengers in the event of an overhead cable failure.



Figure 1.35 Low-platform “Cobra” streetcar produced completely from fiber composite materials in sandwich construction [1.32]
(Photograph: Schindler Waggon)



Figure 1.36 Insertion of a prefabricated interior-fittings module made from fiber composite materials as part of the complete renovation of an old railroad car [1.32]
(Photograph: Schindler Waggon)

This concept also extends to the renovation of out of service cars by introducing totally wound passenger cells into the old cars (see Figure 1.36).

In *electrical engineering*, polymeric materials, especially those resistant to high temperatures, are viewed as good prospects. These will overcome insulation problems when power is increased and components are made smaller. There are also unimagined opportunities in *microcircuitry* with regard to the miniaturization of components and subassemblies.

Most polymeric materials are good electrical insulators. On the other hand, thermoplastic polymeric materials are rendered electrically conducting by the use of suitable fillers in order to achieve a certain degree of electrical conductivity (e.g., for shielding applications). In these cases, the ease of processing by injection molding should be largely retained.

Inherently electrically conducting polymeric materials (e.g., polyacetylene or polypyrene) are also available [1.23, 1.24, 1.25]. They may have applications in battery construction and solar technology.

It is thought that in the future, information will be transferred by means of photons rather than electrons and the fiber-optic cables and devices will be made from polymers. Polymers having nonlinear optical properties allow frequency doubling and hence open up many technical opportunities and new technologies.

In *medicine* and *medical technology*, polymeric materials contribute to the preservation of life and to the quality of life. Reference will only be made here to the development of membranes for dialysis, but there are scores of other developments.

In other fields of technology (valve and fittings manufacture, pneumatics, hydraulics and textile machinery) steady growth will be observed, in particular due to applications in fields which to date were the exclusive preserve of metals, especially nonferrous metals. At the same time, problems of demonstrating and predicting service life will still have to be solved.

Consumer-related fields involve intensive use of polymeric materials but they are also subject to scarcely predictable fashion trends.

References

- [1.1] EHRENSTEIN, G. W.: Polymerwerkstoffe (Polymeric materials), Hanser-Verlag, Munich Vienna 1978
- [1.2] EHRENSTEIN, G. W. and G. ERHARD: Konstruieren mit Kunststoffen – Ein Bericht zum Stand der Technik (Building with plastics – A report on the state of the art), Hanser-Verlag, Munich Vienna 1983
- [1.3] BRENNER, H.: Bauteilentwicklungen von Leichtbau-Faserverbundkonstruktionen (Structural parts developments in lightweight fiber composite structures), *Kunststoffberater* **36** (1991) 9, pp. 38/41
- [1.4] BECKER, H. and E. NEISE: CFK befähigt den Flugzeugbau (CRP lends wings to aircraft construction), *Kunststoffe* **88** (1998) 4, pp. 488/492
- [1.5] GERLACH v., G.: GFK-Bauweisen für Raketenbrennkammern (GRP construction methods for rocket combustion chambers), 20th Intern. Chemical Fiber Conference, Dornbirn, 1981
- [1.6] STÖFFLER, G. and H. WURTINGER: Zug-Druck-Strebe aus CFK aus Verarbeiten und Anwenden kohlenstofffaserverstärkter Kunststoffe (Compression-tension struts made from CRP by processing and using carbon-fiber reinforced plastics), VDI-Verlag, Düsseldorf, 1981
- [1.7] VORBACH, G.: Anforderungen an das Spritzgußteil aus der Sicht des Entwicklers und Konstrukteurs (Requirements on injection-molded parts from the point of view of the developer and designer), *VDI-Gesellschaft Kunststofftechnik Jahrbuch* (Plastics Technology Yearbook) 1980, pp. 89/116
- [1.8] HERZIG, K.: Konstruktionsbeispiele aus der Feinwerktechnik (Design examples from precision engineering), *Kunststoff-Berater* **18** (1973) 4, pp. 231/238
- [1.9] PUCK, A.: GFK-Drehrohrfedern sollen höchstbelastete Stahlfedern substituieren (GRP tubular torsion springs to substitute maximum stress steel springs), *Kunststoffe* **80** (1990) 12, pp. 1380/1383

- [1.10] KARSCH, U. A.: Permeationsminderung, dargestellt am Beispiel des Systems Kunststoffkraftstoffbehälter (KKB) (Permeation reduction illustrated with reference to the plastic fuel tank (PFT) system), *VDI-Gesellschaft Kunststofftechnik Jahrbuch* (Plastic Technology Yearbook) 1996, pp. 165/189
- [1.11] KRANNICH, W.: Kunststoffe im technischen Korrosionsschutz (Plastics in industrial corrosion protection), Hanser-Verlag, Munich Vienna 1943/1949
- [1.12] NESTLER, W.: Der Kunststoff-Apparatebau – Stieflkind der Kunststoffverarbeitung (Plastics in technical equipment – Cinderella of plastics processing), *Chemie-Technik* **10** (1981) 11, pp. 1167/1169
- [1.13] NESTLER, W.: Beitrag zum Thema Auskleidungstechnik (Contribution to the subject of cladding technology), *Plastverarbeiter* **28** (1977) 2, pp. 71/76
- [1.14] NEITZEL, M., W. SCHNEIDER and R. LAUX: Gestaltung von Apparaten aus glasfaserverstärkten Kunststoffen für Chemieanlagen (Design of equipment made from glass-fiber reinforced plastics for chemical plants), *Plastverarbeiter* **30** (1979) 1, pp. 3/6
- [1.15] DÜRKOPP, J.: Beitrag zur Stabilität gebetteter Zylinderschalen aus glasfaserverstärkten ungesättigten Polyesterharzen (Contribution to the stability of bedded cylindrical casting shells made from glass-fiber reinforced unsaturated polyester resins), Diss. TH Aachen (Dissertation, Technical University of Aachen) 1974
- [1.16] VDI-Richtlinie (VDI guideline) 2012: Gestalten von Werkstücken aus GFK (Design of GRP workpieces)
- [1.17] EHRENSTEIN, G. W. et al.: Glasfaserverstärkte Kunststoffe (Glass-fiber reinforced plastics), Expert-Verlag, Grafenau 1981
- [1.18] ANON.: Aus glasfaserverstärktem UP-Harz gewickelter 1000 m³-Tank (1000 m³ tank wound from glass-fiber reinforced UP resin), *Industrie-Anzeiger* **105** (1982) 6, p. 19/19
- [1.19] CARSTENS, H.-H. and J. NIELEBOCK: Guter Wärmeschutz bei Fenstern durch Kunststoffe (Good thermal insulation in windows by means of plastics), *Kunststoffe im Bau* **14** (1979) 3, pp. 117/120
- [1.20] German Offenlegungsschrift 2729692: Vorrichtung zum Einbau in eine Bahngleisweiche (Device for installation in a railroad switch) July 1, 1976
- [1.21] HORNBÖGEN, E.: Werkstoffe im Jahr 2000 (Materials in 2000), *Umschau* **76** (1976) 20, pp. 645/650
- [1.22] FRITZ, G.: Rohstoffprobleme und ihre Auswirkungen auf die Kunststoffindustrie (Raw materials problems and their effects on the plastics industry), *Kunststoffe* **65** (1975) 1, pp. 41/47
- [1.23] WEGNER, G.: Polymere mit metallähnlicher Leitfähigkeit – Ein Überblick über Synthese, Struktur und Eigenschaften (Polymers having metal-like conductivity – Review of synthesis, structure and properties), *Angew. Chemie* **93** (1981), pp. 352/371
- [1.24] NAARMANN, H.: Elektrisch leitfähige Polyaromaten (Electrically conducting polyaromatics), *Ber. Bunsenges. Phys. Chem.* **83** (1979), pp. 427/432
- [1.25] WEDDING, G.: Elektrisch leitende Kunststoffe (Electrically conducting plastics), *Physik i. u. Zeit* **14** (1983) 4, pp. 98/106
- [1.26] ANON.: PTFE für Wärmetauscher in Kraftwerken (PTFE for heat exchangers in power plants), *Kunststoffe* **81** (1991) 2, p. 150
- [1.27] HAUCK, CH. and A. SCHNEIDERS: Optimieren der Schmelzkerntechnik für das Thermoplast-Spritzgießen (Optimizing the fusible core technique for injection molding of thermoplastics), *Kunststoffe* **77** (1987) 12, pp. 1237/1240
- [1.28] RAU, TH.: Zur Entwicklung hochfester Drehstabfedern aus Faser-Kunststoff-Verbunde (On the development of high-strength torsion rod springs made from fiber-plastic composites), Diss. Uni (GH) Kassel (Dissertation, University of Kassel) 1988
- [1.29] MEHRLE, W., O. SEIDLER and W. WEBER: Blattwurzelkonstruktionen von FWV-Rotorblättern für Windturbinen (Blade holder designs for fiber-composite rotor blades in wind turbines), *Kunststoffe* **81** (1991) 1, pp. 63/66

- [1.30] BRÜNINGS, W.-D., CH. HAUCK and D. MÜLLER: Entwicklung von Kfz-Pedalen aus glasfaserverstärktem Polyamid (Development of automobile pedals composed of glass-fiber reinforced polyamide), *Kunststoffe* **79** (1989) 3, pp. 251/254
- [1.31] TELGENBÜSCHER, K.: Neue Eigenschaften durch Aufbringen dünner Schichten – Plasmapolymerisation und Coextrusion polymerer Lichtwellenleiter (New properties by applying thin layers – Plasma polymerization and coextrusion of polymeric optical waveguides) in Tagungshandbuch 16. Kunststofftechnisches Kolloquium des IKV (Conference proceedings of 16th Plastics Engineering Colloquium of the IKV (Plastics Processing Institute)), Technische Hochschule, Aachen 1992
- [1.32] ANDERECK, K.: Composites – Strukturwerkstoffe der Zukunft (Composites – Structural materials of the future), *ETR* **45** (1996), No. 7/8, pp. 433/438
- [1.33] LAND, H.-T. and D. NIEDERNBERG: CD zukünftig aus COC? (CDs made from COC in the future?), *Kunststoffe* **85** (1995) 8, pp. 1048/1054
- [1.34] LANGIUS, L. J. M.: Hochkristallines Polyolefin (Highly crystalline polyolefin), *Kunststoffe* **85** (1995) 8, p. 1122
- [1.35] ANON.: Bayer und GP wollen Autoscheiben aus Polycarbonat marktreif machen (Bayer and GP aim to bring polycarbonate automobile windows to market maturity), *Kunststoffe* **87** (1997) 7, p. 833
- [1.36] ANON.: In Zukunft jährlich ein neues Outfit fürs Auto (In future a new outfit for the automobile every year), BASF information 5/97, p. 5
- [1.37] ANON.: Erste thermoplastische Heckklappe (First thermoplastic tailgate), *Kunststoffe* **87** (1997) 12, p. 1803
- [1.38] GRIGANT, E. et al.: Biologisch abbaubar in 60 Tagen (Biodegradable in 60 days), *Kunststoffe* **87** (1997) 1, pp. 63–65

2 Structure and Properties

Polymeric materials are now almost exclusively manufactured synthetically from organic compounds (monomers) by various processes, such as polymerization, polycondensation, or polyaddition. The monomers are linked together to form macromolecules which are the characteristic feature of the microstructure of polymeric materials (HERMANN STAUDINGER, 1881–1965). Chemical composition, structure, and morphology are parameters which have a close relationship with the macroscopic properties of these materials. Therefore, it will be helpful to have a fundamental understanding of the chemistry of these materials to briefly illuminate some of the most important structure-property relationships. For an in-depth study, the reader is referred to [1.1] and to other review works [2.1 to 2.5].

2.1 Chemical Structure (Constitution)

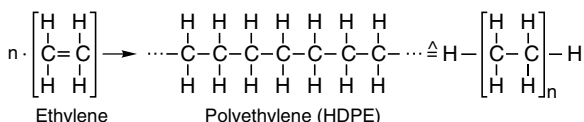
Only a few different elements form the basic building blocks of organic polymeric materials (or polymer chains). In general, these are C and H, supplemented by O, N, Cl, F, and S.

The principle of the structure of a macromolecule may be illustrated by linear polyethylene (HDPE). Under specific polymerization conditions, the polyethylene macromolecule forms by repeated addition of ethylene molecules to one another. In doing so, the ethylene monomer carbon double bonds are broken open and react. In this way, a linear molecular chain is produced which, when stretched, can extend to a length of up to several μm (Figure 2.1).

Figure 2.1 also shows some other structural elements and components typical of polymers, which are plotted on a scale to allow comparison of sizes.

Polymeric materials composed of such linear macromolecules are fusible and are called *thermoplastics*.

The structures of the ethylene and polyethylene molecules are illustrated below by their structural formulae*:



* In reality the angle subtended between the singly bonded C-C atoms is not 180° as shown but rather the tetrahedral angle of 109° between the longitudinal axes of the four superimposed orbitals. Thus, the axis of the C-C main chain assumes a zigzag shape. The angle is referred to as the valence angle.

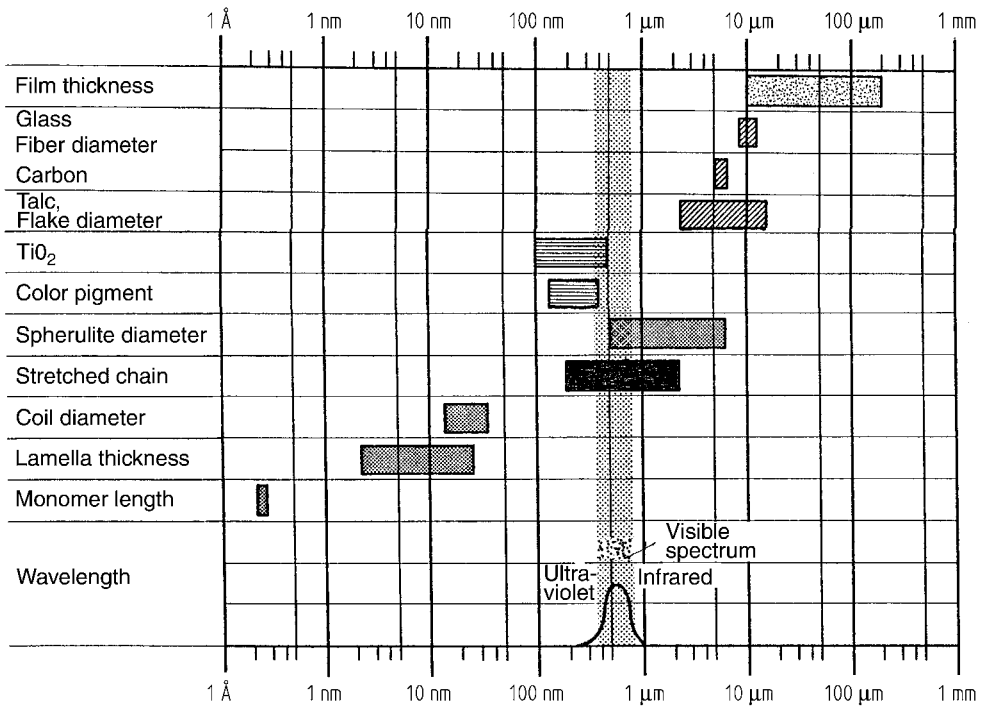


Figure 2.1 Comparison of sizes of some typical polymer structural elements and components

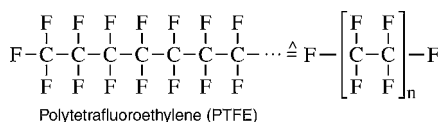
Table 2.1 Comparison of Theoretically and Empirically Determined Values for the Modulus of Elasticity and Tensile Strength of Selected Materials [2.6]

Material	Modulus of elasticity (MPa)			Tensile strength (MPa)	
	Theoretical	Experimental		Theoretical	Experimental
		Fiber	Material	Fiber	Material
HDPE	300 000	100 000 (33%)	1 000 (0.33%)	27 000	1 500 (5.5%)
PP	50 000	20 000 (40%)	1 600 (3.2%)	16 000	1 300 (8.1%)
PA 66	160 000	5 000 (3%)	2 000 (1.3%)	27 000	1 700 (6.3%)
Glass	80 000	80 000 (100%)	70 000 (87.5%)	11 000	4 000 (36%)
Steel	210 000	210 000 (100%)	210 000 (100%)	21 000	4 000 (19%)
Aluminum	76 000	76 000 (100%)	76 000 (100%)	7 600	800 (10%)
					600 (7.9%)

Each link indicated by a dash represents a chemical bond formed by a pair of electrons having opposite spins (covalent bond or primary valence bond). The binding energy of such a C-C bond is approx. 250 kJ/mol. Application of stress along the chain axis would yield a theoretical material strength in the order of 27,000 MPa. In reality, however, this level of strength is not attained, not even in highly oriented polyethylene fibers (1,500 to 2,000 MPa).

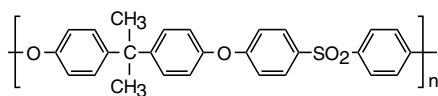
In Table 2.1 the theoretical tensile strength and modulus of elasticity for some materials are compared with the values actually found experimentally [2.6].

Polytetrafluoroethylene (PTFE) is a polymeric material which has a similar structure to polyethylene (PE). However, fluorine atoms are bonded to the carbon atoms instead of hydrogen atoms. It has the following structural formula.

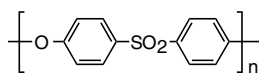


Despite its formal similarity to polyethylene, PTFE differs markedly from PE, particularly in properties such as heat resistance and resistance to chemicals. Practically the only substance capable of attacking PTFE is hydrofluoric acid. This change in properties is attributed to the presence of the relatively large F atoms*, which provide a very effective shield for the C-C chain. The bonding energy of a C-F bond amounting to 460 kJ/mol is much greater than that of a C-H bond at 370 kJ/mol [2.5]. This is another reason for the stability of the PTFE molecule. Although PTFE is composed of linear chains, it cannot really be regarded as a thermoplastic (from a practical point of view). The melt viscosity of PTFE, even at 380 °C, is still so extremely high that it cannot be processed in the molten state by standard thermoplastic processing equipment (*e.g.*, injection molding machines). It has to be converted into moldings by pressing and sintering**.

Polymeric materials whose linear chain structure is not made up of aliphatic C-C bonds but which instead contain aromatic ring compounds in the main chain may also be classified as fusible thermoplastics. However, their heat resistance and heat distortion temperature is distinctly higher, because these chains are much more rigid, especially when there are no “flexible” hetero atoms between the aromatic ring compounds. Examples of polymers with hetero atoms between chains are polysulfone (PSU) and polyether sulfone (PES), which have the following structural formulae.



Polysulfone,
Glass transition temperature
 $T_g = 187^\circ\text{C}$

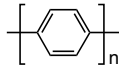


Polyether sulfone,
Glass transition temperature
 $T_g = 225^\circ\text{C}$

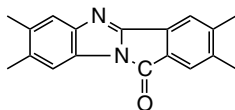
* Due to the large F atoms, the even zigzag alignment found in HDPE is impeded so that the main chain is twisted at each change of direction by 15° and this is associated with a small widening of the valence angle [1.1].

** There are also modified forms of PTFE that can be processed by injection molding.

There are no hetero atoms between rings in the case of polyphenylene, resulting in a material with a very high T_g , but a lack of processability. A similar situation exists for polypyrrone in which the ring compounds are located close together. Despite the formally linear chain structure, such substances are not fusible or melt processable.



Polyphenylene, not fusible



Polypyrrone, not fusible

2.1.1 Degree of Polymerization – Relative Molecular Weight

During the process of producing a polymeric material, chain growth is generally terminated randomly, *i.e.*, the number of monomer units linking up with one another varies from chain to chain; the average number of monomer (or repeat) units is referred to as the *average degree of polymerization*.

The *relative molecular weight* is defined as the sum of the relative atomic masses of the atoms forming the molecule.

Substances of low molecular weight are uniquely identified by their relative molecular weights. For example the relative molecular weight of an ethylene (C_2H_4) molecule is $M = 28^*$.

In the case of the macromolecules (*i.e.*, polymeric materials) the situation is different, because the different sizes of the macromolecules formed also entail different relative molecular weights. Accordingly, polymeric materials are said to have low molecular weight or high molecular weight or even ultrahigh molecular weight. The latter are of some importance especially for polyethylene under the designation UHMW-PE (Ultra High Molecular Weight PE). UHMW-PE has outstanding wear and chemical resistance. It is used, for example, in medical technology for endoprostheses and in chemical engineering for wear-resistant linings.

Thus, the relative molecular weights of the macromolecules exhibit no standard value. On the contrary, there is a more or less broad distribution. Usually, however, when characterizing the relative molecular weight of a polymeric material, it is not its distribution function which is specified, but rather only a mean value. This value may be determined from the number of macromolecules n_j at each degree of polymerization P_j with reference to the total number of macromolecules. This yields the number average molecular weight W_n . Alternatively, it may be determined from the weights for each degree of polymerization and the total weight as the weight average molecular weight W_w .

$$\text{Number average: } W_n = \frac{\sum n_j P_j}{\sum n_j} \quad (2.1)$$

$$\text{Weight average: } W_w = \frac{\sum m_j P_j}{\sum m_j} \quad (2.2)$$

* In accordance with the atomic weights of C = 12 and H = 1 it follows that $(2 \cdot 12) + (4 \cdot 1) = 28$.

Example

Figure 2.2 illustrates the principle and the key parameters of such distribution functions with reference to a graphic example drawn from coin distributions. The individual monetary values of coins W_m symbolize the relative molecular weights of the individual molecules. If the coin values, which go up by a factor of 2 to 2.5 at each step, are lined up more or less equidistantly the common logarithmic abscissa scale is obtained.

The curve on the left shows the number n of coins (molecules) at each value level (degree of polymerization), that is to say the frequency distribution. Assuming the coins all have the same thickness this also corresponds to the height of the pile of coins in each case. The center of the frequency distribution is the number average W_n which in this case lies at 0.61.

The curve on the right traces the value of the pile $W_s = n \cdot W_m$ for each of the piles. Accordingly, it is raised for the higher-value coins relative to the frequency distribution and lowered for the lower-value coins. For that reason it is shifted to the right. Thus the weight average W_w – corresponding in this example to the value average – as the center of the weight distribution is greater than the number average W_n . In Figure 2.2, $W_w = 2.60$.

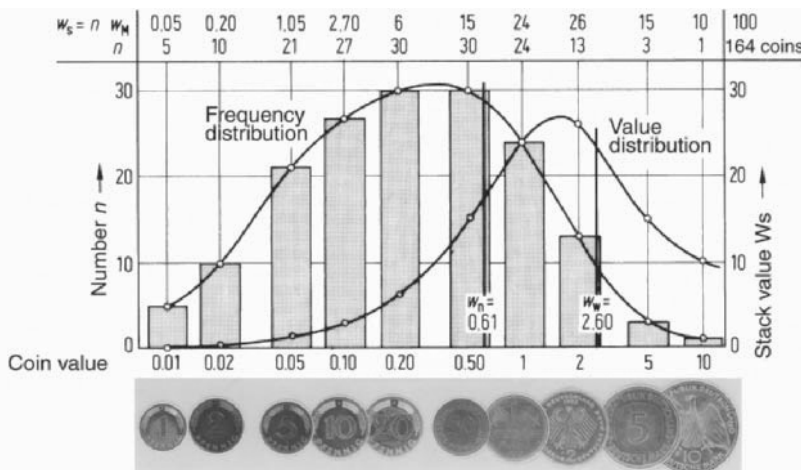


Figure 2.2 Distribution of relative molecular weights illustrated in terms of the frequency and value distributions of coins

$$W_n = \frac{\sum n_j P_j}{\sum n_j} = \frac{(5 \cdot 0.01) + (10 \cdot 0.02) + \dots + (3 \cdot 5) + (1 \cdot 10)}{5 + 10 + \dots + 3 + 1} = \frac{100}{164} = 0.61$$

$$W_w = \frac{\sum m_j P_j}{\sum m_j} = \frac{(0.05 \cdot 0.01) + (0.2 \cdot 0.02) + \dots + (15 \cdot 5) + (10 \cdot 10)}{0.05 + 0.20 + \dots + 15 + 10} = \frac{260.027}{100} = 2.6$$

A narrow distribution of the relative molecular weight results in greater uniformity of the properties of the material, e.g., a narrower range of softening temperatures, lower susceptibility to stress cracking and higher resistance to chemicals. A broad distribution, on the other hand, will affect processability and performance. The low molecular weight fractions improve the flow properties of the melt and the high molecular weight fractions increase the impact-resistance of the finished parts, but they also increase the tendency to warpage.

In order to combine the processing advantages of a low relative molecular weight with those of a high relative molecular weight, polymeric materials having bimodal distributions are also produced. Their distribution curves exhibit two maxima. Figure 2.3 illustrates different molecular weight distributions.

The value of the relative molecular weight of a polymeric material affects many macroscopic properties, sometimes decisively. As the length of the individual macromolecules increases, crystallization can eventually be impeded, as indicated schematically in Figure 2.4, so that the material becomes less densely packed. The density decrease can be attributed to the greater free volume in the amorphous regions of the semi-crystalline polymer.

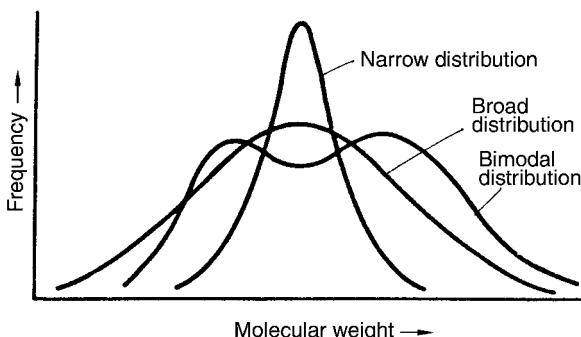


Figure 2.3 Schematic illustration of narrow, broad, and bimodal distribution functions

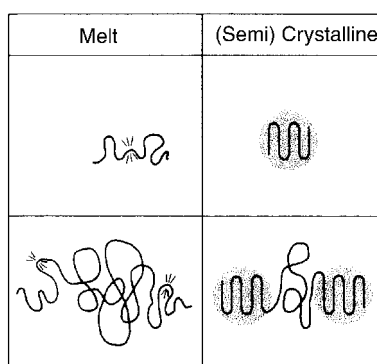


Figure 2.4 Lamellar crystallization of single chains of low molecular weight (top) and high molecular weight (bottom)

In crystalline regions, the intermolecular binding forces come into operation more strongly so that they can make a greater contribution to strength and rigidity (since the molecules are closer together). The strength and modulus of elasticity of a material increase, as might be expected, from low molecular weight substances to those of higher molecular weight. In the case of molecules having very long chains, however, once the degree of crystallinity drops off again, there is no further increase in these properties, indeed a slight drop in strength and rigidity is rather more likely to be found (see Figure 2.5).

On the other hand, because of the greater entanglement of chains in the case of high relative molecular weights, the extent to which the molecules slip over one another increases and as a result, elongation at break rises more sharply than any fall in tensile stress at yield. This has the consequence that energy absorbing capacity (impact-resistance), which may be regarded as the area under the stress-strain curve, increases as the relative molecular weight rises. According to [2.8], the wear caused by sliding friction in the course of the deformation of combinations of polymeric materials and steel is inversely proportional to the energy absorbing capacity of the polymeric material. Accordingly, as the relative molecular weight rises resistance to wear also increases (see also Chapter 4).

As expected, the viscosity of the melt also rises as the chain length of the polymeric material increases (see Figure 2.5). This is due to the greater number of entanglements and the more hindrances to slippage of the chains over one another when the relative molecular weight is high. This interrelationship is of great importance to the processing of polymeric materials. The cavity of an injection mold, in which the ratio of length to wall thickness is high, can be satisfactorily filled only by a polymeric material of low relative molecular weight. On the other hand, in the case of blow molding and profile extrusion, where melt strength is important (since the polymer melt must support its own weight), the polymer melt must have a substantially higher viscosity and hence better shape retention. Polymeric materials having a relative molecular weight greater than approx. 10^6 are left only with sintering as a means of processing (see Figure 2.5).

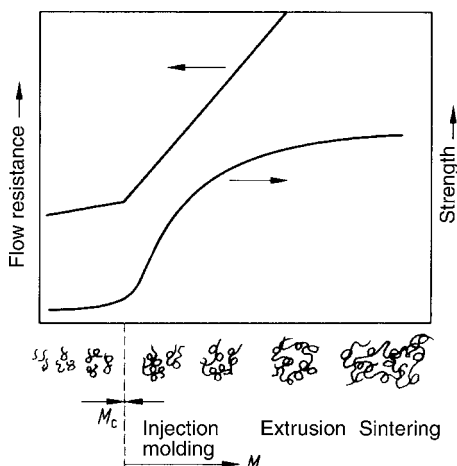


Figure 2.5 Schematic diagram showing flow resistance and strength as a function of relative molecular weight

The uniquely defined number and weight averages are unfortunately rather difficult to measure. Therefore, it is common practice to determine the solution viscosity (*viscosity number* [η]* or the melt viscosity (*melt flow rate MFR* or *melt volume rate MVR***) as technical single-point values so that primarily the ease of flow of different polymeric materials can be compared.

The following relationship exists between the viscosity number $[\eta]$ and the mean relative molecular weight:

$$[\eta] = K_\eta \cdot M^a \quad (2.3)$$

where K_n and a are values specific to the polymer and solution. The mean relative molecular weight M is approximately equal to the weight average value M_w .

2.1.2 Homopolymerization and Copolymerization

When only one type of monomer is used as the starting material for building a polymer, the process is called homopolymerization. Polyethylene is a homopolymer, as indeed are most polymeric materials. It is, however, also possible to build a macromolecule by polymerizing two or more different types of monomer, for example, to combine different properties or to modify particular properties selectively. This is referred to as copolymerization (or heteropolymerization).

Three variants are distinguished depending on the arrangement of the individual components in the molecular structure.

A substance is said to be a random copolymer when its different monomer units, identified here as A and B, occur in a random or irregular sequence in the macromolecule.



In such irregularly constructed polymer chains a crystalline state is very nearly impossible. SAN is an example of a random copolymer.

A block or sequence copolymer is a copolymer in which the individual components occur in relatively large blocks.

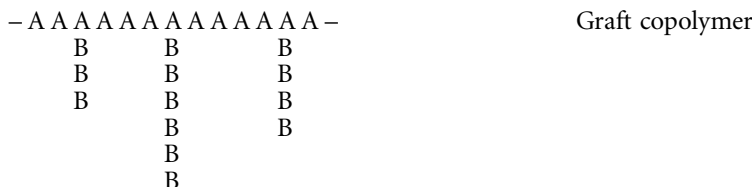


Such polymeric materials are certainly capable of forming crystalline regions in the A and/or B block sequences. Examples include thermoplastic elastomers, in which the A block consists of an amorphous polymer having elastic properties and the B block is, for example, a crystallizable rigid phase which functions as a “physical” (rather than chemical) pseudo cross-link site (see Chapter 3).

- * The viscosity number is the quotient of the relative increase in the viscosity of a solvent due to a polymer dissolved in it and its concentration in g/100 ml. Related standards include ISO 307, ISO 1157, and ISO 1628.

** The melt volume rate (MVR) in $\text{cm}^3/\text{10 min}$ specifies the volume of a polymer melt which, under a specified load and at a specified temperature, can be pressed through a standardized orifice in 10 minutes. Low numerical values are characteristic of high relative molecular weights. Standard: ISO 1133.

Graft copolymers are polymeric materials composed of a uniform backbone chain onto which the second polymer chain segment is grafted in the form of side chains by covalent bonding.



As an example, the grafting process plays an important role in the impact-modification of polystyrene. To produce impact polystyrene, uncrosslinked polybutadiene is polymerized with styrene. Because the two components are incompatible with one another, demixing occurs in such a way that spheres of butadiene rubber form in the hard polystyrene matrix. These spheres in turn contain polystyrene domains (see Figure 2.6). Both components are joined together by grafting, that is to say, by covalent bonds. The effect achieved by this is a distinct increase in the impact resistance and energy-absorbing capacity of the polystyrene*. It is also possible to control other properties, such as stress-cracking resistance or transparency, through the physical size of the rubber particles.

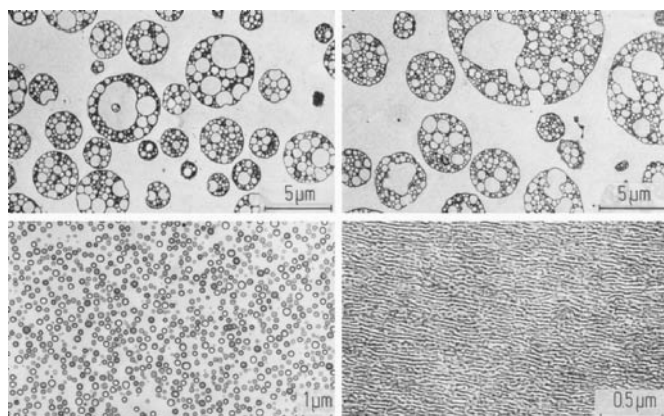


Figure 2.6 Structure of impact-resistant polystyrene containing grafted butadiene rubber (dark areas) [2.9]. Electron micrographs of 0.1 µm thick microtome sections
 Top left: High impact resistance Top right: Stress-cracking resistant
 Lower left: Translucent Lower right: Transparent

- * In contrast with the block copolymer styrene-butadiene rubber (SBR), this effect is not based on the high impact resistance intrinsic in butadiene rubber, because the styrene matrix remains coherent in impact-resistant polystyrene (SB). When an external load is applied to the impact-resistant polystyrene (SB) stress peaks are produced at the perimeter of the butadiene particles resulting in widespread crazing in the polystyrene and hence increased energy absorption.

2.2 Intermolecular Binding Energies (Secondary Valence Bonds)

In polymeric materials that are not crosslinked (thermoplastics, thermoplastic elastomers), cohesion among the macromolecules is achieved by secondary valence bonding of a physical nature as opposed to chemical valence bonds. These *intermolecular* binding forces are based on electrostatic forces. They are responsible for many properties, such as thermomechanical properties, dielectric properties, solubility and swelling behavior, and for all properties related to surface activity such as paintability and sliding friction.

The following binding forces are distinguished:

- Van der Waals forces
- Dipole interactions (permanent and induced)
- Hydrogen bonding, and
- Ionic forces.

Intermolecular binding forces among electrostatically neutral macromolecules are called van der Waals forces. They are attributed to movements of electrons which generate instantaneous dipoles. Although such physical bonds occur in all polymeric materials, they are the sole form of intermolecular binding in some polymeric materials, *e.g.*, PTFE and PE. They are two to three orders of magnitude lower in strength than covalent bonds.

In contrast, the strength of such van der Waals forces is greatly exceeded by interactions based on the presence of permanent dipoles. The latter occur when shifts in charges in the electron cloud give rise to positive and negative poles (electronegativity). Permanent dipoles are found in the molecular structures of PVC, PMMA, PBT, and POM, for example. While stronger than van der Waals forces, their strength is still more than an order of magnitude lower than that of a covalent bond. A permanent dipole can also generate a dipole in an initially nonpolar neighboring molecule or reinforce an existing dipole. Binding forces produced by such induced dipoles are called induction forces.

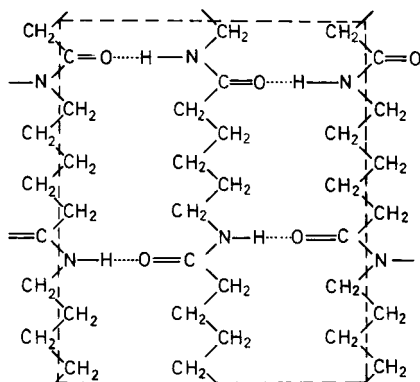


Figure 2.7 Hydrogen bonding in polyamide 6 (PA 6)

Hydrogen bonding generates even stronger intermolecular forces. This occurs, for example, in polyamides (PA), in which a hydrogen atom covalently bonded to a nitrogen atom acts as a bridge between the N atom and an O atom in a neighboring chain (see Figure 2.7). The high electronegativity of N and O gives rise to forces of attraction in the order of 20 kJ/mol.

Ionic bonding is based on electrostatic interactions among differently charged ions. Among polymers it occurs only in specialty materials known as ionomers.

2.2.1 Absorption of Water by Polyamides

Mechanism and Effects of Water Absorption

Polar polymeric materials have an affinity for water. Therefore, water molecules diffuse into these materials to an extent determined by the polymer polarity and environmental conditions. If the water molecules do not react with the polymer molecules nor interact physically with them, absorption of water would be limited and is associated only with limited swelling (but no substantial changes in mechanical properties).

There is a fundamentally different mechanism when water molecules penetrate into polymers having intermolecular binding forces in the form of hydrogen bonds. This is the case in polyamides. In these substances the water molecules interact with the existing hydrogen bonds by forming hydrogen bonds with the acid amide groups themselves (see also Section 2.4.2).

This has two consequences:

1. There is a marked increase in free volume as absorption of water proceeds. The following rule of thumb applies to unreinforced PA:

$$\frac{\Delta l}{l} = \frac{\Delta G}{4 G} \quad (2.4)$$

where l = length

G = PA weight

Δl = change of length

ΔG = weight of water absorbed

In the case of glass-fiber reinforced grades, the change in length is dependent on the amount of fiber present and the orientation of the fibers. If the fibers are aligned (typical of the flow direction on molded parts), moisture induced length changes may only be one quarter of those observed with heat (unreinforced PA). In the transverse direction, the dimensional change is about equal to that of the PA matrix, less the proportion by volume of the fibers.

2. If the tight cohesion between the molecular chains is partially reduced by moisture absorption, mechanical properties such as strength and modulus of elasticity decrease. At the same time ductility is increased. The properties of dry (as molded) and wet PA can vary significantly, as shown in Figure 2.8. Wet can mean moisture absorption of up to 10% by weight. The energy-absorbing capacity (impact resistance) passes through a maximum (see Figure 2.8).

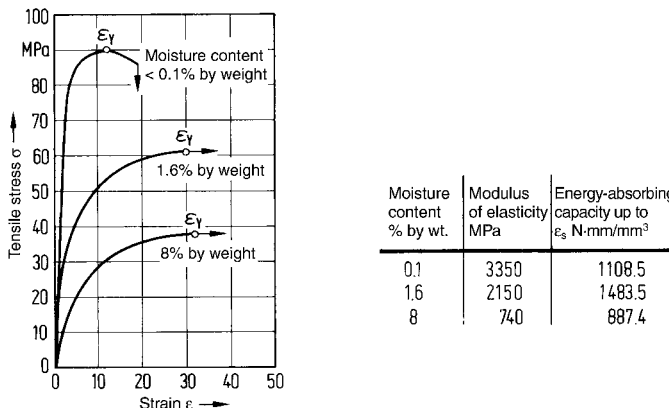


Figure 2.8 Stress-strain curves for PA 66 at different moisture contents; strain rate 50 mm/min, test atmosphere 23/50 [2.8]

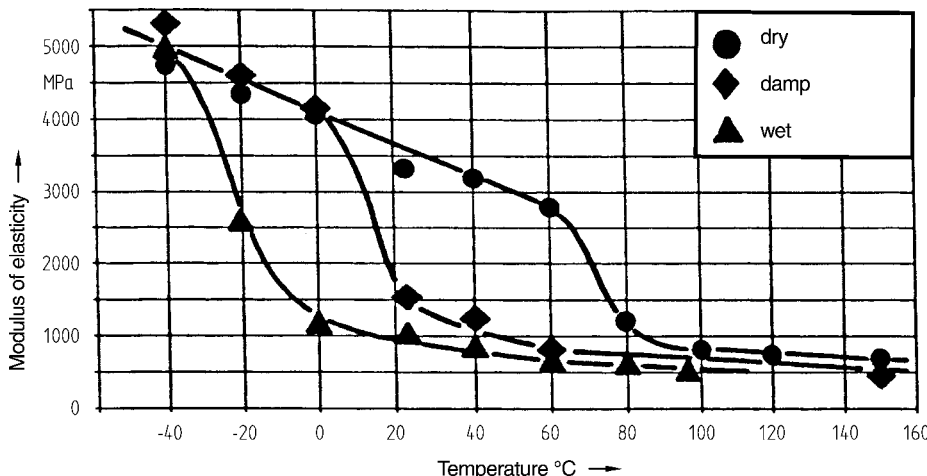


Figure 2.9 Plot of modulus of elasticity against temperature for PA 66; the position of T_g is identified by the steep drop in each modulus for curve

This transition from brittle to tough and finally to flexible behavior of the material with increasing absorption of water is also reflected in the shift in glass transition temperature T_g , which changes from 70 °C (dry), to 10 °C (damp), to -20 °C (wet) (see Figure 2.9 and also Section 2.6).

Since the water molecules attach themselves to the hydrogen bonds in the polyamide, types of polyamide having fewer amide groups per unit chain length (e.g., PA 11, PA 12*) also absorb less water. Accordingly, changes in properties are less marked for these PAs.

* The number identifies the spacing of the amide groups within the molecule by showing the number of C atoms between them. This is the case in the upper part of Table 2.2. Below the double line, the amide groups are not arranged at uniform intervals. For example, in PA 610 the intervals are 6 C atoms and then 10 C atoms, etc. and correspondingly, in PA 46 they are 4 C atoms then 6 C atoms, and so forth. PA 66T is a partly aromatic PA.

Table 2.2 Absorption of Water by Various Grades of Polyamide Measured in Accordance with ISO 62 [2.7]

Polymeric material	Saturation in weight-%	
	in water 23 °C	in standard 23/50 atmosphere
PA 6	9.5	3
PA 6 GF 30	6.6	2.1
PA 6 Cast	8	2.8
PA 11	1.8	1
PA 12	1.5	0.7
PA 12 Cast	1.4	0.9
PA 66	8.5	2.8
PA 66 GF 30	5.5	1.7
PA 610	3.3	1.4
PA 46	13.5	3.7
PA 6/6T	7	1.8
PA 6/6T GF 30	4.5	0.8
PA 66 + PA 6 32% Mineral	6	1.6

Water is more easily absorbed in the less densely packed, amorphous regions of the semi-crystalline PA structure so that the degree of crystallinity also affects the degree and rate of water absorption.

Absorption of water can be regarded as a diffusion process, *i.e.* the moisture content of the polyamide tends towards an equilibrium state corresponding to the prevailing ambient humidity (see Table 2.2). The process of water absorption is reversible, as is the change in macroscopic properties, as long as no hydrolysis or aging due to additional diffusion of oxygen takes place [2.10].

In addition, very thin-walled parts rapidly reach saturation across their entire cross section, whereas this process takes correspondingly longer in parts with “thick walls”. Figure 2.10 shows the effect of wall thickness on the variation of yield stress and modulus of elasticity as a result of exposure in a standard 23 °C/50% RH atmosphere. In “very” thick-walled parts it can take years until the entire cross section exhibits a uniform moisture content (see Figs. 2.11 and 2.12).

Conditioning of Polyamide Parts

Immediately after production by injection molding, PA parts are dry and relatively brittle. In order to adjust them to the desired moisture content and hence set an acceptable level of impact resistance in the shortest possible time and also to preempt dimensional changes, the parts are often conditioned, *i.e.*, water absorption is accelerated by exposing the parts to high ambient moisture levels and higher temperatures. In practice, conditioning parts in hot water (40 to 90 °C), in a warm humid atmosphere (up to 40 °C and as high a relative humidity as possible), or in saturated steam has proved to be effective. The simplest method requiring no outlay on equipment is (hot) storage in sealed PE bags having a wall thickness > 0.1 mm into which 10% water with reference to the weight of the part has been added.

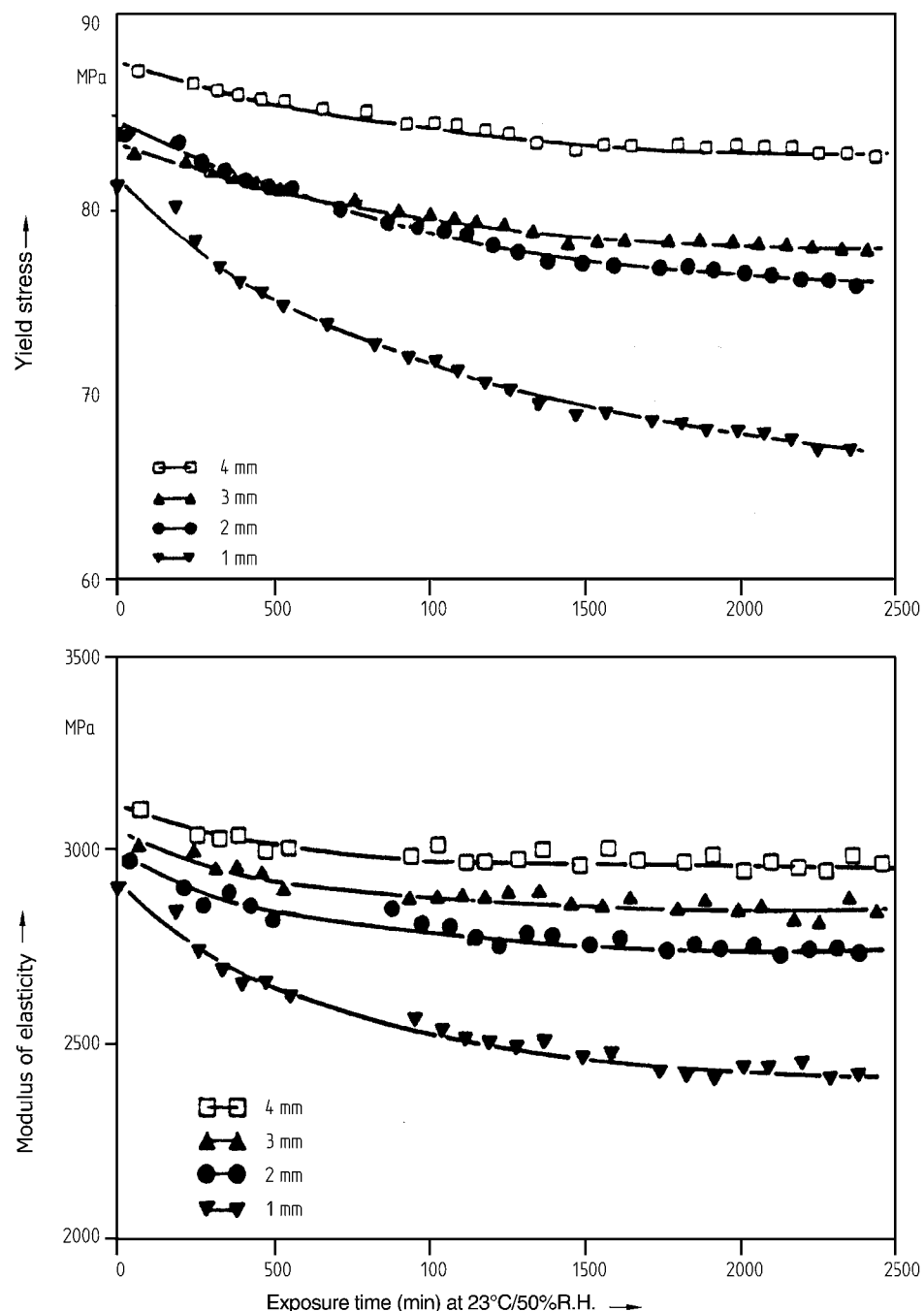


Figure 2.10 Effect of wall thickness on the rate of change of properties of PA 66 stored in a standard 23 °C/50% RH atmosphere

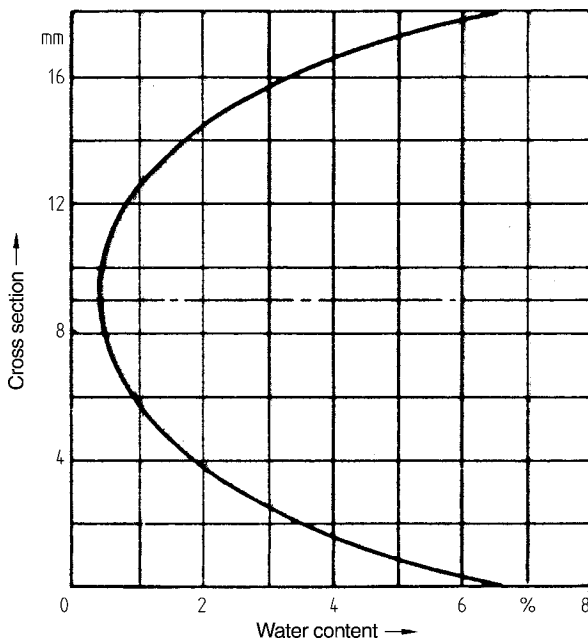


Figure 2.11 Distribution of moisture across the 18 mm cross section of a marine screw propeller made from a highly crystalline cast polyamide (PA 6 casting grade) after use for three years

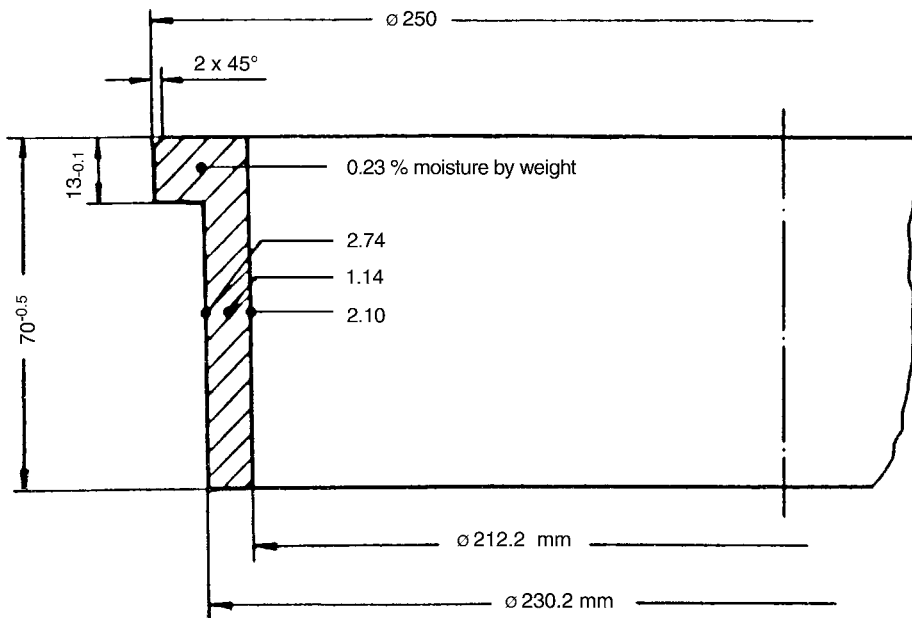


Figure 2.12 Distribution of moisture in a bearing bush made from PA 6 after operating for several years in a construction crane

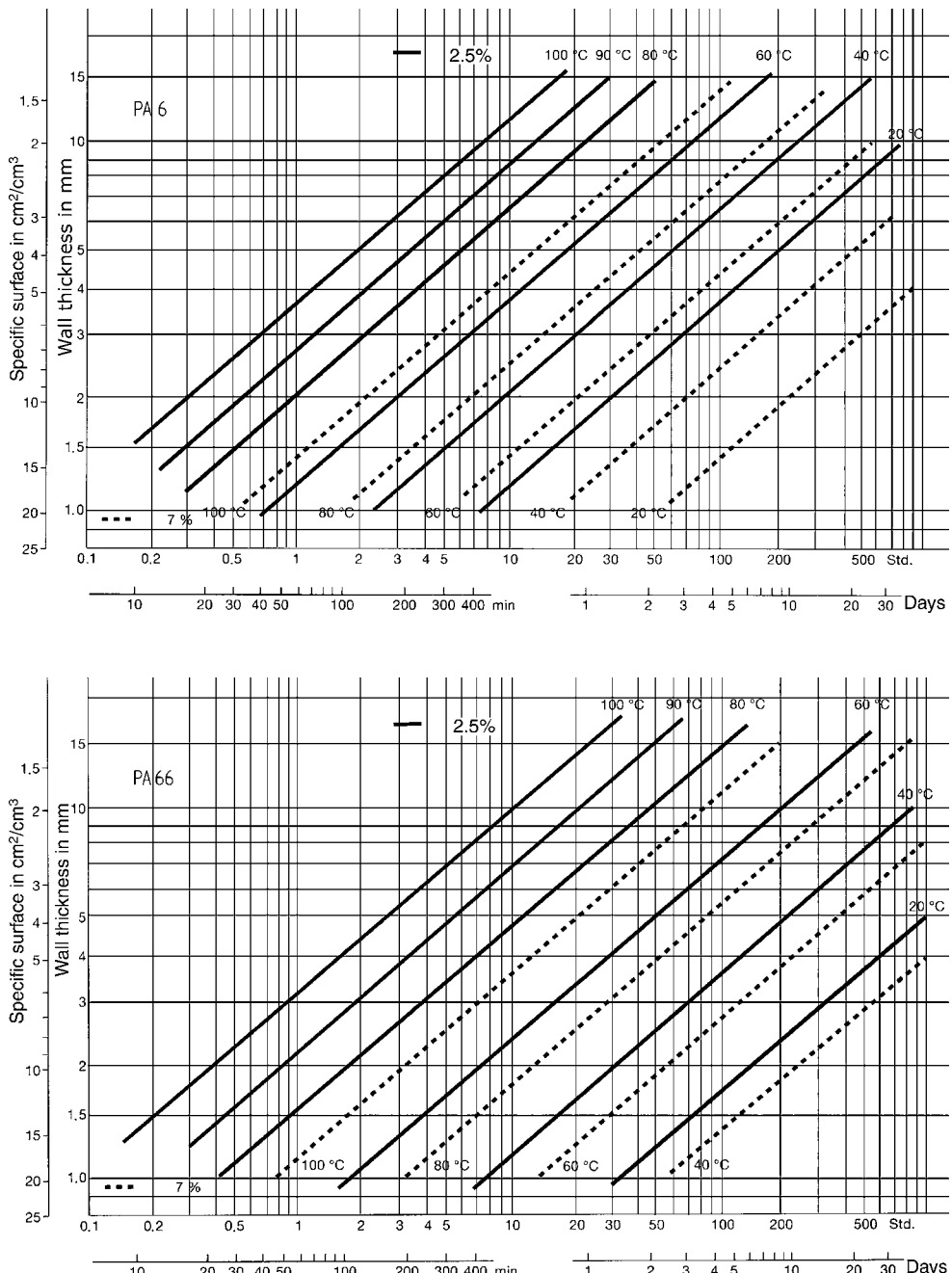


Figure 2.13 Time for conditioning to a moisture content of 2.5% and 7% for PA 6 and PA 66 as a function of wall thickness and water temperature [2.23]

The moisture content that conditioning is intended to achieve depends on the subsequent end use conditions or the degree of impact resistance required for the part, e.g., assembly by means of sufficiently ductile snap-fit hooks. Figure 2.13 provides examples of required conditioning times as a function of wall thickness and water temperature.

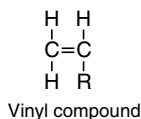
If PA parts contain inserts made of steel, there is a risk of corrosion which can be prevented by adding 0.2 to 0.5% of hexamethylene tetramine, following proper safety precautions [2.23].

When the conditioning process involves heat treatment, discoloration may occur. This is most common in the case of brightly colored PA. Materials containing reclaimed plastic are particularly prone to discoloration. A tried and tested countermeasure is to add 0.2 to 1% of sodium bisulfite. PA parts which have already become discolored may be decolorized again by this means. Storage for several days in solution at approximately 80 °C may be necessary for this purpose [2.23].

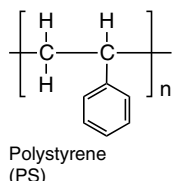
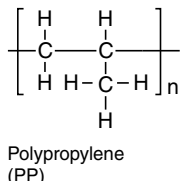
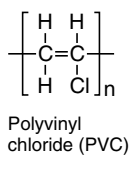
In the course of conditioning a white deposit may also be formed. This is attributed to the migration of any low molecular weight fractions which may be present in the PA. The deposits are readily soluble in alcohols mixed with water.

2.3 Spatial Arrangement of Atoms and Groups of Atoms in Molecules (Configuration)

Vinyl compounds are important starting monomers for polymeric materials. They have the following general structural formula:



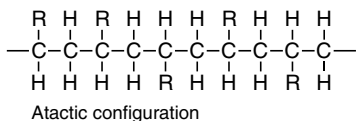
Here, R stands for various groups which can attach themselves at this point. Key examples for industrial polymeric materials are Cl, CH₃, and C₆H₅. The corresponding monomers give rise to the polymeric materials polyvinyl chloride, polypropylene, and polystyrene (when R represents H, polyethylene is obtained).



2.3.1 Tacticity

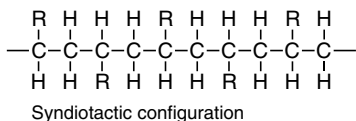
In contrast with polyethylene, these polymeric materials no longer have a symmetrical structure. Depending on the spatial arrangement of the side groups, atactic, syndiotactic, and isotactic configurations are distinguished.

In the atactic arrangement, the position of the side groups relative to the hydrogen atoms is random.

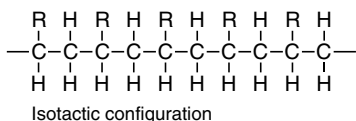


Due to this irregular chain structure, atactic polymeric materials are scarcely capable of the order needed for crystallinity. This is especially the case when the side groups are of relatively large volume (as in the case of PVC and PS).

The term syndiotactic refers to a regularly alternating sequence of side groups on either side of the polymer chain or backbone as shown below.



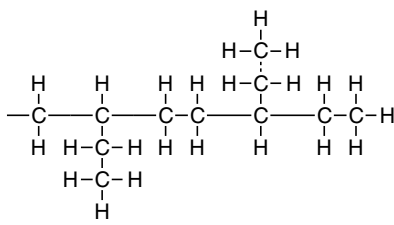
The isotactic configuration is characterized in that the side groups are aligned regularly on one side of the backbone.



In these two “regular” configurations, it is now possible once again for ordered crystalline regions to form. This order manifests itself in the macroscopic properties of the material, such as higher strength, higher modulus of elasticity, and a slightly higher density. Tacticity has a dramatic effect on properties. For example, atactic PP is a gumming substance, while isotactic PP is a widely used, rigid, but ductile semi-crystalline thermoplastic.

2.3.2 Branching

Even in a homopolymer, it is possible for the monomer to attach itself to the side of the polymer main chain to form side chain branches of the same chemical constitution as the main chain. The process is called branching. Branched LDPE (low density polyethylene) is a typical example of this phenomenon.



Branched polyethylene (LDPE)

Branching seriously impairs the regularity of the structure of the macromolecule so that by comparison with linear polyethylene (HDPE) the ability for regions of crystalline order to form is markedly reduced. Accordingly, branched polyethylene (LDPE) has a lower density than linear polyethylene (HDPE). Because the molecules cannot pack together as tightly, the intermolecular binding forces do not come into effect as strongly and this results in lower strength and a lower modulus of elasticity. At the same time, the ductility of the material rises. In tensile strength tests, branched polyethylene can exhibit elongations at break of up to 1,000%. Linear low density polyethylene (LLDPE) is actually a more regular short branch PE formed by copolymerization with an α -olefin comonomer. LLDPE has replaced LDPE in many applications.

2.3.3 Cross-Linking

Cross-linking, the interconnection of the individual macromolecules by means of primary valence bonds to form a permanent network, takes place either during the polymerization of multifunctional monomers or, in the case of linear or branched macromolecules, it is achieved subsequently by chemical means, e.g., by adding peroxide, or by physical means using high-energy radiation. The term relative molecular weight becomes essentially meaningless in relation to such network structures. Instead, the term “degree of cross-linking” is defined as a measure of the number of cross-linkage points per unit volume.

Flexible polymeric materials having a low degree of cross-linking are typically called *elastomers*.

Elastomers are materials that are easily deformed under the action of external forces. Elastomers are useful if they have elongations as high as 100% and more that are reversible. The deformation characteristics of elastomers, however, are not determined solely by the primary valences, as physical binding energies also come into play at the same time (see also Section 2.2). In contrast with thermoplastics having a linear or branched chain structure, cross-linked polymers cannot make the transition to the molten state. This is particularly true when the cross link density is high.

The relative mobility of the chains is greatly restricted. Deformation levels of more than a few percent are just as impossible as melting. Polymeric materials having a high degree of cross-linking are referred to as *thermosets* or *thermosetting plastics*. The cross linking of thermosetting plastics typically occurs after the part shape is formed to facilitate processing.

Apart from *chemical* cross-linking, *physical* cross-linking is also known in sequence or block copolymers (see Section 2.1.2), which are built up of rigid and flexible domains. In the rigid domains, physical binding forces are relatively stronger than in the flexible domains so that these physical interconnections are referred to as “cross-linking” of the flexible domains (see also Section 3.2). These materials exhibit thermoplastic processing characteristics.

2.4 Architecture of Polymer Systems

2.4.1 Homogeneous and Heterogeneous Polymer Mixtures

Many commercial polymers are actually “blends” or mixtures of polymers. As in the case of mixtures of two low molecular weight substances, polymeric two-component systems may take the form of:

- A single-phase system, *i.e.*, a homogeneous mixture (solution) or
- A two-phase system, *i.e.*, a heterogeneous mixture.

In homogeneous mixtures of two or more substances of chemically different composition, the physical properties of the mixture differ from those of the individual pure components depending on the nature of the components and the ratio in which they are mixed. In such homogeneous mixtures, the components of the mixture are said to be perfectly compatible with one another. This situation, however, is extremely rare among polymeric materials.

Heterogeneous mixtures are characterized by the fact that the components are partially or completely incompatible with one another and the properties of the individual components are retained. That is to say, the properties coexist separately side by side.

An example of a heterogeneous blend is the mixture of polyamide 66 (PA 66) with linear polyethylene (HDPE) as shown in Figure 2.14. The HDPE is added in a proportion of approximately 10% in the form of a polymer powder, which is distributed through the polyamide matrix. Aggregates of particles ranging in size up to 100 µm can be seen (see Figure 2.14).

This mixed material is used for sliding bearings because it combines the advantages of both the nonpolar HDPE (good slipping properties) and PA 66 (good wear characteristics) (see also Chapter 4). Other examples related to this are dealt with in Chapter 3 under Blends.

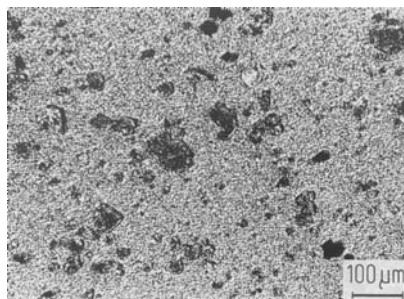


Figure 2.14 Microtome photomicrograph in polarized light of a heterogeneous polymer mixture of polyamide 66 with 10% high molecular weight HDPE (dark areas) [2.11]

2.4.2 Plasticization

Plasticization is achieved by mixing of polymeric materials with polar substances of (typically) low molecular weight, whose purpose it is to break dipole bonds between the macromolecules in the polymeric material and to attach themselves to the poles they liberate. In this way, the rigid molecular association is loosened and groups of chains are rendered more mobile. This manifests itself at the macroscopic level in softening of the material (see also Section 2.2.1).

The plasticization of poly(vinyl chloride) (PVC) is very important in industry. Using suitable plasticizers, PVC's properties can range from rigid to extremely flexible.

The smaller the plasticizing molecules are the greater is their plasticizing effect. This, however, is also associated with the disadvantage known as plasticizer migration. Due to their relatively high vapor pressure, small molecules can diffuse out from the surface of the material. This causes diminution of the plasticizing effect. Plasticizers are also widely used with cellulosic plastics.

2.4.3 Fillers and Reinforcement

In order to selectively improve certain properties, polymeric materials can also be filled or reinforced by the addition of inorganic, usually nonmetallic, substances. Reinforcement occurs when the values for the mechanical strength and modulus of elasticity of the composite are higher than the corresponding values for the unreinforced matrix [2.12]. If the additive does not achieve this, but rather is intended to render the material less expensive, change its electrical properties, make it easier to process, etc., the additive is typically described as a filler. However, it is not always possible to make a clear-cut distinction between fillers and reinforcing materials, because fillers may also have a reinforcing effect on certain properties. As a general rule, if sufficient filler is added, properties such as compressive strength and modulus are also increased. Table 2.3 presents some industrially important fillers, together with the properties they are intended to improve. A variety of other additives are also used with polymeric materials.

Glass fibers are the most important reinforcements for polymeric materials. They take the form of continuous fibers for reinforcing UP, EP, and vinyl ester resins. Short fibers having

Table 2.3 Selection of Industrially Important Fillers, Reinforcing Materials, Other Additives, and the Properties They Improve

Filler or reinforcing material	Most common matrix materials	Properties to be improved
Glass fibers	UP, EP, vinyl ester (VE), PA, PC, POM, PP, PBT	Strength, modulus of elasticity; heat resistance, and a decrease in thermal expansion
Carbon fibers Aramid fibers	EP, UP, vinyl ester (VE), PA	Modulus of elasticity ($E/\rho!$), strength; but not compressive strength in the case of aramid fibers
Inorganic polyhedrals or particulates (glass spheres, chalk, silicates)	Semicrystalline thermoplastics, UP	Isotropic shrinkage (less susceptible to warping), abrasion, compressive strength, possibly price
Sawdust, wood flour	Type 31 phenolic resin, PP	Price, processing, mechanical properties
Lubricants (zinc stearate)	All polymeric materials	Processing, sliding friction
Flame retardants (aluminum hydroxide, halogen compounds)	All polymeric materials as required	Flame resistance
Carbon black	PA, PBT, PE, ABS	Electrical conductivity
Pigments and dyes	All polymeric materials	Color

lengths of approximately 0.2 mm and diameters of approximately 10 μm are used for reinforcing thermoplastics. Despite their high prices, carbon fibers and aramid fibers are increasingly attracting interest in the context of lightweight construction. There is also a trend towards using melt processable thermoplastics with fiber lengths of > 10 mm.

A necessary precondition for a reinforcing effect is that the reinforcing material must have higher strength and a higher modulus of elasticity than the matrix. Its elongation at break should be of the same order of magnitude as the elongation of the matrix under yield stress. In addition, there must be a sufficient degree of adhesion between the reinforcing material and the matrix. If these preconditions are met, forces can be transmitted from the matrix via shear stresses to the reinforcing material accepting the load. In the case of filament-like reinforcement, the principle of the transmission of force and the possible instances of failure can be demonstrated on the basis of a single embedded fiber (see Figure 2.15).

Tensile stresses acting on the matrix stretch it more than the fiber because of its lower modulus of elasticity so that elongation at the surface of the fiber is impeded (provided adhesion is high enough). As a result, shear stresses arise in the boundary surface (interface) and these have high peak values at the ends of the fiber. At the same time, tensile stresses build up in the fiber from the ends of the fiber inwards. When the shear stresses at the fiber end exceed the shear strength of the boundary surface and the matrix, the matrix begins to flow. The shear stress distribution in the matrix and the tensile stress distribution in the fiber illustrated at the top in Figure 2.15 set in across the fiber.

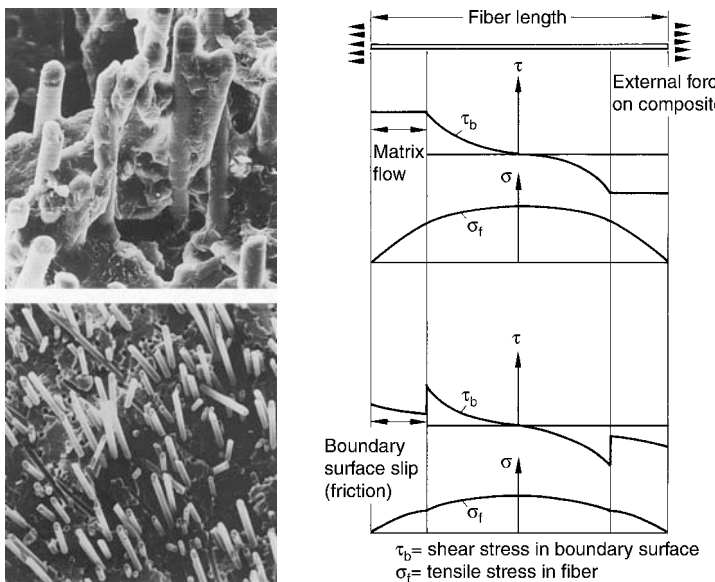


Figure 2.15 Distribution of stress along and in a fiber with shear stress flow in the matrix (top) and interface slippage (bottom) [2.12]

When adhesive conditions are inadequate, boundary surface slippage occurs before shear stress flow, likewise starting at the fiber ends (see Figure 2.15, bottom).

The third possible mode of failure of the composite is fiber fracture when the tensile stress in the fiber rises so high that its own strength is exceeded [2.12]. For this to happen, the fiber must have a certain critical length so that sufficient force can be introduced into the fiber via the summation of shear stresses. In this case, however, the anisotropy of some properties is even more strongly marked. Longer fibers increase performance, but also increase mold wear during processing. Long fibers may also have a problem flowing into thin wall sections.

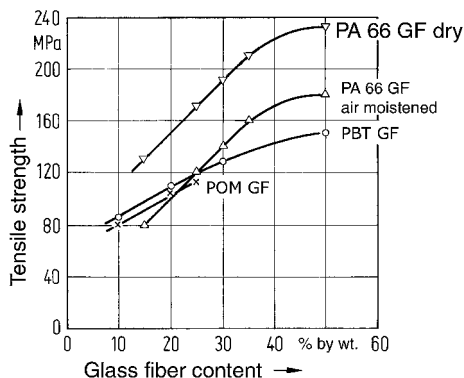


Figure 2.16 Tensile strength as a function of glass fiber content for some thermoplastics; the fibers are predominantly oriented lengthwise (i.e., with improved adhesion)

Accordingly, standard commercial thermoplastics are reinforced with fibers in the subcritical length range in most cases, although longer, higher performance fiber reinforced thermoplastics are available. Apart from the length/diameter ratio of the fibers, the proportion of fibers also determines the reinforcing effect as might be expected (see Figure 2.16).

2.5 Morphology (Supermolecular Structures)

2.5.1 Amorphous Microstructure

The amorphous (random) type of microstructure is characterized by the fact that the polymer macromolecules are positioned relative to one another in such a way that there is no order extending beyond a few chains, *i.e.*, the distance between neighboring chains is constantly changing*. A consequence of this absence of parallel or other ordered alignments in regions of a size corresponding to the wavelength of visible light (400–750 nm) is that no change in refractive index and no diffuse scattering occur within the material. Accordingly, unfilled, homogeneous polymeric materials having an amorphous microstructure are generally optically transparent (unless they contain other non-transparent additives).

There are two points of view regarding the arrangement of the individual macromolecules in the material. A common structural model assumes complete coil interpenetration (see Figure 2.17, a), while the cell structure model assumes single molecular coils which overlap only at the edges (see Figure 2.17, b).

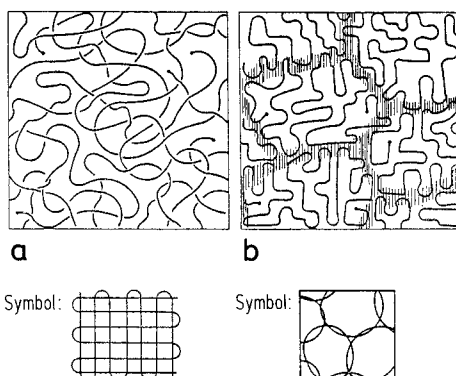


Figure 2.17 Schematic illustration of amorphous types of microstructure in polymeric materials [2.13]
 a) Structure with complete interpenetration of coils
 b) Cell structure with coil interpenetration limited to the peripheral zone
 (Vollmert-Stutz model)

* Comparison of theoretical densities with measured values, however, suggests the conclusion that even in an amorphous type of microstructure there must be a certain degree of short-range order in submicroscopic domains [2.14].

Apart from the transparency already referred to, other overall characteristics of amorphous polymeric materials are energy-elastic brittle deformation behavior below their glass transition temperature (see also Section 2.6.1) and marked ductility of an entropy-elastic nature at temperatures above their glass transition temperature. Their linear thermal coefficient of expansion is approximately $70 \cdot 10^{-6}/\text{K}$ and their mold shrinkage in processing is approximately 0.5%. The mold shrinkage for amorphous polymeric materials is significantly lower than that observed for most semicrystalline polymeric materials (see also Table 7.4).

2.5.2 Crystalline Microstructure

In the molten state, macromolecules (for both amorphous and semi-crystalline thermoplastics) are in an amorphous state of complete disorder. When crystallizable polymeric materials are cooled down to their crystallite formation temperature, certain ordering processes come into operation. The tendency for minimization of the free enthalpy between two neighboring molecules drives the alignment of these molecules into a parallel or otherwise ordered position. This process, which results in a higher state of order, is called crystallization. Such a parallel or ordered arrangement is found, for example, in the weakly crystallizing polymeric materials PVC and EVA. This short-range ordering is referred to as fringed micelle formation (see Figure 2.18).

The more common crystal form is the folded lamella, which is more likely to be exhibited by short macromolecules of uniform constitution and with a regular configuration (see also Figure 2.4). Folding sets in on cooling of the melt at preferred points and the lamellae grow in a direction perpendicular to the fold faces. Several macromolecules may also form part of a folded lamella. In this way, helical crystal lamellae are produced, emanating from a central point to form a spherulitic superlattice. Besides these, there are less symmetrical spherulites in which the radially outwardly growing lamellae branch a number of times. Figure 2.19 shows schematically the individual structural elements for polyethylene, which give rise to a crystalline and spherulitic microstructure.

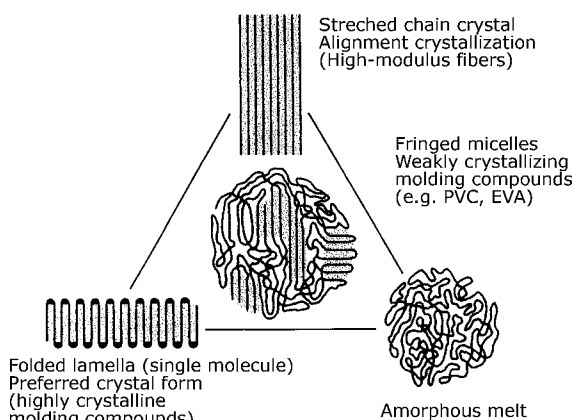


Figure 2.18 Crystalline and amorphous structures

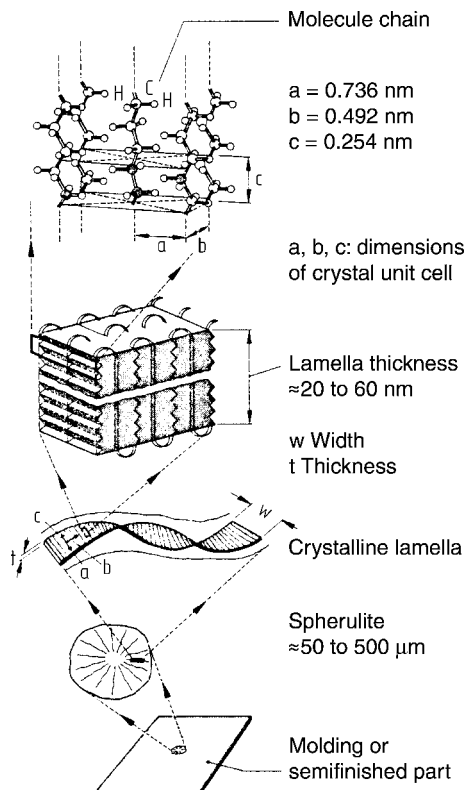


Figure 2.19 Architecture of crystalline structures for polyethylene as described in [2.1]

However, in the polymeric materials commonly used for industrial applications, a perfect crystalline state is not attained. On the contrary, a two-phase system consisting of amorphous and crystalline regions is found. The term “semicrystalline microstructure” is used to describe this. Here, the amorphous regions composed of unordered segments of molecules are found at the surfaces of the crystal lamellae, between the lamellae in the spherulites, and at their boundaries.

The following degrees of crystallization are typically formed during melt processing (injection molding):

High-density polyethylene (linear)	HDPE	70–80
Low-density polyethylene (branched)	LDPE	45–55
Polypropylene (isotactic)	PP	70–80
Polytetrafluoroethylene (sintered)	PTFE	60–80
Polyamide	PA	35–45
Polybutylene terephthalate	PBT	40–50
Polyoxymethylene	POM	70–80

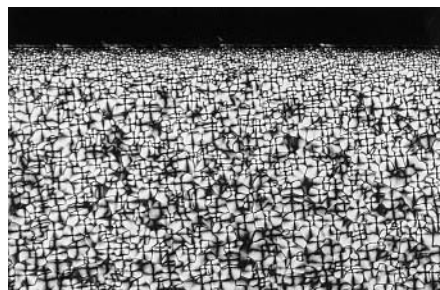
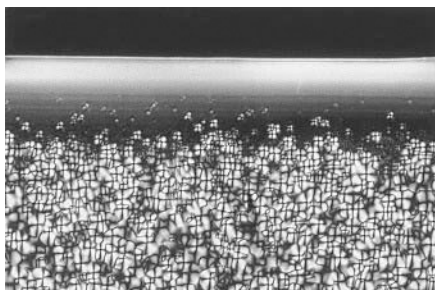


Figure 2.20 Section through the peripheral region of an injection-molded polyamide part
Top: peripheral layer devoid of crystal structure due to rapid cooling of the melt
Bottom: spherulites form right up to the surface at higher mold wall temperatures
(Microtome photomicrograph in polarized light)

The growth conditions for the ideal crystallite and spherulite structures shown rarely exist in practice under the circumstances in which moldings are produced. As an example, Figure 2.20 shows the peripheral region of a polyamide part from a microtome photomicrograph in polarized light. In the left image, the peripheral layer, markedly devoid of structure, is clearly discernible. This is due to rapid cooling of the polymer melt on the wall of the mold. In the right image of the same part, spherulite growth right up to the surface was made possible by a higher mold temperature. This, however, results in a slower production rate. As might be expected, the size of spherulites increases with distance from the surface because of the lower rate of cooling towards the interior of the part. This is also demonstrated in Figure 2.20.

Because of the higher packing density in the crystalline regions, the intermolecular binding forces increase. This manifests itself at the macroscopic level in higher strength and modulus of elasticity values, but lower deformability.

When evaluating deformation behavior it is essential to know the state the amorphous phase is in, because of the two-phase nature of the semicrystalline polymeric materials. If its glass transition temperature is above the temperature at which deformation behavior is to be assessed, the amorphous phase is rigid and brittle, and overall the semicrystalline polymeric material will exhibit high strength and modulus of elasticity values while ductility will be low.

However, if the glass transition temperature of the amorphous phase is below the evaluation temperature, the amorphous fractions will exhibit predominantly entropy-elastic deformation characteristics. The high toughness observed in many semicrystalline polymeric materials is explained by the interactions between amorphous, entropy-elastic components and crystalline, energy-elastic components. A further characteristic feature of polymeric materials having a semicrystalline structure is their good resistance to wear and improved chemical resistance.

The dense packing of the ordered molecules causes increased density, which in turn causes higher shrinkage in processing (up to 3%). Because shrinkage processes due to crystallization start out from the spherulite centers, high tensile stresses may arise at the boundaries of the spherulites. As a result, weak points are built into the structure. To avoid this effect, efforts are made to obtain as fine a spherulite structure as possible. This is done in practice by adding nucleating agents to the polymeric material. These elevate the temperature of crystallization so that the melt begins to crystallize earlier on cooling, resulting in a larger number of small spherulites.

Figure 2.21 shows in summary the different structural and morphological forms of the polymeric material, while in Table 2.4, the effects of the chain structure and morphology on temperature limit, modulus of elasticity, and strength are shown for some typical examples.

Table 2.4 Effects of Structure and Morphology on Some Selected Properties

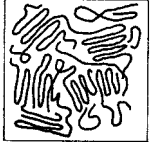
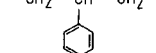
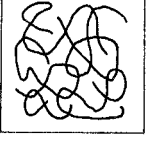
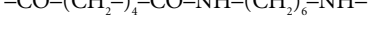
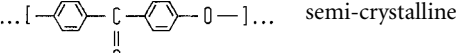
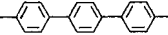
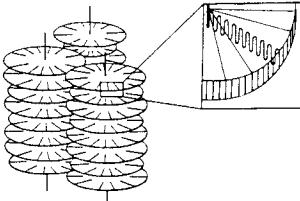
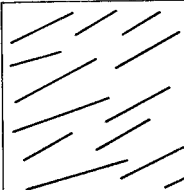
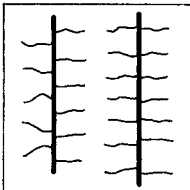
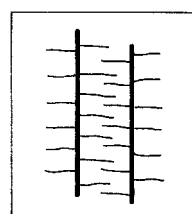
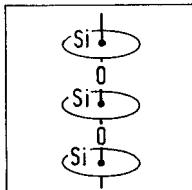
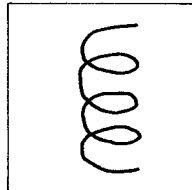
Chain structure	Example	Morphological structure	Material properties
			Tempera- Modulus Strength ture limit of elastic- (MPa) (°C) city (MPa)
Standard polymers			
	$-\text{CH}_2-\text{CH}_2-\text{CH}_2-$		
Linear with C-C chain	Polyethylene (PE)	semi-crystalline	90 1400 30
	$-\text{CH}_2-\text{CH}(\text{C}_6\text{H}_5)-\text{CH}_2-$		
	Polystyrene (PS)	amorphous	90 3200 60
	Polyamide (PA 66)	semi-crystalline	120 3200 85
High temperature polymers			
	$\dots [\text{---}\text{C}_6\text{H}_4\text{---S}(=\text{O})_2\text{---C}_6\text{H}_4\text{---}] \dots$	amorphous	
Linear with aromatic groups and hetero-atoms in the chain	Polyether sulfone (PES)		200 2800 90
	... [---C(=O)---C_6H_4---O---] ...	semi-crystalline	
	Polyaryl ether ketone (PAEK)		260 4000 100
$-\text{A}-\text{A}-\text{A}-$		amorphous	600
Linear aromatic	Polyphenylene		

Table 2.4 (continued)

Chain structure	Example	Morphological structure	Material properties		
			Temperature limit (°C)	Modulus of elasticity (MPa)	Strength (MPa)
Internally reinforced polymers					
Linear with C-C chain	$-\text{CH}_2-\text{CH}_2-\text{CH}_2-$ Polyethylene (PE)		Increase of melting point by 10 K to 146 °C	7500	140
Aromatic chain	Liquid crystalline polyester (LCP)		200	20000	120 40 ⊥
Research objectives					
Internally reinforced polymers with “brush structure”					
solid			molten		
					
Si-O chain			Helix-structure		
					

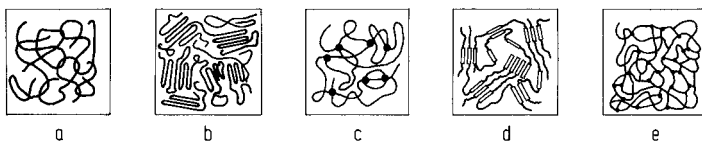


Figure 2.21 Schematic illustration of the structural and morphological forms of polymeric materials

- a) Linear, amorphous thermoplastic
- b) Linear, semicrystalline thermoplastic
- c) Chemically cross-linked elastomer
- d) Physically cross-linked elastomer
- e) Chemically cross-linked thermoset

2.5.3 Anisotropy

Components made from polymeric materials rarely display a morphology with perfectly isotropic properties. Either molecular states of order and states of internal stress are induced by processing [2.15], or the material itself is already biased towards anisotropy due, for example, to the fact that it is a two-component system containing added unidimensional fibers.

Anisotropy can take the following forms:

- Anisotropy in strength, producing different strengths in different directions
- Anisotropy in elasticity, resulting in direction-dependent moduli of elasticity
- Anisotropy in breaking behavior. In multicomponent systems the type of break in the components present (cohesive fracture or boundary surface fracture) may be dependent on direction [2.16].

2.5.3.1 Molecular Alignments

Molecular alignments and alignment stresses arise in processing (e.g., during injection molding) in that shearing due to the flow of the polymer melt causes deformations of the coil structure. The molecules deformed in this way, even whole aligned rows of crystallites, solidify in this position as a result of rapid cooling, especially in the peripheral regions* (see Figure 2.22).

The number of shear-induced alignments in a part that remain depends on the length of time for which the macromolecules remain above their glass transition temperature during cooling. During this period, they can resume their unaligned coil structure. Frozen alignment stresses produce no deformations below the glass transition temperature. Only at temperatures above the glass transition temperature do the deformed molecules once again take on the thermodynamically favored coil shape.

This means that a component encumbered by alignments shrinks or becomes warped only when its temperature is raised above the glass transition temperature of the polymeric material.

* In addition, there are expansion forces operating in the interior of the incoming melt, which bring about alignment of the molecular chains in a direction perpendicular to the main flow direction [2.17] (e.g., radial flow).

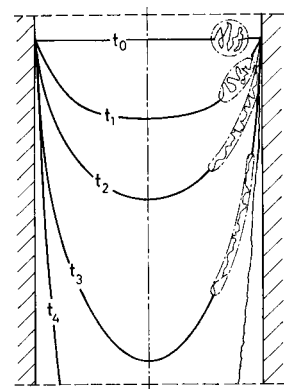


Figure 2.22 Production of molecular alignments due to deformation by shear flow of an originally circular surface element having a coiled structure [2.18]
 $t_0 < t_1 < t_2 < t_3 < t_4$

However, if it is divided below this temperature, by mechanical cutting for example, into two parts with different alignment potential, the two parts retain their shape*.

The macroscopic strength properties of parts aligned in this way exhibit anisotropy in that the strength in the direction of the molecular alignment is distinctly higher than in the unaligned state** and that in the direction transverse to the molecular alignment the strength may even be less than in the unaligned state.

The situation is different for films that are uniaxially or biaxially oriented by mechanical stretching processes***. In these cases (e.g., in what are known as shrink-wrap films), the shrinking effect produced by orientation on heating above the softening point is used.

In addition, stretching processes in the energy-elastic range can increase strength, especially in semicrystalline polymeric materials. This refers to the strengthening effect, due to the rearrangement of the crystalline folded blocks into alignment in the direction of stretching, obtained by mechanical forces after the apparent yield limit has been exceeded.

The stretching operation proceeds at a controlled temperature (often room temperature) but in the localized stretching zone, high temperatures occur which favor the rearrangement process (see also Table 4.1, Type C). A further point to be noted is the high tendency to split in the direction perpendicular to the direction of stretching. In practice, stretching is used for textile fibers, monofilaments, and to produce film or tapes for packaging purposes.

The molecules of liquid crystal polyesters (LCP) are rod-like and as such already exhibit chain rigidity. During the molding process, they tend to align themselves in the direction of flow.

* In contrast with alignment stresses, internal stresses are states of tension which, even in the energy-elastic range, relax or cause deformations. Internal stresses need not necessarily be apparent from the outside, but this will certainly happen if a part is divided into two halves. Causes of internal stresses include constraints to shrinkage, nonuniform cooling, and excessively high holding pressure in injection molding.

** A largely unaligned state can be achieved by casting or compression molding.

*** Stretching here is the selective introduction of molecular alignments in the entropy-elastic state and fixing them by freezing [1.1]. Such shrink-wrap films, typically made of polyolefins, are used for packaging and securing goods during transportation (see Figure 2.23). The goods to be packaged are wrapped in the film and heated. Because of the thermal expansion in the energy-elastic range, the packaging film may first become loose. However, on reaching the softening temperature, the shrinkage forces liberated cause the oriented film to shrink and as a result of thermal contraction on cooling, a firm seating of the film around the packaged goods is achieved.



Figure 2.23 Palletization and security in transport by means of polyethylene shrink-wrap film

The term self-reinforcement is used for semi-crystalline polymers exhibiting stress-induced crystallization; a high degree of alignment is produced (see also Table 2.3) [2.22, 2.26]. However, this latter type of self-reinforcement has so far not gained much significance commercially.

2.5.3.2 Filler or Fiber Alignment

In addition to molecular alignments, other distinct alignments occur, particularly in “short” or “long” glass-fiber reinforced thermoplastic polymeric materials (fiber length approx. 0.2 mm or more). Alignment of the fibers occurs during processing, typically in the direction of flow (see also Section 7.1.2). Such alignments have a much greater impact on strength and deformation characteristics than molecular alignments. However, the technical difficulties are found once again in:

- Predicting the fiber alignment which will establish itself in a molding having a complex shape
- Controlling the molding process to achieve, for instance, an orientation of the fibers in the component in keeping with stresses
- Preventing the occurrence of weaknesses at critical points due to transverse orientation at the same time

The differences in strength and modulus of elasticity in the direction of fiber alignment and the direction transverse to it are shown in an example of a polyamide reinforced with 25% by weight of short glass fibers presented in Figure 2.24. During the preparation of the test specimens, no perfect alignment of the fibers is achievable in short glass-fiber reinforced thermoplastics. In the specified preferred directions of the fibers, there are still some fibers lying in the transverse direction. Measured values perpendicular to the preferred alignment of the fibers are therefore higher than those for the unreinforced material.

When a fiber/matrix composite is placed under load perpendicular to the longitudinal axis of the fibers, concentrations of stress occur at the crest of the circular cross section of the fibers

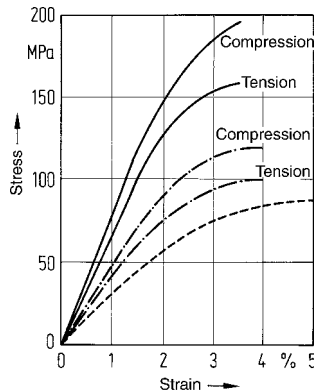


Figure 2.24 Stress-strain curves for glass-fiber reinforced PA 66 (25% by weight of short glass fibers) and unreinforced PA 66. The samples were cut out from plates along and transverse to the primary direction of fiber alignment (direction of flow).

— along the flow direction
- - - transverse to the flow direction
- - without added fibers; "along" and "transverse to" are identical

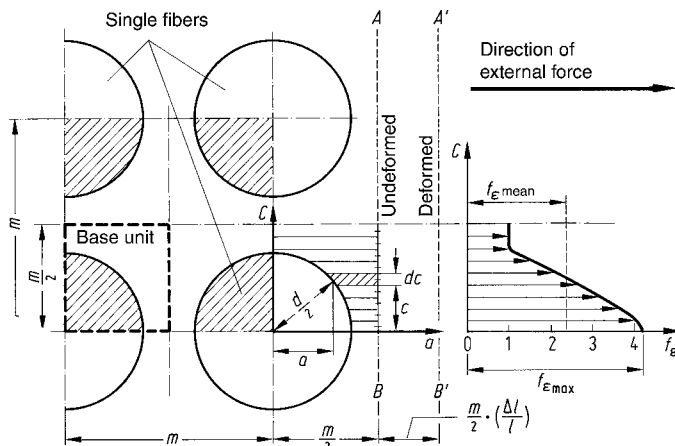


Figure 2.25 Increased elongation of the matrix under load perpendicular to the longitudinal axis of the fibers [2.20]

f_ε = elongation scale-up factor
 $\Delta l / m/2$ = external elongation

with maximum values appearing in the region of the boundary surface [2.19]. At the same time, excessive elongation of the matrix occurs where several fibers lie parallel to one another [2.20]. The model illustration in Figure 2.25 shows the effect of this increased elongation of the matrix at the crest of the fibers. The large difference in modulus of elasticity between the glass fiber and polymer matrix causes the sections of the matrix between the fibers to take on 4 to 10 times the external expansion of the whole composite. The strength and modulus of elasticity of a fully uniaxial fiber composite perpendicular to the orientation of the fibers are even lower than in the unreinforced matrix.

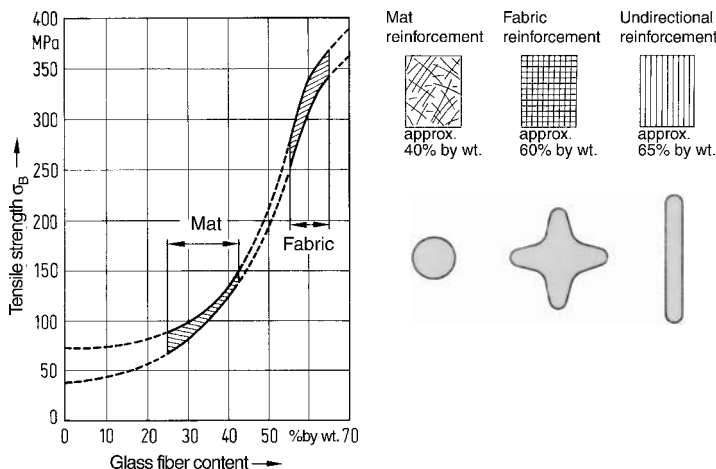


Figure 2.26 Polar diagrams (illustrated schematically) showing the tensile strength of reinforced resin composite systems as a function of the orientation of the reinforcing material (top) and tensile strength ranges of a polyester laminate (UP GF) under standard conditions (23 °C/50% RH) as a function of the glass content

In contrast to short fiber reinforced composites, cast resin composites (UP, EP) can be reinforced by woven fabric, non-woven fabric, or unidirectional strands. The orientation of the fibers can be selectively employed as a design principle. Figure 2.26 shows plots of tensile strength as a function of the orientation of the reinforcing material in the form of polar diagrams. When mats are used for reinforcement, a quasi isotropic state is assumed.

2.6 Thermomechanical Ranges

Polymeric materials are characterized by various thermomechanical states and thermal transitions. Each polymeric material has certain temperature intervals in which the polymeric materials exhibit distinctly different mechanical properties.

These relationships are usually presented graphically for engineers in the form of the torsional modulus $G = f(T)$ [2.21]. Fusion, glass transition, and crystallization are physical processes that are either caused by or lead to a change in specific heat. Accordingly, the temperatures associated with these may also be measured easily by thermal analysis (differential calorimetry, DSC).

2.6.1 Thermoplastics with Amorphous Structure

The thermo-mechanical behavior of amorphous thermoplastics, such as polystyrene, is described in the following section. At low temperatures*, polymeric materials tend to respond

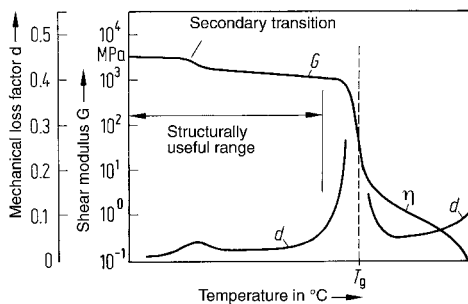


Figure 2.27 Schematic illustration of the variation of the torsional modulus and loss factor of amorphous thermoplastics with temperature

to mechanical loads in an energy-elastic mode. This means that in their force-deformation properties they approximately obey Hooke's law. In doing so, reversible changes in the spacing of atoms and shifts in valence angles take place in the form of atomic and molecular processes. At the macroscopic level this manifests itself in high modulus of elasticity values, while at the same time, brittle fracture behavior is exhibited. Even materials that are soft or elastomeric at room temperature become brittle at "low" temperatures.

With rising temperature, *i.e.*, as thermal energy is supplied, a softening range specific to the polymer is reached which is characterized by the glass transition temperature T_g . The position of T_g can be clearly seen at the maximum of the loss factor d^{**} in Figure 2.27.

Above this temperature, free volume has increased to the point where atomic and molecular movement mechanisms now include rotation and segments of chains and side groups can rearrange themselves. It is quite clear that bulky side groups impede these movements. Accordingly, under mechanical load, a deformation of the original coil structure will occur. Countervailing restoring forces, however, will restore the thermodynamically favored coil structure. This effect lends the polymeric material entropy-elastic (rubber-like) properties. Therefore, they are said to have an entropy-elastic range^{***}. At the same time, however, perceptible irreversible viscous deformations also take place, regardless of the level of stress. In this range, values of the modulus of elasticity fall by several orders of magnitude.

As the temperature rises further, the mobility of the chain finally becomes so high that chains can slide over one another and the material passes over into the molten state. Viewed in strictly thermodynamic terms, only crystalline structures can melt, amorphous ones cannot. The term molten describes a state where an amorphous polymer will flow sufficiently to be processed.

* The term "low temperature" has to be understood in relative terms here. For some polymeric materials, the term may mean temperatures below $-70\text{ }^\circ\text{C}$ (polyisobutylene, PIB), while for others it may be about $+100\text{ }^\circ\text{C}$.

** The loss factor d is the name given to the tangent of the phase angle δ which appears under dynamic, sinusoidal loading of polymeric materials between the stress σ and the elongation ε . The complex modulus of elasticity E formed from the peak values of σ and ε can be divided into a real part E' (= measure of the stored elastic energy) and an imaginary part E'' (= measure of the lost energy converted into heat).

The following relationship applies: $d = E''/E' = \tan \delta$.

*** The terms "rigid" and "flexible" or "rubber-like" are not thermodynamically correct and are usually replaced by "energy-elastic" and "entropy-elastic", respectively. However, from the thermodynamic point of view, rubber has predominantly energy-elastic properties.

In this “fluid” state, the modulus of elasticity is replaced as the characterizing mechanical variable by the melt viscosity η . Like modulus, melt viscosity falls as the temperature rises. Structural parameters, such as bulky side groups and high relative molecular weight, tend to increase viscosity at any given temperature. Higher hydrostatic pressures also cause an increase in viscosity.

The transitions that occur as the temperature rises from the energy-elastic to the entropy-elastic state (and then into the molten state) can in theory be repeated any number of times. In practice, however, frequent repetition (e.g., multiple reprocessing) could lead to chemical changes (e.g., oxidation, degradation, etc.) that affect these values.

2.6.2 Thermoplastics with Semicrystalline Structure

Semicrystalline thermoplastics have both amorphous and crystalline regions. At low temperatures, polymeric materials having a semicrystalline structure respond in essentially the same way as those having an amorphous structure. However, as the temperature rises above the glass transition temperature T_g , only the amorphous components of the structure initially make the transition to the entropy-elastic state. The ordered crystalline regions retain their energy-elastic nature (see Figure 2.28).

In the plot of the torsional modulus against temperature, the softening of the amorphous phase manifests itself as a drop in modulus, which is all the more pronounced when the degree of crystallinity of the polymeric material in question is low. The softening temperature range of the amorphous phase of a semicrystalline polymer is fairly broad. The crystallite melting point of the crystalline regions (T_m) eventually reached as the temperature rises higher, is relatively sharp because the ordered molecular domains break up at a well-defined activation energy (potential energy threshold).

Rigid amorphous thermoplastics have no practical use at temperatures above their T_g . They can be processed by thermoforming (thermoforming of sheet material) at temperatures above their T_g . Semicrystalline polymeric materials, on the other hand, are widely used in the temperature range between their T_g and T_m . In this temperature range, they still have adequate rigidity (as a result of the intact crystalline structure) and exhibit good impact resistance or toughness.

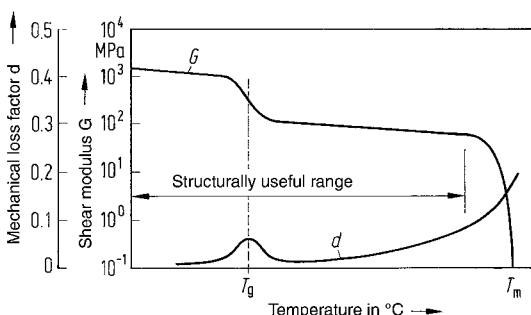


Figure 2.28 Schematic illustration of the variation of the torsional modulus and loss factor of semicrystalline thermoplastics with temperature

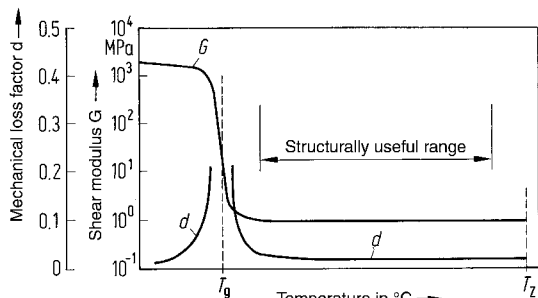


Figure 2.29 Schematic illustration of the curve of torsional modulus and loss factor versus temperature for elastomers

2.6.3 Elastomers

The class of materials known as elastomers are used, because they exhibit their desirable rubber-elastic properties even at low temperatures. Most elastomers have glass transition temperatures well below $0\text{ }^{\circ}\text{C}$. In the case of crosslinked or thermoset elastomers, a feature of their thermomechanical behavior is the absence of the molten state. Above the glass transition temperature, they exhibit low but almost constant values of modulus of elasticity (depending on the material type, $G = 0.1$ to 100 MPa) up to the temperature of thermal decomposition T_z (see Figure 2.29). Their chemical cross-linking allows these materials to be used over a wide temperature range, even when under stress. Thermoplastic elastomers have a more limited temperature use range.

2.6.4 Thermosets

Rigid thermosets (thermosetting plastics) are close-meshed, cross-linked polymers whose glass transition temperature, in contrast with elastomers, is as high as possible (typically $> 50\text{ }^{\circ}\text{C}$). The close-meshed cross-linking ensures that even above the glass transition temperature there is no significant drop in the modulus of elasticity at T_g . Once crosslinked, thermoset plastics do not melt or reach a molten state. On reaching T_z , thermal decomposition sets in (see Figure 2.30). Thermoplastics offer processing advantages relative to thermoset plastics. However, thermoset plastics are used in demanding applications.

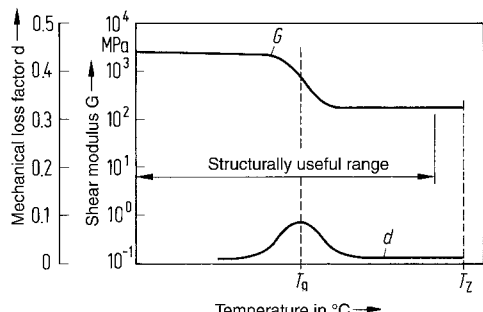


Figure 2.30 Schematic illustration of the curve of torsional modulus and loss factor versus temperature for thermoset plastics

References

- [2.1] MENGES, G.: Werkstoffkunde der Kunststoffe (Materials Science of Plastics), Hanser-Verlag, Munich Vienna 1979
- [2.2] VOLLMERT, B.: Grundriß der makromolekularen Chemie (Outline of Macromolecular Chemistry), Springer-Verlag, Berlin Heidelberg New York 1962
- [2.3] SCHURZ, J.: Physikalische Chemie der Hochpolymeren (Physical Chemistry of High Polymers), Springer-Verlag, Berlin Heidelberg New York 1974
- [2.4] MORRISON, R. T. and R. N. BOYD: Lehrbuch der organischen Chemie (Textbook of Organic Chemistry), Chemie-Verlag, Weinheim 1974
- [2.5] HOLZMÜLLER, W.: Struktur der makromolekularen Körper (Structure of Macromolecular Substances), in Holzmüller/Altenburg: Physik der Kunststoffe (Physics of Plastics), Akademie-Verlag, Berlin 1961
- [2.6] MARTIN, CL. G.: Zur Eigenverstärkung von Polyethylen im Spritzguß (The Self-Reinforcement of Polyethylene in Injection Molding), Dissertation, University of Kassel, 1988
- [2.7] CAMPUS 4 Database, 1997 (BASF, DSM, DUPONT, HUELS), *Kunststoffe* **69** (1979) 9, pp. 575/625
- [2.8] ERHARD, G.: Zum Reibungs- und Verschleißverhalten von Polymerwerkstoffen (The Friction and Wear Properties of Polymeric Materials), Dissertation, University of Karlsruhe, 1980
- [2.9] BREUER, H., HAAF, F. and J. STABENOW: Stress Whitening and Yielding Mechanism of Rubber-Modifier PVC, *J. Macromol. Sci.-Phys.*, B **14** (1977) 3, pp. 387/417
- [2.10] RETTING, W.: Kunststoffe, Ordnungszustände und Eigenschaften (Plastics, States of Order and Properties) in Ullmanns Enzyklopädie der technischen Chemie, 4th ed., Vol. 15, p. 247, Chemie-Verlag, Weinheim 1978
- [2.11] ERHARD, G.: Entwicklungstendenzen der Kunststoffverwendung für Maschinenelemente (Development Trends in the Use of Plastics for Machine Parts), *Kunststofftechnik* **8** (1969) 6, pp. 199/200
- [2.12] EHRENSTEIN, G. W. and R. WURMB: Glasfaserverstärkte Thermoplaste Theorie und Praxis (Glass-Fiber Reinforced Thermoplastics Theory and Practice), *Angewandte Makromolekulare Chemie* **60/61** (1977), pp. 157/214
- [2.13] VOLLMERT, B.: Strukturbedingte Belastungsgrenzen von Polymerwerkstoffen, Belastungsgrenzen von Kunststoff-Bauteilen (Structure-Based Loading Limits of Polymeric Materials, Loading Limits of Plastic Components), VDI-Verlag, Düsseldorf 1975
- [2.14] NORTH, A. M.: Molecular Motion in Polymers, Molecular Behaviour and the Development of Polymeric Materials, Chapman Hall, London 1975, ref. in [1.8]
- [2.15] WINTERGERST, S.: Orientierungen und Spannungen in Spritzgußteilen (Alignments and Stresses in Injection-Molded Parts), *Kunststoffe* **63** (1973) 5, pp. 636/642
- [2.16] SCHNEIDER, W. and R. BARDENHEIER: Versagenskriterien für Kunststoffe (Failure Criteria for Plastics), *Zeitschrift für Werkstofftechnik* **8** (1975), pp. 269/280
- [2.17] WOEBCKEN, W. AND E. SEUS: Die Schwindung von Polyäthylen und ihre Abhängigkeit von den Verarbeitungsbedingungen (Shrinkage of Polyethylene and its Dependence on Processing Conditions), *Kunststoffe* **57** (1967) 5, pp. 637/644 and pp. 719/723
- [2.18] SCHREYER, G.: Konstruieren mit Kunststoffen (Designing with Plastics), Hanser-Verlag, Munich Vienna 1972, Vol. 1, p. 160
- [2.19] EHRENSTEIN, G. W.: Grenzflächenenergetische Vorgänge und Eigenspannungszustände in glasfaser-verstärkten Kunststoffen (Boundary Surface Energy Processes and States of Internal Stress in Glass-Fiber Reinforced Plastics), Dissertation, Technische Hochschule, Hanover 1968

- [2.20] PUCK, A.: Zur Beanspruchung und Verformung von GFK-Mehrschicht-Verbund- Bauelementen (Loading and Deformation of GRP Multilayer Composite Building Elements), *Kunststoffe* **57** (1967) 12, pp. 965/73
- [2.21] SCHMIEDER, K. and K. WOLF: Mechanische Relaxationserscheinungen an Hochpolymeren (Mechanical Relaxation Phenomena in High Polymers), *Kolloid-Zeitschrift* **134** 2/3, pp. 149/189
- [2.22] EHRENSTEIN, G. W.: Eigenverstärkung von Thermoplasten im Schmelze-Deformationsprozeß (Self-Reinforcement of Thermoplastics in the Melt Deformation Process), *Die Angew. Makromolek. Chemie* **175** (1990), pp. 187/203
- [2.23] ANON.: Konditionieren von Fertigteilen aus Ultramid (Conditioning of Finished Parts made from Ultramid), BASF, company brochure, 1993

3 Brief Description of the Properties of Generic Polymeric Materials

3.1 Thermoplastics

Thermoplastics are polymeric materials made up of linear or branched macromolecules. Macromolecules having a regular structure are capable of the order required to form crystals, while an irregular arrangement of polymer chains gives rise to an amorphous structure. Polymeric materials are said to be semi-crystalline (partially crystalline) when they contain both domains of crystalline order as well as amorphous phases.

Macromolecules attach themselves to one another by means of physical binding forces (*e.g.*, van der Waals forces and hydrogen bonding). These binding forces can be overcome when sufficient thermal energy is supplied, *i.e.*, these polymeric materials can make the transition to the molten state. In doing so, a crystalline structure is converted into an amorphous phase. The processing of thermoplastic polymeric materials from the powdery or granular form of the raw materials into finished or semi-finished parts is most commonly accomplished by heating the polymer to the molten state in one of many different processes (see also Figure 7.1).

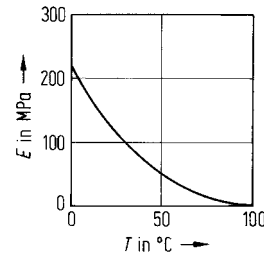
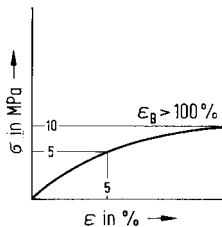
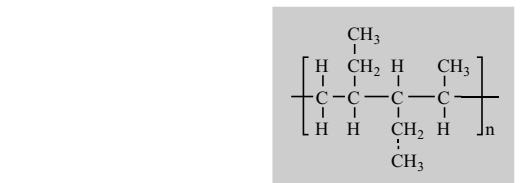
The following section provides a brief description of the properties of some of the most widely used and important polymeric materials. These descriptions are intended to provide only a general guide. Those listed are the standard grades, some of which can be varied in numerous ways using additives, such as fillers, reinforcing materials, stabilizers, flame retardants, pigments, and other additives.

Databases, such as CAMPUS®, set up by several plastics manufacturers, provide information about the numerous grades and modifications of these products.

Several of the figures below contain stress-strain diagrams (σ - ϵ diagrams) describing the deformation behavior determined by short-term tensile stress testing conducted at room temperature. The characteristic relationship between the modulus of elasticity and temperature, $E = f(T)$, is also shown to describe the effect of temperature on deformation behavior. In addition, some general information on structure and morphology is provided. The stated temperature limits of application are values derived from experience in numerous practical situations. The guide values labeled “short-term” relate to a temperature-time limit of up to a few hours, while “long-term” refers to thermal loads lasting for years. Over this time period, the physical properties of the materials change due to thermal aging to an extent that can be very variable depending on the exact conditions and additives. None of these maximum use temperature values should be considered absolute, because they are load dependent. Testing is always recommended.

Low-Density Polyethylene (LDPE)

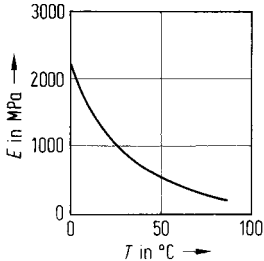
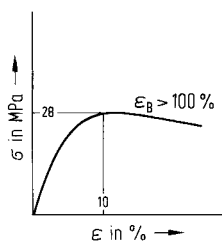
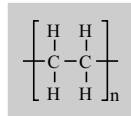
Microstructure	semi-crystalline
Degree of crystallinity	45–55%
T_g	< -100 °C
T_m	108–115 °C
Molecular structure	branched
Temperature limits of applications:	
Short-term	~100 °C
Long-term	~80 °C



Note: Linear low-density polyethylene (a short branch polyethylene copolymer) is now widely used in applications previously dominated by LDPE.

High-Density Polyethylene (HDPE)

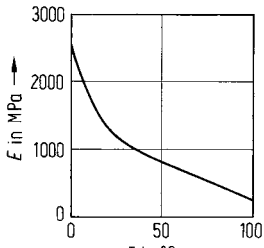
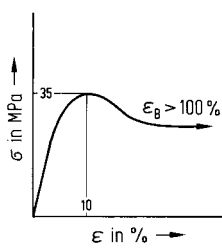
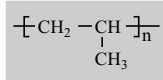
Microstructure	semi-crystalline
Degree of crystallinity	70–80%
T_g	< -100 °C
T_m	130–140 °C
Temperature limits of applications:	
Short-term	~110 °C
Long-term	~90 °C



Note: High-density polyethylene copolymer is also widely used, especially in applications where additional chemical resistance is required. It has a slightly lower density and level of crystallinity.

Polypropylene (PP)

Microstructure	semi-crystalline
Degree of crystallinity	70–80%
T_g	~5 °C
T_m	160–165 °C
Tacticity	isotactic
Temperature limits of applications:	
Short-term	~140 °C
Long-term	~90 °C



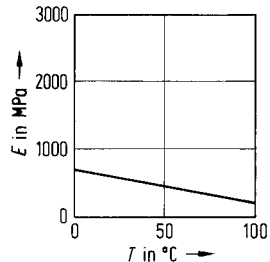
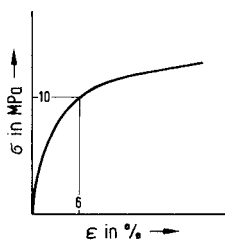
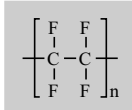
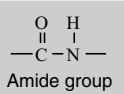
Note: Copolymer grades of polypropylene are also widely used, especially in applications requiring improved low temperature toughness.

Polytetrafluoroethylene (PTFE)

Microstructure	semi-crystalline
Degree of crystallinity	60–80%
T_g	~320 °C
T_z	~500 °C
Temperature limits of applications:	
Long-term	~260 °C

Special characteristics:

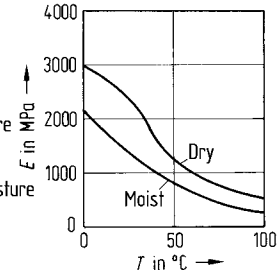
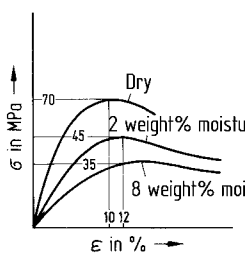
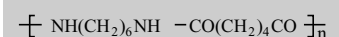
Processing by compression sintering or ram extrusion, high resistance to chemicals, extremely low surface energy

**Polyamide 6 (PA 6)**

Microstructure	semi-crystalline
Degree of crystallinity	35–45%
T_g (dry)	60 °C
T_g (2.8% by wt. moisture)	15 °C
T_g (11% by wt. moisture)	-10 °C
T_m	220 °C
Temperature limits of applications:	
Short-term	~180 °C
Long-term	~80 °C

Special characteristics:

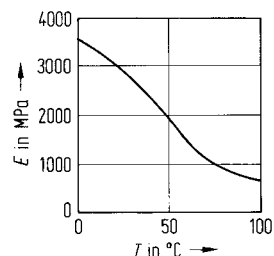
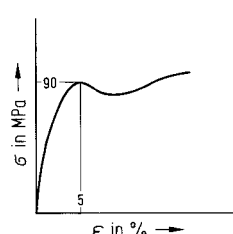
Properties dependent on water absorption

**Polyamide 66 (PA 66)**

Microstructure	semi-crystalline
Degree of crystallinity	35–45%
T_g	70 °C
T_m	255 °C
Temperature limits of applications:	
Short-term	~200 °C
Long-term	~90 °C

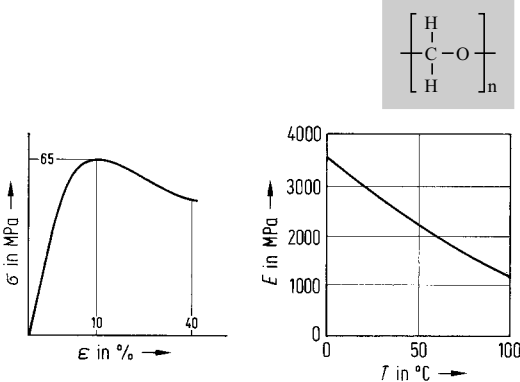
Special characteristics:

Properties dependent on water absorption

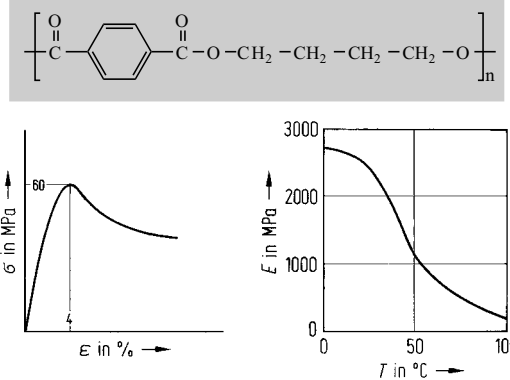


Polyoxymethylene (POM)

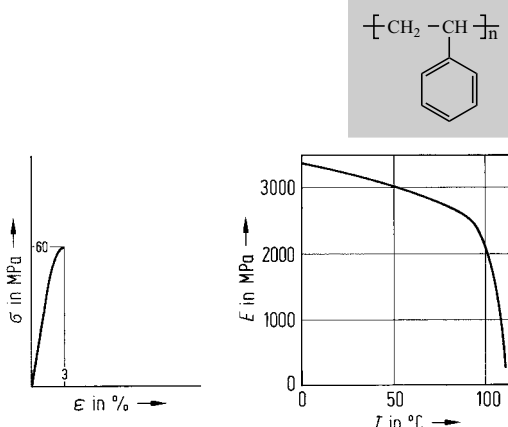
Microstructure	semi-crystalline
Degree of crystallinity	70–80%
T_g	–60 °C
T_m	165–175 °C
Temperature limits of applications:	
Short-term	~150 °C
Long-term	~100 °C

**Polybutylene Terephthalate (PBT)**

Microstructure	semi-crystalline
Degree of crystallinity	40–50%
T_g	60 °C
T_m	225 °C
Temperature limits of applications:	
Short-term	~170 °C
Long-term	~120 °C

**Standard Polystyrene (PS)**

Microstructure	amorphous
T_g	~100 °C
Temperature limits of applications:	
Short-term	~90 °C
Long-term	~60 °C



Impact-Resistant Polystyrene (SB)

Microstructure amorphous

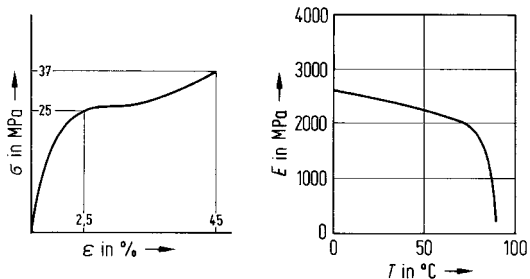
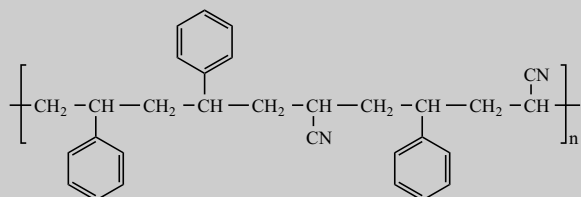
T_g ~95 °C

Heterogeneous mixture of polymers
(polystyrene with grafted butadiene
rubber)

Temperature limits of applications:

Short-term ~80 °C

Long-term ~70 °C

**Styrene-Acrylonitrile (SAN)**

Microstructure amorphous

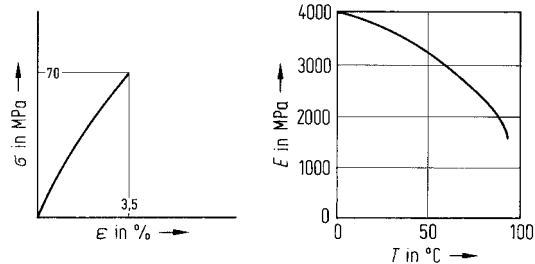
T_g 105 °C

Copolymer of styrene and acrylonitrile

Temperature limits of applications:

Short-term ~95 °C

Long-term ~85 °C

**Acrylonitrile-Butadiene-Styrene (ABS)**

Microstructure amorphous

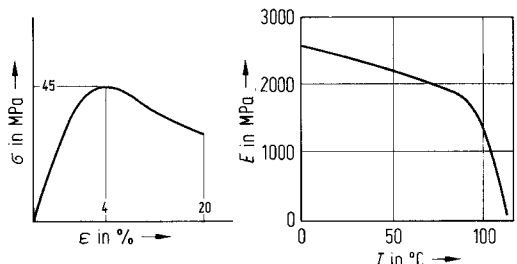
T_g 105–125 °C

Heterogeneous mixture of polymers
(acrylonitrile-butadiene-styrene)

Temperature limits of applications:

Short-term ~95 °C

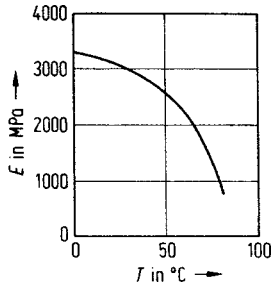
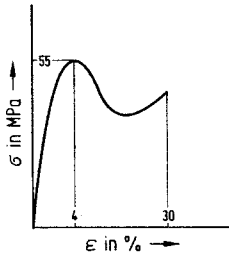
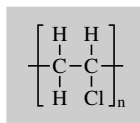
Long-term ~85 °C



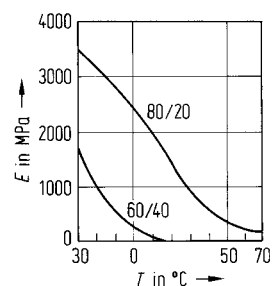
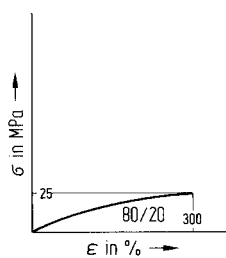
Poly(Vinyl Chloride) (PVC)

Microstructure amorphous
 T_g 90 °C

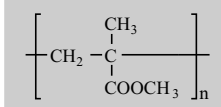
Temperature limits of applications:
 Short-term ~70 °C
 Long-term ~60 °C

**Plasticized Poly(Vinyl Chloride) (pPVC) [3.14]**

Microstructure amorphous
 Temperature limits of applications:
 Long-term up to ~90 °C depending on type and concentration of plasticizer

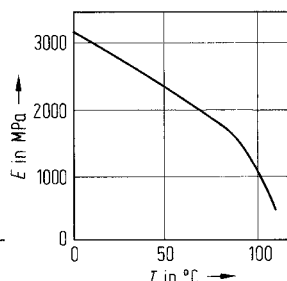
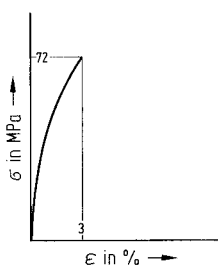
*Special characteristics:*

Mechanical properties controllable over a wide range by varying the plasticizer type and concentration

Poly(Methyl Methacrylate) (PMMA) [3.15]

Microstructure amorphous
 T_g 100 °C

Temperature limits of applications:
 Short-term ~90 °C
 Long-term ~65 °C



Polycarbonate (PC)

Microstructure

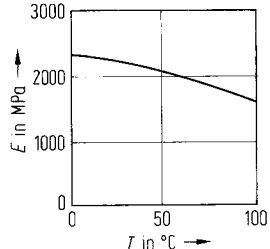
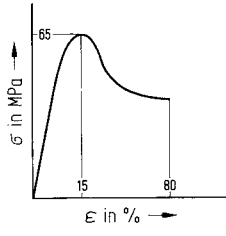
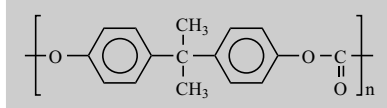
amorphous

 T_g 158 °C

Temperature limits of applications:

Short-term ~135 °C

Long-term ~100 °C

**Polyphenylene Sulfide (PPS GF40)**

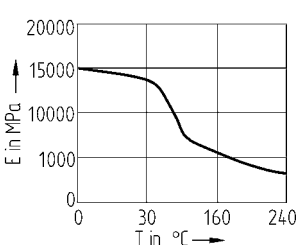
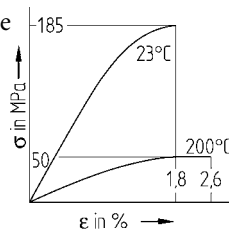
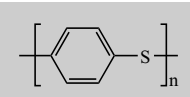
Microstructure semi-crystalline containing 40% by weight of glass fibers

 T_g 85–100 °C T_m 280 °C

Temperature limits of applications:

Short-term ~260 °C

Long-term ~240 °C

**Polyether Sulfone (PES), 0.7% moisture**

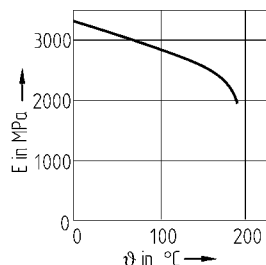
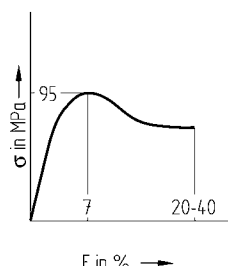
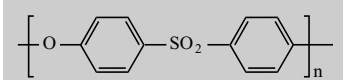
Microstructure amorphous

 T_g 228 °C

Temperature limits of applications:

Short-term ~220 °C

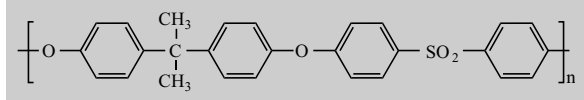
Long-term ~180 °C

*Special characteristics:*

Absorption of water

Saturation in 23 °C/50% RH atmosphere approx. 0.7%
in water approx. 2.1%

Properties slightly dependent on water absorption

Polysulfone (PSU)

Microstructure

 T_g

amorphous

128 °C

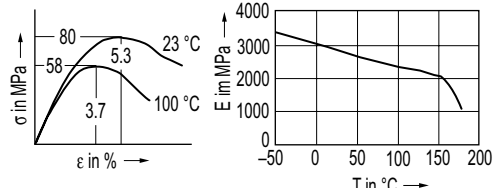
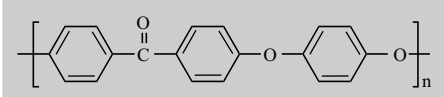
Special characteristics:

Absorption of water

Saturation in 23 °C/50% RH atmosphere approx. 0.3%

in water approx. 0.8%

Properties almost independent of water absorption

**Polyaryl ether ketone (PAEK)**

Microstructure

Degree of crystallinity

 T_g T_m

semi-crystalline

35–50%

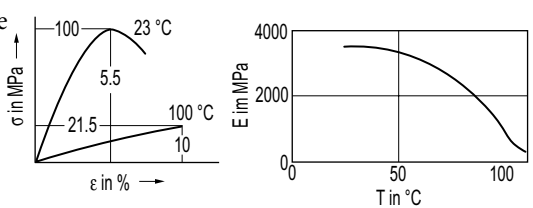
143 °C

344 °C

Temperature limits of applications:

Short-term ~300 °C

Long-term ~240 °C

*Special characteristics:*

High resistance to chemicals, hydrolysis and radiation.

Liquid Crystal Polymer (LCP GF30)

Microstructure

 T_g

rod-shaped molecules, with 30% by weight of glass fibers

280 °C

Temperature limits of applications:

Short-term ~260 °C

Long-term ~240 °C

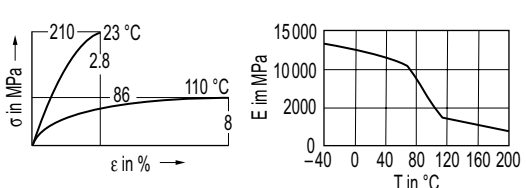


Table 3.1 Properties of Selected Engineering and High Performance Thermoplastics (Source: Campus 4.5)

Polymer	Trade name	Glass Fibers % by weight	$\sigma_b/(\sigma_y)$ MPa	$\varepsilon_b/(\varepsilon_y)$ %	E_t MPa	T_m °C	T_g °C	T_d (HDT) (1.8 MPa) °C
Semicrystalline Thermoplastics								
PA 66	Ultramid A3HG6 dry/moist	30	190/120	3.2/5.4	10 000/6800	260	72	250
PA 46	Stanyl (TE 250 F6) dry/moist	30	180/125	2.5/3.5	12 500/8000	295	75	290
PA6T/6I/66 (PPA)	Amodel (A1133HS) dry/moist	33	221/193	2.5/2.1	13 100	312	127	285
PA6/PA6I (PPA)	Grivory (HTV-33HI) dry/moist	33	200/185	2/2	12 000	325		280
PA6/PA6T (PPA)	Ultramid T (KR 4355 G7) dry/moist	35	210/200	3/3	12 000	295	105	270
PPS	Fortron (1130L4)	30	150	1.9	11 700	280	90	265
PEEK	Victrex 450 G	–	(97)	(4.9)	3600	340	143	152
	Victrex 450 GL30	30	156	4.9	9700	340	143	315
LCP	Vectra (A 130)	30	190	2.1	15 000	280		235
Amorphous Thermoplastics								
PEI	Ultem (1000)	–	(105)	(6)	3200	–	215	190
PES	Ultrason E (2010)	–	(90)	(6.7)	2700	–	225	195
PAI	Torlon (5030)	30	220	2.3	10 800	–	285	282

3.1.1 Polymer Blends

Polymer blends are physical mixtures of polymers, usually two thermoplastics, which may or may not be compatible with one another. This means that combinations of properties reflecting those of the individual components can be achieved. Sometimes, the poly blend can have a range of properties unmatched by either constituent polymer. As an example, there is a synergy manifested in impact resistance for blends of ABS with PC. Blends of PC and ABS have exhibited good impact performance as shown in Figure 3.1. At temperatures higher than 0 °C, the impact behavior reflects that of the constituents. However, at lower temperatures, the impact resistance of the blend is higher than that of the components.

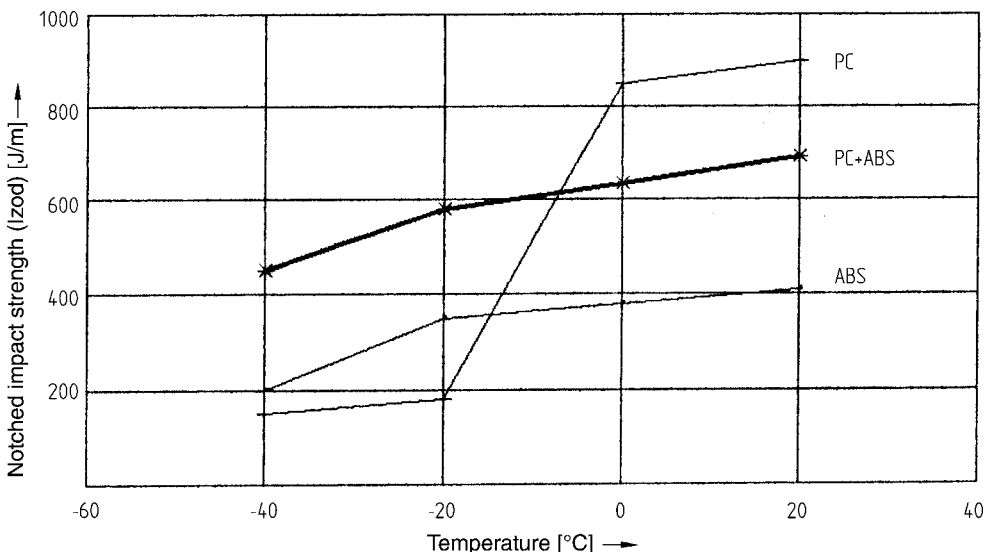


Figure 3.1 Notched impact resistance (Izod) versus temperature for a PC-ABS blend and for the individual components

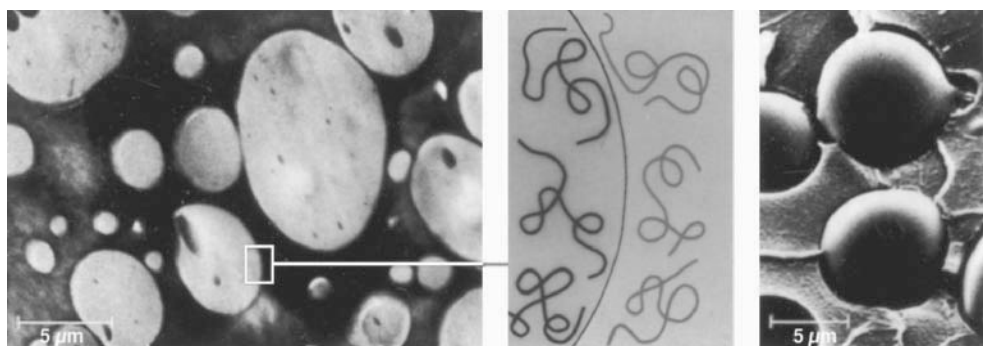


Figure 3.2 Mixing incompatible polymers results in coarse morphology (left) with low phase adhesion (center, schematically), and brittle adhesive fracture at the phase interface (right) [3.21]

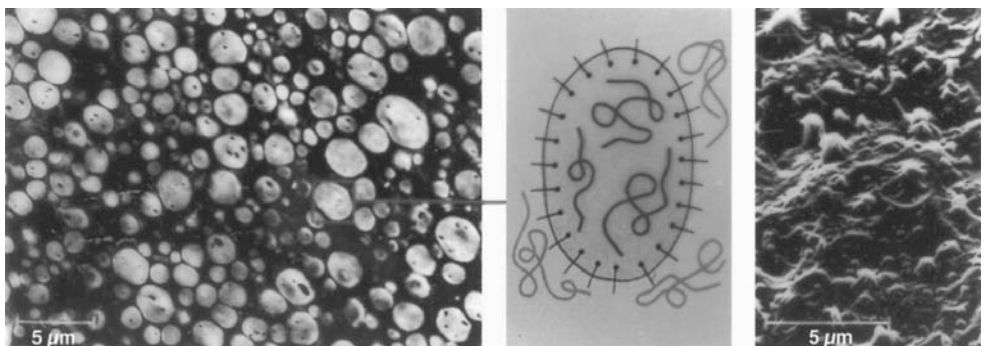


Figure 3.3 Modification by means of compatibilizing bonding agents affording good phase adhesion (center, schematically) and tough cohesive failure (right) [3.21]

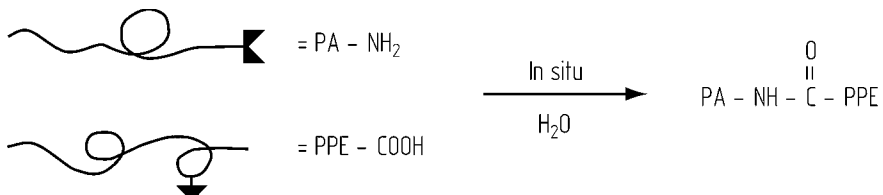


Figure 3.4 Mechanism (schematic) for the formation of junction molecules in the mixing process for a PPE + PA blend

When incompatible polymers are mixed, the result tends to be coarse separation into phases which adhere poorly to one another. This gives rise to brittle adhesive fracture at the phase boundary (see Figure 3.2).

Phase adhesion is improved by adding what are known as compatibilizing bonding agents including, for example, block and graft copolymers (see Figure 3.3).

It is even more efficient when such block or graft copolymer molecules are produced in situ during the mixing process by chemical reaction of suitable functional groups across the boundary surfaces (see Figure 3.4). The PPE + PA blend shown in Figure 3.4 is an example of this.

Examples of Polymer Blends

Blending of polymers first started with the development of impact-resistant polystyrene (SB). When polybutadiene rubber is finely dispersed through the polystyrene matrix, it effectively stops the propagation of cracks and the brittle fracture behavior of general purpose polystyrene (PS) is changed to tough or ductile fracture behavior. The micromechanism responsible for increasing impact resistance is not based on the high intrinsic toughness of butadiene rubber, because the styrene matrix in impact-resistant polystyrene (SB) is coherent. Due to the different coefficients of thermal expansion of polystyrene and rubber, considerable internal stresses occur at the perimeter of the butadiene particles. Under the action of external forces, these give rise to stress peaks which cause widespread crazing in the polystyrene and hence increased absorption of energy. The discrete rubber particles can also stop matrix crack propagation.

In the 1980s, the range of polymer blends was extended considerably. Some examples are presented in bullet-point style below.

Polymer Blend of Polyphenylene Ether and Impact-Resistant Polystyrene (PPE + SB)

Components miscible in all proportions, so selective changes in properties are possible
Range of properties determined very largely by the PPE component.

Heat distortion temperature increases with proportion of PPE (from 90 °C to 160 °C)
Improved processing due to SB component

Polymer Blend of Polyamide and Polyphenylene Ether (PA + PPE)

Increase in heat distortion temperature from 170 °C to 220 °C.

Reduced water absorption (saturation in 23 °C/50% RH atmosphere approx. 1% by weight).
Improved stress-cracking resistance.

Polymer Blend of Acrylonitrile/Butadiene/Styrene and Polycarbonate (ABS + PC)**Polymer Blend of Acrylonitrile/Styrene/Acrylate Rubber and PC (ASA + PC)**

Heat resistance rises in direct proportion to PC content.

Impact resistance, especially at low temperatures, rises in proportion to PC content
(see Figure 3.1).

Aging resistance (yellowing) improved by ASA compared with ABS.

Polymer Blend of Polycarbonate and Liquid Crystal Polymer (PC + LCP) [3.12]

High flow length/wall thickness ratio for thin-walled parts.

High rigidity due to LCP reinforcement.

High impact resistance and high heat resistance.

Susceptible to warping due to LCP reinforcement.

Polymer Blend of Polybutylene Terephthalate and**Acrylonitrile/Butadiene/Styrene (PBT + ABS)****or Polymer Blend of Polybutylene Terephthalate****and Acrylonitrile/Styrene/Acrylate Rubber (PBT + ASA)**

Range of properties determined predominantly by PBT component.

ASA/ABS component reduces shrinkage and tendency to warp.

Commercial grades are usually glass fiber reinforced.

Surface quality very good, even with glass fiber reinforcement.

Polymer Blend of Poly(Methyl Methacrylate) and Acrylonitrile/Butadiene/Styrene (MABS), also (PMMA + ABS)

High transparency due to PMMA component.

Improved heat resistance.

High impact resistance due to ABS component.

Good processability.

Polymer Blend of Polar Polymers (PA, POM, PAEK, etc.) and HDPE or PTFE

Good materials for slip/sliding applications.

Polar matrix affords high wear resistance.

Nonpolar component has lubricating action.

Other examples are blends of HDPE and PA in which the PA component acts as a diffusion barrier, *e.g.*, in fuel tanks, or the mixture of polypropylene (PP) with an ethylene-propylene-diene rubber (EPDM). The EPDM component improves the entropy-elastic deformation properties while the melt processability of the polypropylene is retained.

3.1.2 Functional Polymers

Polymers for Optical Purposes

Polymers have long been used as “functional” materials. Specifically, materials in which the material itself fulfills certain functions, without any special functional design, are described as functional materials.

Polymers already enjoy widespread use in the field of optics and along with lenses, prisms, light pipes, etc., the compact disc (and now the DVD) may be identified as the most popular optical application. Without polycarbonate, this new technology would not be the brilliant success it is. PC serves not only as the storage medium for the microscopically small sequences of pits (features) having dimensions in the range of 0.1 µm, but it also provides the optical conditions for the CD or DVD player’s laser beam [3.11]. Most optically transparent thermoplastics are amorphous, although some semi-crystalline polymers (such as PP) exhibit good light transmission.

Thermotropic polymers alter their light transmittance at certain temperatures. The switching temperature can be set precisely to 1 degree within the range of 20 to 100 °C. The optical effect is based on the fact that starting at the switching temperature, polymer particles in a blend separate out in the polymer, resulting in scattering of about 50% of visible light. Transparency is lost and the thermotropic layer turns milky. The process is reversible. The following molecular processes are involved: partially compatible polymer blends exhibit an immiscibility gap, that is, they are completely soluble in one another at low temperatures and demix at a temperature that is dependent on concentration (see Figure 3.5) so that they are

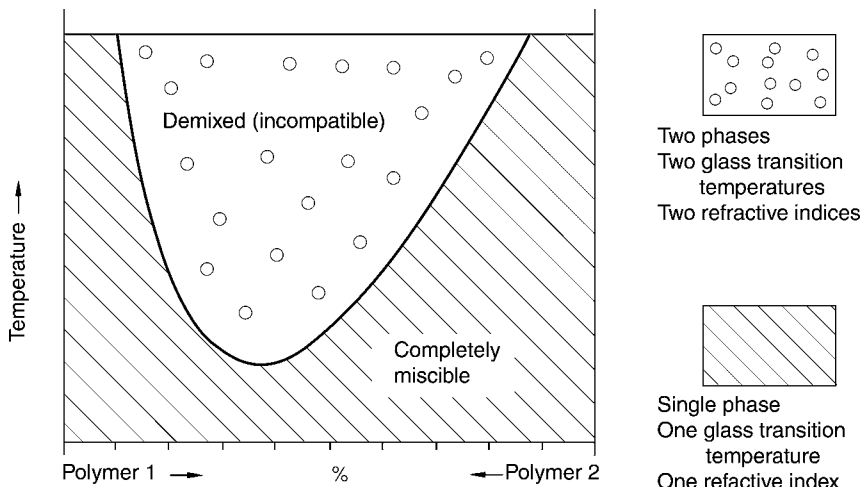


Figure 3.5 Immiscibility gap of a partially compatible polymer blend

transparent at low temperatures. Above the switching demixing temperature, the blend becomes a two-phase system and the blend exhibits a milky or cloudy appearance [3.13].

Electrically Conducting Polymers

As a general rule, polymers are electric insulators. As a result, polymeric materials have found widespread application in electrical engineering and electronics as insulators. It is, however, of great interest to combine the ease of processing of thermoplastics with electrical conductivity. The following section provides only a fundamental overview of this specialized field. The reader is directed to [3.14] for more detail.

There are three primary methods for rendering inherently insulating polymers conductive:

- Filling them with conductive additives,
- Coating them with conductive paints or metal layers, or
- Synthesizing polymers which are intrinsically conductors of electricity.

Depending on the level of conductivity, different goals can be achieved:

- Antistatic properties,
- Electromagnetic screening, and
- Electrically conducting properties.

Conductive Properties

The classic method of achieving a limited level of electrical conductivity consists in mixing conductive additives into the polymer matrix. In doing so, the conductive filler concentration must be high enough to produce a continuously conducting network (known as a percolation

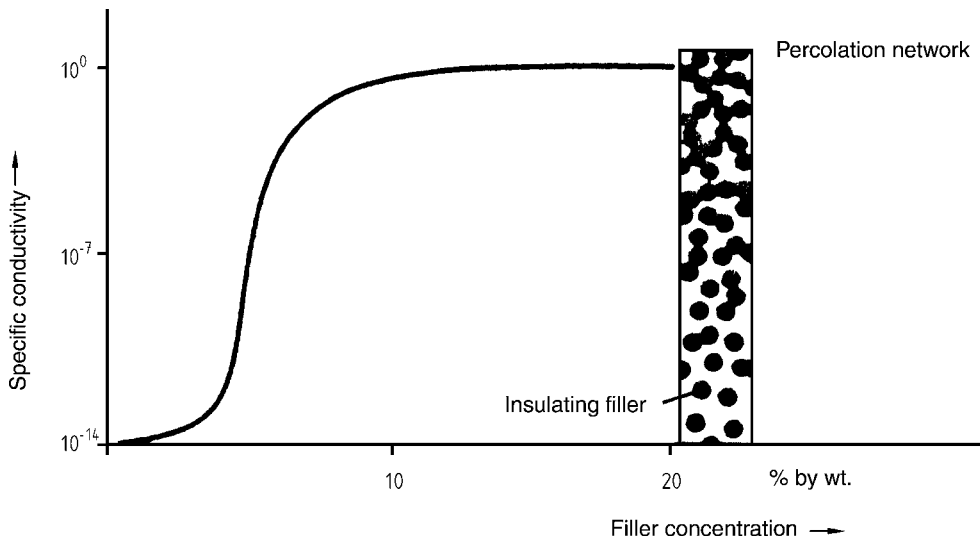


Figure 3.6 Principle of the percolation curve [3.15]

network). Figure 3.6 shows the concentration required for a globular filler with a random distribution. In the case of spherical particles, this threshold lies at about 15% by volume, while it is considerably lower for flake-like or needle-shaped particles. Even when the particles line up with one another due to shear forces associated with injection molding, the percolation threshold can still be at substantially lower concentrations. Conductivity is temperature dependent and can fall as the temperature rises due to the greater thermal expansion of the polymer matrix relative to the conductive particles. The process should be reversible, but there is some evidence that the particles, on cooling, do not necessarily come back into complete contact with one another.

Conductive carbon black is the most commonly used conductive filler (80% of conductive fillers used) followed by carbon fibers, nickel-coated mica, aluminum platelets and steel fibers. Typical levels of conductivity are shown in Table 3.2.

Table 3.2 Typical Values for the Electrical Conductivity of Filled Polymeric Materials [3.15]

Fillers	Conductivity S/cm
Conductive carbon black	0.01–0.1
Carbon fibers	0.1–10
Mica (Ni-coated)	1–10
Aluminum flakes	1–50
Steel fibers	1–50

Application of Conductive Layers

As electronics have evolved, government standards have been devised to help ensure that the electromagnetic compatibility (EMC) of an electronic system with its electronic environment. Such EMC problems can be solved by coating the insides of housings of plastic electronic devices with a conductive substance. These can be conducting paints, vacuum vapor-deposited metal coatings, or electrodeposited layers, all of which involve an additional manufacturing operation. Paints or coatings also have a negative impact on recyclability of thermoplastics. Under certain circumstances, plastics containing conductive additives can be used. For example, a thermoplastic containing very fine stainless steel fibers (diameter 8 to 10 µm), which produce conductivities of 1 to 20 S/cm at concentrations as low as 1 to 1.5% by volume, has been used. The screening effect using a PC + ABS blend as the matrix is 40 to 65 dB for a wall thickness of 3 mm [3.16]. Conductive fillers and fibers can have an impact on color and/or appearance. Sheet metal shields are also widely used with molded thermoplastic enclosures.

Intrinsically Electrically Conducting Polymers

The structural prerequisite for intrinsic conductivity is a molecular structure containing conjugated double bonds, *i.e.*, a regular alternating sequence of single and double bonds as in the polymers shown in Figure 3.7. When double bonds are broken, open radicals containing an unbonded electron are produced. These electrons can give rise to electrical conductivity. By a moderate change in the concentration of the electrons (doping) by oxidation, electric conductors are obtained. One primary problem with these materials is their lack of thermoplastic processability and the instability of the conductivity at high temperatures.

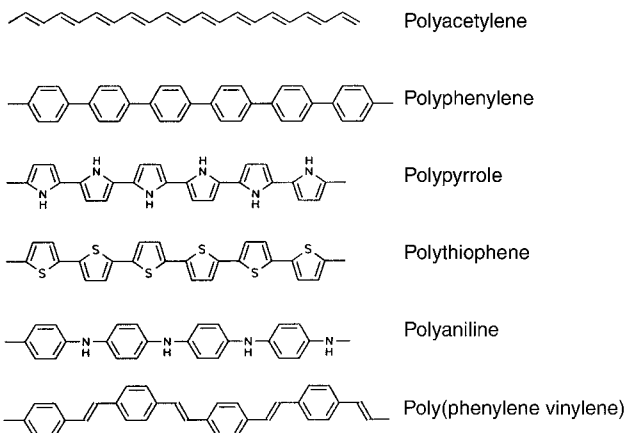


Figure 3.7 Chemical structures of polymers which become electrically conducting on oxidation (doping); undoped these materials are semiconductors [3.17]

Biodegradable Polymers

Most polymeric materials are relatively inert and stable under ambient conditions. However, some plastics are “biodegradable”. Test methods have been established to quantify the degradability of polymers under specific conditions of composting [3.18].

In order to be classified as truly biodegradable, the chain of a degradable polymeric material should be capable of complete degradation through enzymes produced by microorganisms (bacteria, fungi) to CO₂, H₂O, and biomass in the composting process. In some cases, the polymer is produced from natural raw materials, while in others it has been synthesized by chemical means, e.g., from crude oil.

Some degradable polymers and their manufacturers are listed in Table 3.3.

Table 3.3 Biologically Degradable Polymeric Materials and Their Manufacturers [3.19, 3.22]

Polymer	Manufacturers
<i>Based on renewable raw materials</i>	
Polylactides	Cargill, Mitsui & Co.
Poly(hydroxybutyrate/hydroxyvalerate)	Monsanto, Biomer
Starch-based polymers	Biotec, Montedison
Cellulose acetate	Mazzucchelli, Eastman Chemical
<i>Based on chemical synthesis</i>	
Polyester amides	Bayer AG
Copolymers	BASF, Eastman Chemical
Polycaprolactone	Union Carbide, Solvay

The most obvious market for these polymeric materials is in the packaging sector; however, there are many other applications. For packaging applications, biodegradable polymeric materials, whose range of properties approximates that of LDPE, are of significant interest. In addition, they should be processable in thermoplastic manner for films, hollow articles, and injection-molded parts. The properties of polyester amide are quite similar to LDPE, as shown in Table 3.4.

Table 3.4 Properties of Polyester Amide (BAK 1095) in Comparison with LDPE [3.20]

Property	Unit	Polyester amide	LD polyethylene
Modulus of elasticity (tensile)	MPa	220	240
Yield stress	MPa	12	11
Elongation at break	%	400	280
Breaking stress	MPa	25	22
Melting point	°C	125	115
Heat distortion temperature (Vicat A)	°C	95	96

3.2 Elastomers

Elastomers are polymeric materials which are cross-linked by either chemical or physical means. Accordingly, their deformation properties are characterized by a high level of entropy-elasticity (rubber elasticity) in association with a high degree of deformability. Even relatively small external forces can bring about large but mostly reversible changes in shape for some elastomers.

The treatment of linear or branched polymers with cross-linking agents such as sulfur, peroxides, or other reactive vulcanizing agents produces a *chemically cross-linked elastomer*. The polymer chains are linked together by primary valence bonds at discrete points (see Figure 3.8). As a result of this crosslinking, it is no longer possible for the long-chain molecules to flow or slide past one another when heat is supplied.

Physically cross-linked elastomers are block copolymers or what are called segmented elastomers. These are macromolecules composed of both rigid and flexible segments. These rigid and flexible segments are immiscible and each forms its own morphological phase (see Figure 3.8 bottom). At the same time, the flexible segments are regions of amorphous structure having low glass transition temperatures. The rigid segments can be domains having an amorphous structure but having glass transition temperatures which are as high as possible. Alternatively, they are crystalline structures having high crystalline melting points. Accordingly, the rigid segments may be viewed as physical cross-linking points but only in the sense of intermolecular binding forces. As a result of this structure, these segmented elastomers retain their thermoplastic nature. At temperatures above the glass transition temperature of the rigid amorphous segments (or the crystallite melting point of the rigid crystalline segments), they pass over into the molten state. They can, therefore, be processed by conventional thermoplastic processing methods, such as injection molding. The elastomeric material properties are determined by the flexible segments, while the temperature limits in the end use applications are determined by the rigid segments.

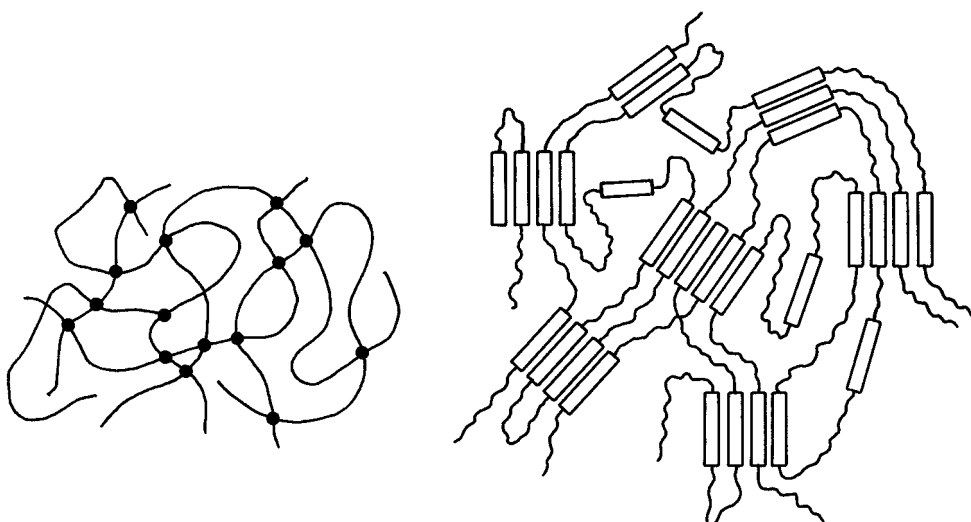


Figure 3.8 Schematic illustration of the structures of chemically and physically cross-linked elastomers

Table 3.5 Common Elastomers and Their Principal Fields of Application

Elastomers	Abbreviation	Typical fields of application
Natural rubber	NR	Linings in chemical engineering
Styrene-butadiene rubber	SBR	Vehicle tires, technical articles Vehicle tires, shoe soles, technical articles Vehicle tires, thin rubber articles Industrial rubber products
Butadiene rubber	BR	
Isoprene rubber	IR	
Chloroprene rubber	CR	
Acrylonitrile-butadiene rubber (nitrile rubber)	NBR	
Polyurethane	PU	
Ethylene-propylene terpolymers (diene)	EPDM	
Butyl rubber	IIR	
Silicone rubber	Q	
Fluororubbers	FR	Seals having high resistance to heat and chemicals
Thermoplastic polyolefin elastomers (ethylene-propylene block copolymers)	EPR (EPM)	Energy-absorbent exterior automobile parts, spoilers, bumpers
Styrene-butadiene block copolymers	SBS	Shoe industry, soles, blend component for thermoplastics
Thermoplastic polyurethanes	TPU	Ski boots, protection against wear, damping members
Thermoplastic polyether esters		Hydraulic systems, pneumatic systems, resistance to oil and heat
Thermoplastic polyamide elastomers		

Table 3.6 Comparison of Properties of Thermoplastic Elastomers

Property	Unit	SBS	TPU	EPR (EPM)	Polyether ester elastomer	Polyamide elastomer
Modulus of elasticity	MPa	10–1,500	20–250	200–1,600	80–260	70–360
Tensile strength	MPa	8–30	5–30	9–30	26–39	12–24
Elongation at break	%	700–900	200–700	200–600	350–450	200
Compression set	%	25–75	12–70	40–75	20–60	20–60
Shore hardness	–	35 A–50 D	70 A–76 D	80 A–60 D	40 D–70 D	33 D–62 D
Temperature limits in applications	°C	–40 to 110	–60 to 60	–40 to 90	–40 to 135	–40 to 135
Abrasion resistance	–	Good	Very good	Average	Average	Average

An ethylene-propylene block copolymer (EPR) composed of approximately 70% crystalline ethylene blocks is a typical example of such a physically cross-linked elastomer. By incorporating a third comonomer, a diene (*e.g.*, ethylidene norbornene) containing a reactive double bond, vulcanization, *i.e.*, chemical cross-linking, is made possible. This material is referred to as EPDM. EPDM can be added as a blend component (in a limited concentration) to a thermoplastic such as polypropylene; thus, a material processable in the conventional thermoplastic manner is once again obtained.

Polystyrene-butadiene-styrene (SBS) is an example of a thermoplastic elastomer composed of two amorphous phases in which the polystyrene (having a high glass transition temperature) represents the fixed physical cross-linking regions and the butadiene the flexible regions.

Table 3.5 presents an overview of some common elastomers and their principal fields of application. Table 3.6 provides characteristic ranges for the properties of thermoplastic elastomers.

3.3 Thermosets

Close-meshed cross-linked polymeric materials are called thermosets or thermosetting plastics. The cross-linking reaction occurs during the molding process once the shape is formed. The reaction can be limited by additive or, most commonly, by an energy source such as heat. Alternatively, in the case of light-curing UP resins, the reaction can be limited by exposure to UV light. The semi-finished products SMC and BMC and pourable molding compounds are ready-to-use compounds composed of resin, curing agent, fillers, and/or reinforcing materials. Cross-linking takes place at the temperature of the molding process or, in the case of light-curing resins, by exposure to UV light. In newly developed resin systems, light from standard fluorescent tubes may be used [3.1].

Table 3.7 Characteristic Values for Selected Thermoset Construction Materials

	Tensile strength (MPa) DIN 53 455	Elongation at break (%) DIN 53 455	Modulus of elasticity (MPa) DIN 53 457	Flexural strength (three-point support) (MPa) DIN 53 452	Impact resistance (kJ/m ²) DIN 53 453	Notch impact strength (kJ/m ²) DIN 53 453	Creep tracking (CTI/M) IEC 112	Density (g/cm ³) DIN 53 479	Source
Standard UP resin, unreinforced	60	2.0	4,800	90	9	1.2	600	1.219	[3.6]
Standard UP resin, 40–45% glass fiber mat (quasi-isotropic)	160	3.3	12,400	250	300	240	600	1.58	[3.6]
Standard UP resin, 60–70% glass fiber fabric	340	3.4	27,000	420	380	—	600	1.88	[3.6]
Standard UP resin, 70–75% unidirectional glass roving fabric	630	2.7	33,000	420	390	—	600	1.98	[3.6]
EP resin, 50–60% glass fiber fabric (same in longitudinal and transverse directions)	300	2	14,000 (C fibers 70,000)	300			600	1.7	[3.7]
UP resin molding compound, type 801 (*min. values as per ISO 14 530)	25		12,000 — 15,000	60*	22*	22*	600*	1.8	[3.7] [3.8]
Phenolic resin molding com- pound, type 31 (* min. values as per ISO 14 526)	30		6,000 — 8,000	70*	6*	1.5*	100	1.4	[3.7] [3.9]
Melamine resin molding com- pound, type 150 (* min. values as per ISO 14 528)	30		6,000 — 10,000	70*	6*	1.5*	600*	1.5	[3.7] [3.9]
Semirigid PU systems (RIM)	14	250	55		with- out failure	Shore D hard- ness 35–67		1.0	[3.7]
	—	—	—					—	
	30	140	700					1.1	
Glass-fiber reinforced PU sys- tems (RRIM); values measured along injection direction	25	65	1,750		75	65		1.23	[3.7]
Rigid PU integral-skin foam RIM systems	8	50	500		7	60		0.1	[3.7]
	—	—	—		—	—		—	
	24	8	1,400		60	80		0.7	
Rigid PU casting resins (alicyclic isocyanate system)	87	4		170	25		600		[3.7]

Table 3.8 Important Thermosets with Their Usual Processing Methods and Some Typical Applications [3.2 to 3.9]

Thermoset (matrix) material	Form as supplied (state prior to processing to finished parts)	Usual form of reinforcing materials (any additional fillers not shown)	Usual processing methods	Typical applications
Unsaturated polyester resins (UP) Vinyl ester resins (VE)	Liquid resin	Without reinforcing materials	Casting (gravity casting)	Moldings for the electrical industry, casting compounds for coils, electronic components, reactive concrete, reactive wall plugs
		Chopped glass fiber strands, mat-shaped or woven reinforcement composed mainly of glass fibers and also carbon and aramid fibers	Hand lay-up, spray lay-up, compression molding	Web-form or shell-shaped parts, containers, bumper supports, seat shells, auto body parts, motor cycle helmets, boats
		Continuous fibers (roving) made from glass, carbon or aramid	Filament winding, pultrusion (profile extrusion)	Pipes, containers, profile sections, optical cable
	Paste-like molding materials (BMC)	Chopped glass fiber strands	Injection molding	Moldings ranging up to large-area auto body parts
	Sheet semi-finished products of leathery consistency, flowable (SMC)	Chopped glass fiber strands of cut roving	Hot press molding	Web-form and shell-shaped high-volume parts (also including ribs, lugs, etc.)
	Pourable molding materials (e.g., type 801 as per ISO 14 530)	Cut glass fiber fabric	Injection molding, transfer molding, injection-com- pression molding	Moldings in the engine compartment, fuel pumps, parts subject to electrical stress having high tracking resistance

Table 3.8 (continued)

Epoxy resins (EP)	Liquid resin	Without reinforcing materials	Casting (gravity casting)	Moldings for the electrical industry, insulators, casting compounds, reactive concrete, slideways in machine tool construction, prototype tools
		Mat-shaped or woven reinforcement composed of glass, carbon or aramid fibers	Compression molding	Web-form and shell-shaped parts, linings and functional parts in the aviation industry
		Continuous fibers composed of glass, carbon or aramid	Filament winding, pultrusion (profile extrusion)	Pipes, torsion shafts, rotor blades, containers, leaf springs, profile sections
Polyurethane (PU)	Liquid	Without reinforcing materials	Casting (reaction injection)	High load capacity electrical insulators, cable end terminators, high-tension insulators in open-wire carrier equipment
		Chopped strands < 0.3 mm, up to 40%	Reaction injection molding (RIM)	Density > 0.8 g/cm ³ : semirigid large RIM parts, "soft-face" auto body parts, front and rear parts, automobile spoilers Density < 0.8 g/cm ³ : rigid integral-skin foam parts having an expanded core and dense outer skin, thick-walled parts, housings in information technology
			Reinforced reaction injection molding (RRIM)	Web-form parts, linings and auto body parts, fenders
Phenolic resin	Pourable molding compound (e.g., type 31 as per ISO 14 526)	Sawdust, wood flour	Compression molding, transfer molding, injection molding	Dark-colored moldings of all kinds, housings, electrical insulating parts
Melamine resin	Pourable molding compound (e.g., type 150 as per ISO 14 528)	Sawdust, wood flour	Compression molding, transfer molding, injection molding	Light-colored moldings, electrical and wiring materials

The relatively high strength, high modulus values, good creep resistance, plastic deformation properties, and heat resistance of these materials are rooted in their close-meshed cross-linking. Thermosetting polymeric materials are available in numerous forms, e.g., as casting resins, semi finished products such as fiber-reinforced paste (bulk molding compound, BMC), fiber-reinforced flowable products (sheet molding compound, SMC), pourable molding compounds with high proportions of fillers and reinforcing materials, or as pellet or powdered molding compounds. Depending on their different physical states, these thermosetting plastics are processed to moldings by different methods. Their properties are dependent on the processing method and the types and quantities of fillers and reinforcing materials employed (see Table 3.7). Table 3.8 provides an overview of the most common thermosets and the usual methods of processing each type of material. Due to the diversity of thermoset chemistry, in particular among the reactive resins UP, EP, and PU, numerous variations and modifications are possible. Table 3.7 presents characteristic values for the properties of some materials.

3.4 Fibrous Reinforcements

Reinforcing additives are materials which, when embedded in a polymer matrix, result in an increase in the tensile strength and tensile modulus of elasticity of the composite compared to the neat matrix (see Section 2.4.3). In order to achieve this reinforcing effect the following conditions must be met [3.10]:

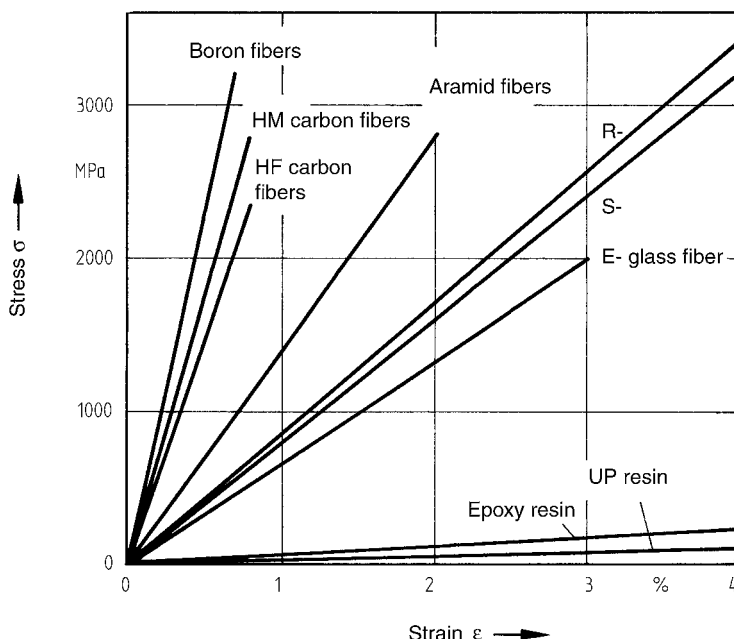


Figure 3.9 Stress-strain curves for various reinforcing fibers and matrix materials [3.5]

- The reinforcing material must have a direction aspect ratio; usually unidimensional and fiber-shaped with adequate fiber length to diameter ratio,
- A critical minimum fiber content must be exceeded,
- The strength and rigidity of the reinforcing material must be greater than those of the matrix, and
- There must be optimum bonding between the matrix and the reinforcing material.

Glass fibers are by far the fibers of greatest importance for reinforcing polymeric materials. Carbon fibers, organic aramid fibers, and even natural wood fiber, play a secondary role. Other fibers of some industrial interest but only limited commercial significance are boron, beryllium, steel fibers or whiskers and short-fibered single crystals obtained from Al_2O_3 . Figure 3.9 provides an overview of the force-deformation properties of some common reinforcing fibers.

3.4.1 Glass Fibers

3.4.1.1 Production and Reinforcing Forms of Glass Fiber Material

Glass fibers are produced by the highly developed technology of the direct melt process. The powdered starting materials (SiO_2 , Al_2O_3 , B_2O_3 , CaO , MgO), mixed in precisely defined ratios, are fused and drawn from dies at approximately 1,300 °C at the rate of 3,000 to 4,000 m/min to form threads with a diameter of 9 to 17 μm^* .

A large number of these filaments are then bound together in a parallel arrangement to form a strand and immediately afterwards, the size (lubricants, wetting agents, polymer-specific bonding agents, etc. to facilitate further processing and the bonding between the matrix and fibers) is applied to the surface of the fiber in the form of an aqueous emulsion. The strand treated in this way is finally wound onto a bobbin, which is usually the starting point for further processing into the various forms used for reinforcement. The most important forms of reinforcement [3.5] are described briefly below:

Roving: Spun filaments are combined to form a strand of a desired degree of thickness expressed in tex (g/km) (see Figure 3.10). Roving is the form of fiber used for unidirectional reinforcement, filament winding, pultrusion of thermosets, and for producing woven material. Chopped roving is used in the spray lay-up process, in the production of preforms, preimpregnated semi-finished products (SMC), and in other processes.

Glass fiber fabric: Web-form reinforcing material having a warp direction and a weft direction (see Figure 3.10). In unidirectional roving fabric, the warp direction of the fabric is rather weak so that the web-form reinforcing material acts only in the weft direction.

Glass fiber mat: Web-form but nonwoven form of reinforcing material with reinforcement properties independent of direction (see Figure 3.10). Glass fiber mats can be produced in the form of cut mats made from chopped spun glass filaments (25 and 50 mm) or in the form of continuous mats from uncut filaments held together by a binder. While the hand lay-up process

* The fibers produced are called textile fibers to distinguish them from insulating glass fibers, e.g., glass wool, glass wadding, which are not suitable for polymer reinforcement.

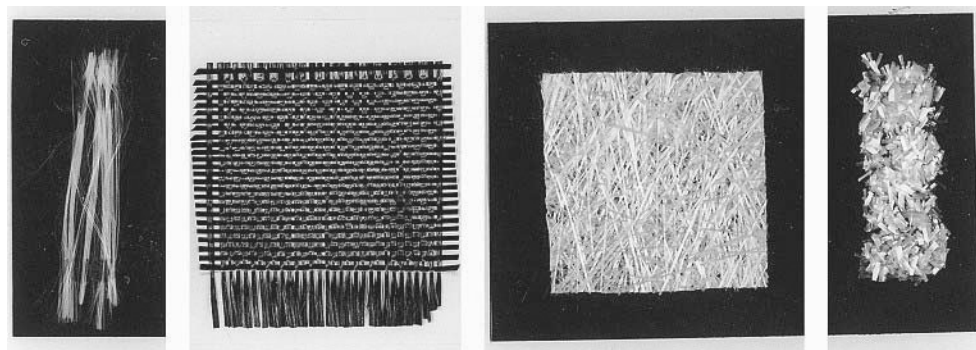


Figure 3.10 Various forms of glass fiber used for reinforcement.
From left to right: roving, fabric, a mat, and chopped strands.

for thermosets employs cut mats, continuous mats are used in compression molding and for the continuous production of sheet material.

Chopped fiber glass: Lengths of fiber glass measuring 3 to 26 mm, which are used for reinforcing molding compounds (e.g., type 801).

Glass fiber short strands: Milled fibers having an average length ranging from 0.2 to 0.3 mm used mainly for reinforcing thermoplastics (see Figure 3.10). Such short glass strands are also suitable for reinforcing PU processed by the reaction injection molding method (RRIM).

3.4.1.2 Types of Glass and Fiber Properties

Different types of glass are used for reinforcing fibers; each type distinguished according to its chemical composition. Some key properties of glass fibers are given in Table 3.9. The low-alkali E glass is used most frequently for reinforced plastics while R glass and S glass have better mechanical and thermal properties.

Table 3.9 Properties of Selected High-Strength Reinforcing Fibers

Type of fiber	Density (g/cm ³)	Tensile strength (MPa)	Modulus of elasticity (MPa)	Melting point (°C)
Glass fibers				
E glass	2.52	2,400	73,000	700
R glass	2.55	3,600	86,000	800
S glass	2.50	3,400	88,000	840
Carbon fibers				
HM fibers	1.90	2,000	500,000	
HS fibers	1.75	2,500	240,000	
Aramid fibers (Kevlar 49)	1.45	3,200	133,000	Temperature limit 230
Boron fibers	2.63	3,200	420,000	

3.4.2 Carbon Fibers

Compared to glass fibers, carbon fibers have greater stiffness and lower specific gravity. The starting material for producing high-grade carbon fibers (C fibers) is almost exclusively polyacrylonitrile fibers (PAN fibers). These fibers are first converted at 200 to 300 °C in an oxidizing atmosphere into a ladder polymer structure. In a ladder polymer, the macromolecules consist of a periodically linked double chain. Carbonization then follows at approximately 1,000 to 1,300 °C in an inert atmosphere. The fibers “char” without melting under these conditions. This step produces a carbon fiber in its normal strength (NS) form. Production of high-strength (HS) and high-modulus (HM) carbon fibers requires an additional process (graphitizing and stretching) at 2,000 and 3,000 °C, respectively.

To facilitate handling in the later stages of processing and to improve adhesion between the surface of the fibers and the polymer matrix, C fibers are treated with size in a manner analogous to glass fibers. The size is usually based on an epoxide resin. The key properties of HS and HM carbon fibers are presented in Table 3.9.

The most important class of polymeric materials reinforced by carbon fibers are epoxide resins. They are used for particularly rigid and strong structures in aerospace, in the construction of high-performance sports equipment, and more recently in automotive engineering. To a lesser extent they are used for thermoplastic reinforcement, mainly in polyamides. Polyamide is reinforced using short C fibers and processed by injection molding to obtain, for example, very rigid components having good lubricity.

3.4.3 Aramid Fibers

High-strength aramid fibers suitable for reinforcing polymeric materials are synthetic organic fibers derived from an aromatic polyamide. The aromatic polyamide is spun from concentrated sulfuric acid where the polymer exists in the liquid crystal, oriented form. The best known trade name for high-strength and high-rigidity aramid fiber is Kevlar® (Dupont). Three grades, Kevlar standard, Kevlar 29, and Kevlar 49, are employed for reinforcing polymers. The strength and rigidity of the grades vary. Characteristic properties of the highest-strength grade are presented in Table 3.9. It is noticeable that this fiber has the highest specific strength of those listed. Limitations however, are its low compressive and shear strengths, and the temperature dependence of its mechanical properties. Therefore, aramid fibers are usually combined with carbon fibers to produce a hybrid composite. In such a hybrid composite, the toughness of the aramid fibers contributes to the overall toughness of the composite. Hybrid reinforcing materials involving different combinations of fibers are also common. Due to their high toughness, aramid fibers are difficult to cut.

3.4.4 Metal Fibers, Whiskers, and Ceramic Fibers

The following fibers have only limited commercial significance as high-performance fibers for fiber-composite materials because of their evidently very high production costs.

- Boron and silicon carbide fibers
- Steel and beryllium fibers
- Whiskers (small-fibered single crystals based on Al_2O_3 , SiC, graphite or Fe)
- Ceramic fibers derived from Al_2O_3

Of these reinforcing materials, boron fibers have the most commercial significance (as epoxide resin composite for applications in military and aerospace). Most of these structures are primarily built using carbon fiber composites, where the boron fiber is added for even greater stiffness.

References

- [3.1] NICOLAUS, W., A. HESSE, D. SCHOLZ: Neue Verarbeitungstechniken durch lichthärtende Ein-komponentensysteme (New Processing Techniques by Means of Light-Curing Single-Component Systems), *Plastverarbeiter* **34** (1983) 1, pp. 31/36
- [3.2] SCHÖNTHALER, W. and K. H. DECKER: Härtbare Formmassen (Curable Molding Compounds), *Kunststoffe* **74** (1984) 10, pp. 601/606
- [3.3] FEUERHAHN, M.: Epoxidharze (EP) (Epoxide Resins (EP)), *Kunststoffe* **74** (1984) 10, pp. 604/606
- [3.4] KOSER, W.: Ungesättigte Polyesterharze (UP-Harze) (Unsaturated Polyester Resins (UP Resins)), *Kunststoffe* **74** (1984) 10, pp. 606/610
- [3.5] EHRENSTEIN, G. W. et al.: Glasfaserverstärkte Kunststoffe (Glass-Fiber Reinforced Plastics), expert-Verlag, Grafenau 1981
- [3.6] BASF Technisches Merkblatt (BASF Technical Leaflet), Palatal P6 M 2144 d
- [3.7] SAECHTLING, H.: Kunststoff Taschenbuch (Plastics Handbook), 22nd ed., Hanser-Verlag, Munich Vienna 1983
- [3.8] DIN EN ISO 14 530 Parts 1, 2 and 3
- [3.9] DIN EN ISO 14 526 and 14528
- [3.10] EHRENSTEIN, G. W. and R. WURMB: Verstärkte Thermoplaste – Theorie und Praxis (Reinforced Thermoplastics – Theory and Practice), *Angew. Makromol. Chemie* **60/61** (1977), pp. 157/214
- [3.11] PIELARTZIK, H. et al.: Funktionskunststoffe bestimmen neue Technologien (Functional Plastics Determine New Technologies), *Kunststoffe* **86** (1996) 9, pp. 1302/1306
- [3.12] RÖMER, M.: Neuland erschlossen (New Territory Opened Up), *Kunststoffe* **86** (1996) 9, pp. 1310/1316
- [3.13] Thermotrope Schichten: Intelligente Schattenspender (Thermotropic Layers: Intelligent Providers of Shade), BASF press release, February 19, 1996
- [3.14] MAIR, H. J. and S. ROTH (Eds.): Elektrisch leitende Kunststoffe (Electrically Conducting Plastics), 2nd ed., Carl Hanser Verlag, Munich Vienna 1989
- [3.15] MÜNSTDEDT, H.: Elektrisch leitfähige Polymere mit neueren Füllstoffen (Electrically Conducting Polymers Containing Novel Fillers), paper, 7th Symposium, Elektrisch leitende Kunststoffe (Electrically Conducting Plastics), Techn. Akademie Kunststoffe, Esslingen, June 1997
- [3.16] BORGMAN, C. and S. ELTINK: Der Faradaysche Kunststoffkäfig (The Plastic Faraday Cage), *Kunststoffe* **87** (1997) 4, pp. 494/496
- [3.17] ROTH, S. and H. J. MAIR: Elektrisch leitende Kunststoffe (Electrically Conducting Plastics), GAK **48** (1995) 9, pp. 634/638

- [3.18] DIN 54 900, Parts 1–4, Draft 1997, Prüfung der Kompostierbarkeit von polymeren Werkstoffen (Testing the Compostability of Polymeric Materials)
- [3.19] PANTKE, M. et al.: Normentwurf: Biologisch abbaubare Kunststoffe (Draft Standard: Biodegradable Plastics), *Kunststoffe* **87** (1997) 1, pp. 10/12
- [3.20] GRIGAT, E. et al.: Biologisch abbaubar in 60 Tagen (Biodegradable in 60 Days), *Kunststoffe* **87** (1997) 1, pp. 63/65
- [3.21] SCHMITT, B.: Aus der Arbeit des Kunststofflaboratoriums (The Work of the Plastics Laboratory), BASF company publication, BASF's 125th Anniversary Jubilee Symposium, 1990
- [3.22] SCHROETER, J.: Biologisch abbaubare Werkstoffe (Biodegradable Materials), *Kunststoffe* **90** (2000) 1, pp. 64/70

4 Physical Properties – Characteristic Values – Test Methods and Procedures

4.1 Deformation Behavior under Uniaxial Dynamic Tensile Stress (Stress-Strain Experiments)

4.1.1 Molecular Deformation and Fracture Mechanisms

When polymeric materials are deformed under the action of an external force, three different components of deformation can be distinguished.

Spontaneous elastic deformation	= spontaneously reversible
Time-dependent viscoelastic deformation	= reversible over time
Time-dependent viscous deformation	= irreversible over time

These are superimposed on one another but each has a varying degree of importance depending on the particular regions of deformation. These different forms of deformation found at the macroscopic level are characterized by molecular deformation and fracture mechanisms taking place in the material. Purely elastic deformation is attributable to changes in the spacing of atoms and valence angle shifts. The contribution from this component is very low at high deformations. The time-dependent viscoelastic deformation component is characterized by the relaxation times of the macromolecules in the polymeric material. For each load to which the molecules or molecular segments are exposed, they need a certain length of time, sometimes a very long time, to reach a state of equilibrium at that level of stress applied. Accordingly, the material responds to an applied stress with a certain time delay (viscoelasticity). If the external load is removed, there is once again a delay before the corresponding equilibrium state is restored.

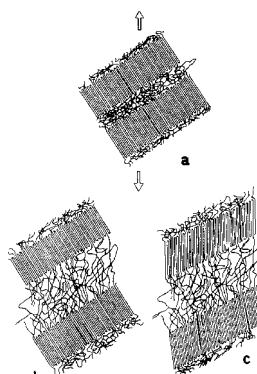


Figure 4.1 Model of the reversible deformation of semi-crystalline lamellar structures [4.2]

These processes tend to play themselves out more in the amorphous microstructural domains. The model in Figure 4.1 illustrates how such processes may occur in a semi-crystalline lamellar structure. However, in semi-crystalline polymeric materials having a spherulitic superlattice, spherulites have been observed to deform to almost 80% under increasing load and then assume nearly their original spherical shape once the load is removed [4.1].

As loading steadily rises, irreversible deformation processes set in which cause even more marked, nonlinear deformation behavior. When this happens, polymeric materials respond in two typical ways: the appearance of normal stress craze zones and shear stress craze zones. Normal stress craze zones are locally bounded domains of highly aligned molecular chains which line up to a marked degree parallel to the direction of loading. Compared to the rest of the matrix, these regions exhibit much lower densities (lower by as much as 60%). The boundary surfaces are still bound to one another by the stretched chains. Nevertheless, these craze zones can turn into cracks if loading is increased further. Figure 4.2 shows a craze zone at this stage.

Normal stress craze zones run perpendicular to the prevailing tensile stress. Shear stress flow lines also form under certain conditions and due to these being superimposed on normal stress flow lines, they usually run at an angle greater than 45° to the direction of loading.

Figure 4.3 reproduces a model-based view of the further course of deformation and fracture for semi-crystalline lamellar structures. Under increasing tensile stress, single lamellae are aligned in the direction of this stress. Folded blocks are pulled out and unraveled until finally more and more primary valences break and macroscopic fracture ensues.

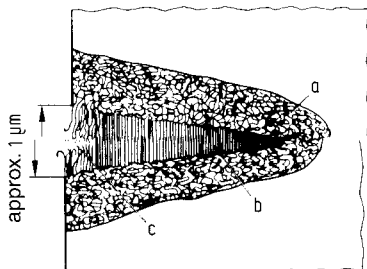


Figure 4.2 Schematic illustration of a normal stress craze zone [4.3]
 a) Undisturbed amorphous structure
 b) Highly aligned molecular structure
 c) Incipient crack

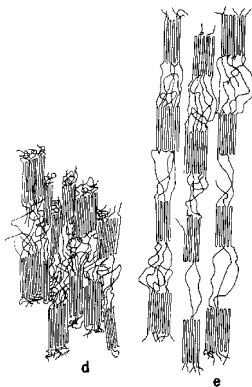
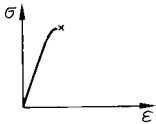
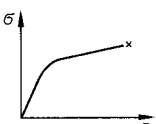
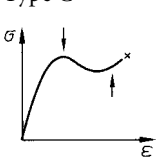
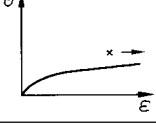
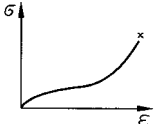


Figure 4.3 Model-based simulation of the irreversible deformation of semi-crystalline lamellar structures [4.2]

4.1.2 Characteristic Stress-Strain Curves

Naturally, temperature (and time) plays an important role in these deformation processes, particularly with regard to the glass transition temperature T_g of the polymer being deformed. For purposes of a fundamental consideration of the deformation behavior of polymeric materials, room temperature will be assumed. A systematic classification of stress-strain curve shapes is shown in Table 4.1. Since the position of the glass transition temperature depends on the deformation rate, Table 4.1 also applies to uniform strain rates.

Table 4.1 Forms of Stress-Strain Curves

Relative position of T_g for the amorphous phase	Typical shape of stress-strain curve	Notes	Examples of polymeric materials in this class
$T_g > RT$	Type A 	Predominantly energy-elastic deformation with relatively brittle fracture (x)	PS PMMA SAN
$T_g > RT$	Type B 	Craze deformation (with increase in volume)	SB
$T_g \approx RT$	Type C 	Transitional shape. Elastic start due to frozen amorphous phase or high crystalline fraction. Local temperature increase with local necking (↓) followed by shear deformation and partial solidification (↑).	PA PP PBT
$T_g < RT$	Type D 	Shear deformation with uniform necking of sample. Fracture (x) at high strain values.	LDPE
$T_g < RT$	Type E 	Entropy-elastic deformation of a chemically cross-linked polymeric material of high mesh width ($\nu = 0.5$)	Elastomers

4.1.3 Determination of Stress-Strain Diagrams and Characteristic Properties of Materials

Because national and international standards for determining characteristic values permit a wide latitude for the test conditions, it is often difficult to make comparisons among materials or even to choose a material from among similar materials. The objectives of two tensile test standards, namely ISO 10 350 (single-point data) [4.4] and ISO 11 403 (multipoint data) [4.5] is to specify, from the large number of possible measured values, a limited set of reliable values and functions. These are determined under specified environmental conditions. The shape of the test specimens and the production parameters must also be specified. As a result, ISO 10 350 is particularly suitable for the preliminary screening of materials and for drawing up specifications. The functional correlations of ISO 11 403 permit a more far-reaching assessment of a material for structural product design.

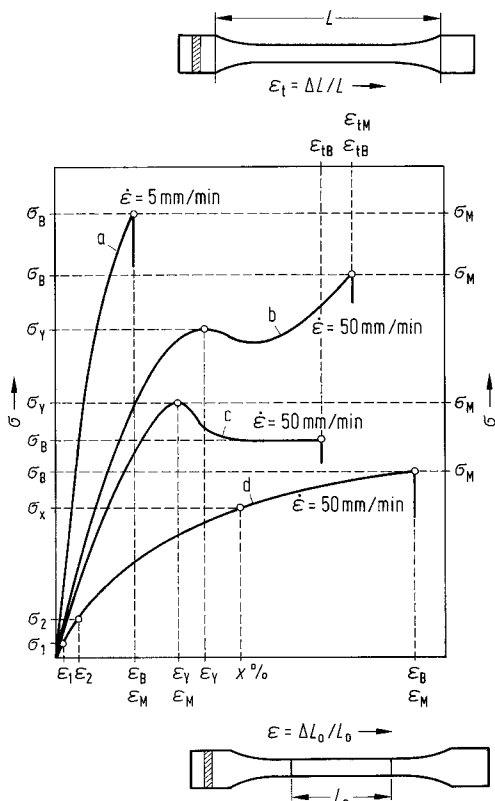


Figure 4.4 Terms, characteristic values, and designations in stress-strain curves as defined in ISO 10 350 [4.4]

- a) Brittle materials
- b) Tough materials having a yield point
- d) Tough materials without a yield point

Stress-strain behavior under short-term uniaxial tensile stress can be determined by the tensile strength test specified in ISO 527 [4.6]. These values are illustrated with reference to the characteristic curve shapes given in Figure 4.4.

The values listed above are defined as follows:

Strength Properties

- *Yield stress* σ_y is the tensile stress at which the gradient of the stress-strain curve first assumes the slope of zero;
- *Tensile stress* σ_M is the maximum tensile stress at maximum force;
- *Tensile strength at break* σ_B is the tensile stress when failure occurs;
- *x% offset yield stress* $\sigma_{x\%}$ is that tensile stress at which the stress-strain curve deviates from the initial linear plot by x% strain (Figure 4.5). This may be used as a strength variable when the stress-strain curve of a material does not exhibit a distinct yield stress and fracture occurs only at high strain values, that is to say, when the material exhibits highly nonlinear behavior.

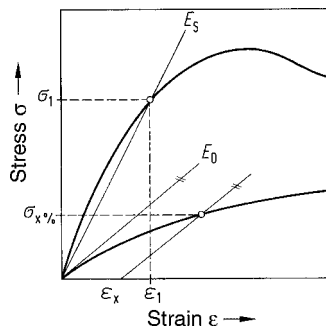


Figure 4.5 Definition of secant modulus E_s and x% offset yield stress

Deformation Properties

- *Yield strain* ϵ_Y is the strain corresponding to the yield stress;
- *Elongation at break* ϵ_B is the strain corresponding to the tensile stress at break as long as the material has not previously passed through a yield point;
- *Nominal elongation at break* ϵ_{tB} is the strain at failure of the material after it has passed through a yield point; the nominal strain ϵ_t is the ratio of the current clamp spacing (between the tensile testing jaws) to the original clamp spacing ($\epsilon_t = \Delta L/L$), extensometers of various design can also be used to determine strain;
- The area under the stress-strain curve is a measure of the *energy-absorbing capacity* (toughness) of the polymeric material in question; a large area means a high energy-absorbing capacity;
- *Modulus of elasticity* E (in a tensile test $E_t = \text{tensile modulus}$) describes the relationship between tensile stress and the corresponding strain in the linear region by means of Hooke's law $E = \sigma/\epsilon$. E is a measure of the material's "rigidity".

Tensile Strength Test		
Standard	ISO 527	
Test specimen geometry		
Dumbbell	1A	1B
Overall length		≥ 150 mm
Parallel distance	80 ± 2 mm	60 ± 0.5 mm
Radius	20 to 25 mm	60 mm
Width of parallel section		10 ± 0.2 mm
Thickness of parallel section		4 ± 0.2 mm
Test length		50 ± 0.5 mm
Principle of Measurement		
The test specimen is stretched along its longest major axis at constant rate (usually until fracture ensues). Throughout the test, changes in length are continuously measured. The stress is defined as the tensile load applied to the initial cross section and the strain as the change in length with respect to the initial test length. In this illustration the actual increase in stress due to the steadily decreasing cross section of the sample is not taken into account. This is commonly referred to as "engineering" stress as opposed to "true" stress.		
Test Results		
Stress-strain function		
Yield stress	σ_y in MPa	
Yield strain (or elongation)*	ε_y in %	
Tensile stress at break	σ_b in MPa	
Break strain (or elongation)	ε_b in %	
Tensile strength	σ_m in MPa	
Strain at tensile strength	ε_m in %	
Nominal strain	ε_n in %	
Modulus of elasticity	E in MPa	
Poisson's ratio	μ (dimensionless)	
* Note: Elongation (%) = $E \cdot 100$		

In some cases, it can be difficult to define the initial slope of a stress strain curve. The slope of the tangent through to origin as a secant passing through the points of 0.05% and 0.25% strain are used. Thus, the relationship $E_t = (\sigma_2 - \sigma_1) / (\varepsilon_2 - \varepsilon_1)$ applies.

This relationship can be used for polymeric materials having marked nonlinear deformation characteristics so that a unique measurement can be carried out, allowing different materials to be compared with one another. Figure 4.6 shows the measured stress-strain curve for a HDPE that illustrates the problems of specifying a "modulus of elasticity". In the case of polymeric materials having an initially linear range up to 0.25% strain, there is no difference

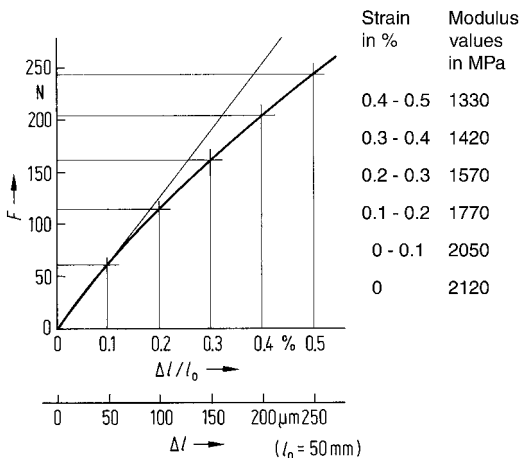


Figure 4.6 Stress-strain curve in the lower strain range for a HDPE. Secant moduli (tangential moduli) for various strain ranges are shown

with respect to the modulus of elasticity as conventionally defined. Strictly speaking, the term modulus of elasticity is not appropriate for visco-elastic materials. However, it is commonly used to describe the rigidity of polymeric materials in practice.

Designers or engineers can use the modulus values measured by the standard described above only for comparing or selecting candidate materials. Because structures made from polymeric materials are frequently loaded to strain levels beyond 0.25%, the *secant modulus* E_S is introduced for design calculations on such structures. The secant modulus is formally defined as the quotient of the stress σ_1 produced by the load and the associated strain ε_1 , *i.e.*, $E_S = \sigma_1 / \varepsilon_1$ (see Figure 4.5). Thus, the nonlinear properties of the material are taken into account for load deformation calculations (see also Section 5.3.2.1).

4.1.4 Effects of Temperature, Time, and Humidity on Stress-Strain Curves

The effects of temperature, the rate at which stress is applied (time), and absorption of water on the molecular cohesion of polymeric materials are reflected in the shape and characteristics of their stress-strain curves. Accordingly, the variation of these functions, as these conditions are altered, has to be taken into account for the reliable design of polymeric components. The formulation and empirical confirmation of laws describing the visco-elastic, nonlinear behavior of materials in a manner which takes time, temperature, and moisture content into consideration are currently focal points of research. The underlying concepts, some derived from empirical studies and others from considerations of failure mechanisms, are typically based either on the principle of temperature-time shifts or the theory of free volume (see, for example [4.7–4.12]). A fundamental understanding of this behavior is important for product designers. However, some of these concepts can be difficult to implement in practice. Designers often rely on simplifications, which can hopefully be backed up by some experimental results.

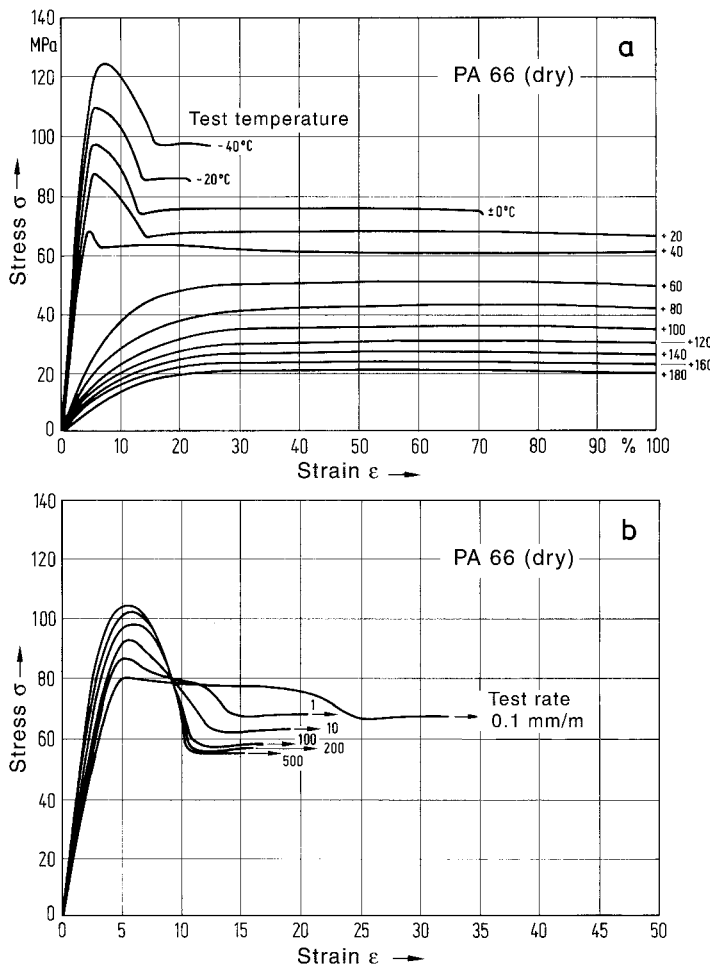


Figure 4.7 Stress-strain diagrams for polyamide 66 at different temperatures (a) and strain rates (b) [1.1]

Temperature

The same polymeric material can assume several of the characteristic stress-strain patterns shown in Table 4.1, depending on the temperature of the sample. This can even occur within a relatively limited range of temperatures, as shown at the top in Figure 4.7. Accordingly, all strength properties of importance for structural design exhibit some degree of temperature dependence. This renders any theoretical calculation of strength or deformation difficult, especially when temperatures are not constant in the end use application.

Strain Rate

Strain rate or rate of deformation is also an important factor. As the strain rate increases, the material responds with reduced relaxation, on the one hand, the stress-strain diagrams become

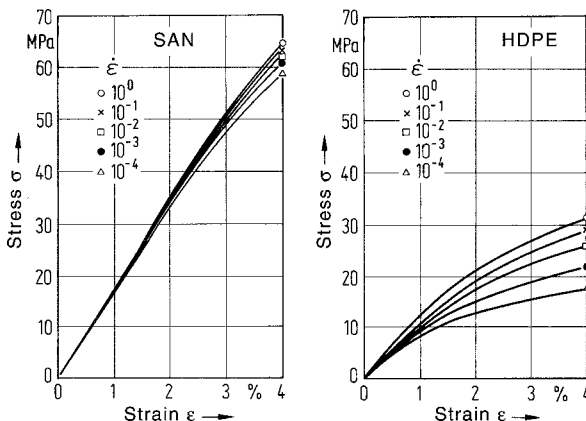


Figure 4.8 Stress-strain curves at room temperature for different strain rates

steeper, yield stress or tensile strength rising, and, on the other hand, ductility or elongation values decrease. Moreover, a change in deformation characteristics can occur in that, at a constant test temperature, the glass transition temperature can be shifted by varying the strain rate [4.13].

The stress-strain curves at the bottom in Figure 4.7 were recorded at different strain rates. They reveal a more marked yield point at high strain rates, while in the curve plotted for the lowest strain rate the yield point is scarcely noticeable. As the strain rate increases, the value of the yield stress also rises. The effect of strain rate is more pronounced above the glass transition temperature than below it. This may be seen in the comparison of the group of curves for HDPE (T_g of the amorphous phase $< -100^\circ\text{C}$) in Figure 4.8 with the group of curves for SAN ($T_g = 105^\circ\text{C}$).

Absorption of Water

When hygroscopic polymers, such as polyamides, absorb water (see also Section 2.2.1), their glass transition temperature shifts to lower values. While the relaxation maximum characterizing the glass transition temperature is found to be at approximately 60°C for dry PA 6, the maximum after absorption of 2.8% water has already shifted to approx. 15°C . When 11% water has been absorbed the glass transition temperature shows even lower values – approx. -10°C (see also Figure 3.5). This is also expressed by the different shapes of the stress-strain curves for these levels of moisture content (see Figures 2.8 and 3.5). Increasing moisture content has a similar effect on stress-strain behavior as increasing temperature. This effect is only important for hygroscopic polymers.

4.1.5 Mathematical Description of Stress-Strain Curves

Stress-strain curves can also be described using mathematical models. For strain values of up to approx. 4%, the stress-strain curves can be reproduced with sufficient accuracy by a

Table 4.2 Polynomial Coefficients for Reproducing Stress-Strain Curves [4.14]

Tempe- rature (°C)	K_0	K_1	K_2	K_3	K_4	Elongation ε_y or ε_b (%)	Stress-Strain Diagram			
	-	-	-	-	-	-	T °C	σ_y MPa	ε_y %	
ABS (Terluran 877 T)	-40	36.68	-7.25	0.64	0.0	0.0	4.6	<p>The graph plots Stress (MPa) from 0 to 72 against Strain (%) from 0 to 4.0. Seven curves are shown, each labeled with its corresponding temperature: -40°, -20°, 0°, 23°, 40°, 60°, and 80°. All curves start at the origin (0,0) and show an increasing stress-strain relationship, with higher temperatures resulting in lower yield stresses and elongations.</p>		
	-20	31.11	-4.09	0.11	0.0	0.0	3.7			
	0	26.81	-1.43	-0.52	0.0	0.0	3.6			
	23	22.49	5.75	-7.71	2.78	-0.38	3.1			
	40	21.12	5.15	-6.25	1.52	-0.12	2.8			
	60	24.23	-7.38	0.71	0.0	0.0	2.7			
	80	19.03	-6.57	0.71	0.0	0.0	2.2			
PA6-GF (Ultramid B3EG5) 23/50 RH atmosphere	-40	139.42	-29.39	0.31	0.58	0.0	(2.8)	<p>The graph plots Stress (MPa) from 0 to 187.5 against Strain (%) from 0 to 4.0. Ten curves are shown, each labeled with its corresponding temperature: -40°, -20°, 0°, 23°, 40°, 60°, 80°, 100°, 120°, and 150°. The curves show a significant increase in yield stress and yield elongation as the temperature increases, with the 150° curve reaching the highest stress levels.</p>		
	-0	112.64	-14.47	-3.47	0.72	0.0	(3.2)			
	0	98.98	-17.80	-0.61	0.28	0.0	(3.8)			
	23	64.40	-12.64	0.24	0.09	0.0	(5.8)			
	40	55.94	-20.85	4.65	-0.44	0.0	(6.3)			
	60	42.26	-11.06	1.64	0.11	0.0	(6.5)			
	80	39.20	-11.13	2.03	-0.19	0.0	(5.8)			
	100	36.79	-10.04	1.68	-0.14	0.0	(5.0)			
	120	33.99	-8.49	1.22	-0.09	0.0	(4.7)			
	150	34.41	-14.00	2.76	0.21	0.0	(5.4)			

polynomial of, at most, order 5. This can be fed to a suitable computer program, which then allows very simple derivation of $x\%$ offset yield stress, secant moduli, and so forth.*

In Hooke's law equation $\sigma = E \cdot \varepsilon$, the proportionality factor E is substituted as a function of strain as follows:

$$\sigma(\varepsilon) = E(\varepsilon) \cdot \varepsilon = (K_0 + K_1 \varepsilon + K_2 \varepsilon^2 + K_3 \varepsilon^3 + K_4 \varepsilon^4) \cdot \varepsilon \quad (4.1)$$

As an example, Table 4.2 contains the polynomial coefficients for a ductile ABS material and rigid, non-ductile glass fiber reinforced PA 6 (containing 25% glass fiber by weight) over a broad temperature range along with the corresponding stress-strain curves [4.14].

4.2 Deformation Behavior under Uniaxial, Long-Term, Static Tensile Loads (Tensile Creep Testing)

All polymeric materials have a tendency to deform or "creep" when subjected to long-term loading. The time-dependence of deformation behavior can be determined by standardized tests. In the tensile creep test (creep or retardation test) specified in ISO 899 [4.15], the sample is placed under load by a static force and the deformation caused by this force is measured as a function of time. The samples are usually subjected to tensile stress because the tensile test can be carried out more reliably; however, compressive and bending creep tests are sometimes conducted. Regardless of stress type, the tests are carried out at different levels of stress and sometimes at different temperatures or relative humidity levels.

Stress relaxation is another time dependent phenomenon exhibited by polymeric materials. Stress relaxation tests are conducted by holding specimens at fixed (constant) deformation values (several values) for long periods of time. The force required to maintain the deformation is measured over time. These tests require considerable technical resources and are expensive to perform and as a result, these data are not widely available. Therefore, static creep performance is usually evaluated for technical purposes and the results of tensile creep tests are used to predict relaxation behavior even though creep and stress relaxation are physically quite different processes.

The tensile creep test provides data that can be very useful for structural product design:

- *Creep curves, stress-time curves, or isochronous stress-strain curves (isochrones for short)* each obtained by cross plotting the parameters stress, strain and time (see Figure 4.9).
- The *linear visco-elastic range*, which is characterized by the relationship between stress and strain in the isochronous stress-strain diagram.
- The *tensile creep strength* $\sigma_{B(t)}$ as the stress at which the sample fails after time t . Creep failure at lower stress levels can take years and such data are not available from relatively short-term tests. Tensile creep strength has only limited usefulness as a design characteristic since failure frequently occurs only at very high strain levels which would hopefully not be used in many engineering structures (see also Section 4.2.1).

* e.g., The CAMPUS program for PCs (multipoint)

Tensile Creep Test

Standards

ISO 899

Test Specimen Geometry

Dumbbell: 1A or 1B (preferred now); older measurements on dumbbells of differing dimensions are still common because of the cost of the test.

Principle of Measurement

The test specimens are subjected to a constant (weight) load in a constant test atmosphere, usually 23/50, 40/35, or 60 and higher/0. Deformation is measured as a function of time under load. Stress is defined with respect to the tensile load acting on the initial cross section. Strain is likewise the change in length relative to the initial length.

Due to their high cost, stress-relaxation tests (decrease in stress under sustained strain) are much less common.

Test results

Creep curves $\varepsilon = f(t)$; $\sigma = \text{constant}$

from these are derived

Relaxation curves $\sigma = f(t)$ $\varepsilon = \text{constant}$

Isochrones $\sigma = f(\varepsilon)$ $t = \text{const}$

Creep modulus $\sigma / \varepsilon = f(t)$

Creep strength $\sigma_b = f(t)$

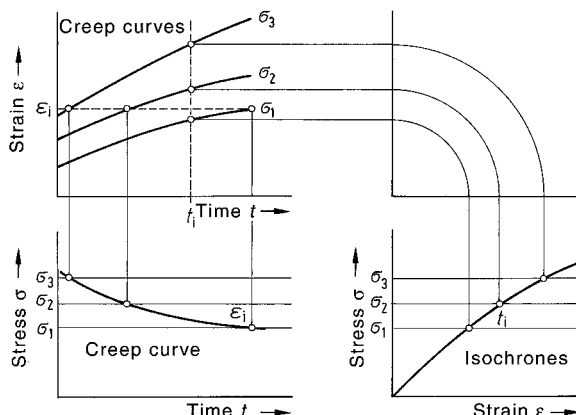


Figure 4.9 Methods of presenting the measured variables σ , ε , and t from the results of tensile creep tests

- The *creep modulus* E_c which is determined by formal analogy with the modulus of elasticity as $E_c = \sigma / \varepsilon(t)$. This modulus applies only to a specific time under load. In the linear visco-elastic range, the creep modulus is dependent only on temperature and time, but not on stress. The introduction of the creep modulus into deformation calculations is an attempt to take time-dependent deformation into account in the simplest possible manner (see also Chapter 5). Stress is a variable for non-linear stress-strain curves.

4.2.1 Mathematical Description of Creep Curves

Creep behavior can be described by models based on empirical observations. Such models are reviewed in [4.17]. At present, two simulation approaches are favored [4.18]. The mechanical substitute or analogy models are composed of combinations of elements such as elastic springs and viscous dampers. Although they do not fully depict the molecular deformation mechanisms, they allow for a simple mathematical description of creep behavior. The parameters E_0 , E_r , η_0 , and η_r are determined by approximation of measured creep curves. The procedure is illustrated in Figure 4.10 with reference to the example of the *4-parameter model* (Burgers model [4.19]). The model assumes linear visco-elastic behavior. In this deformation range, the Boltzmann superposition principle applies. This principle states that a strain $\varepsilon_1(t)$ caused by a stress σ_1 and a strain $\varepsilon_2(t)$ caused by a stress σ_2 may be added when σ_1 and σ_2 are superposed.

In the region in which linear visco-elasticity applies, the three components of deformation shown in Figure 4.10 may be added together to yield the total strain shown below.

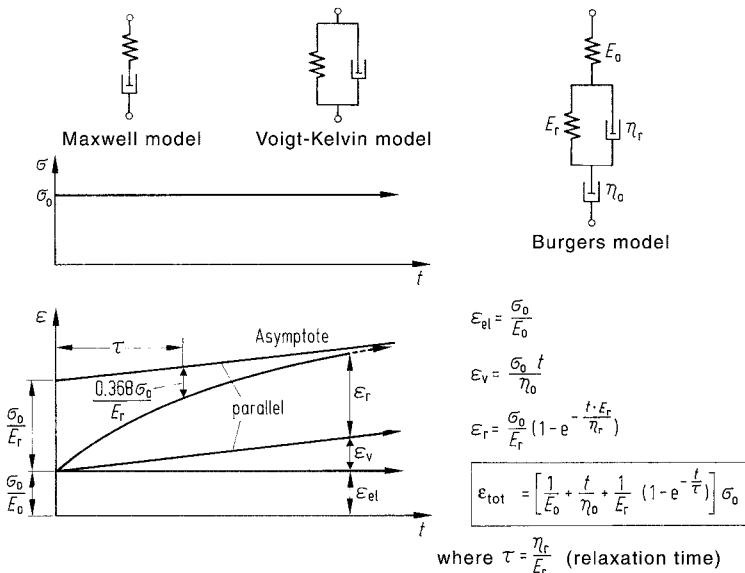


Figure 4.10 Substitute models on the basis of Hooke-type springs and Newtonian dampers for describing the deformation behavior of polymeric materials (top) and their behavior in the event of discontinuous loading together with their mathematical description (below)

$$\varepsilon_{\text{tot}} = \varepsilon_{\text{el}} + \varepsilon_{\text{relax}} + \varepsilon_{\text{visc}} \quad (4.2)$$

The advantage of *Findley's power function* [4.20] lies primarily in the simplicity of the mathematical treatment. It states:

$$\varepsilon_{\text{tot}} = \varepsilon_{\text{el}} + m \cdot t^n \quad (4.3)$$

As may be seen the visco-elastic relaxation component and the viscous deformation component are combined to form the inelastic term $m \cdot t^n$.

In logarithmic terms, Eq. (4.3) yields a straight line:

$$\log(\varepsilon_{\text{tot}} - \varepsilon_{\text{el}}) = \log m + n \log t \quad (4.4)$$

The fitting of measured values and determination of the parameters m and n can be done by linear regression.

To represent the creep behavior of a polymeric material for any level of stress, Eq. (4.3) must be modified by the dependence of the parameters m and n on stress.

$$\varepsilon_{\text{tot}} = \varepsilon_{\text{el}} + m(\sigma) \cdot t^{n(\sigma)} \quad (4.5)$$

Above this limiting value (end of the linear viscoelastic range) referred to as σ^* [4.21], the creep rate increases appreciably due to the effects of structural changes and the approximation loses its validity. At the same time it can be established that $n(\sigma)$ can be depicted as a straight line up to a certain value of σ (see Figure 4.12).

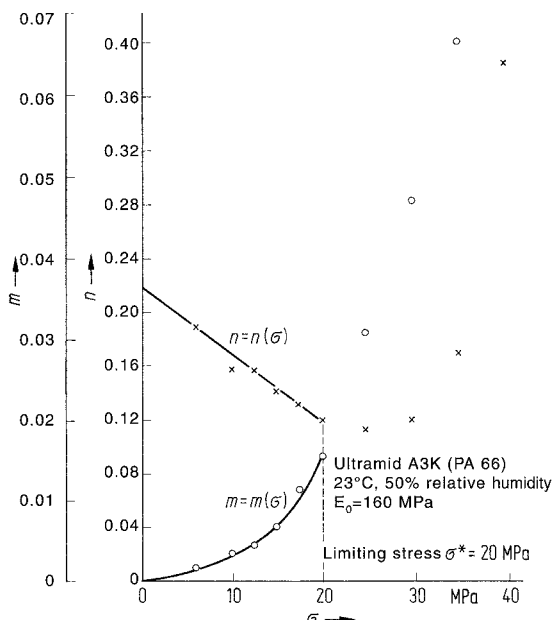


Figure 4.11 Approximations of parameters m and n and determination of limiting stress σ^* [4.21]

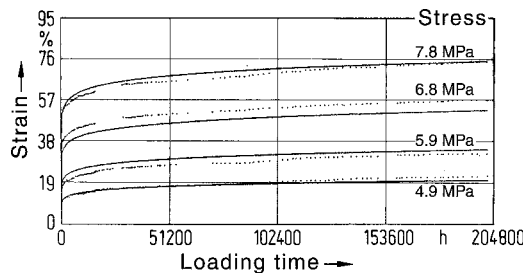


Figure 4.12 Creep functions for LDPE (Lupolen 1800 H, $\sigma_y = 9$ MPa, $E_0 = 200$ MPa) in a standard 23 °C/50% RH atmosphere [4.23]

A similar discontinuity, although not as significant, is found in the stress-dependent function $m(\sigma)$ represented as a power function or polynomial (see Figure 4.11).

With regard to the onset of increased creep rate, the limiting value σ^* may be regarded as a design stress limit for structures subject to long-term static loading.

Another useful performance characteristic can be defined as a stress value at which the inelastic strain component

$$m(\sigma) \cdot t^{n(\sigma)} = 0.5\% \text{ for semicrystalline thermoplastics and}$$

$$m(\sigma) \cdot t^{n(\sigma)} = 0.3\% \text{ for amorphous thermoplastics [4.22].}$$

The finding also demonstrated experimentally for LDPE (a polymeric material with very limited creep resistance) that there is no unexpected rise in creep rate, even over very long test periods (see Figure 4.12). This supports the conclusion that the long-term static deformation of thermoplastics may be extrapolated as a power of ten, for instance, with the aid of Findley's power function [4.24].

4.3 Toughness and Impact Resistance

The toughness or ductility of a material is defined as

The product of its capacity for deformation and its resistance to this deformation.

Toughness is a variable expressed in units of work. Like all properties of polymeric materials, toughness depends on the rate or duration of loading, moisture content, and as for all properties, age can be a factor.

4.3.1 Determination of Tensile Stress-Strain Toughness

The area under the curve in a stress-strain diagram provides a measure of the material's toughness. Tensile tests are often conducted at a rate of 5 mm/min for brittle materials and 50 mm/min for tough or ductile materials. The quantitative evaluation of the fracture toughness of tough materials can be associated with a great deal of scatter, because break strain values tend to have high standard deviation values. In order to evaluate toughness *prior to failure by flow*, that is to say, in the strain range useful for most designs, the area under the stress-strain curve up to the yield strain is available*. This measure can also be used as a performance value for components subject to impact stresses (see Section 5.5).

4.3.2 Determination of Toughness by Flexural Impact Test

A number of test methods are preferably used for assessing toughness under conditions of sudden stress (impact speed of between 1 and 3.4 m/s). These include:

Charpy impact test (unnotched)	ISO 179
Charpy notched impact test	ISO 179
Tensile impact test	ISO 8256

The Charpy impact test is a 3-point, high rate, flexural impact test. While the Izod impact test has been widely used in the past, the Charpy test is in widespread use today.

The impact behavior of very tough, ductile, soft materials is not easily evaluated using the Charpy test. For these materials, the **tensile** impact test can be used.

The quantitative results of impact strength tests for many individual polymeric material grades at 23 °C and -30 °C may be found in the CAMPUS database, or other material supplier or third party databases.

Temperature Dependence of Toughness

When impact tests are carried out as a function of temperature, high and low levels of impact resistance are found which exhibit tough and brittle behavior, respectively. Significant changes in impact behavior are observed at the glass transition temperature at the rate in question.

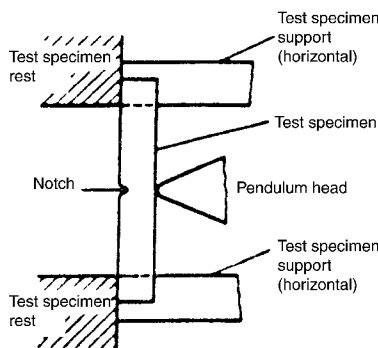
The effect of temperature on impact behavior can be very significant. Figure 4.13 shows the results of such a series of tests with a polypropylene. In addition, the figure shows force-deformation diagrams obtained from instrument-based flexural impact tests.

* The simple rule of calculating toughness from the single-point values of the modulus of elasticity and the yield strain in accordance with $W_Y = \frac{1}{2} E \cdot \epsilon_Y$ is at best permissible for brittle materials. This value would overestimate toughness for materials which deviate markedly from linearity.

Flexural Impact Test

Standards

ISO 179 (Charpy)



Test Specimen Geometry

$80 \times 10 \times 4 \text{ mm}^3$ (preferably), notched if necessary on narrow side; 45° , $r = 0.25 \text{ mm}$ (preferred notch)

Principle of Measurement

The measured variable in the test method is the energy loss on deceleration of a pendulum hammer after it has broken a test specimen.

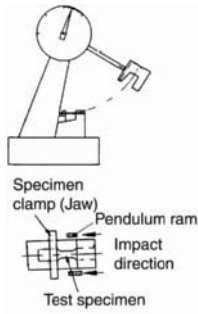
- The impact energy is defined as the fraction of the kinetic energy of the pendulum hammer consumed for deformation and fracture.
- Impact preferably ensues edgewise (e), i.e., on the narrow side of the test specimen. In the case of laminated materials, impact may be flatwise (f).
- There are 9 pendulum hammers for ISO 179 (0.5; 1; 2; 4; 5; 7.5; 15; 25 and 50 J).
- The permitted utilization interval is between 10% and 80% of the energy of the pendulum used. When utilization intervals overlap, the higher energy hammer should always be used.

Test Results

Impact strength as the integral measure of the energy of the pendulum hammer consumed up to fracture with reference to the initial cross section in kJ/m^2

Impact strength of an unnotched test specimen	a_{cu} in kJ/m^2
Notched impact strength of a notched test specimen	a_{cn} in kJ/m^2

This test provides comparative values of the resistance of the material to impact stress. These values are not used directly in design calculations.

Notched Tensile Impact Test	
Standards ISO 8256	
Test Specimen Geometry Various, preferably $80 \times 10 \times 4 \text{ mm}^3$ having double V notch, $45^\circ / r = 1 \text{ mm}$	
Principle of Measurement One end of the test specimen is fastened to a rigid portal structure, the other to a movable jaw. The pendulum hammer strikes the movable jaw (method A) so that the test specimen is subjected to tensile impact stress along its longitudinal axis. The test is preferably used when no break (NB) occurs in the flexural impact test with notches.	
Test Results Notched tensile impact strength a_t in kJ/m^2 As impact energy with reference to the initial cross section	

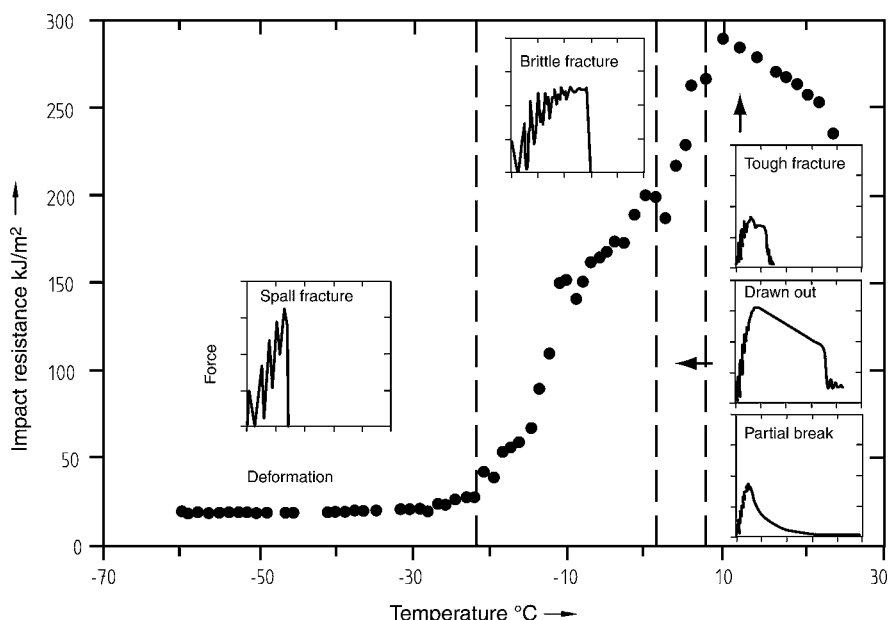


Figure 4.13 Temperature-dependence of the results of flexural impact tests for a polypropylene (Novolen 3240 HX)

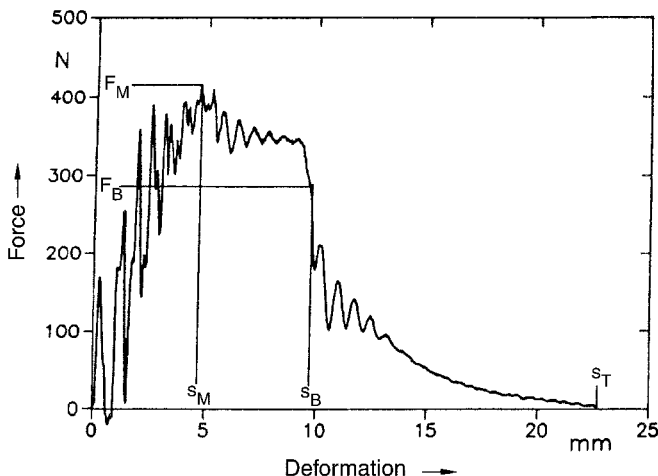


Figure 4.14 Characteristic variables from the instrumented Charpy flexural impact test

F_M = maximum force

s_M = deformation under maximum force

F_B = breaking force

s_B = deformation under breaking force

s_T = total deformation

a_M = impact resistance at maximum force as area up to s_M

a_B = impact resistance at breaking force as area up to s_B

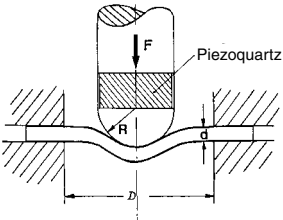
a_T = impact or notched impact resistance as area up to s_T

Instrumented Flexural Impact Test

Standard Charpy impact tests provide an integral value of impact resistance. If the pendulum striking face is equipped with a suitable instrument, measurements of force and deformation can be obtained along with the integral value of the impact resistance and more informative force-deformation data (see Figure 4.14, and also Figure 4.13).

4.3.3 Penetration or Dart Drop Impact Test

Penetration or dart drop impact tests provide a highly practical measure of toughness in which sheet or plaque like test specimens are subjected to a penetration impact stress. These test data supplement those obtained by flexural impact and notched flexural impact tests. While in the latter tests there is a uniaxial or, at the bottom of the notch, a triaxial state of stress, the penetration test provides a first approximation of a biaxial state of stress at high rates. A variety of different dart drop or penetration tests are commonly conducted, including ISO 6603-2.

Penetration or Dart Drop Impact Test		
Standards ISO 6603-2		
Test Specimen Geometry Round disk 60 mm in diameter (pin gate) Square plate 60 × 60 mm ² (film gate) Each preferably 2 mm thick		
Principle of Measurement		
A spherical punch having $R = 10$ mm penetrates the test specimen under hydraulic power or as a free-falling mass at an impact velocity of 4.5 m/s. The test specimen is either seated freely or clamped in place. In the instrument-based test, the head is provided with a high-speed force-deformation measuring device.		
Test Results		
Penetration energy up to break in Nm as a measure of biaxial toughness. Other variables as per the instrument-based flexural impact test; particularly suitable for materials development. The characteristic variables determined are dependent on thickness. The penetration energy up to break is roughly proportional to sample thickness. During penetration, biaxial flexural and tensile deformation together with frictional components are superimposed.		

4.4 Behavior under Cyclic Loads

The behavior of polymeric materials under cyclic, alternating, or repeated stresses is typically measured in protracted tension-compression or flexural fatigue tests. The results are generally presented in the form of Wöhler curves (Figure 4.15) or Smith diagrams (Figure 4.16), in which failure of the test specimen is plotted for different stress amplitudes over the number of load cycles in question (typically called an S/N curve). Because samples under cyclic loads may heat up due to viscous dissipation, the test frequency should be selected or regulated in such a way that the temperature of the test specimen remains constant. The tests are often run for as many as 2 to $4 \cdot 10^7$ load cycles before termination.

The test results have limited predictive power in terms of acceptable design stress values. Accordingly, as in the case of creep strength, Wöhler curves are suitable for design to protect against failure due to fracture. From the knowledge of the failure stress, designers must set a maximum permissible stress for their application. These tests provide no indication of the strain occurring leading up to failure nor any other clues about the structural changes in the material associated with fatigue, e.g., about the onset of fracture. Application of the test results to structural parts under cyclic stress must, therefore, be done with some caution.

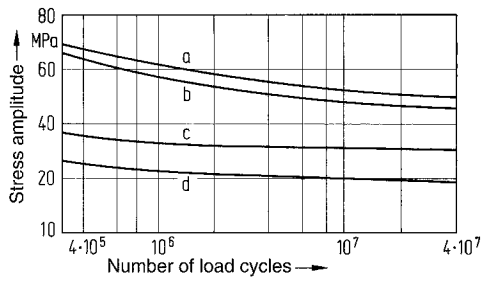


Figure 4.15 Wöhler curves from flexural fatigue tests [4.25] for

- a) PA 66 GF (35% by wt.), c) PA 66,
- b) PA 6 GF (35% by wt.), d) PA 6

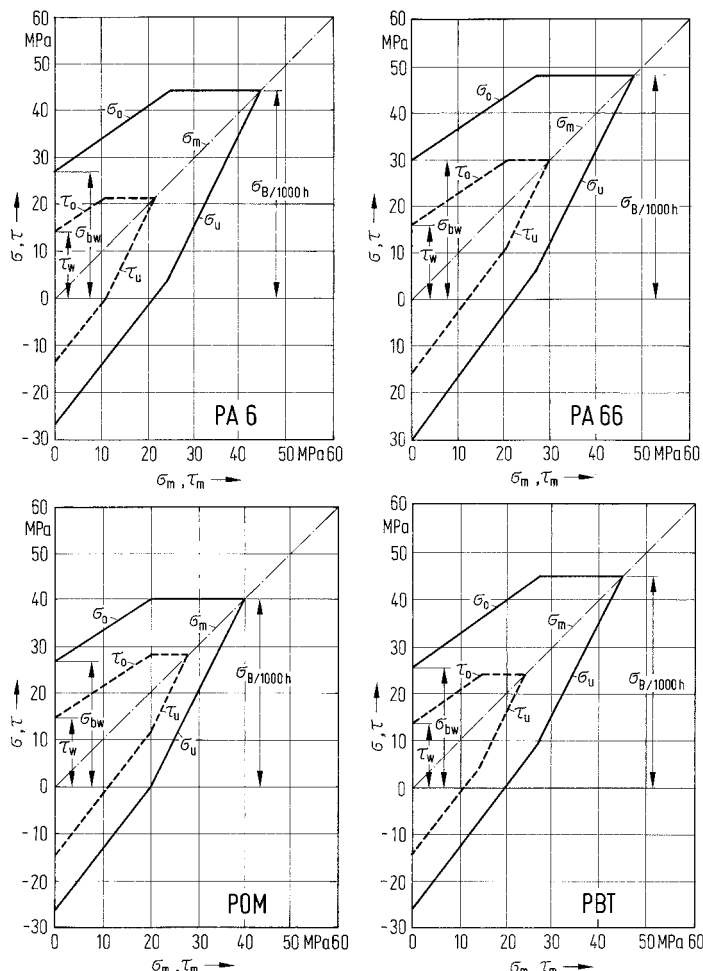


Figure 4.16 Smith diagrams; flexural and torsional stress for $2 \cdot 10^7$ load cycles [4.26]

However, Wöhler curves can certainly be used as a comparative basis for selecting a material. These test data can be expensive to generate, and therefore are available only for a limited number of polymeric materials.

4.4.1 Determination of Characteristic Features of Fatigue

Crack Growth Studies. Fracture-mechanical studies can provide valuable information about crack growth in samples susceptible to cracking. Thus, fracture mechanics has the potential to afford a promising method for designing structures subjected to cyclic stresses [4.27–4.30]. In general practice, however, this approach is not yet common.

Acoustic Emission Analysis. Examples of the successful use of acoustic emission measurements include the demonstration of crack formation, preferably in fiber-reinforced polymeric materials subjected to cyclic loading [4.31–4.32].

Hysteresis Measurements. Hysteresis in stress-strain tests under cyclic loading is a significant feature of visco-elastic materials. Stress and strain are staggered relative to one another by the phase angle δ (see Figure 4.17).

Accordingly, the time-dependent stress and strain are given by:

$$\sigma_{(t)} = \hat{\sigma} \cos(\omega t) \quad (4.6)$$

$$\varepsilon_{(t)} = \hat{\varepsilon} \cos(\omega t - \delta) \quad (4.7)$$

or in complex number notation by:

$$\sigma_{(t)} = \hat{\sigma} \cdot e^{i(\omega t)} \quad (4.8)$$

$$\varepsilon_{(t)} = \hat{\varepsilon} \cdot e^{i(\omega t - \delta)} \quad (4.9)$$

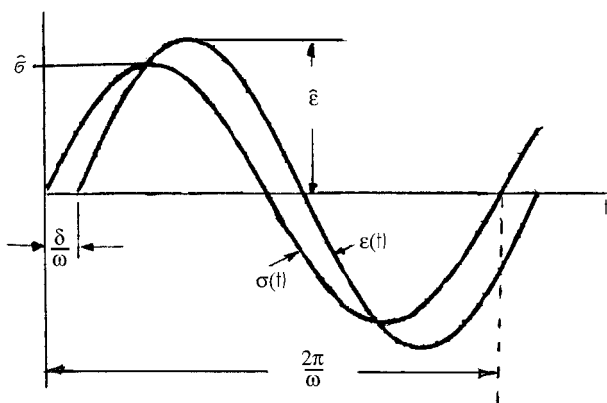


Figure 4.17 Under cyclic loading, stress and strain are staggered relative to one another by the phase angle δ

Therefore, the modulus is a complex number as follows:

$$|E| = E' + i E'' \quad (4.10)$$

where

$|E|$ = complex modulus

E' = storage modulus

E'' = loss modulus

and

$$E'' / E' = \tan \delta = d = \text{mechanical loss factor} \quad (4.11)$$

Suitable instrumentation in the form of servohydraulic test machines allows fatigue behavior to be described with the aid of hysteresis measurements. These in turn make it possible to draw conclusions about the potential for fracture [4.33–4.37]. Values for strain, rigidity, and energy-related properties may be obtained from such measurements.

In the case of linear visco-elastic behavior, the hysteresis loop assumes a typical elliptical shape, the area of the ellipse being a measure of the loss energy W (see Figure 4.18). The storage energy is obtained as the area under the center line that bisects the loop at the same strain value in each case. At the same time, the gradient of this center line characterizes the rigidity of the sample.

The material damping behavior is determined with Eq. 4.11 from the quotient of the loss energy and the storage energy (W_L/W_S).

The change in rigidity and in particular in damping, with the number of cycles may be a measure of the damage occurring during fatigue. The causes of the damage may be, for example, cracks, changes in morphology, creep processes, or temperature effects.

Figure 4.19 shows the effects of an incremental loading test in changing the hysteresis loop of an SMC material. The initially symmetrical loop (± 10 MPa) becomes flatter as the stress amplitude increases to ± 30 MPa and exhibits a kink in the compression range at -12 MPa, which becomes much more evident when the load is increased to ± 40 MPa. As expected, the

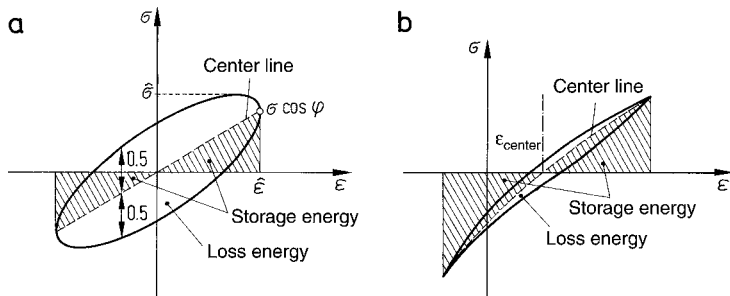


Figure 4.18 Determination of characteristics for describing fatigue phenomena [4.34]

- a) Elliptical hysteresis loop (linear viscoelastic behavior)
- b) Hysteresis loop for nonlinear viscoelastic behavior

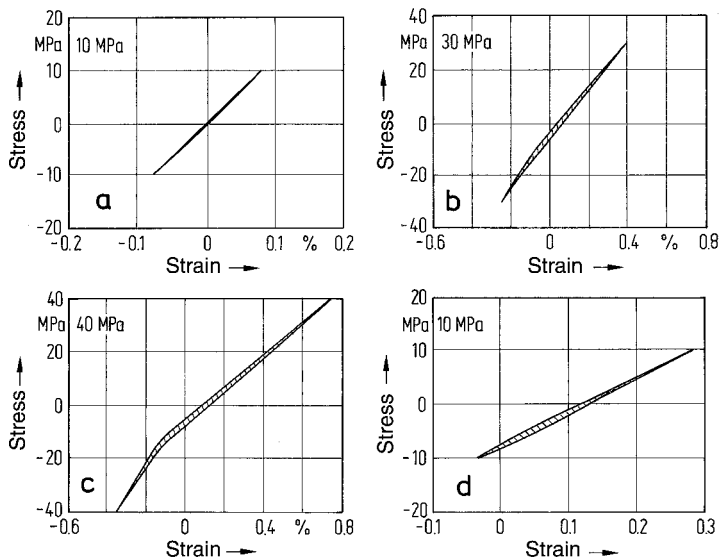


Figure 4.19 Hysteresis behavior of SMC in an incremental loading test.
Test frequency: 10 Hz; test duration: 2 h in each case [4.36].

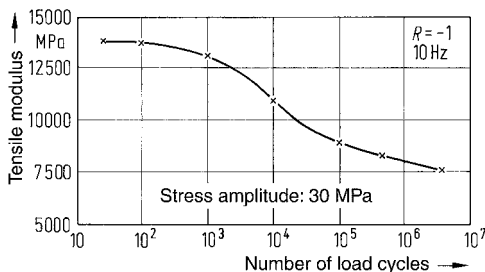


Figure 4.20 Decrease in tensile rigidity as a criterion for evaluating the fatigue behavior of a SMC material [4.36]

strain increases. The loss in rigidity is explained by a high degree of microcracking which is particularly discernible in the tensile stress cycle. In the compression cycle, the cracks close so that the rigidity is apparently restored. After reducing the load to the initial level of ± 10 MPa, changes in shape, rigidity, and position (cyclic creep) of the hysteresis loop are clearly found. Accordingly, such cyclic tests supported by instruments permit reliable conclusions to be drawn about the start of fracture*. The central strain describes the tendency to creep under cyclic loading and the decrease in rigidity (see Figure 4.20) is more useful for evaluating fatigue behavior for engineering purposes than the number of load cycles in a Wöhler curve.

* In the case of glass-fiber reinforced thermoplastics (e.g., glass-fiber reinforced PBT), sensitive measurements of damping already identify the first signs of damage at numbers of load cycles which can be extended further by about a factor of ten up to catastrophic failure [4.37]. In this way, dynamically loaded structural components can be designed more reliably than with conventional Wöhler curves.

Table 4.3 Limiting Values for the Dynamic Loading of Glass-Fiber Reinforced PBT.

Fiber Length: 140–165 µm, Test Frequency: 1 Hz,
Expected Service Life: 10^6 Load Cycles [4.37].

Glass-fiber reinforced PBT Fiber content [% by wt.]	Limiting stress σ_{limit} [MPa]	Limiting strain $\varepsilon_{\text{limit}}$ [%]
14.8	28	0.9
26.9	31	0.4
43.8	36	0.25

4.5 Poisson's Ratio

Poisson's ratio μ is defined by ISO 527 as:

$$\mu = \frac{-\varepsilon_w}{\varepsilon_l} = \frac{-\varepsilon_t}{\varepsilon_l} \quad (4.12)$$

where

ε_w = strain in the width direction

ε_t = strain in the thickness direction

ε_l = strain in the longitudinal direction

It is a characteristic of a material with a relationship between stresses and strains along multiple axes. For example, in a state of planar stress, the strains in the x and y directions are calculated from the stresses in these directions via Poisson's ratio using Hooke's law.

$$\varepsilon_x = \frac{1}{E} (\sigma_x - \mu \sigma_y) \quad (4.13)$$

$$\varepsilon_y = \frac{1}{E} (\sigma_y - \mu \sigma_x) \quad (4.14)$$

For materials that behave isotropically, Poisson's ratio can be determined by measuring the strain occurring under uniaxial loading with the tensile test in the longitudinal direction (direction of action of the tensile force) and the strains (contractions) occurring in the width and thickness directions. Alternatively, it may also be calculated when, for example, the modulus of elasticity E and the modulus of rigidity G or the bulk modulus K are known (assuming same rate and test temperatures). The following two equations show examples of relationships between these variables and Poisson's ratio.

$$\mu = \frac{E}{2G} - 1 \quad (4.15)$$

$$\mu = 0.5 - \frac{E}{6K} \quad (4.16)$$

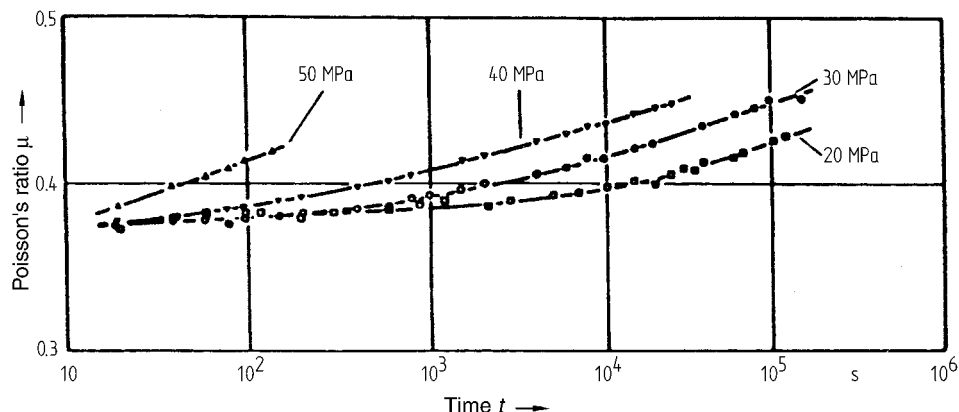


Figure 4.21 Poisson's ratio for PMMA at 50 °C as a function of time under different stresses [4.53]

Table 4.4 Literature Values for Poisson's Ratio for Selected Common Polymeric Materials at Room Temperature

LDPE	HDPE	PP	PVC	PS	SB
0.5	0.5	0.41–0.45	0.37–0.4	0.33	0.35–0.37
ABS	SAN	PMMA	PBT	POM	PA 6
0.39–0.41	0.33–0.36	0.33–0.36	0.41–0.42	0.42–0.45	0.38–0.42
PA 66	PC	PSU	PES	Steel	Aluminum
0.38–0.42	0.35–0.36	0.42	0.43	0.3	0.33

Poisson's ratio for polymeric materials having visco-elastic behavior is, like all elastic variables, not a constant but rather a function of the degree of deformation (or stress) and time and, of course, temperature. Over long periods, it tends towards the value of 0.5 and the same applies correspondingly to the time-temperature equivalent, even at elevated temperatures [4.53, 4.54]. Figure 4.21 illustrates these relationships for PMMA. Table 4.4 presents a compilation of literature values for Poisson's ratio for selected thermoplastics.

Anisotropic Materials

Polymeric materials can exhibit anisotropic behavior for a variety of reasons. For example, injection-molded parts made from fiber-reinforced thermoplastics exhibit a typical layered structure, each layer having a preferred alignment (see also Chapter 7). The layers most important for strength and rigidity are the peripheral layers which tend to be aligned in the direction of flow of the melt. The central layers tend to be oriented perpendicular to the direction of flow of the melt. In thin-walled parts, the orientation of the peripheral layers is more pronounced. Accordingly, Poisson's ratio in these cases likewise exhibits directional dependence.

Table 4.5 Poisson's Ratio Values for Glass-Fiber Reinforced PA 66 at Different Angles to the Direction of Flow

Angle to direction of injection	0 degrees		45 degrees		90 degrees	
Wall thickness in mm	2	4	2	4	2	4
PA 66 (35% glass fiber)	0.5	0.4	0.45	0.45	0.23	0.25
PA 66 (15% glass fiber)	0.5	0.45	0.42	0.4	0.33	0.33

In the case of unidirectionally reinforced fiber composites, the difference between the value parallel to and perpendicular to the orientation of the fibers is even more marked.

Table 4.6 Poisson's Ratio for Unidirectionally Reinforced PU Laminates, Each Containing 60% by Weight of Reinforcement: Glass, Carbon, and Aramid Fibers (At Room Temperature) [4.55]

Loading	In the direction of the fibers	Perpendicular to the fiber direction
Glass fibers	0.28	0.075
Carbon fibers	0.25	0.02
Aramid fibers	0.34	0.025

The values in Table 4.6, however, are less relevant to practical situations, because such highly reinforced resins are not loaded transversely relative to the orientation of the fibers. It is common practice to use a value of $\mu = 0.1$ (assumed) for loading perpendicular to the alignment of the fiber for Poisson's ratio figures for UP glass mat laminates (see Figure 5.17).

4.6 Thermal Properties

4.6.1 Thermal Expansion

The coefficient of thermal expansion is an important parameter in many end use applications. The coefficient of linear expansion α is the percentage change in length of a dimension for a given temperature difference ΔT :

$$\alpha(T) = \frac{\Delta l}{l} \frac{1}{\Delta T} \quad (4.17)$$

This is a material-specific variable which, as shown in Figure 4.22, tends to be inversely proportional to the modulus of elasticity of the material. Many relatively flexible polymeric materials expand due to the effects of temperature by an order of magnitude more than many metals. Accordingly, measures taken to increase the modulus of elasticity, such as orientation, filling, fiber reinforcement, etc., tend to reduce the degree of thermal expansion.

As an example, Figure 4.23 shows the effect of fiber reinforcement on thermal expansion. Reinforced polymeric materials have thermal expansion values in the same range as aluminum.

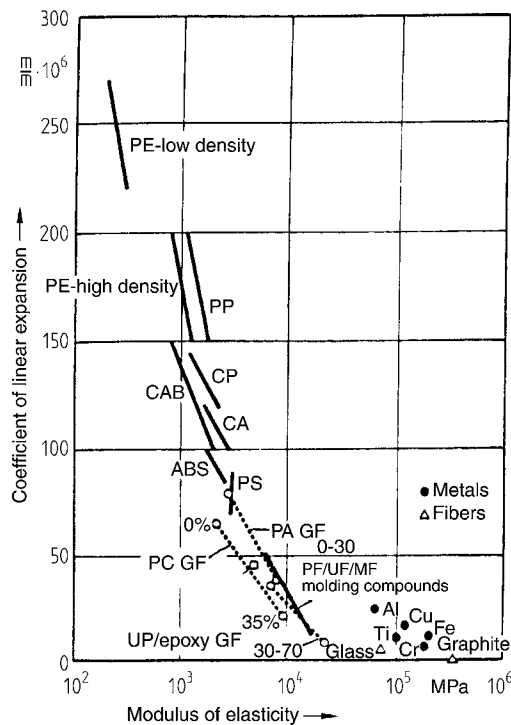


Figure 4.22 Relationship between the coefficient of linear expansion and modulus of elasticity

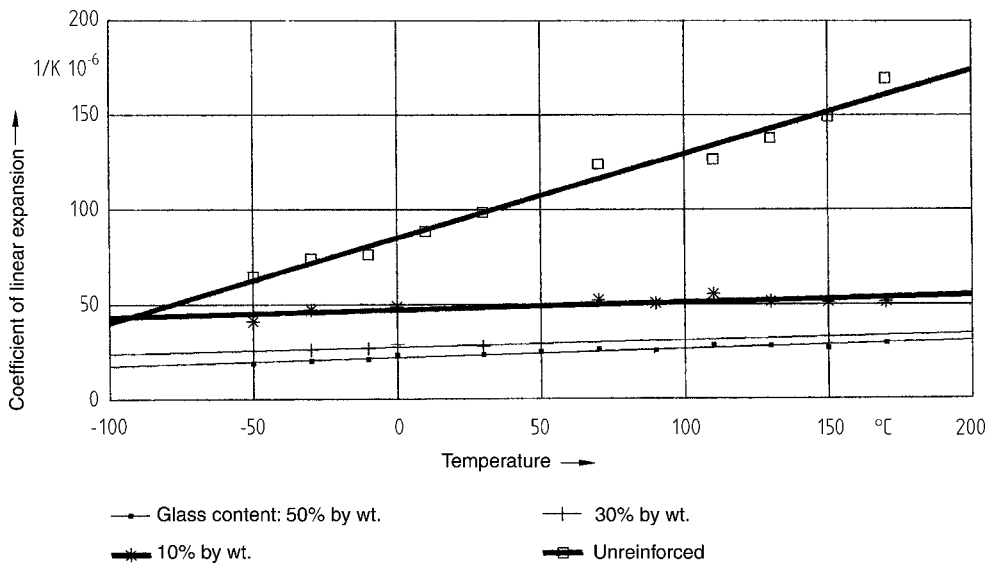


Figure 4.23 Coefficient of linear expansion of PBT and glass-fiber reinforced PBT versus temperature

The coefficient of expansion in the injection direction (preferential orientation) of the test specimens is plotted here against temperature. The coefficient of expansion perpendicular to the direction of fiber orientation assumes approximately the same value of the unreinforced matrix material.

Measured values for coefficients of linear expansion parallel and transverse to the injection direction may be found in databases such as CAMPUS.

The relatively high coefficient of thermal expansion for polymeric materials can lead to a variety of design problems. Measures for controlling thermal expansion in design are provided in Chapter 6.

4.6.2 Dimensional Stability

4.6.2.1 Modulus of Elasticity and Modulus of Rigidity as a Function of Temperature

The relationship between rigidity and temperature has already been discussed in principle in Section 2.6.2. The usual logarithmic presentation employed there, however, may be quite misleading regarding the high loss in rigidity as the temperature rises – even within a sometimes very limited temperature range. This is particularly the case for thermoplastics.

A precise evaluation of the properties of a polymeric material for design purposes must be made on the basis of modular functions of temperature and strain in the form of the secant modulus (see Figure 4.5) and as a function of time in the form of the creep modulus (see Section 4.2).

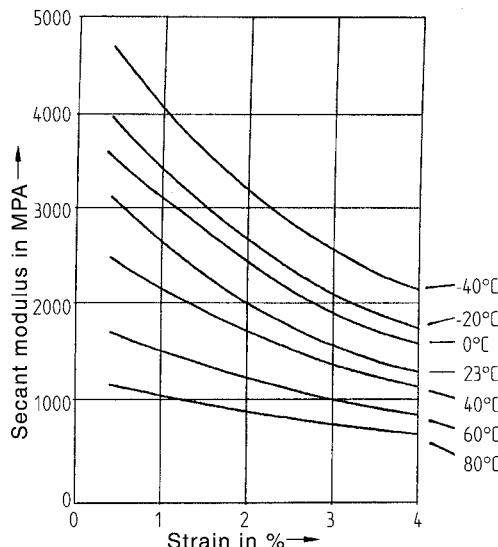
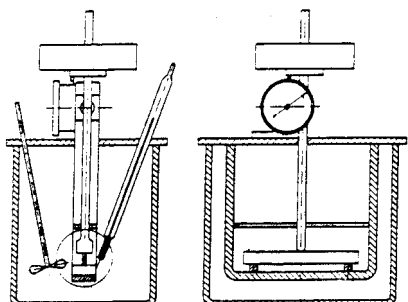


Figure 4.24 Secant modulus at different temperatures for POM (H 2320)
(Source: CAMPUS database, BASF)

As an example, the strain dependent secant modulus for a POM at different temperatures is illustrated in Figure 4.24. These curves form a part of the CAMPUS multipoint database.

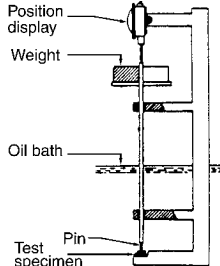
4.6.2.2 Deflection Temperature

A simple and relatively fast technical test for the temperature at which a polymeric material deforms to a standard deflection under load provides a basis for comparing the upper use temperature of different materials. This test, commonly referred to as heat deflection temperature (HDT) or deflection temperature under load (DTUL) does not provide a full indication of maximum use temperature. However, it is widely used as a screening test.

Deflection Temperature	
Test for Temperature at which Bending under Load Occurs	
Standards	
ISO 75 Temperature of deflection under load	
Test Specimen Geometry	
80 × 10 × 4 mm ³ flatwise (110 × 10 × 4 mm ³ edgewise)	
Principle of Measurement	
The test specimen is subjected to three-point bending.	
Bending stress	Method A: 1.8 MPa
	Method B: 0.45 MPa
	Method C: 8.0 MPa
The temperature of the test specimen is raised in an oil bath at a steady rate of 120 K/h.	
The temperature at which the strain in the outer fibers reaches 0.2% is referred to as the temperature of deflection under load.	
Test Results	
Temperature of deflection under load, e.g., method Af _(flatwise) = 95 °C.	
Information Use	
Comparison of materials	
Indication of upper working temperature	
Not a characteristic or fundamental property for use in design equations.	

4.6.2.3 Softening Point

The determination of the Vicat softening point or temperature is also a relatively fast technical test. It provides a measure of the resistance to indentation or penetration at higher temperatures. Like the previous test, it provides some indication of upper use temperature, particularly for amorphous thermoplastics.

Vicat Softening Temperature	
Vicat Softening Point Test	
Standards	
ISO 306	
Test Specimen Geometry	<p>$> 10 \times 10 \times 4 \text{ mm}^3$ (taken from the center of the $80 \times 10 \times 4$ all-purpose test specimen)</p>
Principle of Measurement	<p>A 1 mm^2 needle under a load of 50 N (test method B) – in exceptional cases under a load of 10 N (method A) – is set up on the surface of the test specimen. The temperature of the test specimen is raised in an oil bath – in special cases in air – at a constant rate of 50 K/h. The temperature at which the needle has penetrated 1 mm into the test piece is referred to as the Vicat softening temperature (VST).</p>
Test Results	<p>Vicat softening temperature, e.g., VST / B 50 = 82 °C</p>
Information Use	<p>Most meaningful for thermoplastics having an amorphous structure. Identifies the start of softening and corresponds approximately to the glass transition temperature (for amorphous thermoplastics). Rule of thumb: Vicat – 20° = max. working temperature Not a fundamental property for use in design equations.</p>

4.6.3 Heat Aging

All irreversible intramolecular and intermolecular changes occurring in high polymer materials due to environmental effects can be described using the general term “aging”. Aging can be caused by thermal, mechanical, and dynamic energy, light and radiation, and also chemical environments. Heat aging will be examined in more detail.

Heat Aging	
Standards	IEC 216 ISO 306 (UL 726 B)
Test Specimen Geometry	<p>Various tensile or other specimen geometries, type 4 preferred in future (as per ISO 8256), and taken from a $60 \times 60 \times 3 \text{ mm}^3$ plate.</p>
Principle of Measurement	<p>Storage of the test specimens at a number of constant temperatures without mechanical loading, removal after certain times and checking the changes in the properties of interest.</p> <p>Common properties of interest in the case of thermoplastic materials:</p> <ul style="list-style-type: none"> • tensile strength • tensile impact strength • dielectric strength.
Test Results	
<p>Plot of the change in the characteristic property values over the heat aging period. Arrhenius diagram of time versus heat exposure temperature for a selected percentage drop in the characteristic value (usually 50%).</p> <p>Temperature index (TI) in accordance with IEC 216, as the temperature at which the characteristic value falls to 50% after 20,000 h of exposure.</p> <p>Relative temperature index (RTI) in accordance with UL 726 B relative to a reference material.</p> <p>Halving interval (HIC) as the temperature difference relative to TI when the exposure time is halved (10,000 h).</p>	
Information Use	
<p>Results are dependent on sample thickness.</p> <p>Estimation of loss in strength under long-term exposure to the action of heat.</p> <p>Early selection of materials for high temperature applications.</p>	

As a consequence of heat aging, structural changes can occur (breaking of chains, oxidation, etc.) which in turn give rise to alterations in the macroscopic properties of the material. This is a factor that the designer of a plastic part has to consider. A number of test protocols (IEC 216 or UL 726) specify the conditions for testing a material's performance under prolonged exposure to the action of heat.

The change in a characteristic property value as a function of time can be plotted for any condition of temperature exposure. A point in time can be determined at which this characteristic value has fallen to a certain percentage (*e.g.*, 50%) of its initial value (see Figure 4.25). It is common to illustrate this in the form of an Arrhenius plot, *e.g.*, for a reduction to 50%, in which the time for this percentage drop is plotted against the corresponding exposure temperatures (see Figure 4.26). The thickness of a sample has a significant effect on the aging processes and this variable has to be taken into account when possible. Thermal degradation in the form of a first order chemical reaction includes depolymerization. Depolymerization proceeds uniformly across the cross section of the test specimen once initiated.

A typical second order reaction associated with aging is oxidation. In contrast to depolymerization, oxidation sets in at the surface and penetrates more slowly into the interior of the sample. Accordingly, in the case of thick-walled samples or structural parts, the aging mechanism of oxidation only has an effect after a relatively long time when significant portions of the cross section have been oxidized. Thin-walled parts, on the other hand, may oxidize more quickly.

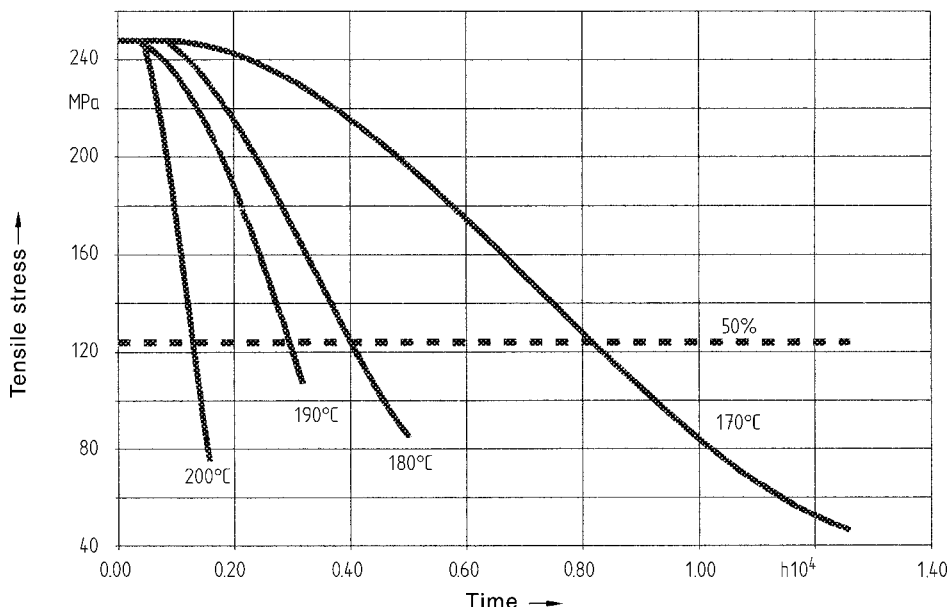


Figure 4.25 Results of heat aging tests. Variation in tensile strength over the exposure period at four different temperatures. Material: PA 66 C4 (A3WC4); sample thickness: 3.2 mm (Source TEP Aging program, BASF)

Figure 4.27 presents some results of heat aging tests. These clearly show the effect of heat stabilization.

Given this type of information, the designer can determine reduction factors that take the effect of the prolonged action of heat into account. It should be noted here that these data do not include the temperature dependence of properties (e.g., mechanical performance) while the samples are at the elevated temperature.

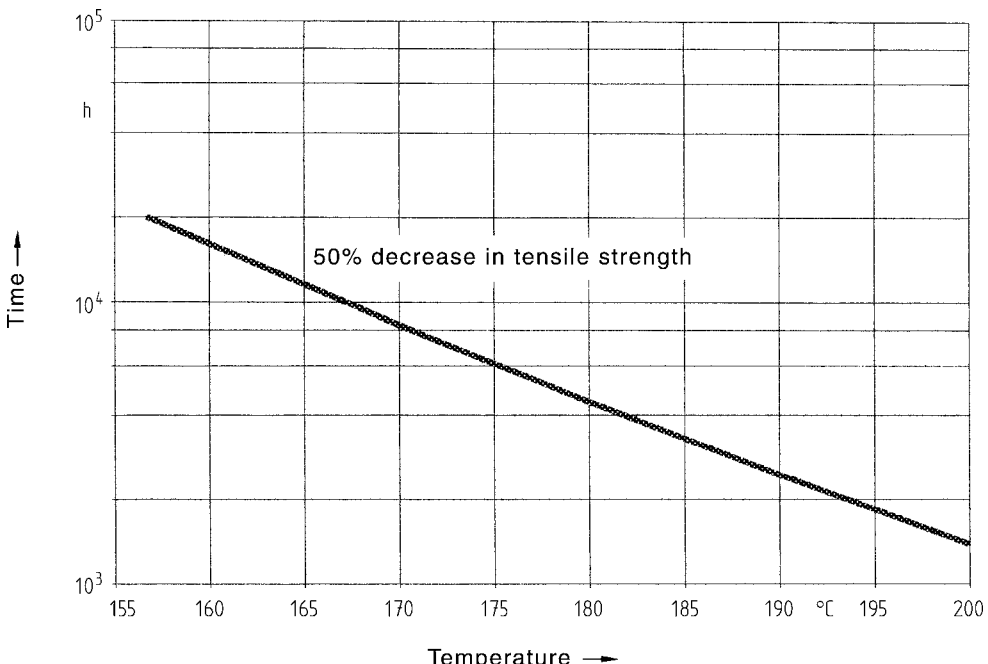


Figure 4.26 Arrhenius plot describing the reduction of tensile strength to 50% of its initial value.
Material: PA 66 C4 (A3WC4); sample thickness: 3.2 mm (Source TEP Aging program, BASF)

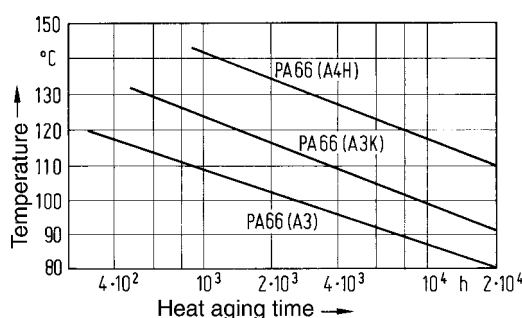


Figure 4.27 Drop in tensile strength to 50% of its initial value after heat aging for three grades of polyamide with different forms of heat stabilization. Sample thickness: 3.2 mm (Source TEP Aging program, BASF)

4.6.3.1 Safety Considerations and Standards

Many industrial or consumer devices and tools must be tested in accordance with safety standards for heat aging (and fire characteristics) in order to ensure minimal risk to the consumer. This applies, for example, to electrical equipment, building supplies, packaging, and a variety of other applications. It is generally not possible to test the aging properties of finished equipment or products under operating conditions due to the usually long service lives involved.

Materials testing protocols, such as IEC 216 or UL 726, are particularly important for evaluating heat aging. They allow for the preliminary screening of materials used in the manufacturing of new products. This screening helps to simplify, shorten, and partially replace the safety testing of the product.

The temperature index (TI) described earlier can be used as a single-point value for screening. It is defined as the temperature in °C at which a limiting value (typically 50%) of a change in a property (compared with the unaged sample) is reached after a certain time (*i.e.*, 20,000 h); this is depicted in Figure 4.28.

In addition to the temperature index, a value known as the halving interval (HIC) can also be specified. This is a measure of the gradient of the Arrhenius plot. It is the temperature difference relative to TI when the time is halved, *i.e.*, to 10,000 h (see Figure 4.28).

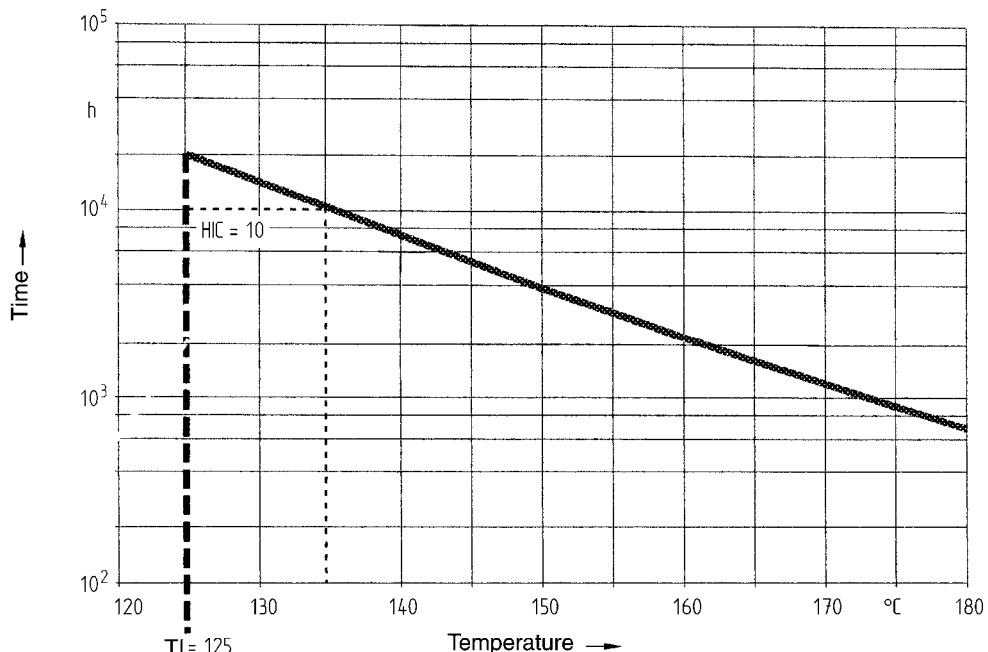


Figure 4.28 Determination of the temperature index (TI) and halving interval (HIC) from the Arrhenius diagram.

Material: glass-fiber reinforced PBT 30, containing flame retardant (B 4406 G6); sample thickness: 3 mm (Source: TEP Aging program, BASF).

As a single-point characteristic, the temperature index is suitable for comparing materials. However, it does not provide any direct relationship with the service life of a product because it applies only to the specific underlying test conditions. The TI can be used to help select materials for electrical equipment requiring agency approval.

4.6.4 Summary Analysis of the Effects of Temperature

Although the effects of temperature on the properties of polymeric materials have already been presented, Table 4.7 summarizes once again the effects of temperature, time, and loading together with the appropriate test methods.

Table 4.7 Possible Effects of Exposure to High Temperatures and Suitable Test Methods for their Evaluation

Duration of exposure to heat	External mechanical loading	Main effects	Suitable assessment variable and tests on material or finished parts
Short	No	Change in dimensions	<ul style="list-style-type: none"> • Linear thermal expansion (ASTM E 831) • Measurement of shrinkage and warpage
Short	Yes	Softening	<ul style="list-style-type: none"> • Glass transition temperature • Mech. property (e.g., tensile test) at high temperature (ISO 527) • Temperature of deflection under load (ISO 75)
Long	No	Heat aging, yellowing, embrittlement	<ul style="list-style-type: none"> • Heat aging (IEC 216, UL 726) • Weathering (ISO 4892) • Heat aging of structural parts and serviceability test
Long	Yes	Intensified creep, stress, relaxation, aging	<ul style="list-style-type: none"> • (Tensile) Creep test at high temperature (ISO 899) • Structural part investigations

4.7 Tribological Properties

Friction and wear are unavoidable consequences of the nonpositive mating of pairs of materials when they are moved relative to one another, even if they are separated from one another to a certain degree by intermediate layers. The law of friction as formulated by Coulomb (1736–1806) states:

$$F_f = f F_n \quad (4.18)$$

This shows that the required frictional force F_f is related to the normal force F_n by the coefficient of sliding friction f .

In friction and wear, material-related and force-related interactions are dependent on numerous influencing variables that take place between the mated materials.

Accordingly, tribology deals with *system properties* and not just the properties inherent in a single material (bulk properties) as shown in Figure 4.29.

Measurements of tribological variables are tied to the tribological system in which the measurements were made. The simplest experimental system for evaluating tribological properties is the pin-on-disk arrangement, which clearly reveals distinct differences among different pairs of materials.

The friction process is associated with the irreversible dissipation of energy, as the energy supplied to a friction system in the form of mechanical work is completely converted into other forms of energy. The major proportion is lost as frictional heat. Other processes consuming energy include deformation, fracture processes, changes in structure, emission of sound, and chemical reactions. Polymeric materials, especially thermoplastics, are very important as materials for parts subject to friction and wear because they can be used as slip materials, especially in *lubricant-free* applications for critical functional parts (see Chapter 12). While semi-crystalline thermoplastics are most widely used in friction and wear applications, amorphous thermoplastics, particularly those containing lubricating additives, are also used.

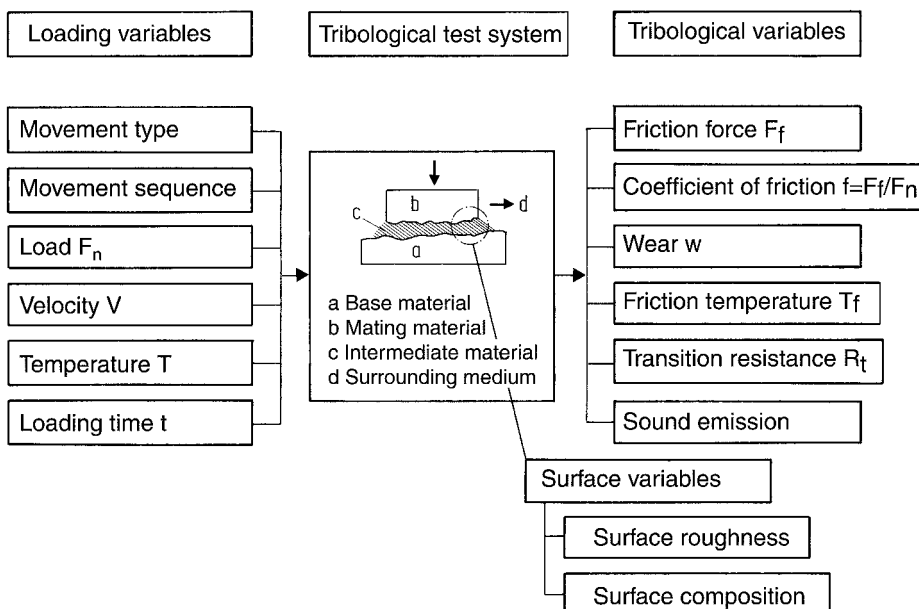
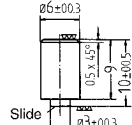


Figure 4.29 Tribological system as described in [4.38]

Tribological Properties	
Standards	ISO 7148-1 ISO 7148-2
Test Systems	
Various; ISO 7148-1 test A: <i>pin-on-disk</i> preferred and used here (disk-on-disk arrangements for pairs of polymeric materials are not standardized)	
Test Specimen Geometry (Pin-on-Disk)	
Polymer pin 6 mm in diameter, contact surface area 3 mm in diameter Steel disk 110 mm in diameter	
	
Principle of Measurement	
The pin slides under constant pressure at constant slipping speed on the steel contact surface.	
Test Results	
Coefficient of sliding friction f Wear due to sliding friction; e.g., linear wear rate W_l Mean sliding surface temperature T	
Information Use	
Results are highly dependent on the tribological system employed. Estimation of tribological properties and initial comparison of materials. Screening of materials for friction and wear applications.	

4.7.1 Fundamentals

The friction force F_f to be applied at the macroscopic level in the sliding process is composed according to current knowledge of an adhesion term $F_{f\text{ adh}}$, a deformation term $F_{f\text{ def}}$ and, in cases of slipping under conditions highly conducive to wear, of a term describing crack formation and crack propagation [4.39–4.42].

This is expressed formally as:

$$F_f = F_{f\text{ adh}} + F_{f\text{ def}} + F_{f\text{ cra}} \quad (4.19)$$

Using this expression, friction and wear phenomena observed in mated pairs of materials involving polymeric materials can be explained to a satisfactory degree of accuracy.

Accordingly, there are three principal factors ruling the sliding friction of solids:

- Adhesion of interfacial layers
- Deformation of microcontact points and surface layers
- Crack initiation and crack propagation.

1. Adhesive Friction

$$F_{f\text{ adh}} = \frac{dW_{ab}}{dx} \cdot A_a = f_{\text{adh}} \cdot \frac{F_N}{H} = \mu_{\text{adh}} \cdot F_N$$

$$F_{f\text{ adh}} = f(W_{ab}, H)$$

W_{ab} = adhesion energy

A_a = actual contact area

f_{adh} = specific adhesive force

H = hardness

μ_{adh} = coefficient of adhesive friction

2. Deformative Friction

$$F_{f\text{ def}} = \frac{dW_{def}}{dx} \cdot A_a \geq \tau_y \cdot \frac{F_N}{H} = \mu_{\text{def}} \cdot F_N$$

$$F_{f\text{ def}} = f(W_{def}, H)$$

W_{def} = deformation energy

τ_y = flow shear stress

3. Friction Due to Cracking and Crack Propagation

$$F_{f\text{ cra}} = \frac{G_{IC}}{\Delta h} \cdot A_a = \frac{K_{IC}^2}{\Delta h \cdot H \cdot E} \cdot F_N = \mu_B \cdot F_N$$

$$F_{f\text{ cra}} = f(G_{IC}, H)$$

G_{IC} = crack propagation force

K_{IC} = fracture toughness

Δh = depth of plastically deformed zone

The first two are generally the most important. The problem, however, is that although the friction mechanisms act simultaneously (but with different intensities and cannot be isolated from one another), they are attributable to completely different physical properties.

The above chart sets out the relationships and identifies the physical properties of the material which come into play in each case. These are the adhesion energy (which is simplified to polarity), the deformation energy (which is simplified to toughness), surface hardness, and crack propagation force.

4.7.1.1 Adhesion and Surface Energy of Solids

In the regions, in which the surfaces of solids sliding over one another come sufficiently close together (intimate contact), atomic or molecular interactions occur between the surfaces.

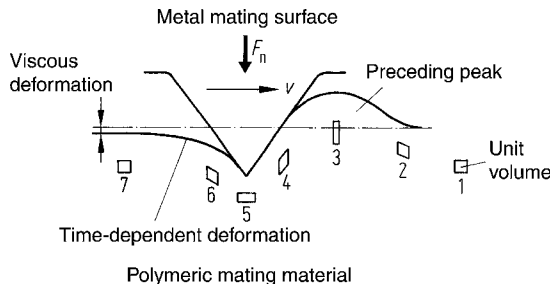


Figure 4.30 Model of deformation by tangential movement of the tip of a *hard* uneven surface peak. The volume elements close to the surface are subjected to alternating deformations during passage of the peak [4.40]

This is the case, for instance, in the region of the actual contact area* but also at the tip of a hard peak in a rough surface as shown in the model in Figure 4.30.

Such an interaction in the frictional contact of mating surfaces involving polymeric materials is the build-up of physical adhesion energy between the surfaces in contact due to their surface energies. If it is assumed that relatively low-energy polymeric materials do not form adsorption layers on the surface, this effective adhesion energy is attributable to electrostatic energy as found in the intermolecular binding energies in the polymers themselves.

The key forms of intermolecular binding energy in order of increasing strength are:

- Dispersion energy
- Dipole interactions and
- Hydrogen bonds.

Surface Energy of Solids

The intermolecular energies of a polymeric material also determine its surface energy γ . By analogy with the action of dispersion energies and dipole interactions, this can be broken down into a disperse component γ^d and a polar component γ^p ** so that:

$$\gamma = \gamma^d + \gamma^p \quad (4.20)$$

Polymeric materials having exclusively disperse surface energy components or those having only minimal polar components (e.g., PTFE or PE) are also referred to as being “nonpolar”, while those having polar components are said to be weakly or strongly polar depending on their values.

* The sum of the contact areas in which technically permanently rough surfaces are actually in contact is referred to as the actual contact area, whereas the projection of the counterpart body onto the base body is usually identified as the contact area.

** The polar and disperse surface energy components of a polymeric material can be determined analytically [4.43, 4.44] or graphically [4.45] with Eqs. (4.20) to (4.23) by angle of contact measurements using at least two test liquids whose surface energy components are known.

The Dupre equation governs the contact of two bodies a and b, having surface energies γ_a and γ_b .

$$\gamma_a + \gamma_b = \gamma_{ab} + W_{ab} \quad (4.21)$$

Here W_{ab} is the adhesion work performed per unit area, which is converted to “contact heat”, and γ_{ab} is the interfacial energy of the surfaces in contact. To separate the two bodies a and b, an amount of energy W_{ab} has to be applied per unit area.

When the polar and disperse surface energy components for the mated pair a and b are known, the adhesion energy W_{ab} can be calculated either by the Owens and Wendt relationship [4.43]:

$$W_{ab} = 2 \sqrt{\gamma_a^d \cdot \gamma_b^d} + 2 \sqrt{\gamma_a^p \cdot \gamma_b^p} \quad (4.22)$$

or by that proposed by Wu [4.44]:

$$W_{ab} = \frac{4 \gamma_a^d \cdot \gamma_b^d}{\gamma_a^d + \gamma_b^d} + \frac{4 \gamma_a^p \cdot \gamma_b^p}{\gamma_a^p + \gamma_b^p} \quad (4.23)$$

The surface energy γ_{SL} is obtained from Young's equation*:

$$\gamma_{SL} = \gamma_S - \gamma_L \cos\theta \quad (4.24)$$

where θ is the measured angle of contact.

In Tables 4.8 and 4.9, the surface energies γ of selected polymeric materials determined by angle of contact measurements are presented. Their polar components γ^p and disperse components γ^d calculated according to Owens and Wendt, and Wu respectively are included.

The polymeric materials listed do not differ significantly in their surface energies γ , with the notable exceptions of PTFE and HDPE. The polar component γ^p , however, allows for a clear distinction to be made between nonpolar materials ($\gamma^p < 1 \text{ mN/m}$) and polar materials ($\gamma^p > 1 \text{ mN/m}$). The tables also show that there are sometimes considerable differences in the values obtained by different authors. This is likely due, on the one hand, to the extremely sensitive method of measurement and, on the other hand, to the fact that the materials used are not absolutely identical despite having the same designation. Therefore, representative average surface energy values are given in Table 4.10.

The surface energies of polymeric materials may be used to help assess the slipping process, because the adhesive contacts established when solids come into contact are broken again when they move relative to one another. The adhesive forces are constantly reestablished with the length of slip. This is associated with a loss of energy, which provides information about the adhesion energy W_{ab} of the polymeric materials involved.

* In cases of contact between solids and liquids the indices S (solid) and L (liquid) are commonly used instead of a and b respectively.

Table 4.8 Surface Energy of Various Polymeric Materials

Author	ERHARD [4.48]			OWENS and WENDT [4.43]			RABEL [4.45] Friedrich			KOERNER [4.49]		
Material	Surface energy in [mN/m]											
	γ^d	γ^p	γ	γ^d	γ^p	γ	γ^d	γ^p	γ	γ^d	γ^p	γ
PTFE							18.5	0	18.5			
HDPE	34.5 33.1	0.1 0.1	34.6 33.2				31.6 30.3	0.2 0	31.8 30.3	32.1 32.1	0	32.1
LDPE				33.2	0	33.2				35.1	0	35.1
PP	42.1	0.3	42.4				30.5	0.7	31.2			
POM	36.0 42.2	6.1 5.1	42.1 47.3									
PA 6	36.8	10.7	47.5				38	5	43			
PBT	39.6	4.2	43.8				41.8	3.3	45.1			
PET				43.2	4.1	47.3	32.9	4.5	37.4	37.8	3.1	40.9
PAEK	36.0	3.8	39.8				36	3.8	39.8			
SAN	40.5 42.1	2.7 3.6	43.2 45.7									
PMMA	38.8 44.2	6.4 6.1	45.2 50.3	35.9	4.3	40.2						
PVC	37.7	7.5	45.2	40.0	1.5	41.5	36.5	1.6	38.1	36.0	3.9	39.9
PS	44.6	0.8	45.4	41.4	0.6	42.0						
PSU	42.1	4.2	46.3									
PES	42.1	5.1	47.2									
PPE	44.7 42.7	2.1 3.2	46.8 45.9									
PC							37.0	1.8	38.8			
TPU							35.2	3.8	39			
PFA							19.1	3.4	22.5			
PVB							36	4.7	40.7			

Table 4.9 Surface Energy of Various Polymeric Materials Calculated by the Method of Wu

Author	ERHARD [4.48]			WU [4.44]			POTENTE [4.46]		
Material	Surface energy in [mN/m]								
	γ^d	γ^p	γ	γ^d	γ^p	γ	γ^d	γ^p	γ
HDPE				35.0	0.7	35.7			
PP							25.8	1.3	27.1
POM	36.8	11.1	47.9						
PA 6	39.2	15.4	54.6				25.6	12.7	38.3
PBT	39.4	9.4	48.8						
SAN	39.5	7.7	47.2				27.1	4.0	31.1
PMMA	39.6	11.7	51.3	29.8	11.6	41.4	25.7	14.6	40.3
PVC	39.0	12.7	51.7				26.0	11.3	37.3
PS				33.8	6.9	40.7	23.3	5.7	29.0
PC							27.3	6.0	33.3

Table 4.10 Representative Average Surface Energy Values for Various Generic Polymeric Materials

Polymeric material	Surface energy in mN/m		
	γ^d	γ^p	γ
PTFE	18.5	0	18.5
HDPE	34.5	0.1	34.6
PS	41.4	0.6	42.0
PP	30.5	0.7	31.2
SAN	41.5	3.3	44.8
PAEK	36.0	3.8	39.8
PBT	39.6	4.2	43.8
PES	42.1	5.1	47.2
POM	36.0	6.1	42.1
PMMA	38.8	6.4	45.2
PVC	37.7	7.5	45.2
PA 6	36.8	10.7	47.5

The adhesion energy W_{ab} affords a direct measure of the effects of adhesive contacts between mated pairs of polymeric materials.

The surface energy of a metal sliding surface is determined by its surface layers, which differ quite markedly from those of polymeric materials; therefore, its measurement in the solid state has little value. Thus, no reliable value for adhesion energy can be determined for mated pairs involving metal surfaces. However, for a qualitative assessment it may be assumed that the surface energy of a metal surface is very high relative to that of most polymeric materials.

Consideration of adhesion leads to the expectation that under *adhesive conditions*, mated pairs of polymeric materials should give rise to low friction when at least one of the pair is a nonpolar polymeric material. In addition, there should be no wear induced by adhesion when adhesion forces are weaker than cohesion forces in one of the mating materials.

4.7.1.2 Deformation and Hysteresis Loss

Deformation at the tips of peaks in rough areas already occurs as the area of actual contact between two bodies is being established. Even when adhesive contact bridges are pulled apart, there are inevitably complex dynamic processes of deformation associated with hysteresis losses in molecular segments and domains as a result of this deformation.

In the case of contact between materials having very *different moduli of elasticity*, the tips of uneven peaks in rough areas of the harder material will penetrate into the surface of the softer material [4.40]. When the materials move relative to one another, a bulge like a bow wave will be produced ahead of each rough peak. As sliding continues, this frontal bow wave precedes the uneven peak and, at the same time, appears to be continuously swallowed up below it. As a result of this process, the material or its surface layers are subjected to a constantly shifting stress and work is done, *i.e.*, energy is lost.

These processes are illustrated by the model in Figure 4.30. The longitudinal section through a single uneven peak shows the alternating deformation of a volume element close to the surface during the passage of the tip of the peak.

Under *deformative conditions*, a mated pair involving a polymeric material should give rise to lower friction when the surface hardness or modulus of elasticity of the polymeric material is high, because the tip of the uneven peak will penetrate less deeply. Less wear is to be expected for materials with higher energy absorption capacity (toughness), because the alternating deformations are less likely to result in cracking and fracture phenomena.

4.7.1.3 Boundary Conditions for Adhesive and Deformative Sliding

When screening materials for friction applications, it is helpful to know at least approximately the conditions under which either adhesive sliding or deformative sliding will *predominate*. It may be assumed, for instance, that adhesive sliding will predominate when the surfaces of the paired materials are very smooth and the contact pressure is low. On the other hand, deformative friction mechanisms, as shown in Figure 4.30, become evident as contact pressure and surface roughness increase. This is particularly the case when polymeric materials are mated with rough metal surfaces.

The role of surface roughness is illustrated in principle in Figure 4.31. Here, the curves of adhesive friction and deformative friction are plotted against surface roughness to reflect the hypothesis given above. These results are based on experimental measurements. Experimental confirmation of the postulated relationships is provided in Section 4.7.2.1.

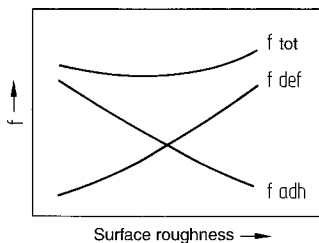


Figure 4.31 Schematic plot of adhesive and deformative components of the coefficient of sliding friction as a function of surface roughness [4.48]

A tried and tested remedy for steel/polymeric material pairs is to harden a steel sliding surface.

Abrasions between sliding surfaces can play an unforeseen role. However, abraded particles of a nonpolar polymeric material are generally more favorable for sliding than abraded particles of a polar polymeric material. This improved sliding effect can be seen in particular in the abrasion of PTFE. In this case, it is thought that material transfer takes place which renders the surface of steel more “nonpolar”.

4.7.2 Friction and Wear in Mated Polymer and Steel Surfaces

If the adhesion energy of a pair of materials cannot be determined (e.g., in combinations involving metals), the *adhesive sliding component* can be estimated at least qualitatively. It may be assumed that low-energy, nonpolar polymeric materials (e.g., PTFE, HDPE) will make only a small contribution to the adhesive component of friction under adhesive sliding conditions (smooth steel surface, low contact pressure). Conversely, the adhesive component will be high for more highly polar polymeric materials (e.g., POM, PVC, PA). Wear caused by adhesion is generally low compared with that caused by deformation.

In line with the model concept in Figure 4.30, the *deformative component* of friction is higher for polymeric materials having a lower surface hardness (or modulus of elasticity). When the material is soft, the sliding tips of peaks can penetrate deeper into the material and produce greater deformation. The degree of polymer wear to be expected under deformative sliding conditions is a function of the polymer's energy absorption capacity under this sliding stress. Deformation and fatigue processes in sliding, however, are extremely complex and it is, therefore, very difficult to reproduce and describe these by means of a material test.

Although a simple stress-strain test cannot measure the fatigue of a material, it may be assumed that the material is irreversibly damaged at the yield stress. Accordingly, energy absorption up to the yield point may serve as a very early indication of the wear resistance of a polymeric material.

For a polymeric material, the area under the stress-strain curve up to the yield point is a simple but representative measure of energy absorption and hence of its resistance to wear.

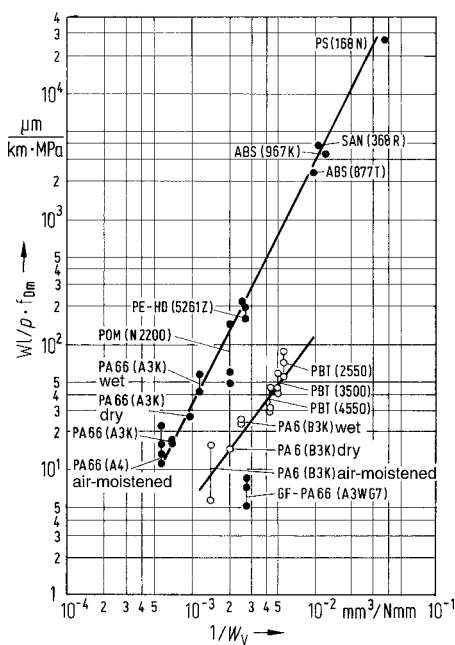


Figure 4.32 Rate of wear of different polymeric materials expressed as the product of the mean contact pressure and coefficient of friction of the mated pair. This is plotted as a function of the reciprocal of energy absorption capacity up to the yield point of the polymeric material in question.

- Strain rate = 0.02 min^{-1}
- Strain rate = 0.5 min^{-1}

Tribological system: pin-on-disk apparatus; $v = 0.5 \text{ m/s}$; technically dry; 23°C ; mated with: 100 Cr6 steel; R_z of steel sliding surface = $2.4 \mu\text{m}$ [4.48]

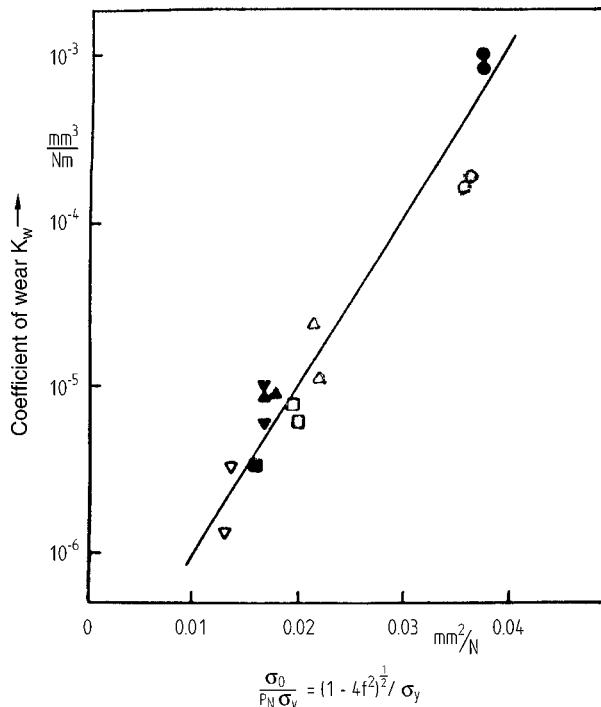


Figure 4.33 Wear characteristics of some thermoplastic polymeric materials under abrasive deformative conditions [4.50]

○ HDPE	△ PA 6	▽ PI	□ PBT
● PTFE	▲ POM	▼ PA 66T	■ PET

Figure 4.32 demonstrates this relationship for mated pairs involving either semi-crystalline or amorphous thermoplastics. This relationship does not hold up so well in the case of filled or reinforced polymeric materials, because their higher hardness evidently plays a greater role for these materials.

In [4.50], the assumption is made that there is a relationship between wear and the ratio of the stress in the sliding plane σ_0 .

$$\sigma_0 = p_N (1 + 4 f^2)^{\frac{1}{2}} \quad (4.25)$$

With this force-based approach a good correlation can be achieved (see Figure 4.33).

4.7.2.1 Effect of Steel Surface Roughness on Steel/Polymer Combinations

HDPE is a very low-energy polymeric material; it has a small polar surface energy component of $\gamma^P = 0.1 \text{ mN/m}$ and as a result is nonpolar. Under predominantly adhesive sliding conditions (*i.e.*, when mated with smooth steel surfaces), there are few possibilities for interactions in the

contact surface and these are weak. This explains the low measured coefficients of friction of $f_{Em} \leq 0.24^*$ for mean roughness heights of $R_z < 0.3 \mu\text{m}$ as shown in Figure 4.34. The rise in the coefficient of friction as R_z increases is most likely the result of an increase in deformative sliding energy. At contact pressures of $p = 8.8 \text{ MPa}$ (on the right in Figure 4.34), the coefficient of friction rises less steeply with R_z than at $p = 1 \text{ MPa}$ (on the left in Figure 4.34). At the higher pressure, powdery abraded material forms due to abrasion from the rough steel surface. It is thought that the powdery abraded material forms an intermediate lubricating layer.

Because for HDPE, the adhesive friction component is largely absent, the relationship $F_f \approx F_{def}$ applies to this soft, non-polar material.

The effect of the different friction mechanisms also emerges from the wear characteristics, depending on whether the mating surface is smooth or rough steel. In the smooth range, the weak adhesive bonds are easily broken again on sliding without the occurrence of much adhesive wear. In the rough range, the deformative sliding mechanism comes into operation, thereby explaining the higher rate of wear**.

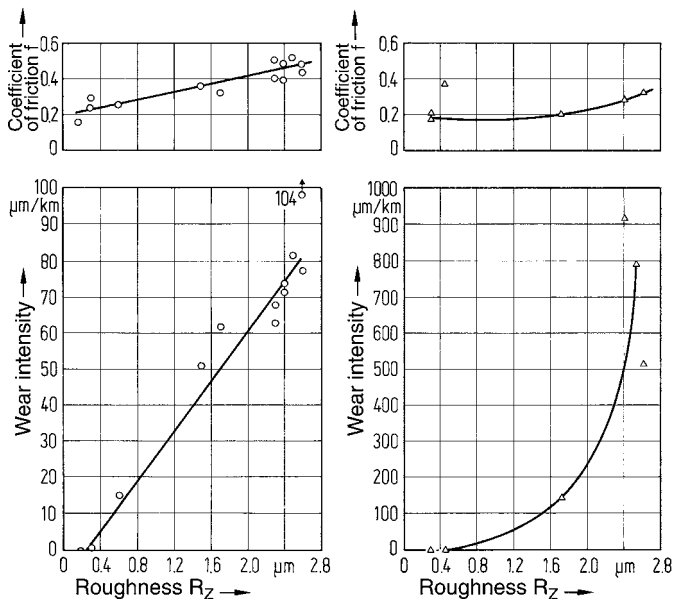


Figure 4.34 Plots of the coefficient of friction and rate of wear for the mated pairing of HDPE (5261 Z) with steel (100 Cr6) as a function of the roughness of the mating steel surface.
Experimental conditions: pin-on-disk apparatus, $v = 0.5 \text{ m/s}$, technically dry, 23°C .
Left $p = 1 \text{ MPa}$, right $p = 8.8 \text{ MPa}$ [4.48]

* The notation f_{Em} is used for the coefficient of friction when f is determined as a mean value in endurance tests after initial effects have subsided.

** For the test equipment used (pin-on-disk and ring-on-ring), the wear rate is given as the decrease in length of the test specimen in μm per km of slide path. The total slide path per measurement is at least 20 km . It is also usual to specify the coefficient of wear K_W as the volume of wear per unit force and unit slide path in mm^3/Nm .

In the case of POM, permanent dipoles act between the C-O groups of the individual macromolecules. The effects of these are revealed in the polar surface energy component of $\gamma^P = 6.1 \text{ mN/m}$. On friction contact, these molecular interactions result under adhesive sliding conditions ($R_z < 0.3 \mu\text{m}$) in relatively high friction losses and coefficients of friction of $f_{Em} = 0.5$ to 0.7 (see Figure 4.35).

As roughness increases, the adhesive sliding mechanism is less favored and the coefficient of friction falls to lower values. A simultaneous increase in the deformative sliding mechanism in direct proportion to R_z cannot be clearly identified from the shape of the curve. However, the increase in the rate of wear as R_z increases points unambiguously to the presence of a deformative component.

PA 66 is highly polar due to its ability to form hydrogen bonds. Accordingly, under predominantly adhesive sliding conditions (smooth steel surfaces and low pressure), high coefficients of friction of $f_{Em} = 0.5$ to 0.7 are measured, which decrease as expected as R_z increases (see Figure 4.36). Rougher surfaces result in less contact area and therefore less overall adhesion.

At $p = 1 \text{ MPa}$ there is only a weak indication of a minimum in the curve of the coefficient of friction. The low value of the deformative component is also evident from the wear, because the relatively low adhesive wear rate on a smooth steel surface remains almost constant over the range of R_z .

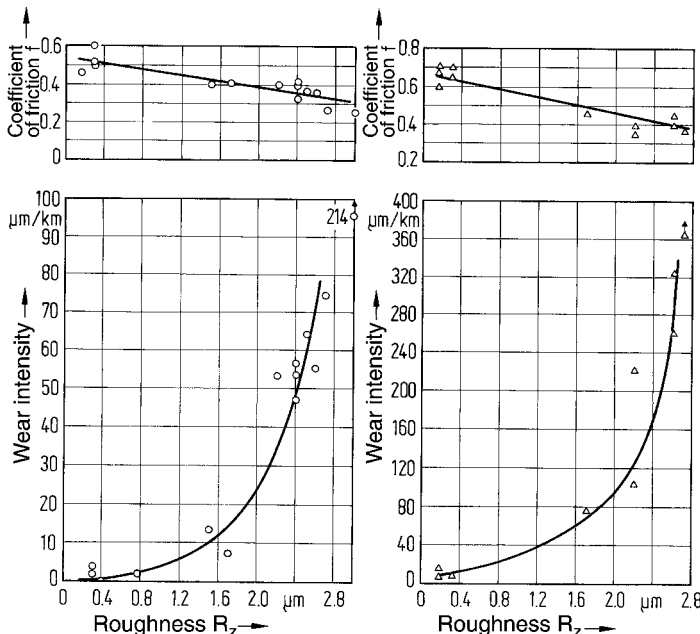


Figure 4.35 Plots of the coefficient of friction and rate of wear for the mated pairing of POM (N 2200) with steel (100 Cr6) as a function of the roughness of the mating steel surface.
Experimental conditions: pin-on-disk apparatus, $v = 0.5 \text{ m/s}$, technically dry, 23°C .
Left $p = 1 \text{ MPa}$, right $p = 8.8 \text{ MPa}$ [4.48]

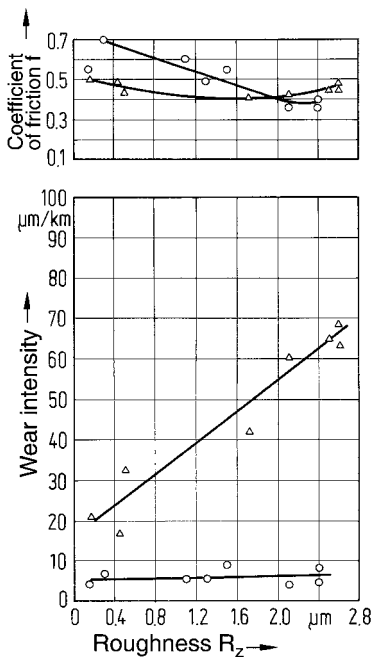


Figure 4.36 Plots of the coefficient of friction and rate of wear for the mated pairing of PA 66 (A4) with steel (100 Cr6) as a function of the roughness of the mating steel surface.
Experimental conditions: pin-on-disk apparatus, $p = 1 \text{ MPa}$ (\circ) 8.8 MPa (\triangle), $v = 0.5 \text{ m/s}$, technically dry, 23°C [4.48]

There is a minimum in the coefficient of friction curve generated at $p = 8.8 \text{ MPa}$. This indicates the superposition of the deformative sliding mechanism, which is confirmed by the increase in the rate of wear in direct proportion to R_z .

4.7.2.2 Effect of Relative Molecular Weight on Friction and Wear

A polymeric material's molecular weight can have a significant effect on wear properties under certain conditions. The coefficients of friction and rates of wear under different contact pressures are plotted for three grades of PBT having different relative molecular weights in Figure 4.37. Because surface energy values are very largely independent of the relative molecular weight, neither the coefficient of friction nor the rate of wear are dependent on the relative molecular weight as is expected under adhesive sliding conditions ($p = 1 \text{ MPa}$, $R_z = 0.3 \mu\text{m}$ on the left in Figure 4.37). Only as the contact pressure, and hence the deformative sliding mechanism, increases is there a significant decrease, especially in the rate of wear.

In the right-hand part of the figure, the corresponding values for mating with rough steel surfaces are plotted. Under these deformative sliding conditions the effect of the relative molecular weight becomes much more apparent, especially in wear resistance. This relationship also applies to thermoplastic polymeric materials.

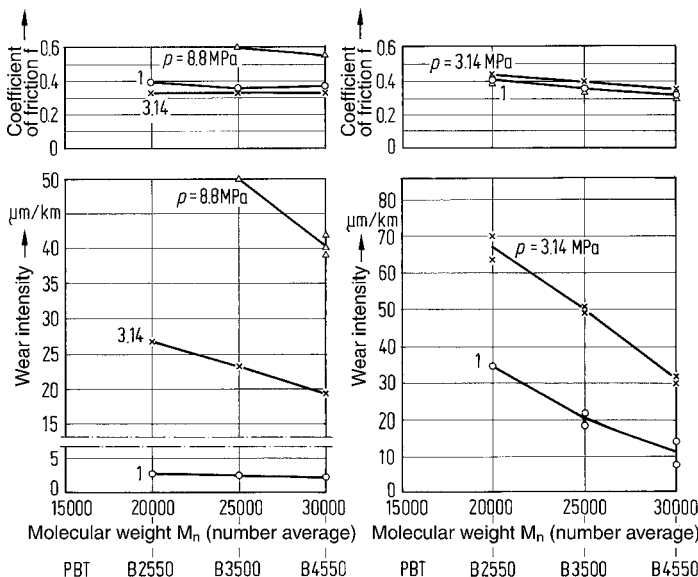


Figure 4.37 Coefficient of friction and rate of wear for three grades of PBT having different relative molecular weights

PBT B 2550: film grade

PBT B 3500: injection-molding grade

PBT B 4550: extrusion grade

Experimental conditions: pin-on-disk apparatus, $v = 0.5 \text{ m/s}$, technically dry, 23°C , mated with 100 Cr6 steel, $R_z = 0.3 \mu\text{m}$ on the left, $R_z = 2.4 \mu\text{m}$ on the right [4.48]

A higher relative molecular weight is synonymous with greater energy absorption capacity and hence lower wear rates.

4.7.2.3 Effect of the Moisture Content of Polyamides on Friction and Wear

As stated previously, moisture content can have a significant effect on the properties of a hygroscopic polymer. Figure 4.38 shows the effect of the presence of moisture in samples of a PA 66 on its tribological properties under deformative sliding conditions ($R_z = 2.4 \mu\text{m}$). Here, the minimum in the rate of wear (or total wear after a 20 km slide path) corresponds to the maximum energy absorption capacity over the range of moisture content (see Figure 4.39).

In the case of mating with rough steel surfaces, plasticization with water does not result in either a drastic lowering of the coefficient of friction or a corresponding reduction in wear. On the other hand, when mated with smooth steel surfaces ($R_z = 0.3 \mu\text{m}$) under otherwise identical conditions, the coefficient of friction decreases to $f \approx 0.05$ and the rate of wear to $< 0.1 \mu\text{m}/\text{km}$.

The stress-strain diagrams in Figure 4.39 show that “dry” PA 66 (moisture content < 0.1% by weight) exhibits brittle behavior, whereas “moist” PA 66 (moisture content of 1.6% by weight)

is distinctly tough and “wet” PA 66 (moisture content 8% by weight) is significantly more flexible. Thus, the energy absorption capacity (toughness) integrated over the range up to the yield point exhibits a pronounced maximum over the moisture content range.

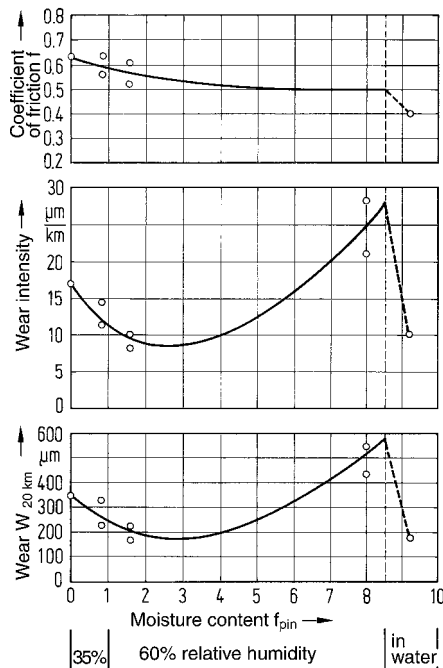


Figure 4.38 Coefficient of friction, rate of wear, and total wear after 20 km for PA 66 (A3K) as a function of moisture content.

Experimental conditions: pin-on-disk apparatus, $p = 1 \text{ MPa}$, $v = 0.5 \text{ m/s}$, 23°C , mated with 100 Cr6 steel, $R_z = 2.4 \mu\text{m}$ [4.48]

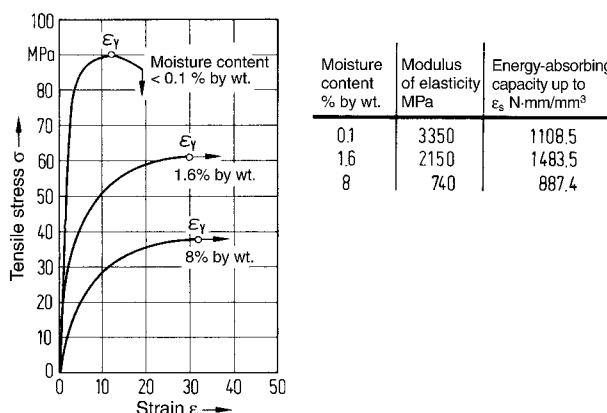


Figure 4.39 Stress-strain diagrams for PA 66 having different moisture contents; $23^\circ\text{C}/50\%$ RH test atmosphere

4.7.2.4 Effect of High-Energy Radiation

The microstructural changes that occur when a polymeric material is exposed to high-energy radiation include chain scission and cross-linking. The specific reactions will depend on the type of polymer and the conditions of exposure.

When oxygen is excluded during irradiation, the cross-linking process can dominate if the free radicals formed bond to one another. Depending on the degree of cross-linking, the polymer may exhibit rubber elastic to hard brittle properties.

When oxygen is present during irradiation, there can be a marked increase in degradation due to oxidation. The oxygen reacts with the free radicals formed, resulting in chain scission and a decrease in the relative molecular weight or a change in structure. At the macroscopic level this is reflected in a decline in mechanical properties, especially in toughness. Here, cross-linking may be strongly or completely suppressed.

In HDPE, high-energy radiation has the effect of cleaving C-H bonds, which results in cross-linking in parallel with the formation of vinylene double bonds. At higher radiation doses, cross-linking increases. This explains the mechanical behavior of irradiated HDPE as shown in Figure 4.40. The modulus of rigidity increases with the radiation dose above the melting point of the unirradiated HDPE.

The consequences of this change in mechanical performance (and microstructure) for friction properties are illustrated in Figure 4.41.

Under deformative sliding conditions (on the left), no significant effect on the coefficient of friction is evident, but there is a marked decrease in wear as cross-linking increases. On the right of the figure, friction and wear are plotted for smooth steel surfaces (adhesive sliding conditions). There is a significant increase in the coefficient of friction with radiation dose. The surface of the HDPE evidently becomes more polar after irradiation due to attachment of oxygen, this being supported by the plot of the loss factor $\tan \delta$. Wear, which is already quite low, decreases even further.

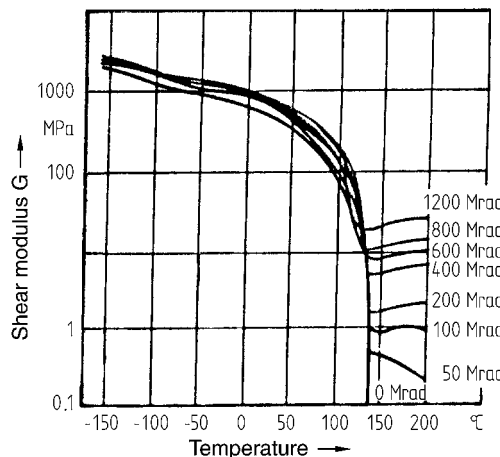


Figure 4.40 Plots of modulus of rigidity versus temperature for HDPE after exposure to different doses of electron beam radiation in the absence of oxygen [4.57]

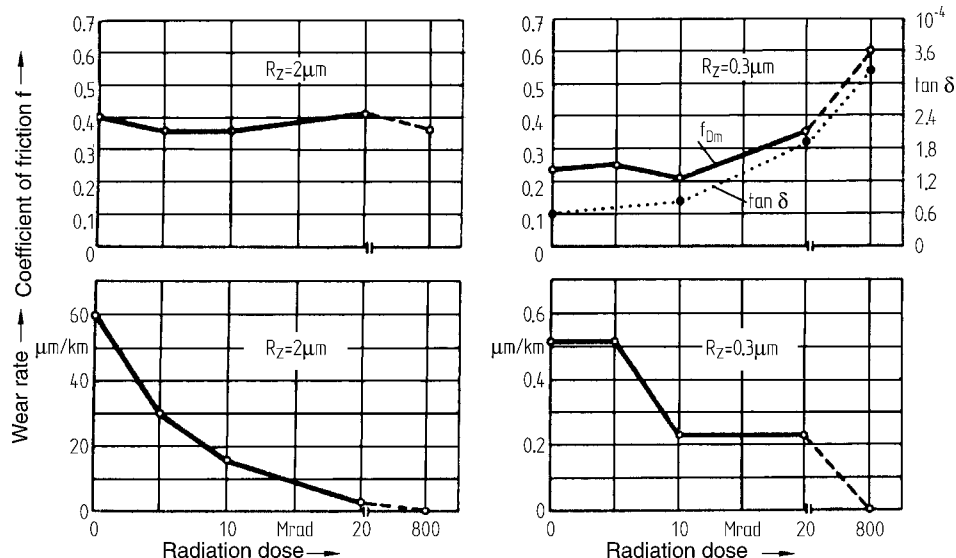


Figure 4.41 Coefficient of friction and rate of wear for HDPE (5261 Z) after irradiation with different doses of 2 MeV electrons

Tribological system: pin-on-disk apparatus

Mating surface: 100 Cr6 steel

Experimental conditions: $p = 1 \text{ MPa}$, $v = 0.5 \text{ m/s}$, 23°C , technically dry

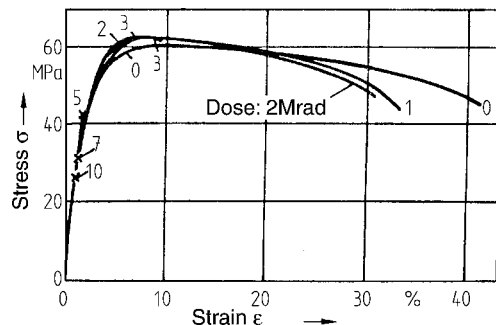


Figure 4.42 Stress-strain diagrams for POM after exposure to different doses of electron beam radiation; strain rate 0.5 min^{-1} [4.56]

Studies have also been conducted on irradiated POM. When POM is irradiated, both C-H bonds and C-O bonds are broken so that even in an inert environment the intramolecular oxygen allows for degradation reactions. The consequence of irradiation is a dramatic decrease in elongation and hence in toughness as may be seen in Figure 4.42.

Figure 4.43 shows the effects of irradiation on the tribological properties of POM. When mated either with smooth or with rough steel surfaces, the rate of wear increases dramatically due to chain degradation and the related material embrittlement.

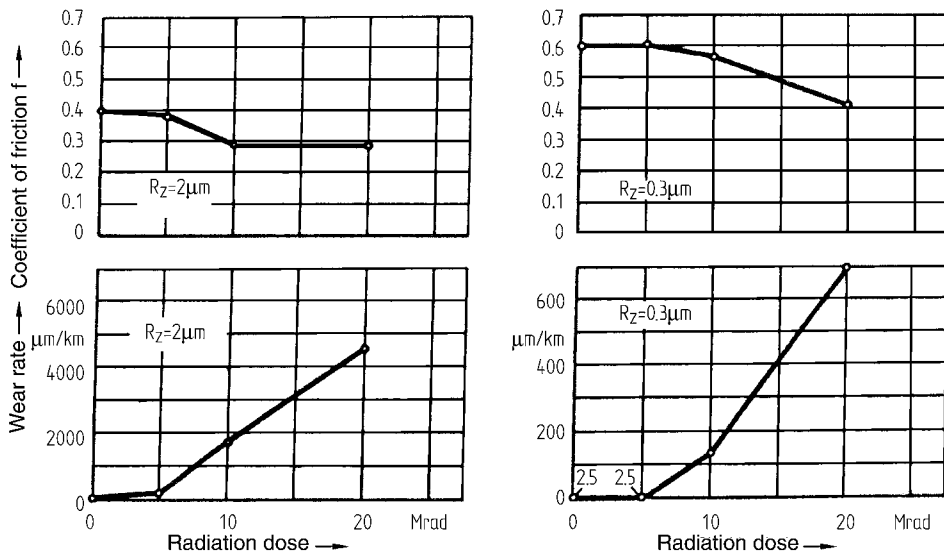


Figure 4.43 Coefficient of friction and rate of wear for POM (N 2200) after irradiation with different doses of 2 MeV electrons
 Mating surface: 100 Cr6 steel
 Experimental conditions: pin-on-disk apparatus, $p = 1 \text{ MPa}$, $v = 0.5 \text{ m/s}$, 23°C , technically dry, RT

4.7.2.5 Effect of Form and Sequence of Motion on Friction and Wear

The form and sequence of motion are parameters affecting the behavior of a system (see also Figure 4.29). Table 4.11 shows that under reversing and oscillating sliding motions PA, for example, exhibits a substantial increase in the rate of wear. Wear is generally reduced by adding reinforcing carbon fibers but its tendency to increase remains, if the matrix material is unchanged. In nonpolar ultrahigh molecular weight HDPE, a different type of behavior is found. Oscillatory wear turns out to be lower here than for uniform and reversing motion [4.51]. Whether this can really be explained on the basis of polarity or whether other factors are at work has not been adequately studied yet.

Table 4.11 Effects of Form and Sequence of Motion on the Rate of Wear

Material	Rate of wear in $\mu\text{m}/\text{km}$		
	Uniform motion	Reversing motion	Oscillatory motion
PA	9	100	120
PA-CF 20	4	12	14
UHMW HDPE	14	14	8

Uniform: $v = 0.5 \text{ m/s}$, $p = 1 \text{ MPa}$ (pin-on-disk)

Reversing: $x_s = \pm 4 \text{ mm}$, $f = 1 \text{ Hz}$, $p = 1 \text{ MPa}$

Oscillatory: $x_s = \pm 2 \text{ mm}$, $f = 10 \text{ Hz}$, $p = 1 \text{ MPa}$

Mating surface: 100 Cr6, 800 HV 10, $R_z = 3 \mu\text{m}$

4.7.3 Friction and Wear in Mated Pairs of Polymeric Materials

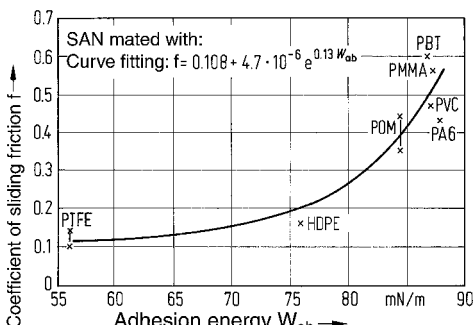
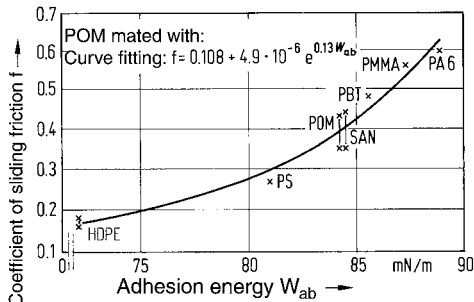
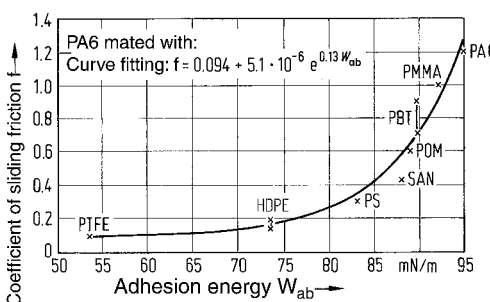
4.7.3.1 Sliding Friction

The results of friction experiments on various combinations of polymeric materials are presented in Figures 4.44 to 4.46. The plots of the coefficient of friction against adhesion energy (evaluated by the Owens and Wendt method) reveal a similar exponential relationship for all combinations of materials. As the adhesion energy rises, the coefficient of sliding friction rises steeply. The fitting functions specified in the figures provide a good approximation to the measured values in the individual cases.

These results of friction experiments on mated pairs of polymeric materials under predominantly adhesive sliding conditions substantiate the relationship established earlier between friction work (or the coefficient of friction) and the adhesion energy needed to separate the surfaces in contact.

Adhesion and hence the coefficient of friction is low when a nonpolar material provides one of the mating surfaces.

The observation that the coefficient of friction for a mated pair increases exponentially can be explained by the fact that if a high W_{ab} is needed to separate the adhesive contacts, the deformation of molecular domains also increases proportionately.



Figures 4.44–4.46
Coefficient of sliding friction f_{Em} as a function of adhesion energy W_{ab} for various mated pairs of polymeric materials
Tribological system: ring-on-ring apparatus
Experimental conditions: $p = 0.29$ MPa,
 $v = 0.12$ m/s, technically dry, 23 °C

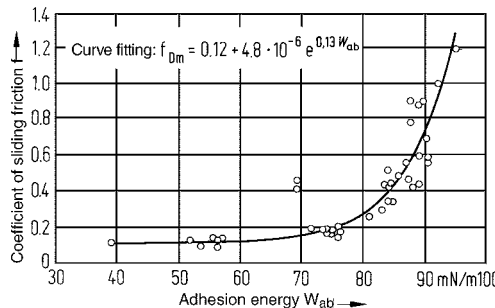


Figure 4.47 Coefficient of sliding friction f_{Em} as a function of the adhesion energy W_{ab} for various mated pairs of polymeric materials along with an empirically fitted curve

Figure 4.47 summarizes the findings from a large number of friction experiments and determinations of adhesion energy. Major deviations usually occur when wear is observed on both materials in the friction experiment. It is thought that abrasion particles in the sliding plane interfere with the assumed adhesive sliding mechanism.

4.7.3.2 Wear Due to Sliding Friction for Mated Polymeric Material Pairs

When considering abrasion in mated pairs of polymeric materials, it can be expected that the member of the pair having the higher cohesion (binding energy) will undergo less wear [4.47]. This is revealed unambiguously by Figure 4.48, in which POM undergoes less wear than HDPE,

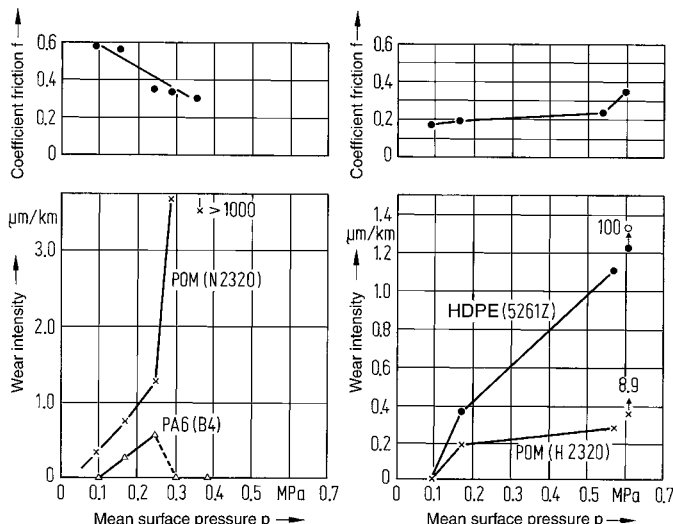


Figure 4.48 Coefficient of sliding friction and rate of wear for mated pairs composed of POM/PA 6 and POM/HDPE

Tribological system: ring-on-ring apparatus

Experimental conditions: $v = 0.12 \text{ m/s}$, technically dry, 23°C

but more than PA. Therefore, when choosing materials for a mated pair of polymeric materials, the component which is hardest to replace or has higher exposure to wear should be chosen from among the polar materials. A typical example of this is a mated pair for a gear system in which the (smaller) pinion is composed of PA and the (larger) wheel is composed of POM.

4.7.4.2 The Effects of Physical Properties on Friction and Wear System Properties

The discourse so far has shown that although friction and wear are system properties, the physical properties of the members of the system do indeed exert a certain influence on friction and wear. Table 4.12 shows in summary the direction in which some physical properties develop. Here, a distinction is made once again between adhesive and deformative sliding.

Table 4.12 Physical Properties and the Trend with which They Affect Friction and Wear in Mated Sliding Pairs of Polymeric Materials

System property	Adhesive component	Deformative component
Sliding friction	Intermolecular binding energies (polarity): • nonpolar ↘ • polar ↗ Adhesion energy: • high ↗ • low ↘	Modulus of elasticity (hardness): • high ↘ • low ↗
Wear due to sliding friction	Adhesion – cohesion: • Adhesion < cohesion ↘ • Adhesion > cohesion ↗	Modulus of elasticity (hardness): • high ↘ • low ↗ Fatigue resistance, energy absorption capacity (toughness): • high ↘ • low ↗

↗ Physical property magnifies the system property

↘ Physical property reduces the system property

4.7.5 Effect of Additives on Friction and Wear Properties

Additives, such as glass fibers, carbon fibers, graphite, molybdenum disulfide (MoS_2), chalk, metal powder, PTFE, or PE all have an effect on a polymeric material's tribological properties. In fact, they are commonly used to selectively alter friction and wear properties. The values given in the following figures have been determined in the laboratory and show trends of the direction in which additives alter these properties.

4.7.5.1 Effect of Fibers on Wear

Glass fibers are the most frequently used reinforcing material. They can bring about a distinct increase in the modulus of elasticity, strength, and hardness of the material. Carbon fibers lead to even greater stiffness and lubricating.

Table 4.12 shows that both tribological values are improved under deformative conditions when glass fibers are incorporated into the polymeric material. The reduced intensity of wear caused by glass or carbon fiber reinforcement (under a low contact pressure of $p = 1 \text{ MPa}$) is also clearly revealed in Figure 4.49.

Effect of Fiber Orientation

The effect of fiber orientation can be seen in Figure 4.50 depicting the example of a carbon-fiber reinforced PAEK (A 2000 C6). If the fibers are aligned perpendicular to the slide plane, the rate of wear is lower than when they are parallel or even at right angles to the sliding direction.

Wear of Steel Mating Surface for Reinforced Polymeric Material/Steel Pairing

Polar polymeric materials containing glass and carbon fibers tend to abrade steel mating surfaces under dry conditions and change the steel topography. Studies in the laboratory and under practical conditions yielded different and sometimes contradictory results. It was found, on the one hand, that an originally rough steel surface ($R_z = 2.0 \mu\text{m}$) mated with PA 66 GF 35 is rubbed smooth in the course of friction contact (see Figure 4.51). However, despite uniform samples taken from the same piece of semi-finished product, the same final values are not obtained. As expected, the rate of wear of the polymer decreases as the roughness of the steel is reduced.

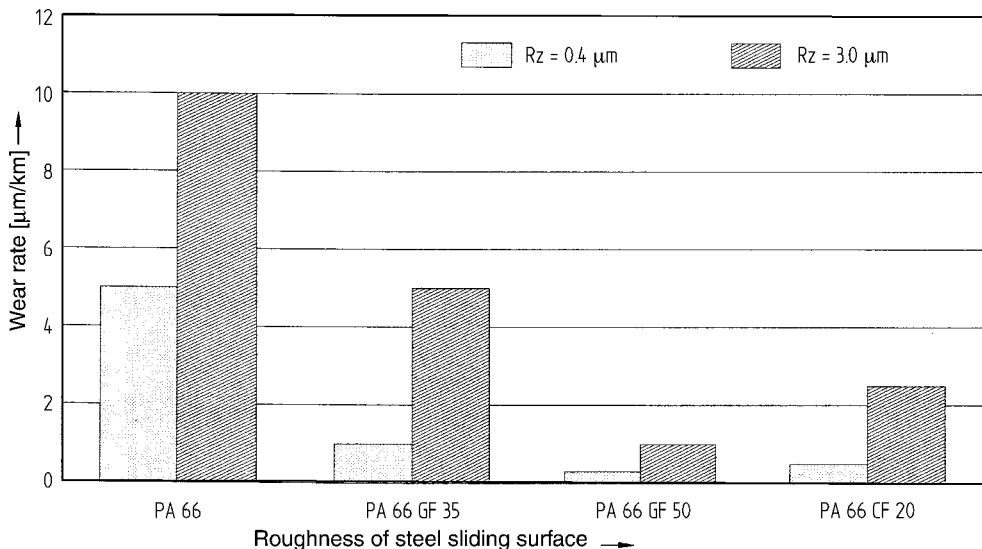
However, cases are also known in which hardened corrugated steel sheet mated with glass-fiber reinforced PA or mated even with unreinforced PA became furrowed after a few km of slide path.

Catastrophic wear occurs when polar, fiber-reinforced polymeric materials are paired with non-hardened steel.

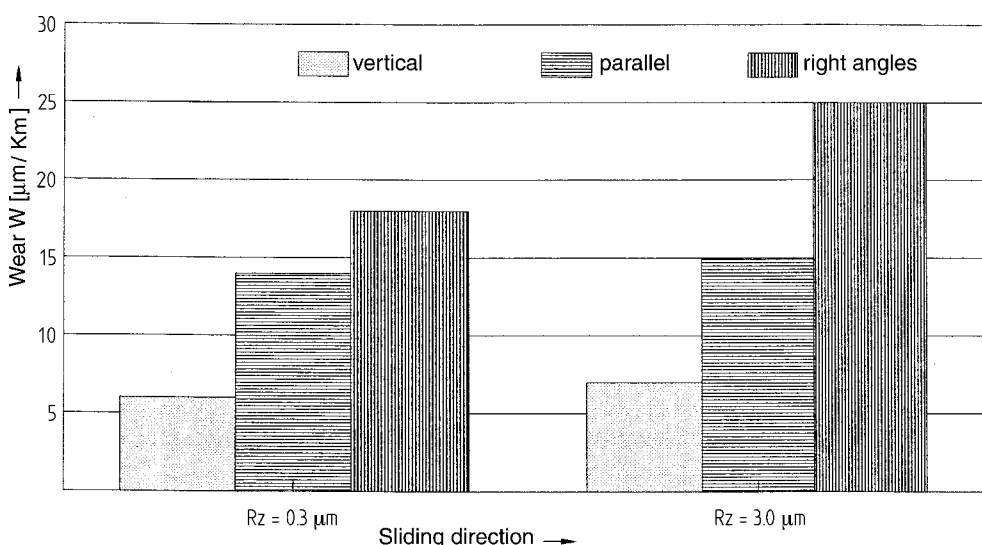
Figure 4.52 shows the test results for two journal bearings composed of glass-fiber reinforced PA 66 (50) mated with non-hardened (left) and hardened steel (right). In the left-hand part of the figure, the high wear on the steel journal and the rusty abraded particles can be clearly seen.

It is essential to harden the steel to approximately 700 HV 10 (HRc 60). Wear of the steel may also be reduced by external lubrication or incorporated lubrication by means of HDPE or PTFE additives.

Glass-fiber reinforced polymeric materials are suitable for high loads and low overall slide distance.

**Figure 4.49** Wear rate of glass-fiber and carbon-fiber reinforced PA 66

Tribological system: pin-on-disk

Mating surface: 100 Cr6 steel, 700 HV 10, $R_z = 0.4$ and $3.0 \mu\text{m}$ Experimental conditions: $p = 1 \text{ MPa}$, $v = 0.5 \text{ m/s}$, mean of 3 measurements, technically dry, RT**Figure 4.50** Effect of fiber orientation on the wear of PAEK CF 30

Tribological system: pin-on-disk

Mating surface: 100 Cr6 steel, 700 HV 10, $R_z = 0.3$ and $3.0 \mu\text{m}$ Experimental conditions: $p = 11 \text{ MPa}$, $v = 0.5 \text{ m/s}$, mean of 3 measurements, technically dry, 23 °C

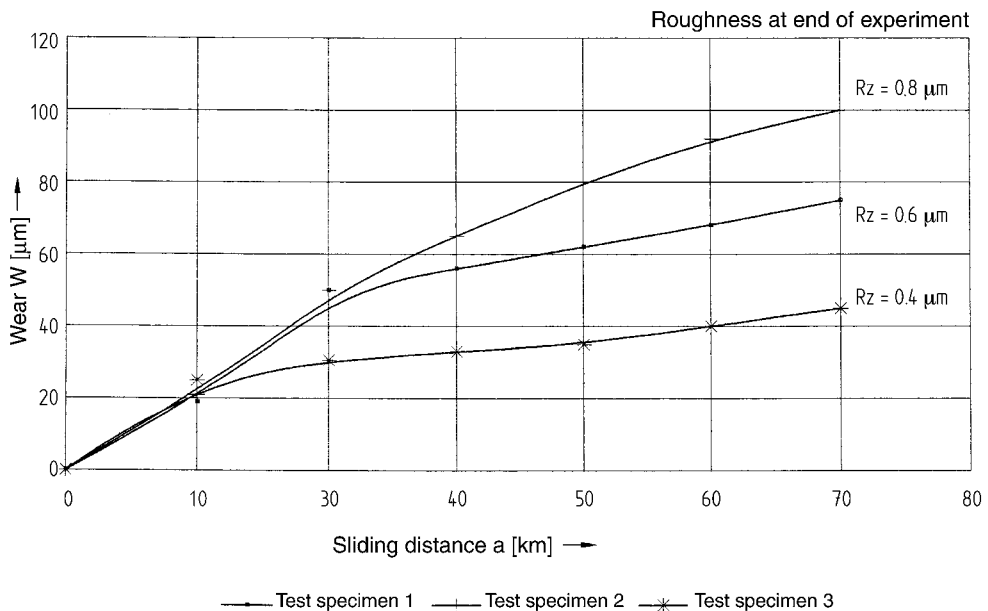


Figure 4.51 Reduction of wear due to smoothing of the surface of the steel
 Tribological system: disk-on-disk, steel (100 Cr6, 700 HV 10) mated with glass-fiber reinforced PA 66 (35)
 Experimental conditions: $p = 0.25 \text{ MPa}$, $v = 0.12 \text{ m/s}$, fibers predominantly perpendicular to the direction of sliding, technically dry, 23°C , initial roughness $R_z = 2.0 \mu\text{m}$

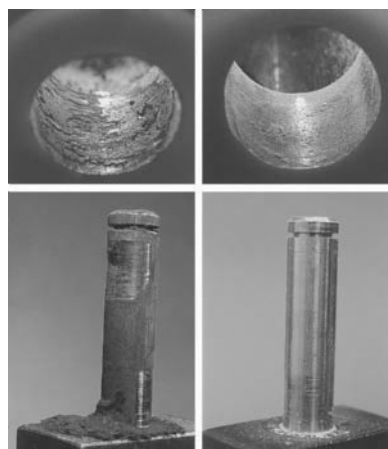


Figure 4.52 Test bearings under dynamic load – steel and glass-fiber reinforced PA 66 (50)
 Experimental conditions: $p_{\min} = 0.1 \text{ MPa}$, $p_{\max} = 2.0 \text{ MPa}$, pivot angle $\pm 30^\circ$, at 15 load cycles per min after 600,000 load cycles
 Bearing bush (top of figure): glass-fiber reinforced PA 66 (50)
 Journal: 200 HV 10 steel (left), 800 HV 10 steel (right)

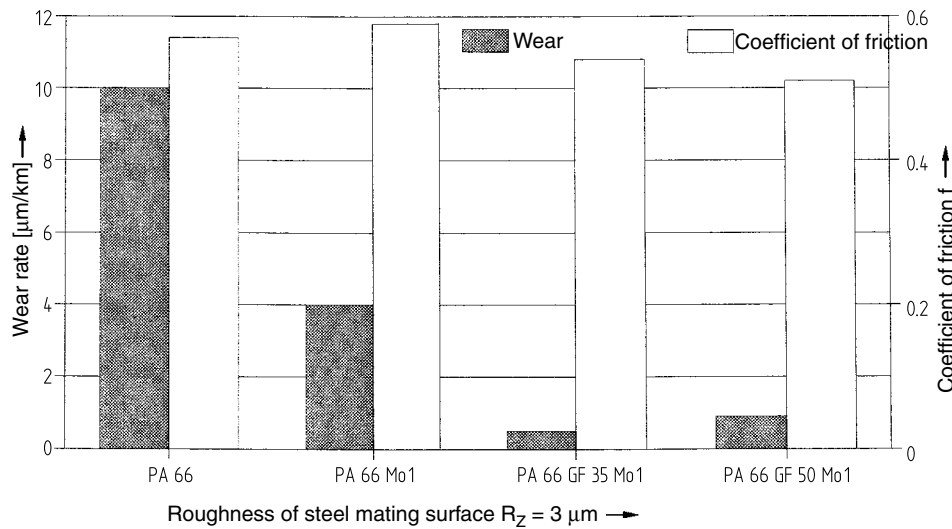


Figure 4.53 Effect of MoS_2 on friction and wear in PA 66
 Tribological system: pin-on-disk
 Mating surface: 100 Cr6 steel, 700 HV 10, $R_z = 3.0 \mu\text{m}$
 Experimental conditions: $p = 1 \text{ MPa}$, $v = 0.5 \text{ m/s}$, technically dry, RT;
 $\text{Mo1} = 1\%$ of molybdenum sulfide (MoS_2)

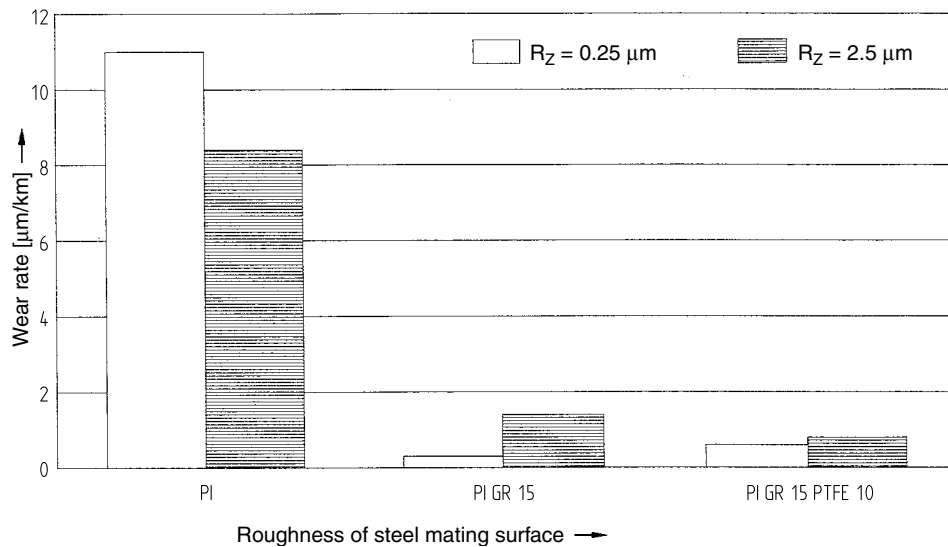


Figure 4.54 Effect of various fillers on the wear of polyimide
 Tribological system: pin-on-disk
 Mating surface: 100 Cr6 steel, 700 HV 10
 Experimental conditions: $p = 3.14 \text{ MPa}$, $v = 0.1 \text{ m/s}$, technically dry, 23 °C
 Graphite reinforcement 15 = 15% graphite
 PTFE 10 = 10% polytetrafluoroethylene

4.7.5.2 Effect of Other Inorganic Additives

Fillers, especially lubricious fillers, have a positive effect on sliding properties for polymeric materials. They increase the modulus of elasticity in compression and surface hardness – and hence their deformative sliding properties are enhanced. The combination of polymeric material and fibers with graphite or MoS₂ also yields good tribological properties. In such combinations, the graphite and MoS₂ do not actually function as lubricants because they are tightly bound in the polymer matrix. However, the abraded material has a better lubricating effect than that of the unfilled matrix material or when it is filled only with fibers. This is shown in Figure 4.53. While MoS₂ reduces wear considerably, it has only a small effect on the coefficient of friction.

A similar relationship may be seen in Figure 4.54 for polyimide as the matrix material. Here, the wear of an unfilled PI is compared with that for a PI containing 15% graphite and one containing 15% graphite plus 10% PTFE. The wear reduction is significant when the additives are used. Although there is somewhat higher wear in the material filled with PTFE under adhesive conditions, which is counterintuitive, the overall wear is extremely low.

4.7.5.3 Effect of Polymeric Additives

The recognition that (1) nonpolar materials make a useful contribution to adhesive sliding but have little resistance to wear under deformative conditions, and (2) that polar materials behave in exactly the opposite way, results in combinations of both types of material in one formulation. This is referred to as *incorporated lubrication*.

These lubricant materials are generally mixtures composed of a coherent polar matrix and up to 20% non-polar lubricating additive (e.g., PTFE or HDPE). Mixtures based on PAEK or PI yield particularly good results.

Wear and the coefficient of friction can also be lowered using lubricant additives of low molecular weight, but this is most effective only under adhesive conditions (see Figure 4.55, $R_z = 0.4 \mu\text{m}$). The effect is not observed with rough steel mating surfaces. However, this form of incorporated lubrication appears to have a perceptible effect only in relatively highly crystalline polymeric materials (e.g., POM).

In the case of PTFE additives, on the other hand, the “lubricant effect” is also observed when paired with rough surfaces. This is evidently due to transfer of PTFE to the steel surface and in the end, to smoothing of the surface.

Even more diverse properties are obtained using mixtures of three or more components (see also Figures 4.49 and 4.50). In these cases, the underlying idea is to reduce adhesion by means of nonpolar substances and at the same time to modify the deformative component by increasing hardness. Wear-inducing, fiber-reinforced lubricant sliding materials should, to the extent possible, also contain some non-polar polymeric additive (10 to 20% of PTFE or PE) in order to keep wear low, especially on steel mating surfaces. Although these mixed materials often produce no major reduction in the coefficient of friction, they can bring about a distinct improvement in wear.

Figure 4.56 illustrates the example of PAEK and how wear can be significantly reduced by adding graphite and PTFE. Values for unfilled PA 66 and fiber-reinforced PA 66 are also plotted for comparison.

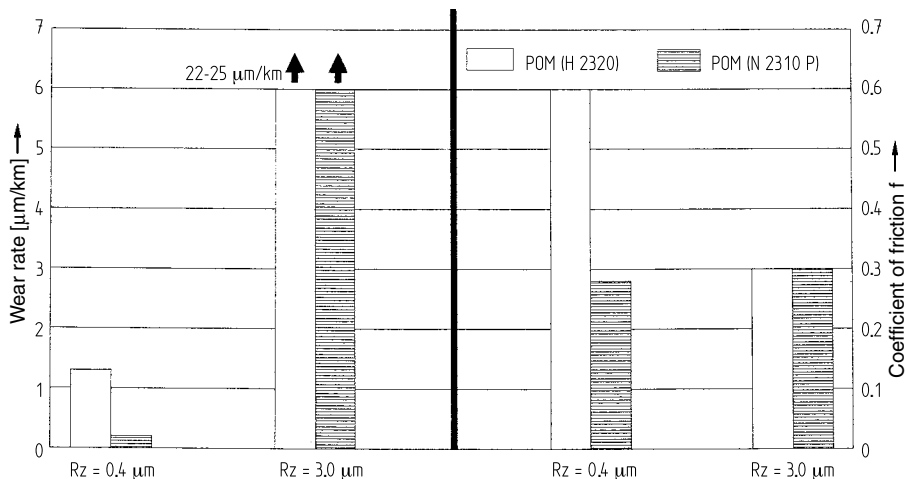


Figure 4.55 Friction and wear in POM (H 2320) and in slip-modified POM (N 2310 P) containing a low molecular weight lubricant (stearate ester)
Tribological system: pin-on-disk
Mating surface: 100 Cr6 steel, 700 HV 10
Experimental conditions: $p = 1 \text{ MPa}$, $v = 0.5 \text{ m/s}$, technically dry, 23°C

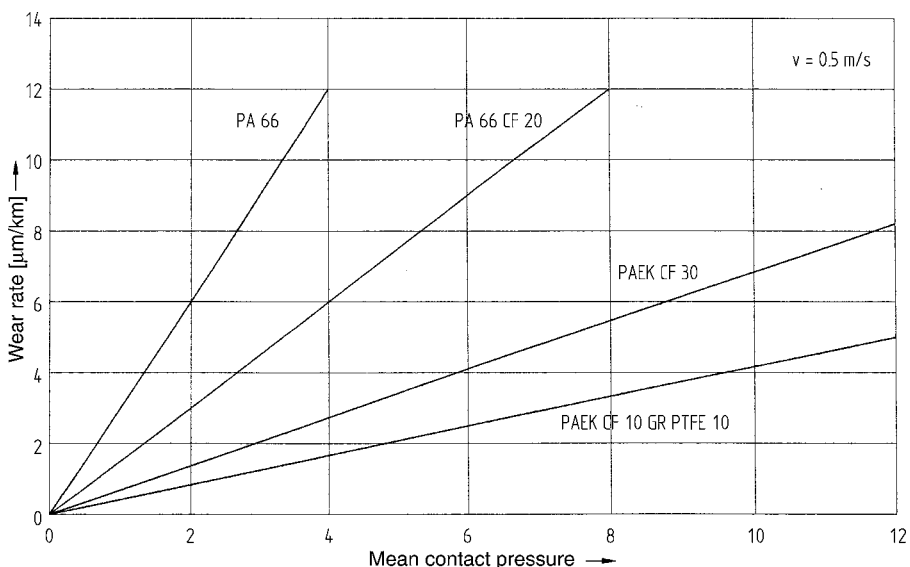


Figure 4.56 Rate of wear as a function of the mean contact pressure for carbon-fiber reinforced PAEK (CF 30) and a four-component lubricant material based on PAEK containing 10% each of carbon fibers, graphite and PTFE. Reinforced and unreinforced PA 66 are plotted for comparison.
Tribological system: pin-on-disk
Mating surface: 100 Cr6 steel, 700 HV 10, $R_z = 3 \mu\text{m}$
Experimental conditions: $v = 0.5 \text{ m/s}$, technically dry, 23°C

4.7.6 Stick-Slip

Stick-slip is a special feature of sliding. It occurs because the coefficient of friction may not remain constant during the course of motion. It is a dynamic process in which adhesion, tensioning, separation, and restoration of linked surfaces or parts of surfaces damped by one another occurs in rapid succession. Depending on the system parameters, the system is excited into oscillation, which may result in audible emissions from a resonating participating surface in the form of whistling, squeaking, or grating noises*.

A simple spring-and-weight system provides a model for understanding the stick-slip processes [4.52]. A body on a level base is acted upon by an elastic force. When the elastic force exceeds the adhesive friction force F_0 , the body starts to move. It slides when the coefficient of friction becomes smaller at the speed of sliding, faster than the spring so that the latter slackens. When the expended elastic energy is consumed by the sliding work, the body comes to a relative standstill. It sticks again, the spring is tensioned once again and the process starts over. The plot of elastic force versus time shown in Figure 4.57 is characteristic of this stick-slip behavior.

Starting at a certain threshold velocity v_{thresh} , the bodies no longer come to rest relative to one another and continuous sliding sets in. Assuming the mass of the body is m , the spring constant c , the instantaneous elastic force F , the coefficient of friction f , and the velocity of propulsion v , the following equilibrium relationship is obtained:

$$m \ddot{x} + c x = (F_0 - F) + c v t = F_N \cdot \Delta f + c v t \quad (4.26)$$

Provided that the slip velocity is greater than zero, integration yields the limiting value for the velocity of propulsion at which stick-slip no longer occurs.

$$v_{\text{limit}} \geq \frac{F_N \cdot \Delta f}{\sqrt{c \cdot m}} \quad (4.27)$$

It is more useful to describe the stick-slip properties of polymers by means of a model in which spring-damper elements are arranged in parallel or in series. These provide a better

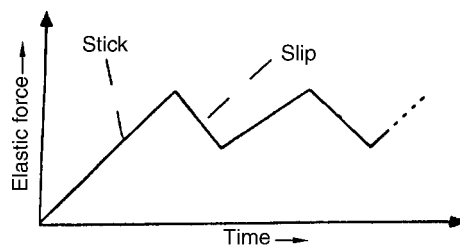


Figure 4.57 Schematic plot of elastic forces versus time

* The generation of such noise is not limited to pairs of sliding surfaces involving polymeric materials. The creaking of a door, the screech of chalk on a board or of brakes, the squeaking of windscreens wipers, and many other noises are caused by the stick-slip effect. The production of sound on stringed instruments is also the result of cyclical changes in friction between the string and bow.

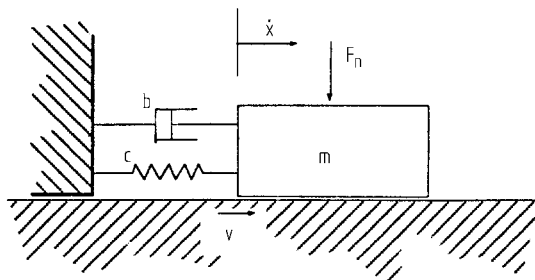


Figure 4.58 Model of sliding, including a Voigt-Kelvin element for describing visco-elastic behavior

representation of the visco-elastic behavior. The system can be illustrated by a Voigt-Kelvin element as sketched in Figure 4.58. The differential equation of motion for this model is:

$$m \ddot{x} + b \dot{x} + c x = F_R \quad (4.28)$$

The parameters b and c are not only variables characteristic of the material but also *characteristic system variables*, which each apply only to a specific oscillatory system and cannot be arbitrarily transferred to others.

These considerations make it clear that the entire system must be taken into account when evaluating noise emissions induced by stick-slip.

Although the system is excited by the restorative sequence of movements by the mated slipping surfaces, the response to these excitations depends on the resonance properties of the total system.

4.7.6.1 Changing Stick-Slip Behavior by Modifying the Parameters of the Sliding System

Slip Velocity

The plot of the coefficient of friction against slip velocity has a characteristic shape. In the low velocity range, the gradient is negative and becomes positive starting at the limiting velocity v_{limit} . The limiting velocity is dependent on the system. Stick-slip occurs in the range of negative gradients. Therefore, reversing and oscillating sequences of movement are particularly critical.

These velocity relationships in a pin-on-disk apparatus are reproduced in Figure 4.59 for four polymeric materials. The steeper the gradient and the higher the initial value of the coefficient of friction, the more susceptible the system is to stick-slip. In the case of HDPE (Figure 4.59 bottom), no noises are heard in the lower velocity range.

Magnitude of the Coefficient of Friction

Sliding conditions causing high coefficients of friction (approx. $f > 0.4$) are evidently more conducive to stick-slip than mated pairs having a low coefficient of friction (approx. $f < 0.25$).

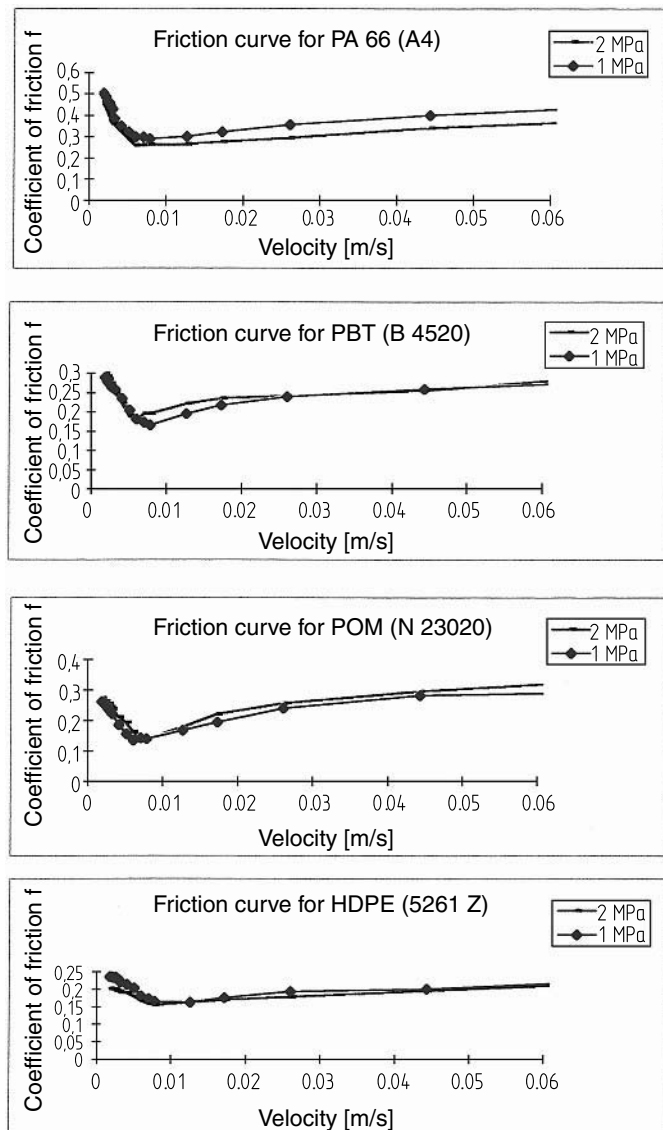


Figure 4.59 Coefficient of friction as a function of velocity
 Tribological system: pin-on-disk
 Mating surface: 100 Cr6 steel, 700 HV 10, $R_z = 0.4 \mu\text{m}$
 Experimental conditions: technically dry, 23 °C [4.52]

Therefore, lubrication of a slip point is the most effective countermeasure. However, on the material side, a sufficiently low coefficient of friction and sliding free of stick-slip is usually achieved using nonpolar materials such as PTFE or HDPE as the sliding material or in the form of an incorporated component.

Contact Pressure

The effect of contact pressure on stick-slip behavior is not fully understood. It appears that the tendency to stick-slip decreases at higher contact pressures so that for the same external load, a reduction of the area of the sliding surface would be advisable. However, this would likely result in increased wear, which increases in an approximately linear manner with pressure.

Roughness of Steel Sliding Surface

Polar materials paired with very smooth steel surfaces ($R_z < 0.5 \mu\text{m}$) are susceptible to stick-slip, because under these conditions high coefficients of friction (as a precondition for stick-slip) are to be expected. Therefore, very smooth steel surfaces should be avoided. However, if surfaces are very rough, the problem of higher wear arises once again.

Acoustics of the Entire System

If excitation to oscillation cannot be prevented at the point of origin, that is, in the mating surface, it may be possible to dampen the ability of the entire system to resonate, e.g., by changing its rigidity in such a way that troublesome noise emissions are suppressed. As an example, a Stradivarius violin will not resonate if it is filled with cement.

4.7.7 Jet Erosion

Granular particles entrained in streams of air or liquid cause wear of components exposed to such streams. The amount of wear depends on:

- The nature of the particles, their size, hardness, shape, and concentration
- The carrier medium
- The angle of impact and the velocity
- The material of the component exposed to the stream

As the duration of exposure increases, characteristic erosion cavities form on the impact surface. This is illustrated in Figure 4.60. The rate of wear is lower at stage c than at stages a and b.

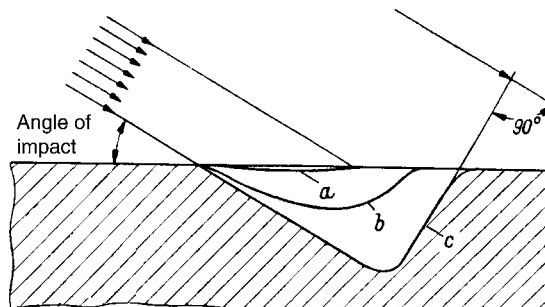


Figure 4.60 Characteristic shape of cavities formed by jet erosion showing the three stages of wear [4.58]

The modulus of elasticity is generally regarded as the primary variable for ranking wear resistance. Materials having a modulus of elasticity ranging from 5,000 to 50,000 MPa are least resistant to wear, while materials having a lower modulus of elasticity, especially elastomers, prove to be resistant to wear. Steels, on the other hand, having a very high modulus of elasticity are also resistant to wear (see Figure 4.61).

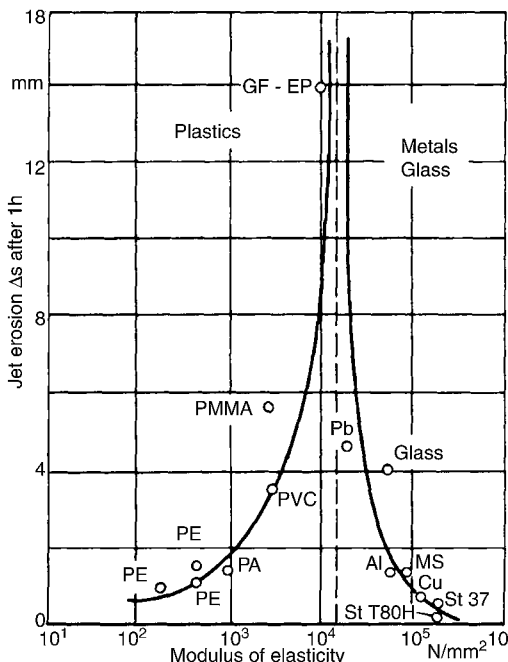


Figure 4.61 Relationship between jet erosion and modulus of elasticity [4.58]

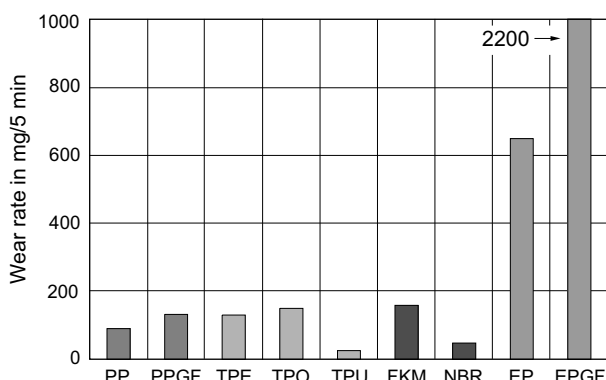


Figure 4.62 Rates of wear of various polymeric materials exposed to jet erosion

Jet material: sharp-edged corundum

Particle size: 60 to 120 µm

Velocity: 70 m/s [4.59]

More recent studies confirm these findings in principle. Figure 4.62 also shows that elastomeric materials with a low modulus of elasticity are significantly more resistant to jet erosion wear than thermosets.

Figure 4.63 reveals a similar picture for selected other materials under different wear conditions. Both illustrations are useful for selecting materials for jet wear applications.

The dependence of wear on the angle of impact shown in Figure 4.64 for ductile and brittle materials is also worthy of note. While the ductile materials exhibit little variation with the angle of impact, the brittle materials show a marked dependence on the angle of impact.

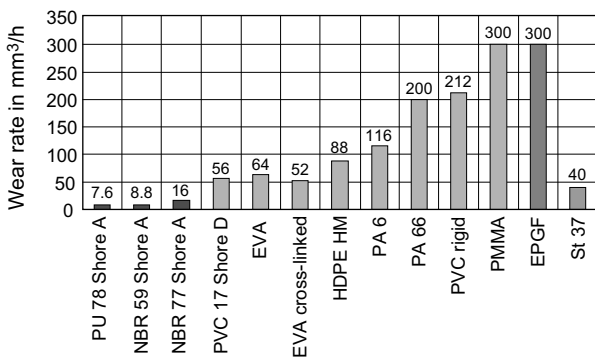


Figure 4.63 Rates of wear of various polymeric materials exposed to jet erosion

Jet material: sharp-edged steel grit

Particle size: approx. 750 μm

Velocity: 40 m/s [4.59]

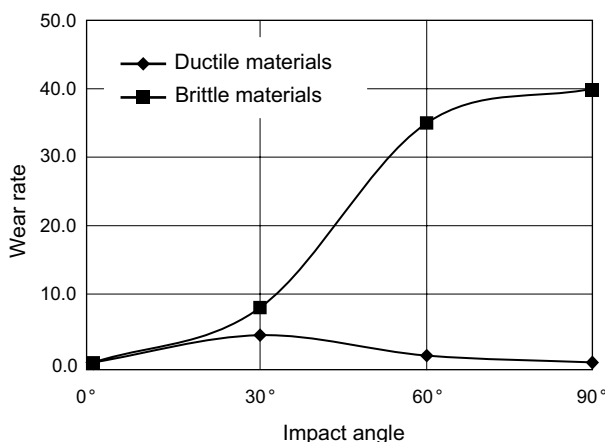


Figure 4.64 Schematic illustration of rate of wear as a function of impact angle [4.59]

References

- [4.1] KARGIN V. A. and YU TSAREVSKAYA I.: Deformation of Crystalline Polybutylene, *Polymer Science (USSR)* **9**, 1967, pp. 289/322
- [4.2] INGRAM P., KIHO H. and PETERLIN A.: The Morphology of Fibers from Deformed Polymer Crystals, *Journ. of Polymer Science, Part C* **16** (1967), pp. 1857/1868
- [4.3] KAMBOUR, R. P.: Die Rolle des Crazing beim Bruchmechanismus von glasartigen Polymeren (The Role of Crazing in the Failure Mechanism of Vitreous Polymers), *Z. Werkstoffe und Korrosion* **18** (1967) 5, pp. 393/400
- [4.4] ISO/DIS 10350: 1992 Kunststoffe – Ermittlung und Darstellung vergleichbarer Kennwerte – Einpunktswerte (Plastics – Determination and Presentation of Comparable Properties Data – Single Point Data)
- [4.5] ISO/DIS 11403: 1992 Kunststoffe – Ermittlung und Darstellung vergleichbarer Kennwerte – Vielpunktswerte (Plastics – Determination and Presentation of Comparable Properties Data – Multipoint Data)
- [4.6] ISO/527: Bestimmung der Zugeigenschaften Teil 1: Allgemeine Grundlagen, Teil 2: Prüfbedingungen für Form- und Extrusionsmassen (Determination of Tensile Properties, Part 1: General Principles, Part 2: Test Conditions for Molding and Extrusion Compounds)
- [4.7] WARD, J. M.: Mechanical Properties of Solid Polymers, John Wiley, New York 1983
- [4.8] SCHLIMMER, M.: Werkstoffanstrengung bei zeitabhängiger Spannungs-Verformungs-Beziehung (Material Strain in a Time-Dependent Stress-Deformation Relationship), *Z. Werkstofftechnik* (1977) 8, pp. 130/139
- [4.9] DÖLL, W. and L. KÖNCZÖL: Bruchmechanische Kurzzeitmessungen zur Bestimmung der Langzeiftfestigkeit (Short-Term Mechanical Failure Measurements for Determining Long-Term Strength), *Kunststoffe* **70** (1980), 9, pp. 563/567
- [4.10] KNAUSS W. G. and J. EMRI: Pressure Induced Ageing of Polymers, *Polymer Engineering and Science* Mid-January 1987, Vol. 27
- [4.11] FINDLEY W. N., J. S. LAI and K. ONARAN: Creep and Relaxation of Nonlinear Viscoelastic Materials, North-Holland, 1976
- [4.12] ROSKOTHEN H. J. and H. F. SÜSSMANN: Zum Spannungs-Deformationsverhalten von Kunststoffen im Feststoffbereich (On the Stress-strain Properties of Plastics in the Solid State), *VDI-Fortschrittsberichte, Series 5, No. 38*, 1978
- [4.13] RETTING, W.: Das mechanische Verhalten von Thermoplasten bei mittlerer und hoher Deformation bis zum Bruch (Mechanical Properties of Thermoplastics at Medium and High Levels of Deformation up to Failure), *Rheologica Acta* Vol. **8** (1969), 3, pp. 259/267
- [4.14] AUMER, B.: Einführung in die Handhabung des Rechners (Introduction to Computing), VDI Seminar "Berechnen von Kunststoff-Formteilen (Computation of Plastic Moldings)" 1987
- [4.15] ISO 899 (DIN 53 444: Prüfung von Kunststoffen Zeitstand-Zugversuch(Testing Plastics, Tensile Creep Test), Beuth Verlag, Berlin 1990
- [4.17] LEWIN, G. and T. WAGNER: Analyse von Beschreibungsmöglichkeiten des Spannungs-Verformungs-Verhaltens von Thermoplasten (Analysis of Methods for Describing the Stress-Strain Properties of Thermoplastics), *Wis. Z. d. TH Otto von Guericke Magdeburg* **23** (1979) 2, pp. 159/166
- [4.18] EHRENSTEIN, G. W. and G. ERHARD: Konstruieren mit Polymerwerkstoffen (Designing with Polymeric Materials), Hanser-Verlag, Munich Vienna 1983
- [4.19] BURGERS, J. M.: First Report in Viscosity and Plasticity, Academy of Science at Amsterdam 3 (1935)
- [4.20] FINDLEY, W. N.: Creep and Stress Relaxation of Plastics, Pergamon Press 1958

- [4.21] MÜLLER, D., SCHMITT, D. and W. SCHNEIDER: Untersuchung des Verhaltens von Kunststoffen bei langzeitiger, statischer Beanspruchung (Study of the Behavior of Plastics under Long-Term Static Loads), *Materialprüfung* **23** (1983) 12, pp. 581/585
- [4.22] EHRENSTEIN, G. W. and B. SARABI: Numerische Auswertung der Kriechversuche zur Ermittlung von Bemessungskennwerten, Schlussbericht zum AIF-Forschungsvorhaben 4934 (Quantitative Evaluation of Creep Tests for Determining Dimensioning Data, Final Report of AIF Research Project 4934) (1983)
- [4.23] ERHARD, G.: Assessing long-term behaviour, *Plastics & Rubber No.* **953** Sept. 4, 1982, p. 12
- [4.24] SARABI, B.: Das Anstrengungsverhalten von Polymerwerkstoffen infolge ein- und zweiachsigem Kriechens (The Strain Behavior of Polymeric Materials as a Result of Uniaxial and Biaxial Creep), Hanser-Verlag, Munich Vienna 1984
- [4.25] BASF-Werkstoffblätter (BASF Materials Sheets) published by BASF, Ludwigshafen
- [4.26] ERHARD, G. and E. STRICKLE: Maschinenelemente aus thermoplastischen Kunststoffen (Machine Components Made from Thermoplastics), VDI-Verlag, Düsseldorf, 2nd ed. 1986
- [4.27] HECKEL, K.: Einführung in die technische Anwendung der Bruchmechanik (Introduction to the Technical Applications of Failure Mechanics), Hanser-Verlag, Munich Vienna 1970
- [4.28] KAUSCH, H. H.: Polymer Fracture, Springer-Verlag, Berlin 1978
- [4.29] DÖLL, W.: Kinetics of creep tip zone before and during fracture, *Polymer Eng. Sci.* **24** (1984), pp. 798/808
- [4.30] KERKHOF, F.: Anwendung der Bruchmechanik auf Hochpolymere (Application of Failure Mechanics to High Polymers), *Kolloid Z. and Z. für Polymere* **251** (1973) 8, pp. 545/553
- [4.31] BARDENHEIER, R.: Schallemissionsuntersuchungen an polymeren Werkstoffen (Noise Emission Studies on Polymeric Materials), *Z. Werkstofftechn.* **11** (1980), pp. 41/46 and 101/110
- [4.32] BARDENHEIER, R., J. WOLTERS and G. MENNING: Schallemissionsuntersuchungen zum Einfluß des Verbundaufbaus auf Schädigungsvorgänge bei verstärktem Polycarbonat (Noise Emission Studies of the Effect of Composite Structure on Degradation Processes in Reinforced Polycarbonate), *Kunststoffe* **73** (1983) 4, pp. 208/214
- [4.33] RENZ, R.: Zum zügigen und zyklischen Verformungsverhalten polymerer Hartschaumstoffe (On the Dynamic and Cyclical Deformation Behavior of Rigid Foam Materials), Diss. Uni Karlsruhe 1977
- [4.34] v. BERNSTORFF, B., R. RENZ and V. ALTSTÄDT: Neuere Untersuchungen zur Schwingfestigkeit von SMC-Werkstoffen (Recent Studies on the Resistance to Vibration of SMC Materials), 20. AVK-Tagung (20th AVK Conference) 1985, pp. 15-1/15-8
- [4.35] RENZ, R., V. ALTSTÄDT and G. W. EHRENSTEIN: Schwingfestigkeitsverhalten von faserverstärkten Kunststoffen (SMC), Faserverbundwerkstoffe Bd. III (Vibration-Resistant Behavior of Fiber-Reinforced Plastics (SMC), Fiber Composite Materials Vol. III), Springer-Verlag, Berlin 1986
- [4.36] EHRENSTEIN, G. W. et al.: Hysteresis-Meßverfahren für die dynamische Werkstoffprüfung (Hysteresis Measurement Method for Dynamic Materials Testing), Conference Proceedings, March 5, 1987, Ed.: Prof. Dr.-Ing. G. W. Ehrenstein, Institut für Werkstofftechnik – Universität (GH) Kassel (Institute of Materials Technology, University of Kassel)
- [4.37] JANZEN, W. and G. W. EHRENSTEIN: Bemessungsgrenzen von glasfaserverstärktem PBT bei schwingender Beanspruchung (Sizing Limits of Glass-Fiber Reinforced PBT under Cyclical Loads), *Kunststoffe* **81** (1991), 3, pp. 231/236
- [4.38] CZICHOS, H.: The principles of system analysis and their application to tribology, *ASLE Trans.* **17** (1974), pp. 300/306
- [4.39] BOWDEN, F. P. and D. TABOR: Reibung und Schmierung fester Körper (Friction and Lubrication of Solid Bodies), Springer-Verlag, Berlin 1959

- [4.40] KRAGELSKI, I. W.: Reibung und Verschleiß (Friction and Wear), Hanser-Verlag, Munich Vienna 1971
- [4.41] RABINOWICZ, E.: Friction and wear of Materials, John Wiley, New York 1965
- [4.42] TANAKA, K.: A review of recent studies on polymer friction and wear in Japan, Proceedings of Intern. Solid Lubrication Symp., Tokyo 1975, pp. 57/66
- [4.43] OWENS, D. K. and R. C. WENDT: Estimation of the Surface Free Energy of Polymers, *Journal of Applied Polymer Science* 1969, **Vol. 13**, pp. 1741/1747
- [4.44] WU, S.: Polar and Nonpolar Interactions in Adhesion, *J. Adhesion* 1973, Vol. 5, pp. 39/55
- [4.45] RABEL, W.: Einige Aspekte der Benetzungstheorie und ihre Anwendung auf die Untersuchung und Veränderung der Oberflächeneigenschaften von Polymeren (Some Aspects of Wetting Theory and their Application to Investigating and Changing the Surface Properties of Polymers), *Farbe und Lack* 77 (1971) 10, pp. 997/1006
- [4.46] POTENTE, H. and R. KRÜGER: Bedeutung polarer und disperser Oberflächenspannungsanteile von Plastomeren und Beschichtungsstoffen für die Haftfestigkeit von Verbundsystemen (Significance of Polar and Disperse Surface Tension Components in Plastomers and Coating Materials for the Bonding Strength of Composite Systems), *Farbe und Lack* 84 (1978) 2, pp. 72/75
- [4.47] ERHARD, G.: Sliding Friction Behaviour of Polymer-Polymer Material Combinations, *Wear* 84 (1983), pp. 167/181
- [4.48] ERHARD, G.: Zum Reibungs- und Verschleißverhalten von Polymerwerkstoffen (On the Friction and Wear Properties of Polymeric Materials), Diss. Uni Karlsruhe 1980
- [4.49] KOERNER, G., G. ROSSMY and G. SÄNGER: Oberflächen und Grenzflächen (Surfaces and Boundary Surfaces), *Goldschmidt-Hauszeitschrift* 2/1974, **No. 29**, pp. 2/41
- [4.50] SANTNER, E. and H. CZICHOS: Tribology of Polymers, *Tribology International* Apr. 89, **Vol. 22**, No 2, pp. 103/109
- [4.51] BERRINGER, H.-P., G. HEINKE and E. STRICKLE: Lösung tribotechnischer Probleme mit Hilfe von Polymerwerkstoffen (Solution of Tribological Problems with the Aid of Polymeric Materials), *Mat.-Wiss. u. Werkstofftechnik* 22 (1991), pp. 168/173
- [4.52] URBANSKY, E.: Untersuchungen von Einflußgrößen auf Stick – Slip induzierte Schwingungen bei Gleitpaarungen mit Polymerwerkstoffen (Studies of Variables Influencing Stick-Slip-Induced Oscillations in Mated Pairs Involving Polymeric Materials), Diploma thesis, University of Karlsruhe, Nov. 1996
- [4.53] FRANK, U.: Die Querkontraktionszahl von Kunststoffen, dargestellt am Beispiel amorpher Thermoplaste (Poisson's Ratio in Plastics Illustrated with Reference to the Example of Amorphous Thermoplastics), Diss. Uni Stuttgart 1984
- [4.54] PEREPECHKO, I. I. and GOLUP, P. D.: Viscoelastic Parameters of Certain Polymers, *Mekhanika polimerov* (1973) 4, pp. 604/609
- [4.55] EHRENSTEIN, G. W.: Mit Kunststoffen konstruieren (Designing with Plastics), Carl Hanser Verlag, Munich Vienna 1995
- [4.56] KNAPPE, W. AND A. ZYBALL: Strahlenbeständigkeit von Polyoximethylen (Resistance of Polyoxy-methylene to Radiation), *Kunststoffe* 63 (1973) 8, pp. 536/539
- [4.57] HEINZE, D.: Das Verhalten von Hochpolymeren gegenüber energiereicher Strahlung (Behavior of High Polymers on Exposure to High-Energy Radiation), *Kolloid-Zeitschrift* 210 (1966), pp. 45/54
- [4.58] BRAUER, H. and E. KRIEGEL: Untersuchungen über den Verschleiß von Kunststoffen und Metallen (Studies of Wear in Plastics and Metals), *Chem. Ing. Technik* 36 (1963) No. 10, pp. 697/701
- [4.59] Moos, E. et al.: Verschleiß bestimmen (Determining Wear), *Kunststoffe* 91 (2001) 4, pp. 113/115

5 Calculations for Structures under Mechanical Load – Examples of Geometrically Simple Structural Parts under Static Loads

5.1 Specific Materials and Processing Problems

The mechanical properties of polymeric materials, especially those of thermoplastics, depend to a much greater extent on temperature, time, and on the magnitude and nature of an applied load than those of metals. In addition, many environmental effects, such as UV radiation or exposure to certain chemicals, play a significant role in aging and related changes in properties. This can be difficult to quantify in strength-related calculations. The conditions used in processing (e.g., injection molding process) can have an effect on the properties of the finished product.

Because the strength of most polymeric materials is an order of magnitude less than that of metals, components made from these materials may be highly stressed even under relatively low loads. On the other hand, a component made from a polymeric material is more likely to be rendered unusable by a high degree of deformation than by catastrophic failure due to fracture (in the case of ductile polymeric materials). The modulus of elasticity of these materials differs by as much as two orders of magnitude. The complexity of deformation behavior, however, leads to the expectation that deformation can only be calculated precisely with the aid of computer support and that the empirical determination of physical properties for this purpose will be very costly. There are, however, a limited number of design tasks for which such extensive design work is necessary. Not all designers have the extensive knowledge required to optimize structural elements with the aid of FEM. This task is best performed by an engineer who specializes in computer aided finite element structural design. However, there are a large number of applications where routine structural design calculations can be done by the average designer to help determine optimum part geometry. These are carried out using justifiable simplifications [5.2]. Knowledge of some specific properties of polymers is needed for this purpose.

5.1.1 Deformation Behavior under Uniaxial Dynamic Tensile Stress

The deformation of polymeric materials under the action of an external force, can be described by three components, which to some extent are superimposed, but at the same time predominate in certain ranges of deformation (see also Section 4.1).

Linear elastic, spontaneously reversible deformation is restricted in most polymeric materials to a total strain range of less than one tenth of one percent. This marks the end of the range of applicability of Hooke's law of elasticity for many polymeric materials. Most strains observed

in practice exceed this range. In many unreinforced thermoplastics, it is not even possible to demonstrate (by way of stress-strain experiments) the existence of a range in which Hooke's law is obeyed.

As strain increases, visco-elastic deformation processes appear. These are said to fall into the *linear visco-elastic range* when the laws of linear visco-elasticity apply. This range is characterized in that two strains ε_1 and ε_2 may be added when the corresponding stresses σ_1 and σ_2 are superposed (Boltzmann's law of superposition).

$$\begin{array}{rcl} \sigma_1 & \Rightarrow & \varepsilon_1 \\ \sigma_2 & \Rightarrow & \varepsilon_2 \\ \hline \sigma_1 + \sigma_2 & = & \varepsilon_1 + \varepsilon_2 \end{array} \quad (5.1)$$

In isochronous stress-strain diagrams, this range is marked by the end of the straight-line rise of the isochrones. This range also ends for most polymeric materials at stresses which cause strains of 0.5 to 1%. As strain increases further, the relationship of stress to strain no longer depends only on time (and of course on temperature), but rather on the applied stress itself. The deformation processes become increasingly nonlinear and also irreversibly (or partially irreversibly) viscous.

These deformation phenomena found at the macroscopic level are characterized by the molecular deformation and damage mechanisms occurring in the material (see also Chapter 4).

In some applications, thermoplastic polymeric materials are subjected to loads which take them into the nonlinear stress-strain range. As a result, calculations based on the laws of elasticity inevitably yield results which diverge to a greater or lesser extent from actual behavior. As long as the stresses are at least close to the linear viscoelastic range, the formulae of the theory of elasticity afford a satisfactory degree of accuracy. Therefore, their use is certainly justifiable and may indeed be essential, based on time available and on economic grounds.

In addition, the calculation of structural elements made from polymeric materials is rendered more difficult and uncertain due to the fact that the condition of a homogeneous, isotropic continuum is not fulfilled. Here, the different types of anisotropy should be taken into account whenever possible (*i.e.*, when anisotropic data is available). The causes of these may lie in the material itself (reinforcement by unidimensional fibers, for instance) or be due to processing. Examples of the latter include residual molecular alignments and internal stresses imposed during the molding operation (see also Chapters 2 and 7).

Internal stresses can be caused by impediments to shrinkage in macroscopic domains. A number of primary causes of internal stress may be distinguished. Cooling internal stresses are the result of different rates of cooling over the cross section of the molding. Holding-pressure related internal stresses are due to the holding pressure acting in the interior of the molding in the injection molding process when the outer contours have already solidified. Embedding internal stresses arise from shrinkage impeded by the shape of the molding due, for example, to metal inserts or due to the constraints imposed by the shape of the mold itself. Secondary internal stresses are also known. These include structural internal stresses brought about by curing reactions (in thermosets) or crystallization (in semi-crystalline thermoplastics). Embedding internal stresses can be produced, for example, by the incorporation of fillers.

Cooling internal stresses give rise to compressive stresses on the surface of the molding. These compressive internal stresses can have a positive effect in the event of tensile loads in the outer zone (e.g., during bending). On the other hand, excessive holding pressure causes compressive internal stresses in the interior of the molding and tensile internal stresses in the outer zone. These are superimposed on the cooling internal stresses so that when the holding pressure is high enough, tensile internal stresses may also be apparent on the surface of the molding. These internal stress states, which are also very difficult to describe quantitatively, represent a further uncertainty factor in calculations of strength.

5.2 Determination of Strength

5.2.1 Basic Procedure for Structural Part Design

The basic procedure for structural part design is given in Figure 5.1. An analysis of stress provides information about the magnitude and nature of the stresses at work in the theoretical cross section in question. Multiaxial states of stress are transformed using suitable failure criteria into a uniaxial reference stress having the same effect which is compared with the permissible level of stress. The latter is obtained from a characteristic property value specific to the material being considered for the application (e.g., tensile yield strength etc.). This property value is further reduced by an appropriate safety factor and any applicable reduction factors.

According to this analysis, the fundamental equation for determining strength may be written down as:

$$\sigma_{v \max} \leq \sigma_{\text{perm}} = \frac{K}{S \cdot A} \quad (5.2)$$

where

$\sigma_{v \max}$ = maximum stress occurring in section being analyzed

K = characteristic strength property of the material

S = safety factor

A = material-specific reducing factor

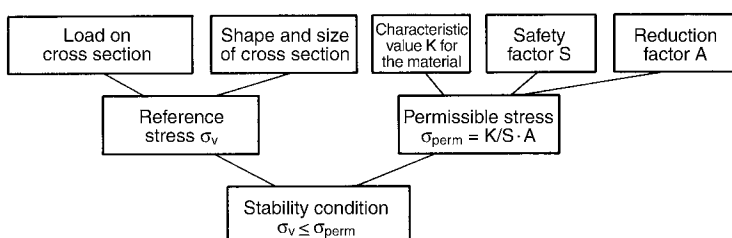


Figure 5.1 Basic procedure for structural part design [5.1]

5.2.1.1 Characteristic Strength

A number of different (material specific) strength parameters can be used for structural design, depending on the specific material behavior.

Figure 5.2 shows the most important failure characteristics.

Materials exhibiting largely brittle failure (see Figure 5.2a, corresponding to type A in Table 4.1) or having a distinct yield point (see Figure 5.2b, corresponding to types B and C in Table 4.1) have a clear-cut characteristic value that can be used as a “failure stress”. This is more difficult to define when there are no such prominent features in the stress-strain behavior, as is the case for many thermoplastics, especially at elevated temperatures. In these cases, a stress is proposed that causes a deformation or strain of a certain magnitude (0.5% offset has proved to be useful) in the nonlinear range (see Figure 5.2c, corresponding to type D in Table 4.1). In amorphous (transparent) polymeric materials, craze zones form when a certain damage stress is exceeded. Although in the initial stages these craze zones (see also Figure 4.2) are still capable of bearing loads, macroscopic cracks form in the course of further strain. This craze limit stress (onset of crazing) can be used as the failure value if available (see Figure 5.2d). Knit or weld line strength may be the limiting factor for structural parts containing weld lines (especially for reinforced thermoplastics).

In the case of sustained static loads, the creep strength is selected as the failure value (see Figure 5.3a) or the value σ^* in Section 4.2.1.

Under dynamic loads, the characteristic failure value is correspondingly obtained from the Wöhler curve or the Smith diagram (see Figures 5.3b and c). Alternatively, a limiting value as shown in Table 4.3 or a load-cycle-dependent rigidity value (see Figure 4.20) is introduced.

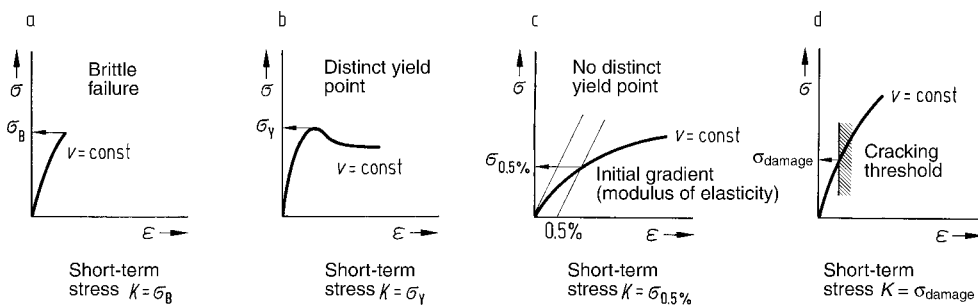


Figure 5.2 Some common short-term stress values that may be suitable as “failure stress” values [5.1]

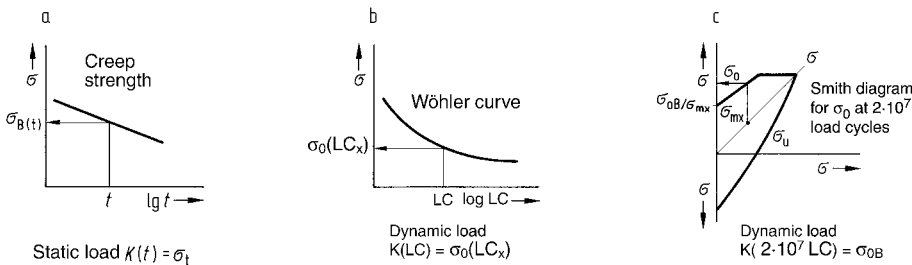


Figure 5.3 Common dimensioning characteristics for long-term loads

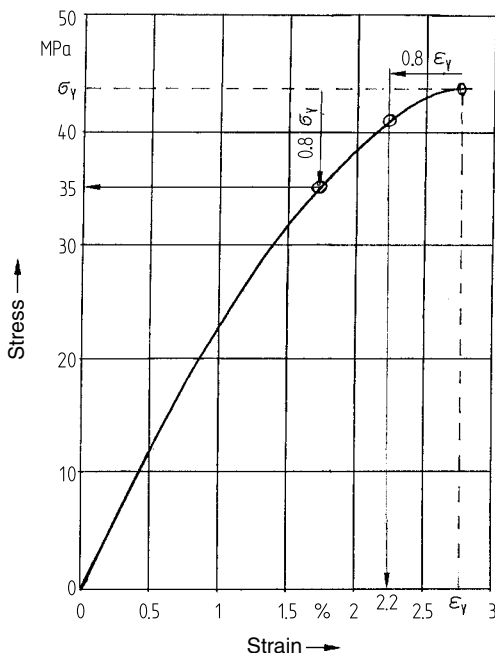


Figure 5.4 A percentage safety interval in a strain-based analysis affords a permissible value different from that in a stress-based analysis for materials that exhibit non-linear stress-strain behavior

Of course, in determining characteristic failure values, the high temperature-dependence of thermoplastics must be taken into account. Here, heat may arise as an external effect or be generated by friction or damping. This situation generates problems in determining and using characteristic values for dynamic failure. This is especially true if long-term aging is a significant factor.

In many cases (e.g., in snap-fit connections), strain-based structural design is more appropriate than stress-based designs. Design calculations are done on the basis of a limiting strain that must not be exceeded. It should be noted that in cases of nonlinear deformation behavior, there is a difference between operating, for example, at 80% of the yield *strain* and operating at 80% of the yield *stress*. Different values are obtained as depicted in Figure 5.4.

In [4.18] Oberbach proposes that permissible stress values be determined using a type of nomograph. The nomograph makes a distinction between short-term, long-term, and dynamic stresses; short-term stress being subdivided into single and multiple loading. A distinction is also made between ductile semi-crystalline, brittle amorphous, and glass-fiber reinforced thermoplastics. The procedure is illustrated in Figure 5.5.

The nature of the load and the group into which the material falls lead to an A-factor on the right ordinate of the left-hand part of the figure (in the example, single loading/glass-fiber reinforced thermoplastic = 0.68). The breaking load (in the example $\sigma_B = 144$ MPa) is multiplied by this factor to obtain the design stress at room temperature. The ordinate of the stress-strain diagram on the right-hand part of the figure is divided into fractions of the

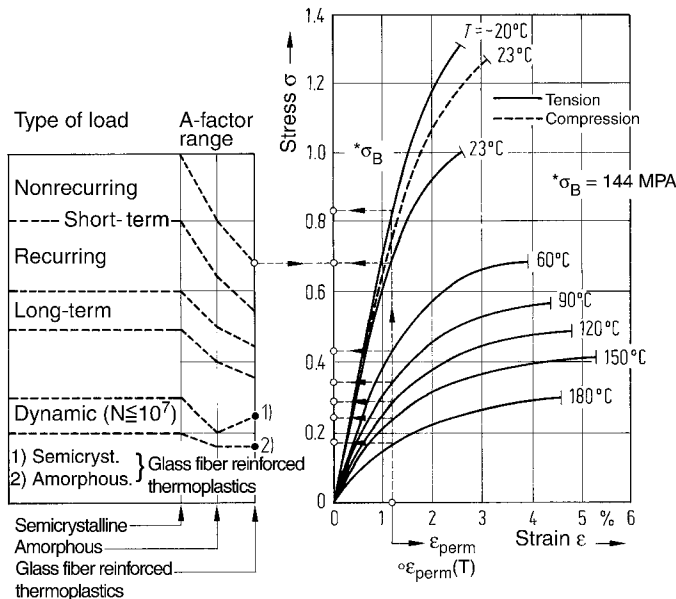


Figure 5.5 Estimation of permissible stresses and strains for a glass-fiber reinforced PBT (30% by weight)

breaking load at 23 °C. From the isotherms a permissible strain value can be determined at the requisite temperature for the design stress determined in this way (in the example $\varepsilon_{perm} = 1.2\%$). While keeping this strain value constant, the A-factor at any other temperature can now be determined at the point of intersection with the corresponding isotherm. This allows the calculation of the permissible stress at this temperature. The same procedure may be used to determine the effect of time for isochronous stress-strain curves.

5.2.1.2 Safety Factors

The magnitude of the safety factors used in structural design of load bearing plastic parts depends on a number of variables, including the various uncertainties in calculating and determining the characteristic values of a material. Such uncertainties often arise, for example, when a load is first applied and are further complicated by simplified assumptions concerning geometry, stress, or previous processing. Secondly, the magnitude of safety factors depends on the seriousness of the damage which would occur were the structural part to fail. It is also influenced by the specific characteristic failure value against which the theoretical calculation is intended to provide a safeguard. It may be the designer who determines the magnitude of the safety factor in some applications. In some cases, agencies also prescribe minimum levels of safety for load-bearing structural parts.

The designer is responsible for the first group of safety factors identified above. He or she must estimate the effect of the simplifications made and the unquantifiable processing operations and rate them according to importance. For the second category of safety factors, the following guide values apply, provided they have not been previously described or agreed differently.

- $S_{\min} \geq 2$ for calculations safeguarding against fracture
 $S_{\min} \geq 3$ for calculations safeguarding against bending and buckling
 $S_{\min} \geq 1.2$ for calculations safeguarding against fracture stresses due to cracking with the additional condition that $S_{\min} \geq 2$ for strength
 $S_{\min} = 1.0$ for calculations of $S_{0.5\%}$, with the additional condition that $S_{\min} \geq 2$ for strength.

5.2.1.3 Reducing Factors

Other uncertainties attributable to the lack of physical properties data under special conditions should not be considered as safety factors but rather be taken into account in the form of what are known as reducing factors in order not to obscure the focus on strength. These material-specific reducing factors have values greater than one.

$$\sigma_{\text{perm}} = \frac{K}{S} \cdot \underbrace{\frac{1}{A_T} \cdot \frac{1}{A_{\text{st}}} \cdot \frac{1}{A_{\text{dyn}}} \cdot \frac{1}{A_A} \cdot \frac{1}{A_W} \dots}_{\text{material-specific}}$$

\downarrow
not specific
to material

(5.3)

A_T takes account of the effect of temperature on the yield stress and/or tensile strength and can be determined between 0 °C and 100 °C by the following relationship when K at 20 °C is inserted into equation (5.2).

$$A_T = \frac{1}{1 - [k(T - 20)]} \quad (5.4)$$

Values for k in this equation are as follows:

PA 66	= 0.0112
PA 6	= 0.0125
PBT	= 0.0095
PA GF and PBT GF	= 0.0071
POM	= 0.0082
ABS	= 0.0117

These values were obtained by linear interpolation of the plot of strength or yield stress in the temperature range between 0 and 100 °C. It is of course more sensible to safeguard against the characteristic failure value at the temperature in question, because these values are often available. On the other hand, Eq. 5.4 can also be employed to provide a rough estimate of the effect of temperature on other characteristic mechanical properties, if no experimental data are available at the required temperature. Testing does provide another option.

A_{st} takes account of the duration of a static load and can be substituted by the values of:
1.3 for a loading time of a few hours
1.6 for a loading duration measured in weeks
1.7 for a loading duration measured in months
2.0 for a loading period of a few years.

A_{dyn} takes account of the effect of dynamic loading and may be taken to be approximately 1.3 to 1.6.

A_A can also cover any aging effects (see Section 4.6.3).

Properties of materials which undergo change due to the absorption of water must be reduced by the reducing factor A_W . For unreinforced polyamides, this can be obtained starting from the value for strength in the dry state from:

$$A_W = \frac{1}{1 - 0.22 w} \quad (5.5)$$

where w is the moisture content in percent by weight assuming uniform distribution over the cross section. This applies within the limits $0\% < w < 3\%$. Above a moisture content of 3% by weight $A_W = 3.4$, likewise starting from strength in the dry state.

Under other conditions (e.g., chemical exposure etc.), it may be necessary to consider other reducing factors.

The process of differentiation should cause the designer to ponder deeply about any possible effects which may reduce strength. Discussions with other members of the design team can be helpful here.

5.2.2 Uniaxial State of Stress

The general equation of stress for uniaxial tensile loads having uniform distribution of stress is as follows:

$$\sigma = \frac{F}{A} \quad (5.6)$$

Another uniaxial, but inhomogeneous, state of stress occurs in the case of bending, e.g., when a beam or similar cross section has a bending moment applied at its ends.

Due to the transverse forces produced by bending loads, nonuniformly distributed shear stresses additionally appear over the cross section of the beam. These shear stresses originating from cross-force bending are, however, negligible when $l/h \geq 1$. Accordingly, pure bending may be assumed in the design of spiral springs and elastic hooks (snap-fit connections), as long as they fulfill the aforementioned condition. In practical applications, these structural parts are likewise frequently loaded beyond the linear viscoelastic range. It has, however, proved effective to use the equation for the elastic case even in such cases and in this way to determine a theoretical outer fiber stress. The values determined using elastic theory are greater than the actual stresses. When quantified, the non-linear behavior can be taken into account for a more realistic prediction.

5.2.2.1 Example of a Thin-Walled Pipe under Internal Pressure

It is extremely rare for components to be in a simple, uniaxial state of stress, although it is sometimes the case. An example is provided by a thin-walled pipe under internal pressure when only the mean tangential stress is considered. This may be regarded in approximation as a thin-walled hub mounted on a metal bolt. Under constant pressure, the stress in the interior of the pipe remains constant and the permissible maximum stress to avoid bursting of the pipe is given by:

$$\sigma_{\text{perm}} = \frac{\sigma_B(T, t)}{S \cdot A} \quad (5.7)$$

where σ_B for the bursting failure is taken from the stress-strain diagram or, in the case of creep failure, from the creep diagram. In Table 5.1 some results from bursting tests on thin-walled pipes are presented together with the tangential stress calculated using what is known as the “boiler formula”

$$\sigma_t = p \frac{r}{s} \quad (5.8)$$

using the tensile strength measured in tensile tests.

It may be seen that this comparison reveals very good agreement for a variety of different thermoplastic materials.

Table 5.1 Comparison of Calculated Burst Stress for Thin-Walled Pipes and Measured Tensile Strength Values for Several Thermoplastics

Material	Wall thickness s [mm]	Mean radius r_m [mm]	Bursting pressure p [bar]	Stress in pipe σ_i [MPa]	Tensile strength σ_r [MPa]
HDPE (5261 Z)	1.5	5.0	85	28.3	28
HDPE (5261 Z)	1.0	4.5	64	28.8	28
HDPE (5261 Z)	0.75	4.25	50	28.3	28
PVC	0.75	5.25	91	63.7	58
PVC	0.75	5.25	89	62.3	58
PMMA (G 55)	0.75	6.25	72	60.0	62
PMMA (G 55)	0.75	4.75	96	60.8	62

Example

What is the bursting pressure of a pipe made of POM GF20 at RT for which

$$s = 1.5 \text{ mm}$$

$$r_m = 5.0 \text{ mm}$$

and what is the approximate increase in diameter when this happens?

From CAMPUS, single-point data, Ticona, for Hostaform C 9221 GV1/20:

$$\sigma_B = 105 \text{ MPa}$$

$$\varepsilon_B = 2.5\%$$

$$p = \frac{\sigma_B \cdot s}{r_m} = \frac{105 \cdot 1.5}{5} = 31.5 \text{ N/mm}^2 = 315 \text{ bar}$$

$$\Delta d = d \cdot \varepsilon = \frac{5 \cdot 2.5}{100} = 0.125 \text{ mm}$$

The pipe ruptures at approximately 315 bar and the increase in diameter is approximately 0.125 mm.

5.2.3 Multiaxial State of Stress

Most engineering components are subjected to a multiaxial state of stress due to the external forces acting on them. The question whether this state of stress will result in failure is answered with the help of a suitable failure criterion. Using mathematical formulae for all possible states of stress resulting in failure, a multiaxial state of stress is converted to a theoretical, uniaxial resultant load, which acts on the material in a manner comparable with the actual multiaxial load and may cause failure. As a general rule, this theoretical load is taken as the characteristic tensile failure value. Failure criteria can be developed on the basis both of physical models of the failure event as well as mathematical approaches derived from empirical observations.

Because the effort involved in verifying test data experimentally is considerable, there are few confirmed results to verify that this approach can be used reliably to design polymeric material structures subjected to multiaxial stresses. References [5.3] and [5.4] provide an overview of currently known criteria.

5.2.3.1 Failure Criteria

“Classical” engineering failure criteria do not describe the behavior of polymeric materials with sufficient accuracy. Nevertheless, the shear experiments discussed in Section 5.2.3.2 show, for example, that some states of stress involving only shear may be described with sufficient apparent accuracy by Tresca’s simple mathematical shear stress criterion:

$$\sigma_v = \sigma_1 - \sigma_3 \quad (5.9)$$

This yields:

$$\tau = 0.5 \sigma \quad (5.10)$$

In addition, experience shows that results of sufficient accuracy are usually obtained using the HMH criterion (criterion of the greatest strain energy proposed by Huber, von Mises and Hencky, or the strain energy hypothesis). According to this, the reference stress is given by:

$$\sigma_{v \text{ HMH}} = \frac{1}{\sqrt{2}} \sqrt{(\sigma_1 - \sigma_2)^2 + (\sigma_2 - \sigma_3)^2 + (\sigma_3 - \sigma_1)^2} \quad (5.11)$$

When this hypothesis is employed it should be noted that the tensile behavior of polymeric materials may be overestimated, while in the compressive range, more reliable values are generally obtained (see also Figures 5.6 and 5.7). The reason for this discrepancy may be due to the fact that polymeric materials are more or less compressible and hence the effect of the hydrostatic stress tensor on the failure event comes into operation. This, together with the difference due to compressibility in the properties of the material under compressive and tensile loads, is not covered by the criterion of the greatest strain energy. Accordingly, materials whose compressive strength is greater than their tensile strength are better described by two alternative criteria. One is the conical fracture criterion:

Reference Stress	
m	$\sigma_{v_{I/II}} = \frac{m-1}{2m}(\sigma_1 + \sigma_2 + \sigma_3) \pm \frac{m+1}{2\sqrt{2m}} \sqrt{(\sigma_1 - \sigma_2)^2 + (\sigma_2 - \sigma_3)^2 + (\sigma_3 - \sigma_1)^2}$
t	$\sigma_{v_{I/II}} = \frac{\sqrt{3}t-1}{\sqrt{3}t}(\sigma_1 + \sigma_2 + \sigma_3) \pm \frac{1}{\sqrt{6t}} \sqrt{(\sigma_1 - \sigma_2)^2 + (\sigma_2 - \sigma_3)^2 + (\sigma_3 - \sigma_1)^2}$
p	$\sigma_{v_{I/II}} = \frac{2-\sqrt{3}p}{\sqrt{3}p(\sqrt{3}-1)}(\sigma_1 + \sigma_2 + \sigma_3) \pm \frac{3p-2}{\sqrt{6}p(\sqrt{3}-1)} \sqrt{(\sigma_1 - \sigma_2)^2 + (\sigma_2 - \sigma_3)^2 + (\sigma_3 - \sigma_1)^2}$
$m = \frac{\sigma_{CB}}{\sigma_{TB}}; \quad t = \frac{\tau_B}{\sigma_{TB}}; \quad p = \frac{\sigma_p}{\sigma_{TB}}; \quad \sigma_p = \sigma_{tan} = \frac{p_i \cdot d_m}{2 \cdot s}$	

The other is the parabolic fracture criterion:

Reference Stress	
m	$\sigma_{v_{I/II}} = \frac{m-1}{2m}(\sigma_1 + \sigma_2 + \sigma_3) \pm \sqrt{\left(\frac{m+1}{2m}\right)^2 (\sigma_1 + \sigma_2 + \sigma_3)^2 + \frac{1}{2m}[(\sigma_1 - \sigma_2)^2 + (\sigma_2 - \sigma_3)^2 + (\sigma_3 - \sigma_1)^2]}$
t	$\sigma_{v_{I/II}} = \frac{3t^2-1}{6t^2}(\sigma_1 + \sigma_2 + \sigma_3) \pm \sqrt{\left(\frac{3t^2-1}{6t^2}\right)^2 (\sigma_1 + \sigma_2 + \sigma_3)^2 + \frac{1}{6t^2}[(\sigma_1 - \sigma_2)^2 + (\sigma_2 - \sigma_3)^2 + (\sigma_3 - \sigma_1)^2]}$
p	$\sigma_{v_{I/II}} = \frac{4-3p^2}{6p(2-p)}(\sigma_1 + \sigma_2 + \sigma_3) \pm \sqrt{\left(\frac{4-3p^2}{6p(2-p)}\right)^2 (\sigma_1 + \sigma_2 + \sigma_3)^2 + \frac{3p-2}{3p(2-p)}[(\sigma_1 - \sigma_2)^2 + (\sigma_2 - \sigma_3)^2 + (\sigma_3 - \sigma_1)^2]}$
(see [5.4]).	

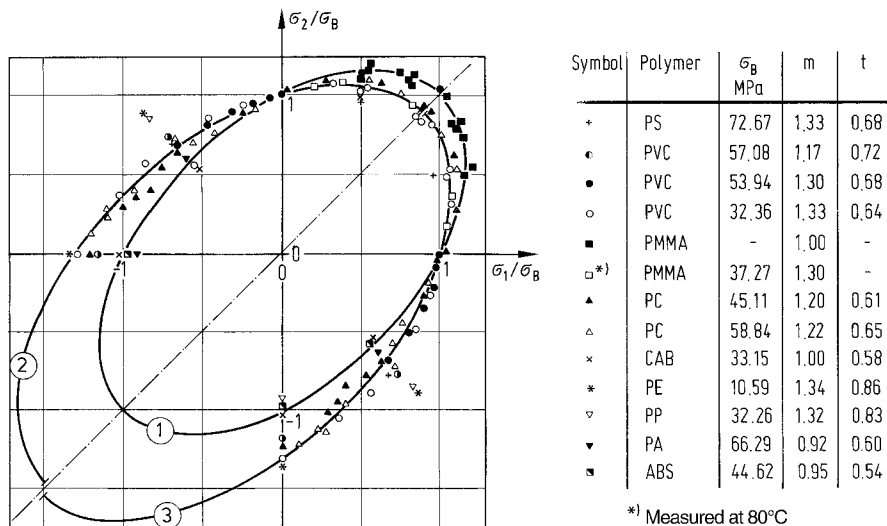


Figure 5.6 Failure due to yielding under biaxial stress. Illustration in the standardized principal normal stress plane at room temperature [5.4]

HMH criterion (1) $m = 1$

Conical criterion $m = 1.3$

Parabolic criterion $m = 1.3$

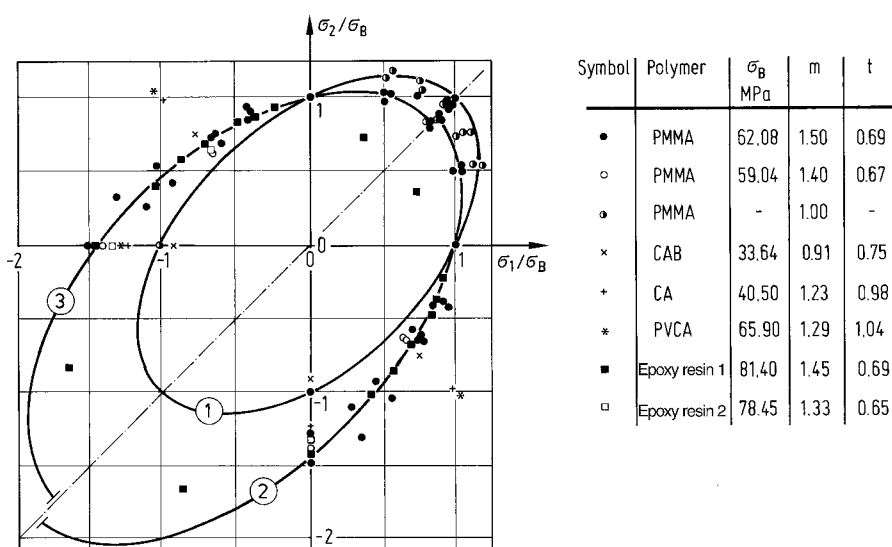


Figure 5.7 Failure due to fracture under biaxial stress. Illustration in the standardized principal normal stress plane at room temperature [5.4]

HMH criterion $m = 1$

Conical criterion $m = 1.45$

Parabolic criterion $m = 1.45$

These alternative criteria must be correlated with the actual behavior of the material through two characteristic values for the material. For this purpose, the ratio of compressive to tensile strength (m), shear strength to tensile strength (t), and the ratio of the peripheral stress of a hollow body subjected to internal pressure to tensile strength (p) are introduced as options.

When $m = 1$, the two alternative criteria transform into the HMH criterion. Figures 5.6 and 5.7 present comparisons of the three criteria in the principal stress diagram for the state of biaxial stress together with some measured values for test pieces subjected to biaxial stress [5.3].

It is recommended that structural parts subjected to biaxial tensile stress be designed by introducing the ratio p into the failure criterion. However, structural parts exposed to a combined biaxial tensile/compressive principal normal stress should be designed by incorporating only the ratio m or t into the failure criterion in question.

5.2.3.2 Examples of Shear Loads

In contrast to normal stresses, which act at right angles to the cross-sectional area, shear stresses are generated by forces whose planes of action coincide with the cross section. Accordingly, they also occur in the extension of the sectional plane considered.

Torsion is a form of shear stress of some importance in engineering. Although polymeric materials are rarely used for structural parts under torsional loads (shafts for example), they are quite commonly exposed to shear loads. Examples include riveted joints, threads under tensile loads, and splined press fits (see Figure 5.8).

Such shearing is generally accompanied by a bending component. If the latter is ignored, the shear strength can be simply converted by the shear stress hypothesis to a resultant stress. The shear stress hypothesis yields the result as shown in Eq. 5.10 that $\tau = 0.5 \sigma$ (use of the HMH criterion yields $\tau = \sigma/\sqrt{3} = 0.58 \sigma$).

In the following examples, results calculated on the basis of this assumption are compared with corresponding empirical results. As expected, the results exhibit better agreement the more the load approximates to unadulterated shear as found, for example, in a splined press-fit connection or a fine screw thread (see Figure 5.8).

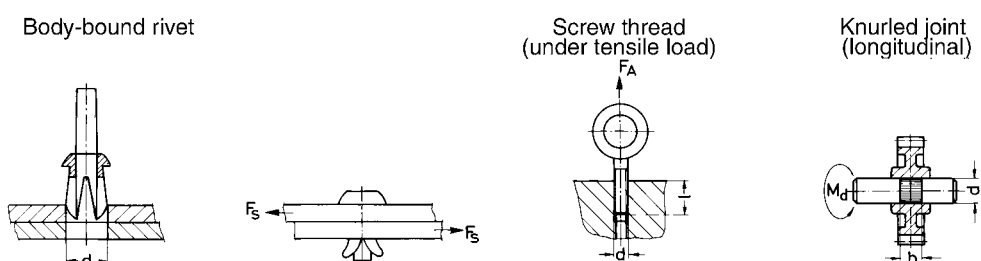


Figure 5.8 Examples of structural parts exposed to shear

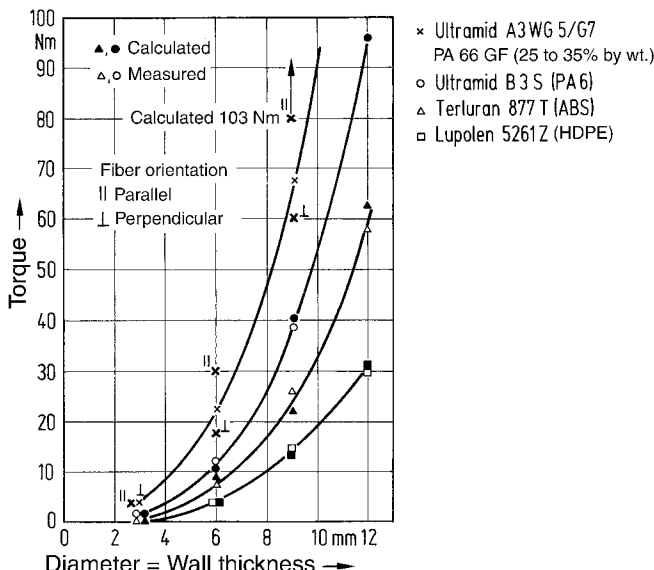


Figure 5.9 Maximum transmissible torque for steel bolts in different polymeric materials.
Ratio of diameter:length in the press fit = 1 [4.26].

Table 5.2 Comparison of Measured and Calculated Values for the Withdrawal Force for Several Screw Types Having Different Thread Configurations in ABS (877 T). Calculated Using $\tau = 0.5 \sigma$ ($\sigma_y = 46.3 \text{ MPa}$); Thread Engagement $l = 2 d$. Metric Threads Cut in Advance; Self Threading Screw Thread Tapped as Driven in [4.26].

Type of screw		Withdrawal force [N]	
		Mean of five measurements	Value calculated from $F_w = \pi d l \tau$
Metric fine thread	M4 × 0.5	2400	2327
	M6 × 0.5	5325	5236
Metric coarse-pitch thread	M4 × 0.7	1788	2327
	M6 × 1	4800	5236
Metal screw thread	4.2 dia.	3125	2566
	4.8 dia.	4400	3351
	6.3 dia.	5825	5773

The calculated failure torque, M_t , is given by:

$$M_t = \frac{\pi d^2}{2} \cdot b \cdot t \quad (5.14)$$

where d is the diameter and b is the width.

The discrepancy in glass-fiber reinforced PA 66 should be noted. The orientation of the glass fibers adds a level of uncertainty to design calculations for fiber reinforced plastics.

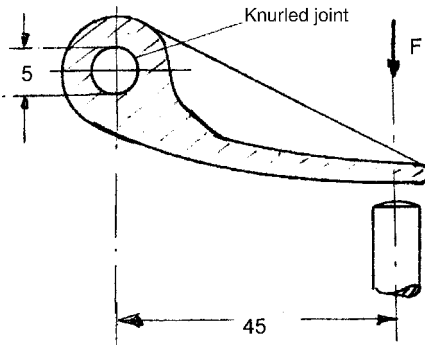
In unscrewing tests on screws with a metric fine thread, there is also good agreement (see Table 5.2), whereas experimental values for metric coarse-pitch screws are well below the calculated values, most likely due to the additional bending stresses in the tests resulting from the greater thread height. In both cases, the threads were cut into the polymeric material. Self-tapping screws have higher withdrawal values than those calculated. This may be due to the more complex state of stress caused by the furrowing of the threads.

When designing components under shear loads with a superimposed bending component, as is the case, for example, in riveted joints, it has proved useful to carry out calculations using the empirical value $\tau = 0.8 \sigma$. The same procedure may also be adopted when die cutting forces are to be roughly estimated.

Example

Using a lever made from POM as shown in the diagram, a trip-hammer force of 14 N is to be exerted. A rough estimate has to be made whether this lever can be fastened to the shaft by a knurled seating and how wide the knurled seating must be so that a safety factor of $S = 2.5$ with respect to failure is obtained.

Impact coefficient $a_{\text{imp}} = 3.0$
Ambient temperature $T_a = 40^\circ\text{C}$



From CAMPUS, multipoint data, BASF, for Ultraform N 2320: $\sigma_Y = 49.5 \text{ MPa}$

$$M_t = F \cdot l = 14 \cdot 45 = 630 \text{ N mm}$$

From Eq. 5.13:

$$b = M_t \cdot \frac{2}{\pi \cdot d^2} \frac{2}{\sigma_Y} \cdot S \cdot a_{\text{imp}} = 630 \cdot \frac{2}{\pi \cdot 5^2} \frac{2}{49.5} \cdot 2.5 \cdot 3 = 4.86; \quad b_{\min} = 5 \text{ mm}$$

5.3 Calculation of Strains and Deformations

The fact that the modulus of elasticity of polymeric materials is relatively low indicates that structures are frequently rendered unusable by excessively high levels of deformation and not just by failure due to fracture. If it is desired to take nonlinear viscoelastic deformation characteristics into account, the calculation effort becomes more difficult but can be done accurately if the loads and temperatures can be specified.

The behavior of relatively rigid and fiber-reinforced thermoplastics can generally be replicated with a good degree of accuracy. The behavior of more ductile materials with non-linear stress-strain behavior can be more difficult to predict. Linearizing the curvature of the stress-strain curve using secants is helpful. The agreement between the deformation behavior calculated in this way and the actual deformation is adequate for all practical purposes. This is the case for structural parts under either static or dynamic loads [5.5]. In fiber-reinforced thermoplastics, the orientation of the fibers has a very much greater effect than nonlinearity.

5.3.1 Linear Elastic Behavior

Linear elastic behavior of a material is described by Hooke's law for the uniaxial state of stress.

$$\varepsilon = \frac{1}{E} \sigma \quad (5.15)$$

The reciprocal of E (modulus of elasticity) defines the gradient of the linear relationship between strain and stress. In generalized form, with the material behaving differently in the x, y, and z directions, this law takes the following form in conventional notation.

$$\varepsilon_x = \frac{1}{E_x} \sigma_x - \frac{\mu_{xy}}{E_y} \sigma_y - \frac{\mu_{xz}}{E_z} \sigma_z \quad (5.16)$$

$$\varepsilon_y = \frac{1}{E_y} \sigma_y - \frac{\mu_{yz}}{E_z} \sigma_z - \frac{\mu_{yx}}{E_x} \sigma_x \quad (5.17)$$

$$\varepsilon_z = \frac{1}{E_z} \sigma_z - \frac{\mu_{zx}}{E_x} \sigma_x - \frac{\mu_{zy}}{E_y} \sigma_y \quad (5.18)$$

$$\gamma_{yz} = \frac{1}{G_{yz}} \tau_{yz} \quad (5.19)$$

$$\gamma_{zx} = \frac{1}{G_{zx}} \tau_{zx} \quad (5.20)$$

$$\gamma_{xy} = \frac{1}{G_{xy}} \tau_{xy} \quad (5.21)$$

For the biaxial state of stress and assuming isotropy, the following well known form is obtained.

$$\varepsilon_x = \frac{1}{E} (\sigma_x - \mu \sigma_y) \quad (5.22)$$

$$\varepsilon_y = \frac{1}{E} (\sigma_y - \mu \sigma_x) \quad (5.23)$$

Due to nonlinear deformation behavior, these relationships apply to thermoplastic polymeric materials with any precision only in the lowest strain ranges (up to a few tenths of one percent). Due to the real need for design calculations it is essential – and also readily justified in the case of fiber-reinforced thermoplastic polymeric materials – to extend the application of these laws into the linear-viscoelastic range. Calculations for fiber-reinforced thermosets are carried out using Eqs. 5.16 to 5.21 in which the different behavior of the materials in the three directions is taken into account [5.6].

5.3.2 Nonlinear Elastic Behavior

In stress-strain diagrams for a uniaxial state of stress, the deviation of the curve from its original linear course is readily observed*. This form of nonlinearity is relatively easy to describe by the secant method by introducing a secant modulus E_s , (*i.e.*, strain-dependent modulus) to replace the modulus of elasticity E (see also Sections 4.1.3 and 4.1.5).

The following steps are necessary: The strain occurring in the cross section under consideration ε_{act} (or stress σ_{act}) may be derived from the geometric circumstances, from a stress analysis, or as a set limit (*i.e.*, the maximum permissible value). Taking the corresponding stress value σ_{act} (or strain value ε_{act}) from the stress-strain diagram the quotient $\sigma_{act} / \varepsilon_{act}$ for the secant modulus is calculated. Two examples illustrate this concept.

* This nonlinearity is due to the fact that in the stress-strain experiment, each pair of stress-strain values is based on a different loading time. As a result, viscoelastic creep processes have come into effect during the test. In the dynamic test, linear behavior is more discernible in the lower range of stress.

Example 1

The mating force (F_C) for a closed annular snap-fit joint as shown in the diagram with a rigid steel internal section and an outer section composed of moist PA 66 is to be calculated.

The mating force can be calculated using the equation

$$F_C = 0.62 \cdot \Delta d \cdot d \cdot E \left(\frac{2s}{d} \right)^{\frac{3}{2}} \cdot \eta$$

where

$$\eta = \frac{\tan \alpha + f}{1 - f \cdot \tan \alpha}$$

Which value for the modulus E should be substituted into this equation?

For this specific geometry, the maximum strain associated with the snap-fit process can be determined using:

$$\varepsilon_{act} = \frac{\Delta d}{d} = \frac{51 - 50}{50} = 0.02$$

The strain value is 0.02 m/m or 2%.

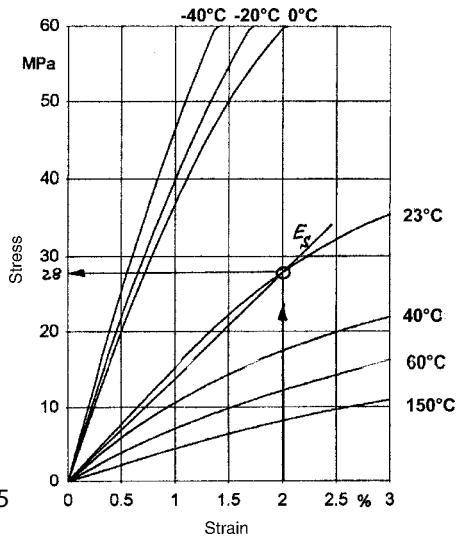
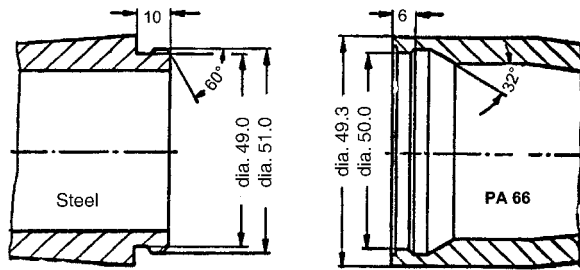
The stress at $\varepsilon_{act} = 2\%$ is obtained from the stress-strain diagram as being $\sigma_{act} = 28 \text{ MPa}$. This value is used to determine the secant modulus:

$$E_S = \frac{\sigma_{act}}{\varepsilon_{act}} = \frac{28}{0.02} = 1400 \text{ MPa}$$

This modulus value $E_S = 1400 \text{ MPa}$ is substituted into the earlier equation and with

$$\eta = \frac{\tan 60 + 0.35}{1 - 0.35 \cdot \tan 60} = 5.2$$

$$F_E = 0.62 \cdot 1 \cdot 50 \cdot 1400 \cdot \frac{2 \cdot 5}{50}^{\frac{3}{2}} \cdot 5.2 = 20,185$$



The force required to close the snap-fit joint is of the order of 20 kN.

Example 2

1. A spiral spring of rectangular cross section made from POM and fixed at one end is to be extended frequently by a force $F = 5 \text{ N}$. The spring excursion f is specified to be 4.5 mm and the length of the spring l is limited by design to 50 mm. The cross section of the spring is to be calculated.

Due to the frequent extension, a **maximum permissible stress** is specified, e.g., $\sigma_{0.5\%}$. From the stress-strain diagram for POM, the modulus of elasticity $E = 3200 \text{ MPa}$ using the method specified in Figure 5.2c.

The permissible maximum stress is specified as:

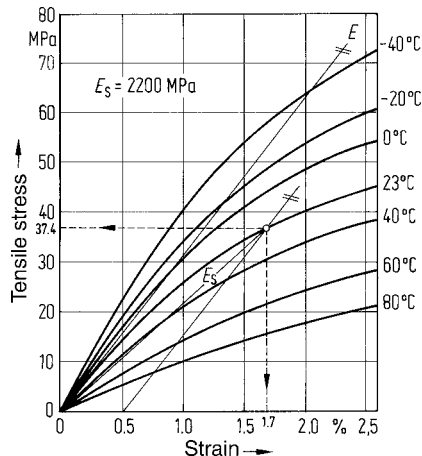
$$\sigma_{\text{perm}} = \sigma_{0.5\%} = 37.4 \text{ MPa} \\ (\text{i.e., a safety factor of } 2)$$

The corresponding maximum permissible strain is

$$\varepsilon = \varepsilon_{\text{perm}} = 1.7\%$$

The secant modulus at this point on the stress-strain diagram is given by:

$$E_S = \frac{\sigma_{0.5\%}}{\varepsilon_{\text{perm}}} = \frac{37.4}{1.7} \cdot 100 = 2200 \text{ MPa}$$



The deflection of a cantilever beam fixed at one end, with a single point load at the free end is given by:

$$f = \frac{F \cdot l^3}{3 \cdot E \cdot I}$$

For a rectangular cross section and with:

$$F \cdot l = M; \quad \sigma = \frac{M}{W}; \quad I = W \cdot \frac{h}{2} \quad \text{and} \quad E = \frac{\sigma}{\varepsilon}$$

The equation can be rewritten as:

$$f = \frac{2}{3} \cdot \frac{l^2}{h} \cdot \varepsilon$$

Thus, designing solely on the basis of strain is possible as long as the condition $\varepsilon \leq \varepsilon_{\text{perm}}$ is adhered to. The height/breadth (h/b) ratio for the cross section of the beam is now varied iteratively until height and breadth values acceptable for production are obtained. This is easily accomplished using a programmable calculator or spread sheet using stress-strain functions (see also Section 4.1.5).

The first step is to determine h_1 for $\varepsilon_1 = \varepsilon_{\text{perm}}$:

$$h_1 = \frac{2}{3} \cdot \frac{l^2}{f} \cdot \varepsilon_1$$

$$h_1 = \frac{2}{3} \cdot \frac{50^2}{4.5} \cdot \frac{1.7}{100} = 6.3 \text{ mm}$$

$$l = \frac{F \cdot l^3}{3 \cdot f} \cdot \frac{\varepsilon_1}{\sigma_1}$$

$$l_1 = \frac{5 \cdot 50^3}{3 \cdot 4.5} \cdot \frac{1.7}{100 \cdot 37.4} = 21 \text{ mm}^4$$

$$b_1 = \frac{l_1 \cdot 12}{h_1^3}$$

$$b_1 = \frac{21 \cdot 12}{6.3^3} = 1.0 \text{ mm}$$

$$h_2 = h_1 - x$$

$$h_2 = 6.3 - 2.8 = 3.5$$

$$\varepsilon_2 = \frac{3}{2} \cdot \frac{h_2}{l^2} \cdot f$$

$$\varepsilon_2 = \frac{3}{2} \cdot \frac{3.5}{50^3} \cdot 4.5 = 0.00945 \approx 1\%$$

σ_2 for ε_2
from stress-strain diagram

from stress-strain diagram
is read off $\sigma_2 = 26 \text{ MPa}$

The 2nd moment of area
(moment of inertia) I_2 is then given by

$$I_2 = \frac{5 \cdot 50^3}{3 \cdot 4.5} \cdot \frac{1}{26 \cdot 100} = 14.5 \text{ mm}^4$$

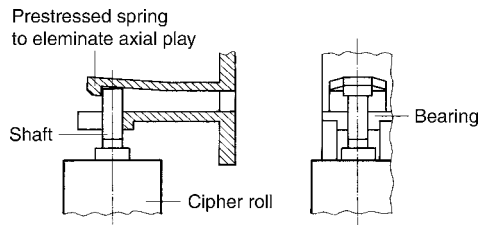
and b_2 by

$$b_2 = \frac{14.5 \cdot 12}{3.5^3} = 4.04 \text{ mm}$$

Accordingly, a technically feasible design would be:

$h = 3.5 \text{ mm}$
 $b = 4.0 \text{ mm}$
with
 $\varepsilon = 1.0\%$
 $\sigma = 26 \text{ MPa}$

2. In a situation like the one shown in the diagram, what is the residual force exerted by the cantilever spring after 104 hours assuming a deflection, $\Delta f = 2 \text{ mm}$?



First, the outer fiber strain $\varepsilon_{\Delta f}$ for the deflection $\Delta f = 2 \text{ mm}$ is determined for a beam of depth, h and length, l .

$$\varepsilon_{\Delta f} = \frac{3}{2} \cdot \frac{h}{l^2} \cdot \Delta f$$

$$\varepsilon_{\Delta f} = \frac{3}{2} \cdot \frac{3.5}{50^2} \cdot 2 = 0.0042 = 0.42\%$$

From the isochronous stress-strain diagram for 10^4 hours and $\varepsilon_{\Delta f}$ a modulus value (creep modulus E_{10000}) is determined. It should be noted that this is a stress relaxation application (rather than creep). However, as mentioned in Section 4.2, stress relaxation data is not as widely available as creep data which can be substituted as a practical option.

This procedure is shown for $\varepsilon_{\Delta f} = 0.4\%$ in the adjacent figure.

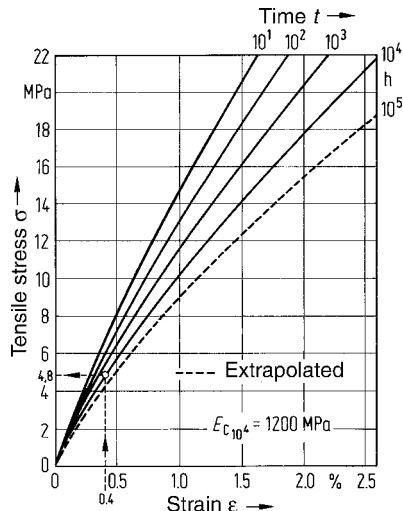
$$E_{10000} = \frac{4.8}{0.4} \cdot 100 = 1200 \text{ MPa}$$

This modulus value is finally substituted into the equation for the force required to cause the 2 mm deflection.

$$F = \frac{3 \cdot E \cdot l}{l^3} \cdot \Delta f$$

$$F = \frac{3 \cdot 1200 \cdot 14.5}{50^3} \cdot 2 = 0.84 \text{ N}$$

The residual force exerted by the spring after 10^4 hours is, accordingly, of the order of 1 N.



5.4 Analysis of Stress and Deformation in Structures under Flexural Loads with the Aid of a Simple FE Approach

Flexure or bending is one of the most common states of stress in parts made from polymeric materials. Examples of this are provided by snap-fit hooks, levers of all kinds, chair backs, armrests, clutch and gas pedals, to name just a few. Such components, however, can often not be designed using self-contained analytical approaches because either the shape is too complex, the loading is nonuniform (*i.e.*, not easily idealized), or the deformation too great.

Parts subjected to flexural stress and in a state of biaxial deformation can be readily analyzed by means of finite bending elements, each of which is easy to solve. Reference [5.7] describes such a computer program capable of running on a commercial programmable calculator or PC*. Only a basic knowledge of the theory of the strength of materials is needed to understand the considerations set out below.

A bending beam fixed at one end is used as the finite beam element. This is acted upon by a moment that is constant over the length of the beam (see Figure 5.10).

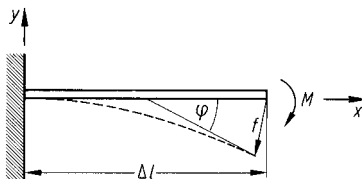


Figure 5.10 Finite beam element as the base element

The following relationships apply to small displacements of the end of the beam.

$$\text{Change of angle at free end of beam} \quad \varphi = \frac{M \cdot \Delta l}{E I} \quad (5.24)$$

$$\text{Displacement of the free end} \quad f \approx \frac{\varphi \cdot \Delta l}{2} \quad (5.25)$$

$$\text{Outer fiber stress} \quad \sigma = -\frac{M \cdot e}{I} \quad (5.26)$$

$$\text{Outer fiber strain} \quad \varepsilon = \frac{\sigma}{E} \quad (5.27)$$

where

M = Bending moment in Nmm (negative in clockwise direction)

Δl = Length of element in mm

I = 2nd moment of area (moment of inertia) in mm⁴

E = Modulus of elasticity in MPa

e = Outer fiber distance in mm

* An example of an easy-to-use PC program is supplied by BASF under the name of BEAMS.

The entire structure under flexural stress is now subdivided into elements which become smaller as the change in bending moment, moment of inertia, or outer fiber distance increases. Equation 5.25 alone involves an approximation applying only to small displacements. Therefore, if there is a sufficiently large number of elements, all undergoing a small displacement, conclusions can readily be drawn about a large displacement. Because the neutral or unaffected fiber need not necessarily be located in the center of the element e_u and e_l are introduced for calculating the upper and lower outer fiber stress values respectively. Nevertheless, if M , I , e_u , and e_l are not constant in the element, the mean value in the center of the element is used for the calculation. Calculation always starts at a point at which bending and angular deflection are zero. This is usually the fixing point or a plane of symmetry with respect to the load. The origin of a Cartesian coordinate system is placed at this point.

In the first step, the change of angle φ_1 is calculated using Eq. 5.24 and the displacement of the end point f_1 using Eq. 5.25. In this way, the displacement of the end point A in Figure 5.11 is determined. Equations 5.26 and 5.27 then yield the outer fiber stress and strain respectively. The latter apply most accurately to the center of the element.

The coordinates of the new end point $\Delta x_1^{f_1}$ and $\Delta y_1^{f_1}$ form the starting point for calculating the next element.

Bending Element 1

$$\Delta y_1^{f_1} = \Delta l_1 / 2 \cdot \sin \varphi_1 \quad (5.28)$$

$$\Delta x_1^{f_1} = \Delta y_1^{f_1} \cdot \tan \varphi_1 \quad (5.29)$$

While the analysis of the outer fiber stresses and strains is very straightforward, the end positions of the succeeding elements must each be determined by a rather complicated geometric procedure, which can, however, be readily performed using a computer.

Figure 5.11 shows the geometric relationships by which the positions of the displaced end points are described for the general case.

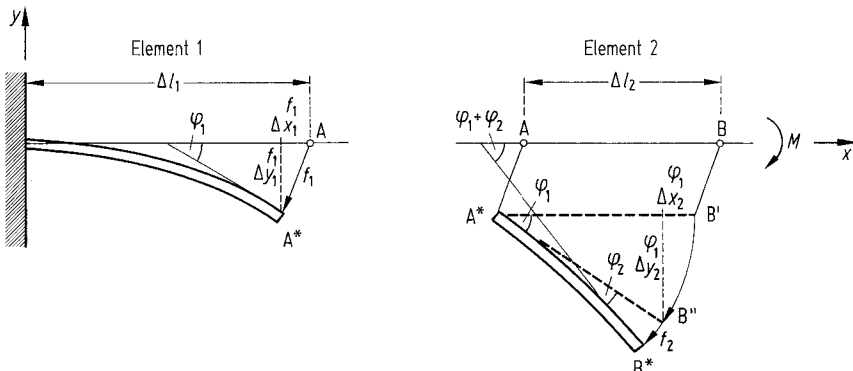


Figure 5.11 Deformation of the first and second elements of the beam

Once the coordinates of the point A* have been obtained from the preceding step in the calculation, the change in the position of B can be concluded with the following contributory displacements:

$B \rightarrow B'$ = parallel displacement of the undeformed element 2 by ($A \rightarrow A^*$)

$B' \rightarrow B''$ = rotation by the angle φ with A* as the pivot.

Rotating element 2 by A*

$$\Delta y_2^{\varphi_1} = \Delta l_2 \cdot \sin \varphi_1 \quad (5.30)$$

$$\Delta x_2^{\varphi_1} = \Delta y_2^{\varphi_1} \cdot \tan \varphi_1 \quad (5.31)$$

$B'' \rightarrow B^*$ = bending of the element as a result of application of the moment analogously to Eqs. 5.28 and 5.29. In this way, the starting point B^* for calculating the next element is established and calculation can proceed in stepwise manner.

This method of calculation also allows the nonlinearity of the material to be taken into account in a simple manner by substituting in Eq. 5.19 the secant modulus for the stress calculated by Eq. 5.18. This can again be done using a computer program by means of a subroutine containing the stress-strain functions (see also Section 4.1.5). Creep under static loads can also be taken into account by substituting the appropriate time-dependent creep modulus.

In a step-by-step calculation, the change in the moments as deformation of the beam increases can also be taken into account. The moments acting through the load forces in the individual elements change as deformation progressively shortens the length of the lever arm.

5.5 Calculation of Structural Parts Subjected to Impact Loads

In the case of impact loads, short-term stress peaks occur in the component. These can be a multiple of the stresses occurring under a static load of the same magnitude. The ratio of stress caused by impact to stress under a static load is referred to as the impact factor. It is calculated essentially from the rigidities of the colliding mass, the component, and the elastic support. Using the impact factor it can be determined whether the load arising is below the failure stress of the material with the requisite margin of safety. In this approach, the instance of an impact load is reduced to a quasi-static one. This is conditional on the material exhibiting linear elastic behavior.

In [5.8] a different and simpler method of impact stress calculation is presented which compares the deformation energy converted in the structural part with the specific energy-absorbing capacity of the material. The specific energy absorption is obtained by integrating over the stress-strain curve.

Figure 5.12 shows the theoretical view of a bending support struck in the center by a mass m at a velocity v . The kinetic energy W of the mass must be converted into deformation work in the beam or plate.

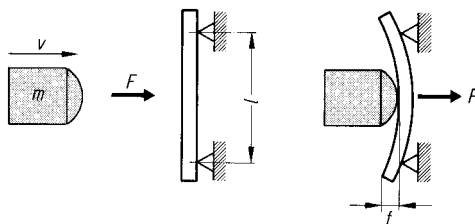


Figure 5.12 Energy conversion in a bending support subjected to an impact load [5.8]

$$W = \frac{1}{2} m v^2 = \int F df \quad (5.32)$$

The force-deformation integral is proportional (factor K) to the stress-strain integral. Given conservation of energy this yields the following equation.

$$\frac{1}{2} m v^2 = K \int \sigma d\epsilon \quad (5.33)$$

ϵ_{\max} is chosen with a sufficient safety interval from the failure strain so that there is still a high enough energy reserve up to failure*.

The factor K for a support of rectangular cross section subjected to load at three points (see Figure 5.14) is given by:

$$K = \frac{b \cdot h \cdot l}{9} \quad (5.34)$$

The corresponding K factors for different geometries and support conditions can be determined from the appropriate equations for elastic deformation and bending moments.

5.6 Structural Design of Fiber-Composite Structures

Structural parts made of fiber-resin composites are often flat structures subjected to load within the plane and, therefore, must be reinforced in at least two directions. They are built up of several layers of material in the form of mats, fabrics and/or unidirectional material (UD). These are saturated usually with a thermosetting resin and thermally cured under pressure. This layered structure is also referred to as laminate.

* The stress-strain diagrams usually available have often been generated at a strain rate (or rate of cross head travel) of 50 mm/min and do not reflect behavior under a high-speed impact load. However, in the case of nonlinear deformation behavior, a strain-based or energy-based approach affords higher reliability than a stress-based one [5.9].

5.6.1 Mechanical Properties of Laminates

5.6.1.1 Deformation Behavior under Uniaxial Tensile Load, Damage Limit

- A composite having a uniaxial *roving reinforcement* (continuous fibers) exhibits a largely linear relationship between stress and strain (in line with Hooke's law) when subjected to stress along the direction of the fibers until fiber breakage (because fibers such as glass fiber exhibit highly elastic behavior).
- In the case of *fabric reinforcement* (fibers lying at right angles to one another), Hooke's law is likewise obeyed initially up to an elastic limit. At this point, cracks in the resin occur in the layers perpendicular to the direction of the load. This is followed by a linear range once more due to the long fibers running in the direction of the force. The transition point between the two ranges is referred to as the damage limit or, according to Puck [5.10], as the "elbow". As would be expected, the position of this elbow depends on the glass fiber content transverse to the direction of loading.
- In the case of *mat reinforcement*, the forces are transmitted through the fibers, which typically have a length of less than 50 mm, and from fiber to fiber through the resin matrix. In the lower region of the stress-strain diagram there is a linear rise which then drops off at higher stresses due to more frequent cracks in the resin. There is no distinct elbow as in the case of fabric reinforcement because of the random distribution of the fibers.

Stress-strain curves for these three forms of reinforcement are presented in Figure 5.13.

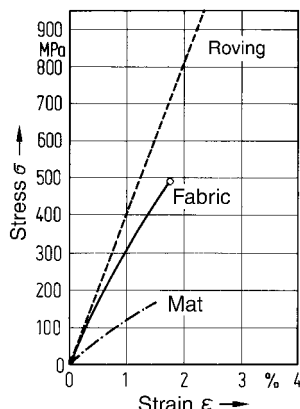


Figure 5.13 Stress-strain curves for mat, fabric, and UD reinforced thermoset plastic laminates

5.6.1.2 Fundamental Elasticity Variables in a UD Layer

The anisotropy of the individual laminate layers determines their strength and elasticity variables, and contributes to those of the entire laminate. This means, on the one hand, that the load-bearing fibers are aligned in the direction of the stresses in operation. This means that weight-optimized structural parts can be manufactured (e.g., pressure vessels, see also Section 1.1.2). On the other hand, the dramatic decrease in strength and rigidity transverse to

the direction of the fibers must be considered. Overall, design calculations for such composite structures are relatively demanding.

The elasticity and strength variables of a UD layer can be calculated from the characteristic values for the individual constituents: the matrix (M) and the fibers (F) [5.11]. This is done on the basis of more or less idealized cross-sectional models using, for example, the linear proportionality rule. The relationships normally applicable for this purpose are given in Eqs. 5.35 to 5.43 and are illustrated in Figure 5.14. Table 5.3 presents the fundamental elasticity variables for fibers.

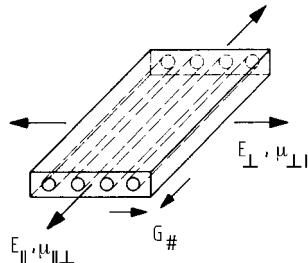


Figure 5.14 Model of a UD layer showing fundamental elasticity variables

$$E_{\parallel} = \varphi E_{\parallel F} + (1 - \varphi) E_M \quad (5.35)$$

$$E_{\perp} = \frac{E_M}{1 - \mu_M^2} \cdot \frac{1 + 0.85 \varphi^2}{(1 - \varphi)^{1.25} + \varphi \frac{E_M}{(1 - \mu_M^2) \cdot E_{\perp F}}} \quad (5.36)$$

$$\mu_{\perp\parallel} = \varphi \mu_{\perp\parallel F} + (1 - \varphi) \mu_M \quad (5.37)$$

$$\mu_{\parallel\perp} = \mu_{\perp\parallel} \frac{E_{\perp}}{E_{\parallel}} \quad (5.38)$$

$$G_{\#} = G_M \frac{1 + 0.6 \varphi^{0.5}}{(1 - \varphi)^{1.25} + \varphi \frac{G_M}{G_{\parallel\perp F}}} \quad (5.39)$$

The tensile strength of a UD layer in the fiber direction is estimated by the linear proportionality rule.

$$\sigma_{\parallel B} = \varphi \sigma_{\parallel F} + (1 - \varphi) \sigma_M \quad (5.40)$$

When $\sigma_M \ll \sigma_{\parallel F}$, this is simplified to:

$$\sigma_{\parallel B} = \varphi \sigma_{\parallel B} \quad (5.41)$$

Table 5.3 Fundamental Elasticity Variables for Fibers [5.12]

Fiber	$E_{ F}$ MPa	$E_{\perp F}$ MPa	$G_{ \perp F}$ MPa	$\mu_{\perp F}$
E glass	73,000	73,000	30,000	0.25
Aramid	130,000	5,400	12,000	0.38
C fibers				
HF	240,000	15,000	50,000	0.28
HM	500,000	5,700	18,000	0.36

At right angles to the loading direction the following relationship applies:

$$\sigma_{\perp B} \approx \frac{1}{2} \sigma_M \quad (5.42)$$

Because the fiber content is usually given as a percentage by weight (ψ), it must be noted that the above equations require the fiber content to be specified as a percentage by volume.

$$\varphi = \frac{1}{1 + \frac{1 - \psi}{\psi} \frac{\rho_F}{\rho_M}} \quad (5.43)$$

Indices used in Eqs. 5.33 to 5.42 have the following meanings:

\parallel parallel to the fibers (or direction of loading)

\perp perpendicular to the fibers

shear parallel and perpendicular to the fibers.

In Poisson's ratio, the first index refers to the direction of contraction.

5.6.1.3 Averaged Characteristic Values for Mat Laminates

To determine physical properties, in particular for quasi-homogeneous mat laminates, the usual measurements in materials testing are carried out on samples cut out of laminates. Values averaged over the cross section for matrix and fiber behavior are then obtained for different levels of fiber content. All variables dependent on temperature, time, and aging are normally determined in this manner. Figures 5.15 to 5.18 show examples of the results of such measurements.

If the mechanical properties of fiber composites are related to the corresponding density, a clear illustration of the good performance of fiber reinforced polymeric materials is obtained (see Table 5.4).

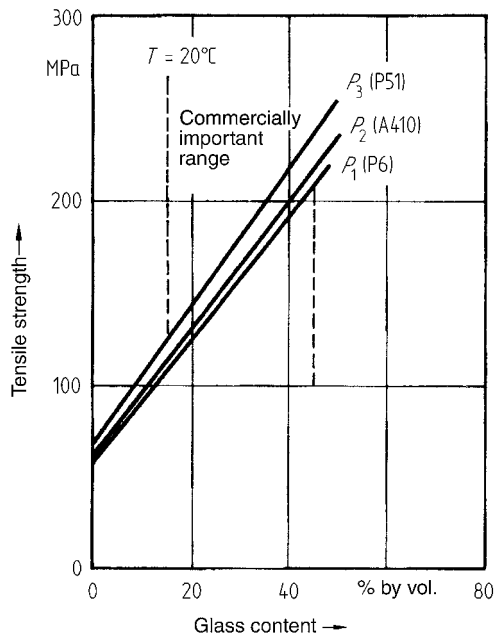


Figure 5.15 Tensile strength of various UP mat laminates [5.13]

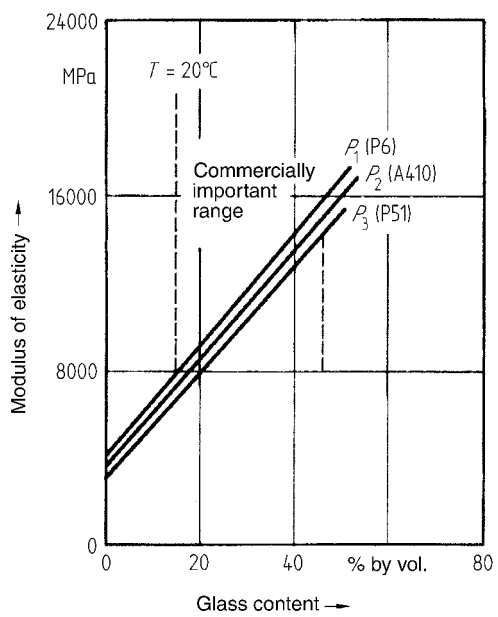
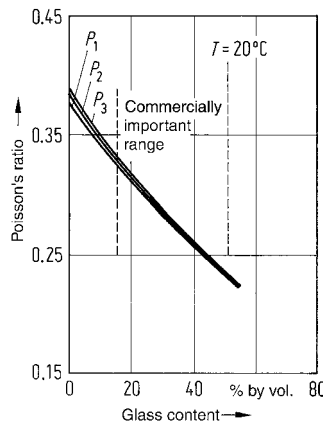


Figure 5.16 Modulus of elasticity of UP mat laminates [5.13]

**Figure 5.17** Poisson's ratio for UP mat laminates [5.13]**Table 5.4** Standardized Quality Indices of Various Lightweight Construction Materials with Reference to Aluminum

Property	Quality index	Wood (spruce, pine)	Mg alloy	Al alloy	Ti alloy	Steel	Glass-fiber reinforced plastic	Carbon-fiber reinforced plastic HM	Carbon-fiber reinforced plastic HT
Static strength • tensile, compressive, bending	σ/γ	1.25	1.06	1	1.38	1.12	1.94	2.19	2.94
Longitudinal rigidity • tensile, compressive	E/γ	0.92	0.96	1	0.94	1.04	0.50	2.27	1.77
Shear rigidity • torsion	G/γ	—	0.94	1	0.93	1.04	0.32	1.47	1.12
Bending resistance of rods	\sqrt{E}/γ	2.32	1.26	1	0.79	0.63	0.81	1.95	1.77
Buckling resistance and bending strength of plates	$\sqrt[3]{E}/\gamma$	3.06	1.33	1	0.73	0.53	1	1.84	1.76
Elastic energy absorption capacity	$\frac{\sigma_{\text{prop.}}^2}{E}$	0.47	0.52	1	3.4	3.4	8.4	2.1	4.5
Impact strength	A	0.2	2.5	1	1.5	2.5	0.75	0.2	0.2
Fatigue strength $R = -1$ $N = 10^6$	$\sigma_{\text{bw}}/\gamma$	1.2	1.2	1	2.2	1.3	1.7	2.8	3.2

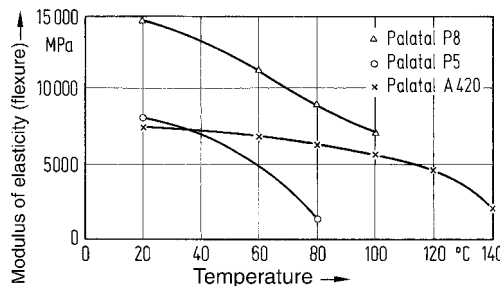


Figure 5.18 Modulus of elasticity of UP mat laminates as a function of temperature [3.5]

5.6.2 Methods of Calculation

Fiber composite structures can be designed using different methods according to the end use requirements.

5.6.2.1 Calculation of Averaged Values

In industrial practice, calculations for most structural parts are simplified in the early design phase of the product development process. This, however, does not suffice as proof of strength for safety purposes.

5.6.2.2 Continuum Theory

Continuum theory is based on the premise that the individual layers of a laminate form a quasi-homogeneous orthotropic continuum. The rigidities of these layers are calculated from the moduli of the constituent matrix and fibers (Eqs. 5.34 to 5.38) and in the case of multilayer composites transformed to the common reference direction and summed. Depending on the external loads the deformation and finally the stresses in the individual layers and in the composite are obtained. These computations may require a great deal of effort. The extensive literature on this, e.g., [5.10] to [5.16], should be consulted for more complete coverage.

It is assumed that each layer is part of a homogenous continuum, so this theory applies only up to the proportionality limit (damage limit, see Section 5.6.1.1). In addition, the nonlinearity resulting from the change in rigidity would have to be taken into account. Nevertheless, this theory applies to all resins and all types of reinforcement.

5.6.2.3 Network Theory

Network theory assumes that the forces are absorbed solely by the fibers. Accordingly, this theory is not applicable to short-fiber mat laminates. In addition, it applies only above the damage limit, but for that reason it can usefully be employed for designing for fiber breakage. The calculated results are generally lower than actual (experimental) values, which means that design by this method has an additional built-in safety factor.

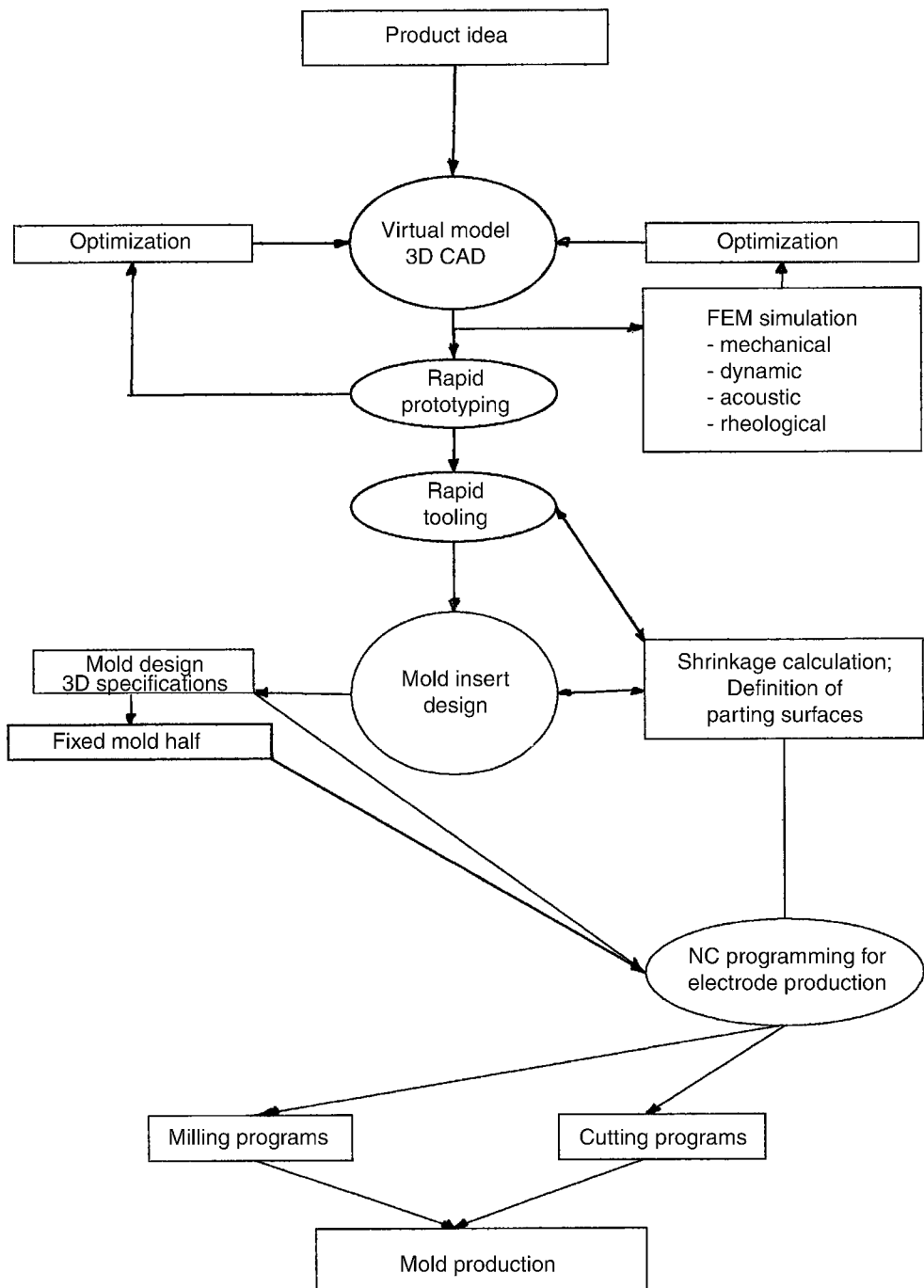


Figure 5.19 Flow diagram for computer support from product concept through tooling

5.7 Computer-Aided Development

The computational methods described so far provide only approximate results, depending on the degree of simplification and quality of data. These basic analytical calculations for structural parts having complicated geometries are possible only if numerous simplifying assumptions are made with respect to the geometry.

Today, however, designers and development engineers are able to call on computer-aided methods in all phases of product development. These make it possible at an early stage to avoid dead-end development directions and to achieve optimized results. This is of critical importance for productivity, competitiveness, and safety for polymeric material parts subject to structural loading.

The flow diagram in Figure 5.19 shows the development stages in which such computer support can be employed.

5.7.1 Computer-Aided Design (CAD)

While initial product concepts are usually sketched by hand, it is important to develop CAD files early in the product development process. Models and drawings should be prepared using a 3D CAD system, because only in that way can a complete and unambiguous definition of the geometry be provided. This is indispensable for visualization and other engineering functions.

FE Structural Analysis (Finite Element or Finite Difference Calculations)

FE methods can now be used to address the most varied problem areas. Just a few years ago, such problem areas had to be solved exclusively by time-consuming experimental tests on prototypes. With FE analysis, the following tasks can be carried out in reasonable periods of time.

- Finding weak points in a design
Computation provides information about the state of stress over the entire component so that all zones, which appear weak or not functional, can be immediately optimized.
- Optimization of strength, rigidity, and weight
The effectiveness of the design measures incorporated into the first draft to provide adequate strength, rigidity, and stability (bending, buckling) can be evaluated and, if necessary, optimized very reliably and quickly. At the same time, weight minimization can be set as a product development objective.
- Investigation of the vibrational behavior of parts and control of acoustic properties. In the case of structural parts exposed to oscillations and vibrations, it is important at the early design stage to understand the vibrational behavior of the parts. This allows points of resonance to be shifted into noncritical areas, *e.g.*, by adding ribs. The boundary element method (BEM) affords the possibility of calculating the acoustic properties of a component, *i.e.*, the propagation of sound waves in air, and if necessary of taking measures to optimize the design.

Rheological Simulations

High-performance simulation programs [5.17] are available today which allow part designers to simulate the molding process. Potential problems that may arise in processing can be evaluated early in the design process (see also Chapter 7). In the simplest form, the molding simulation software can be used to determine mold filling pressure drops, temperature changes, and so forth. This information is particularly helpful for determining the optimum gating scheme.

- When fiber-reinforced thermoplastics are injection molded, fiber-alignment effects arise, which can be predicted by process simulation software. If possible, the part should be gated in such a way that the fiber alignment direction (close to the part surface) coincides with the direction of the highest principal normal stress. The alignment direction can be controlled within limits by the choice of the position of the gate or by other measures, such as flow promoters or flow inhibitors.
- The position of weld lines or air traps that reduce strength can be identified and altered by design.
- Shrinkage and warpage as a consequence of anisotropy of the materials or cooling conditions, which vary from point to point, can also be computed so that appropriate countermeasures can be taken.
- Special molding processes, such as gas assist molding, can be simulated. Simulation of gas pressure during molding reveals the diffusion of the gas bubbles during the injection molding process so that the effectiveness of the gas channels and the gas injection points can be evaluated.
- Two-component injection molding processes can also be simulated by numeric methods.

5.7.2 Rapid Prototyping

Solid computer models can also assist in the development of prototype parts using conventional CNC machining and rapid prototyping techniques. Generally speaking, rapid prototyping is a generative production method in that the prototype parts are built up “layer by layer” in contrast with machining, in which the parts are produced by removal of material. It is necessary to have an unbroken volumetric description of the component in a suitable solid modeling format. Once the computer model is available, a prototype can then be produced within hours. Most of these processes form parts using some type of polymeric material.

A brief review of the more common rapid prototyping methods is provided below. Detailed information may be found in [5.18].

Stereolithography

Stereolithography is the most widespread rapid prototyping method and perhaps the earliest method available commercially. Its high degree of precision, which is only slightly constrained by physical limits, is outstanding.

A tank in the stereolithography apparatus contains a liquid, light-curable polymer, which is cured point by point in layers by a computer-controlled laser scanner. The laser scanner traces

Table 5.5 Mechanische Eigenschaften von ausgehärteten Harzen für die Stereolithographie [5.18]

Polymer	Modulus of elasticity (MPa)	Tensile strength (MPa)	Elongation at break (%)	Impact resistance (kJ/m ²)	Manufacturer
Acrylic resin (SL 5149)	1150	35	10	23	Ciba
Epoxy resin (SL 5180/SL 5170)	2500	60	10	37	Ciba
Acrylic resin (2110)	37	7	46	150	Du Pont
Epoxy resin (6100/6110)	2700	55	9	34	Du Pont

the contours of a layer in accordance with the required cross-sectional geometry on the surface of the resin bath. The cured layer is lowered by about 0.1 mm using a porous elevator which is movable in the z direction. The next cross-sectional layer is formed on top of the previous layer. Each layer cured in this way joins with the one below until the prototype has been completely built up.

In a secondary treatment, the “green” part is placed in a chamber under UV radiation where it becomes fully cured. It can be reworked mechanically by machining or bead blasting and, if necessary, painted or dyed. A variety of UV-curable polymeric resins can be used with this process. Their properties can range from elastomeric to very rigid. The prototypes then possess the properties of these resins (see Table 5.5).

Solid Ground Curing (SGC)

Solid ground curing is another process that makes use of a liquid, light-curable resin. Curing of the cross-sectional area, however, does not take place by point by point or line irradiation, but rather by area exposure. A computer-controlled mask generator produces a negative for each layer of the component’s cross section on a glass plate coated with toner. This mask is positioned over the resin bath and exposed to UV light for a few seconds. This causes curing of the resin beneath the transparent sections of the mask. In the next step, any remaining liquid resin is drawn off by suction and replaced by wax. Subsequent milling over the surface ensures that the layer thickness is accurate and registration is maintained. The surface produced by this serves as the base for the next layer. On completion of the final part layer, the supporting wax is dissolved.

Fused Deposition Modeling (FDM)

FDM is another popular rapid prototyping method. Here, a thermoplastic material, in “monofilament” form, is fed to a traveling, temperature-controlled heating and winding head where it melts. A thin bead of this molten material is then deposited by a nozzle onto the

previous cross-sectional layer where it solidifies. ABS, PC, and PPS are common thermoplastic materials used for this rapid prototyping method.

Selective Laser Sintering (SLS)

The selective laser sintering process uses a CO₂ laser which in each pass sinters a thin layer of a powdered thermoplastic material and builds up a prototype part in this generative manner. The entire process is carried out in a chamber under an atmosphere of inert gas. Models or patterns having good mechanical properties are obtained. The powdered materials used for this process include ABS, PA, PC, PS, and elastomeric materials. Metal powders coated with thermoplastic binders can also be used to produce powder metal preforms for subsequent high temperature sintering. [5.20].

Laminated Object Manufacturing

Laminated object manufacturing is a combined cutting and bonding process. The geometry of the molding is built up from paper or plastic film coated with a hot-melt adhesive. These sheets are applied by a roller and pressed by a heated pressure roller onto the layers already in place. A CO₂ laser then cuts the actual cross-sectional contour out of the uppermost film. In the end, a block containing the finish part and unwanted surrounding material is formed. The unwanted material is broken away, leaving the prototype part.

5.7.3 Rapid Tooling

While rapid prototyping techniques can be used to produce single or multiple prototype parts quickly and economically, the parts are not fully functional with respect to material performance. When possible, prototype parts produced from the “production material” (*i.e.*, the polymeric material to be used in manufacturing) are preferred for performance testing. In addition, it is best if the performance prototypes are produced using the same (or similar) manufacturing process as that planned for production. The issue that usually arises here is tooling cost. The cost of prototype tooling cannot always be justified.

The point here is that rapid prototyping techniques can also be used for production of “rapid tooling”. For example, in some instances it is possible to produce mold cavities and cores directly by rapid prototyping as opposed to prototype parts. There can be issues, such as size limitation, limited durability, heat transfer, surface finish, and the like. However, as this rapid tooling concept evolves, these problems will be solved using techniques, such as powdered metalizing, hard coatings, platings, among others. Further discussion of these techniques is beyond the scope of this text, but they are mentioned here as significant developments are likely to occur in this field over the next decade.

References

- [5.1] ERHARD, G.: Berechnen von Bauteilen aus thermoplastischen Polymerwerkstoffen (Calculation of Structural Parts made from Thermoplastic Polymeric Materials), VDI-Z 121 (1979) 19, pp. 179/190
- [5.2] RICHTER, W.: Wünsche an die Konstruktionslehre (Requirements of Design Theory), *Konstruktion* 42 (1990) 8, pp. 331/319
- [5.3] SCHNEIDER, W. and R. BARDENHEIER: Versagenskriterien für Kunststoffe (Failure Criteria for Plastics), *Z. f. Werkstofftechn.* 6 (1975) 8, pp. 269/280 and 6 (1975) 10, pp. 339/348
- [5.4] BARDENHEIER, R.: Das Anstrengungsverhalten polymerer Werkstoffe infolge mechanisch mehraxialer Beanspruchungen (Strain Behavior of Polymeric Materials under Multiaxial Mechanical Loads), Diss. TH (University of) Darmstadt 1981
- [5.5] HAUCK, CH.: Optimieren mechanisch beanspruchter Bauteile aus Thermoplasten mit der Finite-Element-Methode (FEM) (Optimizing Structural Parts under Mechanical Load by the Finite Element Method), *Konstruktion* 42 (1990) 12, pp. 421/427
- [5.6] SCHARR, G.: Experimentelle Bestimmung des kompletten Stoffgesetzes von anisotropen faser verstärkten Kunststoffen (Experimental Determination of the Complete Set of Laws Governing Anisotropic Fiber-Reinforced Plastics), *Meßtechnische Briefe* 21 (1985) 1, pp. 7/11
- [5.7] WÜBKEN, G.: Kunststoffteile rechnen und gestalten (Calculation and Design of Plastic Parts), *Techn. Rundschau Nr.* 47 (1978) 1, p. 33
- [5.8] OBERBACH, K.: Zur Aussagekraft von Stoßversuchen an Probekörpern für das Zähigkeitsverhalten von Plastformteilen (The Predictive Value of Collision Tests on Test Pieces for the Toughness Properties of Plastic Moldings), *Plaste und Kautschuk* 29 (1982) 3, pp. 178/182
- [5.9] SARABI, B.: Kunststoffkennwerte im Spiegel von Konstruktionspraxis und Werkstoffprüfung (Key Properties of Plastics as Reflected in Construction Practice and Materials Testing), *Kunststoffe* 81 (1991) 5, pp. 440/445
- [5.10] PUCK, A.: Einführung in das Gestalten und Dimensionieren (Introduction to Design and Dimensioning), in Ehrenstein/Märting: Konstruieren und Berechnen von GFK-Teilen (Design and Calculation of GRP Parts), Supplement to Kunststoff-Berater Umschau-Verlag, Frankfurt 1969
- [5.11] PUCK, A.: Zur Beanspruchung und Verformung von GFK-Mehrschichtenverbund-Bauelementen (The Loading and Deformation of GRP Multilayer Composite Structural Elements), *Kunststoffe* 57 (1967) 4, pp. 284/293; 7, pp. 573/582 and 12, pp. 965/973
- [5.12] KLEINHOLZ, R. and J. MOLINIER: Verstärkungswerkstoffe nach Maß (Made-to-Measure Reinforcing Materials), *Textilglas Report* 1/1986, pp. 13/20
- [5.13] SCHUMACHER, G.: Die mechanischen Eigenschaften durch Glasseidenmatten verstärkter Polyester- und Epoxidharze (Mechanical Properties from Glass-Mat Reinforced Polyester and Epoxide Resins), Diss. TH (University of Stuttgart) 1966
- [5.14] WIEDEMANN, J.: Elastizität und Festigkeit von Bauteilen aus GFK (Elasticity and Strength of GRP Structural Parts), in Ehrenstein et al.: Glasfaserverstärkte Kunststoffe (Glass-Fiber Reinforced Plastics), Volume 62, Expert-Verlag 1981
- [5.15] WURTINGER, H.: Entwurf und Vordimensionierung tragender Konstruktionen aus glasfaserverstärkten Kunststoffen (Design and Initial Dimensioning of Load-Bearing Structures Made from Glass-Fiber Reinforced Plastics), VDI-Z 109 (1967) 24, p. 1121 and 36, p. 1710
- [5.16] VDI-Richtlinie (VDI Guideline) 2014, Bl. 3 Entwicklung von Bauteilen aus Faser-Kunststoff-Verbund (Development of Structural Parts Made from Fiber-Plastic Composite), Beuth-Verlag, Berlin 1992

- [5.17] MPA and MPI Molding Simulation Software, Moldflow Corporation, Wayland, MA, USA.
www.moldflow.com.
- [5.18] GEBHARDT, A.: Rapid Prototyping, Hanser Verlag Munich Vienna 1996
- [5.19] SONNEFELD, F.: Schmelz- und Lösekerntechniken für Klein- und Nullserien (Melt and Lost Core Techniques for Short and Trial Runs), Diploma thesis, University (TH) of Karlsruhe 1997
- [5.20] ANON.: Elastomere für das Lasersintern (Elastomers for Laser Sintering), *Der Zuliefermarkt* **11** (1997)

6 Design and Material Considerations for Parts Subjected to Mechanical Loads

There are a variety of technical tools available to designers, including computer-aided design tools (CAD and CAE) to relieve the burden of routine tasks and perform complex analyses. There is also design methodology that organizes and classifies design principles in systematic manner, thereby making it easier to find optimum solutions [6.1–6.3]. Nevertheless, a design emerges not only from theoretical technical knowledge, but also from an individual's thought processes that relate to both form and function, as well as manufacturability [6.4, 6.5].

Unfortunately, all that can be described here is information about materials, stresses, manufacturing processes, methods of joining, and so forth. Therefore, designers are concerned about designing for the material, for the manufacturing process, for the joint, or for the load and so on. However, when pursued systematically, these objectives are often at odds with one another. Against this background, the following sections present some embodiments of designs, where mechanical loads are important design criteria. It is hoped that this section will provide some general knowledge about tried and tested examples of structural polymeric material parts. These examples are structured in accordance with the overriding design task [4.18].

6.1 Flexible Structures

Polymeric materials are so versatile that they can be used for both rigid and flexible items. There are at least three possible methods for rendering a cross section or an entire structure flexible in the sense of achieving high deformation under a predetermined force. These are:

- Use of a material having a low modulus of elasticity;
- Having a low geometrical moment of inertia in the cross section; and
- Exploiting the nature of the loading force as it relates to geometry.

While each of these factors (material, design, and external force) can be used to achieve a desired result, flexibility in this case, it is usually some combination of these variables that leads to the optimum solution.

6.1.1 Modulus of Elasticity

Elastomers are examples of polymeric materials having a relatively low modulus of elasticity. Using thermoplastic elastomers, particularly elegant designs can be realized by two-component, or multi-shot, or insert injection molding (see Chapter 7).



Figure 6.1 Shutter consisting of rigid bars composed of a blend of ABS and PC and a flexible connecting web composed of TPU.

The right-hand section of the figure shows how this part is installed to act as a closure for a glove compartment (Manufacturer: Fischer-Werke, Waldachtal-Tumlingen).

As an example, Figure 6.1 shows a shutter consisting of individual rigid crossbars, composed of a blend of ABS and PC, which are back-injected overmolded in the same process with a web produced from a flexible TPU. The detached runner for the ABS/PC crossbars can be seen in the top left portion of the figure, while the detached runners for the TPU are shown in the top right and lower left quadrants. This shutter is used in automobiles (BMW 5 series) for closing a small glove compartment, shown in the picture on the right. It functions much like a roll-top desk.

6.1.2 Design Geometry – Moment of Inertia

Flexibility can also be obtained using geometry as a variable. Very thin-walled structures or parts of structures are naturally extremely flexible. Examples of such structures include integral hinges and flexible couplings (see also Section 8.3). They act as integral connecting links between parts that have to move relative to one another while maintaining a certain alignment. Figure 6.2 shows an example of this type of design solution for an integral joint between a housing and its lid. It should be noted in the design that the transition from the parts into the thinner cross section of the hinge is characterized by radii of curvature promoting flow and reducing stress concentration effects. This in turn favors the marked longitudinal alignment of the molecules needed in the flexible hinge region, thereby imparting high flexural fatigue strength. Stress concentrations and cracking would likely arise if the transition is too abrupt.

Molecular alignment (and thus hinge life) can be further enhanced by flexing the hinges several times after demolding (while still warm) to provide additional orientation.

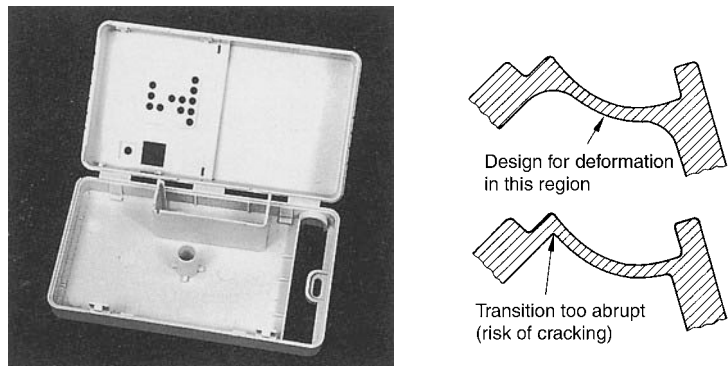


Figure 6.2 A flexible integral hinge connecting a housing and its lid; material: PA 6 [6.7]

Hinged parts of this type are generally injection molded. If the part is gated into the base, melt must flow through the hinge area to fill out the lid. If the flow length is too long, the lid may not fill out (*i.e.*, a short shot). Gates must be provided on both the housing and the lid to ensure filling. The invariably forming weld or knit line must not be located in the hinge area, because weld lines are generally weaker.

6.1.3 Load-Geometry Interactions

When designing for flexibility, it is obvious to consider the use of materials having a low modulus of elasticity or to utilize thin wall sections. However, the flexibility of a structure is not simply a function of the modulus of elasticity and the geometry of the part; it can also be determined by the nature of the load and its interaction with the part's geometry.

Figure 6.3 illustrates an example of a beam having a rectangular cross section, where the deformation produced by a force acting on it is higher in bending (provided $l > h$) or in torsion (see Eq. 6.2) than in compression or tension, because the numerical factor ζ in Figure 6.3 also assumes values greater than one [6.6].

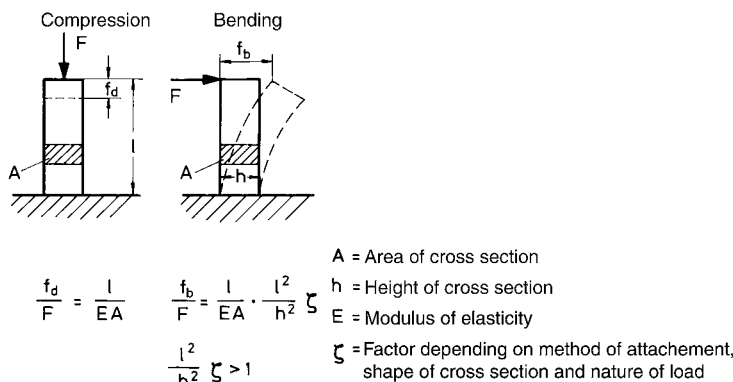


Figure 6.3 Effect of the direction of a force on deformation according to Muller [6.6]

If high degrees of deformation are to be achieved in a predetermined direction, a structure should be designed in such a way that the forces in action cause bending (or torsion) in the structure. On the other hand, rigid structures result when the forces in action produce tensile or compressive stresses.

Snap-Fit Joints

Examples of polymeric material structures where high levels of deformation are desirable include springs and snap-fit joints. Snap-fit joints, especially those constructed from thermoplastic polymeric materials, afford a simple, economical, and reliable type of joint connection. When the parts to be joined are pushed together, ribs, bulges, or hooks engage in corresponding undercuts and produce a largely positive joint without any additional structural elements or extra pieces. The use of snap-fit joints is a key element of design for enhanced manufacturability (see also Section 8.1). The effective height of the hook region (snap-fit height or interference) can be greater for structures or beams subject to bending stresses than for structures subject only to compressive or tensile stresses. Accordingly, in what are known as “annular” snap-fit joints, the relatively rigid circular cross section can be modified with a series of longitudinal slots resulting in a series of semi-circular segments subject to bending (rather than tensile) stresses as shown in Figure 6.4.

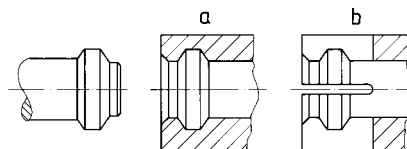


Figure 6.4 Schematic view of an annular and slotted annular snap-fit joint

- a) Annular snap joint is predominantly under tensile stress
- b) The slotted annular snap joint has a higher bending component due to segmentation

Rollers, Wheels

Flexible plastics or elastomers are often used for rollers of various types. The phenomenon of “flattening” in rollers is usually undesirable, because this can increase rolling friction, create non-uniform contact pressure, and so forth. On the other hand, a higher degree of flattening is desirable in some cases to increase friction. This can be achieved by coring out regions just below the roller surface so that the thinner web sections will flex and hence greater deformation is produced (see Figures 6.5 and 6.6). The thin web sections “bend” rather than the usual “compression” for a solid roller.

Pressure Bars (Printing Webs)

The element in Figure 6.7 is also based on the design principle of flexible construction. When the bars between the two plates are vertical, they rigidly fix the spacing between the two plates. A small lateral displacement of the plates relative to one another suffices, however, to produce a bending moment in the bars which are connected to the plates by integral hinges so that the rigidity is lost.

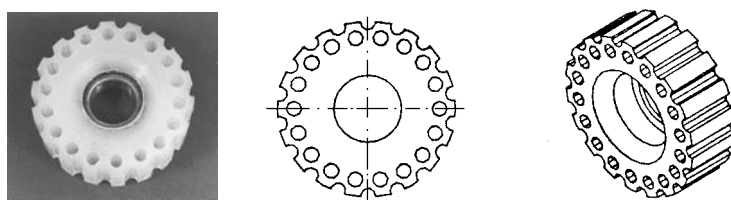


Figure 6.5 Roller made of PU (Shore hardness approx. 88 A) for feeding paper.
The combination of the surface profile and cored-out section results in improved performance.
(Courtesy: Räder-Vogel, Hamburg)

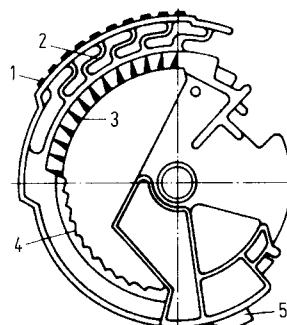


Figure 6.6 A typical face roller produced using the same concept.
The outer typeface support is attached to the inner frame by a series of flexing elements, demonstrating the use of flexing elements instead of compression [6.16].

- 1: Typeface
- 2: Flexing elements
- 3: Toothed segment
- 4: Ratchet
- 5: Limit stop

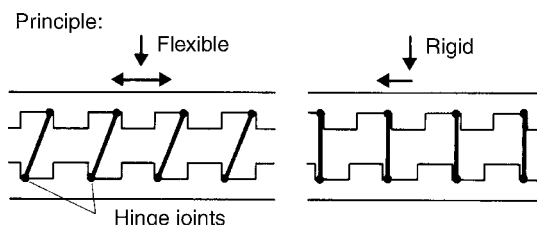


Figure 6.7 Spacer in rigid position (right) and yielding position (left)

6.2 Flexurally Rigid Structures

The distribution of stress over the cross section of a beam subject to flexural loading is linear in the case of materials obeying Hooke's law. However, in the case of most polymeric materials, the distribution of stress departs from linearity to the extent that the material exhibits nonlinear behavior. The actual outer fiber stress becomes smaller than the theoretical linear elastic stress and the state of stress becomes increasingly multiaxial, because shear stresses now appear in the interior of the beam.

Cross sections with most of their cross-sectional area in the peripheral regions are particularly flexurally rigid.

Figure 6.8 shows a ranking of the flexural stiffness of various cross-sectional shapes, each having the same cross-sectional area, *i.e.*, each cross section consuming the same amount of material.

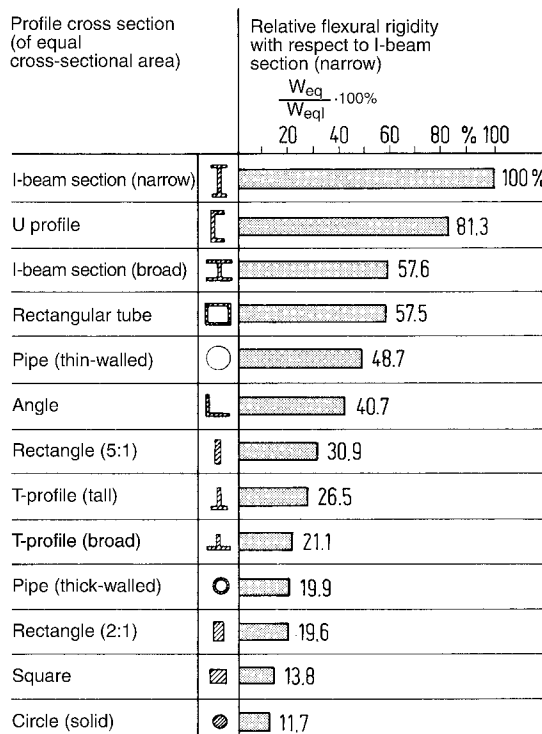


Figure 6.8 Ranking of different cross-sectional shapes in terms of their flexural stiffness for the same cross-sectional area [6.8]

As a result of the processing technology employed, moldings made from polymeric materials are frequently sheet- or shell-like structures. Because of the “relatively” low modulus of elasticity of these materials, they are considerably less rigid than metal structures of the same shape. The following possibilities are available for increasing the rigidity of components:

- Increasing the modulus of elasticity, e.g., by reinforcement with glass, carbon or aramid fibers
- Increasing the thickness of the walls
- Introducing ribs or corrugations (see also Chapter 10).

The following relationship for the flexural stiffness of a plate or sheet, shows that only a linear stiffening effect can be achieved by increasing the modulus of elasticity.

$$D = \frac{E \cdot s^3}{12(1 - \mu^2)} \quad (6.1)$$

where

s = Thickness of the plate or sheet

μ = Poisson's ratio

However, increasing the wall thickness will increase the stiffness by a power of three. Even more effective than a uniform increase in wall thickness is the attachment of ribs to the plate surface (see also Section 10).

Example

How much can the wall thickness of a plate be reduced by using a 35% glass fiber reinforced polyamide 66 compared to a neat polyamide 66?

$$E_{PA\ 66} = 1600\text{ MPa}$$

$$E_{PA\ 66GF35} = 8500\text{ MPa}$$

$$\frac{s_{unreinf}}{s_{reinf}} = \sqrt[3]{\frac{E_{reinf}}{E_{unreinf}}}$$

$$S_{reinf} = \frac{1}{\sqrt[3]{\frac{8500}{1600}}} = 0.57$$

Although the modulus of elasticity of the reinforced PA is more than five times higher than that of the neat PA, the wall thickness can only be reduced by about half.

6.3 Flexurally Flexible, Torsionally Rigid Structures

A bar having a circular cross section is rigid both flexurally and torsionally. However, if in a bar with a circular cross section, incisions are made perpendicular to its axis each offset by 90° , and material is removed from the peripheral regions, a flexible element is produced. Its torsional rigidity, however, is not substantially impaired because there is still a continuous closed cross section.

This principle was exploited in the compensating coupling shown in Figure 6.9. The injection molding process allows the efficient production of such a structure from a thermoplastic. The coupling shown is manufactured from POM, an appropriate material in this case, because of its high flexural fatigue strength and good elastic properties.

The joint in Figure 6.10 is based on the same principle. Its double cardanic action is achieved by means of two integral hinges offset by 90° . The coupling shown (for a shaft diameter of 1.5 mm) can compensate for an angular shift of as much as 15° . However, the coupling is limited to a torque transmission of approximately 5 N [6.9].

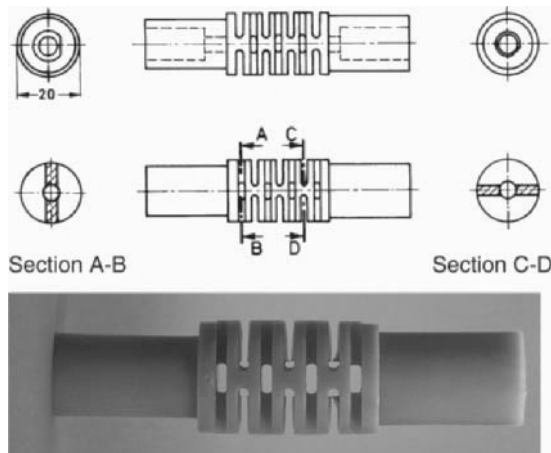


Figure 6.9 Flexible, torsionally rigid compensating coupling made from POM (N 2210) according to [6.9]

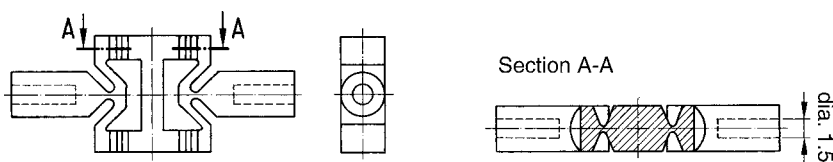


Figure 6.10 Articulated joint made of polypropylene following the principle of two integral hinges offset by 90° , suitable for relatively low torques according to [6.9]

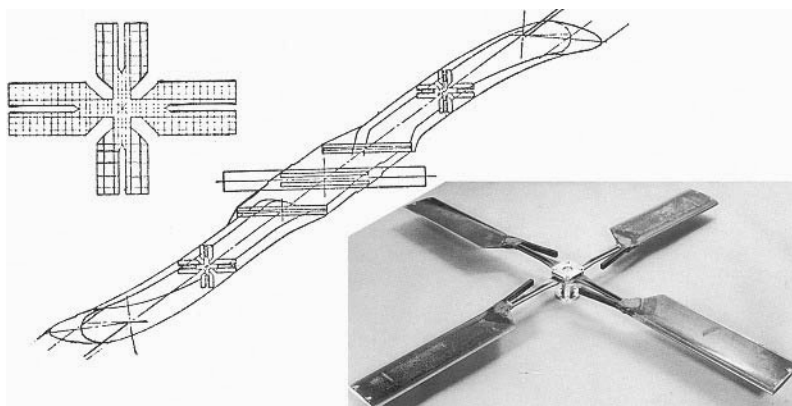


Figure 6.11 Bearingless tail rotor as an example of a flexurally rigid, torsionally flexible design according to [6.10]

6.4 Flexurally Rigid, Torsionally Flexible Structures

A structure having good resistance to bending and torsional flexibility can be achieved with glass-fiber composites simply by arranging the fibers unidirectionally. The glass fibers have high tensile and compressive stiffness, hence bending stiffness. At the same time, however, the shear strength and rigidity parallel to the fiber direction is relatively low so that there is a degree of flexibility under torsional loads. These properties arising from the nature of the material can be magnified considerably by giving the composites an appropriate geometric change in shape. As has been shown, the geometrical moment of inertia of a cross section – a measure of its flexural rigidity – can be increased by arranging as much material as possible at the greatest possible distance from the neutral axis. As long as the cross section is not closed at its outer perimeter, it remains torsionally flexible. This structural principle also applies to thermoplastics.

Figure 6.11 shows a helicopter tail rotor composed of glass-fiber reinforced plastics. The design is referred to as a bearingless design, because the cant angle is adjusted solely by the twisting of the flexurally rigid but torsionally flexible star-shaped profile. Considerable problems may occur in manufacturing of such cross-sectional shapes from fiber composite materials [6.10, 6.11].

6.5 Torsion-Resistant, Torsionally Rigid Structures

If a structural part is subjected to torsion by a torque M_t and the material exhibits elastic properties, there is a linear distribution of the torsional stresses over its cross section.

The maximum torsional stress occurs in the outer fibers.

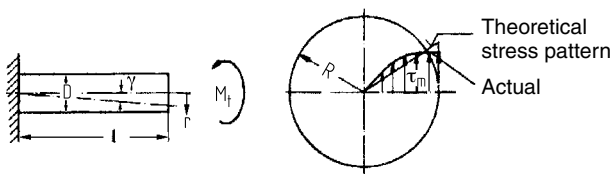


Figure 6.12 Distribution of shear stress for pure torsion

$$\tau_{\max} = \frac{M_t}{W_t} \quad (6.2)$$

The torsional angular displacement ρ is given by:

$$\rho = \frac{180}{\pi} \cdot \frac{M_t \cdot l}{G \cdot J_p} \quad (6.3)$$

where

M_t = Torque

W_t = Polar moment of resistance

J_p = Polar moment of inertia

G = Shear modulus

l = Length

From this distribution of stress it follows that torsional stiffness is best achieved using cross sections having material in the peripheral regions which should form a closed profile.

Under the further requirement of minimum consumption of material, these conditions are best fulfilled by structures, such as a thin-walled pipe. Figure 6.13 shows a compilation of different profile shapes of the same area together with their relative torsional rigidity with reference to the pipe cross section.

Because the stresses in a twisted pipe run at an angle of 45° to the pipe's axis, torsional rigidity can be further reinforced using a fiber composite in which the fiber direction matches the direction of stress. In the case of a pipe subjected to a torsional load, this anisotropy in strength and rigidity can be achieved by means of fibers cross-wound at 45° in a spiral (see also Figure 1.16).

Mutual reinforcement by joining individual parts together affords another possibility for obtaining structural parts or subassemblies having increased torsional rigidity. This is frequently used in the design of housings made from injection-moldable polymeric materials. As an example of this principle, Figure 6.14 shows a drawer box consisting of rigidly ribbed single U-shaped parts. After joining the upper and lower parts by means of molded-in snap-fit elements, a hollow structure of adequate torsional rigidity is obtained.

The use of diagonal ribbing is also a common design practice for rendering planar parts torsionally rigid (see Section 10).

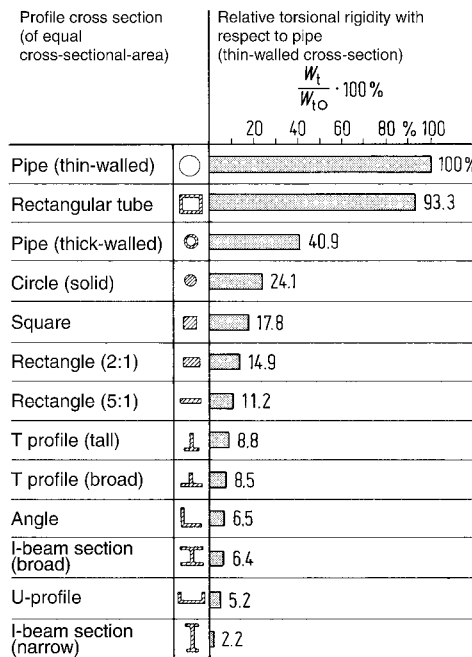


Figure 6.13 Ranking of different cross-sectional shapes in terms of their torsional stiffness or rigidity for the same cross-sectional area [6.8]

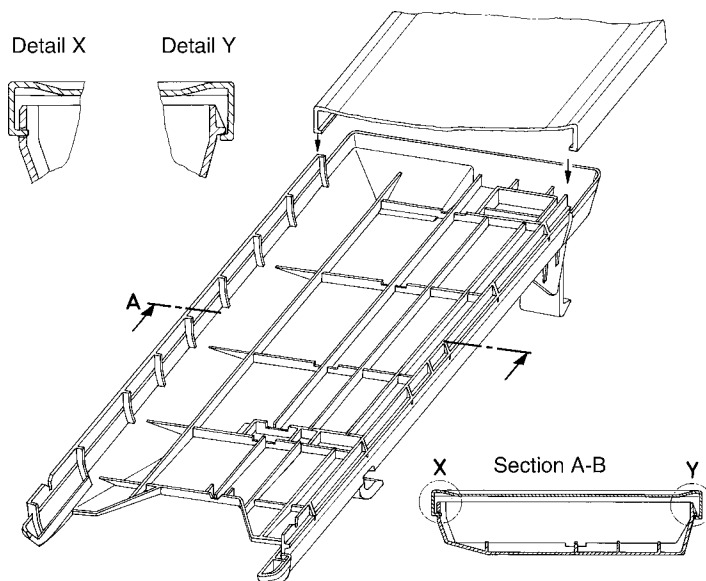


Figure 6.14 Stiffening a housing by joining two injection molded halves to form a torsionally rigid hollow structure

6.6 Flexurally and Torsionally Rigid Structures

Figures 6.8 and 6.13 show that a square tube cross section meets both the optimum requirements for flexural and torsional rigidity. However, problems may be encountered in demolding the core when producing such a shape by injection molding*. Other cross-sectional shapes together with their relative rigidities are presented in Figure 6.15.

A good solution for a structure meeting the above requirements has been found in the design of an angled gas pedal [6.12]. An upright U profile modified with cross ribbing was selected

Profile cross section	Relative rigidity (%)	
	Bending	Torsion
Square tube	100	100
U-profile, vertical, ribbed	56	65
U-profile, horizontal, ribbed	94	65
Double-T-profile, ribbed	94	30
ESUM profile, ribbed	54	20

Figure 6.15 Relative rigidities of different cross sections with reference to the square tube cross section [6.12]



Figure 6.16 Gas pedal with ribbed U profile cross section; at the bend, the open end of the U profile is switched to the other side [6.12]

* A solution may be found under certain circumstances in the gas-assist injection molding process (see Chapter 7).

for this application. In addition, the open end of the U profile was switched to the other side at the bend. In this way, any twisting of the pedal under load from the driver's foot is limited (see Figure 6.16). Such structures should be simulated using a structural analysis program (FEM) to confirm that the design is structurally acceptable.

6.7 Torsionally Flexible Structures

The relatively low shear modulus for most polymeric materials already satisfies the material requirements for torsionally flexible structural elements, such as springs or snap-fit features (see also Sections 6.10, 8.1.2, and 8.2.1.4).

Torsionally flexible cross-sectional geometries are presented in Figure 6.13. These cross sections can be further modified to limit the stiffness imparted by the outer perimeter (*e.g.*, a slotted pipe cross section).

6.8 Tension-Proof, Tensionally Rigid and Torsionally Flexible Structures

Such requirements on a structure can once again be met in part using appropriate materials. Fiber-composite materials having fibers arranged in the direction of the tensile load provide tensional rigidity. Figure 6.17 shows a tension-proof and tensionally rigid structure, but at the same time, it is also a torsionally flexible element made from an epoxide composite material. Torsional flexibility is further enhanced by embedding the fibers in a PU elastomer. This component is known as a Bendix joint, a connector in the main rotor of a helicopter. It is approximately 285 mm long. The reinforcing fiber used was a 0.15 mm thick steel wire, laid in place under pretensioning by a winding process. As mentioned, the wires are sheathed in a polyurethane elastomer in order to increase the torsional flexibility of the composite.

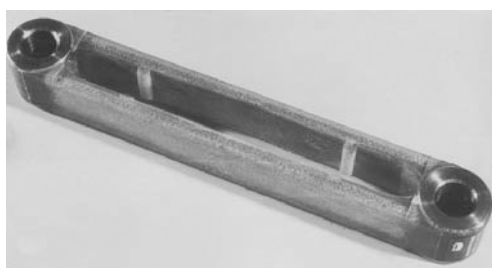


Figure 6.17 Tension-proof, tensionally rigid, and torsionally flexible connecting member (known as a Bendix joint) on the main rotor of a helicopter according to [6.15] (Photograph: MBB, Munich)

6.9 High Shear-Strength, Shear-Resistant Structures

The distribution of shear stress over a rectangular cross section subjected to a transverse force is parabolic. The maximum shear stresses occur in the region of the axis through the center of gravity. The outer edges are free of shear stress (see Figure 6.18).

From this it follows directly that for this type of structure it makes sense

to accumulate as much material as possible in the region of the axis along the center of gravity.

A circular cross section best meets this requirement, whereas a narrow I profile is not effective. It is apparent that structural parts subjected to bending loads and those under shear loads need to be dimensioned from completely contrary perspectives. The effect of the direction of the transverse force with respect to the cross section is also noteworthy. This is made clear by the example of the square cross section in Figure 6.19.

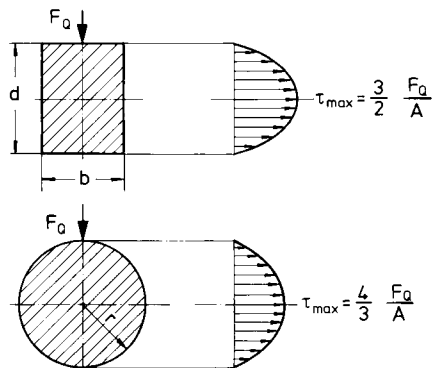


Figure 6.18 Pattern of shear stress over different cross sections subjected to a transverse load

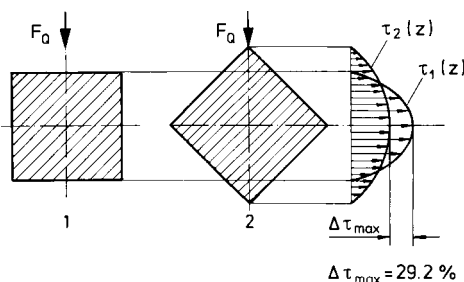


Figure 6.19 Reduction of the maximum shear stress in a profile subjected to a transverse force by altering the direction in which the force is introduced (installation position) [6.8]

6.10 Pressure-Yielding and Compression-Resistant Structures

Structural elements that must respond to low pressure loads with relatively large deformations include, among others, seals to compensate for inaccuracies in shape, flexible compression springs, and shock absorbers. Elastomers with relatively flat pressure/deformation curves meet the material requirements for such structures. Design measures for achieving high levels of deformation (in the direction of an external compression load) include converting the compressive stresses into flexural stresses, as shown in Section 6.1, or into shear stresses. By analogy with Figure 6.3, the angular deformation γ under the action of a torsional moment $M_t = F_t l$ is given by:

$$\frac{\gamma}{F_t} = \frac{l}{E \cdot A} \cdot \frac{\zeta}{d} \quad (6.4)$$

For a circular cross section made from a material with elastic properties $\zeta = 11.2$.

Using this principle in the spring arrangement shown in Figure 6.20, the maximum deformation on the right can be increased by 30% over that on the left for the same consumption of material.

Conversely, the compressive rigidity of a compression spring is increased when lateral expansion is largely impeded. This can be done, for example, by vulcanizing intermediate metal sheets in place as shown in Figure 6.21. In this case, the susceptibility of such a structure to shear is retained. This principle is applied in practice in bridge bearings [6.13].

Examples of structures which yield under pressure are also found when meeting certain tolerance and fitting requirements, in which components interact with other components to a defined level of fit or play.

Setting unrealistically narrow tolerances seldom results in success but rather gives rise to high numbers of rejects.

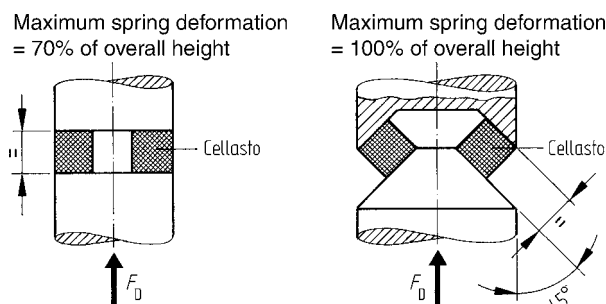


Figure 6.20 Increasing the deformation of an elastomer spring of the same overall height by changing the direction of the load on the spring element

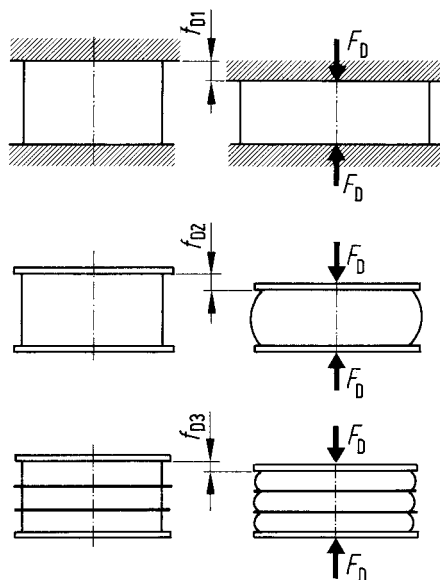


Figure 6.21 Impeding lateral expansion in elastomeric compression springs ($f_{D1} > f_{D2} > f_{D3}$) [6.13]
 Top: Lateral expansion unimpeded at the end faces
 Center: Lateral expansion impeded at the end faces
 Bottom: Lateral expansion largely impeded by vulcanizing intermediate metal sheets in place

On the other hand, certain assembly problems may also be overcome by exploiting the deformability of the polymeric materials when they are being joined together. A tried and tested method of ensuring a tightfit is to attach what are referred to as "adaptor ribs". In doing so, a small overlap is added in some areas; when the parts are joined together, deformation of the material at these points occurs. The principle is illustrated in Figure 6.22 (see also Figure 7.30).

The well known building blocks from Fischer-Technik also carry such adapter ribs on their sliding connector seatings (see Figure 6.23).

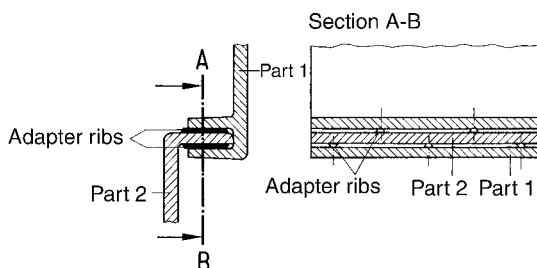


Figure 6.22 Tight-fitting joints by means of adapter ribs

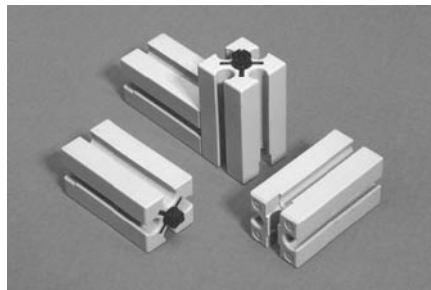


Figure 6.23 PA building blocks from Fischer-Technik with POM adapter ribs at the end faces. The adapter ribs provide a tolerance compensation and improve slip for the connector seatings

6.11 Multifunctional Structures

In the previous sections, some design principles embodying specific structural characteristics have been presented by way of example, usually with reference to single elements. It can be said that an “overall design” is particularly elegant when it is implemented with as few individual parts as possible. When the design possibilities afforded by injection molding are fully exploited together with the possibilities for building-in selective anisotropy (fiber and molecular alignments) and the use of easy-fit connector technologies, multifunctional designs can be implemented, which are not only technically appealing, but may also offer major cost savings. Such multifunctional parts built by integrated methods are referred to in different contexts in other parts of the book (see, for example, Figures 1.8 to 1.10, 6.6, 8.2 and 11.34).

Over and above these, the following two examples should make it abundantly clear just how much can be saved in manufacturing and assembly costs by systematic design.

Figure 6.24 shows the completed design for a grounding contact plug made from PA by integrated technology. The entire housing, including the strain relief, is injection molded as a single part. Pins, contact terminals, etc. are held captive, snapped in, or riveted and by bending about the integral hinges, the finished plug is produced.

A technically and economically interesting development in plastic components in the utility vehicle sector was made by Daimler-Benz, Gaggenau. Figure 6.25 shows a manual gas lever made of glass-fiber reinforced PA 66 (A3WG5) for the MB-Unimog. The previous generation levers were manufactured from steel and consisted of seven individual parts, which were joined together in a series of operations, such as bending, riveting, bonding, and braze welding. The new lever made from polymeric material is produced in one operation by injection molding and can be assembled without any additional secondary operations.

In order to transmit torque to the shaft, the hub is provided with a knurled surface and is slightly undersized. The shaft onto which it is pushed also has a knurled surface. This method of joining a shaft to a hub is particularly efficient, takes advantage of the properties of the material, and at the same time produces a joint which can withstand relatively high loads (see also Section 5.2.3.2).

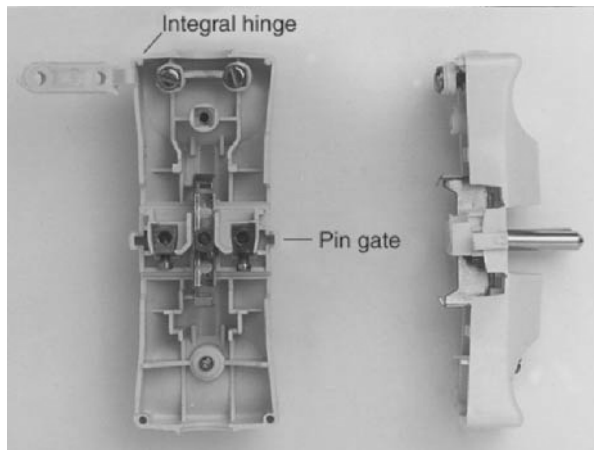


Figure 6.24 Grounding contact plug made from PA by integrated technology

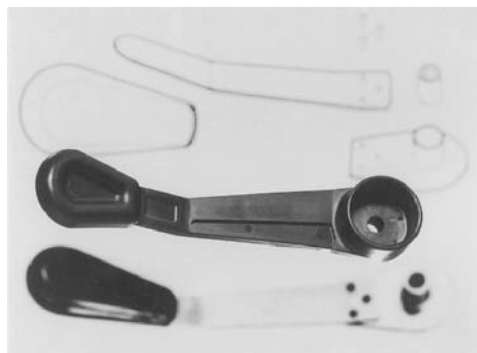


Figure 6.25 Manual gas lever of integrated plastic design (Manufacturer: KABO PLASTIC, Feldkirchen)

6.12 Thermal Expansion and Thermal Stress

If the thermal expansion of a component (see also Section 4.6.1) is impeded, thermal stresses arise. This can have different causes, the most common being:

- Impeded shrinkage due to the dimensions of the mold
- Locally variable thermal loads in the part
- Combinations of materials having different coefficients of thermal expansion

According to Hooke's law, impeded expansion results in a stress σ_T given by:

$$\sigma_T - E \cdot \varepsilon_T = -E \cdot \alpha \cdot \Delta T \quad (6.5)$$

In polymeric materials, the modulus of elasticity E and the coefficient of thermal expansion α are temperature-dependent variables, which should be integrated over ΔT . In most cases, however, it suffices to calculate using an average value.

In addition, thermal stress, like any mechanical stress, is dependent on time as relaxation can occur over time.

Impeded Shrinkage

A ring injected onto a smooth metal shaft is hampered from shrinking on cooling. The molecular processes on cooling are complex. Solidification, crystallization (for semi-crystalline polymers), and cooling cause a build-up of stress due to the rise in the modulus of elasticity. Also, a relaxation of stress is simultaneously superimposed on this. In every case, cooling stresses arise, and if cooling proceeds too rapidly and/or the shaft is not preheated, these can result in hoop fracture. Thermal stresses do arise when shrinkage is impeded by the dimensions of the mold as shown at the bottom of Figure 6.26. Sharp edges give rise to additional notch-related stresses.

As a further example, Figure 6.27 shows overmolded rolling bearing rings in which design solutions A and B result in significant internal stresses, while C, D, and E give rise to low internal stresses [6.17]

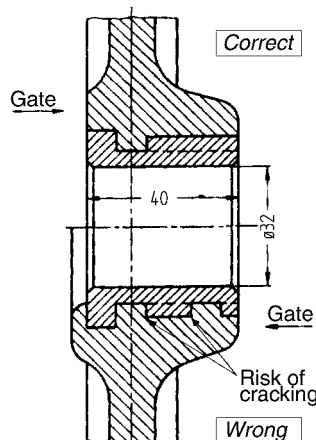


Figure 6.26 Correct and incorrect design of an overmolded metal hub for high load applications

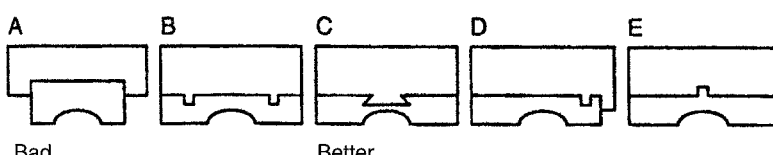


Figure 6.27 Overmolded rolling bearings having distinctly impeded shrinkage (A, B) and less constrained design variations (C, D, E) [6.17]

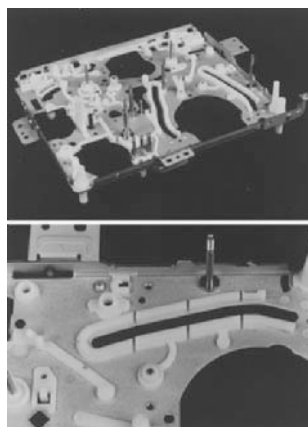


Figure 6.28 A metal circuit board ensures high rigidity and dimensional stability due to its low thermal expansion coefficient. Relatively long elements composed of high CTE POM are provided with expansion joints to compensate thermal expansion and thermal stresses (Photograph: Öchsler, Ansbach)

Combinations of Materials

Combinations of materials are often used to achieve an acceptable division of requirements between the materials employed. Plastic/metal components are often used together. The purpose of the metal is to achieve a low coefficient of thermal expansion (CTE) and high rigidity. Printed circuit boards produced by outsert technology provide a typical example of this (see Figure 6.28).

Figure 6.29 illustrates the difference between the changes in dimensions in an all-plastics design and in an outsert structure over a temperature range of -20 to 80 °C [6.18].

Another thermal expansion example is presented in Figure 6.30. In the large gear wheel shown, the hub is made of sheet steel and only the actual teeth are made of cast PA. Cast PA has very good tribological properties. In the case of an all-plastics wheel, expansion for $\Delta T = 40$ °C would be approximately 4 mm!

Expansion Joints

A tried and tested method for keeping thermal expansion within acceptable limits is to integrate expansion joints. An example of this can be seen in Figure 6.28.

Bearing liners incorporate a diagonal slit (Figure 6.31) or the individual supporting segments are connected by thin film bridges (see Figure 6.32 and also Figure 12.19).

Expansion Compensation

Changes in play or clearance due to variations in temperature can be controlled by simple means when the entire system exhibits the dimensional changes. Figure 6.33 shows such a solution in which small gear wheels are mounted in a yoke made of the same polymeric material so that changes in the play of the teeth are compensated.

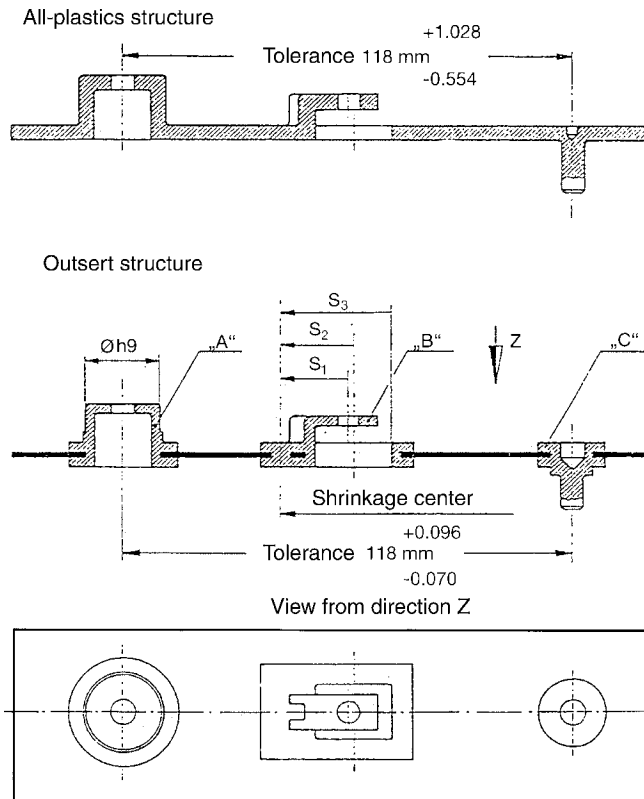


Figure 6.29 Dimensional changes due to thermal expansion in all-plastics and outsert structures for temperatures varying from -20 to 80°C

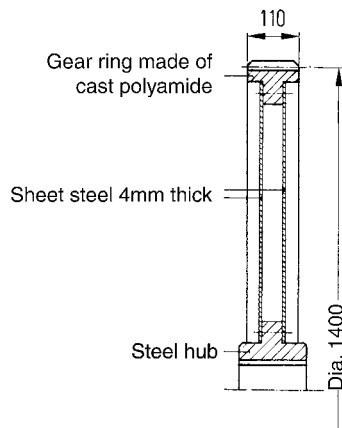


Figure 6.30 In the case of large gear wheels, the hub is made of steel sheet

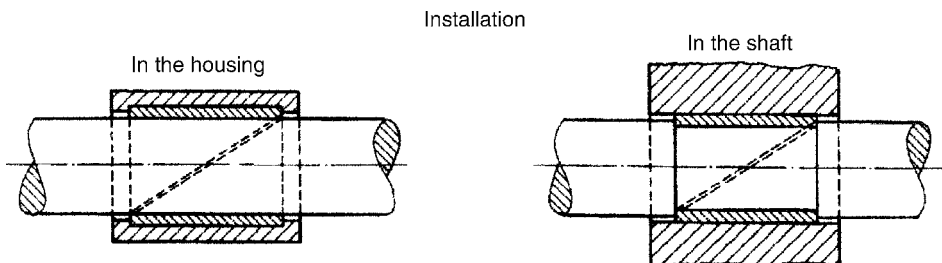


Figure 6.31 Changes in dimensions caused by temperature fluctuations can be absorbed using slit bushings



Figure 6.32 Tight-fitting bearing for linear movements.
The actual sliding region is divided into segments connected by 0.2 mm thick film bridges to allow for thermal expansion compensation.
(Photograph: igus GmbH, Bergisch Gladbach)

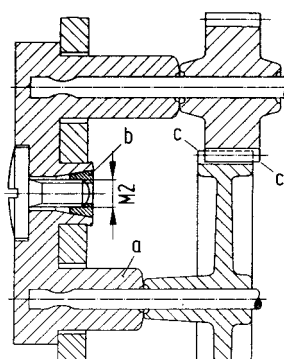


Figure 6.33 Mounting of gear wheels in precision mechanical instruments to compensate for thermal expansion
 a) Yoke made of PA 11
 b) Cone clamp
 c) Gear wheels made of PA 11

6.13 Universal Joints

Two-component injection molding (see also Section 7.4) also allows the production of universal joints in effectively one operation.

To make universal joints, largely incompatible materials with different melting points and different degrees of shrinkage (thermal expansion) can be combined.

A ball-and-socket joint is shown in Figure 6.34. In the first step, the ball is injection molded from PA 66 containing 2% of MoS₂. Because of the precision required, the molded part is machined down to the precise spherical geometry. In a second cavity for forming the socket, the ball is overmolded with glass-fiber reinforced PBT.

In this case, the gate must be positioned so that there is no direct flow of material onto the ball (despite its higher melting point) to be sure that the surface does not melt or distort. The required clearance in operation can be achieved, on the one hand, through the different shrinkages of the materials used and, on the other hand, in that the ball is raised to a higher temperature before overmolding so that it expands to an appropriate dimension. In this case, this temperature was 160 °C [6.7].

When less stringent requirements are imposed on the precision of the joint, the joints can be produced in one operation. The toy shown in Figure 6.35 and the fastener in Figure 6.36 is produced by the conventional multi-component processing without any secondary operations.

To produce the toy monkey, a rotary mold with three cavities is used. In the first cavity, the monkey's head is injection molded in PBT. The mold is then rotated 120° and at the next station, the trunk composed of PA 6-GF15 is injected around the ball at the neck. Because of the incompatibility of these two materials and the lower shrinkage of PA 6-GF, this joint remains slightly articulated after demolding.



Figure 6.34 Ball-and-socket joint as feed-through for the steering column in Unimog vehicles to compensate for twisting of the vehicle [6.7]
(Photograph: Kabo-Plastic, Hartheim)

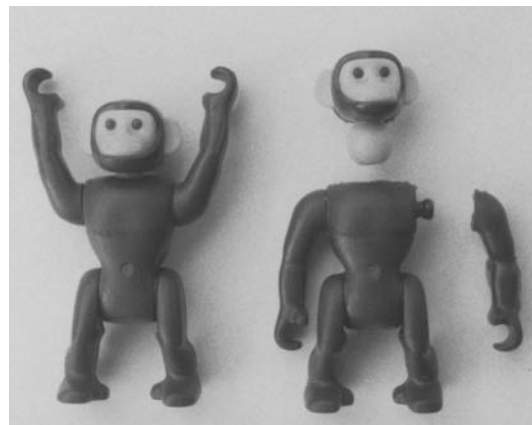


Figure 6.35 Toy monkey with articulated head, arms, and legs obtained by injection molding

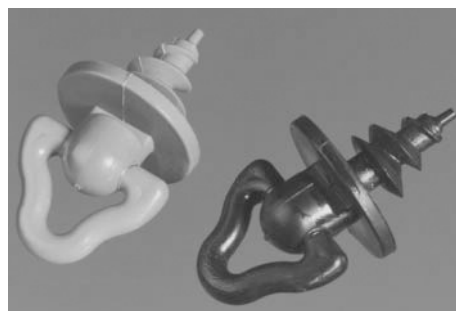


Figure 6.36 Fastener with movable handle (Manufacturer: Fischer Werke, Tumlingen)

After a further rotation, the hair and the extremities composed of POM are injected onto the projections on the trunk. These materials are also incompatible so that relative movement of the parts is ensured. The higher shrinkage of the POM results in a tight fit, which allows stable setting of the extremities in any position.

The fastener in Figure 6.36 is used for fixing floor carpets in automobiles. Here also, the triangular handle made of POM is injection molded first and then the screw section with the thread composed of PA is molded on top so that both parts can move relative to one another.

A conventional universal joint for a rearview mirror in an automobile is conventionally made of several parts (see Figure 6.37, top). Using multicomponent molding technology, this universal joint can be made in a single process. The mirror support is injection molded with the universal joint using ABS filled with glass beads (shrinkage: 0.2%). After rotation into a second cavity, the base plate composed of POM is then injected around the ball. The shrinkage of POM is 2% so that a tight seating is obtained. The entire production cycle takes 40 seconds.

As a general rule, a base or home position can be provided in such universal joints by means of a slight flattening of the ball.

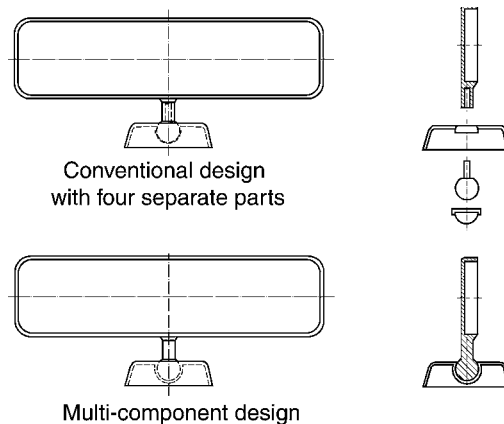


Figure 6.37 Ball-and-socket joint for an automobile rearview mirror as conventionally designed (top) and as produced by two-component molding technology (Ferromatik Milacron GmbH)

References

- [6.1] ROTH, K.: Konstruieren mit Konstruktionskatalogen (Construction using design catalogs), Springer-Verlag, Berlin 1982
- [6.2] PAHL, G. and W. BEITZ: Konstruktionslehre (Design theory), Springer-Verlag, Berlin 1976
- [6.3] RODENECKER, W. G.: Methodisches Konstruieren (Methodical design), Springer-Verlag, Berlin 1976
- [6.4] RUTZ, A.: Konstruieren als gedanklicher Prozess (Design as an intellectual process), Dissertation, TU Munich 1985
- [6.5] EHRLENSPIEL, K. and A. RUTZ: Konstruieren als gedanklicher Prozess (Design as an intellectual process), *Konstruktion* **39** (1987) 10, pp. 409–414
- [6.6] MÜLLER, H. W.: Verformungsgerechtes Konstruieren (Design in line with deformation), *Chem.-Ing.-Techn.* **48** (1976) 7, pp. 594–601
- [6.7] EHRENSTEIN, G. W. and G. ERHARD: Konstruieren mit Polymerwerkstoffen (Designing with polymeric materials), Hanser-Verlag, Munich Vienna 1983
- [6.8] STEINHILPER, W. and KAHLE, U.: Biegung, Schub und Torsion beeinflussen die Gestalt eines Bauteiles (Bending, shear and torsion affect the shape of a structural part), *Maschinenmarkt* **87** (1981) 75, pp. 1548–1550
- [6.9] ERHARD, G. and STRICKLE, E.: Maschinenelemente aus thermoplastischen Kunststoffen, Band 2 Lager und Antriebselemente (Machine components made from thermoplastics, Volume 2: Bearings and drive members), VDI-Verlag, Düsseldorf 1985
- [6.10] BRUNSCH, K.: Rationelle Fertigungsverfahren zur Herstellung von Hubschrauberrotorblättern (Efficient production methods for helicopter rotor blades), MBB Report No. UD-312L80
- [6.11] HUBER, H., FROMMLEIT, H. and BUCHS, W.: Development of a Bearingless Helicopter Tail Rotor, 6th European Rotorcraft and Powered Lift Aircraft Forum, Bristol 1980
- [6.12] BRÜNING, W.-D., C. HAUCK and D. MÜLLER: Kfz-Pedalen aus glasfaserverstärktem Polyamid (Automobile pedals made from glass-fiber reinforced polyamide), *Kunststoffe* **79** (1989) 3, pp. 251–255

- [6.13] GOHL, W.: Werkstoffeigenschaften und Gestaltfestigkeit (Properties of materials and dimensional fatigue strength), *VDI-Zeitschrift* **119** (1977) 24, pp. 1189/1192
- [6.14] VORBACH, G.: Anforderungen an das Spritzgußteil aus der Sicht des Entwicklers und Konstrukteurs (Requirements on injection-molded parts from the point of view of the developer and designer), *VDI-Gesellschaft Kunststofftechnik Jahrbuch* (Plastics Technology Yearbook), 1980, pp. 89–116
- [6.15] BRUNSCH, K.: Personal communication
- [6.16] ROTH, K.: Anregungen zum Einsatz unkonventioneller Gestaltungsmöglichkeiten bei Kunststoffkonstruktionen aus Konstruktion, Fertigung und Anwendung feinwerktechnischer Kunststoffteile (Suggestions for using unconventional design methods in plastic structures from the design, production and use of precision mechanical plastic parts), VDI-Verlag, Düsseldorf 1976
- [6.17] EHRENSTEIN, G. W.: Mit Kunststoffen konstruieren (Designing with plastics), Carl Hanser Verlag, Munich Vienna 1995
- [6.18] ROTHE, J.: Sonderverfahren des Spritzgießens (Special methods of injection molding), *Kunststoffe* **87** (1997) 11, pp. 1564–1580

7 Designing for Production

Polymeric materials can be processed from raw materials to finished parts by a wide variety of manufacturing processes and technologies. An overview of the most important manufacturing processes and manufacturing resources is given in Figure 7.1. The reader may consult the basic literature, *e.g.*, [7.1] to [7.11] for more detailed descriptions of these processes.

Particular attention will be paid to designing for injection molding, because of the great importance of injection molding for processing thermoplastic polymeric materials.

In order to be in a position to exploit the design possibilities of injection-molded parts as fully as possible, the designer should have at least some idea of the significant effort to be invested in constructing the mold that gives the parts their shape. In addition, the operations and consequences of filling the mold, packing and cooling, and demolding have to be thought through in design terms. Otherwise, unforeseen problems may make it necessary to modify the mold, thereby causing extra costs and prolonging development time.

During mold filling, the flow of the melt gives rise to orientations, which, especially in the case of fiber-reinforced thermoplastics, can cause anisotropy in the finished parts and give rise to warpage due to direction-dependent shrinkage. Weld lines or entrapped air can also result, depending on the geometry of the mold.

Locally variable shrinkage and the related warpage can be caused and also prevented by variable control of the temperature of the mold and/or cooling rates. It is therefore important to consider cooling rate at the design stage of product development.

After cooling, the parts must be ejected and taken out of the mold. For this purpose, ejectors must be positioned at suitable points, demolding drafts have to be determined, and in the case of undercuts, acceptable solutions with regard to mold design must be sought. Each of these topics will be discussed in more detail in the following sections.

7.1 Mold Filling

Injection molding is a discontinuous manufacturing process. Specific operations with corresponding consequences for the quality of the finished part can be assigned to each phase of a cycle (see Figure 7.2). These consequences can be controlled within certain limits by the process parameters.

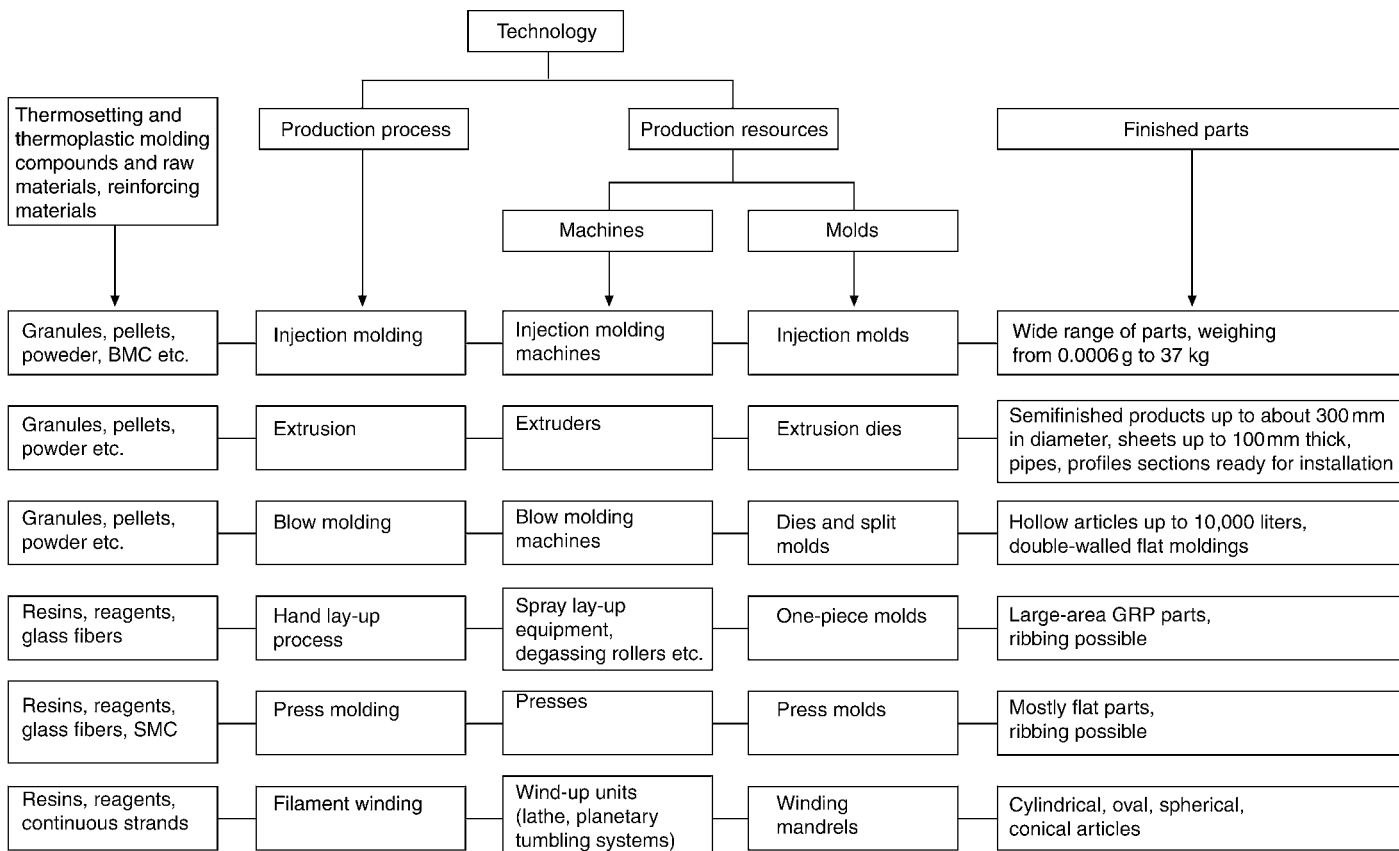


Figure 7.1 The most important manufacturing processes and manufacturing resources for producing industrial structural parts from polymeric materials

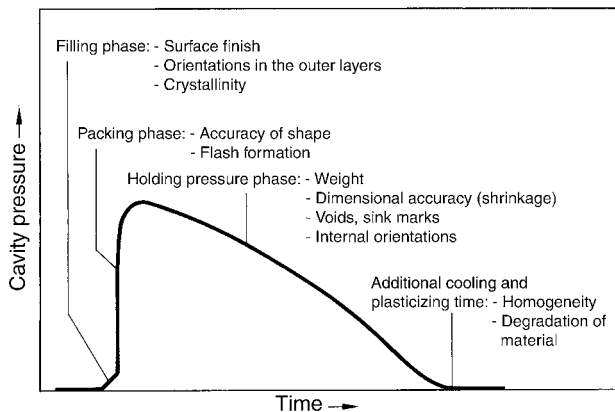


Figure 7.2 Typical variation of the pressure in the injection mold and assignment of quality indicators related to each phase of the process

7.1.1 Simulation of the Filling Operation

While it may be easy to visualize the flow of the melt into the mold cavity for parts of simple geometry, graphical or computer-based methods are necessary in the case of parts with more complex geometries to simulate filling of the mold. The graphical method of replicating the filling process with the aid of compass and ruler as the molding develops (flow pattern method [7.12]) provides initial information about the propagation of the flow front, the position of weld lines, and any air occlusions. This method is still limited to parts with relatively simple geometry and therefore has limited practical use today with the advent of computer simulation. However, it can assist in the fundamental understanding of the process.

The method proceeds on the assumption of an isothermal, Newtonian flow so that changes in the properties of the material dependent on conditions of flow can be neglected. The flow front initially spreads out from the injection point (gate) in the shape of a circle (*i.e.*, radial flow) and the flow path covered in unit time is proportional to the current wall thickness.

$$\frac{\Delta l}{s} = \frac{\Delta l'}{s'} \quad (7.1)$$

The principle of this method is shown in Figure 7.3.

A more accurate analysis of the mold filling process is obtained by numerical methods. There is a range of commercial computer programs available for this purpose. These not only simulate the filling process, but also provide information about important process parameters. For the part designer, however, flow pattern simulation is perhaps the most critical tool as it provides information about where to expect:

- The position of flow lines and weld lines (mechanical weak points)
- Entrapped air (scorch marks/or air traps)
- Local solidification of the melt (flow hesitation or freeze-off due to thin-walled sections)
- Flow direction vectors (indications of orientations)

Figure 7.4 shows the results of a numerical flow pattern simulation of the plate in Figure 7.3 (Moldflow software).

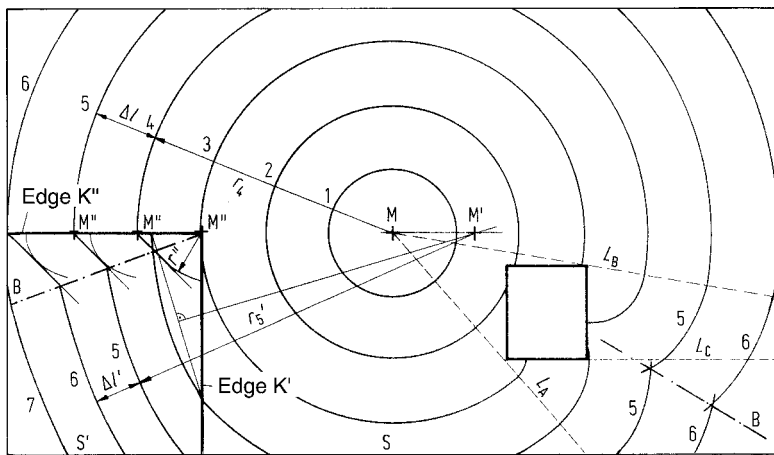


Figure 7.3 Example of a flow pattern prediction for a plate with a rectangular opening and different wall thicknesses

- M: Position of gate, center of unperturbed laminar flow
- M': Theoretical center of laminar flow through the edge K' in the thinner-walled region
- M'': Theoretical centers of laminar flow through the edge K''
- 1, 2, ...: Melt fronts
- Δt : Time interval
- $\Delta t'$: Time interval in thinner region (equation 7.1)
- $r_{1,2,\dots}$: Radii of melt fronts in the unperturbed region
- $r'_{1,2,\dots}$: Radii of melt fronts in the thinner region
- r'' : Radii of melt fronts through $K'' = \Delta t'$
- s: Wall thickness
- s' : Wall thickness in thinner region (here $s' = 0.75$ s)
- L_A, \dots : Radial vectors from gate to the corners of the opening
- B: Weld line

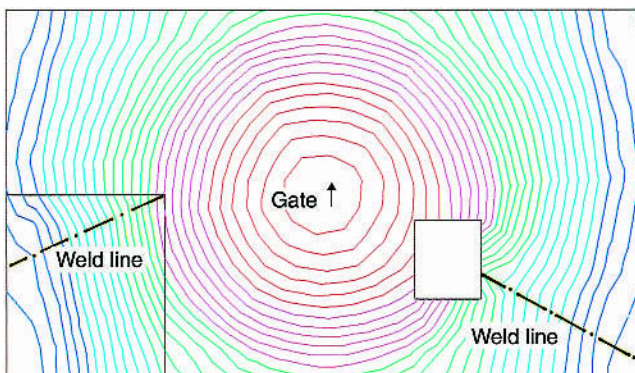


Figure 7.4 Flow pattern simulation for the plate in Figure 7.3

7.1.2 Causes of Orientation in Moldings

When the polymer melt flows into the cavity of the mold, the coiled structure of the macromolecules in the melt is deformed by shearing and stretching forces so that the molecules align themselves. When suddenly cooled, they freeze into this aligned deformed state. This is referred to as molecular orientation (see also Section 2.5.3.1). The number of such orientations that continue to exist in a part depends on the rate of cooling. Specifically, the time in which the macromolecules are at a temperature above the glass transition temperature T_g is important. During this time, the macromolecules have a chance to resume their energetically most favorable state of highest entropy (coiled structure without orientation) or to form crystalline structures.

Parts having molecules that are oriented in this way exhibit anisotropy in their macroscopic strength properties. This takes the form of increased strength in the direction of orientation and weakening in the perpendicular direction.

However, in the case of heterogeneous polymer systems, such as polymeric materials reinforced by chopped fibers, alignment of the fibers can also occur. This can have a far more dramatic effect on properties than molecular orientation.

The analysis of flow-induced preferred orientations, especially of chopped strands in thermoplastics, is the subject of much research work. A good survey is given in [7.13], for example. Although findings sometimes contradict one another, the following relationships may be taken as current state-of-the-art.

While the region around the gate does not permit a description of the orientation of the fibers it is followed by a characteristic build-up of layers having different fiber orientations. In flat moldings with largely uniaxial melt flow, fiber orientations such as those shown in Figure 7.5 can be expected. This layered structure has been confirmed in many studies of rectangular sheets formed by a film gate. According to these studies, the outermost layer consists of a polymer film (1) with few fibers followed by an equally thin unoriented layer (2). The third layer exhibits marked orientation of the fibers in the direction of flow, which can be attributed to the shear flow prevailing there. The fibers in the core layer (5), on the other hand, are oriented predominantly at right angles to the direction of flow. The transition layer between these two highly oriented layers is found to have random orientation.

The layers oriented in the direction of flow (3) have a significant effect on the properties of the part. Due to their proximity to the surface, they determine flexural rigidity more than the core region.

The orthogonally oriented layer (5) reduces strength and to a lesser extent rigidity in the direction of flow, but it also compensates in some degree for the anisotropy caused by the layers of type (3).

The degree of orientation in the individual layers, their thicknesses, and their symmetrical arrangement over the cross section depend in a highly complex manner on:

- Material parameters;
- Process parameters; and
- Geometrical parameters

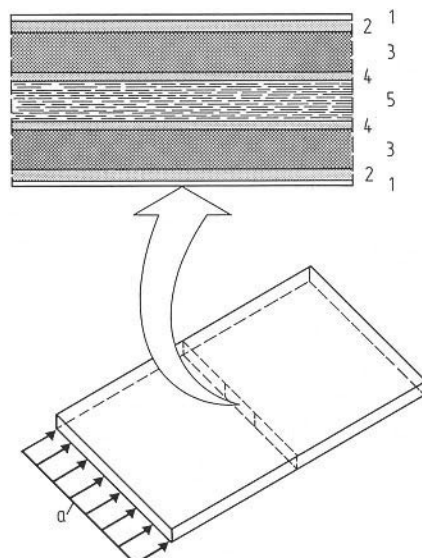


Figure 7.5 Schematic illustration of fiber orientation in a rectangular sheet with a film gate [7.13]

- 1: Outer film with few fibers
- 2, 4: Random fiber orientation
- 3: Fibers aligned predominantly in the direction of flow
- 5: Fibers aligned predominantly perpendicular to the direction of flow
- a: Gate

Material Parameters

The layered structure sketched in Figure 7.5 has been found in particular for PA 66 and applies in principle for all materials having similar flow properties (e.g., PA 6 or PBT). In the case of PP, the outer layers appear to be thinner and the central layer thicker so that taken as a whole, fiber orientation at right angles to the direction of flow can result [7.14]. However, the anisotropy factors from [7.16] given in Figure 7.9 do not verify this reversal. Nevertheless, given comparable fiber contents, PP has been found to exhibit distinctly lower anisotropy than PA. In addition, the reinforcing and stiffening effects of the fibers decrease more rapidly in a PP matrix than in a PA matrix, when measurements are made parallel and perpendicular to the direction of flow.

High fiber contents strengthen the intensity of orientation in the direction of flow (see also Figure 7.10). The effect of fiber length is of secondary importance [7.13].

Process Parameters

Of the various injection molding process parameters, mold filling time has the greatest effect on fiber alignment. Thus, at least in the case of a polyamide matrix, the formation of the central layer (5) can be weakened or even almost completely suppressed by prolonging the mold filling time*.

* However, a low injection speed usually also results in poorer surface quality.

High holding pressures and long holding pressure times likewise weaken the central layer in favor of layers (3), but only as long as the holding pressure still allows flow in the core [7.13, 7.15].

Geometrical Parameters

The principal effect of increasing the wall thickness of a part is to increase the thickness of the central layer (5) [7.14, 7.15].

When the geometry of a part diverges in the direction of flow, stretching flow gives rise to transverse orientations, while constrictions in the cross section reinforce longitudinal orientation, see, e.g., [7.13, 7.15, 7.17].

Figure 7.6 shows the example of a dumbbell-like tensile test bar with a marked fiber orientation in the cross section in the direction of flow. In such bar-shaped geometries, the longitudinal orientation is further reinforced by the lateral perimeter effects.

An obstacle to flow – a core, for example, to form an opening – divides the flow of the melt. In front of the obstacle the fibers increasingly assume a transverse orientation and behind it the two melt streams encounter one another again and form a weld line with strictly longitudinal orientation (see Figure 7.7) [e.g. 7.13, 7.15, 7.18, 7.19].

Ribs provided for stiffening the part do not necessarily disturb the orientation process already described. When the flow front approaches the rib from the side (Figure 7.8, left), the direction of flow is diverted and the rib fills from the base up so that the orientation close to the edge is

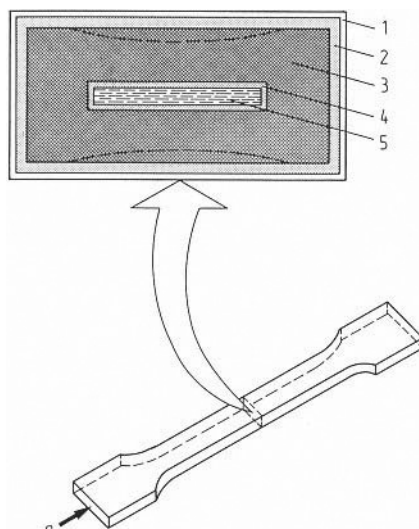


Figure 7.6 Schematic view of fiber orientation in a dumbbell-like tensile test bar [7.13]

- 1: Outer film with few fibers
- 2, 4: Random fiber orientation
- 3: Fibers aligned predominantly in the direction of flow
- 5: Fibers aligned predominantly perpendicular to the direction of flow
- a: Gate

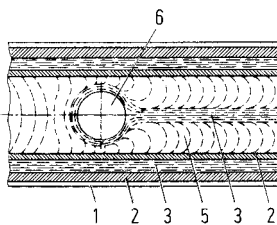


Figure 7.7 Schematic view of fiber arrangement in the central layer, flowing around a core [7.13]
6: Obstacle to flow (core), other labels as in Figure 7.5

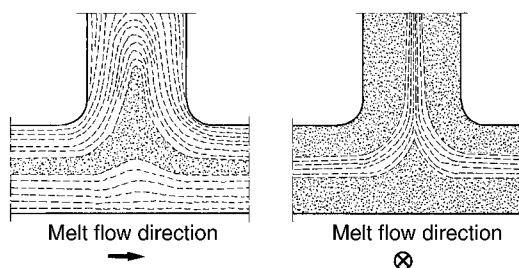


Figure 7.8 Fiber orientation (in principle) transverse (left, disadvantageous) and parallel (right, advantageous) to the longitudinal axis of the rib [7.20]

set transverse to the longitudinal axis of the rib [7.13, 7.20, 7.21]. If the flow front runs along the rib longitudinally, the fibers close to the edge also arrange themselves longitudinally in line with the direction of flow (see Figure 7.8, right).

Such clear-cut flow conditions, however, rarely occur in ribbed structures so that hybrid forms of these ideal states of orientation can be expected. Since the thickness of ribs should be about half the thickness of the plate from which they extend (to avoid accumulation of melt at the base of the rib), the melt will race ahead in the base region, even when fed in longitudinally and lags behind in the thinner rib cross section due to the higher flow resistance in the latter. Consequently, the direction of fiber orientation will assume an angle relative to the direction of the rib. The situation is even more complex at the intersections of orthogonal ribs, where there is no clearly predictable state of orientation (see also Section 10.3.3).

7.1.2.1 Effects of Orientation

Considerable anisotropy in strength and rigidity can result from fiber orientations, particularly those caused by flow (see also Section 2.5.3.2). In addition, there can be significant differences in molding shrinkage (and thermal expansion) parallel and transverse to the direction of orientation (Figure 7.10), which may cause distortion or warpage of the finished part (see also Section 7.2.3).

Because of the numerous parameters at work here, there are major problems in transferring characteristic values measured on geometrically simple test specimens to parts having different shapes. Even the test results obtained by various authors on molded plaques can be compared

to only a limited degree. It is, however, helpful to recognize clearly established trends. Figure 7.9 shows anisotropy factors for strength and the modulus of elasticity (tensile) over ranges of nominal wall thickness. It may be seen from this that:

- Anisotropy in the direction of flow decreases as wall thickness increases, because the transverse-oriented layer (5) becomes thicker; and
- For polymeric materials with marked non-Newtonian flow properties (e.g. PP, SAN) compared with PA, transverse orientation predominates even for thin wall sections so that the anisotropy factors in the flow direction can be less than 1.

The effects of differences parallel and transverse to the direction of flow and the effects of fiber content on molding shrinkage are shown as trends in Figure 7.10. These results relate to shrinkage measured on sheets produced with a film gate.

Largely isotropic shrinkage and freedom from warpage is obtained with particulate fillers (see Table 7.1), even though these fillers do not produce the same reinforcing effects provided by unidimensional fibers.

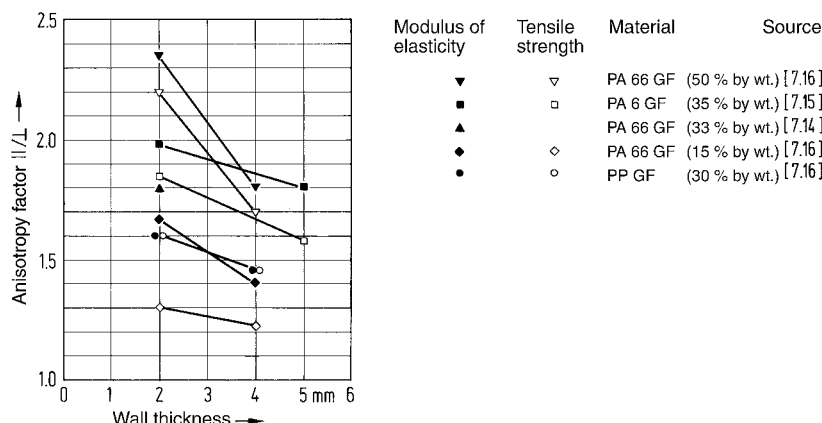


Figure 7.9 Anisotropy factors for strength and rigidity measured parallel and transverse to the direction of flow in injection molded plaques produced with a film gate

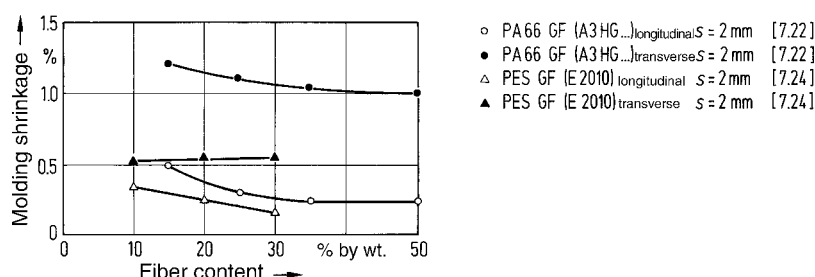


Figure 7.10 Molding shrinkage of PA 66-GF (A3HG) for different glass fiber contents measured on 2 mm thick plaques [7.22, 7.24]

Table 7.1 Molding Shrinkage of PA Filled with Different Inorganic Fillers
Measured on 2 mm Thick Plaques [7.22]

PA reinforced by 30% by weight of:	Shrinkage in %	
	longitudinal	transverse
Glass fibers	0.3	1.0
Glass beads	0.9	1.0
Silicate	0.2	0.3
Chalk	1.3	1.4

7.1.2.2 Controlling Orientation

A simplification justified in design practice is that the layers (3) aligned in the direction of flow determine direction-dependent properties. It may be taken as a general rule that the mold should be filled in such a way that segments of the part susceptible to orientation end up with an orientation compatible with the stresses to which they will be exposed to in service (if at all possible). The direction of orientation in the outer layers (3) can be deduced from the flow pattern method or, even better, from a flow pattern simulation as being normal to the flow front vectors. This is not the case close to the gate and at the ends of flow paths.

Warpage caused by orientation may be counteracted to some degree by filling the mold in a uniform or symmetrical manner so that longitudinal and transverse shrinkage do not impede one another. Some examples of variables that should be considered are discussed in the following.

Gate Position

Open framework structures are particularly susceptible to warpage, when the individual sections making up the structure have differing wall thicknesses and hence give rise to differences in flow resistance, flow rate, and fiber orientation. It is frequently possible to control warpage by suitable choice of gating locations.

Figure 7.11 shows an automobile headlight frame that is gated at two points on the upper frame section. Because the cross-sectional area of the upper frame section is greater than that of the lower frame section, under conditions of constant volume flow rate, the melt initially flows more slowly in the upper frame than in the lower frame. Therefore, the glass fibers at the top tend to be more aligned (see also *Process Parameters* in Section 7.1.2), which results in lower shrinkage compared to the lower frame section. This inevitably leads to warpage of the frame.

The results of a flow pattern simulation confirm this situation. The isochrones in the upper frame section are substantially more tightly compressed than in the lower frame, *i.e.*, the melt front passes through a shorter distance per unit time (see Figure 7.12, top). If the gates are positioned on the inside of the connecting webs, the flow pattern simulation shows that the longitudinal sides are more uniformly filled. From this it may be concluded that fiber orientation is more uniform and the frame will likely be free of warpage (see Figure 7.12, bottom).

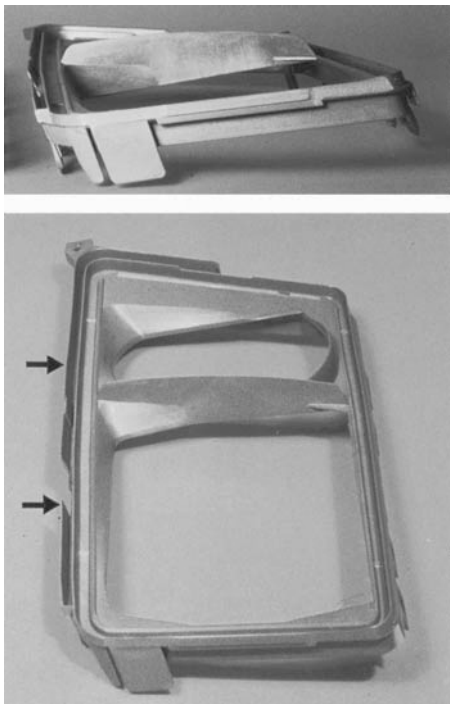


Figure 7.11 Frame composed of glass-fiber reinforced PBT for automobile headlights

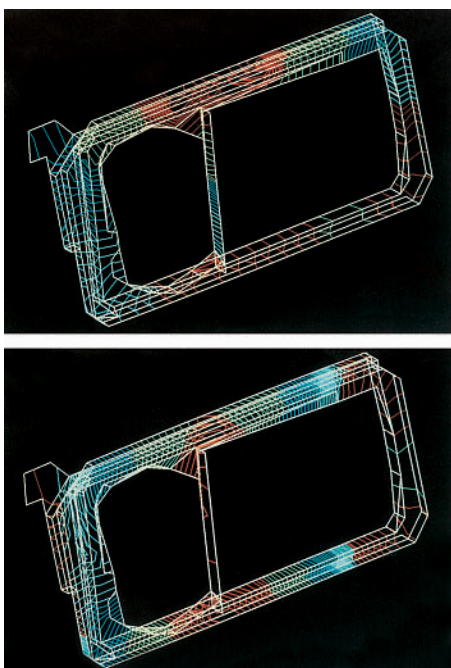


Figure 7.12 Flow pattern simulation of different gate positions [7.23]

Flow Promotion

Nonuniform flow through sections of a molding susceptible to warpage may also be rectified by means of flow promotion. Flow promoters are local increases in wall thickness or depressions in the flow channel having a larger cross section and hence lower resistance to flow.

A computer-based flow pattern study may once again be used as a flow promoter design aid for evaluating the mold filling process.

In Figure 7.13, flow pattern simulations for a bifurcated housing section are compared. Nonuniform filling of the two limbs can be identified from the difference in line density (see Figure 7.13, top). The filling process in both limbs can be rendered distinctly more uniform by means of a flow promoter positioned ahead of the upper leg (Figure 7.13, bottom). This is necessary to ensure freedom from warpage. In this example, however, thermally induced warpage is also involved. This frequently plays a decisive role in parts having edge stiffeners and U-shaped geometries (see also *Surface Temperature of Mold* in Section 7.2.3.2).

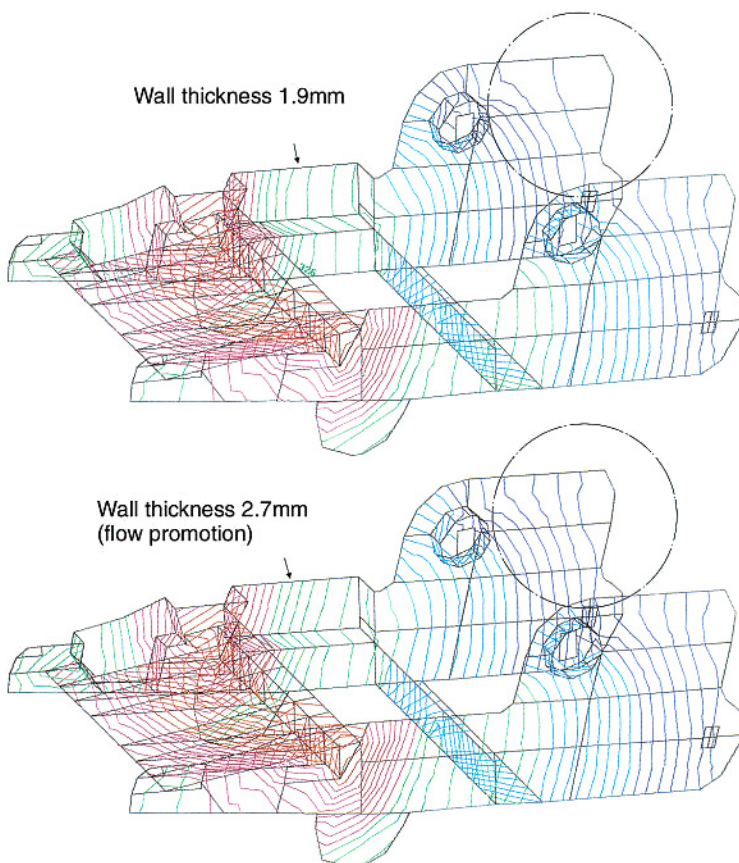


Figure 7.13 Flow pattern simulation without (top) and with flow promotion (bottom) for a bifurcated part made from glass-fiber reinforced PA 6

Flow Inhibition

In contrast to flow promotion, the melt flow can be selectively slowed down or diverted by a flow inhibitor, which is a narrowing of the available cross section. The use of a flow inhibitor for the box-shaped part made of a fiber-reinforced thermoplastic in Figure 7.14 resulted in the melt flowing through both the longitudinal side walls in parallel, even though the gate was located off-center on the underside.

The flow inhibitors in this case are grooves between the base and the lower edge of the side walls so that the melt does not flow obliquely from the base into the side walls (Figure 7.15, top), but rather flows from the end face up through the side walls (Figure 7.15, bottom). As a result, the fibers are primarily aligned in the longitudinal direction to provide freedom from warpage. In addition, cooling of the inside edge is improved (see also Figure 7.41) and as a result, angular distortion is reduced.

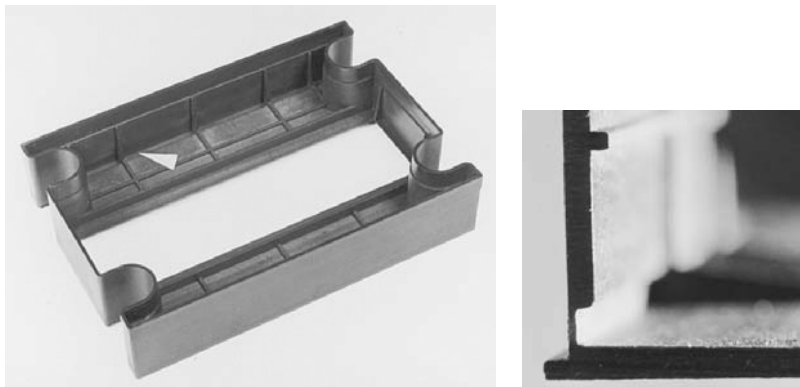


Figure 7.14 Grooves parallel to the edge of the side walls act as flow inhibitors
(Photograph: Jantsch, Stein)

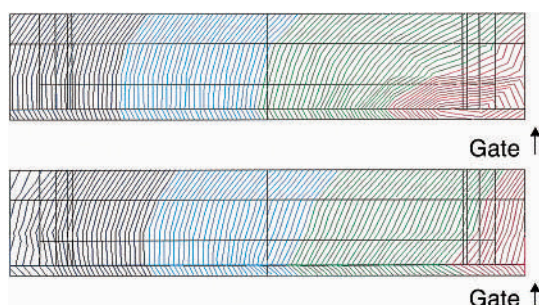


Figure 7.15 Flow pattern simulation of the side wall of the box-shaped part shown in Figure 7.14. Close to the gate, the melt flows from below into the lateral area (top). The flow inhibitor is used to create a more uniform upward flow (bottom)

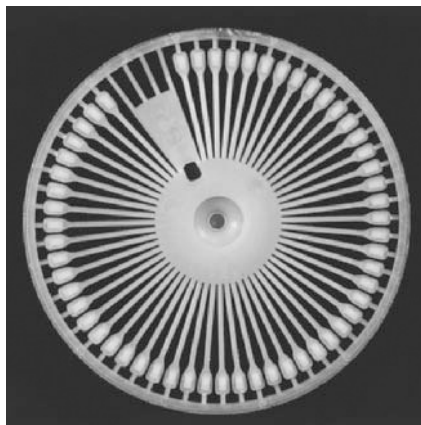


Figure 7.16 Overflow channel on the spring arms of a telex daisy wheel
(Photograph: Siemens, Munich)

Overflow Channel

Fiber orientation is less well defined close to the gate and at the end of the flow path than it is in the pathway between them (assuming the melt flows smoothly through the latter). When a designer wants to obtain a certain degree of orientation right up to the end of the flow channel, an overflow channel can be added to achieve this goal. An overflow channel is an extra section of the mold cavity, extending beyond the actual cavity, comparable, for instance, to a riser in metal die casting.

As an example, this potentially costly measure has been added to the daisy wheel cavity in order to produce a part with a uniform orientation over the entire length of its long narrow springing arms [4.18], as shown in Figure 7.16. The result is improved mechanical performance, but at the cost of an additional secondary operation.

7.1.3 Causes for Formation of Weld Lines and Air Pockets

Weld lines form when the fronts of two or more melt streams encounter one another in the mold. This is inevitable when the melt has to flow around an opening in the molding (*e.g.*, a core in the mold) or when the molding is gated at several points. Differences in wall thickness causing partial acceleration or slowing down of the melt front, or even just different flow lengths, may also result in different melt streams coming together* (see also Figures 7.3 and 7.4).

Correspondingly, an air pocket is formed when the melt fronts enclose a hollow space from which the air can no longer escape.

* Occasionally, a distinction is made between a weld line (frontal meeting of the melt streams) and a flow line (the recombination of more or less parallel streams).

Table 7.2 Weld Line Factors Measured on Tensile Test Specimens and Flexural Impact Test Specimens with and without Weld Lines

Material	Morphology	Weld line factor Nature of stress		Source
		Dynamic	Impact	
PA 6 (B3S)	semicrystalline	≈ 1		[7.27]
PA 6-GF (B3WG6; 30% by wt.)		0.6		[7.27]
PA 66 (A3K)		≈ 1	0.22	[7.27]
PA 66-GF (A3WG7; 35% by wt.)		0.55		[7.27]
HDPE (A120)		≈ 1	0.2	[7.26]
PP (5520)		0.92		[7.32]
PP (5200)		0.85		[7.26]
PBT (B4500)		0.95		[7.27]
PBT (B1505)		0.96		[7.32]
PBT-GF (B3235; 30% by wt.)		0.57		[7.32]
PBT-GF (B4300G6; 30% by wt.)		0.6		[7.27]
PS (143E)	amorphous	0.4($T_m = 180^\circ\text{C}$)*	0.05($T_m = 180^\circ\text{C}$)**	[7.28]
		0.8($T_m = 260^\circ\text{C}$)*	0.4($T_m = 260^\circ\text{C}$)**	[7.28]
PS (203)		0.64($T_m = 210^\circ\text{C}$)		[7.32]
SB (333)		0.9		[7.32]
SB (475K)		0.85		[7.27]
ABS (867M)		≈ 1	0.6	[7.28]
ABS***		0.75 to 0.4		[7.42]
ABS-GF (2803G3; 15% by wt.)		0.55	0.3	[7.28]
PC-GF (10% by wt.)		0.85		[7.29]
PC-GF (20% by wt.)		0.58		[7.29]
PC-GF (40% by wt.)		0.47		[7.29]

* Initial value without weld line decreases from $\sigma_M = 54 \text{ MPa}$ ($T_m = 180^\circ\text{C}$) to $\sigma_M = 44 \text{ MPa}$ ($T_m = 260^\circ\text{C}$)

** Initial value without weld line decreases from $a_{cU} = 27 \text{ kJ/m}^2$ ($T_m = 180^\circ\text{C}$) to $a_{cU} = 12 \text{ kJ/m}^2$ ($T_m = 260^\circ\text{C}$)

*** As the acrylonitrile content rises, the weld line factor drops significantly.

T_m = melt temperature

7.1.3.1 Effects of Weld Lines and Air Pockets

It is likely that weld lines impair the mechanical properties and visual appearance of a part to some variable degree. Reduced mechanical properties may be caused, on the one hand, by insufficient welding of the melt fronts – possibly rendered more difficult by entrapped air. On the other hand, in the area of the weld line an orientation sets in, which differs markedly from neighboring domains, especially in the case of fiber-reinforced thermoplastics. This may result in direction-dependent changes in properties. In particular, when there is a frontal encounter between melt streams, notches causing weakness form on the surface of the part [7.25].

Mechanical Weld Line Factors

Analogously to a welding factor*, a weld line factor is defined as the ratio of a property measured at a weld line to the value of the property in the absence of a weld line. The test specimen most commonly used to measure the weld line factor is a tensile bar gated at one end (without weld line) or gated from both ends (with weld line). Some of the weld line factors determined this way are presented in Table 7.2.

Examination of the individual results in Table 7.2 leads to the following classification.

Table 7.3 Guide Values for Weld Line Factors

Type of material	Weld line factor	
	Dynamic (strength)	Impact (toughness)
Amorphous structure	0.4–0.95	0.1–0.6
Semi-crystalline structure	0.85–1.0	0.3–0.5
Glass-fiber reinforced (dependent on fiber content)	0.5–0.85	

The weld line factors presented in Tables 7.2 and 7.3 were determined for the critical case of two melt streams in frontal collision. If the melt flows around cores in the mold, the weakening caused by this splitting gradually heals some distance after the opening. Even the unappealing appearance can fade.

If the opening is remote from the gate, the cooling of the melt, which has already occurred by that time, results in poorer fusion in the region of the weld line.

Weld Lines as Visible Surface Marks

Weld lines on the surface of the part are visible to various degrees as unnecessary lines. In the case of weld lines with poor venting (air pockets), the high levels of compression can give rise to local thermal damage and unattractive scorch marks.

Even if the surface is subsequently treated by painting, electroplating, etc., these regions still retain an unattractive appearance.

* The welding factors found in thermal sealing tend to be substantially lower than weld line factors.

Weld Lines as Predetermined Failure Region

The weakness of a weld line may also be exploited as a predetermined failure region. This concept is utilized in bottle closures, for example.

7.1.3.2 Controlling Weld Lines and Air Pockets

As a general rule, weld lines caused by part geometry and flow conditions cannot be avoided, but their effects can be controlled by appropriate measures. These include:

- Process conditions
- Mold design
- Other design measures

Process Conditions

Process variables, such as melt temperature T_M , mold cavity temperature T_C , and injection rate over the ranges employed in practice for semi-crystalline and even for glass-fiber reinforced thermoplastics have a very limited effect on weld line strength. Perhaps the most significant variable is T_M , which in the case of materials with an amorphous structure can lead to improved weld strength when increased (see Table 7.2).

Mold Design

By choosing the location of the gate, the position of the weld line is determined. A flow pattern simulation provides information about the expected position of a weld line so that even when the mold is being designed, the weld line can be shifted into noncritical regions by varying the gate location.

As a geometric measure, *a flow promoter or a flow inhibitor* can also be used to control the melt stream so that the weld line is moved away from any undesirable position (see Figure 7.17).

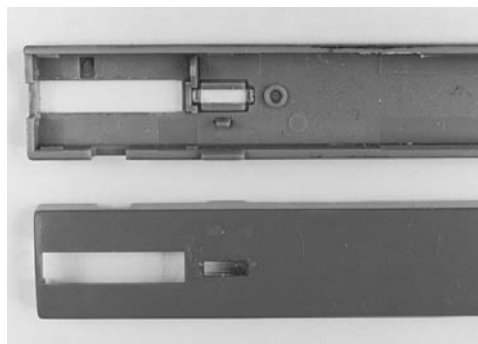


Figure 7.17 Automobile cassette player cover (C-Box). A flow inhibitor was used to shift the weld line away from the narrow section behind the opening.

(Photograph: Fischer, Tumlingen)

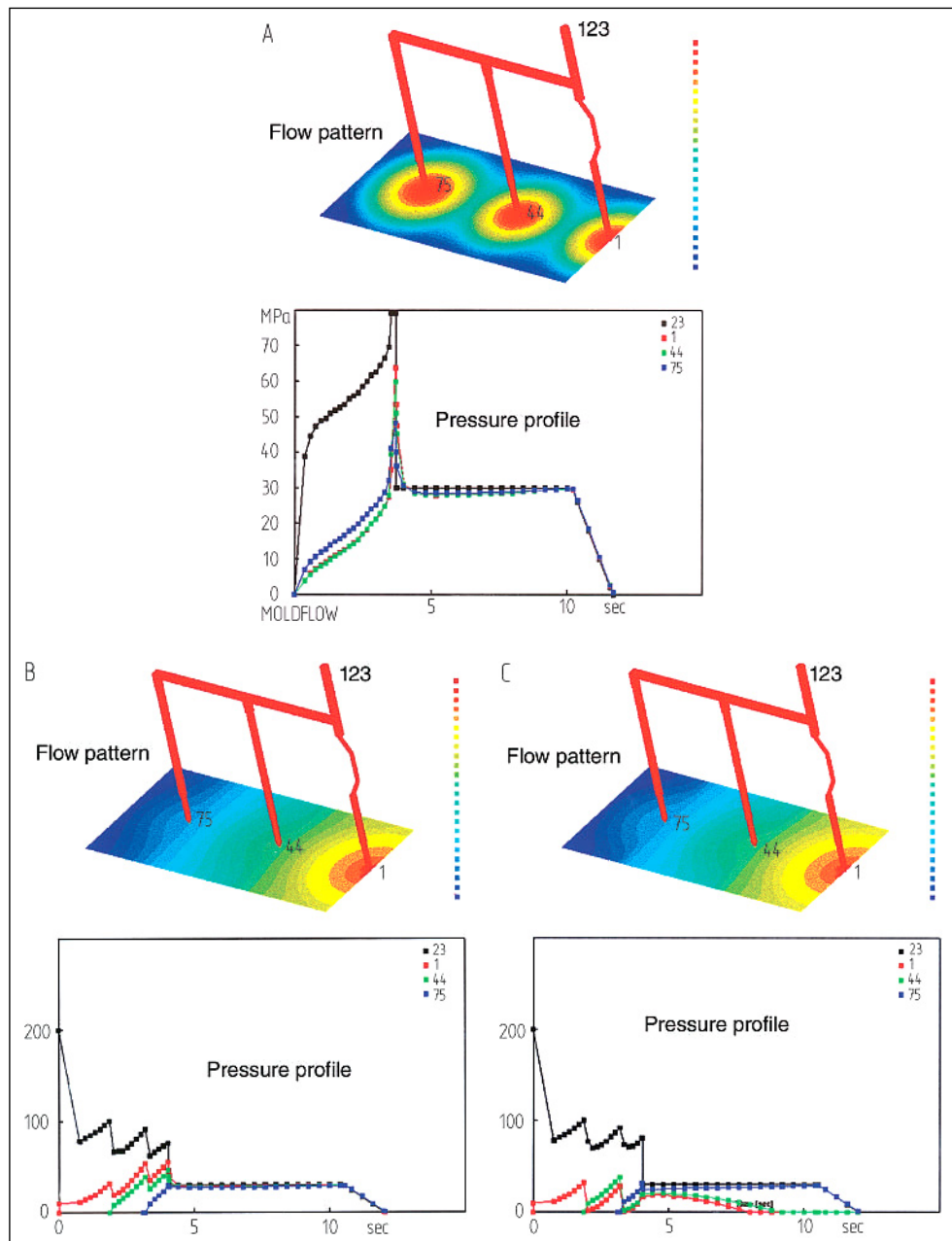


Figure 7.18 Flow pattern simulations and pressures required for a flat plaque measuring $1,200 \times 300 \times 3 \text{ mm}^3$ for conventional injection molding (A) and for the cascade technique (B, C) resulting in no weld lines.
In the pressure curves, node 1 is shown in red, 44 in green, 75 in blue, and 123 in black.

The melt stream may also be controlled by *sequential injection molding* when multiple gates are needed to fill the part. In this technique, which is particularly suitable for large, flat parts, the valve gate pins in a hot runner system are opened and closed in such a way that weld lines are moved into noncritical areas [7.52].

Cascade injection molding is more suitable in the case of elongated parts, for which hot runner valve gate nozzles are arranged in a row. Injection usually starts at the central nozzle and neighboring nozzles are not opened until the melt stream has reached them. In this way, despite having multiple gates, a part externally free of weld lines is produced.

Figure 7.18 shows a simulation of the cascade molding technique for a flat plaque measuring $1,200 \times 300 \times 3$ mm. In section A of this figure, a conventional injection mold filling pattern through all nozzles simultaneously is illustrated. In the diagram at the bottom of the figure, the change of pressure at the individual gates and at the start of the runner is plotted against the mold filling time. Weld lines occur between the individual gating positions.

Sections B and C of this illustration show what happens when the cascade technique is employed. At the start of injection, the nozzle is in the center* (node 1) and the remaining nozzles are opened only after the melt front reaches them. No weld line is visible from the outside. In B, all of the nozzles remain open for the holding pressure, while in C, the preceding nozzle is closed when the next one is opened. This holding pressure procedure has an effect on shrinkage and warpage behavior and has to be optimized for every particular part geometry.

A weld line impacting the appearance of a molded part can be concealed by texturing the surface or, in the case of decorative articles, it can be covered by inserting a printed film in the mold**.

Other Design Measures

The simplest design measure for eliminating the weakening effects of a weld line is to increase the wall thickness or cross-sectional area in the vicinity of a weld line (see Figure 7.19).

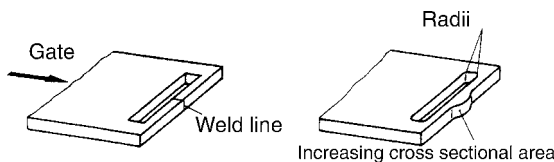


Figure 7.19 Increasing cross-sectional area in the region of a weld line (and increasing radii in corners) [7.30] can lead to improved performance

This is shown in Figure 7.20 for a molded part: the lug for holding a snap-fit hook in place on the mating part is much thicker where the weld line is located.

* Because of symmetry, only half of the plaque geometry has been simulated.

** Plastic decoration in-mold process (PDI)

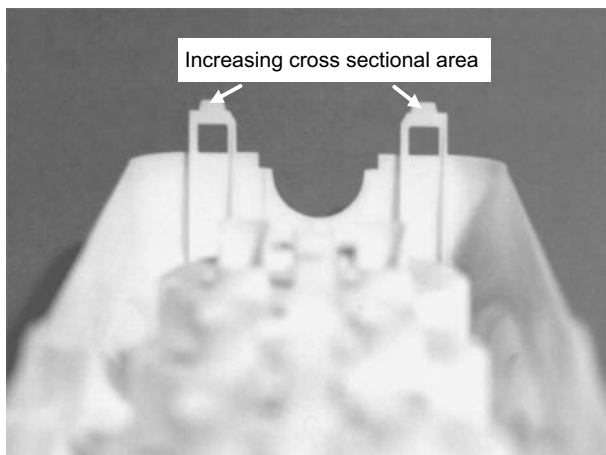


Figure 7.20 The connecting lug on a multiway plug is made thicker to compensate for the loss in strength caused by the weld line (Manufacturer: Kopp AG, Kahl/Main)

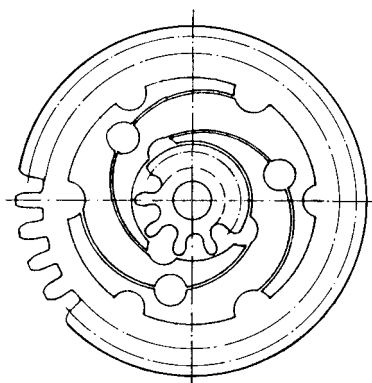


Figure 7.21 Thickened regions in the spring arms serve to enlarge the weld line region and at the same time act as points of engagement for the ejector pins [7.30, 7.31]

This principle can be implemented in more complex parts, e.g., in the spring-mounted gear wheel ($d_k = 11$ mm) in Figure 7.21 on both the hub and the toothed outer ring. The wheel is gated at three points. This inevitably gives causes weld lines in the thin-walled spring arms. The compromised cross section is reinforced in these regions by increasing its area [7.31]. At the same time, these thicker regions serve as points of engagement for ejectors for safely demolding the spring arms (see also Figure 8.57).

In mold cavities with a large cross-sectional area, the melt front runs ahead during the filling process relative to regions of narrow cross section (see also *Flow Promotion* in Section 7.1.2.2).

If a flat part is reinforced and stiffened by a thicker edge stiffener around the perimeter of the part, there is a risk that this edge will be filled first and that an air pocket will form in the thinner region (see Figure 7.22).

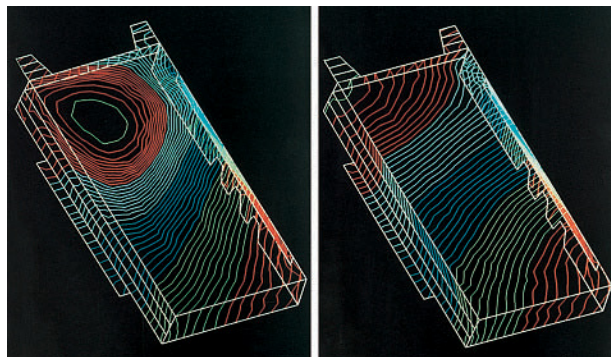


Figure 7.22 The melt flow front runs ahead in the thicker edge stiffener so that an air pocket forms (left). This effect can be prevented by increasing the wall thickness of the interior area (flow promotion, right).

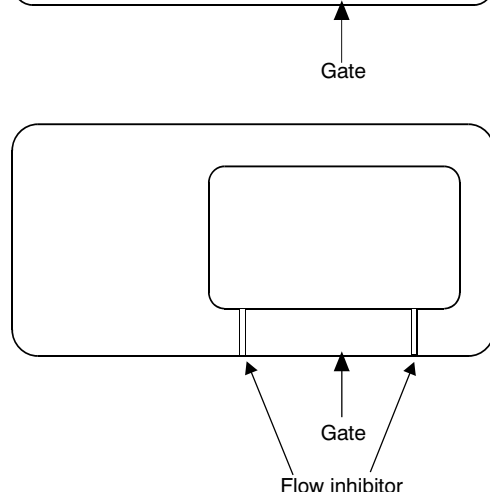
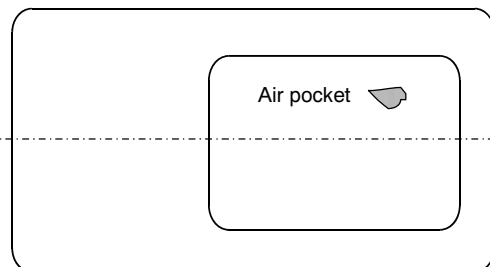


Figure 7.23 The thin viewing region of the Petri dish must be absolutely free of weld lines or air pockets. In the design, in the upper part of the figure, an air pocket forms in the thin central region because the melt fills the thicker edge first. Flow inhibitors (narrow points) prevent this.

Alternatively, an air pocket in such a part can also be prevented by a flow inhibitor (see Figure 7.23). In the Petri dish depicted in the Figure 7.23, the gates are narrowed on the right and left to such an extent that the melt first fills the thin viewing region before it can enclose the latter to form the side walls. This of course causes weld lines to form, but these are located outside the inner viewing area.

A computer-aided flow pattern simulation provides valuable assistance in establishing appropriate wall thicknesses.

Frequently, design considerations have to be matched to the requirements for a structure capable of withstanding stresses or other requirements related to manufacturing.

A bottle cap with a hexagonal outer contour and a cylindrical inner contour presents the melt with cross sections of differing flow resistance, because of the simplicity of producing the mold core (see Figure 7.24). This could give rise to weld lines (flow lines) along the thinner areas, which would impact the visual appearance and might also result in fracture when the cap is pushed on. Therefore, it would be better if the inner cross section were not circular but rather reflect the outer contour, hexagonal with rounded edges.

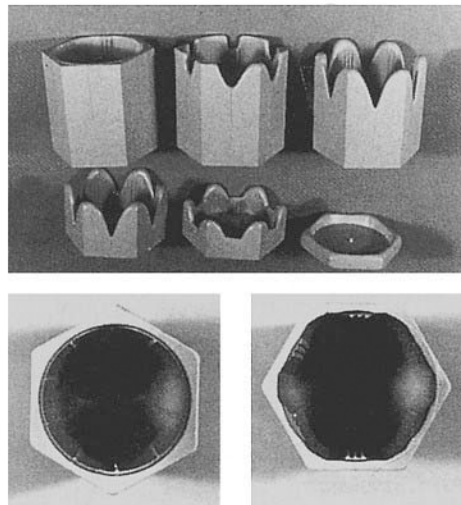
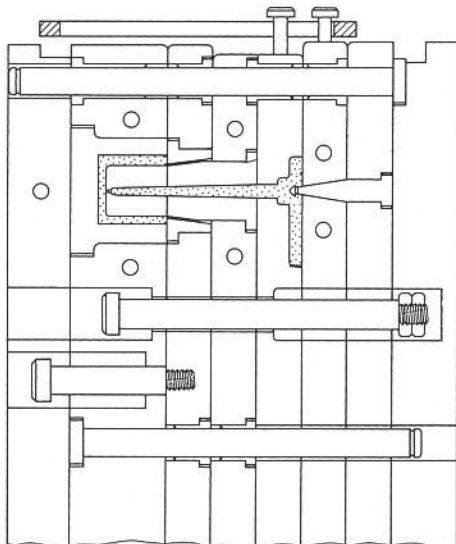


Figure 7.24 Bottle cap made of ABS, position in mold
Experimental filling study using a round core (top)
More advantageous version with hexagonal core [7.33]

7.2 Cooling and Solidification

The injection molding process involves injecting a hot melt into a relatively cold mold. On contact with the mold wall, the polymer melt gives up its heat to the latter and it solidifies or freezes. Volume contraction (shrinkage) is associated with this cooling process.

7.2.1 Cooling Rate

Rapid cooling is desirable from a manufacturing view point to achieve a short production cycle. A variety of factors affect the cooling time required for injection molded parts.

7.2.1.1 Effects of Cooling Rate

As shown in Eq. 7.2, the theoretical solidification time for plate-like parts, t_S , is a function of the thermal properties of the polymeric material, the process parameters, and the geometry of the part.

$$t_S = \frac{d^2}{\pi^2 \cdot a} \cdot \ln \left[\frac{8}{\pi^2} \cdot \frac{T_{MM} - T_C}{T_S - T_C} \right] \quad (7.2)$$

where

d = Thickness of part

a = Thermal conductivity

T_{MM} = Mean temperature of melt in the mold

T_C = Mean temperature of mold cavity

T_S = Mean demolding temperature \approx solidification temperature

If the melt cools on the mold wall so rapidly that the molecules have no time to relax or crystallize, a high degree of orientation becomes frozen in the outer layers (see also Section 7.1.2). In the case of semi-crystalline polymeric materials, the formation of crystalline domains (spherulites) in the outer zones is partly or completely suppressed (see also Section 2.5.2, Figure 2.20) and this generally results in lower strength, hardness, and in particular lower resistance to wear.

7.2.1.2 Controlling the Cooling Rate

In design terms, shortening of the cooling or setting time can only be achieved by means of designing parts with a reduced and uniform wall thickness to the extent possible. This also reduces the consumption of material.

Because the wall thickness governs cooling time by a power of two, differences in wall thickness must be avoided.

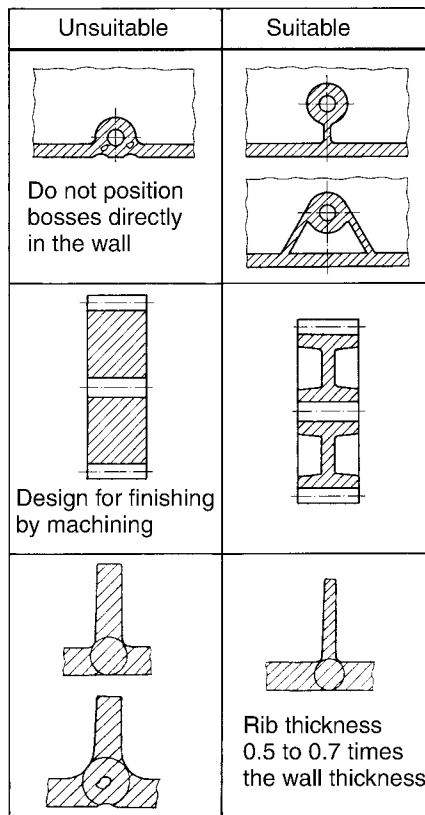


Figure 7.25 Design examples that help promote a more uniform wall thickness

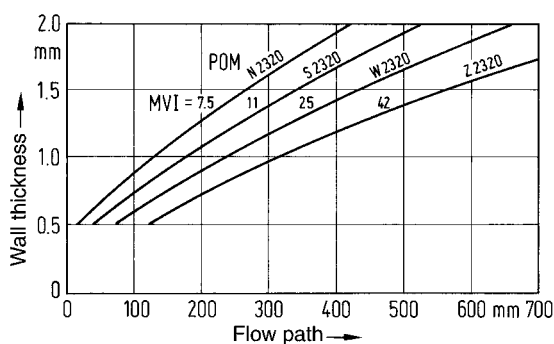


Figure 7.26 Relationship between flow path length and wall thickness for various grades of POM (spiral flow test) [7.51]

The thickest point in a part determines the cycle time.

Differences in wall thickness also cause internal stresses (warpage), voids, and/or sink marks because thicker sections tend to shrink more. Some design examples are provided in Figure 7.25. For each particular thermoplastic material, the minimum wall thickness technically achievable is a function of the viscosity of the melt and, therefore, is related to the length of the flow path. Figure 7.26 makes this relationship clear for selected of POM grades.

“Thin-wall” injection molding technology, which is characterized by a flow path: wall thickness ratio of 100 for wall thicknesses less than 1 mm, is primarily used in cases where material costs account for a high proportion of total part costs (e.g., in packaging) or in technical fields, where it is important to have minimum dimensions and maximum savings in weight while maintaining adequate rigidity. Packaging applications are generally containers, such as cups, boxes, and pill tubes. An example of a technical application is the housing for a mobile phone. In the last 10 years, the wall thickness of such devices has been reduced from 1.8 mm to 0.8 mm [7.66]. This was achieved with blends of PC and ABS, which can have relatively high viscosities. In addition to weight savings, the reduction in cooling time is a further economic advantage for thin-wall moldings (see Figure 7.27).

Extreme examples of very low wall thicknesses and long flow paths include diskette shutters (see Figure 7.28). The maximum flow path for these parts, which are only 0.35 mm thick, is 38 mm. This is only achievable, however, by using extremely free-flowing polymeric materials.

A key prerequisite for the successful use of thin-wall technology is a highly free-flowing type of polymeric material. Because the thin-walled parts can be satisfactorily injected into the mold only by means of high injection rates of up to 1,000 mm/s and injection pressures of up to 3,000 bar, high-precision molds and high-performance injection-molding machines are generally necessary.

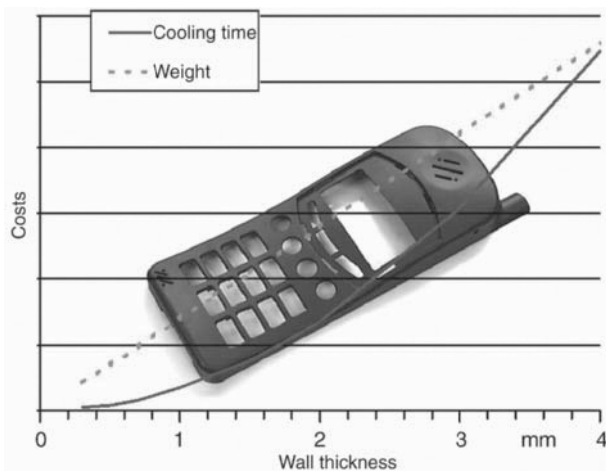


Figure 7.27 Cooling time and weight of a cell phone housing (made of a blend of PC and ABS) as a function of wall thickness of the part



Figure 7.28 Shutter for a 3.5" diskette
 Material: POM (Z 2320; MVI = 42)
 Wall thickness: 0.35 mm
 Flow path: 38 mm
 Weight: 1 g
(Photograph: BASF Magnetics)

7.2.2 Changes in Dimensions and Tolerances

7.2.2.1 Shrinkage

Mold shrinkage is defined as the difference between the dimensions of the cold mold (at 23 ± 2 °C) and those of the part measured either immediately after demolding or after aging for 16 hours in a standard 23/50 atmosphere (DIN 16 901).

pVT diagrams show the relationship between the pressure, specific volume, and temperature of a polymeric material in the molten and solid states. If the change in pressure measured in the mold cavity (see Figure 7.2) and the mean temperature of the molding are mapped onto such a pVT diagram, conclusions about shrinkage may be drawn.

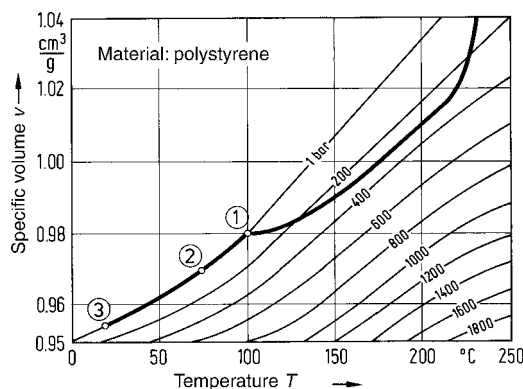


Figure 7.29 pVT diagram for polystyrene (PS) showing change of state during cooling [7.35]
 1. Melt attains atmospheric pressure
 2. Demolding
 3. Part attains ambient temperature

The temperature at point 1 (where the internal pressure of the mold has reached atmospheric pressure) is decisive for the extent of shrinkage and hence the subsequent dimensions of the part. As cooling proceeds, the molding detaches itself from the wall of the mold; it shrinks based on the definition above. Demolding ensues at point 2 and shrinkage comes to an end at point 3 (or 16 h thereafter in accordance with DIN 16 901).

Thus, the volume shrinkage may be defined by the relationship:

$$S_V = \frac{V_M - V_P}{V_M} = \frac{m \cdot v_1 - m \cdot v_3}{m \cdot v_1} \quad (7.3)$$

where

Subscript M = mold

Subscript P = part

Given that m is constant this simplifies to:

$$S_V = 1 - \frac{v_3}{v_1} \quad (7.4)$$

Assuming isotropic shrinkage, linear shrinkage is given by:

$$S \approx \frac{1}{3} S_V \quad (7.5)$$

Linear shrinkage along the individual dimensions of a part, however, is usually different than that given by Eq. 7.5 for a number of reasons:

- Anisotropy of the material (e.g., shrinkage impeded by glass fibers);
- Impeded shrinkage due to the geometry of the mold (dimensions constrained by the mold);
- Impeded shrinkage due to outer layers which have already solidified; and
- Locally variable cooling conditions.

Particular attention has to be devoted to the marked dependence of shrinkage on wall thickness when a part is being designed.

Although a part in the form of a flat plate can shrink freely in all three dimensions, shrinkage in the plane of the plate is impeded by the solidified outer layers, while in the direction normal to this plane there is no impediment to shrinkage [7.35]. Thus, it is apparent that *shrinkage will increase as wall thickness increases*. When the wall thickness is increased at certain points, the solidified outer layer at these points will be drawn inwards and sink marks or voids will result.

When semicrystalline thermoplastics crystallize, they undergo a greater reduction in volume on cooling than thermoplastics with a purely amorphous structure. Accordingly, their linear shrinkage may be expected to be substantially higher (see Table 7.4). The ranges shown there indicate that there are many factors or variables that can influence shrinkage (for the shrinkage of glass-fiber reinforced polymeric materials, see also Figure 7.10).

Table 7.4 Guide Values for Molding Shrinkage

Polymeric material	Morphology	Part shrinkage in %
Polystyrene (PS)	Amorphous	0.3–0.6
Poly(methyl methacrylate) (PMMA)		0.3–0.7
Acrylonitrile-butadiene-styrene (ABS)		0.4–0.7
Acrylonitrile-butadiene-styrene + glass fibers (ABS-GF)		0.2–0.4
Polycarbonate (PC)		0.6–0.8
Polycarbonate + glass fibers (PC-GF)		0.2–0.5
Polyamide (PA)	Semicrystalline	0.7–2.0
Polyamide + glass fibers (PA-GF)		0.2–0.8
Polyoxymethylene (POM)		1.8–3.0
Polyoxymethylene + glass fibers (POM-GF)		0.2–0.6
Polypropylene (PP)		1.2–2.5

The power of modern simulation software suggests that it may be advantageous to determine shrinkage by computer simulation. There are a number of computer programs available for this purpose. These are based on the linear superposition of the various independent variables [7.36], as shown below.

$$S = S_0 + \int_{P_{H0}}^{P_H} \frac{\delta S}{\delta P_H} dP_H + \int_{T_{M0}}^{T_M} \frac{\delta S}{\delta T_M} dT_M + \int_{T_{C0}}^{T_C} \frac{\delta S}{\delta T_C} dT_C + \dots \quad (7.6)$$

where

S_0 = Linear molding shrinkage for defined base parameters

δS = Changes in shrinkage specific to the parameter in question

P_H = Local holding pressure

T_M = Melt temperature

T_C = Cavity surface temperature

While the mathematical effort in solving Eq. 7.6 is no obstacle, the effort involved in identifying the shrinkage function experimentally is significant.

In other computer-based approaches, the part is considered layer by layer and shrinkage and warpage are calculated on the basis of pVT diagrams using FEM. Such computer programs can yield results that are in good agreement with those observed for actual molded parts.

7.2.2.2 Post Molding Shrinkage

Even after a part has cooled to room temperature, secondary shrinkage may still occur. This is referred to as post molding shrinkage or aftershrinkage. These changes in dimensions can be contractions caused by rapid cooling. The melt is supercooled and solidifies at a higher specific volume than is given by the curve at $p = 1$ bar in the pVT diagram. In the case of semi-crystalline thermoplastics in particular, this effect takes the form of secondary crystallization. Dimensions constrained by the mold and subject to impeded shrinkage also tend to compensate for this restraint, at least in part, by post molding shrinkage.

Increases in dimensions are also possible, e.g., when solidification ensues while the cavity pressure is greater than atmospheric. Internal pressure stresses are then frozen in place – especially in amorphous thermoplastics – and these will later relax.

7.2.2.3 Tolerances*

Achievable production tolerances are in part influenced by mold shrinkage. It is not so much the absolute value of shrinkage that is relevant, but rather the unavoidable range of shrinkage caused by the manufacturing process and the part design. Permissible tolerances and deviations in dimensions are specified in DIN 16 901. The experience that has gone into DIN 16 901 has shown that the achievable dimensions in plastic parts have a linear percentage relationship to the nominal dimensions and deviate from the latter by the amounts shown below.

Normal injection molding	< 1%
Technical injection molding	< 0.6%
Precision injection molding	< 0.3%

These relationships are illustrated graphically in Figure 7.30 and compared with the ISO tolerance ranges.

It is of course possible for actual tolerances to be less than those set out in DIN 16 901, provided the higher production costs are justified.

Unnecessarily overstated tolerance requirements do not necessarily result in higher quality; they are more likely to give rise to higher volumes of rejects.

Therefore, narrow or “tight” tolerances important for a part’s function need to be carefully discussed with the manufacturer of the part to ensure that they can be and are achieved.

Figures 7.31 and 7.32 show examples of high-volume parts made from amorphous and semi-crystalline polymeric materials with tight tolerance requirements.

The scale part made from SAN is partially painted after injection molding (Figure 7.31, bottom) after being partially covered by a template. The length of 254 mm determined for the part requires a positive tolerance of < 0.1 mm. Several thousand units of this part were produced daily in different molds and the narrow tolerance limits were successfully adhered to [7.53].

* For a comprehensive treatment of these problems see [7.55].

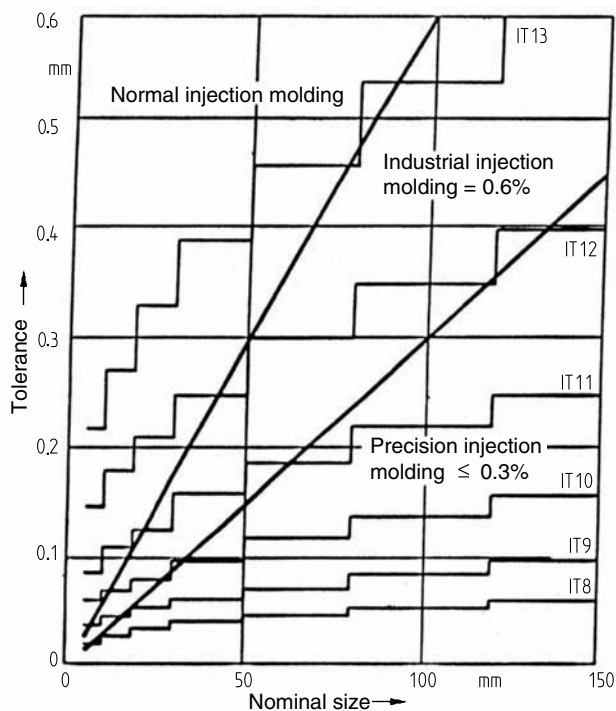


Figure 7.30 Tolerances for plastic parts (linear relationships) compared to the ISO tolerance ranges used for metals



Figure 7.31 Scale part made from SAN (368 R)
(Photograph: Philips, Austria)

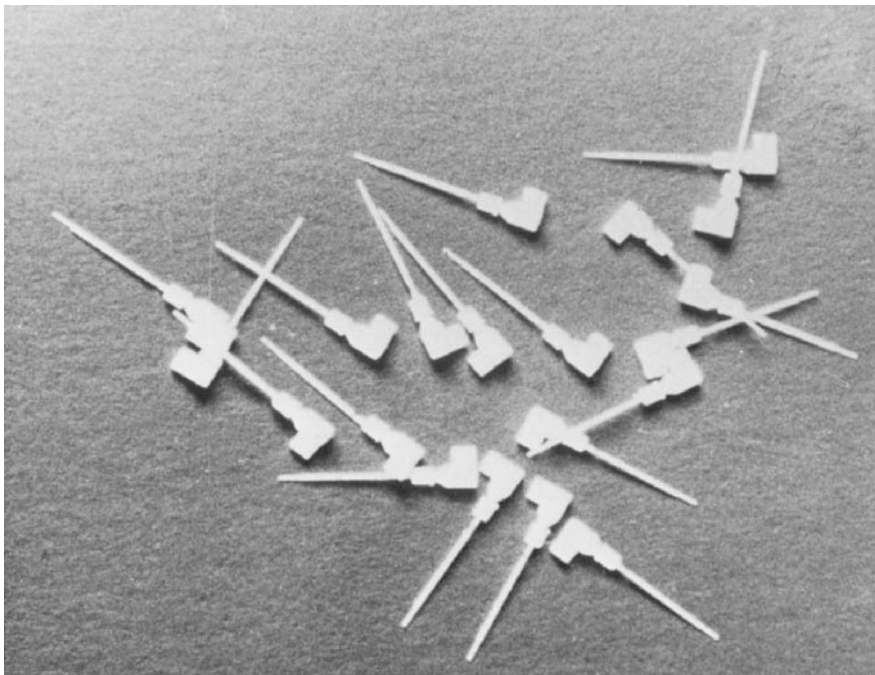


Figure 7.32 Control springs for quartz clocks made from POM
(Manufacturer: Breiter, Dauchingen; Produced for: Gebr. Staiger, St. Georgen)

An example of a semi-crystalline material is shown in Figure 7.32. These parts are control springs for quartz clocks made from POM and are to be held to $0.15 + 0.005$ mm. The thick section at one end of the parts serves solely as a grip, which is pushed into position for assembly and then broken off [7.54].

A further impressive example from the recording industry is a tight tolerance shift rail made from POM, in which an operationally decisive length of $69 + 0.05$ mm has to be adhered to [7.54].

Extreme tolerance requirements arise in imaging optics. These involve departures from specification of no more than 0.5 to 1 μm .

Certain assembly problems may also be solved by exploiting the deformability of polymeric materials when parts are being put together. The use of what are known as adaptor ribs has already been dealt with in Section 6.10. Figure 7.33 shows another variant of this principle.

When dimensions and tolerance limits are being specified, both the actual production tolerances and the changes in dimensions to be expected in operation should be taken into account. The bar charts in Figures 7.34 a–f provide some insight into how different factors theoretically affecting dimensional changes may act.

The theoretical principles underlying this behavior have been verified experimentally with a geometrically simple part of a cylindrical bearing bushing. The findings are reproduced in Figure 7.35.

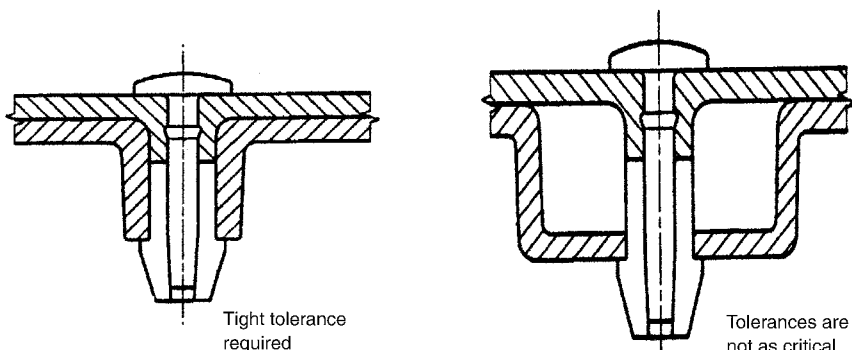


Figure 7.33 The joint at the left has a narrow tolerance range so that a tight-fitting assembly is ensured. The tolerance requirements for the design shown on the right are greatly reduced.

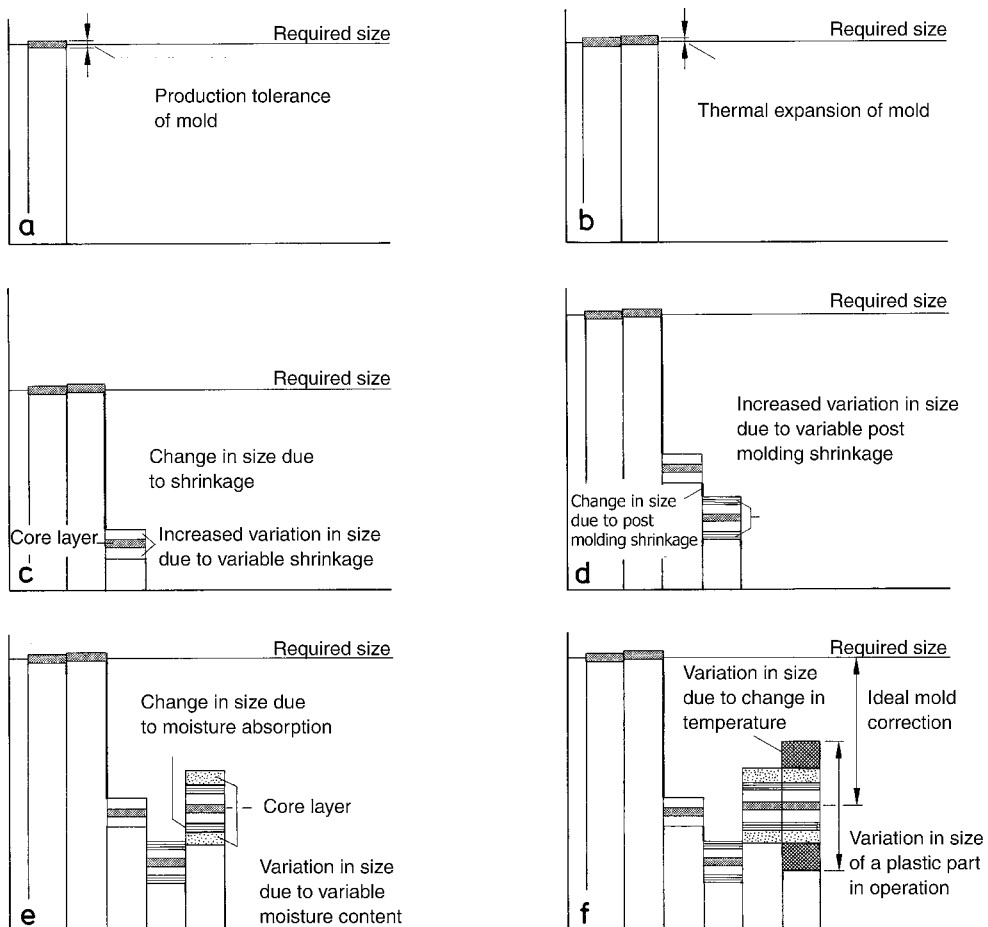


Figure 7.34 Theoretical changes in dimensions in injection molded parts [7.37]

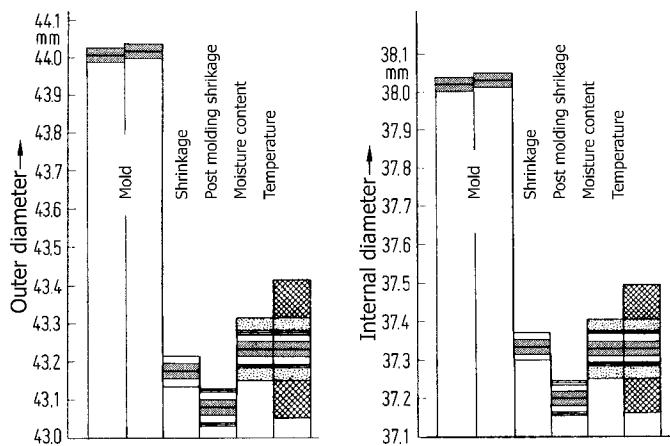


Figure 7.35 Measured changes in dimensions of the outer diameter (left) and internal diameter (right) of an injection-molded bushing made from PA 66 [7.37]

The test specimens were made from PA 66 through a diaphragm gate at a mold temperature of 80 °C. As expected, the impeded shrinkage of the internal diameter of 1.8% is a little less than the unimpeded shrinkage of the outer diameter of 1.9%.

No appreciable post molding shrinkage was found at room temperature. Only after annealing for 10 minutes at 120 °C did the internal diameter decrease by 0.37%, while the outer diameter decreased by 0.23%. The initially impeded shrinkage balanced itself out once again.

Moisture absorption can also be a factor that influences the dimensions of hydroscopic thermoplastics. Moisture absorption levels ranging from 1.3 to 2.3% by weight in polyamide parts are assumed and the temperature differences in operation are taken to be 60 K.

Further examples of solutions to tolerance and assembly problems appropriate to the material and the production process may also be found in Figures 1.10, 6.22, 11.50 and 11.51.

7.2.3 Warpage

Warpage is the deviation of a molding's dimensions from its desired shape when surfaces bow, or twist, or when the angles between faces change.

7.2.3.1 Causes of Warpage

The causes of warpage in production are always due to differences in shrinkage in a molding that are attributable to:

- Anisotropy of the material;
- Locally variable internal pressure in the mold; and
- Locally variable cooling conditions.

Anisotropic behavior of the material and the lengthwise and crosswise differences in shrinkage caused by this have already been discussed in Section 7.1.2.

In the case of parts with relatively long runners, differences in shrinkage and hence the tendency to warp arises along the flow path, because pressure losses increase in proportion to the length of the runner. Shrinkage is greater at points remote from the gate than at points near the gate. Therefore, a long bar-shaped part may tend to bow along its axis.

Nonuniform cooling caused by differences in wall thickness or temperature differences between the cavity and core can cause thermally induced warpage, because shrinkage is greater on the resulting hotter side of the part than on the colder side of the part.

A flat plate cooled more rapidly on one side than the other will arch in a concave manner towards the hotter side as a result of the greater ΔT on that side of the molding after ejection (see Figure 7.36).

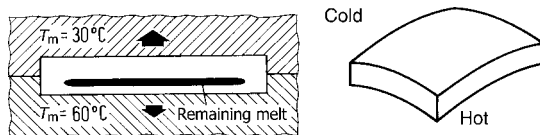


Figure 7.36 Arching of a plate caused by nonuniform heat dissipation [7.50]

Numerous “thin” ribs on a thick plate have the same effect because they cool faster. There is more longitudinal shrinkage for the thicker base plate (see Figure 7.37, right), unless sufficient heat is extracted from the base plate by an appropriate cooling system. Conversely, thick ribs pull a thinner plate in the opposite direction (see Figure 7.37, left). Sink marks, already referred to, also form on the plate’s surface opposite the thick ribs.

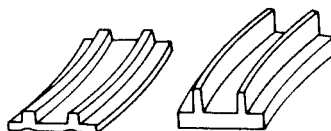


Figure 7.37 Warpage and sink marks in surfaces reinforced by ribs [7.50]

Thick ribs correspondingly pull a reinforced bowl inwards (see Figure 7.38, left). Ribs that are too thin, while not producing any sink marks, are more likely to push the surface of the bowl outwards (see Figure 7.38, right).

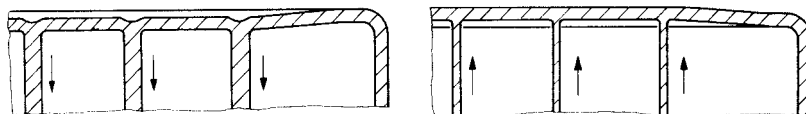


Figure 7.38 Different directions of warpage when bowls are reinforced by excessively thick and excessively thin ribs [7.30]

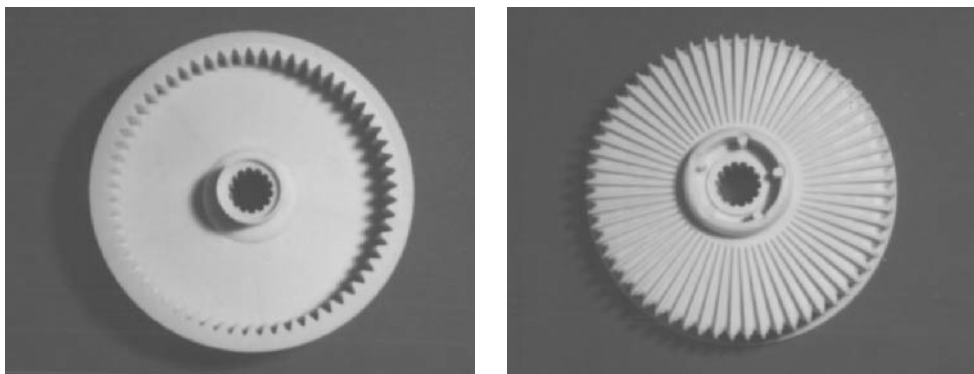


Figure 7.39 Gear wheel composed of PA 66 + PTFE 15 for circular saw drive [7.70]

$$\begin{aligned} D &\approx 100 \text{ mm} \\ n &= 2,600 \text{ min}^{-1} \\ P &= 1.7 \text{ kW} \end{aligned}$$

Circular parts with high requirements for rotational accuracy (*e.g.*, precision gear wheels) should not be reinforced by ribs if possible, because these may distort the toothed wheel into the shape of a polygon (see also Section 11.3.1). The best method of obtaining accurate circularity is to fill the cavity uniformly through a diaphragm gate.

Uniform filling of a rotationally symmetrical part can be achieved by first injecting a thick-walled collar through several pin gates requiring no subsequent finishing. This collar then acts as a diaphragm gate so that the disc can be filled uniformly without weld lines. The collar remains a constituent of the part. This concept is depicted in Figure 7.39.

The ribs, which each run towards the tooth gap on the gear wheel, serve as flow promoters and at the same time as reinforcement for the disc. In the region of the toothed structure, the ribs also produce a uniform wall thickness so that the relatively thick-walled teeth do not cause any warpage. Another collar at the outer perimeter absorbs the mechanical circumferential stresses when the wheel is in operation [7.70]. It is advisable to check the structural characteristics of the part by means of a computer-based filling simulation.

In areas with different wall thicknesses (see Figure 7.40), the thinner area will exhibit warpage, because the thicker sections will shrink more.

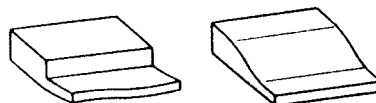


Figure 7.40 Warpage of part with different wall thicknesses (left). In areas where differences in wall thickness are unavoidable, a gradual transition should be provided (right) [7.49].

A thin membrane-like disc enclosed by a thick circular perimeter buckles, as illustrated in Figure 7.41, as a result of the greater shrinkage of the thick perimeter leading to radial compressive stresses build up around the disc circumference.

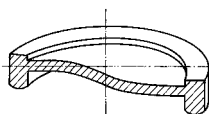


Figure 7.41 Buckling of a thin disc enclosed by a thick perimeter [7.50]

Angular warpage is a particularly common form of thermally induced warpage. Under conditions of constant heat flux, more heat is dissipated on the outside of an edge, because there is a greater surface area available than on the inside. Accordingly, shrinkage on the inside will be greater, causing warping towards the inside (reduction of the angle; see Figure 7.42).

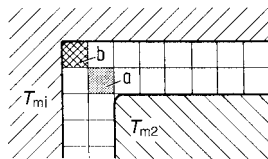


Figure 7.42 Despite the cavity surface temperatures being the same ($T_{m1} = T_{m2}$), cooling rates are different due to the differences in area in contact with the mold wall [7.30]

The unit volume labeled a in Figure 7.42 has no contact with the cavity surface. In this environment, the melt cools substantially more slowly than at the outside edge, where the unit volume b has two of its surfaces in contact with the cavity wall.

7.2.3.2 Controlling Warpage

From the preceding section it follows that thermally induced warpage can be avoided when no differences in shrinkage occur in the molding. This means that on reaching the 1 bar isobar (see pVT diagram), the specific volume would have to be the same in all sections of the molding. The following control parameters are available to this end.

Melt Temperature, Pressure Profile

The melt temperature distribution along the flow path in the molding is not easily controlled. Holding pressure has only a limited effect on warpage, although holding pressure profiles can be used to help promote more uniform shrinkage.

Cavity Surface Temperature (Heat Transfer)

The most effective measure for preventing warpage is selective modification of heat transfer conditions in regions particularly susceptible to warpage. The effect of cavity surface temperature is illustrated in Figure 7.43, where both positive and negative warpage has been induced in a box-shaped part by having different temperatures in the two halves of the mold [7.22, 7.38]. Warpage in this part mainly takes the form of edge warpage. Hotter inner edges result in a reduction of the angle and colder ones cause the angle to increase (see also Figure 7.45 f).

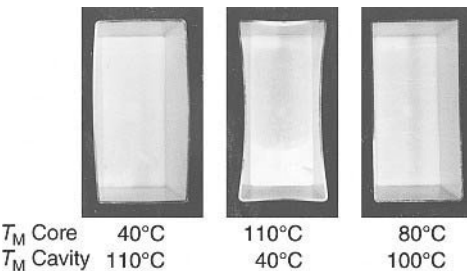


Figure 7.43 Thermally induced warpage and freedom from warpage due to differences in cavity surface temperature T_m for a box-shaped part made from POM (N 2320) [7.22]



Figure 7.44 Console insert made of ABS for the C-Box cassette system
(Photograph: Fischer, Tumlingen)

Thin or small cores can often be insufficiently cooled because of space limitation for cooling lines. Occasionally, however, it is possible to connect freestanding, thin cores to more easily cooled sections of the mold by means of acceptable changes in part design. Figure 7.44 shows a console insert made of ABS for the C-Box cassette system. The prototype mold for this part had a continuous inner wall to provide stability. The various functional elements were formed on this wall. A long narrow core was needed, but it was not cooled. This caused the insert to warp. In the optimized version of the mold, the continuous wall was divided into individual legs so that the narrow core could be connected to the main core resulting in better cooling.

A tried and tested mold making measure for enhanced cooling involves the use of copper or copper alloys to ensure better heat dissipation. This approach is used, for example, to improve dissipation of heat from inside edges and to minimize angular warpage. Figure 7.45 presents some design measures for counteracting angular warpage

In most cases, the goal is to prevent warpage, although sometimes the phenomenon can be exploited. If a relatively narrow core is left deliberately hot between the legs of a U-shaped part, a clasp can be produced whose legs are prestressed to press against one another after demolding. The optimum temperature difference for the part shown in Figure 7.46 was determined experimentally. This production technique can be used, for example, for POM clasps for loose-leaf binders, for fastening clips (see Figure 7.46), and other clamping elements operating under built-in tension.

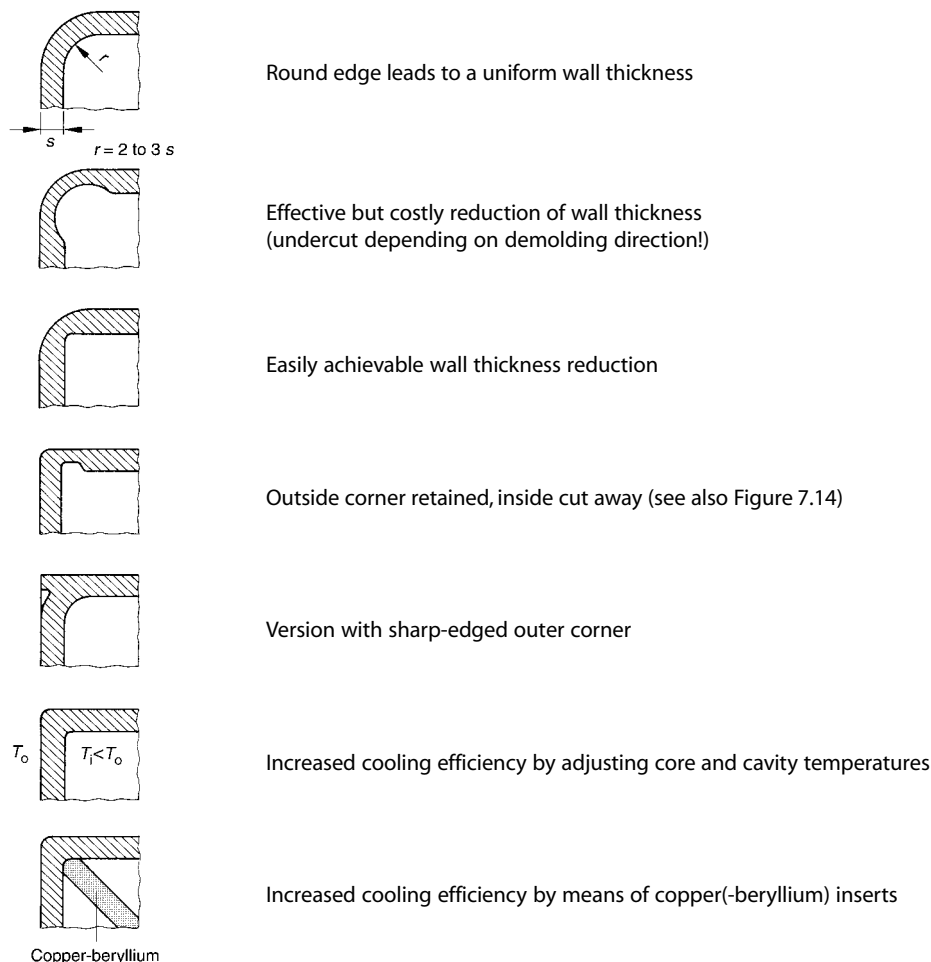


Figure 7.45 Measures for reducing angular warpage at corners

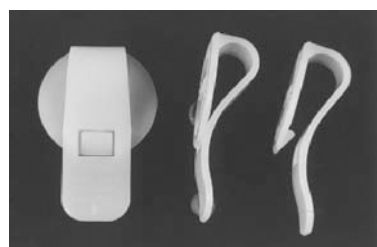


Figure 7.46 Prestressed clip made of POM for fastening identity or name tags to clothing.
The position in the mold is shown on the right.
(Photograph: Jantsch, Stein)

Compensation in the Mold

Compensation of deviations in shape in the mold is costly and usually associated with several mold modification steps. The mold cavity is made with a negative warpage, which compensates for the expected warpage of the part.

Cooling under Cavity Pressure

When differences in shrinkage cannot be avoided, the extent of the effective warpage depends to a degree on the dimensional stability of the part. This increases, as the demolding temperature decreases. Therefore, demolding takes place only after the part has cooled down to a temperature where it has acquired adequate rigidity. The impeded shrinkage caused by this, however, causes a state of internal stress which may relax and result in warpage when the part is in use, especially at elevated temperatures.

Therefore, particularly large flat parts susceptible to warpage are sometimes allowed to cool and relax slowly in specially designed post mold fixtures.

7.3 Demolding

The final phase of the injection molding cycle is the removal of the injection-molded part from the mold. In the simplest injection mold, the mold cavity is cut between two mold plates. For demolding, the two halves of the mold are moved apart and the part is ejected mechanically with the aid of ejector pins, ejector bushes, stripper plates, and the like. Alternatively, it may be ejected pneumatically (or mechanically for initial break away followed by pneumatic ejection).

During the design phase, attention must be paid to ease of demolding to avoid surface damage, such as scratches on visible or functional surfaces, and to avoid excessively expensive tooling. Two examples of relatively simple parts illustrate the complications associated with part ejection.

Bubble Ring

The bubble ring is a well known children's toy for blowing soap bubbles. The ring on which the soapsuds are suspended (Figure 7.47), is connected to the screw cap by a stem. The cap has a base and ribs for stiffening the walls. The diagrams in Figure 7.47 show the complicated demolding sequence in four steps.

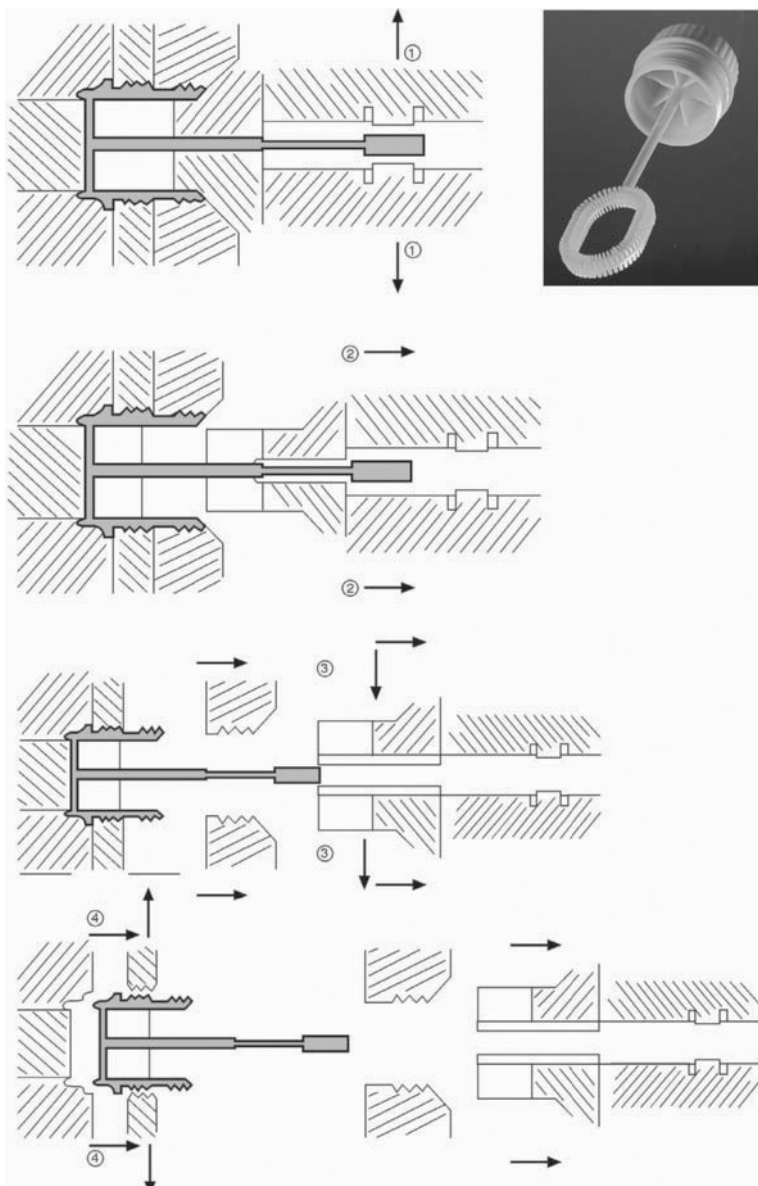


Figure 7.47 Demolding sequence for the bubble ring cap made by Kabus

- ① In the region of the ring opening and the lower end of the stem, the parts of the mold are moved away to demold the ring.
- ② The stem and the ribs are exposed by sliding the mold plate to the right. Therefore, the end of the stem close to the ring is a little thinner.
- ③ The concentric sealing rings are demolded by force.
- ④ The outside thread of the screw cap is exposed after the slides are moved apart and the part can be ejected.

Infusion Bottle Holder

Figure 7.48 shows the demolding sequence for a medical “drip” holder made of PP.

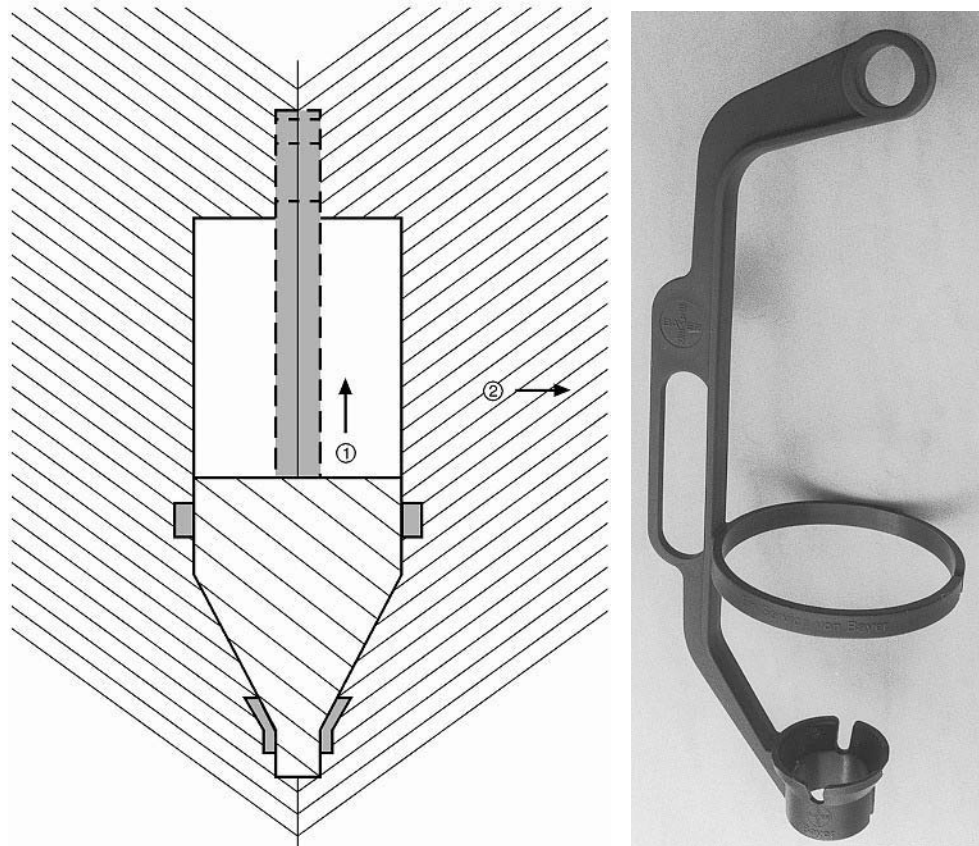


Figure 7.48 Holder for infusion bottles.

Principle of demolding:

- ① The inner contour is formed by a core, which is guided through the slit on the lower bottle support and displaced upwards into the free space. The retaining brackets are likewise opened in the mold by the width of the slit. The inside of the brackets shrink to a greater extent because of the hotter core so that after demolding, they engage over one another.
- ② The moving mold half is moved away and the part is ejected.

7.3.1 Draft

Most molded parts are produced in a mold with a cavity and core. As a result of molding shrinkage, the solidified and cooled melt shrinks onto those parts of the mold forming the inner contours (e.g., onto the cores)*. The part may also adhere by its outer contours to the cavity walls, depending on the material and molding pressures. In order to facilitate demolding or to make it at all possible:

A draft or taper on all surfaces in the demolding direction must be provided.

The recommended draft is specific to the material. Table 7.5 presents guideline draft angle values for short demolding strokes. In the case of long demolding strokes, especially for less ductile polymeric materials and those susceptible to scratches, relatively large drafts are advisable [7.39]. Demolding can be carried out without a draft up to a certain distance (when surface quality is very good), if the demolding surfaces can give way laterally.

Table 7.5 Guide Values for Draft Angles [7.39]

Material	Angle in degrees
PA, POM, HDPE, ABS, PP	0.5
PBT, SB	1
PS, SAN, PC	1.5

Surface roughness is also an important variable with respect to draft angle requirements. Surface texture or surface granularity causes slight undercuts. Therefore, grained surfaces require a slightly larger draft angle to ensure that the surface is not damaged on demolding. In reference [7.6], a draft of 1° is recommended for every 1/100 mm of grain depth.

7.3.2 Demolding of Undercuts

Design efforts to integrate as many functions as possible into a component often have the consequence that straightforward demolding is impeded by undercuts. In such cases, several parting surfaces and opening directions are needed in the mold and demolding becomes more costly and more of a maintenance issue. However, the incorporation of undercut features offers enough advantage in terms of reducing secondary operations or improving performance to make them rather common.

* Injection-moldable thermoset materials are demolded at high temperatures (approx. 170 °C). Therefore, their shrinkage in the demolding phase is low so that there is less shrinking onto the mold cores.

7.3.2.1 Forced Demolding

Some undercuts can be handled by forced demolding. The size of the undercuts or counterdrafts that can still be demolded in this fashion is a question of the strain that can be imposed on the section of the part at the *demolding temperature*, without leaving any permanent deformation. When the part is geometrically simple, this strain can be estimated and its permissibility can be evaluated using the relevant stress-strain diagram (*i.e.*, the yield strain must not be exceeded) for the material to be molded.

Investigations of the demolding characteristics of undercut cylindrical bushings described in [7.40] provide some pointers to the size of force-demoldable undercuts that can be adequately established by a stress-strain diagram (see Figure 7.49).

A distinction is made between a favorable position of the undercut close to the end of the part and an unfavorable position at some distance from the end, in which strain is also impeded by the base. In both cases, a simplified estimate of strain, $\epsilon = H/D_m$, was used.

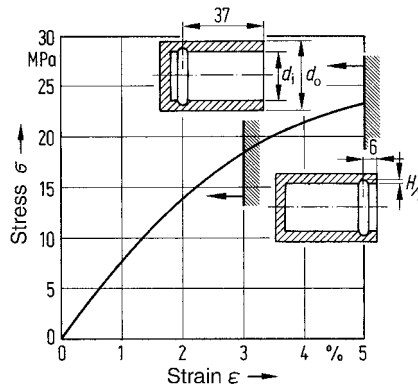


Figure 7.49 Forced demolding of circular undercuts in a cylindrical part.

The limiting values specify the strains up to which forced deformation is possible without damage or permanent deformation. Polymeric material: POM (N 2320); demolding temperature $T_D \approx 100^\circ\text{C}$; $d_o = 43 \text{ mm}$; $d_i = 29 \text{ mm}$; $d_m = 36 \text{ mm}$.

7.3.2.2 Mold-Making Measures

If an undercut that is important to the function of a part is of such a size that it cannot be demolded by force, it must be possible to expose the undercut areas by means of moving mold parts. Splits are used for individual contour regions, which are restricted and separate from one another. Splits (or a split cavity) are employed in the case of two or more external contour regions arranged symmetrically with respect to one another. As a result, the molds are not only more expensive, they also become more susceptible to problems such as flash and require more intense maintenance. In addition, operational reliability decreases as service life is reduced due to wear of movable parts.

The demolding of internal undercuts usually requires even more complicated mold-making measures. The design principle is based on sloping divided cores, which are tightened or released by means of wedges. Collapsible cores, which in the collapsed state have smaller external

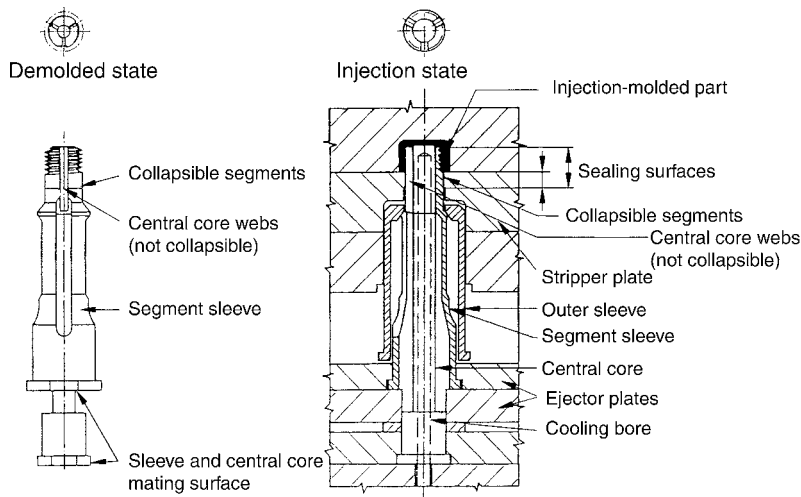


Figure 7.50 Collapsible minicore ($d_{\min} = 13 \text{ mm}$) for demolding small internal threads. By collapsing the three segments, undercuts, for which $\Delta d/d$ is up to 20%, are demoldable [7.41].

dimensions than in the home state (see Figure 8.35), are also used. In Figure 7.50, the cross section of a mold fitted with a very small collapsible core for producing an internal thread is shown schematically.

Hasco's mold rules, with which internal threads or inside undercuts in cylindrical parts having diameters of 12 to 55 mm can be demolded, are based on the same structural principle [7.69].

A low-cost solution can also be achieved using elastic ejectors. Elastic ejectors spring back a distance during the demolding operation, thus releasing the undercut. Figure 7.51 shows a detail of a mold, in which undercuts in a pill container are to be demolded at a total of 7 locations [7.67].

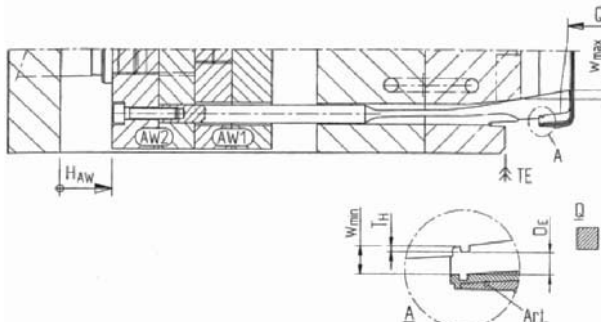


Figure 7.51 Outline diagram of a detail of a mold in which internal undercuts are demolded by means of elastic ejectors

T_H = Undercut depth

D_E = Differential for reliable demolding

$W_{\min} = T_H + D_E$

H_{AW} = Ejector stroke

(Photograph: EOC Normalien, Lüdenscheid)

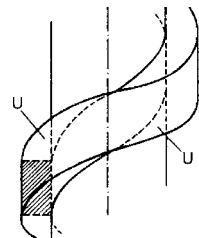


Figure 7.52 Undercuts U in a thread with a rectangular thread profile on demolding with a split mold [7.6]

Depending on the profile and gradient of the thread, external threads may also require undercuts (see Figure 7.52).

The greater the chosen flank angle, the smaller the undercuts turn out to be. The geometric relationships of undercuts and the necessary number of jaw sections must be examined on a case by case basis (see also Section 11.3, Figure 11.38). Split molds can leave undesirable marks and flash behind in the parting line to a greater or lesser degree, depending on the quality and condition of the mold. If flash cannot be tolerated, unscrewing molds can be used. Threaded cores or sleeves release the thread when they are rotated during demolding. This mold expenditure can be avoided in the case of prototypes and possibly in the case of short production runs by using exchangeable cores, which after demolding are unscrewed manually outside the mold.

7.3.2.3 Fusible Cores

The injection molding of parts using conventional, nondemoldable cores was patented as early as 1968 [7.43]. For a time, the method was rarely used. Only when the automobile industry declared an interest in the production of thermoplastic air intake manifolds for vehicle engines in the 1980s, did the breakthrough come for investment casting technology.

In the first step of the process, a metal core is die cast from a low melting point metal alloy. This core will later replicate the inside contours of the part to be manufactured. The metal is usually an alloy of tin, bismuth, or lead whose melting point is below the melting point of the thermoplastic in question. For example, in the case of glass-fiber reinforced PA 66 ($T_m = 255^\circ\text{C}$) a Zn-Bi alloy with a melting point of 138°C is typically used.

In the actual production step for the part, these cores are inserted in the injection mold and the thermoplastic melt is forced around them, filling the space between the core and cavity. The very high thermal conductivity of the metal alloy, the low thermal conductivity of the polymeric material, and a minimum mass of material in the core ensure that the polymer melt solidifies very quickly on the surface of the core and does not cause the core to melt.

After the melt has solidified, the part is demolded together with the core.

In the final step of the process, the metal core is melted out of the molding, usually by inductive heating in a hot liquid bath (e.g., Lutron ES from BASF). The recovered metal alloy can be reused for fresh cores. Figure 7.53 shows an air intake manifold at the three stages described above (see also Figure 1.14).

Detailed descriptions of the process may be found in [7.44 to 7.48].

The diagram in Figure 7.54 gives an impression of the layout of a production cell in which such intake manifolds are mass-produced.

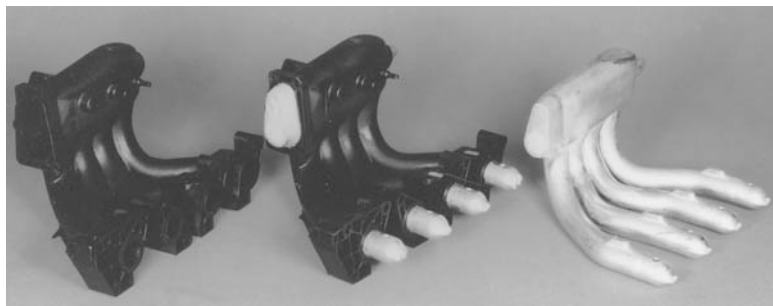


Figure 7.53 Production stages for intake manifolds.
Right: core composed of a tin-bismuth alloy;
center: core and casting;
left: finished intake manifold made from PA 66-GF
(Manufacturer: Montaplast, Morsbach).

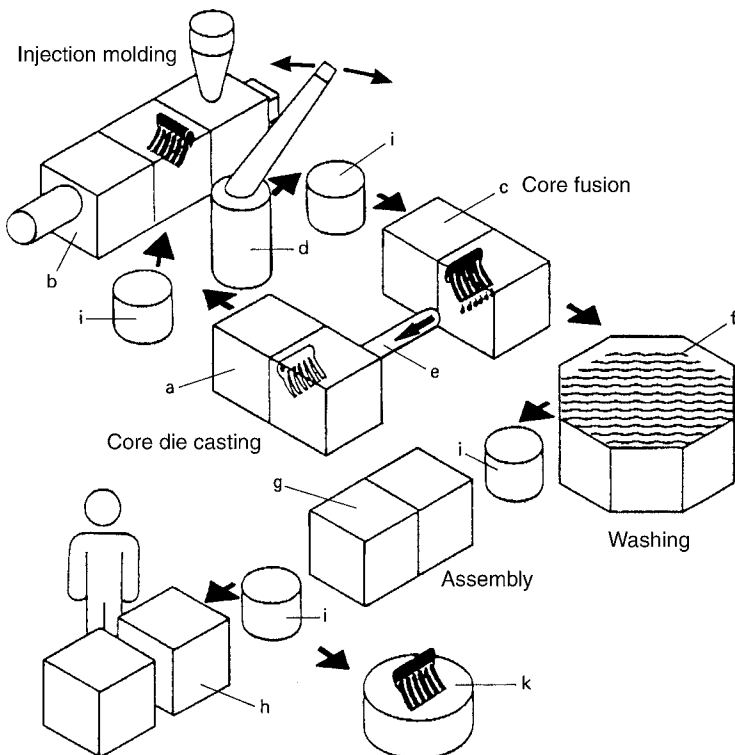


Figure 7.54 Schematic illustration of a production cell for manufacturing intake manifolds by investment casting [7.48].
a: core die casting unit; b: injection molding machine; c: core melting unit; d: robots;
e: melt recirculation; f: washing unit for the injection-molded parts; g: assembly of the
intake manifold (friction weld cover, put inserts in place); h: packaging and shipment;
i: test stations in the course of production; k: additional testing for product audit.

7.3.3 Avoidance of Undercuts

Because the demolding of undercuts is associated with extra costs, it must be considered early in the design phase whether undercuts can be avoided. This can often be achieved by skillful and creative design.

7.3.3.1 Modifying the Design

Design viewpoints are often at odds with straightforward technical implementation. A typical example of this is provided by the screw cap in Figure 7.55.



Figure 7.55 Screw cap with undercut (left) and a simple version without undercut (right) [7.34]

The knob design with biaxial knurling borrowed from metal working (Figure 7.56, left) requires substantially higher costs for the mold than the versions without undercuts in the center and on the right of Figure 7.56.



Figure 7.56 Knob design with (left) and without (center and right) undercuts [7.39]

7.3.3.2 Piercing Cores (Blocking or Shutoffs)

Certain part features can be produced using the cavity core shut-off concept. Shut-offs are designed so that the cavity and the core partly touch one another when the mold is closed so that an aperture is formed in the molding. In this way, apertures in side walls can be demolded without undercuts (see Figure 7.57).

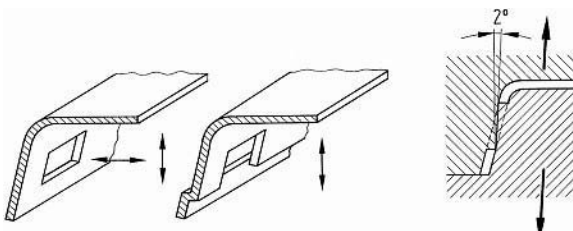


Figure 7.57 Opening on the side of a housing [7.49]. On the left, an additional split is required for demolding. The design in the center and on the right is free of undercuts. When the parting surfaces are stepped (right), a side inclination of 2° is necessary.
↔ Demolding directions

Lattice-like openings at an oblique angle to the demolding direction may be produced without undercuts as shown in Figure 7.58.

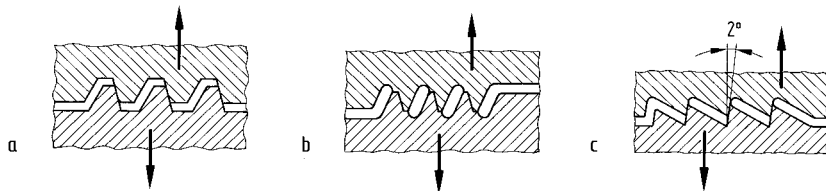


Figure 7.58 Oblique lattice openings [7.34]
→ Demolding directions

The principle of avoiding undercuts on snap-fit hooks by means of piercing cores is appropriate when it is possible to make an opening in the wall, as shown in Figure 7.59 (see also Figure 8.15).

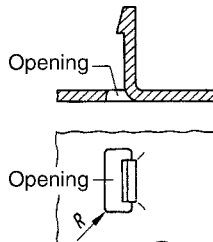


Figure 7.59 Principle of demolding a snap-fit hook without undercuts

In the case of a fork-shaped part with internal lugs (see Figure 7.60), a split may be eliminated if the curved wall above the lugs is pierced.

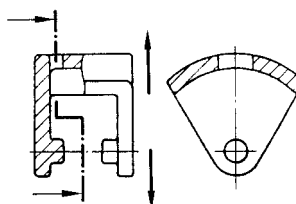


Figure 7.60 Demolding without additional splits by using piercing cores behind the internal lugs
→ Demolding directions

If in the case of internal undercuts, such a measure is not possible because of the constraints imposed by the shape, demolding becomes more complicated. In segmented snap-fit joints with large internal undercuts (see Figure 7.61), the cost can be kept within acceptable limits by keeping the space under the hooks free by means of piercing cores, which then have to be demolded sideways.

A further example of designing for demolding is sketched in Figure 7.62. The part design in the left-hand section of the figure requires splits for demolding the continuous hollow spaces.

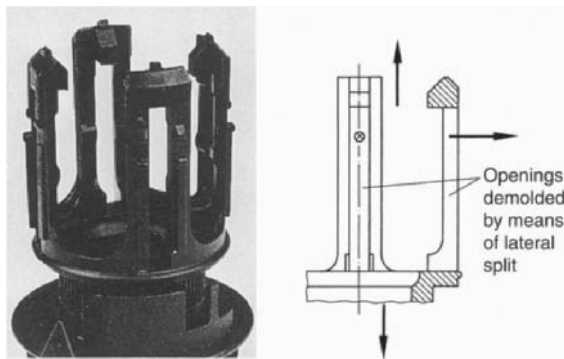


Figure 7.61 Segmented snap-fit joint; demolding of the undercuts by means of piercing cores
→ Demolding directions

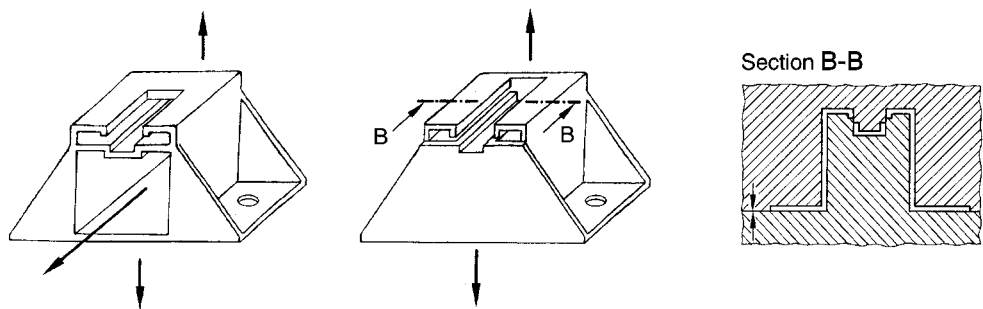


Figure 7.62 Design variants with (left) and without splits (center); position in mold (right)
→ Demolding directions

These splits must be withdrawn sideways. The part in the center of the figure can be demolded without splits when the front and rear walls are closed and the base is left open. The side opening along the guide groove is made by a piercing core inserted from above, as indicated in the right-hand section of the figure.

7.3.3.3 Multipart Designs

Undercuts may also be avoided if components can be designed in several parts in such a way that each part can be produced independently without undercuts. The joining process, which is then necessary, is an additional secondary operation which, of course, must not be a major burden on the overall product cost. The example in Figure 7.63 shows how snap-fit joint elements are molded-in; the two halves are identical so that any two parts can be economically joined to one another simply by interlocking them (see also Figures 11.36 and 11.37).

The economic case is more difficult to make for more complex structural parts. An example is provided by the air intake manifolds mentioned earlier. Because of the relatively high cost of fusible core technology, these are also commonly injection molded in the form of half-shells and joined together by welding (see Figure 7.64); more recently also by means of snap-fit

joints (see Figure 7.65). In the presented snap-fit version, the holes for screwing the two-piece manifold onto the cylinder head is molded through the upper and lower half-shells. With this type of assembly, however, an additional seal between the two halves is needed.

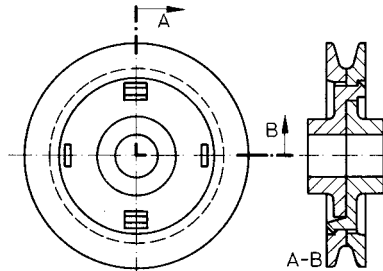


Figure 7.63 V-belt pulley (PA) designed as two identical parts joined by snap-fit hooks

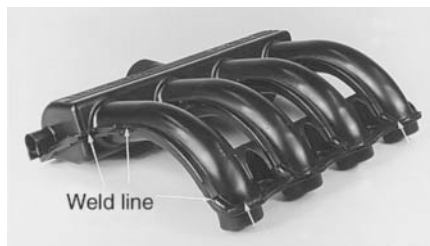


Figure 7.64 Intake manifold made of PA 66-GF (A3WG7), injection molded in the form of half-shells that are welded together



Figure 7.65 The two halves of this intake manifold are connected by means of snap-fit joints
(Manufacturer: Bosch, Waiblingen; User: Opel, Rüsselsheim)

7.4 Sandwich Molding (Co-Injection Molding)

When two or more components are injection molded to produce a “multi-layer structure”, special properties and effects can be obtained by combining different materials. Some of the possibilities afforded by this technology are itemized below.

- *Dense surface – expanded foam core*
Thick-walled moldings without sink marks having surfaces equivalent to solid injected parts.
- *Reinforced surface – unreinforced core*
High flexural rigidity with reduced raw materials costs.
- *Unreinforced surface – reinforced core*
Good surface with increased strength and heat resistance.
- *Multicolored surface*
Abrasion-resistant lettering on keyboards, etc.
- *Flexible surface – hard core*
Flexible surfaces with a rigid hard core, pleasant feel and integration of functions.
- *Hard surface – flexible core*
High compressive and flexural strength; ability to act as vibration damper.
- *Reinforced surface – electrically conducting core*
Good surfaces and simultaneously providing electric shielding.
- *Conducting surface – unreinforced core*
Particularly high shielding values due to two shielding layers.
- *Surface composed of virgin material – core made of recycled material*
Production of high-grade parts using recycled materials.
- *Good surface – core composed of barrier raw material*
Reduction of permeability by means of a barrier layer in the core.
- *Surface composed of polymeric material – core made up of gas*
Thick-walled moldings free of sink marks affording shorter cycle times and weight reductions.

Combinations of polymeric materials, which adhere well to one another are listed in Table 7.6.

7.4.1 Two-Color Injection Molding

In multicolor technology, two or more similar polymeric materials with different colors are injected into one another or over one another. This technology has found widespread use in the production of operating controls such as keyboards (see Figure 7.66). High-quality lettering and, above all, symbols having high abrasion resistance are obtained. For economic reasons, two-color injection molding is only used when considerations of design and aesthetics are of central importance.

Table 7.6 Combinations of Materials [7.56]

	ABS	ASA	SAN	S/B	PS	PMMA	PC	PSU	HDPE	LDPE	PP	EVA	PA 6	PA 66	POM	PBT	PPE + S/B	ABS + PC	PC + PBT
ABS	+	+	+	-	-	+	+	+	-	-	-	-	+	+	-	-	-	-	
ASA	+	+	+	-	-	+	+	+	-	-	-	-	+	+	+	-	-	-	
SAN	+	+	+	-	-	+	+	-	-	-	-	-	-	-	-	-	-	-	
S/B	-	-	-	+	+	-	-	-	-	-	-	-	-	-	-	+	o	o	
PS	-	-	-	+	+	-	-	-	-	-	-	+	-	-	-	+	o	o	
PMMA	+	+	+	-	-	+	o	o	o	o	-	-	-	-	-	+	+	+	
PC	+	+	+	-	-	o	+	+	-	-	-	-	o	-	-	o	o	+	+
PSU	+	+	-	-	-	-	+	+	-	-	-	-	-	-	-	o	+	+	
HDPE	-	-	-	-	-	o	-	-	+	+	+	+	o	o	o	-	o	o	o
LDPE	-	-	-	-	-	o	-	-	+	+	+	+	o	o	o	-	o	o	o
PP	-	-	-	-	-	-	-	-	-	+	+	+	o	o	o	-	o	o	o
EVA	-	-	-	-	-	+	-	-	+	+	+	+	-	-	-	o	o	o	
PA 6	+	+	-	-	-	o	-	o	o	o	-	-	+	+	-	o	+	+	
PA 66	+	+	-	-	-	o	-	o	o	o	-	-	+	+	-	o	+	+	
POM	-	-	-	-	-	-	-	o	o	o	-	-	-	-	+	o	o	o	
PBT	+	+	+	-	-	-	+	-	-	-	-	-	-	-	-	+	-	+	+
PPE + S/B	-	-	-	+	+	-	o	o	o	o	o	o	o	o	o	-	+	o	o
ABS + PC	+	+	+	o	o	+	+	o	o	o	o	o	+	+	o	+	o	+	+
PC + PBT	+	+	+	o	o	+	+	-	-	-	-	-	+	+	o	+	-	+	+

+ = good adhesion

o = poor adhesion

- = no adhesion

On the other hand, laser etching is increasingly gaining importance as an alternative. A mold insert for each single symbol is not needed because the symbols are applied only onto the finished injection molded parts. There are certain restrictions on the range of materials suitable for laser etching*. Table 7.7 provides more details. Figure 7.67 shows a telephone keypad whose lettering was produced by this method.

* Raw material manufacturers supply particularly suitable color formulations optimized for etching.

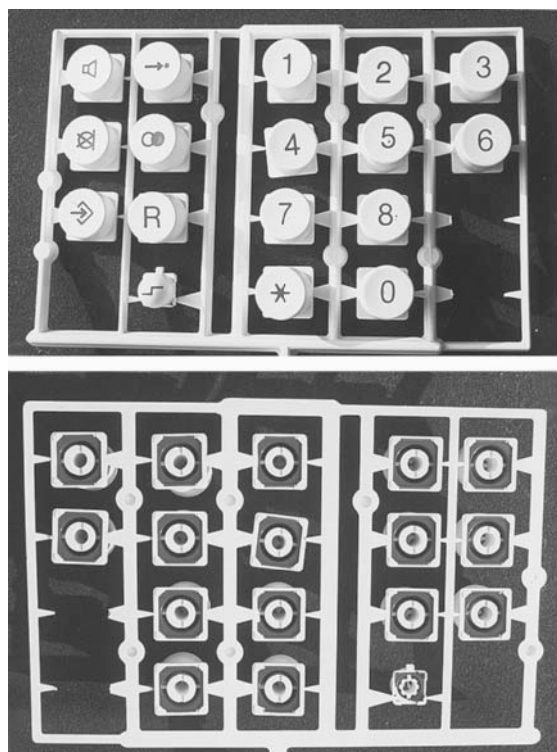


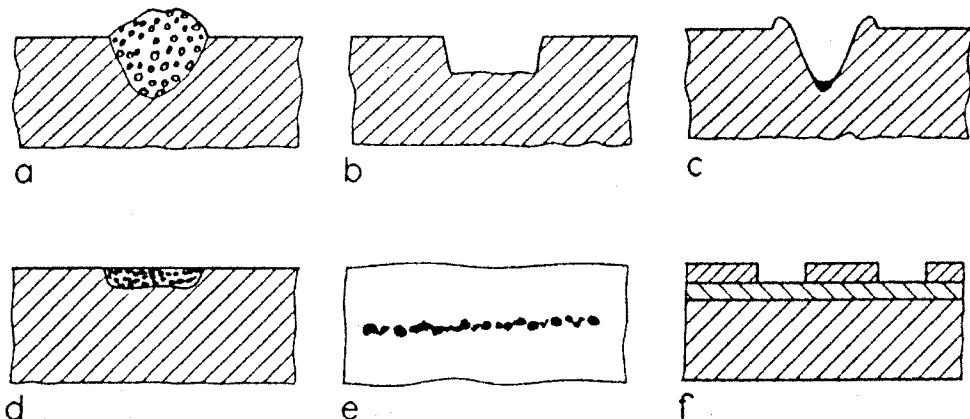
Figure 7.66 Keyboard keys are injection molded from red and white ABS, one after the other, using a molding machine with two injection molding units



Figure 7.67 Laser-etched keypad and housing made from PA 66, black LS23189 (Manufacturer: Bang & Olufsen, Denmark)

Table 7.7 Suitability of Selected Materials for Laser Etching [7.64]

Material	Notes
ABS	Readily etchable, both dark when the material is light and light when the material is dark; laser-optimized colorings readily etchable
ASA	Good results on light color formulations
PA 66	Good light coloring when the material is dark. No contrast in the natural material. Laser-optimized colorings readily etchable.
PC	Good dark coloring on a transparent base. Light on black formulations.
PC + ABS	Very good dark coloring on light color formulations. Beige when the material is dark.
PC + PBT	Both dark on light and light on dark
PBT	Very good dark coloring, light lettering also possible
PPE	Unsuitable on dark color formulations, satisfactory on light color formulations
PPS	Good dark coloring on light backgrounds. Light-colored etching possible.
POM	Hardly any contrast on light colored backgrounds. Laser-optimized color formulations are good to very good for accepting lettering.
SAN	Satisfactory to good etchability on black, gray, white and transparent backgrounds

**Figure 7.68** Effects obtained by laser etching [7.65]

- a = Foaming
- b = Engraving without color change
- c = Engraving with color change
- d = Color change, color loss (bleaching)
- e = Beaded structure
- f = Etching by removal of paint or lacquer

Depending on the material and pigment used, different effects can be produced by laser etching (see Figure 7.68).

- a) In thermoplastics with a suitable dark coloring, the material expands along the irradiated contour. The foam structure extends to a depth of up to 100 µm and rises over the original surface to a height of about 50 µm. The color contrast is very good.
- b) Material can also be eroded by vaporization. However, the lettering is not very legible.
- c) In addition to removal of material, a carbonized black layer can be produced at the bottom of the eroded channel, which produces good contrast in light colorations.
- d) In special pigmentations, a color change yields lettering approximately 100 µm deep with no appreciable damage to the surface. The achievable contrast is a little less than in a) and c).
- e) Another effect gives rise to an irregular dark coloration along the line of exposure.
- f) A particularly powerful effect is obtained by laser-etching transparent materials previously coated with a special dark paint. The laser beam burns the paint off along the exposed contours and in this way, symbols that can be lit from behind are produced. The “day & night” design for illuminated pushbuttons in automobiles are produced by this method. In order to increase the contrast during the day when the pushbutton is not illuminated, a thin light-colored layer of paint that is not attacked by the laser is first applied to the transparent plastic, followed by the dark layer of paint. Alternatively, an opaque base material is used. When the dark-colored layer is taken away, there is good contrast even without back-lighting (see Figure 7.69). A two-pack laser paint may be used for the paint system*.



Figure 7.69 “Day & night” design of pushbuttons in automobiles

7.4.2 Rigid-Flexible Combinations

Using sandwich technology, it is also possible to join thermoplastics to thermoplastic elastomers in a single operation. On the one hand, it is possible to greatly improve the functionality of parts and, on the other hand, to cut down operating and assembly costs. There are also fewer

* For example, SP 2200 two-pack laser paint from Nordwest-Chemie.

tolerance problems when the properties of the flexible component can be used to compensate for tolerances.

The following variants of the process and the tool concepts associated with them have proved to be effective to date [7.57]:

- Transfer method
- Turntable method
- Index plate method
- Split technique

In the *transfer method*, the preform* is transferred by means of handling devices into a second, new cavity in the same machine or in another parallel machine. The method is primarily suitable for large parts.

In the *turntable method*, the complete ejector side of the mold is turned by 180° after injecting the preform. The preform remains on the core and is inserted into a new cavity on the fixed mold half. In this station, the flexible component is injected while at the same time the next preform is produced in the first station.

The *index plate method* affords greater design freedom. In this method, the second cavity can have a different core on both the core and fixed side. With the method, the preform is lifted by a plate, rotated, and inserted into the second cavity.

A particularly efficient method is the *split technique*; however, it does restrict design freedom. With this method, the cavity for the second material is closed initially by a split and is opened only after the first material has been injected. As an example, sealing lips can be injected in place by this method.

Materials

Table 7.8 provides an initial overview of materials that adhere well to thermoplastic elastomers. Within each of the groups of elastomers identified, there also exist special grades with even better adhesion. In addition, the surface temperature of the component injected first plays a decisive role in determining the bonding strength of the composite [7.58].

Table 7.8 Strengths of Composites Made from Combinations of Rigid and Flexible Materials

		ABS	PS	PC	PE	PP	PA	POM	PBT	PVC
TPE-O	Polyolefin elastomers	–	–	–	+	++	+	–	–	–
TPE-U	Polyurethane elastomers	+	–	+	–	–	+	+	+	+
TPE-S	Polystyrene elastomers	+	+	–	+	+	+	–	–	–
TPE-E	Polyester elastomers	+	–	+	–	–	+	–	+	–
TPE-A	Polyamide elastomers	–	–	–	–	–	+	–	–	–

+ = good adhesion – = poor or no adhesion

* The part produced from the first component is the preform component.

Examples

The following figures provide an impression of the numerous possibilities for integrating functions by means of rigid-flexible composite materials. These involve integrated sealing functions, soft-touch surfaces that feel pleasant to the touch, switch panels, and elastic and damping functions to name but a few.



Figure 7.70 Cone for a back-siphonage preventer cartridge in sanitary fittings. The dark cone is first injected from PP (1022), while in a second step the sealing ring from TPE-O is injected. (User: Wildfang GmbH, Mülheim)



Figure 7.71 It is particularly efficient to inject several sealing rings onto a part in a single operation. The sealing rings are connected to one another internally by webs.
Valve body: PA-GF
O-ring seals: TPU



Figure 7.72 Part of a sealing strip. The rigid component made of PP carries the fastening hooks and clips, while the sealing lip is made of SBS (Manufacturer: Weidmann, Rapperswil, Switzerland).

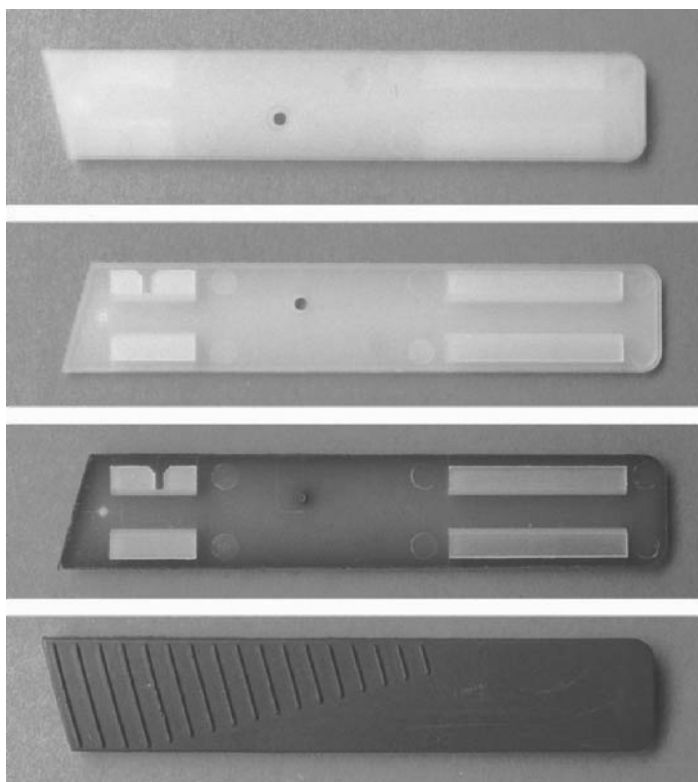


Figure 7.73 Handle made of PA with a grip surface made of TPU.
In the first station, the rigid frame is injection molded from PA.
In the second cavity, the TPU component is injected through the bore in the PA part
(Manufacturer: Philips, Klagenfurt, Austria).



Figure 7.74 Grip of an electric toothbrush made from ABS as the rigid component.
In addition to imparting a good feel to the handle, the flexible component here provides
the seal for the brush head and the cover for the switch mechanism
(Manufacturer: Weidmann, Rapperswil, Switzerland).



Figure 7.75 "Visiotherm" control device on AMC cooking pots. Arranged on the support part made of ABS + PC (right) are small spring arms that actuate setting keys over the three segments (Manufacturer: Weidmann, Rapperswil, Switzerland).

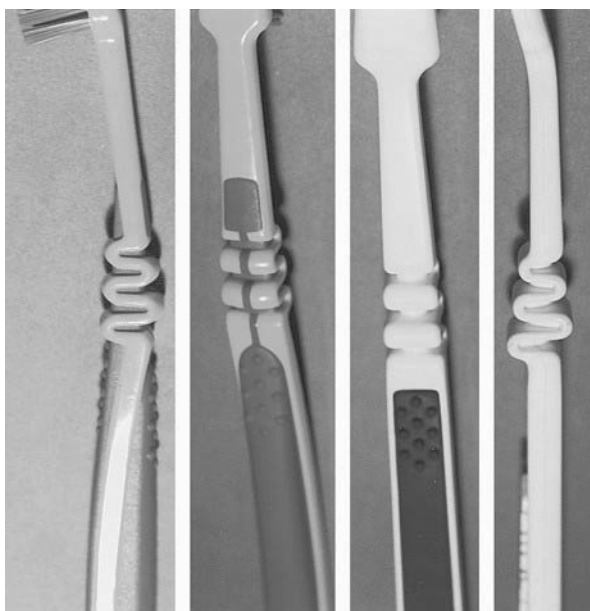


Figure 7.76 "Dr. Best" toothbrushes. Despite its undulating shape, the version on the right is not very effective, because the flexible spring elements are stiffened again by the core. In the improved design on the left, the core is produced by two-component injection molding from a flexible thermoplastic elastomer, as is the handle, which has a pleasant feel.



Figure 7.77 Glove compartment in a Mercedes Benz automobile produced from PP and TPE-O by transfer molding. The interior surface made from elastomer damps any rattling noises from objects stored within (Manufacturer: Weidmann, Rapperswil, Switzerland).

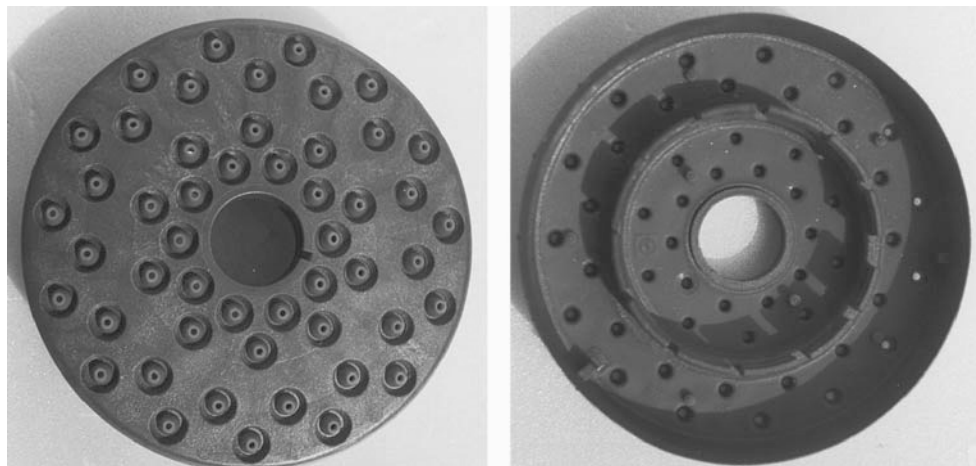


Figure 7.78 Shower head made of POM-GF with jets made of silicone. The problem of shower heads becoming blocked with lime deposits is well known. Here, the jets are made of nonpolar silicone, which minimizes the formation of lime deposits. The parts are made by transferring the thermoplastic preform into a second heated mold in a second machine, in which the liquid thermosetting silicone rubber is injected over it. The vulcanization temperature is approx. 170 °C.

7.4.3 Gas Injection Technology (GIT)*

Sequence of Operations

The standard GIT process involves filling the cavity only partially with melt (see Figure 7.79 left) and then injecting a gas (usually nitrogen) through the machine nozzle (see Figure 7.79 center). The injected gas displaces the still molten plastic material within relatively thick gas channels to the ends of the mold cavity (see Figure 7.79 right). This results in a hollow space in the injection molded part, which from the outside seems to be solid. As might be expected, the surface on the inside is not smooth and the wall thickness is not completely uniform (see Figure 7.80). Applications in which the gas channel is designed as a functional cavity are also possible in principle [7.68].

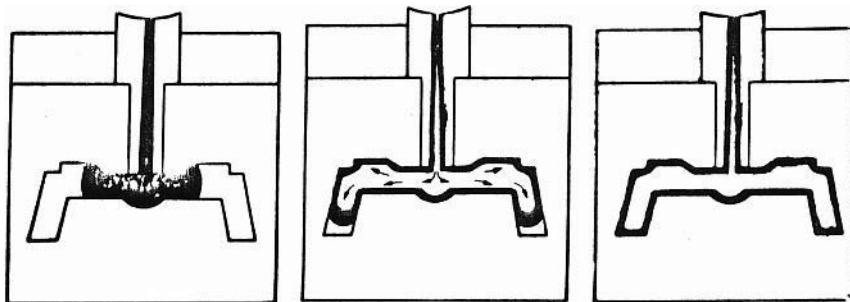


Figure 7.79 Theoretical sequence of operations in the standard GIT process



Figure 7.80 Section through the lower end of a clutch pedal

* A number of variations of this process have been introduced. Most know-how about the process is currently in the hands of the equipment manufacturers and experienced GIT molders. When incorporating GIT processes, the licensing situation has to be taken into account.

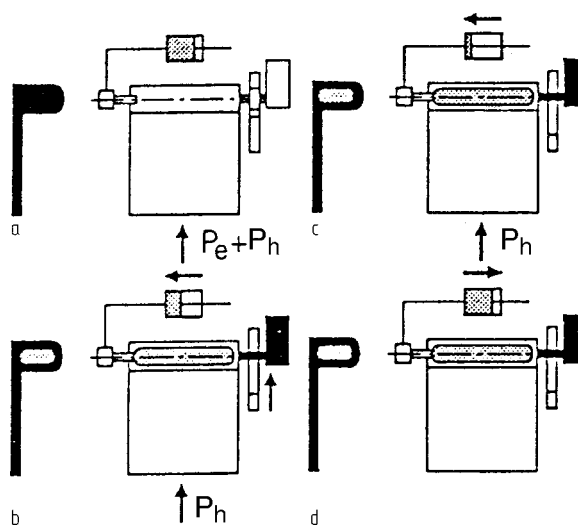


Figure 7.81 Sequence of operations in the GIT secondary cavities process [7.59]
 a Complete filling and brief holding pressure,
 b Injection of gas, opening of secondary cavity and holding pressure,
 c Compression phase under gas holding pressure,
 d Release of pressure and return of gas.

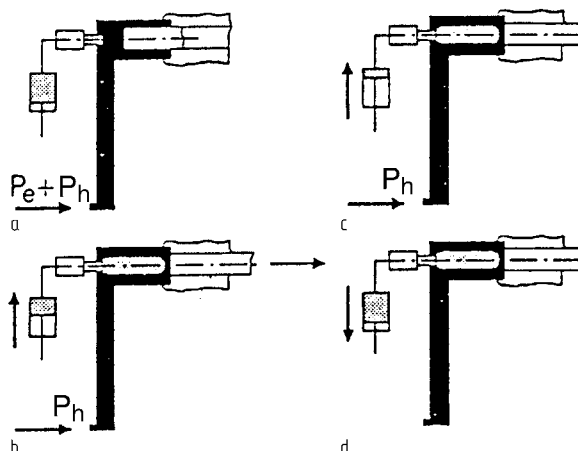


Figure 7.82 Sequence of operations in the GIT core puller process [7.59]
 a Complete filling and brief holding pressure,
 b Injection of gas, core pulling, and holding pressure,
 c Compression phase under holding pressure and gas holding pressure,
 d Release of pressure and return of gas.

The gas pressure acting from the inside prevents the formation of sink marks.

Two variants of the process are illustrated in Figures 7.81 and 7.82 [7.59].

In the *GIT secondary cavities process*, the entire cavity is first filled. The gas is then introduced and pushes the molten plastic material in the core of the gas channels into a secondary cavity opened by a core action. The process is suitable for flat parts having some thicker areas.

In the *core puller process*, the cavity is also first filled completely. One or more cores are then pulled back and the spaces liberated are filled with gas. The gas is not introduced through the machine nozzle but rather directly at the thick sections of the molding. The more expensive construction of the mold is a disadvantage of this process.

Design Notes

Table 7.9 provides an overview of the theoretical suitability of the GIT process for the manufacture of different types of components together with the advantages of the process [7.60].

Table 7.9 Classification of Component Types and the Advantages Afforded by GIT

Component type	Advantages
Bar- or handle-shaped components	Weight reductions of up to 50%, shortening of the cooling time by up to 50%, no sink marks, reduced susceptibility to warpage, and components having high torsional rigidity (and bending strength).
Components having some thickened areas	No sink marks in the thick-walled areas, no warpage due to accumulation of material and good visual appearance of the thick regions by comparison with conventional injection molding.
Plate-like components	No sink marks in ribbed areas and high rigidity due to extensive ribbing. Reduced susceptibility to warpage.

The empirical procedure for GIT component design is difficult. Therefore, it is advisable to carry out numerical filling studies during the design stage*. Nevertheless, some theoretical design rules have to be taken into account because in addition to the advantages there is also a series of restrictions associated with this method.

GIT processes require an unconventional component design. Wherever gas cavities are to be produced, *wall thicknesses must be high* because the gas will go to where the melt temperature is highest and hence viscosity is lowest. Even the slightest inhomogeneities will allow the gas to advance in an uncontrolled manner.

* Most commonly available simulation programs contain modules for GIT process simulation.

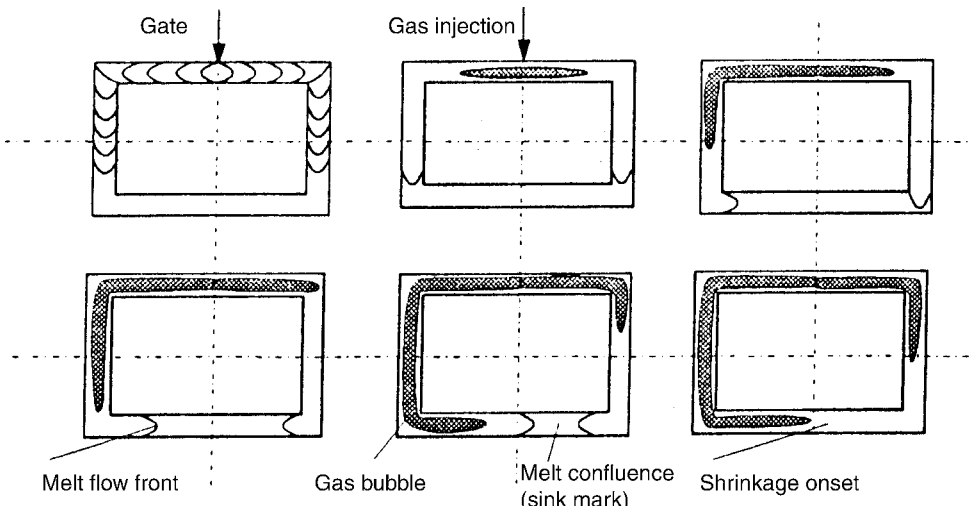


Figure 7.83 Filling study for melt and gas in a closed-ring gas channel (schematic). The slightest inhomogeneity determines the path taken by the gas. When the melt fronts meet, the gas does not break through. At this point, the part is solid and it will be susceptible to sink marks and warpage [7.61].

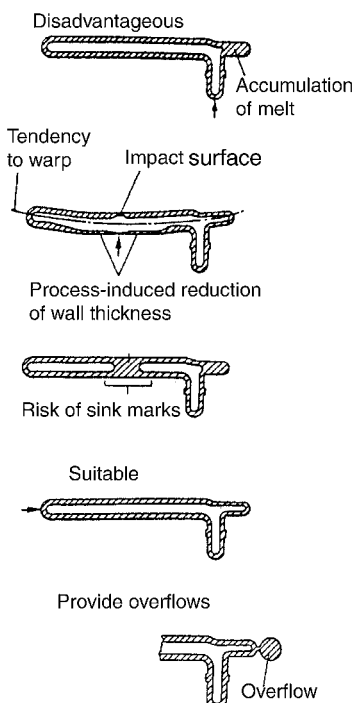


Figure 7.84 Effect of gate position on the propagation of gas bubbles [7.62]

Therefore, sharp inner edges where the gas can break through create problems (see also Section 7.2.3.2). Plate-like or lamellar components of uniform wall thickness cannot be produced by the GIT processes. The gas tends to diffuse nonuniformly, resulting in finger-like shapes in the center of the cross-section. Plate-like parts containing gas channels or gas ribs can be molded with the GIT process. The sandwich process is more suitable for such parts [7.63].

The gas must be guided in well-defined “channels”!

In these thicker channels, the melt temperature at the center of their cross section is relatively high.

Well-defined means that rib intersections or other bifurcations of the gas pathway (see Figure 7.79) cannot be produced (see also Section 10.4).

The position of the gate must be chosen in keeping with the constraints of the GIT method. Figure 7.84 shows some examples.

Peripheral reinforcing elements and all-round beads can be executed far more effectively and in much more visually attractive manner by the GIT process than by conventional injection molding. In addition, undercuts can often be avoided (see Figure 7.85).

For other design rules see the rib design section in Chapter 10.

Example Applications

Figures 7.86 to 7.88 show some components produced by the GIT process.

Water Injection Technology (WIT)

In terms of its operational sequence, water injection technology is very much comparable with gas injection technology. In this variant, water assumes the role of the nitrogen. Because of its better cooling action, water produces shorter cycle times and smoother inner surfaces. Use of the process is not yet widespread but it has great prospects as an injection molding technology [7.68].

7.4.5 External Gas Pressure Technology

External gas pressure technology is currently not in widespread use. In this process, the melt is pressurized to a gas pressure of up to 300 bar after injection. The pressure is applied externally to one side of the part through nozzles fitted flush with the mold surface. The gas then presses the slightly solidified wall inwards and displaces all of the remaining melt uniformly in all directions so that no sink marks appear on the other side of the mold. Of course, the inner side in question must not be a cosmetic surface.

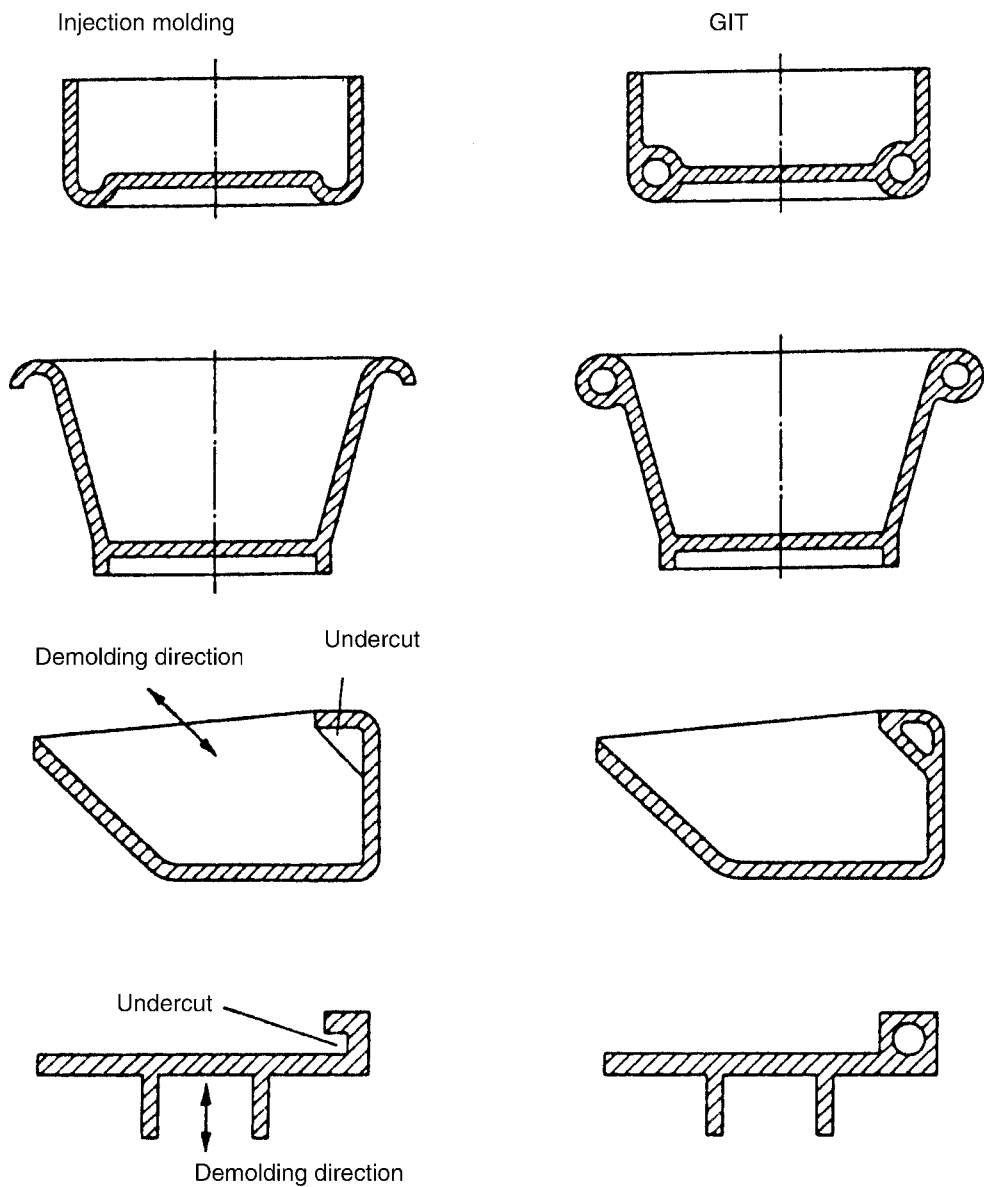


Figure 7.85 Peripheral reinforcements by conventional methods and by the GIT process [7.62]

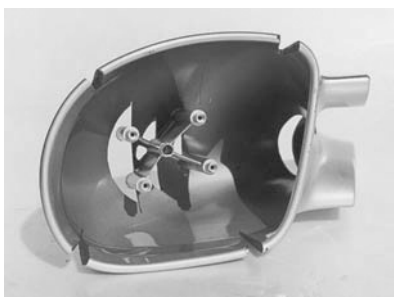


Figure 7.86 Accelerator pedal made from PA 6-GF 30 having high torsional and flexural rigidity throughout its oval tubular cross section. The pedal is distinctly lighter than a ribbed injection-molded version (Manufacturer: BMW, Munich).



Figure 7.87 Exterior rearview mirror for the BMW W3. The gas channels around the edge give the part great stability and a solid appearance.



Figure 7.88 Door handles are ideal for production by the GIT process. The large, hollow cross section exhibits great strength and rigidity and affords a good grip (Manufacturer: BMW, Munich).

References

- [7.1] MENGES, G.: Einführung in die Kunststoffverarbeitung (Introduction to plastics processing), 2nd ed., Hanser Verlag, Munich 1979
- [7.2] SCHWARZ, O. et al.: Kunststoffverarbeitung (Plastics processing), 4th ed., Vogel Verlag, Würzburg 1988
- [7.3] MINK, W.: Grundzüge der Spritzgießtechnik (Fundamentals of injection molding technology), 5th ed., Zechner & Hüthig Verlag, Speyer 1979
- [7.4] HENSEN, F., W. KNAPPE and H. POTENTE: Handbuch der Kunststoff-Extrusionstechnik (Handbook of plastics extrusion technology), Vol. 1 and Vol. 2, Hanser Verlag, Munich 1989/1986
- [7.5] MICHAELI, W. and M. WEGENER: Einführung in die Technologie der Faserverbundwerkstoffe (Introduction to the technology of fiber composite materials), Hanser Verlag, Munich 1989
- [7.6] GASTROW, H.: Spritzgießwerkzeugbau in 100 Beispielen (Injection mold making in 100 examples), 4th ed., Hanser Verlag, Munich 1990
- [7.7] MENGES, G. and P. MOHREN: Anleitung für den Bau von Spritzgießwerkzeugen (How to build injection molds), 3rd ed., Hanser Verlag, Munich 1990
- [7.8] MICHAELI, W.: Extrusionswerkzeuge für Kunststoffe und Kautschuk (Extrusion dies for plastics and rubber), 2nd ed., Hanser Verlag, Munich 1991
- [7.9] Verein Dt. Ingenieure (Association of German Engineers) (eds.) Das Blaswerkzeug (The blow mold), VDI-Verlag, Düsseldorf 1984
- [7.10] JOHANNABER, F. and K. STOECKHERT: Kunststoff-Maschinenführer (Plastics machine guide), 2nd ed., Hanser Verlag, Munich 1984
- [7.11] SAECHTLIN, H. J.: Kunststoff-Taschenbuch (Plastics pocketbook), 24th ed., Hanser Verlag, Munich 1989
- [7.12] MENGES, G., U. LICHUS and H. BANGE: Eine einfache Methode zur Vorausbestimmung des Fließfrontverlaufs beim Spritzgießen von Thermoplasten (A simple method for predetermining the flow front path in the injection molding of thermoplastics), *Plastverarbeiter* **31** (1980) 11, pp. 671/676
- [7.13] HEGLER, R. P.: Faserorientierung beim Verarbeiten kurzfaser verstärkter Thermoplaste (Fiber orientation in the processing of chopped-fiber reinforced thermoplastics), *Kunststoffe* **74** (1984) 5, pp. 271/277
- [7.14] BRIGHT, P. F. and M. W. DARLINGTON: Factors influencing fibre orientation and mechanical properties in fibre reinforced thermoplastic injection mouldings, *Plastics and Rubber Processing and Applications* **1** (1981) 2, pp. 139/147
- [7.15] BAYER, R. K. and G. W. EHRENSTEIN: Einfluß der Verarbeitung auf die mechanischen Eigenschaften von spritzgegossenem GF-PA (Effects of processing on the mechanical properties of injection-molded PA-GF), *Plastverarbeiter* **32** (1981) 10, pp. 1387/1392
- [7.16] EBENAU, A.: Unpublished work 1992
- [7.17] HEGLER, R. P. et al.: Einfluß stofflicher Parameter auf die Faserorientierung beim Verarbeiten kurzfaser verstärkter Thermoplaste (Effects of material parameters on fiber orientation in the processing of chopped-fiber reinforced thermoplastics), *Kunststoffe* **76** (1986) 9, pp. 766/771
- [7.18] PFEFFERKORN, W.: Zur Vorausberechnung des Elastizitätsmoduls kurzfaser verstärkter elastischer Stoffe (Precalculation of the modulus of elasticity of chopped-fiber reinforced elastic materials) I: *Plaste und Kautschuk* **21** (1974) 5, pp. 368; II: *Plaste und Kautschuk* **23** (1976) 2, pp. 115/119
- [7.19] MENGES, G. and P. GEISBÜSCH: Die Glasfaserorientierung und ihr Einfluß auf die mechanischen Eigenschaften thermoplastischer Spritzgießteile – Eine Abschätzmethode (Glass-fiber orientation and its effects on the mechanical properties of thermoplastic injection-molded parts – An estimating method), *Colloid and Polymer Science* **260** (1982), pp. 73/81

- [7.20] MENGES, G. and U. WÖLFEL: Die Faserorientierung kurzfaserverstärkter Spritzgießteile (Fiber orientation in chopped-fiber reinforced injection-molded parts), *Kunststoffe Plastics* (1986) 5, pp. 31/34
- [7.21] DELPY, U.: 7. Stuttgarter Kunststoff-Kolloquium (7th Stuttgart Plastics Colloquium) TU Stuttgart 1981
- [7.22] FRIEL, P.: Die Schwindung thermoplastischer Kunststoffe (Shrinkage of thermoplastic materials), BASF brochure 1990
- [7.23] BOES, D.: Vorgänge im Formteil und deren Simulation durch Rechenprogramme (Processes in moldings and their simulation by computer programs) BASF brochure 1989
- [7.24] ANON.: Ultrason, BASF brochure 1990
- [7.25] WENDT, U.: Untersuchungen der Fließnaht in Spritzgußteilen (Investigations of flow lines in injection-molded parts), *Kunststoffe* **78** (1988) 2, pp. 123/125
- [7.26] BURSIAN, W.: Die Festigkeitseigenschaften von Fließnähten bei gespritzten thermoplastischen Kunststoffartikeln (Strength properties of flow lines in injection-molded thermoplastic articles), *Plastverarbeiter* **16** (1965) 2, pp. 68/71
- [7.27] KEHR, G.: Die Beeinflussung der Bauteileigenschaften durch Bindenähte (Determining component properties by weld lines), BASF brochure 1989
- [7.28] KEHR, G.: Personal communication
- [7.29] HAMADA, H. et al.: Improvement of Weldline Strength in Injection Molded FRTP Articles, *Intern. Polymer Processing* **II** (1988) 3/4, pp. 131/136
- [7.30] ANON.: Richtlinien für das Gestalten von Formteilen aus technischen Kunststoffen (Guidelines for designing moldings made from engineering plastics), Hoechst brochure C.3.4 1991
- [7.31] Patent specification DE 27 14 020 CE
- [7.32] MENGES, G. and Th. SCHACHT: Einfluß der Verarbeitungsparameter auf die mechanischen Eigenschaften von Bindenähten (Effects of processing parameters on the mechanical properties of weld lines), *Kunststoffberater* (1988) 4, pp. 54/57
- [7.33] BEALL, G.: Spritzgußteile neu gestalten (Redesign injection-molded parts), *Kunststoffe* **80** (1990) 8, pp. 911/914
- [7.34] VDI-Richtlinie (VDI Guideline) 2006: Gestalten von Spritzgußteilen aus thermoplastischen Kunststoffen (Design of injection-molded parts made from thermoplastics), VDI-Verlag, Düsseldorf 1979
- [7.35] STITZ, S.: Analyse der Formteilbildung beim Spritzgießen von Plastomeren als Grundlage für die Prozeßsteuerung (Analysis of the formation of moldings in the injection molding of plastomers as a basis for process control), Dissertation RWTH Aachen 1973
- [7.36] HOVEN-NIEVELSTEIN, W. B.: Die Verarbeitungsschwindung thermoplastischer Formmassen (Molding shrinkage of thermoplastic molding compounds) Dissertation RWTH Aachen 1984
- [7.37] ERHARD, G.: Zur Wahl von Toleranzen und Passungen an Kunststoff-Spritzgußteilen (Choice of tolerances and fits in injection-molded plastic parts), *Konstruktion* **18** (1966) 8, pp. 346/350
- [7.38] SCHÜRMANN, E.: Abschätzmethoden für die Auslegung von Spritzgießwerkzeugen (Estimating methods for designing injection molds), Dissertation RWTH Aachen 1979
- [7.39] WIMMER, D.: Kunststoffgerecht Konstruieren (Designing for plastics) Hoppenstedt-Verlag, Darmstadt 1989
- [7.40] FRIEL, P.: Personal communication
- [7.41] ANON.: D-M-E Normalien (D-M-E Standards), D-M-E brochure, Neuenstadt, Kocher 1991
- [7.42] HAGERMANN, E. M.: Weld-line Fracture in Molded Parts, *Plastics Engineering* **29** (1973) 10, pp. 67/69

- [7.43] Patent specification GB 1250476 1968
- [7.44] ROWBOTHAM E. M. and G. D. SUTHURST: Achieving the Impossible – Plastic Intake Manifold, Reinforced Plastic Congress, London 1980
- [7.45] KAMPRATH, A., R. BINDER and T. LANGEHEINEKEN: Kunststoffsaugrohre – erste Erfahrungen und Versuchsergebnisse (Plastic intake manifold – initial experience and test results), *ATZ* **87** (1985) 10, pp. 519/528
- [7.46] HALDENWANGER, H.-G., P. MINEIF, K. ARNEGGER and S. SCHULER: Kunststoff-Motorbauteile in Ausschmelzkerntechnik am Beispiel eines Saugrohrs (Plastic engine components by fusible core technology with reference to the example of an intake manifold), *ATZ* **89** (1987) 3, pp. 139/144
- [7.47] HAUCK, CH. and A. SCHNEIDERS: Optimieren der Schmelzkerntechnik für das Thermoplast-Spritzgießen (Optimizing fusible core technology for thermoplastic injection molding), *Kunststoffe* **77** (1987) 12, pp. 1237/1240
- [7.48] ALTMANN, O. and O. PARR: Scmelzkerntechnik im Motorenbau (Fusible core technology in engine construction), *Kunststoffe* **81** (1991) 3, pp. 179/191
- [7.49] HAACK, W. and J. SCHMITZ: Rechnergestütztes Konstruieren von Spritzgießteilen (Computer-aided design of injection-molded parts), Vogel-Verlag, Würzburg 1988
- [7.50] SCHWEIGER, H.: Schwindung und Verzug (Shrinkage and warpage) in: VDI-K-Jahrbuch (VDI-K Yearbook) 1984
- [7.51] ANON.: Ultraform, BASF brochure 1992
- [7.52] HOMES, W.: Kaskadenspritzgießen vermeidet Bindenähte (Cascade injection molding prevents weld lines), *Kunststoffe* **86** (1996) 9, pp. 1268/1272
- [7.53] EHRENSTEIN, G. W. and G. ERHARD: Konstruieren mit Polymerwerkstoffen (Designing with polymeric materials), Hanser Verlag, Munich Vienna 1983
- [7.54] ANON.: Technische Kunststoffteile Wettbewerb '79 (Industrial plastic parts – Competition '79), Fachverband technische Teile im GKV (Industrial parts specialist group in the Plastics Processing Association), Frankfurt
- [7.55] STARKE, L.: Toleranzen, Passungen und Oberflächengüte in der Kunststofftechnik (Tolerances, fits and surface quality in plastics technology), Carl Hanser Verlag, Munich Vienna 1996
- [7.56] METTLER, R. and P. STEIGER: Zweikomponenten-Spritzguß, Literaturauswertung (Two-component injection molding – A review of the literature), Term project FH Aargau 1996
- [7.57] GATTRINGER, R.: Bahn frei für Designvielfalt bei der Bauteilgestaltung (Way clear for design diversity in parts design), *Kunststoffe-Synthetics* (1998) 2, pp. 16/18
- [7.58] DIJKSTRA, K. et al.: Softtouch-Oberflächen (Softtouch surfaces), *Kunststoffe* **88** (1998) 3, pp. 348/350
- [7.59] KILLERMANN, R.: Sonderverfahren der Gasinnendrucktechnik. Seminar Gasinnendruckverfahren beim Spritzgießen (Special procedures in gas injection technology. Seminar on the gas injection process in injection molding), SKZ Würzburg, 1994
- [7.60] ECKARDT, H.: Anwendungsbereiche, Möglichkeiten und Grenzen beim Gasinnendruck-Verfahren. Seminar Gasinnendruckverfahren beim Spritzgießen (Fields of application, opportunities and limits in the gas injection process. Seminar on the gas injection process in injection molding), SKZ Würzburg, 1994
- [7.61] SCHRÖDER, T.: Optimale Formteilqualität bei der Anwendung der Gasinjektionstechnik (GIT). Seminar Gasinnendruckverfahren beim Spritzgießen (Optimum molding quality in the application of gas injection technology (GIT). Seminar on the gas injection process in injection molding), SKZ Würzburg, 1994

- [7.62] THEISSIG, W.: Anwendung des Gasinnendruckverfahrens für Komponenten im Automobilbau. Seminar Gasinnendruckverfahren beim Spritzgießen (Application of the gas injection process for components in automotive engineering. Seminar on the gas injection process in injection molding), SKZ Würzburg, 1994
- [7.63] JAROSCHEK, CH.: Sandwich- und Gasinnendruck-Verfahren im Vergleich (The sandwich and gas injection processes compared), *Kunststoffe* **87** (1997) 9, pp. 1172/1176
- [7.64] ANON.: Die richtige Partitur macht's (The right score does it), *Kunststoff-Journal* March 1995
- [7.65] ANON.: Laserbeschriften von Thermoplasten (Laser marking of thermoplastics), BASF brochure 01.1998
- [7.66] KUDLIK, N.: Dünnewandtechnik (Thin-wall technology), *Kunststoffe* **89** (1999) 9, pp. 92/96
- [7.67] EMMERICH, H. and D. GIESLER: Federnde Auswerfer – Flexibilität macht sich bezahlt (Elastic ejectors pay for themselves), *Kunststoffe* **89** (1999) 5, pp. 61/65
- [7.68] JOHANNABER, F. et al.: Trends beim Spritzgießen (Trends in injection molding), *Kunststoffe* **90** (2000) 10, pp. 48/59
- [7.69] ANON.: Faltkerne verkürzen Zykluszeiten (Collapsible cores shorten cycle times), *Kunststoffe* **92** (2002) 7, pp. 51
- [7.70] EBERT, K-H.: Der virtuelle Prototyp – Auslegung von Zahnrädern, aus Maschinenelementen aus Kunststoffen – Zahnräder und Gleitlager (The virtual prototype – Design of gear wheels in: Machine elements made from plastic – Gear wheels and sliding bearings), Springer VDI Verlag, Düsseldorf 2001, pp. 36/49

8 Flexing Elements

Structural elements that are required to have high deformability should be designed so that they are capable of withstanding the flexural or torsional loads associated with the application (see also Section 6.1). Two examples of such designs common in parts made from polymeric materials are snap-fit or interlocking joint elements and elastic elements. Another common feature in parts designed for high deformability is their relatively thin wall thickness. For example, integral hinges are structural elements having extremely low wall thicknesses.

8.1 Snap-Fit Joints

Definition

Joint types are defined according to the mechanisms acting at the points of attachment holding the assembled parts together (see Figure 8.1) [8.1]. On this basis, a snap-fit joint is a frictional, form-fitting joint.

The structural features of a snap-fit joint are hooks, knobs, protrusions, or bulges on one of the parts to be joined, which after assembly engage in corresponding depressions (undercuts), detents, or openings in the other part to be joined.

Accordingly, the design of a snap-fit joint is highly dependent on the polymeric material(s). Snap-fit joints are also relatively easy to assemble and disassemble. A key feature of snap-fit joints is that the snap-fit elements are integral constituents of the parts to be joined.

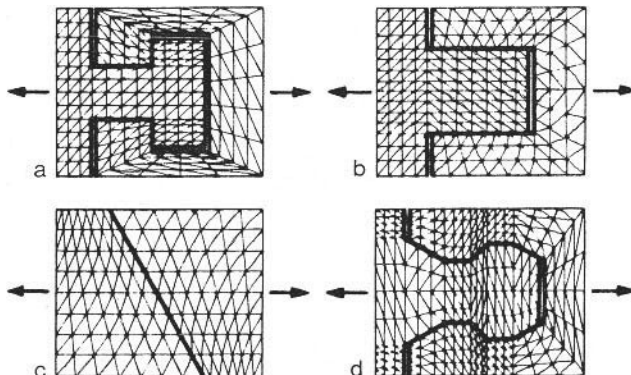


Figure 8.1 Types of joints (schematic) [8.1]

- a) Form-fitting joint
 - b) Frictional joint
 - c) Adhesive joint
 - d) Frictional form-fitting joint
- ↔ Direction of action of forces

Differentiated and Integrated Construction

Design solutions using “differentiated” construction assign certain functions separately to the individual structural elements with the goal of fulfilling all of the functional requirements in an optimum manner. This inevitably means that there are a number of parts in a subassembly. “Integrated” construction, on the other hand, uses fewer parts and consequently results in lower assembly costs but may require the acceptance of restrictions or compromises in functionality. Figure 8.2 shows this trade-off with reference to the example of a bayonet coupling.

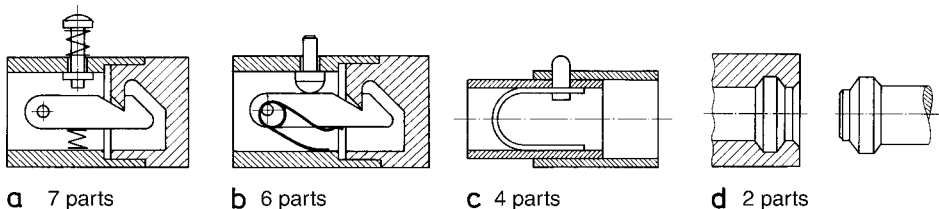


Figure 8.2 Design variants for a coupling as described in [8.12] and [8.16]

The systematic reduction in the numbers of parts finally leads to variant d), a snap-fit joint made from polymeric material. Injection molding technology is so versatile, that it allows for the integration of functions directly into the parts to be joined.

Classification

Snap-fit joints are classified according to the most varied attributes [8.2, 8.3, 8.4, 8.13]. However, a classification based on geometrical considerations appears to be most appropriate here (see Figure 8.3).

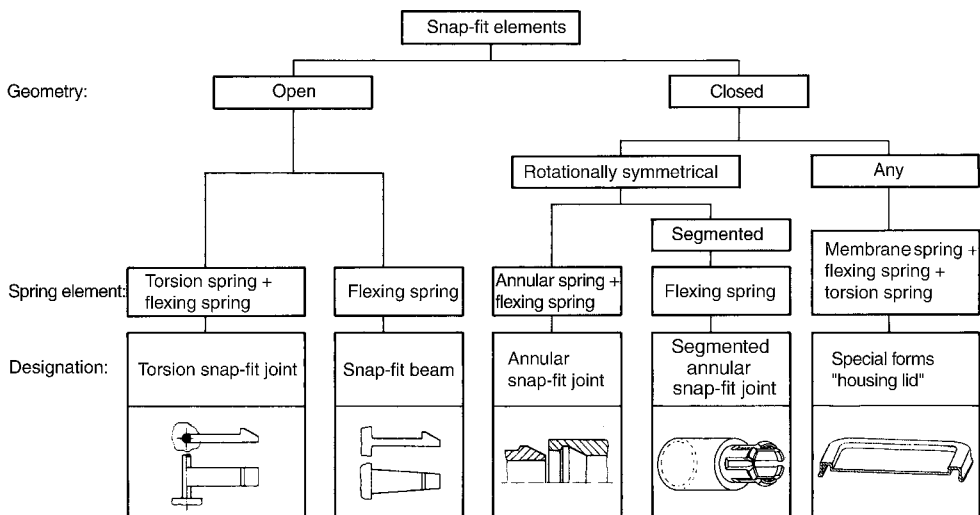


Figure 8.3 Classification scheme for snap-fit elements based on geometrical considerations

Dimensions and Forces

The dimensions and forces associated with assembly/disassembly are discussed in the following figures.

Figure 8.4 Dimensions and their designations for snap-fit hooks

- α_1 = Joining angle
- α_2 = Retaining angle
- b = Breadth of cross section (hook breadth)
- h = Height of cross section
- l = Snap-fit length
- H = Snap-fit height (undercut)

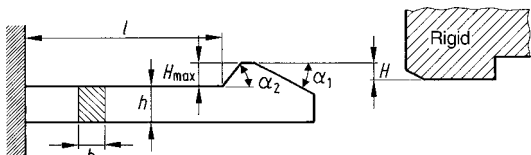


Figure 8.5 Dimensions and their designations in cylindrical annular snap-fit joints

- | | | |
|--------------------------------|---|-----------------------|
| d_{\max} = Greatest diameter | } | of the snap-fit joint |
| d_{\min} = Smallest diameter | | |
| d_o = Outer diameter | } | of the outer part |
| s_o = Wall thickness | | |
| d_i = Inner diameter | } | of the inner part |
| s_i = Wall thickness | | |

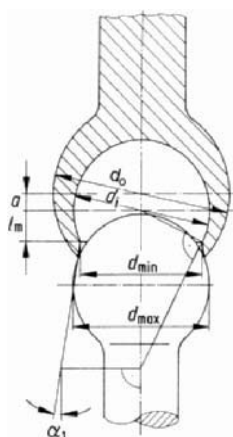
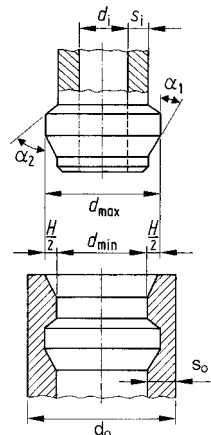


Figure 8.6 Dimensions and their designations in spherical annular snap-fit joints

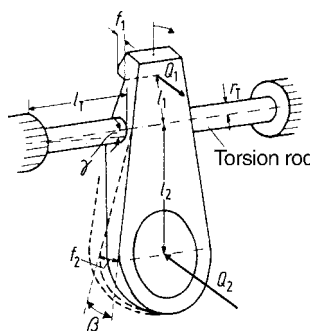
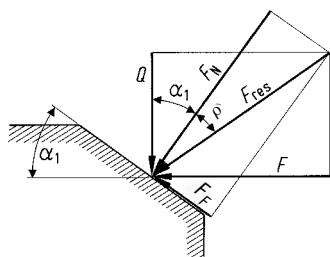


Figure 8.7 Dimensions and their designations in torsional snap-fit joints

- | | | |
|--------------------------------|---|----------------|
| l_T = Length | } | of torsion rod |
| r_T = Radius | | |
| β = Torsion angle | } | of torsion rod |
| γ = Twisting angle | | |
| $l_{1,2}$ = Lever arm lengths | } | of torsion rod |
| $f_{1,2}$ = Elastic excursions | | |
| $Q_{1,2}$ = Deflection forces | } | of torsion rod |
| | | |

**Figure 8.8** Angles and forces at the active surface

- Q = Deflection force
 F = Assembly force
 F_N = Normal force
 F_F = Friction force
 F_{res} = Resultant force
 α_1 = Joining angle (lead-in angle)
 ρ = Friction angle

The forces and angles at the assembly contact surfaces of the joints (see Figure 8.8) apply in an analogous manner for all snap-fit joint design variations.

Assembly Operation

A review of the snap-fit assembly operation is helpful to gain a better understanding of the factors at work and of the calculations discussed below. The assembly force F , generally acting in the axial direction, is resolved at the mating surface in accordance with the mathematical relationships associated with a wedge (see Figure 8.8). The transverse force Q causes the deflection needed for assembling the joint. At the same time, friction and the joining angle determine the conversion factor η .

$$\eta = \tan(\alpha_1 + \rho) = \frac{f + \tan \alpha_1}{1 - f \cdot \tan \alpha_1} \quad (8.1)$$

The relationship in Eq. 8.1 is plotted in Figure 8.9 against $\alpha_{1,2}$ for common values of η .

The retaining or release force of the joint can be altered using the retaining angle α_2 . The use of a value of $\alpha_2 \geq 90^\circ$ creates a self-locking geometric form-fitting joint. Figure 8.10 illustrates that a joint constructed in this way can be released again without forced failure of the joint when the moment of the force couple represented by the retaining and reaction forces is able to overcome the friction force in the active surface.

A design countermeasure to prevent release in this way is to attach a retaining guard or locking ring (see also Sections 8.1.1.3 and 8.1.3.3).

As snap-fit features are being assembled, the assembly force follows the characteristic pattern shown in Figure 8.11. This is also described in [8.11] and [8.23]. After a steep rise, the assembly force reaches a peak, falls to a lower level where it remains fairly constant as the lead angle causes the part to deform, and then falls back to zero, once the joint area of the part snaps into place.

Deformation during the assembly of snap-fit joints can be significant. As a result of these deformations during the assembly operation, the geometric relationships change (e.g., the relative angular positions) [8.21, 8.10]. This, however, is not taken into account in the calculation of the assembly forces in the sections below. The local variation of the plane of action and its effect on transverse force during the assembly operation is likewise not taken into account (see Section 5.4).

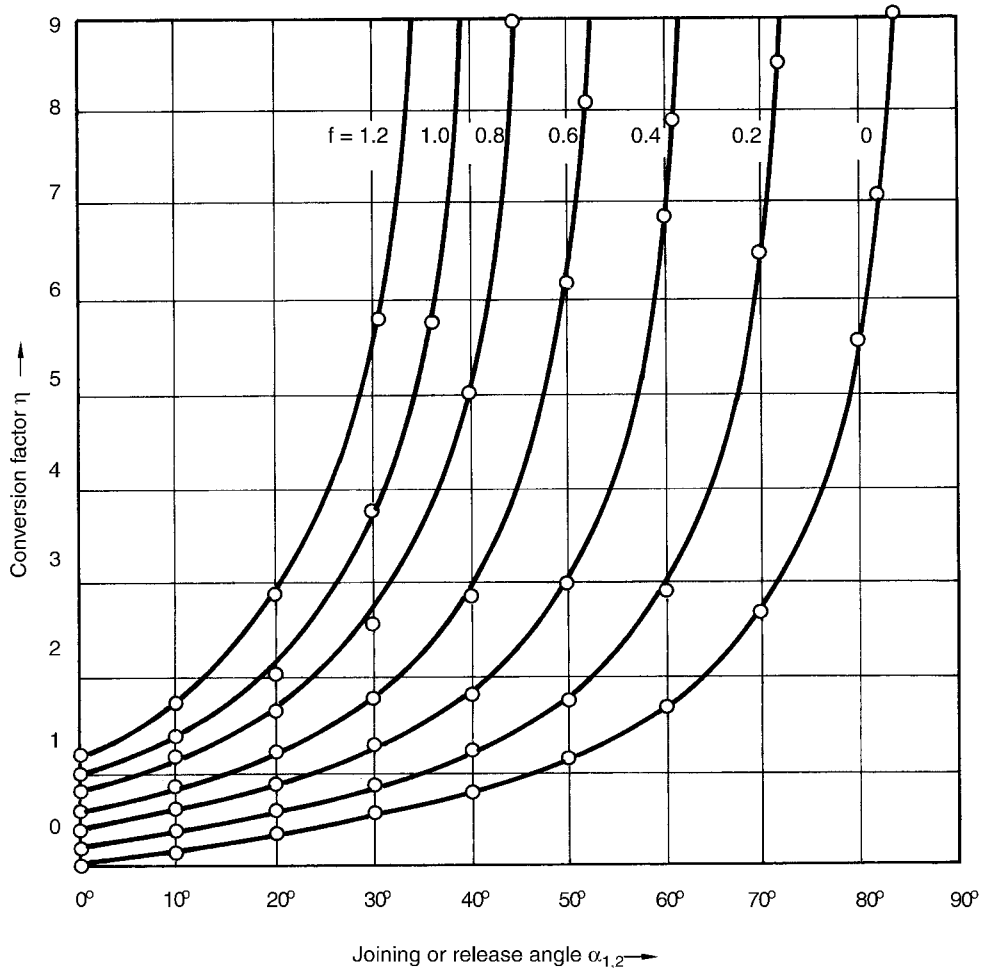


Figure 8.9 Conversion factor η for various coefficients of friction f as a function of the joining (lead-in) angle or the retaining (snap-out) angle [8.11]

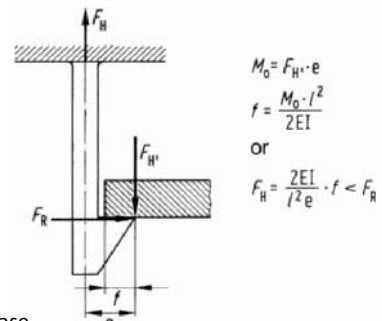


Figure 8.10 Forces and moments acting on a snap-fit hook having a retaining angle of 90° at the time of release

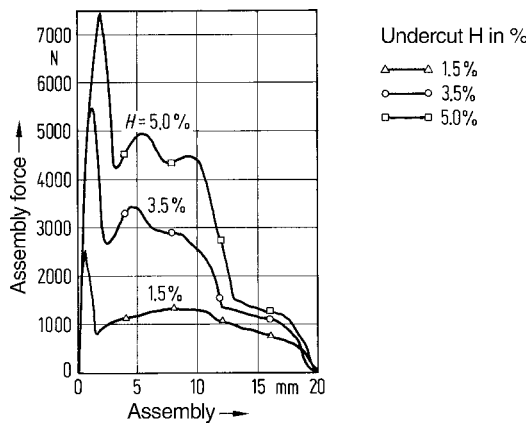


Figure 8.11 Assembly force over the assembly path for cylindrical snap-fit joints having different size undercuts. Outside part is made of POM (H 2200) with $d_{\min} = 40 \text{ mm}$; inside part is made of steel [8.18].

Loss of Retaining Force

In the case of snap-fit elements that are repeatedly joined and separated, or those that remain under a residual stress, the time-dependence of the material properties should be taken into account. In line with viscoelastic behavior, the strain (deformation) imposed during the assembly operation diminishes only gradually. Test results on separated [8.21] and on assembled snap-fit joints made from POM and PP [8.11] have shown that recovery after release of stress can take as long as 4 to 5 hours. The residual strain found in these cases was in the range of 1 to 3% for disassembly strain values of 8 to 10%.

These residual strain values are reached asymptotically after 5 to 10 assembly or release cycles. Lower assembly related strains lead to lower residual strains. In addition, after a large number of assembly cycles, no further loss of retaining force is observed.

If the snap-fit joint element is deformed enough during assembly resulting in a residual stress, this stress relaxes over time after assembly in line with the relaxation behavior of the material. The residual stress or residual elastic force remaining can be estimated theoretically by linearizing the isochronous stress-strain diagram (see the example calculation in Section 5.3.2).

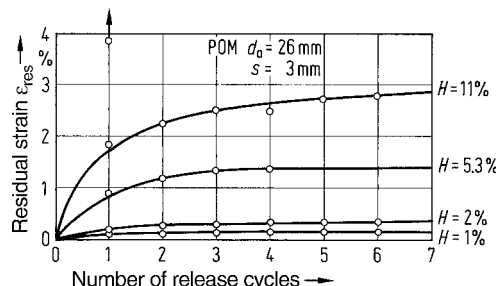


Figure 8.12 Relationship between residual strain and number of release cycles for an annular snap-fit joint made of POM having a rigid inner part for different undercut sizes [8.11]

8.1.1 Snap-Fit Beams

8.1.1.1 Types of Snap-Fit Beams

The most common structural element in snap-fit joints is a beam, subject to a bending load, in the form of a cantilever snap-fit beam with a hook. Its useful snap-fit height (momentary interference) can be altered by changing the cross-sectional shape of the beam and, of course, by its effective snap-fit length.

Good utilization of material is reflected in high values for the geometry factor C (see Figure 8.13).

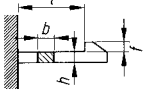
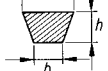
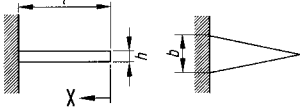
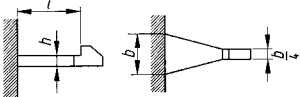
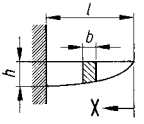
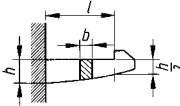
	Rectangular cross section	Trapezoidal cross section
	 $b = \text{const.}$ $h = \text{const.}$ $C = 0.67$	 $a = \text{const.}$ $b = \text{const.}$ $h = \text{const.}$ $C = \frac{a+b}{2b+a}$
	$h = \text{const.}$ $b_x = b \frac{x}{l}$ $C = 1$	
	$h = \text{const.}$ $b \rightarrow b/4$ $C = 0.86$	$h = \text{const.}$ $a \rightarrow a/4$ $b \rightarrow b/4$ $C = 1.28 \frac{a+b}{2b+a}$
	$b = \text{const.}$ $h_x = h \sqrt{\frac{x}{l}}$ $C = 1.33$	
	$b = \text{const.}$ $h \rightarrow h/2$ $C = 1.08$	$a = \text{const.}$ $b = \text{const.}$ $h \rightarrow h/2$ $C = 1.64 \frac{a+b}{2b+a}$

Figure 8.13 Material utilization as reflected by the geometry factor C in snap-fit hooks having different cross-sectional shapes according to [8.5]. The values of C for the trapezoidal cross section apply to the case in which the tensile stress acts in the wide face of the trapezium.

Uniform loading of the material and hence optimum utilization of the material for a cantilever snap beam is achieved by a linear decrease in width or a parabolic decrease in thickness along the length of the beam.

Figures 8.14 to 8.17 indicate some aspects of *importance for production* in the design of snap-fit hooks. For example, two opposing hooks are more easily produced if they have a cross section in the form of a cylinder segment rather than a rectangular cross section. The simpler production due to the cylindrical shape of the geometric envelope affords substantially lower mold production costs. The production costs for drilling, reaming, and polishing the circular cross section may have a cost ratio of 1 : 4 compared to those for producing a rectangular cross section by spark erosion and milling [8.7].

By skillful partitioning of the snap features within the mold and the use of shut-offs or piercing cores (see Figure 8.15), snap-fit hooks can be produced without complicated mold actions. When shut-offs are used to produce snap-fit beams and hooks, the designer must allow for the shut-off angle (0.5 to 1°).

In clamshell housing parts, such as those illustrated in Figure 8.16, the undercuts of built-in hooks are most easily molded if the hook faces outward (top) rather than inward (bottom).

The maximum stress that occurs when a beam bends is usually at the transition from the snap-fit beam to the molding. *Radii of curvature have to be provided here*, even if this increases mold-making costs. Even a radius of 0.5 mm reduces the peak stress at the transition considerably (see Figures 8.17 and 10.4). Generous radius values are also recommended for segmented annular snap-fit joints (Figure 8.17).

Adequate snap-fit hook height can be achieved by *extending the length of the elastic section of a hook* (see Figures 8.18 and 8.19).

Interlocking joints with a series of joining positions arranged one behind the other allow for assembly at various positions. Figures 8.19 to 8.21 show examples of this concept applied to molded parts.

The concept of *an elastic snap-fit beam with a hook and a rigid undercut* may also be “reversed” to form the variant of *a rigid hook and an elastic beam with an undercut*. An example of this is shown in Figure 8.22. Figure 8.23 shows an example of an automobile headlight housing incorporating this concept (see also Figures 8.27 and 7.60).

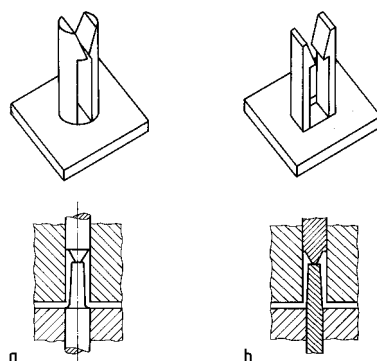


Figure 8.14 Snap-fit hook with circular (a) and rectangular (b) envelope shape and associated details of the injection molds [8.7]

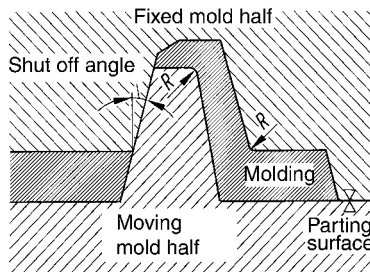


Figure 8.15 Principle of demolding a snap-fit beam and hook without special mold action [8.20]

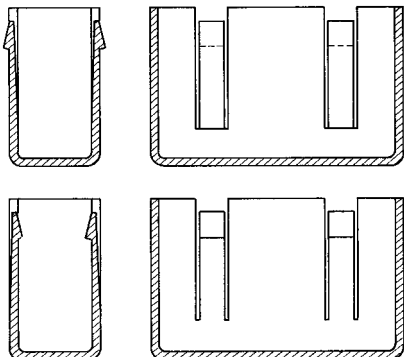


Figure 8.16 Beam hooks (undercuts) on the core side (bottom) cause higher mold costs than those facing outward (top) [8.13]

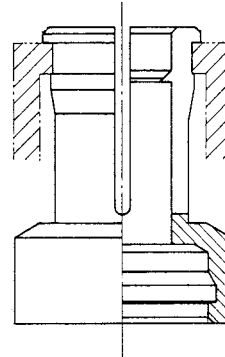


Figure 8.17 Rounding-off the segment gap for slotted annular snap-fit joints to reduce peak stress values

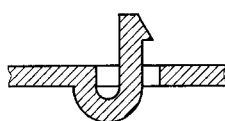


Figure 8.18 Principle of extending the length of the elastic (bending) section of a snap-fit hook [8.9]

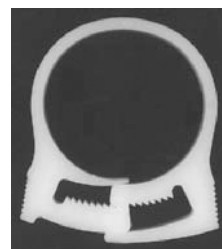


Figure 8.19 Interlocking joint with saw tooth profile and retaining guard on a clamping ring

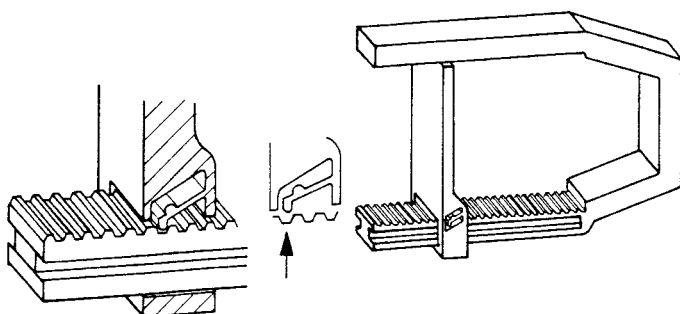


Figure 8.20 Interlocking joint capable of adjustment [8.2]

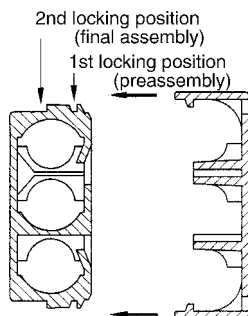


Figure 8.21 Plug housing capable of being fixed sideways in two locking positions

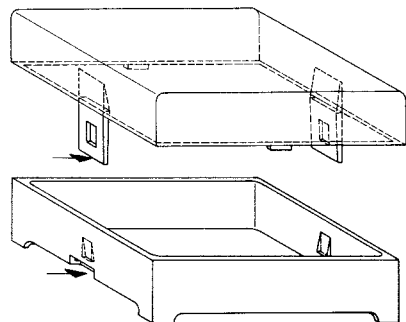


Figure 8.22 Housing cover joint assembled using cantilever beams with undercuts rather than hooks [8.5]

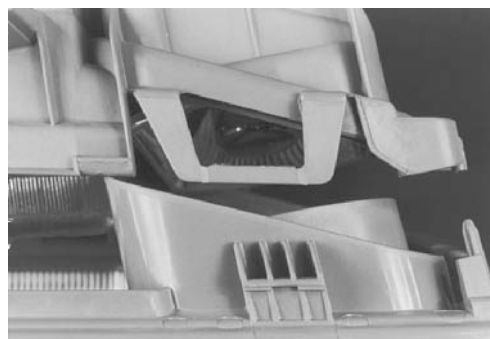


Figure 8.23 Joint composed of a rigid hook and an elastic bracket

8.1.1.2 Snap-Fit Beam Calculations

Permissible Size of Undercut

A snap-fit hook (snap-fit bracket) may be simplified as a bending beam fixed at one end (*i.e.*, a cantilever beam). Calculations can be performed on the basis of classical bending theory*. In the assembly calculations, the beam is theoretically deflected by at least the depth of the undercut. In this rough calculation, the effect of shear stress due to the transverse force is usually neglected because $l \gg h$. Any deflection of the mating surface is usually estimated or neglected in the classical calculations, although it may be considered in Finite Element Simulations.

The permissible size of the undercut (snap-fit height) for a cantilever snap-fit beam can be determined based on the permissible outer fiber strain ϵ_{perm} for the material from which the beam will be made.

$$H_{\text{perm}} = C \frac{l^2}{h} \cdot \epsilon_{\text{perm}} \quad (8.2)$$

where

C = Geometry factor (see Figure 8.13)

ϵ_{perm} = Permissible outer fiber strain as an absolute value (m/m)

Guide values for one-shot assembly:

Semi-crystalline thermoplastics $\approx 0.9 \epsilon_Y$

Amorphous thermoplastics $\approx 0.7 \epsilon_Y$

Reinforced thermoplastics $\approx 0.5 \epsilon_Y$

Guide values for frequent assembly:

Strain at $\sigma_{0.5\%}$ (see Figure 5.2c).

Snap beams having shapes and cross sections other than those shown in Figure 8.13 cannot usually be analyzed in this way. A method for analysis of beams with more complex cross sections is given in Section 5.4.

Assembly Force and Retaining Force

The *assembly force*, F , is calculated from the deflection force Q and the conversion factor η .

$$F = Q \cdot \eta \quad (8.3)$$

where η is obtained from Figure 8.9.

The *retaining force* is calculated by analogy with the retaining (or return) angle α_2 (for $\alpha_2 \geq 90^\circ$ see Figure 8.10). During assembly, plastic deformation may occur so that as a result of changed geometry, the actual retaining force may be smaller than the one calculated [8.11]. Even when the retaining and joining angles are the same, the separating force is a little smaller than the assembly force. This can be attributed to the fact that the bending moment between the planes of action of the actuating forces and the plane of action of the reaction force in the material tends to open the snap-fit connection during assembly.

* Using classical handbook equations or commercially available computer programs such as the SNAPS PC program from BASF or Fittcalc from Ticona.

The *deflection force* is given by

$$Q = W \frac{E_S \cdot \epsilon}{l} \quad (8.4)$$

where

W = section modulus for a rectangular cross section (I/c) where $c = h/z$.

$$W = \frac{b \cdot h^2}{6}$$

for a trapezoidal cross section (with tensile stress in the wider face)

$$W = \frac{h^2}{12} \cdot \frac{a^2 + 4ab + b^2}{2b + a}$$

for other cross sections see Hütte, Dubbel and other reference works.

E_S = secant modulus in MPa for the strain arising associated with the deflection

ϵ = strain arising as an absolute value (m/m)

8.1.1.3 Additional Functions

Overstrain Safeguards

Snap-fit hooks, especially thin fragile ones or those made using brittle materials, must be adequately protected against excessive stress or deflection (see Figures 8.24 and 8.25).

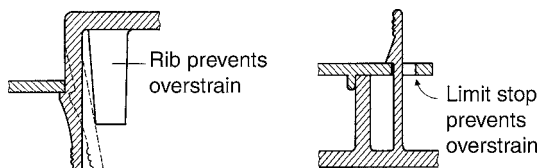


Figure 8.24 Overstrain safeguards for snap-fit hooks [8.19]



Figure 8.25 Snap-fit hooks can be safeguarded against excessive strain or fracture by means of a deflection limit or stop
(Photograph: Siemens AG, Munich)

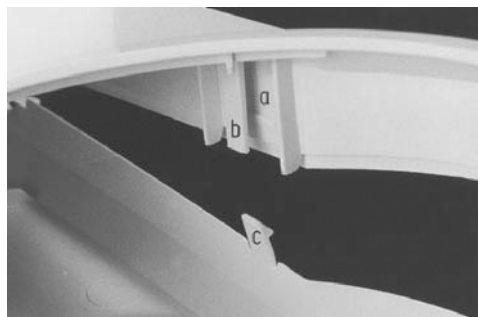


Figure 8.26 Tabs act as retaining guards, guide surfaces, and provide tolerance compensation
 a) Undercut
 b) Tab
 c) Snap-fit beam and hook

Retaining Guards

In order to prevent inadvertent or unwanted release of a snap-fit joint (see also Figure 8.10) with certainty, the snap-fit hook can be secured after assembly by another element in the structural unit. Figure 8.26 shows one of many possibilities by the example of the base of a coffee machine. The hot plate is inserted into the two parts of the housing where it presses the tab against the snap-fit hook and in this way secures it against release. Additionally, these tabs provide guidance for the assembly of the hot plate and compensate for any tolerance variations.

Opening Aids

An extension of the snap beam (beyond the hook) in the form of a recessed grip is a simple way to facilitate release of a snap-fit joint by hand (see Figure 8.24). Designs, such as the one shown in Figure 8.27, have also proved to be effective. In this case, however, the bending stress has to be absorbed by the very short fillet between the housing and the actual connecting element.

In the locking mechanism shown in Figure 8.28, a spring provides the force required to keep the fulcrum snap-fit in place.

In the case of snap-fit opening aids involving tools, appropriate means of access and gripping must be designed into the parts to be assembled (see, e.g., Figure 8.29).

Energy Storage Devices

Permanent pretensioning is not easily obtained with molded snap-fit connections made of polymeric material due primarily to the limitations of polymeric materials. Therefore, stresses in the joint should be released as much as possible after assembly. When, however, only relatively small amounts of energy are to be stored, e.g., for compensating tolerances or obtaining small prestress, this can be accomplished using pretensioned snap-fit elements made of polymeric materials. Glass-fiber reinforced materials are best for these applications, but unreinforced materials such as POM can also be used (see Figure 8.28). The residual pretensioning can be estimated from the creep modulus E_c (see example calculation in Section 5.3.2).

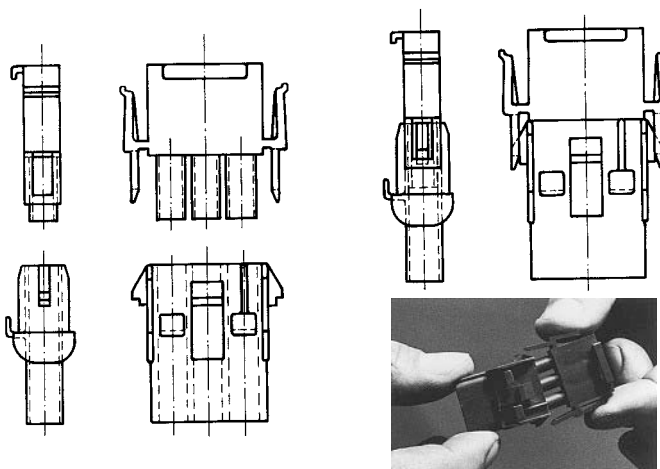


Figure 8.27 During assembly, mainly the snap-fit bracket is deformed, while during separation, only the short fillet is deformed

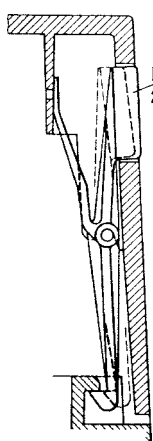


Figure 8.28
Locking mechanism
for a housing cover
(Photograph: Siemens AG,
Munich)

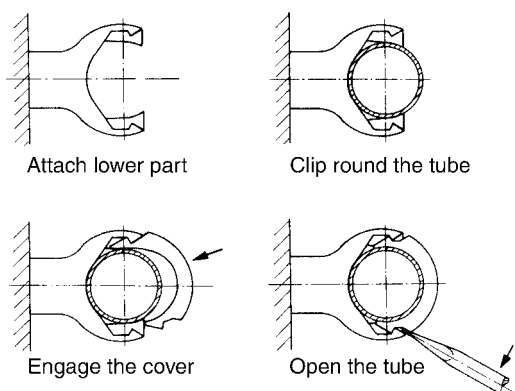


Figure 8.29 Opening a pipe clamp by means of a screwdriver

Seals

Reliable sealing of two components joined by snap-fit beams can be achieved only if a sufficient number of snap-fit beams is provided and if the pressure of the elastic seal is accomplished by tensile stress (not bending stress) in the beam (see Figure 8.30).

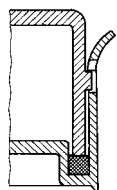


Figure 8.30 Principle for designing an elastic seal

8.1.2 Torsional Snap-Fit Joints

High levels of deformation can also be obtained when plastic parts are subjected to torsional loads (see Section 6.1). As a result, torsion springs are used as deforming elements for snap-fit joints.

8.1.2.1 Types of Torsional Snap-Fit Joints

A torsional snap-fit joint is usually designed in the form of a double rocker, as shown in Figure 8.27. The torsional axis may be rectangular as shown or more cylindrical (see Figure 8.31). This variant allows distinctly greater snap-fit deformations but may result in higher tool costs.

In the torsional joint shown in Figure 8.32, both torsion (about the x-axis) and bending stresses are combined. The cross section subjected to torsion is rectangular in shape to simplify production.

An interesting concept for a torsional snap-fit joint is shown in Figure 8.33. The double rocker is connected in the axis of rotation to a torsion rod, which is located in a surrounding membrane.

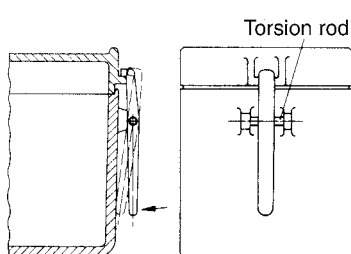


Figure 8.31 Principle of a torsional snap-fit joint on a case [8.5]

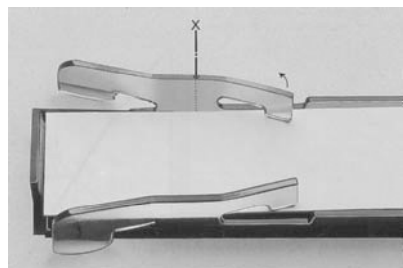


Figure 8.32 Combined torsional and flexural snap-fit joint in the form of a double rocker with an opening aid [8.5]



Figure 8.33 Sealing lid with a torsion-membrane snap-fit joint molded in place. Left: view from above; right: view from below.

8.1.2.2 Torsion Snap-Fit Joint Calculations

Permissible Size of the Undercut

Equations 8.5 to 8.8 are limited to the simple geometrically form of a torsional snap-fit joint with a circular cross section as shown in Figure 8.7.

Assuming that deformation results only from the twisting of the torsion rod, the snap-fit's deformation (height) is given by:

$$H = f_1 = l_1 \cdot \sin\beta \quad (8.5)$$

The following geometric relationship exists between the torsion angle β and the angle of twist γ :

$$\beta = \frac{180}{\pi} \cdot \frac{\gamma \cdot l_T}{r} \quad (8.6)$$

and for a particular material

$$\gamma = (1 + \mu) \cdot \varepsilon \quad (8.7)$$

μ = Poisson's ratio ≈ 0.35 for rigid materials (see Table 4.1, type A), compared with 0.5 for elastomeric materials (see Table 4.1, types B, C and D).

From Eqs. 8.5 to 8.7 it follows that the permissible size of undercut is:

$$H_{\text{perm}} = \sin \left[\frac{180}{\pi} (1 + \mu) \varepsilon_{\text{perm}} \frac{l_T}{r} \right] l_1 \quad (8.8)$$

Equation 8.6 for other cross-sectional geometries for the torsional element may be found in standard mechanical engineering handbooks.

Assembly Force

A moment of $Q_1 l_1 = Q_2 l_2$ is needed to deflect the torsional snap-fit arm.

$$Q_1 \cdot l_1 = Q_2 \cdot l_2 = G \cdot \gamma \cdot W_p \cdot n \quad (8.9)$$

where

G = shear modulus for which an approximation is $G = \frac{E_s}{2(1 + \mu)}$

W_p = Polar moment of resistance

n = Number of torsion rods

μ = Poisson's ratio

8.1.3 Annular Snap-Fit Joints

8.1.3.1 Types of Annular Snap-Fit Joints

From the point of view of production technology, positioning a protrusion on the inside contour of a closed pipe is usually difficult and costly. The following methods are available:

- Machining (costly because of the additional production step; suitable for prototypes or small piece numbers)
- Forced demolding (only small undercut possible, depending on the material rigidity)
- Collapsible core (high-cost mold, many moving parts)

Figure 8.34 shows a mold design for demolding an undercut close to the gate on a hollow, cylindrical sleeve-shaped part. The demolding operation proceeds by the following steps.

1. The mold is opened by the cylinder A at I. The split 1 moves inwards and the undercuts 1.1 are released.
2. The mold opens at II. The cylinder B moves synchronously with this movement and the outer contour is released.
3. As the sleeve is stripped from the core, cylinder C is moved forward, and split 2 slides forward at an angle and releases the remaining undercuts 1.2.

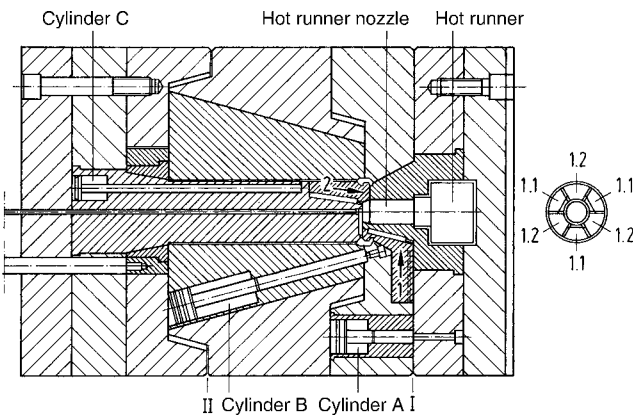


Figure 8.34 Method for demolding an undercut in the inner part of a sleeve-like molding

Common applications for closed annular snap-fit joints are pipe connectors and cap closures. Depending on the position of the bulge or undercut, annular snap-fit joints are said to be terminal or nonterminal. The bulge may be located on the inside or outside of the part, depending on the application (see Figure 8.35).

A greater undercut distance can be used when the snap-fit joint area is designed as shown on the right in Figure 8.36. This permits greater deformation of the wall.

Spherical snap-fit joints are a special case of annular snap-fit joints where their operation as ball-and-socket joints is additionally exploited (see Section 8.1.3.3).

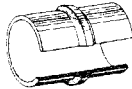
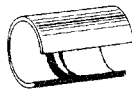
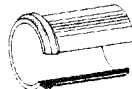
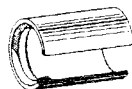
Bulge	Outside (BO)	Inside (BI)
Far from end		
Close to end		

Figure 8.35 Position of the bulge in cylindrical or annular snap-fit elements [8.11]



Figure 8.36 The design on the right permits greater elastic deformation (undercut) in annular snap-fit joints [8.9]

8.1.3.2 Annular Snap-Fit Joint Calculations*

Permissible Size of Undercut

The following calculation assumes that the entire deformation on assembly is absorbed by only one of the mating parts. Also, the simplifying assumption (for a thin-walled cylinder) of a uniaxial state of stress (tangential stress) has been made. In the assembly operation, the permissible size of undercut can be read off directly from the stress-strain diagram as $\varepsilon_{\text{perm}}$ (see explanatory notes to Eq. 8.2).

$$H_{\text{perm}} = \frac{d_{\max} - d_{\min}}{d_{\min}} = \varepsilon_{\text{perm}} \quad (8.10)$$

ε = strain as absolute value (m/m)

Assembly Force and Retaining Force

The assembly force for an annular snap-fit joint is calculated by analogy with Eq. 8.3 supplemented by the geometrical conditions.

$$F = Q \cdot d_{\min} \cdot \pi \cdot \eta \quad (8.11)$$

The widening of the cylinder due to the radially acting deflection force Q may be estimated by comparison with a support on a yielding structure. A detailed derivation is given in [8.22, 8.23]. From this, the assembly force equation for thin-walled annular snap-fit joints is obtained.

* SNAPS PC program from BASF or Fittcalc from Ticona.

$$F = K \cdot H \cdot d \cdot \left(\frac{2 s}{d_m} \right)^{\frac{3}{2}} \cdot \left(\frac{E_{St}}{E_{Sa}} \right)^{\frac{3}{4}} \cdot E_{Sa} \cdot \eta \quad (8.12)$$

where

$$\begin{aligned} K &= \text{Constant} = 0.62 \text{ for terminal position} \\ &\quad = 2.49 \text{ for nonterminal position} \end{aligned}$$

$$H = d_{\max} - d_{\min}$$

$$E_{St} = \text{Secant modulus in the tangential direction with } \epsilon_t = \Delta d/d_m$$

$$E_{Sa} = \text{Secant modulus in the axial direction with}$$

$$\epsilon_a = \epsilon_t \pm \sqrt{\frac{E_{St}}{E_{Sa}} \cdot 3 (1 - \mu_a \cdot \mu_t)}$$

$$d_m = \text{Mean diameter of the mating partner composed of polymeric material}$$

$$s = \text{Wall thickness in the region of the bulge or protrusion}$$

Setting $E_{St} = E_{Sa}$ (permissible for a terminal bulge), Eq. 8.12 simplifies to:

$$F = K \cdot H \cdot d \cdot \left(\frac{2 s}{d_m} \right)^{\frac{3}{2}} \cdot E_{St} \cdot \eta \quad (8.13)$$

From the fundamental equation of an elasticity curve for an infinitely long cylindrical tube, it can be shown that the deformation of the tube occurs substantially only up to the first intersection of the elasticity curve with the x-axis, i.e., Eq. 8.13 applies with sufficient accuracy to tube lengths greater than approximately $(d \cdot s)^{1/2}$ [8.23]. If the tube is reinforced in the vicinity of the joint (sealed by a closed end, for example), the actual assembly force will, as expected, be greater than the one calculated. The retaining force is estimated by introducing α_2 into Eq. 8.1, but it should be pointed out that after repeated assembly and disassembly, the release or retaining force and the assembly force may be considerably less than that calculated, if changes in shape or permanent deformation have occurred. Even for the same retaining and joining angle, the release force is a little lower than the assembly force. The bending moment between the action planes of the actuating forces and the action plane of the reaction force during assembly opens the snap-fit joint and acts in the opposite direction during closure.

The assembly force for cylindrical snap-fit joints can be calculated using the approach commonly used for compression joints. It can be used to determine the assembly force for thick walled annular sections [8.17, 8.23].

On this basis the assembly force is given by:

$$F = K \cdot H \cdot \frac{\sqrt{\frac{2(u-1)}{(u+1)}}}{\frac{(u^2+1)}{(u^2-1)} \pm \mu} \cdot E_{St} \cdot \eta \quad (8.14)$$

where

$$u = d_o/d_{\min} \text{ (outer ring); } d_{\min}/d_i \text{ (inner ring)}$$

$$\mu = \text{Poisson's ratio (+}\mu\text{ for outer ring; -}\mu\text{ for inner ring)}$$

When, however, experimental results are compared with the results of the theoretical calculation using Eqs. 8.12 to 8.14, poor agreement is sometimes reported [8.23, 8.18]. Nonetheless, considering the great uncertainties in the assumptions for the coefficient of friction, Poisson's ratio, and modulus values and the fact that production tolerances and other dimensional and geometric deviations are not taken into account, Eqs. 8.12 and 8.13 seem perfectly adequate for practical purposes.

In reference [8.17], an equation for the assembly force for spherical snap-fit joints is derived starting from the mathematical approach adopted for compression joints. This yields:

$$F \approx \pi \cdot H \cdot \frac{d_i \cdot l_m}{\frac{(u^2 + 1)}{(u^2 - 1)} + 1} \cdot E_{St} \cdot \eta \quad (8.15)$$

where

$$d_{\max} \approx d_i \text{ and } u = d_o/d_i \text{ (see Figure 8.6)}$$

8.1.3.3 Additional Functions

Retaining Guards

Annular snap-fit joints having an inner part composed of polymeric material can be secured more tightly using a filler pin when the end use requirements justify this, as, for example, in the case of clips. Such a filler pin can be linked for ease of assembly directly to the component by thin pieces of webbing attached as an extension of the joining axis (see Figure 8.37, position a) so that after assembly it can be easily pushed into place (position b).

Figure 8.38 shows how a retaining guard is provided in a corresponding assembly sequence by a different part in a subassembly.

The most varied retaining guards are employed in snap-fit closures for blow-molded packaging units (also as a means of safeguarding original quality). The securing element in the sealing cap in Figure 8.39 is formed by a separately inserted bracing ring (a) composed of a stiff material [8.8].

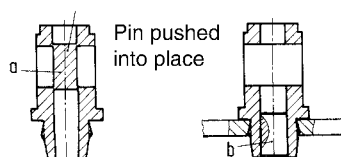


Figure 8.37 Additional retaining force provided by a filler pin

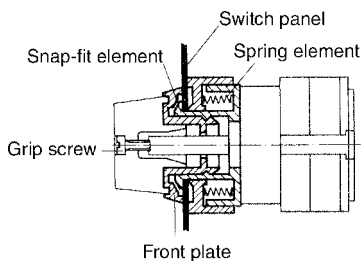


Figure 8.38 Fastening of a switch secured against release by an annular front plate
(Photograph: Kraus & Naimer)

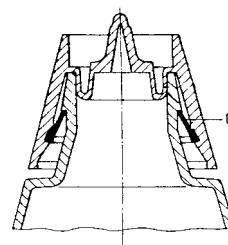


Figure 8.39 Bracing and securing ring (a) on the annular snap-fit joint in a bottle closure [8.8]

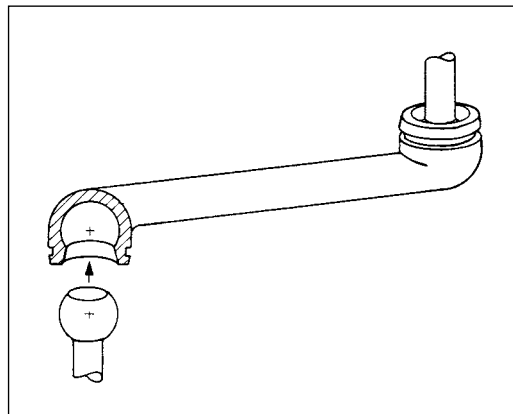


Figure 8.40 Snap-fit ball-and-socket joint [8.2]

Sliding Elements

Due to their rotational symmetry, annular snap-fit joints may also be used as bearings when they can be mounted with adequate bearing clearance. Spherical snap-fit joints are particularly suitable for this purpose (see Figure 8.40).

8.1.4 Segmented Annular Snap-Fit Joints

If the closed circular cross section of an annular snap-fit joint is broken (or slotted), the nature of the stress coping with the undercut changes from tangential tensile stress (in the tube cross section) to bending stresses in the individual segments. Geometrically, the joint remains an annular joint, but it is treated like an elastic beam element (see Section 6.1). The permissible size of the undercut can be significantly greater for the slotted annular sections, but at the same time, the assembly force and the retaining force become smaller.

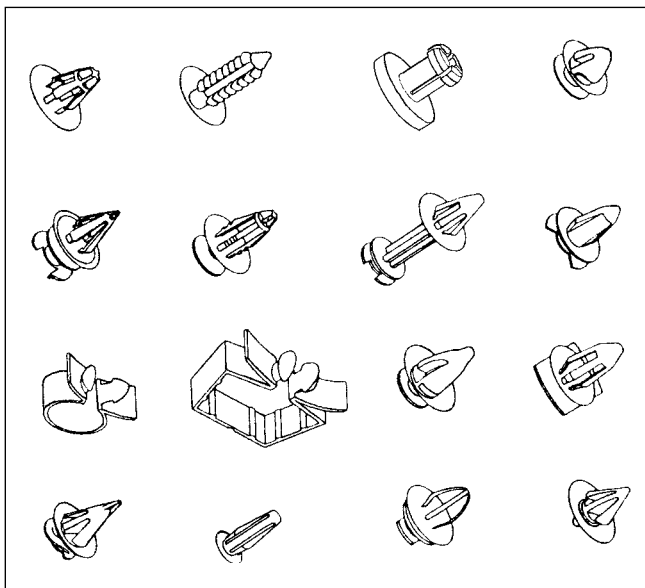


Figure 8.41 Different geometric forms of clips [8.6]

8.1.4.1 Segmented Annular Snap-Fits

The clip is typical of the wide range in which the outer ridge of an annular snap-fit joint can be segmented. Figure 8.41 contains a selection of geometries that can be used as independent connectors or can be integrated into other components.

8.1.4.2 Slotted Annular Snap-Fit Joint Calculations

Permissible Size of the Undercut

The individual segments are formally treated as snap-fit beams (see Section 8.1.1.2). Apart from the beam's cross sections presented in Figure 8.13, a segment in the form of an arc of a cylinder is of particular interest here. The relevant values and equations for design calculation are given in Figure 8.42.

The geometry factor C is plotted against the radius ratio p_1/p_2 for common segment angles in Figure 8.43. C_1 is used when the beam is deformed outwards (tensile stress in the concave surface) and C_2 is used when it is deformed inwards (tensile stress in the convex surface).

Assembly Force and Retaining Force

The assembly force and retaining force are calculated using the method for the elastic beam elements, using Eqs. 8.1, 8.3, and 8.4 for each individual segment. The section modulus values of the segment cross sections may be found in the standard literature.

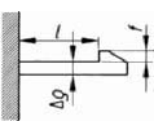
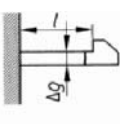
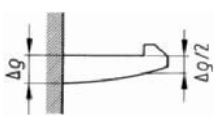
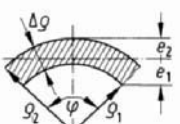
			
Circular arc segment			
	$H_{\text{perm}} = C \frac{\varepsilon_{\text{perm}} \cdot I^2}{\rho_2}$	$H_{\text{perm}} = 1.28 D \frac{\varepsilon_{\text{perm}} \cdot I^2}{\rho_2}$	$H_{\text{perm}} = 1.64 C \frac{\varepsilon_{\text{perm}} \cdot I^2}{\rho_2}$

Figure 8.42 Permissible size of undercuts for beams having a cross section in the form of a cylinder segment [8.5]

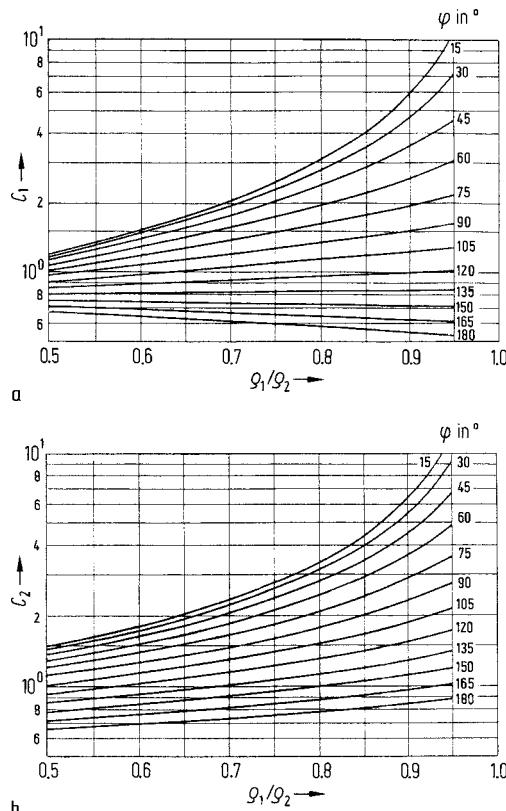


Figure 8.43 Plots for determining C_1 and C_2 [8.5]

8.1.4.3 Additional Functions

Retaining Guards

The easier joining of a segmented annular snap-fit joint results inevitably in easier opening or disassembly. Measures to prevent unwanted opening include filler pins (see Figure 8.37) and stop collars (see Figures 8.44 and 8.45).

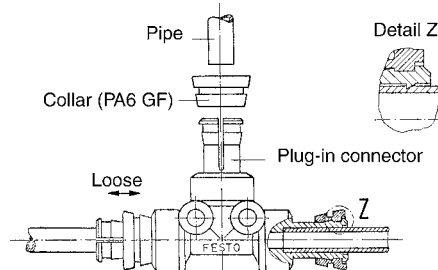


Figure 8.44 Tubing connection by means of a segmented annular snap-fit joint locked into place by a securing collar

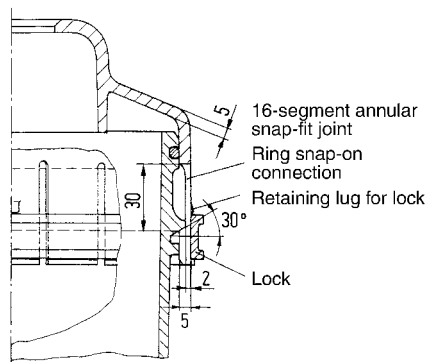


Figure 8.45 Design for a container lid as a segmented annular snap-fit joint having a lock, retaining lug, and radial seal

Seals

When a snap-fit joint is sealed by means of an O-ring, for example, the plane of action of the seal must be sufficiently rigid. A radially acting seal is generally suitable (see Figure 8.45). Figure 8.46 presents an equally good solution.

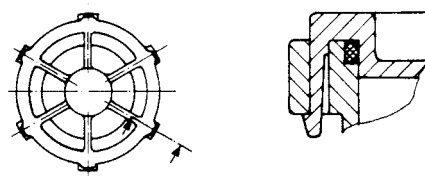


Figure 8.46 Method of sealing a container closed by a segmented snap-fit lid [8.2]

8.2 Elastic Elements

8.2.1 Elastic Thermoplastic Materials

True elastic materials usually exhibit linear stress-strain behavior. Since this is not the case for most thermoplastic polymeric materials, the following general rules apply:

- The elastic element has to be arranged in such a way that it is not under load in the normal (home) position and comes into operation only for short periods of time
- After loading, a load-free period is provided such that adequate time is available for elastic recovery
- In the case of alternating loads, the frequency should be limited to < 20 Hz.

When these material-related restrictions are observed, it is possible to produce elastic elements by injection molding, especially when they are integrated components of structural parts.

Such components are almost exclusively elements subjected to bending stresses and only very occasionally to torsional stresses. When suitably shaped, elements subjected to bending stresses can also be turned into tension or compression springs, depending on the direction of the force (see Figure 8.47). The following discussion of elastic elements is structured according to the nature of the external forces.

Experience has shown that POM is a preferred material for injection-molded elastic elements.

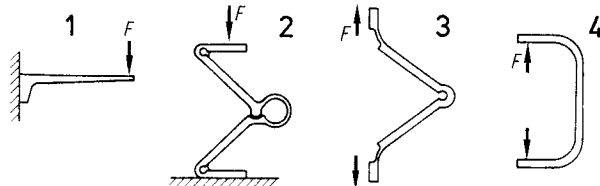


Figure 8.47 Design principles for flexing springs (1), compression springs (2), and tension springs (3, 4) [8.25]

8.2.1.1 Flexing Springs

A bending beam in the form of a snap-fit beam is the most common elastic element and has been discussed at length in Section 8.1.1. In addition, the bending beam, whether straight or curved, may also be employed as an integrated elastic component, as the typical examples in Figures 8.48 to 8.52 demonstrate. Figure 8.48 shows *straight flexing springs* on a daisy wheel made of glass-fiber reinforced PA 66 (35% by weight) used in a telex machine. The thin flexing arms are particularly at risk at the point where they emerge from the central disk. The notch effect is minimized at this point by using radii that also help direct the flow of the melt during injection molding. The chopped strands orient in the flow direction to provide greater resistance to stress. The flow conditions in the long elastic arms lead to a longitudinal orientation in the outer layers, which likewise helps with stresses. Some fibers also line up in the circumferential direction so that there is no serious weakness perpendicular to the longitudinal axis [8.26].

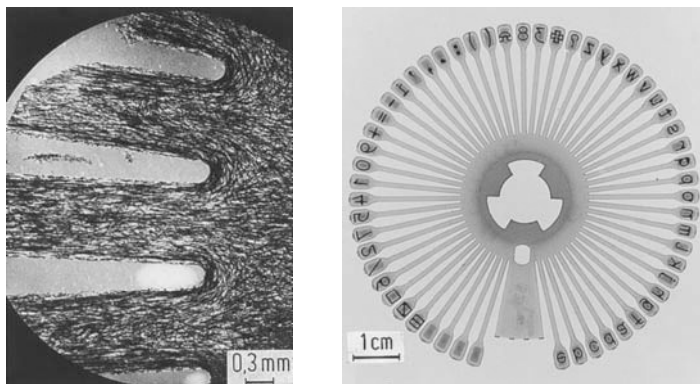


Figure 8.48 Daisy wheel made of glass-fiber reinforced PA 66; alignment of the glass fibers rendered visible by microradiography [8.26]

The deformation of springs having a *center line bent into an arc of a circle* can be calculated from the differential equation for the elasticity curve. This has the following general form:

$$E \cdot I \cdot \left(\frac{d^2 \cdot f}{d \varphi^2} + f \right) = -M \cdot r^2 \quad (8.16)$$

Starting with this equation, the equation for the elasticity curve for an individual material and hence the spring deformation are determined.

A common spring shape is the *semicircular* design shown in Figure 8.49. The solution of Eq. 8.16 for the spring deformation of this shape is:

$$f = \frac{F \cdot r^3}{2 \cdot E \cdot I} \cdot \pi \quad (8.17)$$

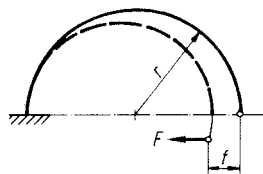


Figure 8.49 Important dimensions in a semicircular flexing spring and their designations

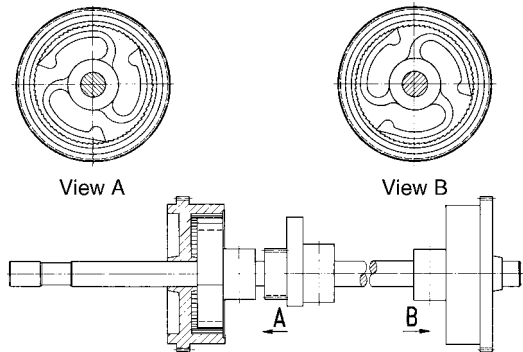


Figure 8.50 Elastic detent pawls in an overdrive gear. Springs and wheels made of POM.
(Photograph: Kienzle Apparate, Villingen)

Springs of this type are used, for example, in ratchet mechanisms (see Figure 8.50 and also Figure 7.20).

8.2.1.2 Tension Springs

A spring element is defined as a tension spring when the forces acting on the element act in opposite directions along an axis (see Figure 8.47). An example of a tension spring is shown in Figure 8.51.

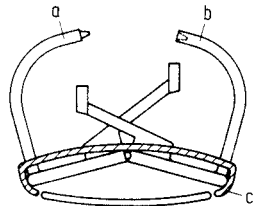


Figure 8.51 Ring binder clips (a, b) are held in position with a tension spring (part c) composed of a polymeric material [8.25]

8.2.1.3 Compression Springs

By definition, compression springs should absorb compressive forces. This requirement may be met structurally in different ways. For example, Principle 2 in Figure 8.47 is implemented in the well known design of a clothes pin (see Figure 8.52).

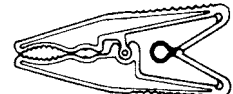


Figure 8.52 Integrated design of a clothes pin with a toggle joint and a compression spring [8.25]

A special type of compression spring takes the form of a *slightly curved* flexing spring that is compressed in the center by a level pressure pad (see Figure 8.53). Springs of this type are usually referred to as leaf springs.

Neglecting friction, the equation for the deformation of the flexing spring is:

$$f_1 = \frac{F \cdot l^3}{3 \cdot E \cdot I} \quad (8.18)$$

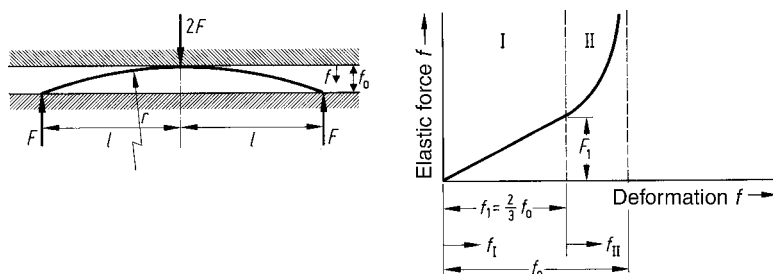


Figure 8.53 A slightly curved flexing spring. Its dimensions, their designations, and the spring's force-deformation diagram are also provided

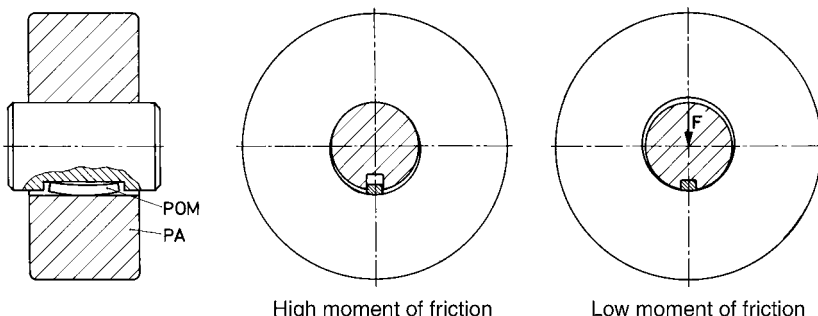


Figure 8.54 Caster for office chairs with a load-dependent rolling resistance

At the end of the linear section of the elasticity curve F_1 is given by:

$$F_1 = \frac{E \cdot I}{l \cdot r} \quad (8.19)$$

In the second section of the curve, the spring becomes increasingly less flexible, following a hyperbolic function.

Figure 8.54 shows a remarkable application of this principle. The POM spring is located in an adjusting spring groove in a shaft and ensures that the roller made of PA runs in the unloaded state with comparatively high friction against the shaft (braked). An external load F counteracts the force of the spring so that it is compressed and creates some clearance between the shaft and the bore of the PA roller. The point of slippage is now shifted substantially to the outer surface of the POM spring, where the POM slides against the PA with a low coefficient of friction.

Other examples of applications, in which the design principle illustrated in Figure 8.53 has been applied can be found in Figures 8.55 to 8.57.

A *disk spring* is a special form of compression spring. When made of a polymeric material (such as POM), they are particularly useful when a relatively large spring deformation is required for an application involving a small force [8.27]. This is not the case for steel disk springs, because to avoid buckling, a certain ratio of spring height to wall thickness must not be exceeded ($h/s \leq 1.35$). Thus, at the low wall thicknesses needed for small elastic forces, steel disc spring deformation is limited.

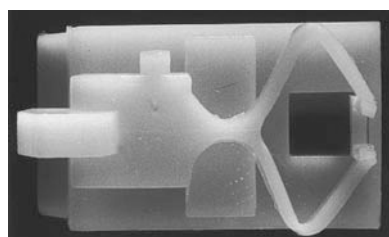


Figure 8.55 POM locking latch with a compression spring molded in situ [8.24]

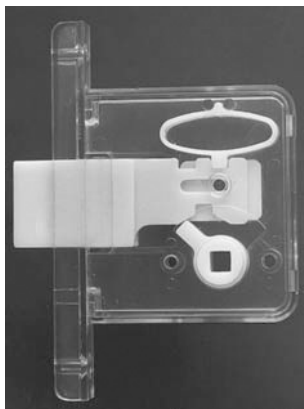


Figure 8.56 POM door lock with a compression spring as a single part



Figure 8.57 Sealing cap on the objective of a camera. The marks of the ejector pins are clearly visible. Small ejectors on the thin springs facilitate demolding and prevent deformation during demolding.

Table 8.1 Comparison of Disk Springs Made of Spring Steel and POM for Small Forces [8.27]

Disk spring dimensions					Material	Characteristic values		
D_o [mm]	D_i [mm]	s [mm]	$h + s$ [mm]	h/s		F_{\max} [N]	f_{\max} [mm]	σ_{\max} [MPa]
14	7.2	0.215	0.495	1.30	Steel	19.4	0.28	910
14	7.2	0.70	1.30	0.86	POM	18.7	0.60	72
14	7.2	0.195	0.445	1.28	Steel	12.8	0.25	718
14	7.2	0.60	1.25	1.08	POM	12.7	0.65	71
14	7.2	0.165	0.375	1.27	Steel	6.7	0.21	533
14	7.2	0.50	1.15	1.30	POM	7.4	0.65	63
14	7.2	0.13	0.30	1.31	Steel	2.6	0.17	234
14	7.2	0.40	0.90	1.25	POM	2.6	0.50	41

The characteristic values given in Table 8.1 for plastic springs refer to short-term loads at room temperature. They were determined theoretically using DIN 2092 using a modulus of elasticity $E = 2,700$ MPa. The stress-dependence of the modulus of elasticity was not taken into consideration in the calculations carried out in [8.27]. Therefore, the stresses shown in the table do not correspond exactly to those expected in real life. Nevertheless, Table 8.1 clearly presents the key characteristics and differences in the two spring materials.

Figure 8.58 shows an application in which disk spring elements provide several functions. In the caster housing sketched, the disk springs made of POM assume the key function of providing the springing action to compensate for play and to damp lateral forces. Simultaneously, they also act as contact seals. The mating of POM with PA guarantees good slip properties (low friction).

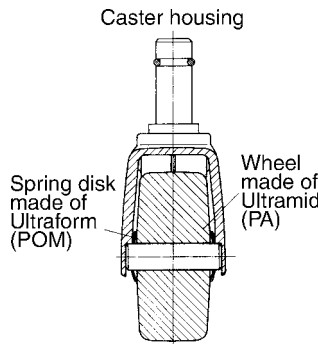


Figure 8.58 The spring disks made of POM ensure compensation for play and damping of noise. At the same time, they act as seals and protect the bearings against dust [8.24].

Another typical form of compression spring is the *spiral spring* for which there are significant complications and limitations on the manufacturing methods that can be employed. The springs with a rectangular cross section can be produced by machining (see Figure 8.59). Injection molding is possible only with special spring designs and molds can be expensive. As an example, the spring in Figure 8.60 is demolded from the core by rotating the core.



Figure 8.59 Spiral springs with a rectangular cross section made from PA by machining [8.24]



Figure 8.60 Injection-molded spiral spring for use as a compression spring in the valve of a bottle closure; closure cap: LDPE; seal and valve: rubber; compression spring: POM [8.24]

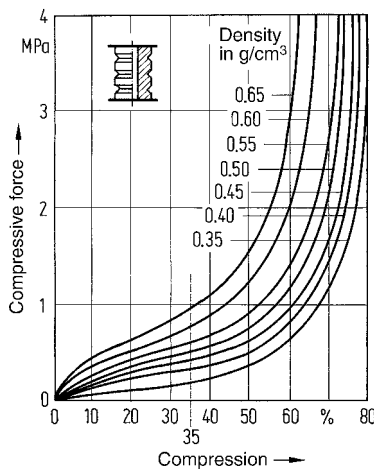


Figure 8.61 Characteristic elastic curves for spring/damping elements made of cellular PU (Cellasto) of different densities [8.28]

Compression springs made from elastomers are also employed as vibration dampers. Such elements made from cellular polyurethane have proved to be effective in automotive engineering. They have a characteristic elastic curve showing progressive compression (see Figure 8.61). In the lower, almost linear, range, the air trapped in the cells is compressed. Once a deformation of about 35% is achieved, the material itself is compressed.

8.2.1.4 Torsion Springs

Torsion springs in the form of a *torsion bar spring* are a type of spring that is only rarely made of polymeric material, although they can be of relatively compact construction. In order to keep the shear stress within permissible limits, however, the torsional element should be designed to be as long as possible (see also Figure 6.27).

The spring deformation or torsion angle can be calculated using Eqs. 8.6 and 8.7.

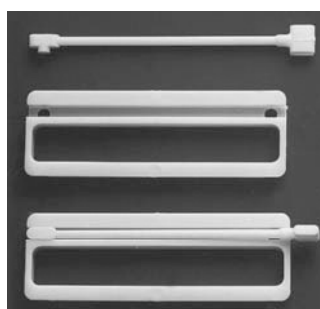


Figure 8.62 Torsion bar spring made of POM [8.24]

8.2.2 Springs Made of Fiber-Plastic Composites (Glass-Fiber and Carbon-Fiber Reinforced Plastic)

While thermoplastic polymeric materials are preferred as materials for springs, because of the efficiency with which they can be molded, higher performance fiber-composite materials can be employed for storing energy. Glass-fiber reinforced plastics with a predominantly parallel fiber arrangement (60 to 80% glass by weight) make it possible to achieve high flexural fatigue strengths for a relatively low modulus of elasticity by comparison with steel. Unidirectional glass-fiber epoxide-resin composites can withstand pulsed flexural loads of 500 to 800 MPa over 10^5 to 10^6 load cycles [8.29, 8.30]. The savings in weight made possible by substituting glass-fiber reinforced plastic springs for metal springs in automotive engineering is of great interest; however, the costs associated with glass-fiber reinforced plastic springs limit their use.

8.2.2.1 Leaf Springs

Designers have considered using fiber-plastic composites for automotive leaf springs as far back as the 1950s. However, these ideas were turned into reality only in 1983, when General Motors fitted a transverse glass-fiber reinforced plastic leaf spring in a sports car [8.31]. A key obstacle to the mass production of glass-fiber reinforced plastic leaf springs is that production methods compatible with large-scale production must first be developed [8.30]. The use of fiber-plastic composite leaf springs in sport utility vehicles is a current development objective.

Materials

Carbon-fiber reinforced plastic containing high-strength carbon fibers behaves even better than glass-fiber reinforced plastic under vibratory loads. Substantial weight savings are also obtained but at a significantly higher materials costs.

The characteristic properties of glass-fiber reinforced plastics, carbon-fiber reinforced plastics, and steel are given in Table 8.2 with reference to a steel leaf spring.

Due to their low compressive strength parallel to the fibers orientation direction, aramid fiber composites come into consideration only for hybrid structures when the compression zone can be built up of glass fibers and the tensile zone of aramid fibers. Thermal stresses are an additional consideration for such structures [8.32].

Table 8.2 Characteristic Values for Modulus of Elasticity E , Permissible Stress σ_{perm} and Breadth b Needed by Comparison with the Breadth of a Steel Spring [8.29]

Steel	GRP	CRP
E [MPa]	210,000	48,000
σ_{perm} [MPa]	1,400	650
b/b_{Steel}	1	0.52
		1.05

Shape of Spring

The simple rectangular spring with a cross section of constant height and width does not make the most effective or efficient use of the material (see Figure 8.13), although the constant cross section would be advantageous when laying continuous fibers from a manufacturing viewpoint. Accordingly, a leaf spring is best designed for support of constant flexural loads. Apart from the tapered beam geometries identified in Figure 8.13, a hyperbolic spring is particularly advantageous due to its good stress distribution and cross section. The thickness of the hyperbolic spring varies linearly, while its breadth varies hyperbolically (see Figure 8.63). For that reason, however, it also forms a very wide structure [8.33].

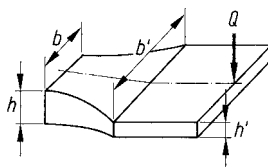


Figure 8.63 Hyperbolic spring

Calculation

Due to their generally simple geometry, flexing springs are still amenable to analytical computation. Fiber composites, on the other hand, are inhomogeneous and distinctly anisotropic. Nevertheless, the preliminary sizing of a leaf spring is generally determined using analytical methods, usually elastic bending theory for small deformations. Most leaf springs are largely reinforced unidirectionally so bending behavior can be calculated using the characteristics of the material having unidirectional fiber orientation (see Section 5.6).

The basic design process for the initial sizing of a single-layer vehicle leaf spring with superimposed vertical forces and longitudinal forces arising from braking and acceleration moments is described below. The detailed derivation may be found in [8.33].

Based on permissible stress, it follows that:

$$\sigma_{\text{perm}} = \frac{3 \cdot Q_V \cdot l}{b \cdot h^2} \cdot \left(1 + \frac{Q_L \cdot a}{Q_V \cdot l} \right) \quad (8.20)$$

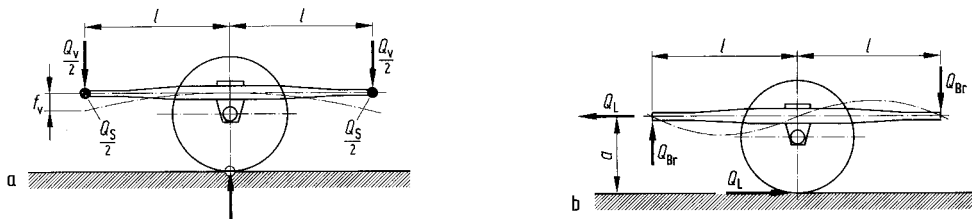


Figure 8.64 Loading of a symmetrical vehicle leaf spring [8.33]

- a) For vertical deflection force (Q_V) and side force (Q_S)
- b) During braking with longitudinal force Q_L from the braking moment and the reaction force Q_{Br} arising from this as supporting force

In addition, the condition for the deflection or deformation (at the spring rate of $C = Q_V/f_V$) must be fulfilled:

$$f_V = f' \cdot \frac{\frac{Q_V}{2} \cdot l^3}{E \cdot b \cdot h^3} \quad (8.21)$$

with f' being taken from Figure 8.65.

From Eqs. 8.18 and 8.19 it follows that for a specified length, l , and spacing, a , the principal dimensions h and b in the central cross section of the spring are given by:

$$h = \frac{1}{6} \cdot f' \cdot \left(\frac{1}{f_V} \right) \cdot \left(\frac{\sigma_{\text{perm}}}{E} \right) \cdot \frac{1}{1 + \frac{Q_L \cdot a}{Q_V \cdot l}} \quad (8.22)$$

and

$$b = 108 \cdot \frac{Q_V}{f_V \cdot f'^2} \cdot \frac{f_V}{l}^3 \cdot \frac{E^2}{\sigma_{\text{perm}}^3} \cdot \frac{1}{1 + \frac{Q_L \cdot a}{Q_V \cdot l}}^3 \quad (8.23)$$

The complete design of a vehicle spring in the form of a primary structure cannot end at this point. The effects of shear stress must be taken into account and finally numerical optimization steps (FEM).

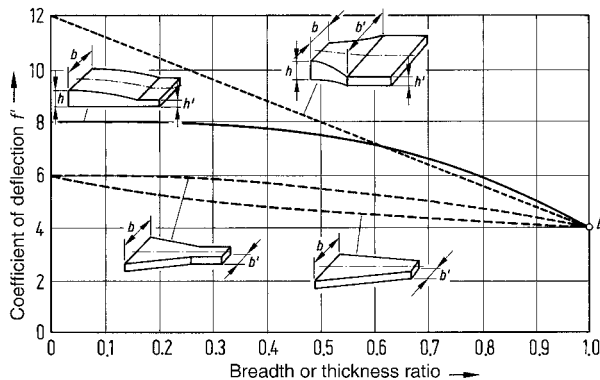


Figure 8.65 Coefficient of deflection as a function of the breadth or thickness ratio [8.33]

8.3 Integral Hinges and Integral Joints

An integral joint is an extremely thin flexible feature connecting two sections of a molded part for the purpose of assembly. Such an articulated joint is therefore a flexible joint that can be made from a thermoplastic, preferably as an integral component of the plastic molding. If the length of such an articulated joint is relatively long, it is referred to as a tape or strap joint. These joints have no sliding surfaces and, thus, when there is little (internal) friction, they are completely resistant to wear. Integral hinges, such as the hinge sections on the box shown in Figure 8.66, are also very common.

A very long service life (flexural fatigue strength) is obtained when these thin sections are kept free of notch effects (see Figure 8.66).

In the thin region of the hinge, which is only a few tenths of a millimeter thick, the molecules are aligned during the injection molding process in the flexing direction by the pronounced shear flow of the polymer melt, particularly in the outer layers. In the case of polypropylene, the central layer exhibits a fine spherulitic structure with spherulite diameters of only a few micrometers. Due to this alignment in the flexing direction, a long service life can be expected. An integral hinge, however, does not respond well to transverse loads.

The most suitable material for integral hinges is polypropylene (PP), with PP copolymers exhibiting even better articulation properties than PP homopolymers.

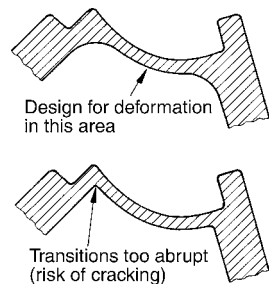
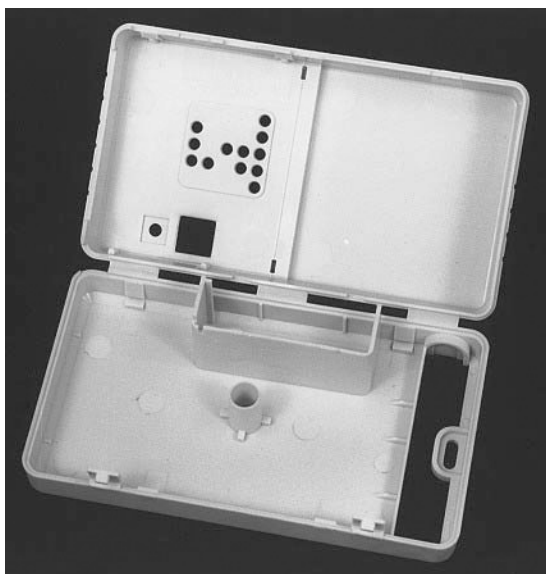


Figure 8.66 Integral hinge joints between a lid and a box molded as one part.

Radii of curvature promoting flow (top right) and favorable molecular alignments capable of withstanding stress also reduce damaging notch stress concentrations.

8.3.1 Manufacture of Integral Hinges and Integral Joints

8.3.1.1 Injection Molding

Thin hinges can be manufactured by the injection molding process as independent structural elements; however, the two halves of the hinge must then be joined in a suitable manner to the two parts to be joined (e.g., a lid and a box).

It is particularly efficient, however, when hinges are injection molded together with the parts to be assembled in a single operation to form truly “integrated” hinges.

Gate Position

During the injection molding of parts having integral hinges, the melt must flow uniformly, quickly, and without delay through the entire width of the thin hinge region so that the required molecular alignment occurs. This can be best achieved by means of a film gate or several pin gates in a row so that, when the melt front reaches the thin section, it advances in a linear fashion (see Figure 8.67).

Under no circumstances should the melt come to a stop in the cross section of the thin hinge area (*i.e.*, there should be no flow hesitation). In the case of multiple gating, the flow pattern should be such that no weld lines form along the axis of the hinge. Therefore, a numerical flow pattern simulation is often very useful and sometimes indispensable when designing parts with integral hinges.

As a technical measure to prevent the formation of a weld line, the gates may also be opened in time-shifted manner (see Cascade Injection Molding in Section 7.1.3.2), if the mold has a valve-gated hot runner system. Using this method, only the gates feeding one half of the hinge joint are opened, until the melt has flowed through the thin hinge cross section and reaches the gates placed at the other side of the thin region. The latter gates are then opened and the remainder of the cavity is filled. In order to find the best position of the gates and the fill pressure requirements, a numerical simulation is advisable.

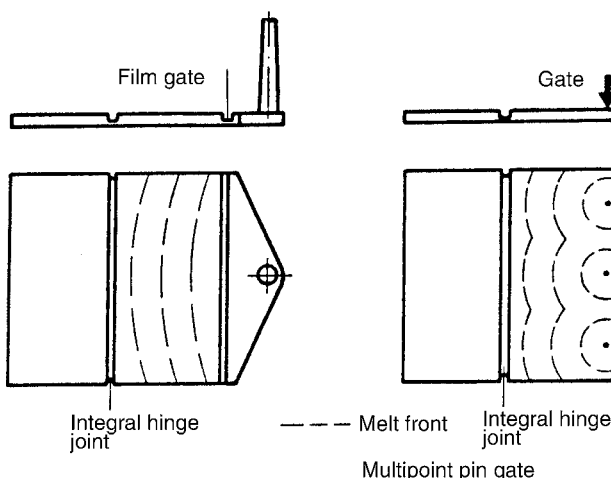


Figure 8.67 The melt front should reach and flow through the thin section in a linear fashion

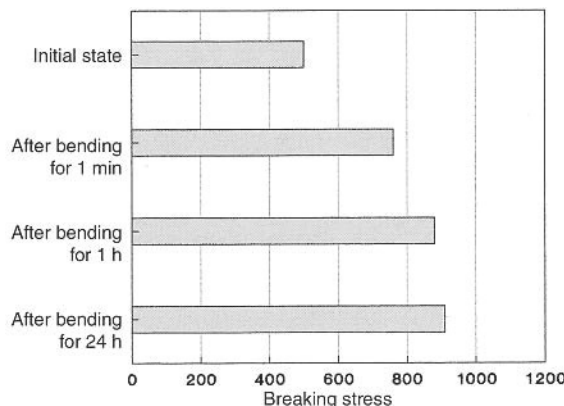


Figure 8.68 Effect of stretching on the tensile strength of integral hinges made from PP (Novolen 1100 L) in comparison with the unstretched, i.e., not previously deformed hinges. Time in this case refers to the time after ejection from the injection mold [8.35].

The positive effects on optimum articulation properties and long service life caused by the shear-induced molecular alignment can be enhanced further by stretching the oriented hinge cross section. The strengthening effect in semi-crystalline plastics, which occurs under the action of mechanical force (after the yield point has been exceeded), is due to the rearrangement of the lamellar crystalline regions that orient in the direction of stretching.

This improved fatigue resistance is found to a significant degree in polypropylene (PP) and modified forms of polypropylene (see Figure 8.73). The effect is less marked in polyethylene (PE), polyamide (PA), and impact-modified thermoplastics. In the cases of polyoxymethylene (POM) and polybutylene terephthalate (PBT), hinge weakening is more likely to occur when the hinge areas are mechanically stretched.

This stretching usually occurs the first time the joint is flexed. It is, however, more reliable and advisable to bend the integral joint by $\pm 90^\circ$ to $\pm 180^\circ$ shortly after demolding, while it is still warm (see Figure 8.68).

In some cases, a double integral hinge joint is utilized (see Figure 8.71, bottom). Here, the cavities located to the right and left of a manifold block must both be filled through the thin hinge sections. This requires free-flowing types of plastic and the volumes of these cavities must not be too large. Otherwise, multiple gates and time-shifted opening may have to be employed.

8.3.1.2 Blow Molding

Parts incorporating integral hinges can also be made by the blow molding process. The mold halves are closed around the parison to form the hinge. The cavity thickness in the area of the hinge may be a little less than the desired hinge film thickness, because there may be some elastic recovery. In this way, the thin region is produced by extreme pinching of the parison but without cutting through it. As a result of this pinching operation, which is equivalent to stretching the material, a fine structure is produced which exhibits even better integral joint

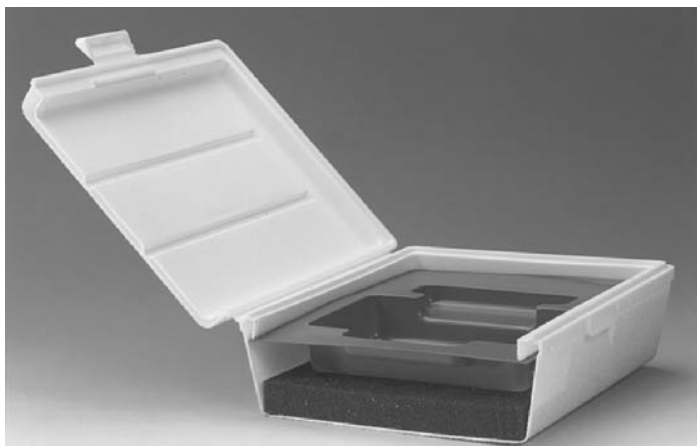


Figure 8.69 The lid and base of this blow-molded PP box are connected by an embossed integral hinge as is the locking latch on the lid (Manufacturer: Fischer Söhne AG, Muri, Switzerland)

properties than are possible by injection molding and subsequent stretching. In addition, there are no weld lines with this molding process and transverse strength is higher than that obtained with the injection molding process. In addition, due to the nature of the process, materials of high molecular weight are employed and as such they have a higher fatigue resistance.

Figure 8.69 shows a blow-molded container in which the lid and box are held together by an integral hinge. The locking latch is also linked to the lid by this method.

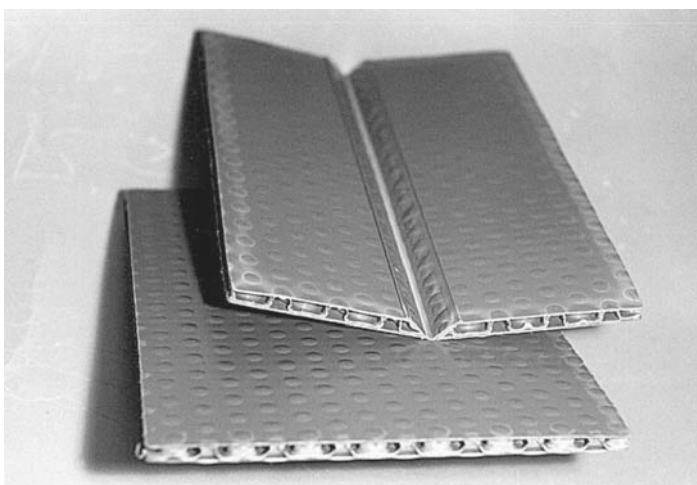


Figure 8.70 PP sandwich panel with embossed hinge and folding edge (Manufacturer: Friedola Holzapfel GmbH, Topfmühle, Germany)

8.3.1.3 Embossing

It is also possible to create hinge geometries by embossing. Even when the hinge joint grooves are put in place after the actual molding process by embossing using a cold or hot embossing die, the material is stretched during bending and integral joints of high durability are obtained. Embossed hinge joints are common in thermoformed packaging containers. This method of hinge formation also works very well with expanded polystyrene (EPS) film, which, when used for packaging goods, need not withstand too many load cycles.

It is also possible to emboss a hinge groove in this way in sandwich panels (see Figure 8.70).

8.3.2 Design

The shorter the thin section of an integral hinge is made – in the extreme case by a V-shaped incision – the more precise the control of the joint performance because its pivot point is more precisely defined. In this case, however, the notch stresses can become so high that less ductile materials will fracture instantly. A more ductile material can adapt to the stresses during bending and respond to the high notch stresses by flowing. As a result of the stretching process, however, the original linear joint groove becomes both broader and thinner. In that case, the pivot point of the joint is no longer fixed as precisely. During compensation, the degree of stretching is increased to such an extent by the flow process that the joint continues to function properly. Nevertheless, such a design is not advisable in principle. This design is possible with PP when the first alternating flexing loads are applied slowly.

Accordingly, the notch base of the thin section should at any rate have a radius of curvature of at least 0.5–1 mm (see Figure 8.71).

The transition to the thin hinge section should not be abrupt, but rather be a steady or curved transition as shown in Figure 8.66.

Figure 8.72 shows two other commonly used designs for integral hinge joints.

It is not absolutely essential for the hinge joint groove to form a straight line – an angled or bent shape is also possible. The movement of the joint is then not exactly uniform but occurs successively along the bend. The operation of the joint requires adjoining elements that are elastic, yielding, or capable of deforming to compensate for the non-linear kinematics.

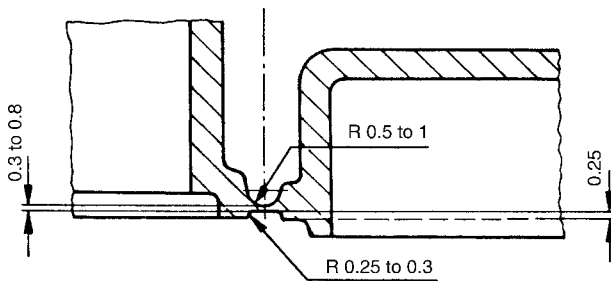


Figure 8.71 Guideline values for the design of an integral hinge made of PP with a hinge groove

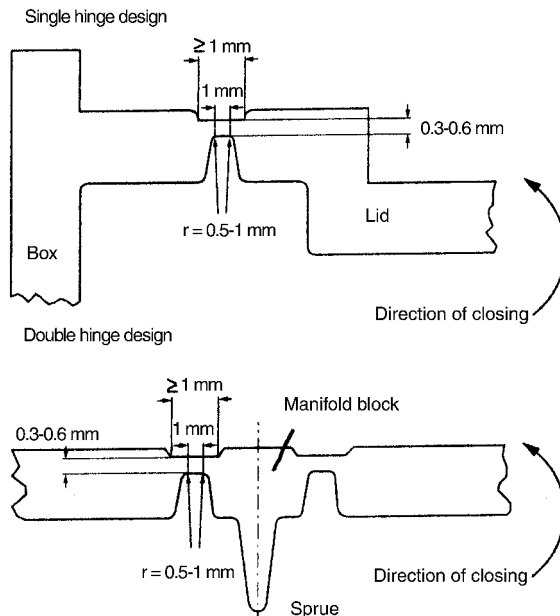


Figure 8.72 Commonly used designs for integral hinge joints [8.35]

8.3.3 Materials

PP is the most suitable material for integral hinges because of its outstanding fatigue behavior when reinforced by stretching. In general, however, integral hinge joints may also be produced from other thermoplastics. Integral hinge joints made of semi-crystalline thermoplastics withstand significantly higher numbers of load cycles and have a longer service life than those made of amorphous thermoplastics. Materials of high molecular weight having a narrow molecular weight distribution exhibit the best mechanical properties, but they can cause filling problems for very thin hinge joint cross sections because of their higher melt viscosity.

Adding fillers and reinforcing materials generally works to the detriment of articulating properties. Rigidity increases, ductility and flexural fatigue strength diminish, and hence the service life of the joint most likely decreases.

The use of particulate fillers such as glass beads or calcium carbonate, and lamellar fillers such as talc, is less of a problem than glass or carbon fibers. Some improvement can be achieved with the addition of impact modifiers.

8.3.4 Integral Hinge Design Calculations

Integral hinges are not amenable to design calculations based on characteristic property values obtained from standardized specimens at low strains because they may not represent the hinge properties. Both material properties and the hinge geometry change as a result of the

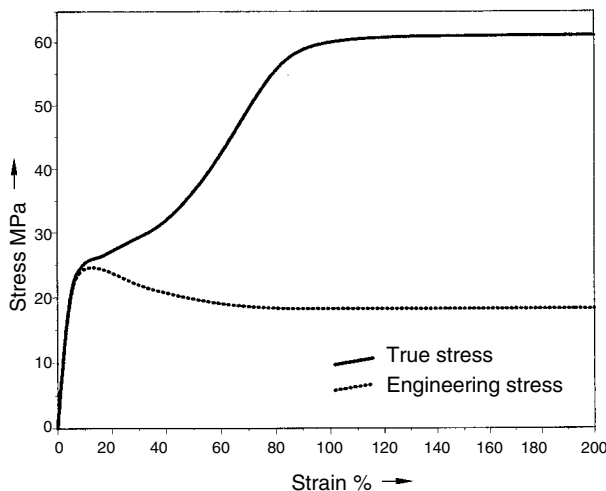


Figure 8.73 “True” stress and stress related to the original cross section (“engineering”) plotted against the instantaneous strain

stretching process. For example, in the standard ISO 527 tensile test at 10% strain, PP exhibits a yield point. This is normally a design limit that must not be exceeded in most applications, because the material begins to flow, the cross section changes, and permanent deformation has occurred. This flow is precisely what happens when the hinge joint is first bent and the operating strain lies above the yield point. The drop in stress after this yield point shown in the stress-strain diagram is spurious, because according to the test standard, the stress acting at any time is based on the initial cross-sectional area of the sample. If, on the contrary, the instantaneous test force is related to the actual tapering cross section, the “true stress-strain diagram” is obtained (see Figure 8.73). It can be seen that the thinner cross section can withstand much higher strains and stresses.

Comparable conditions occur in an integral hinge. As a consequence of stretching in the first bending operation, the cross section likewise tapers and reinforcement takes place so that an integral hinge can also withstand substantially higher strains than are calculated on the basis of the yield point and the initial cross-sectional area.

Polypropylene is an adaptive or ductile material. The material adapts to loading by changing its geometry.

In addition, in hinges with a very sharp joint groove, the theoretical notch stress would be in the non-permissible range even for PP, although actual practice shows that acceptable integral hinges of this type can be made from this material.

The large notches (grooves) have their edges smoothed out by flow in the first bending operation.

Design calculations for integral hinges of length L and thickness s are given in the following section (see Figure 8.74).

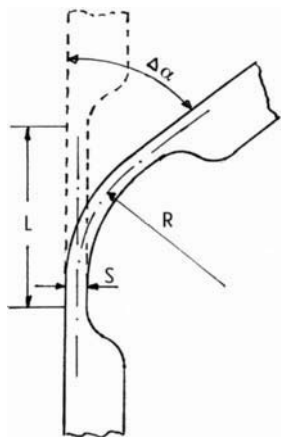


Figure 8.74 Dimensions and designations for an integral hinge

8.3.4.1 Calculation of the Length and Thickness of an Integral Hinge

The outer fiber strain ε_o may be estimated as follows:

$$\varepsilon_o = \frac{s}{2 \cdot R} \quad (8.24)$$

Given that

$$R = \frac{L}{\Delta\alpha} \quad (8.25)$$

we obtain

$$\varepsilon_o = \frac{s \cdot \Delta\alpha}{L \cdot 2} \quad (8.26)$$

The bending angle $\Delta\alpha$ has to be inserted in radians:

$$\Delta\alpha_{\text{rad}} = \frac{\pi}{180} \cdot \Delta\alpha^\circ \quad (8.27)$$

Solving for L , the required length of the thin section, and the film thickness s , yields the following expressions:

$$L = \frac{s \cdot \Delta\alpha}{2 \cdot \varepsilon} \quad (8.28)$$

$$s = \frac{2 \cdot L \cdot \varepsilon}{\Delta\alpha} \quad (8.29)$$

It should be noted that the strain value ε is not the strain value determined from a tensile test, but rather is a characteristic value specific to the type of part. It is determined by experiments on integral hinges and hence also covers the effects of geometric change and stretching. Strain values of this type for some materials are given in Table 8.3.

Table 8.3 Characteristic Strain Values for Selected Polymeric Materials Measured in Accordance with ISO 527 and as Part-Specific Values Measured on Integral Hinges

Material	Yield strain ε_y in %	Nominal strain ε_i in %	Strain amplitude ε_a in % after 10^4 load cycles	Strain amplitude ε_a in % after 10^5 load cycles
PP (1100L)	10	> 50	60	60
PA 6 (B3K, moist)	20	> 50	55	45
PA 66 (A3K, moist)	20	> 50	50	40
PA 66-GF 30 Impact-modified (A3ZG6)	5 elongation at break	*	4	3
POM (H2320)	10	35	35	30
POM GF15 (N 2200 G3)	3 elongation at break	*	3	2
PBT (B 4500)	3.5	> 50	25	20

* Does not apply for this material

Example

What length should an integral hinge have (length of the thin section), if it is to withstand at least 10^4 load cycles in which it is bent by an angle of 180° ?

Thickness of thin section = 0.3 mm

Safety factor = 1.5

Material: POM or alternatively PP

$$\text{for POM: } L = \frac{s \cdot \Delta\alpha}{2 \cdot \varepsilon} = \frac{0.3 \cdot \pi \cdot 100 \cdot 1.5}{2 \cdot 35} = 2.0 \text{ mm}$$

$$\text{for PP: } L = \frac{s \cdot \Delta\alpha}{2 \cdot \varepsilon} = \frac{0.3 \cdot \pi \cdot 100 \cdot 1.5}{2 \cdot 60} = 1.17 \text{ mm}$$

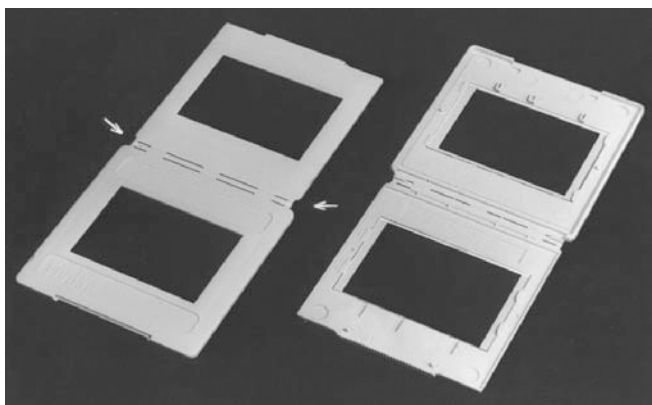


Figure 8.75 Integral hinges in slide frames made of impact-resistant polystyrene (SB)
(Photograph: Oechsler, Ansbach)

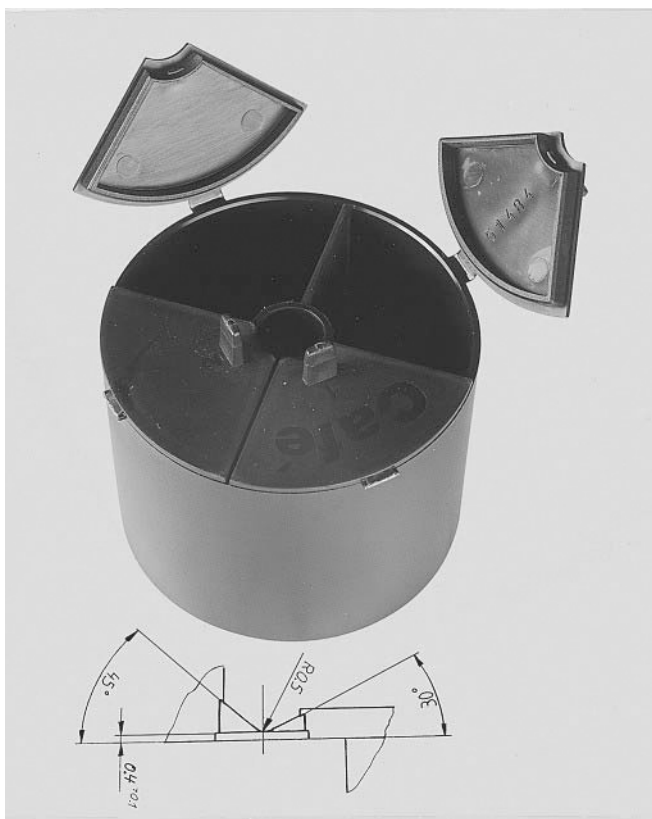


Figure 8.76 Storage container made of polypropylene with an antistatic additive
(Manufacturer: Krups, Solingen)

8.3.5 Applications with Integral Hinges

Examples of the different applications in which such joints are useful include:

- Lid-and-container joints;
- Bi-stable joints;
- Simplified production by the injection molding process;
- Dynamically loaded joints; or
- Acting as an assembly aid and captive binding for small parts.

8.3.5.1 Lid/Container Hinge Joints

Figures 8.66, 8.69, and 8.71 have already presented typical examples of lid-and-container joints using integral hinges, some produced by injection molding and others by blow molding.

In the slide frames in Figure 8.75, the principle shown in the lower part of Figure 8.72 is implemented, that is, the two halves of the part are filled from a manifold block outwards to the right and left through the integral hinges. This small block is of such dimensions that, when the two halves are folded together, they lie flat on top of one another. The material is an impact-resistant polystyrene (SB) which allows only few flexural load cycles, enough for the application.

In the four-part storage container made of PP in Figure 8.76, the lids of the four chambers are linked by integral hinges to the housing. The thickness of the hinges is 0.4 mm and the radius at the hinge joint groove is 0.5 mm.

8.3.5.2 Bi-Stable Hinge Joints

A bi-stable joint (snap-fit hinge) is a joint in which two component parts (e.g., lid and container) come into two stable end positions about an axis of rotation. The end positions (open and closed positions) are reached by moments turning to the right or left with respect to the axis of rotation. The turning direction of these moments changes each time a labile dead center position is passed. The moments are generated by elastic forces from integrated flexing or tension spring elements or by flexing the housing parts. In the course of the kinetic sequence, the elastic force increases from each of the end positions to the dead center position and decreases again after the moment changes direction. At the end positions, the forces acting within the system are in equilibrium. The end positions are stable. In this situation, the joint can be constructed as a pivot joint or, more practically, as an integral joint.

Remarkably, this principle is also found in nature. In Figure 8.77 the principle is illustrated on the basis of the control mechanism when a fly beats its wings. Points 1–3 are articulated links on the fly's body or its wings. The fly's body acts as a flexing spring which can be tensed by its muscles. When points 1, 2, and 3 are aligned in a plane, the system is in labile equilibrium (top position), from which the upbeat or downbeat of the wings can be produced by tensing or relaxing the flexing spring.

In Figure 8.78, the principle is explained in terms of a technical design for a hinge with a tension spring (between A and B) and a flexing spring (lug at A).

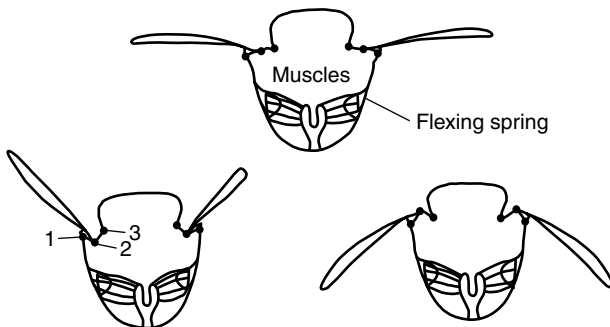


Figure 8.77 Wing-beat control mechanism in flies

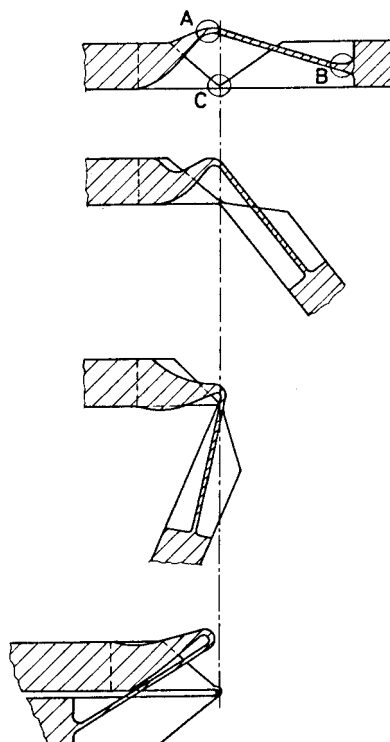


Figure 8.78 Kinetic sequence of events in a snap-fit hinge made of polymeric material including an integral hinge joint [8.36]

This bi-stable snap-fit hinge including an integral hinge joint, is without doubt, one of the most demanding plastic designs. There are now numerous design variants of this design for many types of lid/container closures most of which are patented. Bi-stable joints are also used for industrial products. Figure 8.79 shows such an application for a flap valve in a pipe.

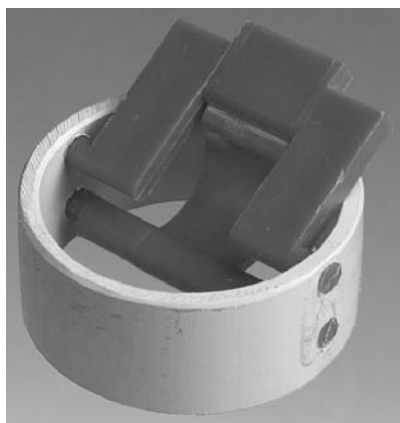


Figure 8.79 Flap movement mechanism for a flap valve in a pipe system

8.3.5.3 Simplified Production

A highly effective design principle is to make box-shaped parts or parts forming otherwise closed shapes using integral hinges. Otherwise, such parts would have to be demolded using splits or other special techniques. As opened-out flat parts, they can be injection molded and then be folded up by means of integral hinges. This approach simplifies mold-making and frequently opens up other design opportunities. Figure 8.80 shows an already half-assembled housing (for accommodating the electronics systems in refrigerators) that was produced this way. The finished part is obtained by folding over the integral hinge planes, fitting the side walls into the grooves, and pressing the pins into the molded hollow bosses.

Another very cleverly executed design concept is reproduced in Figure 8.81. This is a simple travel razor made of polypropylene. Adequate rigidity is obtained by folding up the hinged side walls.

The grounding contact plug shown in Figure 8.82 is another example of a product assembled using this technique.

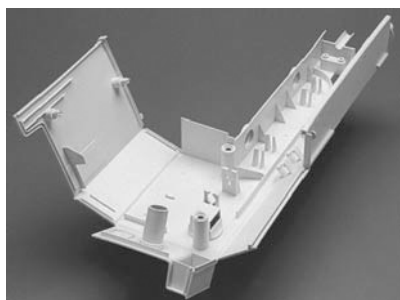


Figure 8.80 The part is produced as two opened-out flat parts connected by an integral hinge and subsequently folded up for assembly

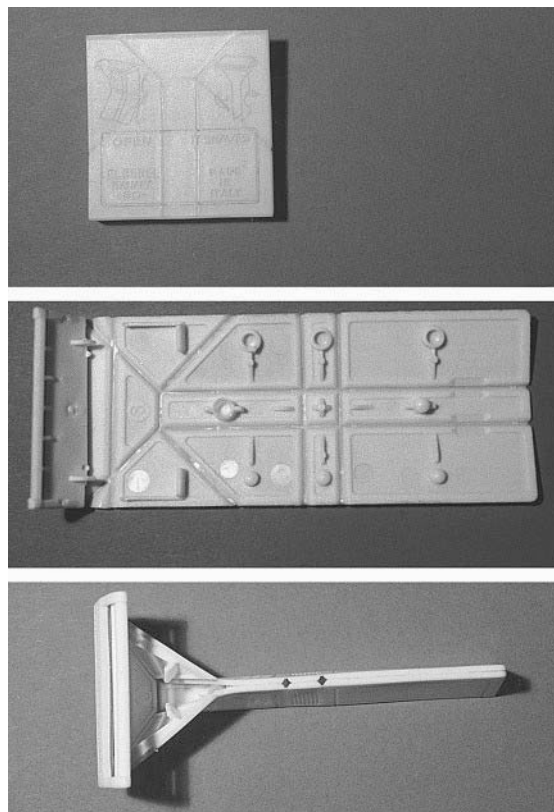


Figure 8.81 PP travel razor containing a number of integral hinges
Top: Folded crosswise using the hinges (for transport)
Center: Position in the injection mold
Bottom: Set up for use by folding via the hinges in the longitudinal direction

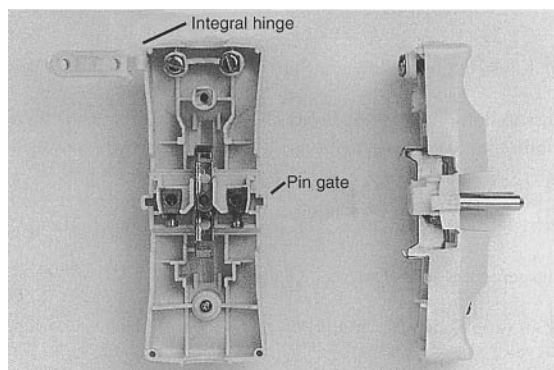


Figure 8.82 Integrated grounding contact plug with integral hinges
(Manufacturer: Kopp AG, Kahl; Design by Bohlender)

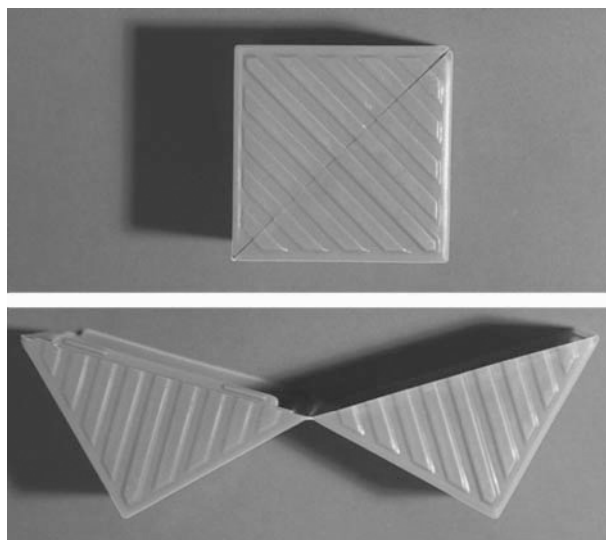


Figure 8.83 Toy cube made of polypropylene; it is injection molded in the diagonally open position and folded together using an integral hinge

Figure 8.83 shows the simple example of a children's toy cube. A clever feature here is that the parting plane runs diagonally and the cube is opened and closed along one edge. This allows the part to be demolded more easily than if one face of the cube were designed as a lid.

Dowels represent a technically demanding application for thermoplastic materials. A particular requirement is for the screw to be screwed in easily while at the same time displacing material. Figure 8.84 shows a new dowel concept in which the plastic dowel part is not constructed as a closed tube, but rather is made up of two separate, asymmetrically arranged spiral segments, which mesh with one another when they are joined together via the integral hinge at the tip of the dowel. Thus, the dowel is rendered substantially more deformable and the force needed to pull it is doubled compared with a conventional dowel.

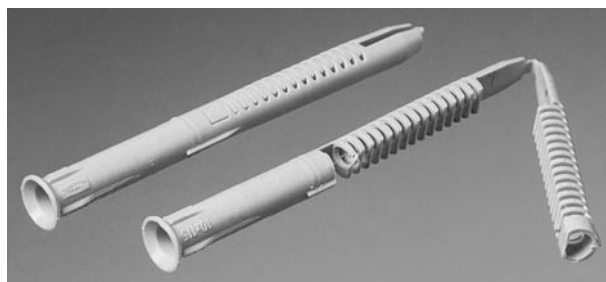


Figure 8.84 In the lower molding, the dowel (PA 6) is injection molded in two halves joined to one another at the tip by an integral hinge. The finished dowel is obtained by fitting the two halves together and welding them (Manufacturer: Fischer Werke, Tumlingen).

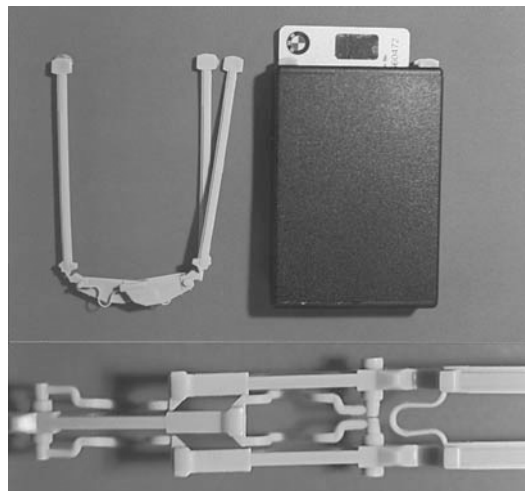


Figure 8.85 Map storage box (Manufacturer: Fischer Werke, Tumlingen)

The box in Figure 8.85 is used for storing maps and can be used in vehicles. When the gray button is pressed, the map moves forward and can be taken out. The complicated release mechanism made of PA is injection molded in one part (see bottom of figure) and is bent into the installation position using an integral hinge (left of figure).

The cable holder in Figure 8.86 is also an interesting design solution. It is manufactured in the open position. When it is assembled, the two slotted annular snap-fit joints in the lower part are first pushed through the holes in the mounting plate. After that, the upper part is held captive by a strap hinge linking it to the lower part which is folded down. On the left, the upper part is held in the opening by its edge and on the right by the snap-fit hook. As this tilting operation proceeds, the two locking pins attached to integral hinges engage in the annular snap-fit joints, thus preventing release of the fastening.

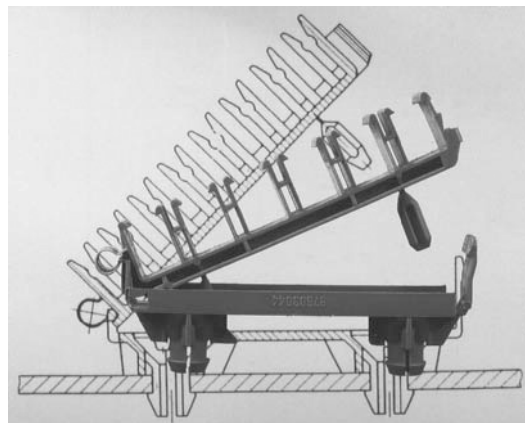


Figure 8.86 Cable holder made of PA 6

8.3.5.4 Dynamically Loaded Integral Hinge Joints

Integral hinges are also very suitable for use as dynamically loaded joints. Figure 8.87 shows an example of such an application in the vibrating head of an electric razor.

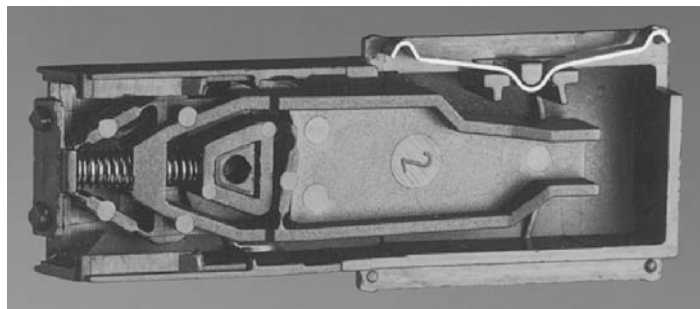


Figure 8.87 The guide joints in the vibrating head of an electric razor are constructed in the form of integral hinges; material: POM (Manufacturer: Philips, Klagenfurt)

Figure 8.88 presents a sketch of a small coupling joint whose function as a universal joint is based on integral hinges offset by 90° with respect to one another. This joint can compensate for an angular displacement of approximately 15° . However, its capacity is limited to a torque of about 5 N-cm.



Figure 8.88 Coupling joint based on the principle of two integral hinges offset by 90° for transmitting very low torques

8.3.5.5 Assembly Aid and Captive Binding Using Integral Hinges

Attaching small parts to a larger part so that they are held captive and cannot easily be lost has long proved to be an effective design practice. This is usually done by means of a strap hinge, a thin-walled flexible band. This facilitates assembly and other obvious advantages are obtained. Examples of this have already been presented in the two preceding figures.

In the grounding contact plug in Figure 8.82, the strain relief clip is linked in this way to the plug housing. In the cable holder in Figure 8.86, the entire upper section is connected to the lower section by a strap hinge. The locking pins are also fastened by shorter integral hinges.

The outlet chamber of a coffee machine provides another example of this technique. It is produced in two parts and the two halves of the tubular part are connected by a strap hinge. During assembly, the two parts are pushed together and held in place by six snap-fit hooks.



Figure 8.89 Coffee machine water outlet made from PP.
It is assembled using a strap hinge and snap-fits (Manufacturer: Krups, Solingen).

References

- [8.1] BEITZ, W. and K.-H. KÜTTNER: *Dubbel, Taschenbuch für den Maschinenbau* (Dubblel, Mechanical engineering handbook), 15th ed., Springer Berlin, Heidelberg, New York, Tokyo 1986
- [8.2] DELPY, U.: *Einführung in Schnappverbindungen*, Lehrgangshandbuch Schnappverbindungen aus Kunststoff (Introduction to snap-fit joints, Course handbook), TAE, Esslingen 1989
- [8.3] KLÄGER, R.: Entwicklung eines Konzeptes zur Unterstützung der Konstruktion von Schnappverbindungen beim Einsatz des volumenorientierten CAD-Systems EUCLID (Development of a concept for supporting the design of snap-fit joints using the EUCLID volume-related CAD system), Diploma thesis, University of Karlsruhe 1986
- [8.4] KÄUFER, H. and M. JITSCHIN: *Katalog schnappbarer Formschlußverbindungen an Kunststoffteilen und beispielhafte Konstruktion linienförmiger Kraftformschlußverbindungen* (Catalogue of form-fitting snap-fit joints on plastic parts and example design of linear frictional form-fitting joints), *Konstruktion* **29** (1977) 10, pp. 387/397
- [8.5] OBERBACH, K. and D. SCHAUF: *Schnappverbindungen aus Kunststoff* (Plastic snap-fit joints), Part 1: Gestaltung und Berechnungsgrundlagen (Design and calculation principles), Part 2: Berechnungs- und Einsatzbeispiele (Examples of calculation and use), *Verbindungstechnik* (1977) 6, pp. 41/46 and (1977) 7/8, pp. 29/33
- [8.6] MILBERG, J. and K. RIESE: *Automatische Montage von Klippen durch Industrieroboter* (Automatic assembly of clips by industrial robots), *Flexible Automation (V)*, Sept. 1986, pp. 249/258

- [8.7] ANEMAAT, A.: Das Berechnen konstruktiver und funktioneller Merkmale für Schnappverbindungen mit Ergebnisübertragung in die Praxis (Calculation of structural and functional characteristics of snap-fit joints and practical application of the results), Conference handbook, "Verbindungs-technik – vt '80", pp. 209/225
- [8.8] HOLZMANN, R. and P. KLÜSENER: Verschlüsse für blasgeformte Kunststoffverpackungen (Closures for blow-molded plastic packaging units), VR-INTERPACK 1969, pp. 650/656
- [8.9] NIEDERHÖFER, K.-H.: Konstruieren mit Kunststoffen (Designing with plastics), TÜV Rheinland, Cologne 1989
- [8.10] SCHÖNEWALD, H.: Schnappverbindungen in der Anwendung (Applications of snap-fit joints), *Kunststoffe* **79** (1989) 8, pp. 732/737
- [8.11] SIEGEMUND, E.: Untersuchung werkstoffspezifischer Beanspruchungsgrenzen, konstruktions-spezifischer Versagensformen und Berechnungsmöglichkeiten dünnwandiger zylindrischer Verbindungselemente (Study of material-specific loading limits, design-specific failure forms and methods of calculation for thin-walled cylindrical connecting elements), Fortschritt-Bericht, Series 1, No. 139, VDI-Verlag, Düsseldorf 1986
- [8.12] ROTH, K.: Konstruieren mit Konstruktionskatalogen (Designing with design catalogues), Springer-Verlag, Berlin, Heidelberg, New York 1982
- [8.13] KOLLER, R. and M. STELLBERG: Ein Weg zu einer systematischen Konstruktion und Ordnung von Schnappverbindungen (Approach to the systematic design and classification of snap-fit joints), *Konstruktion* **39** (1989) 8, pp. 315/320
- [8.14] LAUSCHER, H.-J.: Methodisches Konstruieren mit Kunststoffen (Methodical design with plastics), Dissertation, University of Aachen 1977
- [8.15] SCHMIDT, H. AND H. RÖBER: Thermoplaste – Werkstoffe für Federn? (Thermoplastics – Materials for springs?), *Maschinenmarkt Industriejournal* **78** (1977) 38, pp. 843/846
- [8.16] ERHARD, G. and E. STRICKLE: Maschinenelemente aus thermoplastischen Kunststoffen, Band 1, Grundlagen und Verbindungselemente (Machine elements made from thermoplastics, Vol. 1, Principles and connecting elements), VDI-Verlag, Düsseldorf 1974, p. 106
- [8.17] Berechnen von Schnappverbindungen mit Kunststoffteilen (Calculation of snap-fit joints with plastic parts), Brochure B.3.1, Hoechst AG 1982
- [8.18] REISINGER, H.-D.: Zylindrische Schnappverbindungen aus thermoplastischen Kunststoffen – praktische und theoretische Ermittlung der Montagekräfte (Cylindrical snap-fit joints made from thermoplastics – practical and theoretical determination of assembly force), unpublished study from a practical training course, BASF 1980
- [8.19] BALS, J.: Konstruktive Auslegung von Preß- und Schnappverbindungen. Fügen von Kunststoff-Formteilen (Structural design of press-in and snap-fit joints. Joining plastic moldings), Ingenieurwissen series, VDI-Verlag, Düsseldorf 1977
- [8.20] ADELHARD, H.-G.: Spritzgußgerechte Gestaltung von Schnappelementen. Lehrgangshandbuch Schnappverbindungen aus Kunststoff (Design of snap-fit elements for injection molding. Course handbook for plastic snap-fit joints), TAE, Esslingen 1989
- [8.21] GERTIG, J.: Tragfähigkeit von Gestaltsvarianten linienhafter Kraftformschlusverbindungen aus Thermoplasten (Load-bearing capacity of design variants of thermoplastic frictional form-fitting joints) Dissertation, Technical University Berlin 1981, Konstruktionstechnik series, Ed.: W. Beitz
- [8.22] DELPY, U.: Zylindrische, vom Rohrende abliegende Schnappverbindungen aus Kunststoff (Cylindrical plastic snap-fit joints located away from the end of the pipe), *Konstruktion* **30** (1978) 8, pp. 307/310
- [8.23] DELPY, U.: Zylindrische Schnappverbindungen aus Kunststoff – Berechnungsgrundlagen und Versuchsergebnisse (Plastic cylindrical snap-fit joints – Principles of calculation and experimental results), *Konstruktion* **30** (1978) 5, pp. 179/184

- [8.24] ERHARD, G. and E. STRICKLE: Maschinenelemente aus thermoplastischen Kunststoffen – Lager und Antriebselemente (Machine elements made from thermoplastics – Bearings and drive elements), VDI-Verlag Düsseldorf 1985, pp. 257/281
- [8.25] ROTH, K.: Anregungen zum Einsatz unkonventioneller Gestaltungsmöglichkeiten bei Kunststoff-Konstruktionen Konstruktion, Fertigung und Anwendung feinwerktechnischer Kunststoffteile (Suggestions on the use of unconventional design methods for plastics designs. Design, production and application of precision-engineered plastic parts), VDI-Verlag Düsseldorf 1976
- [8.26] EHRENSTEIN, G. W. and G. ERHARD: Konstruieren mit Polymerwerkstoffen (Designing with polymeric materials), Hanser-Verlag Munich, Vienna 1983, pp. 103/105
- [8.27] WALZ, K.: Tellerfedern aus Kunststoff (Plastic disk springs), *Konstruktion Elemente Methoden* (1969) No. 1, pp. 58/63
- [8.28] Schwingungsdämpfung mit Cellasto (Damping vibrations with Cellasto), Elastogran – Kunststofftechnik brochure, Lemförde
- [8.29] GÖTTE, T., R. JACOBI and A. PUCK: Zur Entwicklung von Nutzfahrzeug-Blattfedern aus Faser-Kunststoff-Verbunden (On the development of leaf springs for utility vehicles from fiber-plastic composites), *Kunststoffe* 75 (1985) 6, pp. 355/361
- [8.30] JACOBI, R., M. MAIER and M. NEITZEL: Zum Stand der Entwicklung von Bauteilen aus Verbundwerkstoffen (Status of developments in structural parts made from composite materials), paper presented at the “Verstärkte Plaste” conference Oct. 16/17, 1990, Dresden
- [8.31] FROMMANN, H. and B. KIRKHAM: Entwicklung und Serieneinsatz einer Kunststoff-Blattfeder am Beispiel der Corvette, in: Kunststoffeinsatz im Automobilbau (Development and series production of a plastic leaf spring for the Corvette in: Employment of plastics in automotive engineering), VDI-Verlag Düsseldorf 1984
- [8.32] SCHNEIDER, W.: Wärmeausdehnungskoeffizienten und Wärmespannungen faserverstärkter Kunststoffe, in: Kohlenstoff- und aramidfaserverstärkte Kunststoffe (Coefficients of thermal expansion and thermal stresses in fiber-reinforced plastics in: Carbon- and aramid-fiber reinforced plastics), VDI-Verlag, Düsseldorf 1977
- [8.33] GÖTTE, T., R. JACOBI and A. PUCK: Grundlagen der Dimensionierung von Nutzfahrzeug-Blattfedern aus Faser-Kunststoff-Verbunden (Principles of the dimensioning of utility vehicle leaf springs made from fiber-plastic composites), *Kunststoffe* 75 (1985) 2, pp. 100/104
- [8.34] Filmgelenke aus technischen Kunststoffen (Integral joints made of engineering plastics), brochure No. B.3.5, Hoechst
- [8.35] Technische Information für Experten (Technical Information for Experts) No. 02/96, BASF
- [8.36] WIESINGER, W.: Patentierte Schnappscharniere aus Kunststoff (Patented snap-fit hinges made from plastic), *Kunststoffe – Plastics* 19 (1972) No. 1, pp. 23/24

9 Mechanical Fasteners

The classical method of mechanical fastening using a metal bolt and a metal nut is comparatively unimportant when joining polymeric materials. Specific advantages, such as the ability to achieve a high and constant force cannot be exploited and such joints require many individual parts making the assembly operation relatively labor-intensive.

Creep or loss of prestress is a common problem when metal fasteners are used to assemble plastic parts. In order to keep the loss of prestress as low as possible, the following guidelines should be adhered to.

A significant reduction of contact pressure can be achieved by means of wide washers or similar hardware.

Transverse strain should be reduced to achieve a largely hydrostatic state of stress (provide lateral support to keep prestressed wall thickness low).

Creep in the polymeric material and differences in dimensions caused by differential thermal expansion of the bolt and the plastic part can be counteracted most reliably using special bolts (Figure 9.1) or metal sleeves (Figure 9.2) for the direct absorption of the assembly stress.

Figure 9.3 shows some common commercial metal casings which are inserted into cylindrical holes in plastic parts. They are split and easily compressed during assembly. They must be a few tenths of a millimeter longer than the overall thickness of the plastic part so that the force flux is transmitted to the metal inserts, not the plastics parts themselves.

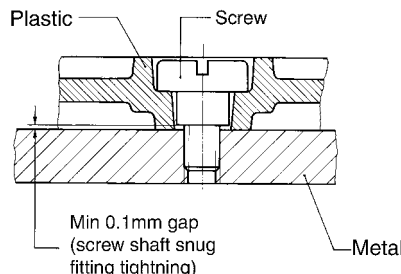


Figure 9.1 Fastening a plastic part using a machine screw with a shoulder

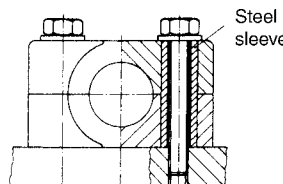


Figure 9.2 Assembly of a bearing block with screw force supported by a steel sleeve [9.1]

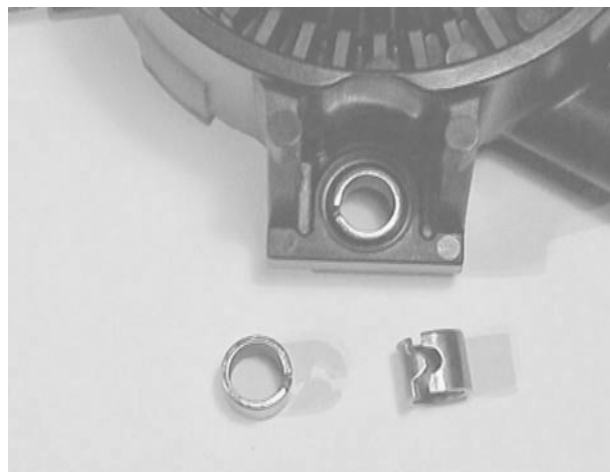


Figure 9.3 A low-cost and acceptable solution can be achieved using split, flexible sleeves that are inserted in cylindrical holes and are a few tenths of a millimeter longer than the overall wall thickness of the plastic parts

9.1 Molded Threads and Threads Produced by Machining

9.1.1 Screws and Bolts Made of Polymeric Material

Screws and bolts made of polymeric materials are more likely to be used for special purposes than for standard friction-based joints. The comparatively low strength, high coefficient of thermal expansion, and tendency to creep (to a degree dependent upon the polymeric material) impose clear limits for polymeric fasteners.

Figures 9.4 and 9.5 provide an initial indication of the load-bearing capacity of injection-molded screws made from dry PA 66 and POM at different temperatures. They relate to fracture loads under short-term, dynamic loading. As a general rule of thumb, approx. 25 to 30% of these values may be taken as the permissible design load.

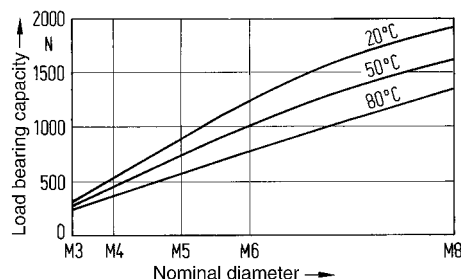


Figure 9.4 Maximum load-bearing capacity of injection-molded screws made from dry PA 66 [9.2]

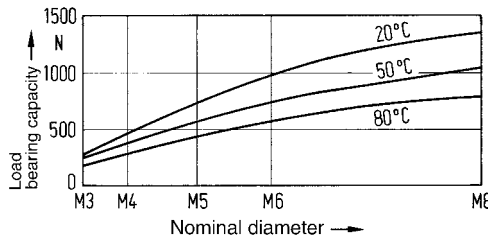


Figure 9.5 Maximum load-bearing capacity of injection-molded screws made from POM

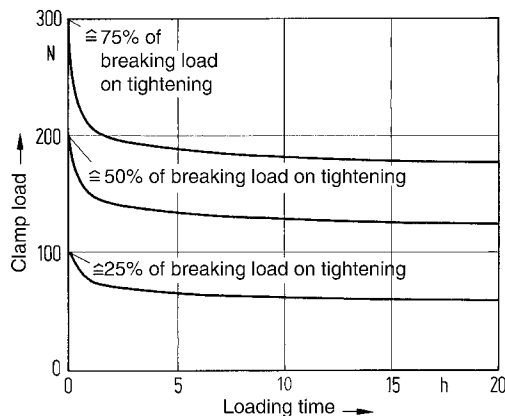


Figure 9.6 Clamp load as a function of time for PA 66 screws tightened to different stress values at room temperature [9.2]

Figure 9.6 shows the loss of clamp load for PA 66 screws tightened to different stress values. Stress relaxation begins to occur immediately after the initial tension has been applied. The clamp load value decreases to almost half its initial value after a relatively short time. At higher temperatures, the rate of stress relaxation is even more pronounced.

Reference should be made to [9.2, 9.3] for more detailed studies on the performance of screws made from polymeric materials.

As mentioned above, the use of screws made of polymeric materials is common in special applications. This is justified based on other properties of the polymeric materials. Polymeric mechanical fasteners are used in applications in which there are requirements for

thermal or electric insulation, corrosion resistance, color matching, or color identification.

Screws made from polymeric materials are useful as sensitive control elements. The fine flash resulting from mold parting on the longitudinal axis of the thread helps give these screws self-locking characteristics (see also Section 1.1.2, Figure 1.11).

9.1.2 Injection-Molded, Blow-Molded, and Machined Threads

Cutting threads in unreinforced polymeric materials is technically possible, but for cost reasons, this is done only for limited production or the production of single units, e.g., in prototype construction from semifinished parts or stock.

The achievable extraction or pull-out force F_E for a metal threaded fastener in a plastic part may be estimated simply and relatively precisely using Eq. 9.1 (see also Section 5.2.3.2).

$$F_E = d_o \cdot \pi \cdot l_s \cdot \tau_Y \quad (9.1)$$

where

d_o = Outer diameter of screw

l_s = Length of engagement

τ_Y = Failure shear stress $\approx \sigma_Y / \sqrt{3}$ to $\sigma_Y / 2$

Ideally, the shape of thread on the fastener has a low included angle, because this gives rise to smaller radial forces. In this respect, a buttress thread, trapezoidal, or round thread is favorable. Such thread shapes are also standardized for threaded closures for blow-molded plastic containers in DIN 6131.

9.2 Threaded Inserts

9.2.1 Encapsulated Threaded Inserts

When metal inserts (usually brass or aluminum) with an internal machine thread and a profiled outer contour are positioned in the injection mold and overmolded, a pretensioned form fit between the threaded insert and the polymeric material is achieved because of shrinkage. This yields a stable thread that can be assembled repeatedly. The shape of the outer profile on the insert should have features that run perpendicular to the stresses acting under load. Therefore, a hexagonal profile is not optimum (see also Section 11.3.3.3). Profiles with circumferential grooves provide improved part-out resistance.

The manual positioning of the inserts in the mold is costly and can increase the cycle time; therefore, automated insertion of the insert(s) into the mold should be considered.

9.2.2 Threaded Inserts Embedded by Ultrasound

Metal parts can be rapidly and firmly embedded in thermoplastic polymeric parts with the aid of ultrasonic technology. The inserts are ultrasonically vibrated and pressed into undersized holes or hollow bosses. At the contact surface, between the polymeric material and the metal insert, the frictional energy liberated plasticizes the thermoplastic and allows the metal insert's external features to penetrate into the material. The melt flows around the features (corruga-

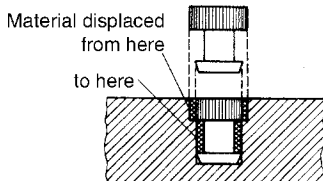


Figure 9.7 Displacement of material when an insert is embedded by ultrasonic vibration

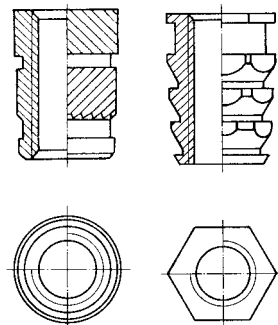


Figure 9.8 Threaded metal inserts suitable for ultrasonic insertion

tions and undercuts) and encapsulates the sides of the metal part in a largely stress-free manner after the area has cooled.

In order to ensure that there is sufficient material available to fill all of the insert's external features, the drilled or molded hole must have a suitably undersized diameter. The principle of ultrasonic insertion is shown in Figure 9.7. Figure 9.8 shows typical threaded inserts suitable for ultrasonic embedding.

Ultrasonic insertion equipment is needed for the secondary operation. The exposure time to the ultrasonic energy is usually less than one second; however, the handling of the parts can be time-consuming.

ABS, PC, PS, and PVC are very suitable material candidates for the ultrasonic insertion process. While semi-crystalline thermoplastics, such as PA and POM, are also suitable, the process is less commonly used for PE and PP parts.

9.2.3 Press-In Threaded Inserts

Inserts can also be pressed into plastic parts to provide threads. Threaded metal inserts, which are pushed mechanically into place, are usually provided with a longitudinal knurled surface for securing them in the radial direction and with a collar for securing them in the axial direction (see Figure 9.9). The inserts are pushed into undersized drilled or molded holes or hollow bosses.

Rigid amorphous materials, such as general purpose polystyrene (PS), styrene-acrylonitrile (SAN), or polycarbonate (PC) are not suitable for this method, because of their stiffness and susceptibility to stress cracking. On the other hand, good results can be achieved with elastomer-modified polymeric materials (SB, ABS, etc.) and with semi-crystalline polymeric materials such as PA, PA GF, POM, PBT, and glass-fiber reinforced PBT. Although HDPE is suitable in principle, its low rigidity results in limited transmission of torsional and pull-out forces.

The maximum tightening torques for pressed-in inserts can be calculated theoretically. See Sections 5.2.3.2 (Figure 5.9) and 11.3.3.3.

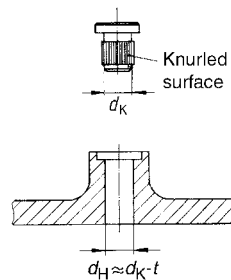


Figure 9.9 Metal threaded insert with collar and longitudinal knurled surface (t = knurling depth) [9.1]

9.2.4 Expansion Inserts

Expanding threaded inserts can also be used with molded or fabricated plastic parts. They are provided with two or more axial slits. When the split inserts are pressed into the predrilled or molded holes, the various segments flex, leading to low insertion force. The insert segments are then spread open by an assembly tool or, depending on the system, directly by the machine screw that is driven into the threaded hole so that it anchors itself in the polymeric material. The outer surface of the segments typically has cross-knurling (Figure 9.10, left) or rings (Figure 9.10, center and right).



Figure 9.10 Expanding threaded inserts

Fitting is quick and easy and requires no expenditure on special equipment.

9.2.5 Screw-In Inserts

Self-tapping inserts are slightly conical at their ends and have cutting ridges or flights (see Figure 9.11) on the external surface. The insert cuts threads in the polymeric material as it is driven into a drilled or molded pilot hole. A screwdriver-like tool is used to drive the self-tapping insert into the pilot hole.

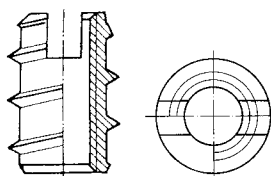


Figure 9.11 Self-tapping insert with cutting ridges or flights

9.2.6 Inserts Made of Polymeric Materials

Inserts made from glass-fiber reinforced polymeric materials are sometimes used in place of metal inserts. They are particularly suitable for applications where recyclability is important. They are commonly used as self-tapping inserts or as ultrasonic inserts. They are available in PA, PC, PP, and SB in sizes from M3 to M8. Figure 9.12 shows an insert for ultrasonic inserting and the blind pilot hole in which it is inserted. The extraction forces achievable using inserts made of glass-fiber reinforced PA 6 are about the same as those of hot-embedded brass inserts [9.12].

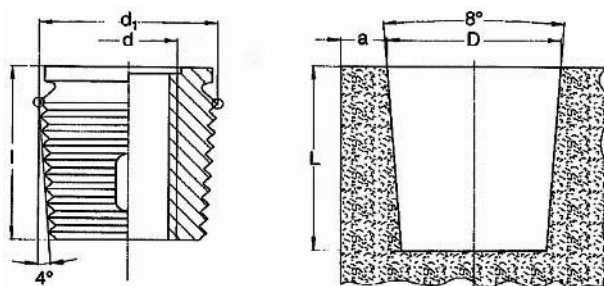


Figure 9.12 Glass-fiber reinforced thermoplastic insert for ultrasonic insertion
(Photograph: Böllhoff, Bielefeld)

9.2.7 Comparative Evaluation of the Various Inserts

There is a very large number of parameters or variables determining the economic efficiency of the various types of inserts. In addition, the mechanical quality of the joint produced with the different inserts is also difficult to quantify. This makes quantitative comparisons extremely difficult. Generally, it can be stated that high strength requires high equipment costs. Table 9.1 provides some guide lines for the qualitative evaluation of some threaded inserts and information about the receiving or pilot hole diameters and boss wall thicknesses [9.5].

Table 9.1 Qualitative evaluation of various threaded inserts with recommendations on core hole diameter and wall thickness of (weld-line-free) screw eyelets [9.5]

Insert type	Method of incorporation/ fixing in place	Equipment needed	Special features	Geometric and mechanical characteristics	Recommended hole diameter [mm]			Recommended wall thickness (boss) [mm]		
					M 4	M 5	M 6	M 4	M 5	M 6
Form R (DIN 16 903)	Overmolding/shrinkage stresses and undercuts	Injection-molding machines – inserts must be placed in position – disadvantageous for high piece numbers	Hexagonal design (risk of stress cracking) Inserts closed, hence distinct limit on screw-in depth	Average to high extraction forces due to deep undercut; average shearing moments; high space requirement; relatively large external diameter	–	–	–	> 3	> 3.3	> 3.5
Form S (DIN 16 903)	As for Form R	As for Form R	Round design with longitudinal knurling, otherwise as for form R	Low extraction forces, high shearing moments due to knurling	–	–	–	> 2.5	> 2.8	> 3
®Hit-Sert 1 (Figure 9.8, right)	Partial fusion of plastic by means of ultrasound or heat. Pressed in. Low shrinkage stresses/ flow around undercuts	Ultrasonic heating unit or hot-embedding machine	Short cycle times; noise due to ultrasonic unit Longer cycle times; noiseless operation	Conical shape with hexagonal profile of outer contours; little sensitivity to core hole variation due to conical shape	8.1					> 3
®Hit-Sert 2 (Figure 9.8, left)	Incorporation as for Hit-Sert 1 Diamond knurling, annular groove and longitudinal knurling; low notch stresses	Ultrasonic heating unit or hot-embedding machine as for Hit-Sert 1	As for Hit-Sert 1	Conical shape facilitates fitting into the receiving bore; round outer contours High shearing moments and high extraction forces. Core hole variations as for Hit-Sert 1	5.5	6.7	8.0	> 2.5	> 2.7	> 3
®Sonic-Lok	Fitting as for Hit-Sert 1 und 2 but cylindrical receiving bore/counter-rotating gear rings	Ultrasonic heating unit or hot-embedding machine	As for Hit-Sert 1	Average to high extraction forces and shearing moments; round outer contours; relatively insensitive to core hole variations	5.5	6.5	7.9	2.5	2.7	> 3
®Mubux-A	Cold press-fitting/ 3 parallel gear rings; plastic stressed beyond the yield point	Press or lever-type hand device	Several parallel gear rings	Moderate to average extraction forces and shearing moments	5.3					> 2.5

Table 9.1 (continued)

Insert type	Method of incorporation/ fixing in place	Equipment needed	Special features	Geometric and mechanical characteristics	Recommended hole diameter [mm]			Recommended wall thickness (boss) [mm]		
					M 4	M 5	M 6	M 4	M 5	M 6
®Ensat IN 22 b (Figure 9.11)	Insert is screwed in/ self-tapping thread; low radial stresses	Low piece numbers by hand using screw-in spindle; high volumes by means of automatic or semiautomatic tools	Fixing thread cuts itself on turning due to cutting edges (slits)	High extraction forces; little security against unscrewing; suitable for repairs; relatively high requirement for space and relatively large outer diameter	5.7	7.0	8.7	> 2	3	4
®Dodge-Standard	Cold press-fitting/ stretcher plate and diamond knurling (radial stresses)	Single or multiple spindle, press	Insert body slit 4 ways in region of diamond knurling; expansion effect by pressing stretcher plate down to the base with a fitting spindle; securing against falling out; insert closed hence screw-in depth distinctly limited	Average extraction forces; high shearing moments; relatively high wall thickness required	5.2	6.3	7.8	> 3	3.5	4
®Mubux E	Cold press-fitting/ gear ring and grooves; threaded insert is stretched when screw is screwed in (radial stresses)	Fitting spindle, press	Slotted threaded insert, screw must be screwed in to the base	Moderate extraction forces and shearing moments; can be improved by constructing with 2 gear rings	5.7			> 2.5		
®Banc-Lok	Cold press fitting/ 5 cutting rings and longitudinal knurling to secure against twisting (radial stresses)	Fitting spindle, press	As for Mubux E	Average extraction forces; different numbers of cutting rings possible	7.8				3.5	
®Spred-Sert	Cold press fitting/ anchor rings and longitudinal knurling (radial stresses)	Fitting spindle, press	As for Mubux E	Moderate to average extraction forces and shearing moments	5.3			> 2.5		

9.2.8 Behavior under Dynamic Loads

Test results under dynamic loading are rare because of the high costs of conducting dynamic tests. Figure 9.13 shows Wöhler curves for two types of inserts.

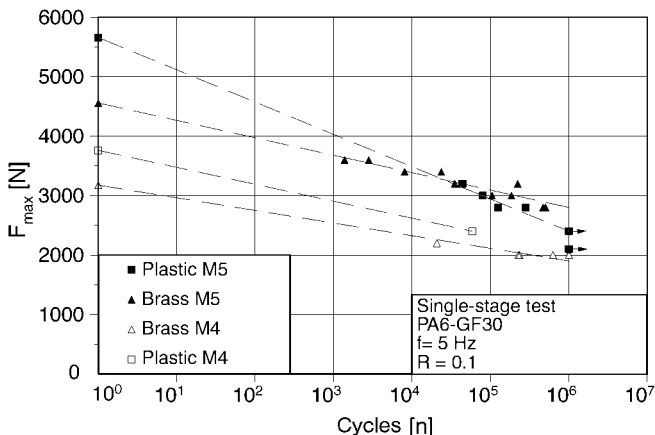


Figure 9.13 Wöhler curves from dynamic single-stage tests on thermally embedded brass inserts and ultrasonically embedded plastic inserts in glass-fiber reinforced PA 6 GF 30 [9.12]

9.3 Self-Threading Screws

Self-threading screws are a widely used assembly method for plastic parts. Historically, this method of assembly has been predominantly used for joints under relatively low loads. However, today there is a great range of screw geometries developed especially for polymeric materials and with proper part design allowing the production of joints that can withstand much higher loads. A summary of the most important variables influencing joints and the characteristics, which they in turn affect, is presented in Figure 9.14.

The self-threading screw assembly process consists of a thread-forming (or sometimes cutting) process, initiated by the screw and a frictional process between the thermoplastic polymeric material and the thread (see Figure 9.15). Thread-cutting screws tend to be used with more rigid, brittle plastics, while thread-forming screws are used with more ductile plastics. Due to high local deformation and frictional processes, the plastic material is additionally subjected to thermal stress in the region close to the thread. During tightening of the screw, an initial stress is achieved in the material surrounding the screw threads. This stress tends to decrease again over time (and with temperature) due to creep and relaxation processes occurring in the plastic.

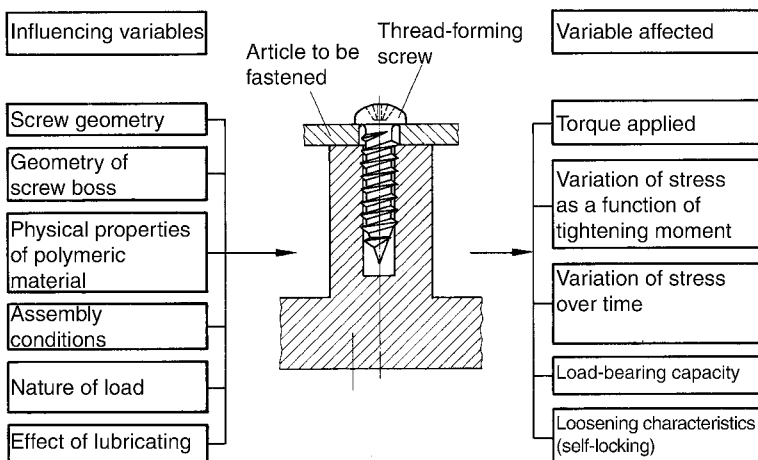


Figure 9.14 Variables influencing joints made with self-threading screws [9.4]

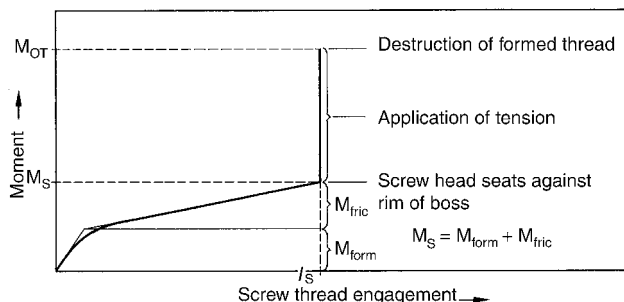


Figure 9.15 Schematic illustration of the self-threading screw assembly process [9.4]

9.3.1 Screw Shapes and Geometries

An ideal self-threading screw thread for use with plastic materials should fulfill the following criteria:

- Low radial expansion;
- Low screw-in torque and high over-turn torque;
- High lateral overlap of thread; and
- Tight tolerances.

Sheet metal screws intended for joining metal sheets having a thread in accordance with DIN 7970 are commonly used with plastic parts but they do not adequately fulfill these requirements and as such do not result in the optimum joint.

It is better to use types of self-threading screws specially developed for polymeric materials (or wood). These have a small included thread angle of 30 to 40°, a smaller root diameter, and hence a greater thread height and greater pitch. Some typical thread geometries are shown in Figure 9.17.

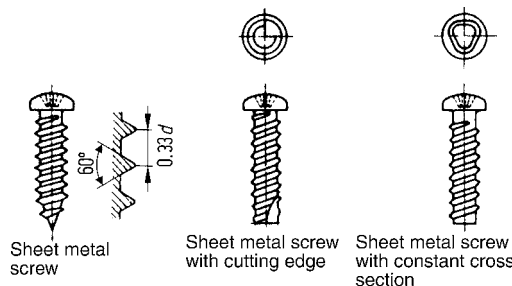


Figure 9.16 Sheet metal screw threads [9.6]

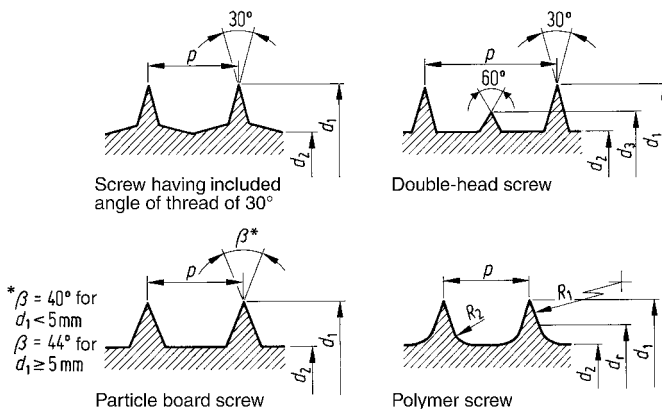


Figure 9.17 Typical thread shapes developed for use in thermoplastic polymeric materials [9.4]

Screws with cutting flights (*i.e.*, thread-cutting screws) (see, for example, Figure 9.16, center) reduce drive torque and boss expansion (and related hoop strain), but not necessarily allow repeat assembly. They are intended for the assembly of very brittle or glass-fiber reinforced thermoplastic polymeric materials as well as rigid thermosets, which are susceptible to cracking at low tensile strains.

A screw geometry with an asymmetric thread profile (see Figure 9.18) has been specially developed for thermoset molding compounds (*e.g.*, type 31, type 181, etc.). The low ductility of glass-fiber reinforced or filled thermosets necessitates the use of a screw with a cutting flight.

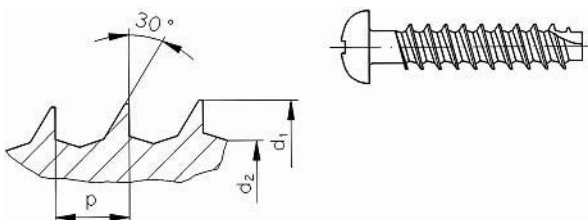


Figure 9.18 Asymmetric thread profile of a thread cutting screw for use with rigid thermosets [9.7]

9.3.1.1 Included Thread Angle

Threads with a small included thread angle make it possible to reduce both the screw-in torque as well as the radial force associated with assembly. This reduces the stress on the plastic boss and, as a result, boss wall thickness can be kept relatively small.

9.3.1.2 Self-Locking Screw Threads

Screws become self-locking when the axial force generates no torque, *i.e.*, when the pitch angle is smaller than the angle of friction. According to [9.8], the self locking limit occurs at thread pitch angles of 8 to 10°. A coating of lubricating agent on the screw has a positive effect on the screw-in torque but it reduces the tendency for self-locking behavior. Unwanted loosening due to vibration is also facilitated when lubricants are used.

Self-locking performance can also be increased by altering the screw geometry. This is the case in special screws whose cross section is not circular, but rather is designed as an orbiform curve (see Figure 9.16, right).

9.3.2 Design of the Screw Boss

Self-threading screws are normally received by a hollow boss (usually with a blind hole) extending up from the nominal wall of the plastic part as shown in Figure 9.19. To facilitate demolding, the boss usually has conical draft angles of 0.5 to 1°.

As in the case of ribs (see also Chapters 7 and 10), accumulations of material (*i.e.*, local increases in wall thickness) inevitably occur at the base of the boss, which can cause sink marks, voids, or warpage. Therefore, the core that forms the blind pilot hole should extend about a third of the way into the nominal wall at the base of the boss. Further improvement is obtained by extending the radius around the base of the boss into the surrounding wall (see Figure 9.20), but this is achieved at the expense of somewhat higher mold costs.

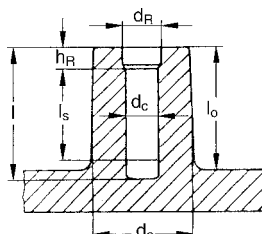


Figure 9.19 Typical self-threading screw boss geometry showing key dimensional parameters

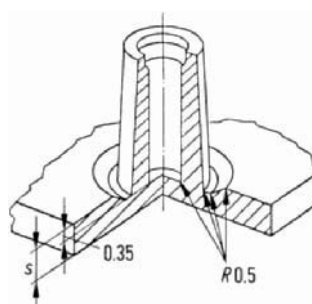


Figure 9.20 Self-threading screw boss with an extended pilot hole recessed and radius (fillet) for reducing sink marks in the base surface opposite the boss [9.9]

9.3.2.1 Screw Engagement Depth

For optimum strength, the screw engagement depth should be as great as possible. The upper practical limit of engagement is determined by the strength of the screw itself. A rule of thumb, the screw engagement depth l_s given by various authors [9.1, 9.6, 9.8 and 9.10] may be formulated as follows:

$$l_s = (2 \text{ to } 2.5) \cdot d_1 \quad (9.2)$$

where

d_1 = Outer diameter of the screw

This empirical relationship is substantiated by measurements, such as those presented in Figure 9.21. While the screw driving (insertion) torque increases slightly with screw engagement depth, the “destruction torque” and the extraction force increase distinctly in proportion with the screw engagement depth. A large difference in these two values is characteristic of a high quality joint.

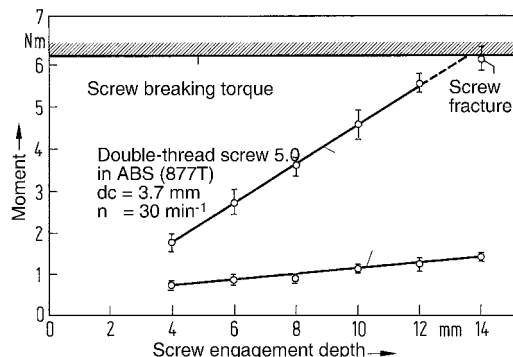


Figure 9.21 Screw engagement torque and destruction (stripping) torque as a function of screw engagement depth [9.4]

In contrast to joints held together with metal bolts and metal nuts, all pitches in the thread of the screw support an applied load more or less uniformly. This has been confirmed by photoelastic studies [9.4].

9.3.3.2 Boss Pilot Hole Diameter

The pilot hole diameter for a particular self-threading screw and plastic material combination is a critical variable. In addition, different pilot core pin cross-sectional shapes (circular, square, triangular, hexagonal, etc.) are occasionally discussed and employed. However, in order to avoid areas of concentrated stress and to ensure that the joint has high load-bearing capacity, circular cross sections should be used preferably for the pilot hole.

The following empirical expression for pilot hole diameters has been established:

$$d_C = 0.8 \cdot d_1 \text{ to } 0.9 \cdot d_1 \quad (9.3)$$

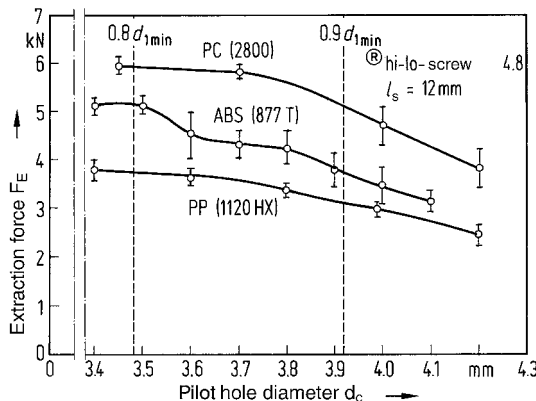


Figure 9.22 Self-threading screw extraction force (pull-out force) for various materials as a function of pilot hole diameter [9.4]

where the smaller value applies to ductile plastic materials and the higher value to more brittle plastic materials. This relationship has proved to be reliable. Figure 9.22 shows that high extraction forces are achieved using pilot hole diameters in this range.

When pilot hole diameters in this range are used, the stress on the boss remains at tolerable levels. Values below this range should not be used, even if a gradual increase in extraction force is associated with the smaller diameter.

9.3.2.3 Boss Relief Bore

It is extremely important that the pilot hole diameter is enlarged at the open end of the boss as shown in Figure 9.19. This is referred to as the relief bore or lead-in. It is advantageous for “starting” the screw during assembly, but it is also needed to relieve stress at the upper boss region (open end), which is under pressure from the screw head and the screw flights in that region. The following rules apply to the sizing of this relief bore.

$$d_R = 1.1 \cdot d_1 \quad (9.4)$$

$$h_R = 0.5 \cdot d_1 \quad (9.5)$$

9.3.2.4 Boss Outer Diameter

The outer diameter of the self-threading screw boss can be determined in a number of ways, but ensuring the boss has sufficient shear strength relative to the thread shear strength is important. The relevant equation for this is:

$$d_{O1} = \sqrt{\frac{4}{\sqrt{3}} \cdot d_1 \cdot l_s + d_1^2} \quad (9.6)$$

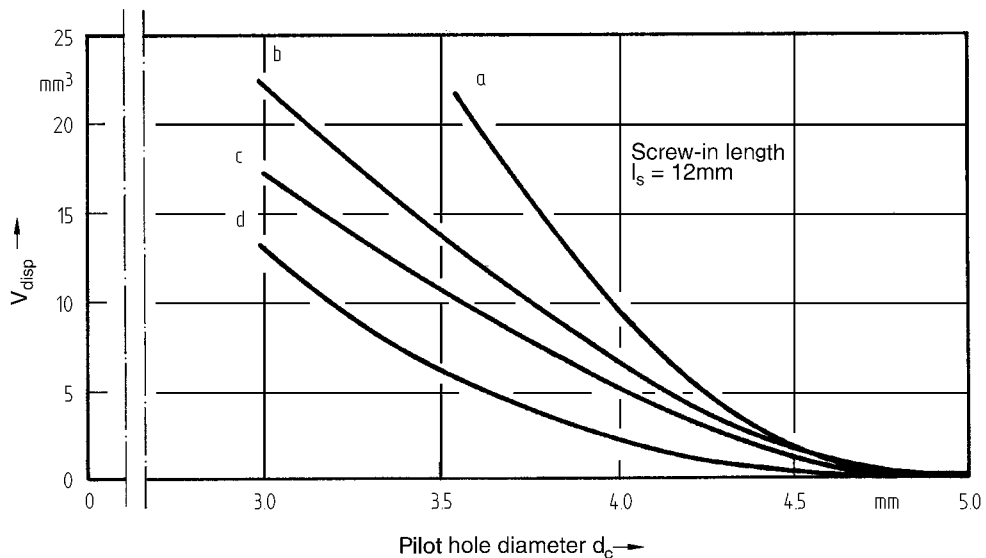


Figure 9.23 Volume displacement of screw as a function of the core hole diameter [9.4]

- a = Sheet metal screw, $d_1 = 4.8\text{ mm}$
- b = Particle board screw, $d_1 = 4.8\text{ mm}$
- c = Screw having an included angle of thread of 30° , $d_1 = 5\text{ mm}$
- d = Double-threaded screw, $d_1 = 4.8\text{ mm}$

Equation 9.6 may yield outer diameters that are unreasonably low when screw-engagement depths are small.

Therefore, the state of stress produced by the tightened screw has to be taken into account additionally. Depending on the screw geometry, a greater or lesser volume is displaced when the screw is driven into the boss. Some of this material flows into the interstices between the screw threads. There is also an increase in boss diameter. In this context, Figure 9.23 clearly shows the advantage of specialty screws designed for use with plastics over standard sheet metal screws.

A simple model* can help to determine the increase in the outer diameter of the boss as a result of driving the screw into the boss. According to this, the minimum outer diameter required for a given value of acceptable circumferential or hoop strain is given by:

$$d_{O2} = \sqrt{\frac{1}{3} \cdot \frac{8 \cdot d_C \cdot (r_S - d_C/2)}{\epsilon} - d_C^2} \quad (9.7)$$

* The simplified model according to [9.4] assumes the boss is a thick-walled hollow cylinder, open at both ends, and the displaced volume is being replaced by an unyielding steel bolt having the radius r_S (Eq. 9.8), which is pushed into the pilot hole of the boss. This view takes into account neither the complex processes of the (desirable) flow of the plastic material into the free interstices between the thread nor the inhomogeneous distribution of stress in different directions.

where

$$r_s = \sqrt{\frac{V_{\text{disp}}}{\pi \cdot l_s} + \left(\frac{d_C}{2}\right)^2} \quad (9.8)$$

V_{disp} = Displaced volume (Figure 9.23)

ϵ = Circumferential strain ($\epsilon_{\text{perm}} \approx 0.3$ to 0.6% depending on the material's elongation at break or strain at yield point, susceptibility of the material to stress cracking, tightening force applied, etc.)

Equation 9.6 focuses on the effect of an external force (torque) while Eq. 9.7 considers the internal stresses caused by the screw. The greater of the two diameters calculated by the two methods should be used as an appropriate value for the outside diameter of the boss.

9.3.3 Calculation of Key Variables in a Self-Threading Screw Joint

9.3.3.1 Screw Drive Torque

The screw drive torque M_s requirements for a self-threading screw being driven in a hollow plastic boss is influenced by both the thread-forming torque and the friction torque as shown in Figure 9.15. These can be estimated on the basis of the simplified assumptions of Eq. 9.9.

$$M_s = \frac{\sigma_Y \cdot (d_1 - d_C)}{\sqrt{3}} \left[\tan \frac{\beta}{2} + \sqrt{\left(1 + \tan^2 \frac{\beta}{2}\right) \left(\frac{d_1 + 2d_C}{3} \cdot \pi\right)^2 + p^2} \cdot \right. \\ \left. \cdot \left(\frac{d_1 + 2d_C}{6} \right) + \frac{(1 + \alpha) \cdot f \cdot l_s \cdot (d_1 - d_C)}{4 \cdot p \cdot \cos \frac{\beta}{2}} \sqrt{\left(\frac{d_1 + d_C}{2} \cdot \pi\right)^2 + p^2} \right] \quad (9.9)$$

where

σ_Y = Yield stress of the polymeric material in MPa

β = Included thread angle in degrees

α = 0.0993 for $\beta = 30^\circ$

p = Thread pitch (cf. Figure 9.17) in mm

f = Coefficient of sliding friction ($f \approx 0.2$ to 0.3)

Unfortunately, the characteristic physical property values in Eq. 9.9 are associated with great uncertainties. Some of these uncertainties are due to the fact that at high screw-in speeds the polymeric material may soften and even melt in some places.

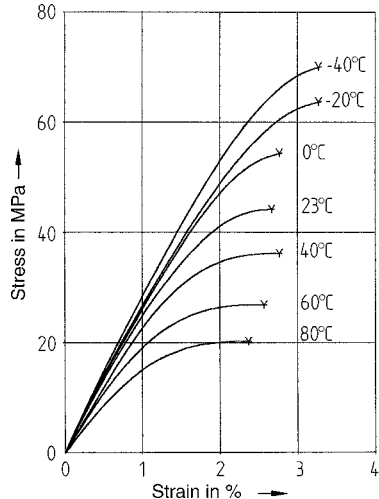
Example

A screw joint is produced using a thread-forming screw with an included thread angle of 30° , it should attain an extraction force of at least 3 kN at an operating temperature of 40°C ; material: ABS (967 K).

The following variables need to be determined:

1. The screw diameter
2. The pilot hole diameter
3. Outer diameter of the boss

1. From CAMPUS, Multipoint (BASF) the failure stress for ABS (Terluran 967 K) at 40°C is given as 36 MPa.



According to Eq. 9.2, $l_s \approx 2 \cdot d_1$

Rearranging Eq. 9.12 in terms of d_1 yields:

$$F_E = \frac{\sigma_Y}{\sqrt{3}} \cdot d_1 \cdot (2 \cdot d_1) \cdot \pi \rightarrow d_1 = \sqrt{\frac{F_E \cdot \sqrt{3}}{\sigma_Y \cdot \pi \cdot 2}} = \sqrt{\frac{3000 \cdot \sqrt{3}}{36 \cdot \pi \cdot 2}} = 4.8 \text{ mm}$$

The next largest standardized **screw diameter** is **5.0 mm**.

2. The **pilot hole diameter** is given in Eq. 9.3 as $0.8 \cdot d_1 = 0.8 \cdot 5 = \mathbf{4.0 \text{ mm}}$.
3. The outer diameter of the boss is calculated from Eqs. 9.6 and 9.7.

Equation 9.6 yields:

$$d_{O1} = \sqrt{\frac{4}{\sqrt{3}} \cdot d_1 \cdot l_s + d_1^2} = \sqrt{\frac{4}{\sqrt{3}} \cdot 5 \cdot 10 + 25} = 11.85$$

Using V_{disp} from Figure 9.23, r_s is calculated as:

$$r_s = \sqrt{\frac{V_{\text{disp}}}{\pi \cdot l_s} + \left(\frac{d_C}{2}\right)^2} = \sqrt{\frac{6.3}{\pi \cdot 10} + \left(\frac{4}{2}\right)^2} = 2.05$$

and Eq. 9.7 yields d_{O2} as:

$$d_{O2} = \sqrt{\frac{1}{3} \cdot \frac{8 \cdot d_C \cdot (r_s - d_C/2)}{\varepsilon} - d_C^2} = \sqrt{\frac{1}{3} \cdot \frac{8 \cdot 4 \cdot (2.05 - 2)}{0.006} - 25} = 8.97$$

The larger value is taken for the **outer diameter of the boss** = **12 mm**.

9.3.3.2 Destruction Torque

Equation 9.10 has proved suitable [9.11] for estimating the destruction or stripping torque M_{OT} .

$$M_{OT} = \frac{\sigma_y \cdot \pi \cdot d_1^2 \cdot l_s \cdot (p + \pi \cdot f \cdot d_1)}{2\sqrt{3}(\pi \cdot d_1 - f \cdot p)} \quad (9.10)$$

Equation 9.10 determines the moment occurring in the thread. The moment of friction between the head of the screw and the surface in contact with it (M_{HF}) must also be taken into consideration. This is given by:

$$M_{HF} = f_A \cdot F_T \cdot \frac{1}{4}(d_{HO} + d_L) \quad (9.11)$$

where

f_A = Coefficient of friction at screw head
(for steel/polymeric material $f_A \approx 0.2$ to 0.3)

F_T = Tensioning force (Eq. 9.14) in N

d_{HO} = Outer diameter of head in mm

d_L = Diameter of the screw receiving hole at the location of contact

Equations 9.10 and 9.11 provide the moments in Nmm.

9.3.3.3 Screw Extraction (Pull-Out) Force

The screw extraction or pull out force F_E may be estimated using Eq. 9.12.

$$F_E = \frac{\sigma_y}{\sqrt{3}} \cdot d_1 \cdot \pi \cdot l_s \quad (9.12)$$

Thus, when load requirements and screw engagement depth are specified in advance, and reduction factors (see Section 5.2.1.3) are taken into account, the necessary screw diameter d_1 can be calculated. Or, when the dimensions of the screw are specified in advance, the screw engagement depth l_s may be calculated.

When other criteria have to be met, e.g., requirements for electric heating devices, these too must be taken into account when sizing screws and bosses.

Behavior under Dynamic Load

Figure 9.24 shows examples of results from tensile fatigue experiments on self-threading screw joints made from PP as the polymeric boss material. Depending on the average load (static creep stress), trends become established in the Wöhler plots describing failure.

These test results show that it is justified in the case of relatively small loads to estimate the permissible average load using Eq. 9.12, taking reduction factors for static and dynamic loading

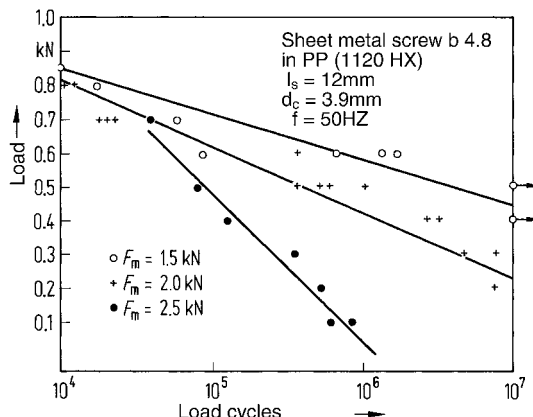


Figure 9.24 Wöhler plots for joints with PP self-threading screw bosses and a sheet metal screw under different median stresses [9.4]

into account. According to Section 5.2.1.3, $A_{\text{stat}} = 2$ and $A_{\text{dyn}} = 1.3$. In this case, an overall reduction factor $A_{\text{stat}} \cdot A_{\text{dyn}} = 2.6$ may be expected.

9.3.3.4 Tightening Moment and Tensioning Force

For most applications, the use of high tensioning (or tightening) forces is not recommended. On the one hand, an increased tensioning force results in higher stress on the self-threading screw boss. On the other hand, the higher the tightening force is, the more rapid is its decline over time due to stress relaxation. It is recommended that the tightening moment M_T be determined in accordance with Eq. 9.13.

$$M_T = M_S + K \cdot (M_{\text{OT}} - M_S) \quad (9.13)$$

The factor K should be between 0.2 and 0.5. It depends primarily on the accuracy of the screw-driving equipment and also on the expected variation in the torque-turn curves. For precision equipment (variation $\pm 3\%$) and low scatter, the factor 0.2 can be used. In such a case, the force required for the destruction of the thread by over-tightening is of the same order as that for the extraction force. This is illustrated in Figure 9.25 for assembling polypropylene parts with a double-helix self-threading screw (Figure 9.17).

It appears that at high screw-in speeds ($n = 570 \text{ min}^{-1}$) somewhat higher tensioning forces can be achieved. For purposes of estimation, however, it suffices to use the extraction force F_E calculated in accordance with Eq. 9.12 and to assume a linear relationship between the tensioning force F_T and the tightening moment M_T . If the tightening moment is determined by Eq. 9.13, then taking head friction into account this yields:

$$F_T = \frac{4 F_E \cdot K (M_{\text{OT}} - M_S)}{4 (M_{\text{OT}} - M_S) + F_E \cdot f_A \cdot (d_{\text{HO}} + d_L)} \quad (9.14)$$

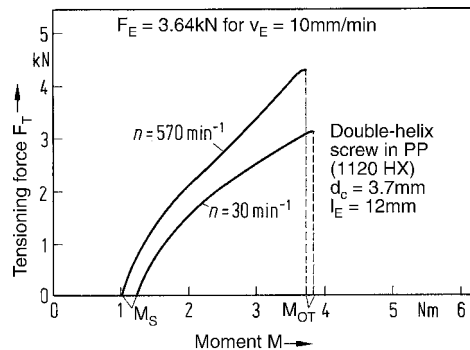


Figure 9.25 Tensioning force as a function of tightening moment

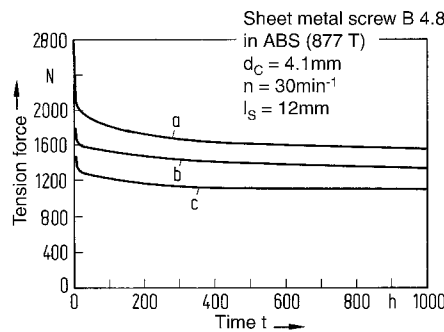


Figure 9.26 Reduction in tensioning force values over time [9.4]

Change of Tensioning Force over Time

The tensioning force applied by the tightening moment decreases over time and as a function of time and temperature due to relaxation of the polymeric material. Examples of this decrease are shown in Figure 9.26 for joints tightened to different torque levels.

It is apparent that, as the tensioning force increases, the rate of time-dependent loss of force increases. Thus, the difference in tightening force ΔF_{T0} at the start of the experiment at time $t = 0$ between Experiment a and Experiment c is 1,270 N. The tensioning force in Experiment c at time $t = 0$ is 54% of that in Experiment a. After an experimental duration of 1,000 h, the difference ΔF_{T1000} is only 500 N. After 1,000 h, the tensing force in Experiment c is about 70% of that in Experiment a. These experimental results indicate that the application of high tightening forces is not necessary in normal applications.

9.3.3.5 Assembly Conditions

In high volume production, precision screw-driving equipment affording high reproducibility of screw-in conditions are invaluable tools for producing high quality self-threading screw joints. This equipment typically has rotary speeds in the range of 600 to 800 min^{-1} , but they

can have rotational speed capability as high as 2,000 min⁻¹. As screwing speed increases, there is a tendency for the screw-in torque to decrease. This is more marked in amorphous thermoplastics than in semi-crystalline materials. This decrease in drive torque is explained by the increased production of heat and the related local softening of the plastic in contact with the screw.

The destruction torque at high screwing speeds does not decrease as rapidly as the screw-in torque and may even rise in some cases. The difference between them is likely to increase with screw driving speed. From this point of view, there is no disadvantage in using high screwing speeds for self-threading screws. It is, however, recommended that high screwing speeds should not be used for low screw-in depths.

It is important that the screwing operation is ended precisely at the appropriate tightening torque. Equation 9.13 is used for determining the appropriate tightening torque moment.

References

- [9.1] ERHARD, G. and E. STRICKLE: Maschinenelemente aus thermoplastischen Kunststoffen (Machine elements made of thermoplastic), Part 1, VDI-Verlag, Düsseldorf 1974
- [9.2] VDI-Richtlinie 2544: Schrauben aus thermoplastischen Kunststoffen (Screws made of thermoplastics), Beuth-Verlag, Berlin 1973
- [9.3] MÜLLER, K.: Stoffliche und konstruktive Gesichtspunkte für die Anwendung von Schrauben und Muttern aus Thermoplasten (Material and design considerations in the use of thermoplastic bolts and nuts), *VDI-Z 111* (1969), pp. 349/353, *VDI-Z 111* (1969), pp. 1328/1335
- [9.4] ONASCH, J.: Zum Verschrauben von Bauteilen aus Polymerwerkstoffen mit gewindeformenden Metallschrauben (On the joining together of components made of polymeric materials using thread-forming metal screws), Dissertation, University of Kassel 1982
- [9.5] EHRENSTEIN, G. W. and H. MOHR: Gewindeeinsätze in Acryl-Butadien-Styrol (ABS) (Thread inserts in acrylonitrile-butadiene-styrene (ABS)), *Verbindungstechnik* 9 (1977) 4, pp. 5/9
- [9.6] EHRENSTEIN, G. W. and J. ONASCH: Fügen von Kunststoffteilen mit gewindeformenden Metallschrauben (Joining plastic parts with thread-forming metal screws), *Verbindungstechnik* 13 (1981) 9, pp. 27/30
- [9.7] WEITZEL, S.: Formteile direkt verschrauben (Screwing moldings together directly), *Plastverarbeiter* 38 (1987) 12, pp. 48/53
- [9.8] GROSSBERNDT, H.: Direktschraubverbindungen an thermoplastischen Werkstoffen (Direct screwed joints in thermoplastic materials), *Kunststoffe* 73 (1983) 11, pp. 701/707
- [9.9] RECKER, H.: Vorteilhafte Gestaltung zum Erreichen optimaler Oberflächen in: Konstruieren mit thermoplastischen Kunststoffen (Good design for achieving optimum surfaces in: Designing with thermoplastics), VDI-Verlag, Düsseldorf 1986
- [9.10] EHRENSTEIN, G. W. and H. MOHR: Gewindeformende Schrauben für Kunststoffbauteile (Thread-forming screws for plastic components), *Verbindungstechnik* 11 (1978) 11, pp. 13/19
- [9.11] KNAPP, H. and H. MOHR: Verbinden von Kunststoffbauteilen mit gewinde-formenden Schrauben (Joining plastic components using thread-forming screws), BASF brochure, Ludwigshafen, B 600d (889) 1990
- [9.12] TOME, A., G. W. EHRENSTEIN and F. DRATSCHMIDT: Gewindeeinsätze aus Kunststoff (Plastic thread inserts), *Kunststoffe* 89 (1999) 5, pp. 72/79

10 Ribbed Structures

Ribs are an efficient design feature for increasing the rigidity and load-bearing capacity of structural parts subjected to flexural or torsional stresses. They provide an alternative to the use of thicker walls. As a result, consumption of material is reduced and production costs in injection molding are lowered. On the other hand, considerations favoring ease of production for ribbed structures are often diametrically opposed to those favoring a good stress distribution.

10.1 Comparison with Other Methods of Reinforcement

The flexural strength and stiffness of a plate is influenced by the modulus of elasticity of the material of which it is composed and by the geometrical moment of inertia of its cross section (or plate constant) as shown in Eq. 10.1.

$$D = \frac{E \cdot s^3}{12(1 - \mu^2)} \quad (10.1)$$

where

s = Thickness of the plate and

μ = Poisson's ratio

On this basis, the following possibilities are available for increasing stiffness or rigidity (see also Section 6.2):

- Increasing the modulus of elasticity;
- Increasing the wall thickness;
- Introducing corrugations or cambers; or
- Applying ribs.

10.1.1 Increasing the Modulus of Elasticity

Considerable increases in the rigidity of polymeric materials can be achieved in particular by means of inorganic fibrous reinforcing additives such as glass or carbon fibers (see also Sections 2.4.3 and 3.4). Nevertheless, the reinforcing effect of the fibers is relatively low because the fibers have only a linear effect on stiffness. Compared to an unreinforced thermoplastic part, it is possible to achieve the same level of rigidity using a glass fiber reinforced thermoplastic at about half the wall thickness as specified in Eq. 10.2.

$$\frac{s_{\text{unreinf}}}{s_{\text{reinf}}} = \sqrt[3]{\frac{E_{\text{reinf}}}{E_{\text{unreinf}}}} \quad (10.2)$$

10.1.2 Increasing Wall Thickness

Because the rigidity of a part increases with the third power of its wall thickness, an increase in wall thickness has a substantially greater effect than switching to a more rigid material. The longer process cycles in injection molding associated with thicker walls do not favor this approach. In addition, wall thicknesses greater than approx. 8 mm can only be achieved by injection molding in special cases.

Significantly greater wall thicknesses are achieved using modified injection molding processes, such as the structural foam molding method. This variant of injection molding makes use of a blowing agent additive, which causes the thermoplastic melt to foam in the mold so that the application of holding pressure through the gate is not needed. The in-mold pressurization is a result of the pressure of the foam. This yields a sandwich-like structure having a dense outer skin and an expanded foam core. The most suitable polymer for this method is impact-modified polystyrene, although the process can be used with many other thermoplastics.

The increase in rigidity brought about by the greater wall thickness for structural foam parts, however, is itself reduced somewhat by comparison with the conventional injection-molded material due to the fact that the rigidity of the structure is inversely proportional to the density of the foam (0.7 to 0.9 g/cm³) [10.1].

Other variants of the injection molding process, which allow the production of thick-walled sandwich structures include two-component injection molding and the internal gas pressure methods in which one injection unit first supplies the material for the outer layers of the part and a second injection unit supplies the material for the core. In the case of the internal gas pressure method, this second component is a gas.

Flat, double-walled parts may also be produced by the blow molding process. In this case, the blow-molded parison is not inflated to form a large-diameter hollow article, but is left as a

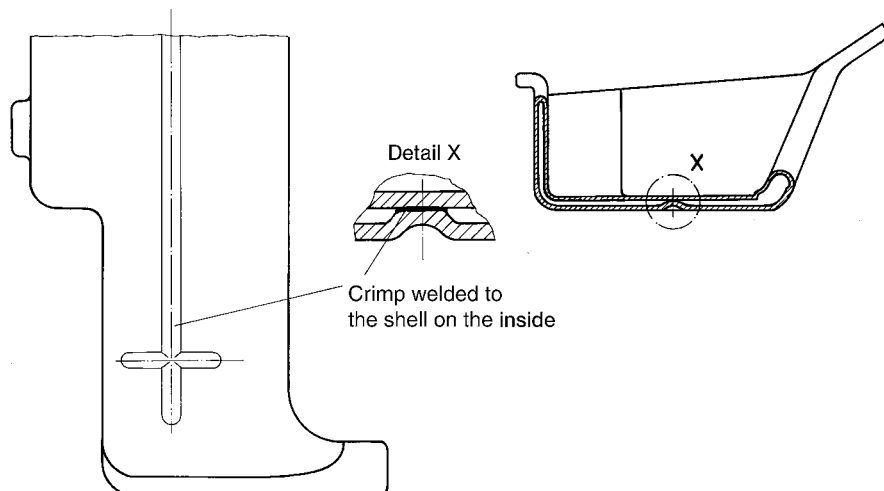


Figure 10.1 Section through a blow-molded, flat part with the embossed crimp (pinch-offs) welded on the inside [10.2]

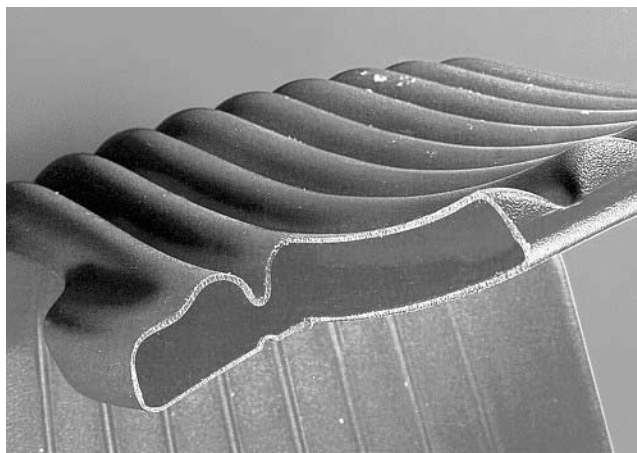


Figure 10.2 Blow-molded seat shell made of PP (1050). The corrugation and partial welding may be seen in the exposed section (Manufacturer: Fischer Söhne, Muri, Switzerland).

double walled shell-like part. In addition, the two walls can be welded together at pinch-off points distributed over the plane of the part. Examples of this are the container boxes in a refrigerator, seat shells, or the glove compartment for an automobile as shown in Figure 10.1. A further advantage of blow molded parts is their inherent toughness in comparison with injection-molded parts. The blow molding process requires polymeric materials of relatively high molecular weight, which generally have good toughness. This means that blow-molded parts are tougher than injection-molded parts of identical construction.

Another example is the blow-molded PP seat shell for a child's chair shown in Figure 10.2.

10.1.3 Crimps and Corrugations

Crimps and corrugations act as reinforcing elements and can substantially increase the rigidity of a part. Even a slight camber on a surface produces a marked increase in rigidity. Crimping and corrugating are the simplest method of stiffening thermoformed parts made from semifinished sheet material and for blow-molded parts.

Comparison of a corrugated surface with a ribbed surface of the same dimensions and weight (see Figure 10.3) clearly shows that the corrugated structure is much stiffer. In this example, the stiffness of the corrugated structure increases by a factor of 1.8.

While corrugated structures are very efficient, they have disadvantages compared to ribbed structures. These include:

- The corrugated surface has a less attractive appearance, unless the corrugations are deliberately exploited as a design feature; and
- Mold costs for corrugated injection molded parts are higher and any subsequent adjustments in height are much easier to carry out in the case of a ribbed structure.

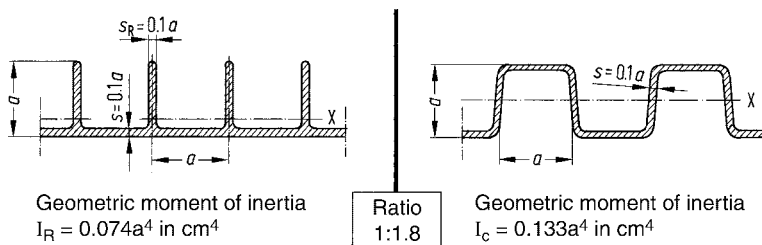


Figure 10.3 Comparison of rigidity for ribbed and corrugated surfaces
 $I_C = 1.8 I_R$

10.2 General Considerations in Ribbed Structures

10.2.1 Rib Height

The stiffening effect of a rib becomes significant when the height of the rib, h_R , is a multiple of the part wall thickness s . It is generally the case that:

$$h_R = (5 \text{ to } 10) \cdot s \quad (10.3)$$

When the ribs are too high there is a risk of bowing of the part as shown in Figure 10.4. This figure presents test results obtained from ribbed strip-like plaques made from impact-modified polystyrene. These plaques measure $400 \times 100 \text{ mm}^2$ and were produced with two rib thicknesses. Each of the curves shows the start of bowing.

The height of a rib used to stiffen the structure can be varied based on the bending moment. The rib height decreases in areas where the bending moment is low (e.g., towards the edges of the plate or part).

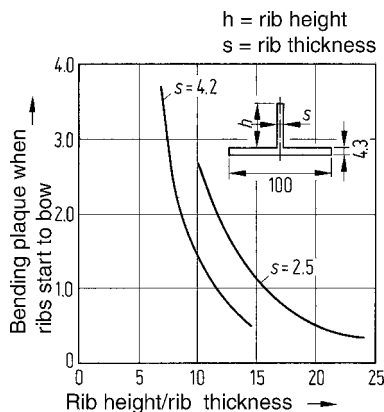


Figure 10.4 Test results on the bowing of ribs of different height as a function of rib height/thickness ratio. Strips $400 \times 100 \text{ mm}^2$ of impact-modified polystyrene sheet [10.3].

10.2.2 Rib Position

Ideally, ribs should be located on the side of the part subjected to tensile stress and aligned in the direction of the stress vector.

Ribs located transverse to the direction of stress represent sudden jumps in cross sectional area which, like notches, act as impediments to strain and magnify stress.

This magnification of stress can be alleviated to a large extent by incorporating transitional radii of curvature at the base of the ribs. Figure 10.5, taken from structural finite element analysis, shows the effect that the magnitude of the transitional radius on magnification has on the stress at a sudden increase in cross-sectional area running transverse to the direction of tensile stress (x-direction). This is comparable to a transverse rib for which the Mises reference stresses are shown. The local stress at the transition point is twice the value of the applied stress for a radius $r = 0.5$ mm. The stress drops off markedly as the radius increases.

In injection molding, however, a large radius of curvature at the base of a rib leads to an undesirable accumulation of material (see also Section 10.3).

Even in the case of ductile materials where dangerous stress peaks will be overcome by local flow processes, sudden increases in cross-sectional area should be avoided if at all possible when designing plastic parts. This is particularly the case for parts subjected to dynamic stress.

When parts have a very complicated geometry, it is almost impossible to predict the optimum position of ribs unless structural design aids are used. Numerical methods (*e.g.*, FEM) are available during the design phase and optical test methods (*e.g.*, holographic interferometry and Moiré techniques) are used when a physical model or prototype has already been made.

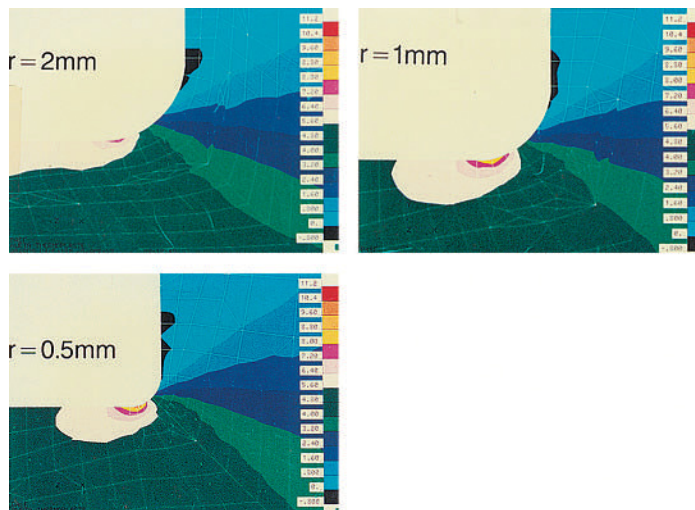


Figure 10.5 Notch effect at a rib running transverse to the direction of stress and having different transitional radii of curvature

In the case of more geometrically regular structures, this effort is not generally needed. Figure 10.6 shows a section of an appliance cover, which when lifted and pushed against a limit stop, is mainly subjected to bending stress. Ribs are added to the part in the region of the hinge points. In addition, however, two ribs are arranged in the transverse direction. Crack formation under load starts just above the rib running transverse to the bending stress near the hinge point. If the transverse ribs are removed and a fillet is added at the transition to the hinge eyelet, the impediment to strain (which magnifies stress) is eliminated as the holographic interferograms* in Figure 10.7 demonstrate.

A ribbed zone within a larger structure acts as an island of high rigidity with stress concentrations around its perimeter.

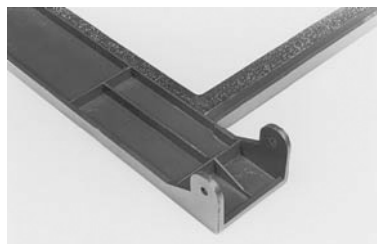


Figure 10.6 Detail of an appliance cover with ribbing at its hinge point

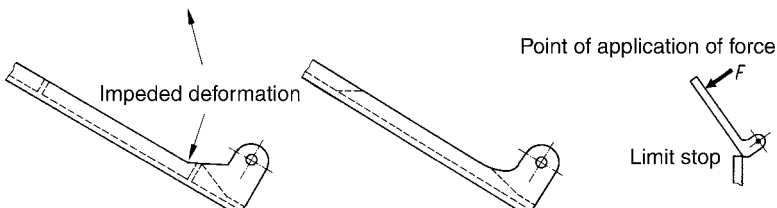
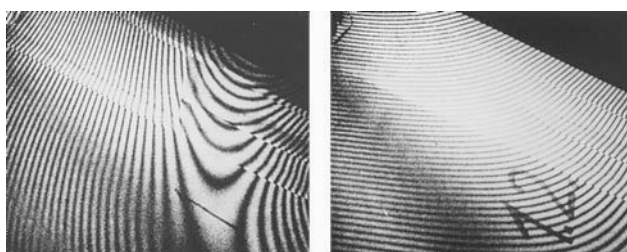


Figure 10.7 Holographic interferograms of the appliance cover shown in Figure 10.6 with stress concentrations in the area of a transverse rib (left) and a more uniform stress distribution after removal of the rib and adding a fillet to the transition region (right)

* Holographic interferometry renders deformations visible in the half-wavelength range of the laser light employed ($\lambda = 514 \text{ nm}$ for an argon laser). This is due to the production of interference patterns of the illuminated object in two states of stress or deformation. A uniformly thick interference pattern indicates uniform deformation while a sudden increase in line width indicates an impediment to strain [10.4 to 10.6].

Failure due to crack formation (see Figure 10.8) usually starts at the ends of the ribs.

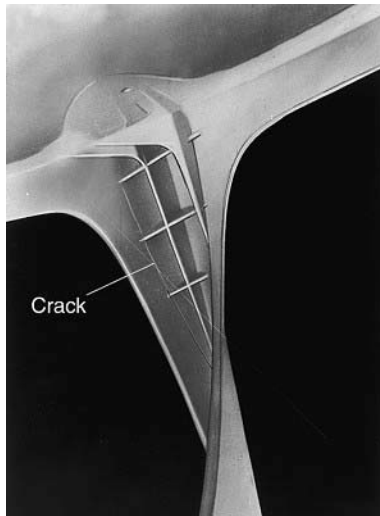


Figure 10.8 Crack formation in a plastic chair caused by a lack of suitable transitions from the ribbed zone to the wall [108]

10.2.3 Number of Ribs (Consumption of Material)

Experimental results [10.1] and the results of FEM calculations [10.7] confirm the expectation that the reinforcing effect increases linearly in proportion with the number of ribs. Along with the number of ribs, the reinforcing effect is also largely determined by the arrangement or orientation of the ribs relative to the direction of stress and the conditions under which they are fixed. The studies relate to panels measuring $400 \times 400 \times 4 \text{ mm}^3$ with rib heights of 30 mm and rib thicknesses of 2.7 mm. The reinforcing effect was quantified using a reinforcement factor E'/E . E' is a hypothetical value of the modulus of elasticity of the ribbed panel (characterizing the higher rigidity of a ribbed panel) relative to one without ribs. The reinforcing effect can be determined from the graphs in Figure 10.9. In this figure, the reinforcing factors attainable with loose-contact panel edges* are plotted for various rib configurations against the consumption of material, *i.e.*, the ratio of the weight of the ribbed panel to that of the panel without ribs.

When the amount of material consumed is low, *i.e.*, for a small number of ribs, there is little difference in the stiffening effect of the different rib configurations. When material consumption is increased in a close-meshed ribbing pattern, the stiffening effect is significant. The diagonal configuration proves to be the most effective.

* When there is loose contact, the edges of the panel (with the exception of the corners) are positioned loosely on a rigid base.

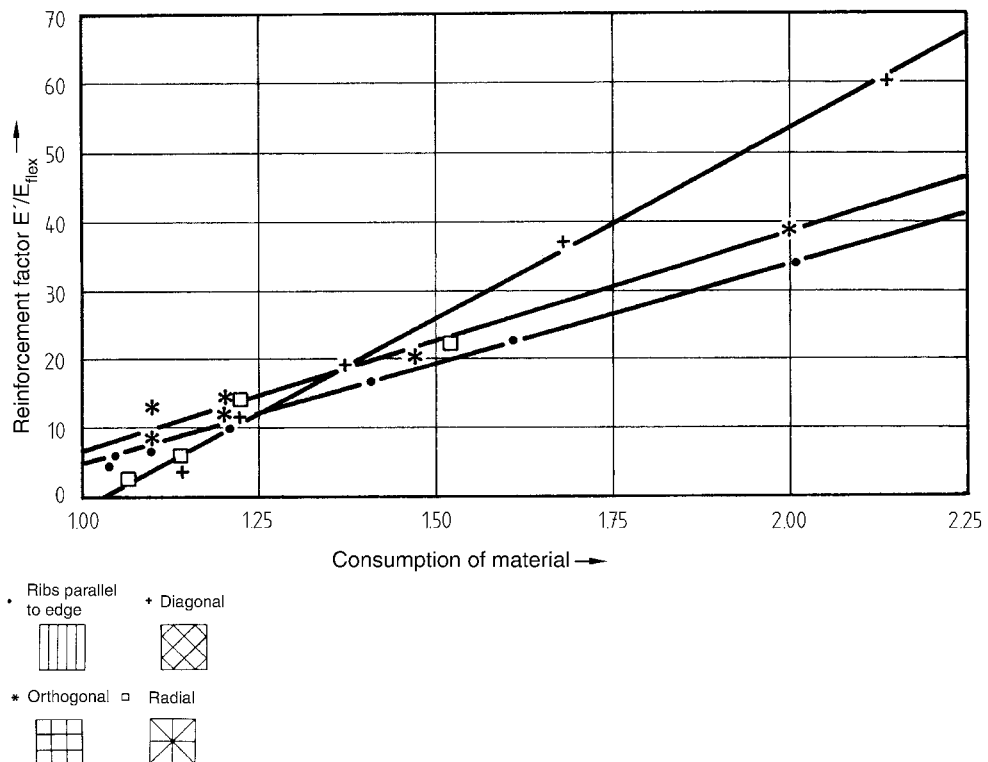


Figure 10.9 Reinforcing factor for ribbed panels under uniform load with simple support on the edges. The corners of the panels are assumed to be fixed [10.7].
(The reference variable for the reinforcing factor is the rigidity of an unribbed, simply supported panel.)

The reinforcing effect is quite different when the edges of the panels are fixed in position (see Figure 10.10).

Ribbing running parallel with the edges of the panel is more effective than the diagonally ribbed configuration.

Comparing the results in Figure 10.9 with those in Figure 10.10, it should be noted that in the unribbed state the deformation of the panel with fixed edges is up to 3.2 times less than that of the simply supported panel. Accordingly, for a direct comparison of rigidity, the results in Figure 10.10 must be multiplied by the factor 3.2.

Since the reinforcing effect increases steadily with the density of ribbing, a close-meshed configuration proves to be particularly effective.

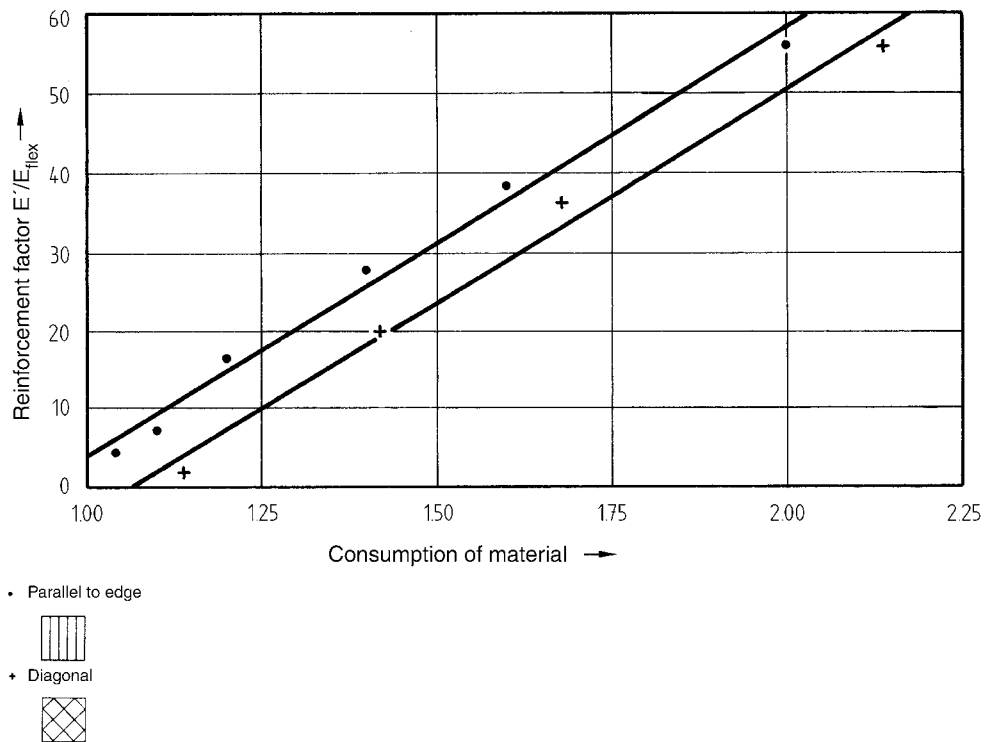


Figure 10.10 Reinforcing factor for ribbed panels under uniform load with the edges of the panels fixed around the entire perimeter [10.7].
(The reference variable for the reinforcing factor is the rigidity of an unribbed panel with fixed edges.)

10.2.4 Support

Figures 10.9 and 10.10 with the different support conditions of the panels show the lower and the upper extremes of support. In the case of real parts, the support is usually somewhere between these two extremes. In addition, the “ribbed panel” is generally a “sub-part” or an element of a larger part. The fixing conditions of support are determined by the shape of the larger part. Figure 10.11 provides some indication of how support conditions affect the stiffness of a diagonally ribbed plate. Here “pressure container” refers to support between high and rigid walls and “tabletop” to fixed support at the four corners only.

In order for the support condition or mounting condition to have any effect on stiffness, the ribs must extend up to the edge and be connected to it. Figure 10.12 shows an example in which this is not accomplished.

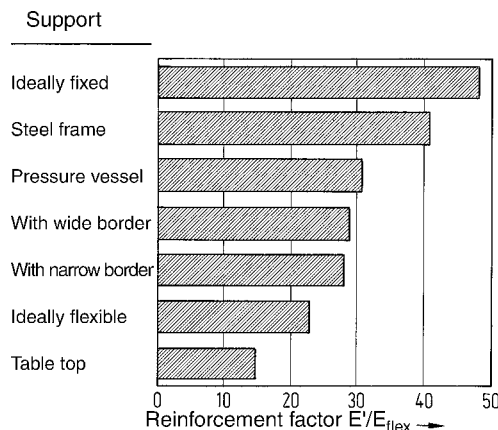


Figure 10.11 Effect of different support conditions on the stiffness of a diagonally ribbed panel (ribbing consumption 1.4) with reference to an unribbed, loosely mounted panel [10.7]



Figure 10.12 To achieve improved stiffness, the ribs should be connected to the perimeter edge

10.3 Design Rules for Injection-Molded Ribs

10.3.1 Rib Thickness

To maximize rigidity, the ribs should be as thick as possible relative to the nominal wall thickness. This, however, contradicts the requirement for a good visual appearance with a smooth surface, free of sink marks. Filling problems can also arise in injection molding for parts with variable wall thickness. Accordingly, to meet production requirements, the nominal wall from which the ribs extend must be thicker than the ribs extending up from the wall. The rule of thumb for rib wall thickness is:

$$s_R \approx (0.5 \text{ to } 0.7) \cdot s \quad (10.4)$$

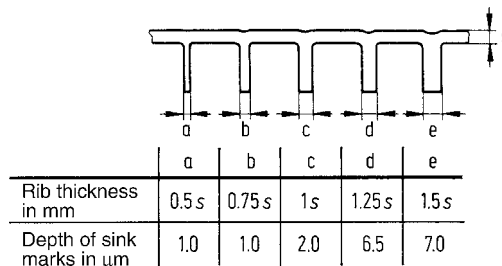


Figure 10.13 Test results of the depth of sink marks for different rib/wall thickness ratios.
Material: PBT filled with glass beads (B 4300 K4).

This is confirmed by the experimental results in Figure 10.13 showing the depth of sink marks for different rib thicknesses. The parts were made of PBT filled with glass beads in a test mold. The test results show that even for $s_R = 0.5 \cdot s$, a slight depression is still obtained but the depression (sink) is not particularly visible or objectionable.

Polymeric materials having high molding shrinkage (e.g., PP) are, as expected, even more critical with regard to the occurrence of sink marks on the surface opposite the ribs.

The size of the sink marks opposite ribs can also be reduced with proper injection mold design (see Section 7.2). Adjustments to the injection mold afford further possibilities for reducing sink marks (see Section 7.2).

To obtain a good visual appearance for a ribbed structure, it is preferable to use a larger number of “thin” ribs.

10.3.2 Cooling Time

Thin ribs are desirable for the purpose of achieving short cooling times. Figure 10.14 shows how cooling time increases with the maximum wall thickness as measured. The maximum wall thickness occurs at the base of the rib. Inscribing a circle in the base region can show how changes in wall thickness, rib thickness, and radius will effect cooling time.

The transition radius at the base of the rib does minimize stress concentration effects, but is not particularly advantageous in terms of production rate.

It should be determined if the stresses expected near the base of a rib make a generous radius or fillet essential, or whether the more efficient solution with a smaller radius is sufficient.

Figure 10.15 exemplifies the fundamental importance of ribbing compared to an equally rigid unribbed structure for efficient production. The unribbed structure would require a cooling time longer by almost a factor of four due to the thicker nominal wall.

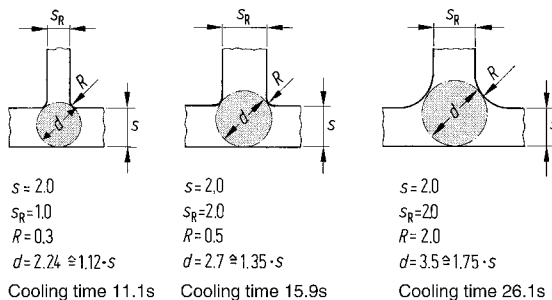


Figure 10.14 Effect of rib thickness and radius of curvature on the cooling time for a ribbed injection-molded part. The diameter of the inscribed circle specifies the maximum wall thickness to be cooled.

Size	Weight of panel g	Cooling time s	Bowing mm
 Size of panel: 400 x 400 Number of ribs: 4 Load: Q = 80 N	808.08	50.11	0.22
 Panel: 400 x 400 x 10 Load: Q = 80 N	1680.0	196.52	$f = 0.00416 \frac{qa^4}{D}$ = 0.22 $(D = 243000 \text{ Nmm})$

Figure 10.15 Cooling times for HIPS panels of equal rigidity ($E = 2,450 \text{ MPa}$)

10.3.3 Injection Direction

The anisotropy of strength and rigidity in glass-fiber reinforced polymeric materials gives rise to differences in behavior in ribbed structures depending on the direction of mold filling relative to the direction of the ribs. This is attributed to the direction of orientation of the glass fibers in the ribs (see also Section 7.1.1). Even in the ideal case of longitudinal flow along the ribs, the orientation of the fibers assumes an angle to the longitudinal axis of the rib. This angle of inclination depends on the ratio of the flow resistance in the part wall to that in the rib and hence, on the ratio of the thickness of the part wall to that of the rib. The thinner the rib is relative to the part wall, the greater the angle of inclination (see Figure 10.16). With thin ribs, the direction of orientation deviates from the direction most favorable for withstanding bending stresses. Therefore, as the relative rib thickness decreases, bending strength and flexural rigidity also decrease. In the case of very thin ribs on a thick surface, the reinforcing effect of the fibers is not fully utilized (see also Figure 7.9).

The experimental findings in Figure 10.16 are confirmed by a numerical flow pattern simulation (Figure 10.17). This shows that the flow front in a rib for which $s_R = s$, advances at approximately the same rate as that in the part wall (top). Thus, the fibers at the surface are aligned in the direction of the rib. When $s_R = 0.5$, however, the flow front in the thinner rib hangs back with the result that the fibers assume an angle to the longitudinal axis of the rib (center).

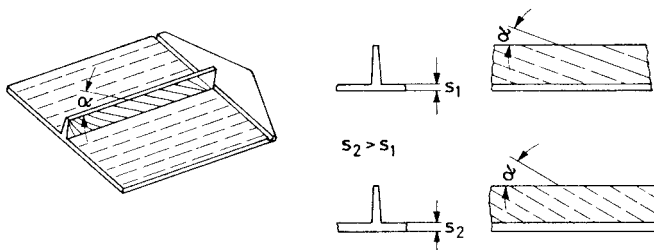


Figure 10.16 Schematic illustration of the orientation of glass fibers at the surface of injection molded ribs with flow along the longitudinal axis of the rib [10.9]

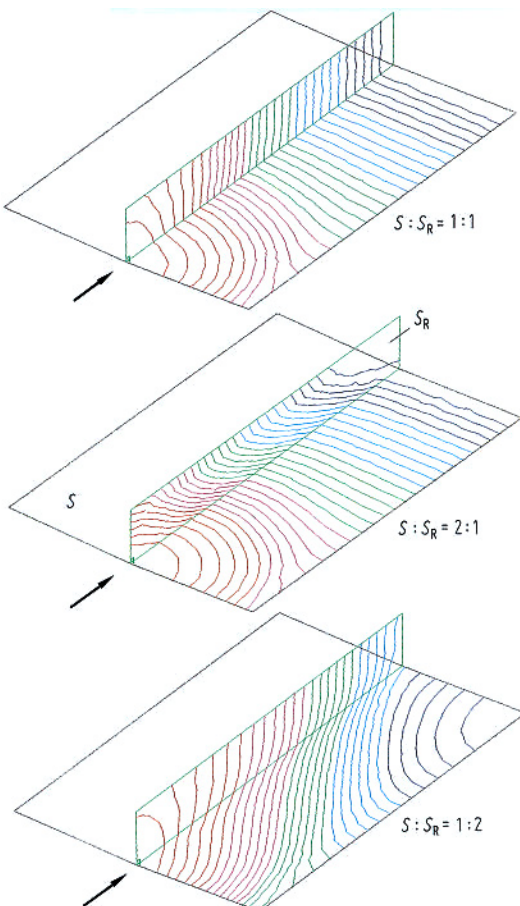


Figure 10.17 Filling studies for ribs with a longitudinal flow direction (gate →) having different wall/rib thickness ratios. For greater clarity, the flow front isochrones have been erased from the rear side of the part wall. The fibers at the surface are aligned perpendicular to the flow front.

10.3.4 Rib Intersection Points (Nodes)

In the design of the rib intersection points (e.g., for orthogonal ribs), requirements favoring efficient production and uniform stress distribution are not completely compatible with one another. For maximum rigidity, the transmission of forces through the nodes must not be interrupted. From this point of view, the design in Figure 10.18, left, is the most advantageous when the local stress concentrations (impediments to strain) occurring under load in the nodal points, are to be kept within tolerable limits. Here too, an adverse alignment of the

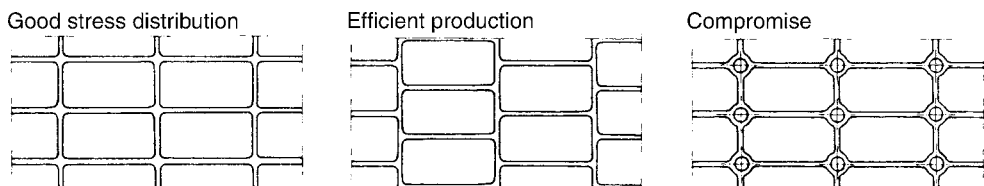


Figure 10.18 Design variations for rib intersections [10.10]

Left: Continuous rib pattern best suited for uniform stress distribution and structural stiffness

Center: Offset ribs for more efficient production

Right: Compromise where thick sections are "cored out"

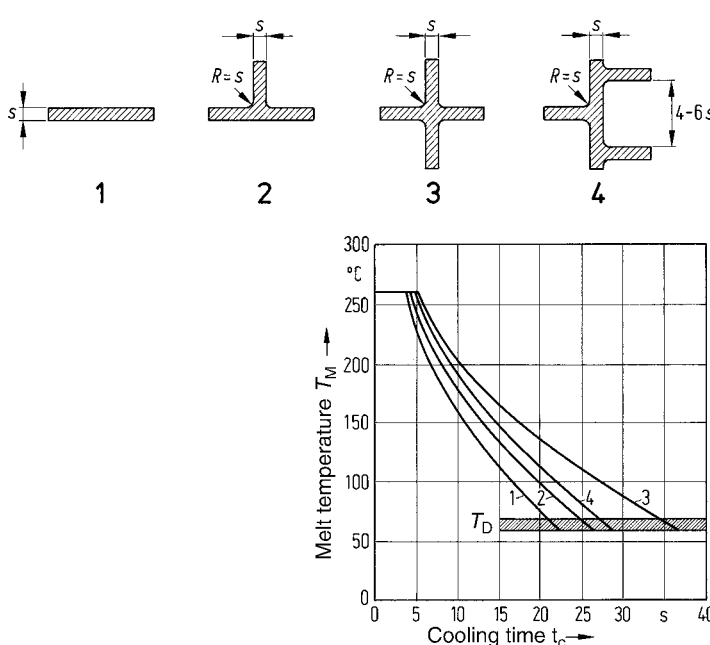


Figure 10.19 Cooling curves for different rib configurations

T_M = Melt temperature

T_D = Demolding temperature

fibers may result in failure of the fiber-reinforced part. Therefore, the rib intersections must have at least some radius. With a relative radius of curvature of $R/s_R = 0.5$, approx. 90% of an impact load relative to $R/s_R = 1$ can be absorbed. When $R/s_R = 0.2$, approx. 80% of the load can be absorbed [10.11] (see also Figure 10.5).

Such nodal points, however, represent accumulations of material which increase the cooling time for the plastic part as shown in the cooling curves in Figure 10.19 (3). This figure shows that an offset rib arrangement is advantageous from a cooling perspective, but due to the interrupted transmission of forces its stiffening action is substantially lower. A commonly used compromise is shown in Figure 10.18 (right). The prerequisite for this solution is that the mold cores forming the blind holes are well cooled. In addition, these cores should extend by about $0.3 \cdot s$ into the thickness s of the base wall (see also Section 9.3.2).

For fiber-reinforced polymeric materials, the weakening effect of any anisotropy resulting from the mold filling pattern should also be considered.

10.4 Design Rules for Ribs Produced by Gas-Assist Molding Methods

The internal gas pressure (IGP) methods require unconventional part designs compared to conventional injection molding. Wherever gas cavities are to be produced, *wall thicknesses must be high* because the gas seeks out those regions where the melt temperature is highest and hence viscosity lowest. The slightest inhomogeneities allow the gas to advance in an uncontrolled manner.

For that reason, other than with conventional injection molding, the ribs in parts produced by IGP injection molding must be thick while the nominal part walls are thin so that the gas is unequivocally conveyed into the thicker ribs. If the base wall thickness is too high, the gas spreads out into the wall on either side of the ribs (see Figure 10.20, right).

Figure 10.20 shows two proven design variants, one of which has a conventional IGP rib design and one an additional rib section extending from the IGP rib. This produces a particularly high stiffening effect.

The schematic illustration in Figure 10.21 shows a method of producing gas channels for ribs by the core puller method. In the upper section of the figure, the areas between the ribs are still closed off by cores. In the lower section, the cores have been withdrawn and the gas expands to fill out the sections between the ribs creating small box beams.

Intersecting ribs are not generally used in gas assist molding because the gas cannot go in a defined direction at the intersection points.

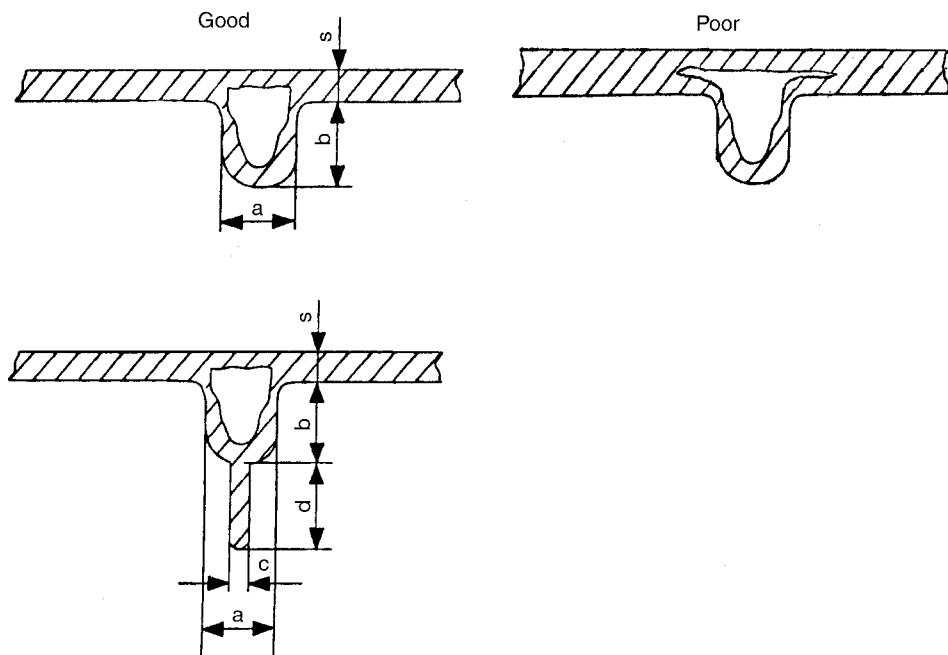


Figure 10.20 Rib designs for the IGP molding method

$$s = 2.5 \text{ to } 3.5 \text{ mm}$$

$$a \approx b = (2.5 \text{ to } 4) \cdot s$$

$$c = (0.5 \text{ to } 1) \cdot s$$

$$d = (5 \text{ to } 10) \cdot c$$

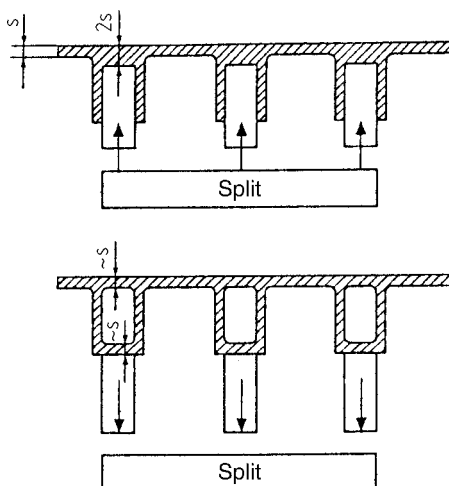


Figure 10.21 Method of forming box ribs by gas assist molding with the core puller method [10.15]

10.5 Design Rules for Blow-Molded Ribs and Corrugations

Freedom of design for blow-molded parts is highly restricted in comparison to injection-molded parts. The extruder of an extrusion blow-molding machine provides a tubular parison of melt, usually having a relatively uniform wall thickness. These parison ends are fully or partially closed off by the two closing halves of the blow mold. While still in the plastic state, the parison is expanded by compressed air against the mold wall. This yields a hollow article with an accurately shaped outer contour. In places at which the parison is stretched more by the inflation process, the wall thickness of the part is correspondingly lower. Therefore, there are extremely limited possibilities for stiffening by means of ribs with this production technology. The formation of corrugations, on the other hand, is feasible within limits.

10.5.1 Blow-Molded Corrugations

Raised corrugations on the outside wall of a blow molded part can be formed only within a limited range of width/depth ratios because the wall thickness would likely become too thin on stretching at greater ratios (see Figure 10.22).

In terms of production technology, it is easier to produce corrugations which extend inward from the outside wall of the part.

While in the case of the *outside corrugations* first mentioned, there is a limit to the ratio of depth to width of somewhere less than 1:1, *inside corrugations* can be made deeper relative to their width. It should be noted that the wall thickness should not be stretched too thin in the transition from the corrugation to the wall. This region should be beveled (see Figure 10.23) and modified with a generous radius of curvature (or be given a parabolic shape).

Blow molded *planar surfaces* can be stiffened using corrugated patterns similar to those used in metalworking. Diagonal corrugations are used to achieve a two-dimensional stiffening effect, while parallel corrugations stiffen uniaxially in their longitudinal direction. The stiffening effect, however, is not particularly efficient in diagonal corrugations because the nodal point cannot be well defined. Parts incorporating parallel corrugations exhibit flexible behavior at right angles to their extension (see also Section 6.1). Therefore, containers under internal pressure (*e.g.*, gasoline canisters) are better constructed with smooth walls to form an oval or octagonal cross section.

A stepped corrugation pattern (see Figure 10.24) provides comparatively effective stiffening in a plane.

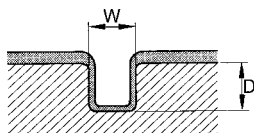


Figure 10.22 Maximum blow-up ratio for an outside corrugation and related decrease in wall thickness; $D : W = 1 : 1$

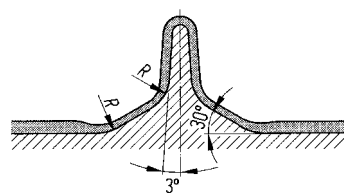


Figure 10.23 Example for an inside corrugation on a typical blow-molded part

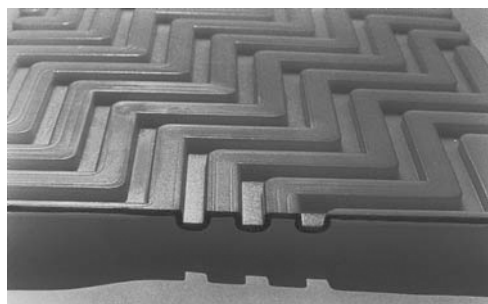


Figure 10.24 Stepped corrugation pattern for stiffening planar surfaces according to Bührle [10.12]

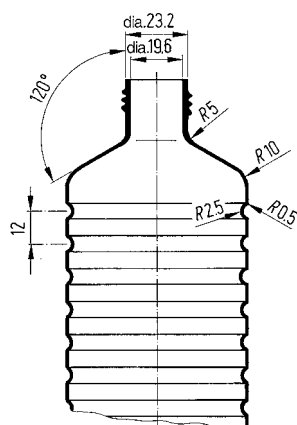


Figure 10.25 Reinforcement of a blow-molded bottle of circular cross section by concentric corrugations

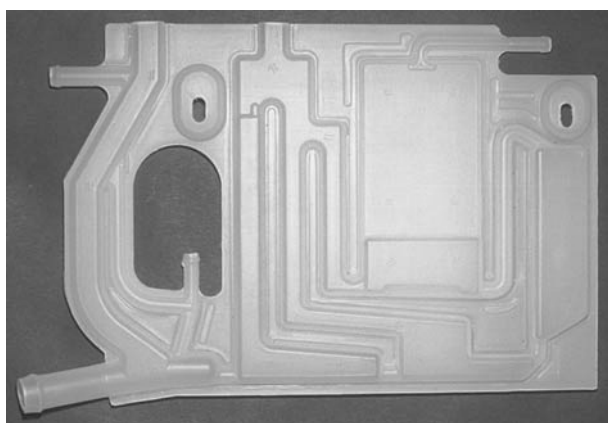


Figure 10.26 Blow-molded tubular system made from PP as a level measuring device in washing machines (Manufacturer: Fischer Söhne, Muri, Switzerland)

A *circular cross section*, as commonly found in bottles and other containers (see Figure 10.25), is commonly reinforced against internal and external pressure using concentric corrugations. The example in Figure 10.26 is also noteworthy. This is a blow-molded flat part which is corrugated and welded at certain points in such a way that not only high rigidity is obtained, but also a tubular system is created. It is employed as a level measuring device in washing machines.

10.5.2 Blow-Molded Ribs

Solid ribs can only be applied to blow-molded parts by special shaping on the inside of the parison.

The die geometry is designed so that a parison having *internal longitudinal ribs* is extruded. Although these ribs lose something of their original shape due to die swell and the blowing pressure, they largely remain in place. In the region of the base, the pinch-off sections of the blow mold force these ribs together on the inside of the part (see Figure 10.27). If a container reinforced in this way is exposed to internal pressures, the ribs are located on the pressure side.

The wall thickness of the parison can also be controlled by changing the die gap as the parison forms. In this way, *concentric thickened regions* can be produced (see Figure 10.28), which afford some reinforcement*.

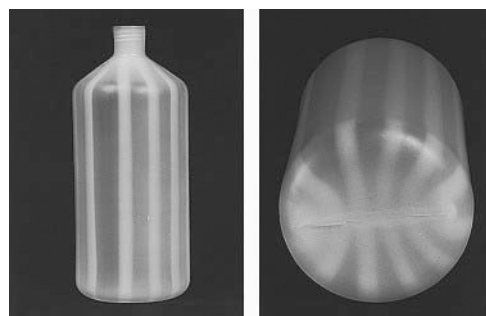


Figure 10.27 Internal ribs in a blow-molded part formed by a profiled die mandrel geometry [10.12]

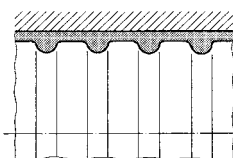


Figure 10.28 Reinforcement of a blow-molded container using concentric rings (i.e., changes in wall thickness) formed by parison profiling [10.12]

* Using the technique known as *partial wall thickness control*, the parison is extruded with a greater wall thickness at discrete points distributed over the length of the parison. This is done by (partially) enlarging the die gap as the parison is formed. Wall thicknesses in regions where the material is subjected to high stretching forces tend to be smoothed out.

10.6 Design Rules for Compression-Molded Ribs

Flat components made from thermosets must be stiffened within the limitations of the processing technologies employed for these polymeric materials. Fiber-reinforced composite materials can be strengthened and reinforced by selective alignment of the fibers in a predetermined direction. However, there are design limitations for ribs produced by compression molding in comparison with injection molding of thermoplastics. Free-flowing SMC semifinished products of relatively complicated geometry can be compression-molded with quasi-isotropic properties for part geometries having astonishingly thin and high ribs.

10.6.1 Manual Processing (Hand Lay-Up Process)

Parts having a relatively small surface can be stiffened by modifying the design of the edges as shown in the example in Figure 10.29.

In most cases, hand lay-up parts containing stiffening ribs are first produced as parts having a relatively uniform wall thickness. After the part is cured, prefabricated rib sections, either made of glass-fiber reinforced plastic or of metal, wood, or rigid foam, are laid on top of the wall and are firmly bonded to the surface to be stiffened by laminating an additional layer of reinforcement over their surface (see Figure 10.30).

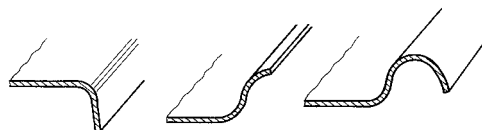


Figure 10.29 Stiffening of a part with a relatively small surface area using an efficient edge design

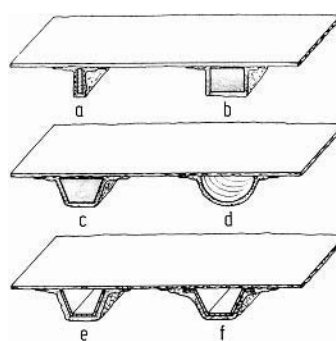


Figure 10.30 Stiffening of a glass-fiber reinforced plastic part using ribs laminated in place by the hand lay-up process [10.13]

- a) wood profile or the like;
- b), c) rigid foam profile;
- d) plastic tube cut in half;
- e), f) metal or glass-fiber reinforced plastic profile

10.6.2 Compression Molding

Figure 10.31 shows examples of common edge designs for compression-molded parts.

SMC semifinished products preimpregnated with glass mats (see Section 3.3) become free-flowing under compression molding conditions (in the mold) to such an extent that rib-forming cavities having high flow length-wall thickness ratios can be incorporated into the mold. Figure 10.32 demonstrates the good flow characteristics of SMC in the example of the engine compartment hood for the Citroën BX. The ribs having wall thicknesses of 1.5 to 2.1 mm and heights of approx. 15 mm are completely filled.

A particular advantage of low-profile SMC materials (*i.e.*, low-shrinkage to non-shrink resin systems) is that thick ribs can be produced effectively without sink marks, even though the local wall thickness at the base of the ribs is greater than that for other sections of the part. A wall thickness ratio of $s_R/s = 1$ is certainly achievable (see Figure 10.33).

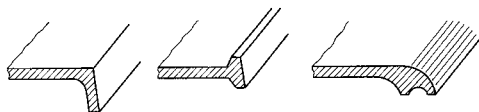


Figure 10.31 Edge designs for compression-molded parts [10.13]



Figure 10.32 SMC ribbing on the inside of the hood of the Citroën BX

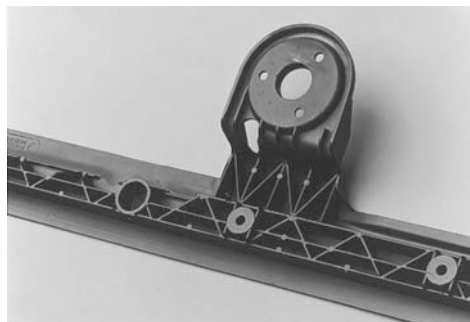


Figure 10.33 Strong and stiff, close-meshed ribbing in a windscreen wiper support made of low-profile SMC for a Daimler Benz truck
 Wall thickness: 4.3 to 4.5 mm
 Rib thickness: 4.1 to 4.3 mm (at the base)
 Rib height: 30 mm
 Draft: ~ 1.2°
(Photograph: BASF, Ludwigshafen)

References

- [10.1] SCHMITT, D. and A. WEBER: Biegesteife, verrippete Platten sowie Platten mit Schaumstoff-Integralstruktur aus thermoplastischen Kunststoffen aus: Belastungsgrenzen von Kunststoff-Bauteilen (Ribbed panels and panels having a rigid integral foam structure made from thermoplastics in: Loading limits of plastic parts), VDI-Verlag, Düsseldorf 1975
- [10.2] EHRENSTEIN, G. W. and G. ERHARD: Konstruieren mit Polymerwerkstoffen (Designing with polymeric materials), Hanser-Verlag, Munich 1983
- [10.3] MOHR, H. and A. WEBER: Rippen- und sickenversteifte Kunststoff-Konstruktionen (Plastic structures reinforced by ribs and corrugations), *Konstruktion, Elemente, Methoden* **11** (1976) 13, pp. 79/84
- [10.4] BRÜNINGS, W.-D., H. KNAPP, E. STRICKLE and D. MÜLLER: Holographische Interferometrie erleichtert das Gestalten beanspruchter Kunststoffteile (Holographic interferometry facilitates the design of plastic parts subjected to loads), *Maschinenmarkt* **88** (1982) 25, pp. 457/459
- [10.5] BRÜNINGS W.-D., H. KNAPP, E. STRICKLE and D. MÜLLER: Optimieren von Bauteilen aus Kunststoffen mit optischen Meßverfahren (Optimization of plastic parts using optical test methods), *Maschinenmarkt* **88** (1982) 18, pp. 307/310
- [10.6] BRÜNINGS W.-D., H. KNAPP, E. STRICKLE and D. MÜLLER: Optische Meßverfahren zum Untersuchen von Bauteilen aus Kunststoffen (Optical test methods for studying plastic parts), *Maschinenmarkt* **87** (1987) 90, pp. 1963/1966
- [10.7] WEBER, A. and W. WILHELM: Anisotropie als Prinzip bei der Entwicklung neuer Kunststoffe und bei der Konstruktion von Bauteilen (Anisotropy as a principle in the development of new plastics and in the design of components)
- [10.8] OEHLER, G. and A. WEBER: Steife Blech- und Kunststoffkonstruktionen (Rigid sheet-metal and plastic designs), Springer-Verlag, Berlin 1972
- [10.9] DELPY, U.: Steifigkeit und Tragfähigkeit spritzgegossener Rippen und rippenversteifter Platten aus glasfaserverstärkten Thermoplasten (Rigidity and load-bearing capacity of injection-molded panels made of glass-fiber reinforced thermoplastics), *Kunststoffe* **67** (1967) 9, pp. 498/502

- [10.10] GEMMER, H.: Werkstoffgerechtes Gestalten von Formteilen aus thermoplastischen Kunststoffen (Material-based design of moldings made from thermoplastics), *Plastverarbeiter* **22** (1971) 11, pp. 793/799 and *Plastverarbeiter* **23** (1972) 1, pp. 12/17
- [10.11] DELPY, U.: Zur Tragfähigkeit verrippter Formteile aus glasfaserverstärkten Thermoplasten (On the load-bearing capacity of ribbed moldings made of glass-fiber reinforced thermoplastics), *Kunststoffe* **74** (1984) 6, pp. 341/344
- [10.12] BÜHRLE, H.: Personal communication 1992
- [10.13] ANON.: Gestalten und Konstruieren mit glasfaserverstärktem Leguval (Design and construction using glass-fiber reinforced Leguval), Bayer AG brochure 1972
- [10.14] ECKARDT, H.: Anwendungsbereiche, Möglichkeiten und Grenzen beim Gasinnendruck-Verfahren. Seminar ‘Gasinnendruckverfahren beim Spritzgießen’ (Applications, possibilities, and limitations of the internal gas pressure method. Seminar on the Internal Gas Pressure Method in Injection Molding), SKZ Würzburg, 1994
- [10.15] THEISSIG, W.: Anwendung des Gasinnendruckverfahrens für Komponenten im Automobilbau. Seminar Gasinnendruckverfahren beim Spritzgießen (Use of the internal gas pressure method for components in automotive engineering), SKZ Würzburg, 1994

11 Gear Wheels

Gear wheels are designed to transmit movements and forces or moments without slippage. In the field of precision engineering, the transmission of movement (at relatively low torques) is frequently the more important task of toothed drives. Accordingly, special gear tooth designs that are particularly free of play, have low friction, and are quiet in operation find application in a variety of products [11.1–11.4]. The tooth depth of such gear wheels is usually less than 1 mm, which leads to problems in moldmaking and in dimensionally accurate production*. These machining problems are not addressed to any significant extent here. Probably the smallest gearwheel** produced from polymeric material (POM) by conventional means today is used for driving the second hand of a wrist watch [4.18]. It weighs 0.00056 g, has eight teeth and an outer diameter of 1.32 ± 0.01 mm. The mold cavity was produced by spark erosion and the electrodes by disk shape milling cutters [11.35].

In contrast to gears for precision engineering applications, gear wheels in traditional mechanical engineering applications ($m > 1$ mm) have the primary task of force transmission as the principal consideration. The largest gear wheel produced in one part by anionic polymerization from cast PA 6 has a number of teeth $n = 76$, a tooth depth $m = 33$ mm, and a reference circle measuring 2,508 mm.

Gear Wheel Materials

Thermoplastic materials with a semi-crystalline morphology are most commonly used as gear wheel materials. Thermoplastics commonly used for gears include:

- Polyamides (PA),
- Polyoxymethylene (POM),
- Polybutylene terephthalate (PBT),
- High molecular weight, high-density polyethylene (HDPE),
- Polyaryl ether ketone (PEEK),
- Polyphenylene sulfide (PPS) and
- Polyurethane (PU) (thermoplastic and elastomeric).

These materials can be used with or without certain additives. Reinforcing PA, POM, PBT, and PEEK with chopped strands increases the strength and modulus of these matrix materials. Therefore, gear wheels made from glass-fiber reinforced thermoplastics can certainly withstand higher static loads. In dynamic operation, however, gear wheels made of these reinforced materials should be lubricated in order to prevent high levels of wear. Friction-reducing additives can also be used in PA, POM, PBT, or PEEK. These additives are usually coarsely

* Erosion machining also allows the production of molds for tooth geometries that are not feasible by mechanical machining or grinding.

** Even much smaller components can now be produced by micromolding technologies, lithography technology, or by means of UV-curing photosensitive layers.

divided particles of HDPE or PTFE or more finely divided low molecular weight lubricants. These are suitable for high-speed gears or types of gears that are predominantly exposed to sliding stresses (e.g., worm gears).

Gear wheels made from thermosetting materials are produced almost exclusively by machining semifinished laminated composites. These include:

Phenolic resin bonded layers of cotton fabric,

Compressed laminates and phenolic resin bonded layers of vulcanized fiber or beechwood,

Other thermoset resin laminated fabrics.

Mating Materials

The highest levels of load-bearing capacity and service life are obtained by mating plastic gears with steel gear wheels whose tooth faces have been hardened. Because the driving pinion is subjected to greater levels of wear, steel is generally used as the material for the pinion. When two polymeric materials are used for meshing gears, the material having greater resistance to wear is generally used for the pinion (see Section 4.7.2).

Lubrication

In principle, gear wheels made from polymeric materials can run without lubrication. Lubrication with oil can, however, substantially improves load-bearing capacity and service life, because, apart from reducing friction and wear, this can also improve heat dissipation. Most gear wheel materials are more compatible with lubricants or greases based on mineral oil. Table 11.1 provides some values for the upper limits of the oil temperature for selected plastic gear materials.

In precision engineering, gears often require lubrication for extended periods of time with minimum amounts of lubricant. The lubricants can become less effective over time due to premature resinification, gelling, and changes in the stabilizer-inhibitor equilibrium in many oils. Special synthetic oils have proved to be less susceptible to these changes [11.13–11.14].

Lubrication with grease, even when applied only once at the time of installation, brings about a lengthening of service life for many plastic gear applications. The circumferential speed of a gear wheel lubricated with grease should be limited to a maximum of 4 m/s, because above this speed lubricant can be thrown off the tooth faces due to centrifugal forces. In a report [11.15] on greased machine elements operating in a dusty environment it was found that grease and dust bonded together to form a sort of “emery paste”, which actually accelerated wear of the gears.

Table 11.1 Guideline Values for Upper Temperature Limits of Oil Used in Contact with Selected Polymeric Gear Wheel Materials over 1,000 h [11.33]

Limiting temperature in °C in contact with lubricating oil containing additives (API-SE)	PA 66, heat- stabilized (A4H)	PA 66, heat- stabilized (A3W), PBT (B 4550)	PA 66, stabilized (A3K), POM (H2320)	PA 66 GF, heat stabilized (A3HG5)	PA/PE (A3R), HDPE (5261Z)
	120	110	100	150	< 60

Water or oil emulsions are not generally regarded as lubricants in the normal sense, but may rather be viewed as coolants. Accordingly, the increase in load-bearing capacity and service life demonstrated in [11.5] for spur gears made of PA and POM operating in oil emulsions is more likely to be attributable to more effective cooling than to lubrication. However, a lubricating effect and reduced wear can be achieved when the surface roughness of the mating steel tooth flank is $< 0.3 \mu\text{m}$ (see also Figure 4.38). Such gear wheels, however, are very costly to produce.

11.1 Calculation of the Tooth and Tooth Face Temperatures in Spur Gears

If the gear temperature is known (ambient temperature) and does not change during operation, the known temperature-dependent properties can be used for the strength calculation. Evaluation becomes more difficult, however, if the temperature of the part in question changes in the course of operation due, for example, to frictional heat or internal damping. The latter is the case for gear wheels, sliding bearings, rollers, and the like. The fundamental procedure for evaluating the strength of such machine elements is shown in Figure 11.1. The first step in creating an energy balance is to determine the heat generated by the system. This heat is compared with the rate at which heat can be dissipated out of the system. Under equilibrium

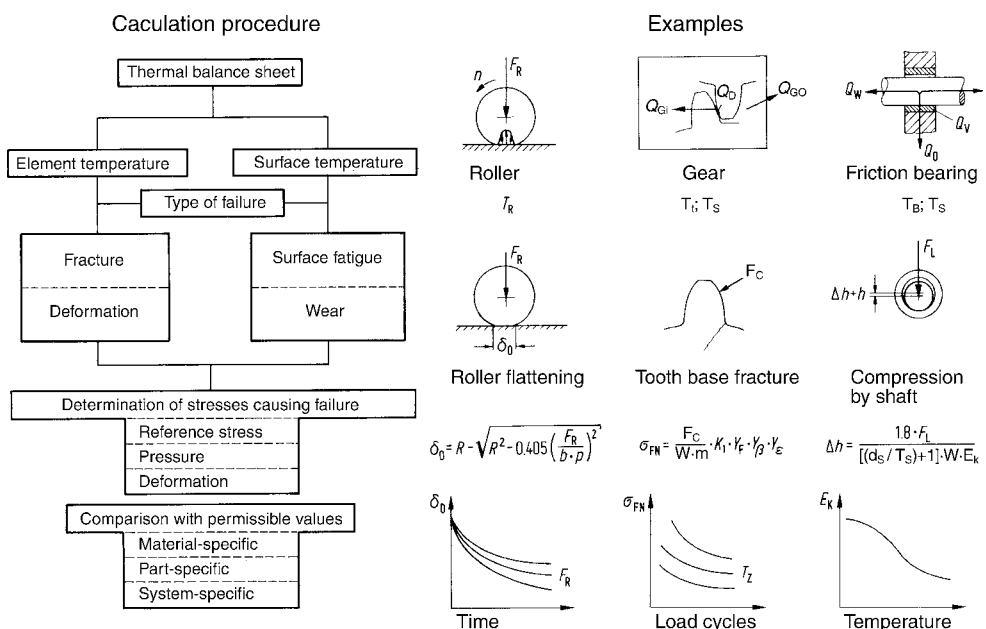


Figure 11.1 Procedure for calculating the strength and performance of meshing gear elements [5.1]

conditions, this yields the temperature being sought. The effort involved in determining the temperature distribution precisely is not easily determined in most cases, but an average temperature of the element or body in question and an average temperature of the surface in question should be determined. The average body temperature can then be related to fracture or deformation failure, while the average surface temperature accounts for surface damage. The various causes of failure are then investigated one after the other on the basis of these temperatures.

When a gear system is in operation, the occurring rise in temperature is due to a combination of causes:

- When the teeth are under dynamic load, viscoelastic deformation causes hysteresis losses, which are converted for the most part into heat and
- A gear wheel pair is a tribological system having sliding and rolling friction components whose frictional losses are likewise converted to heat.

There are several theoretical and semi-empirical approaches for calculating the temperature of a moving meshed gear wheel system. They are based on different physical models.

11.1.1 Blok's Flash Temperature Hypothesis

The calculation proposed by Blok [11.6] is based on the idea that in the Hertzian contact range, a ribbon-like heat source produced by frictional heat losses moves over the tooth face or flank. In [11.7], a modified form of Blok's equation is specified for calculating short-term temperature peaks on polyamide gear wheels. Years of experience have shown, however, that the Blok method is not particularly suitable for gear wheels made of polymeric materials. The Blok method is commonly used in accordance with DIN 3990 [11.8] for calculating the scuffing load capacity (hot scuffing) of metal gear wheels. These typical scuffing phenomena, however, are not as commonly observed in gear wheels made of polymeric materials.

11.1.2 Takanashi Method for Calculating Temperature

The Takanashi model can be used to calculate heat dissipation for parts subject to both friction and deformation [11.9]. This model takes viscoelastic deformation into account using the Voigt model and further includes the coefficient of friction as a function of temperature, the rate of slip, lubrication, and the paired materials. Both components are added together:

$$Q_{\text{tot}} = Q_F + Q_D \quad (11.1)$$

The friction component is determined using the expression:

$$Q_F = \alpha \cdot \frac{1}{42.7} \cdot f \cdot F_C \cdot \sum_{i=1}^4 \beta_i |v_P - v_{St}| \cdot t_i \quad (11.2)$$

where

$$\alpha = \frac{\sqrt{\lambda_p \cdot \rho_p \cdot c_p \cdot v_p}}{\sqrt{\lambda_p \cdot \rho_p \cdot c_p \cdot v_p} + \sqrt{\lambda_{St} \cdot \rho_{St} \cdot c_{St} \cdot v_{St}}}$$

α = the fraction of the heat transferred to the polymer gear wheel,

λ = thermal conductivity in W/mK,

ρ = specific gravity in kg/m³,

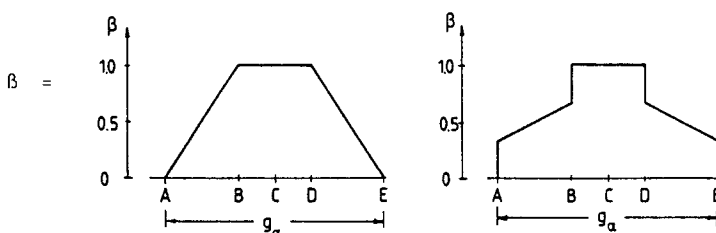
c = specific heat capacity in kJ/kg K,

v = tangential velocity in m/s,

f = coefficient of friction,

F_C = circumferential force in N,

β = load distribution factor for gear wheels with (left) and without (right) profile correction [11.8]



t = meshing time in s.

Indices

p = index for the polymeric material,

St = index for steel,

i = segment A, B, C or D of the load distribution factor.

To calculate the deformation component it is proposed that the tooth be considered as a viscoelastic spring-damper (Voigt model, see Figure 11.2) and that Q_D be determined from the work loss.

$$Q_D = \frac{1}{427} \cdot \frac{F_C^2}{2} \cdot \sum_{i=1}^4 \frac{\beta_i^2}{c_{Fi}} \left(1 - e^{-\frac{t_i}{\tau}} \right) \quad (11.3)$$

where

c_F = spring constant in N/cm,

τ = relaxation time in s.

For the other symbols see Eq. 11.2.

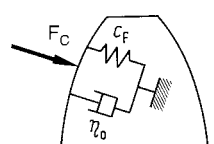


Figure 11.2 Viscoelastic model of tooth [11.9]

The equilibrium temperature of the teeth can now be determined if, in addition to the amount of heat Q_{tot} generated in operation, the amount of heat Q_E given off by the rotating gear wheel to the environment is known. This amount of heat can be calculated from the following equation (heat transfer according to Newton):

$$Q_E = \alpha_T \cdot A \cdot (T_T - T_E) \cdot \frac{60}{n} \quad (11.4)$$

where

A = area of the gear wheel giving off heat in cm^2 ,

T_T = tooth temperature in $^\circ\text{C}$,

T_E = temperature of the environment in $^\circ\text{C}$,

n = speed of rotation in min^{-1} .

To determine the heat transfer coefficient α_T , experiments were carried out on rotating gear wheels. The results of these [11.9] may be summarized as follows:

$$\alpha_T = \frac{10 \cdot \lambda_A}{m} \cdot \left(\frac{m}{10 w} \right)^{0.05} \cdot \left(\frac{m \cdot v}{10 a} \right)^{0.4} \cdot \left(\frac{1}{\text{Pr}} \right)^{0.4} \quad (11.5)$$

where

λ_A = thermal conductivity of air in $\text{cal}/\text{cm s K}$,

m = module in mm ,

w = tooth width in mm ,

v = circumferential velocity in cm/s ,

a = thermal diffusivity of air in cm^2/s ,

Pr = Prandtl number of air between -50 $^\circ\text{C}$ and 100 $^\circ\text{C}$, constant = 0.71.

By equating Eq. 11.1 with Eq. 11.4, the tooth temperature is finally given by:

$$T_T = T_E + \frac{Q_{\text{tot}}}{\alpha_T \cdot A} \cdot \frac{n}{60} \quad (11.6)$$

Difficulties are often encountered in the practical application of this relationship because of a lack of physical data for determining Q_{tot} .

11.1.3 Hachmann and Strickle Method for Calculating Temperature

The Hachmann and Strickle method for calculating the temperature is likewise based on a heat balance sheet [11.10]. The quantity of heat Q_1 produced during meshing is equivalent under steady state conditions to the quantity of heat Q_2 given off to the interior of the gear and hence equivalent to the quantity of heat given off to the outside by the gear housing. Heat dissipation via the shaft is not taken into consideration.

The power loss for 20° meshing is introduced as the quantity of heat Q_1 produced. This is approximated by the expression:

$$Q_1 = 3.54 \cdot P \cdot f \cdot \frac{i + 1}{t_1 + 5i} \quad (11.7)$$

where

P = power in kW,

f = coefficient of friction,

i = transmission ratio t_1/t_2 = number of teeth in pinion/number of teeth in wheel.

Q_2 , the amount of heat transferred by the gear wheel into the interior of the gear, is given by:

$$Q_2 = A \cdot \alpha_T (T_{t1,t2} - T_i) \quad (11.8)$$

where

A = heat exchange area in m^2 ,

T_t = tooth temperature in $^\circ\text{C}$ and

T_i = temperature in the interior of the gear in $^\circ\text{C}$.

Since the heat exchange surface area is not known exactly, a factor k_1 (to be determined experimentally) is introduced:

$$A = k_1 \cdot m \cdot t \cdot w \quad (11.9)$$

and α_T is estimated by a model of a level plate of length $m \cdot \pi$, with longitudinal flow at the circumferential velocity v :

$$\alpha_T = \frac{1}{20} \cdot \frac{\lambda_A}{m} \left(\frac{v \cdot m}{a} \right)^{0.75} \quad (11.10)$$

where

λ_A = coefficient of thermal conductivity in W/mK ,

m = module in mm,

v = circumferential velocity in m/s ,

a = thermal diffusivity of air in m^2/s .

The amount of heat Q_3 dissipated through the gear housing is calculated by analogy with Eq. 11.8, the heat transfer coefficient α_T being replaced by an experimentally determined factor k_3 .

$$Q_3 = A \cdot k_3 \cdot (T_i - T_E) \quad (11.11)$$

Equating Eq. 11.7, 11.8, and 11.11 and with $\lambda_A = 0.028 \text{ W/mK}$ and $a = 0.094 \text{ m}^2/\text{h}$ yields the following equation:

$$T_{t1,t2} = T_E + P \cdot f \cdot 136 \frac{i+1}{t_1+5i} \left(\frac{k_2 \cdot 17100}{w \cdot t_{1,2} \cdot (v m)^{\frac{3}{4}}} + 7.33 \cdot \frac{k_3}{A} \right) \quad (11.12)$$

11.1.4 Comparison of Methods of Calculating Temperature

The coefficient of heat transfer α_T of the rotating gear wheel to the surroundings plays a major role in the temperature calculations, but it is a variable that is difficult to determine. The equations given for it, Eq. 11.5, which is supported by experiment and Eq. 11.10 based on analysis of a model, although similar in principle, yield distinctly different results (see Figure 11.3).

A general evaluative comparison of the methods cited is best carried out on the basis of a specific numerical example whose trends will clarify the results in each case.

The following numerical values are used for this purpose:

Steel pinion	$t_1 = 21$	$x_1 = 0$
PA 6 gear wheel	$t_2 = 26$	$x_2 = 0$
Module	$m = 6 \text{ mm}$	
Meshing angle	$\alpha = 20^\circ$	
Tooth width	$w = 10 \text{ mm}$	

	Example 1	Example 2
Coefficient of friction	$f = 0.2$	$f = 0.2$
Circumferential force	$F_{C1} = 245 \text{ N}$	$F_{C2} = 134 \text{ N}$
Speed of rotation	$n_1 = 570 \text{ min}^{-1}$	$n_2 = 1,040 \text{ min}^{-1}$

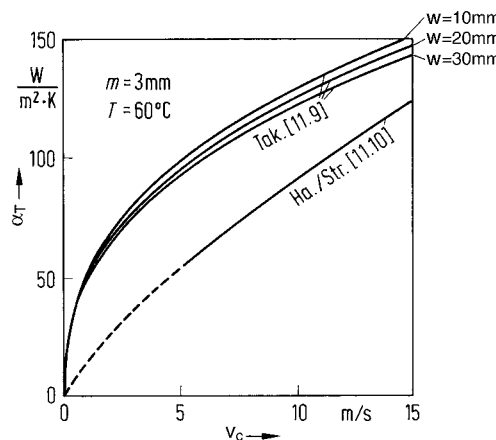


Figure 11.3 Comparison of values of α_T calculated in accordance with references [11.9] and [11.10]

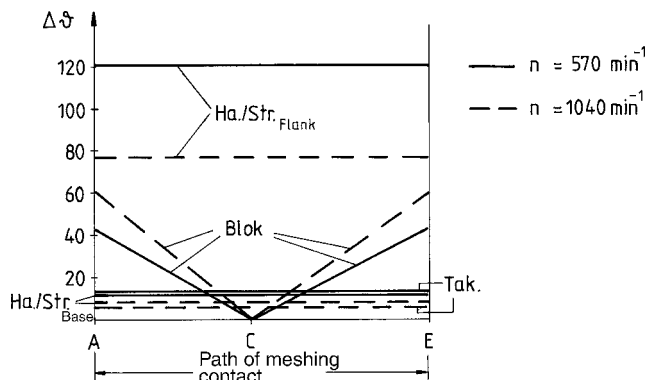


Figure 11.4 Comparison of different methods for calculating the temperature over the path of meshing contact [11.12]

The comparison of the results of temperature calculations presented in Figure 11.4 shows that using Blok's method, the temperature increase disappears as expected in the pitch point because only rolling friction occurs here. It is, however, well known that in the case of gears made of polymeric materials, thermally induced damage occurs precisely in this region.

When constant power is being transmitted but speeds are varied, both the Hachmann and Strickle methods and that of Takanashi show a decrease in temperature when speed is increased, whereas the calculation according to the Blok model shows a temperature increase with increasing speed. It is, however, plausible that the temperature does decrease as a result of the lower circumferential force and the increased heat transfer coefficient at higher speeds.

Calculations performed using the Hachmann and Strickle method yield *very high flank temperatures*. Calculated flank temperatures often exceed the melting point of the polymeric material. However, in bench test experiments, conducted under the same conditions, no melting has been observed.

11.1.5 Optimized Temperature Calculation

The Hachmann and Strickle gear temperature model, which has proved to be effective as a practical design technique, has been investigated experimentally [11.12] in relation to the key variables in Eq. 11.12. Temperature measurements obtained by means of a thermovision camera and infrared thermometry are in good qualitative agreement with the "trends" shown by speed of rotation, gear surface, coefficient of friction, and tooth width. The thermal effects associated with the dimensional inaccuracies and in the material were also investigated. Figure 11.5 provides impressive evidence of the thermal effect of imprecise tooth geometries. After a running time of only 5 minutes, it was possible to record a local temperature increase which continued to be observed as a "thermal balance error" throughout the service life of the gear wheel. In the present case, the temperature increase amounted to approx. 10 K. Similar effects can arise from structural faults in the material, voids, etc. causing thermally induced failure.

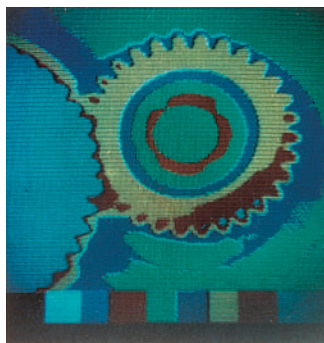


Figure 11.5 Local temperature increase as a result of inaccurate tooth cutting.
Thermal state after 3 h of running time.

11.1.5.1 Speed of Rotation

The sliding speeds investigated ranged from $v = 5$ to 15 m/s.

At sliding speeds of $v \leq 1$ m/s, Eq. 11.12 yields unrealistically high temperatures. Therefore, it is advisable to set the factor $k_2 = 0$ for $v \leq 1$ m/s.

11.1.5.2 Flank Temperature

The accuracy of experimental temperature measurements is limited according to [11.12]. Factors include the poor time resolution, the slowness of temperature measurements on moving objects, and the rapid cooling of the gear. It cannot be expected that the actual temperatures at the base of the tooth or even the addendum flank can be precisely measured. Nevertheless, experimental temperature measurements provide useful relative values. Table 11.2 contains a representative selection of measured and calculated values. The measurements are based on experiments on polymeric material gears mated with steel.

Although the temperatures measured at the base of the tooth are always higher than those calculated, there is no obvious correction which can be made to Eq. 11.12. On the other hand, the tooth flank temperature as calculated by Eq. 11.12 is much higher than the measured values, but these do not represent the actual flank temperatures.

The calculated value should at best be regarded as a *thermal parameter* since flank temperatures higher than the melting point of the polymeric material are frequently calculated. However, control experiments under the same conditions did not show melting of the flank. Since the difference between the measured and calculated values tends to increase linearly with the calculated value (see Figure 11.6), it appears justified to reduce the factor k_2 for calculating the flank temperature by approximately 30% so that:

$k_2 = 7$ for the pairing of steel with a polymeric material

$k_2 = 10$ for a polymeric material mated with a polymeric material

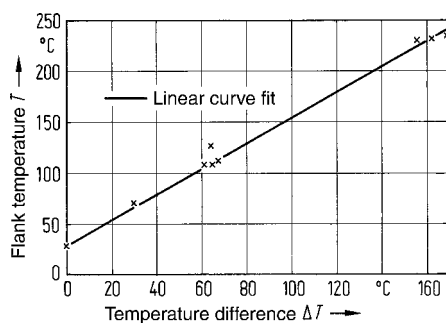
Table 11.2 Comparison of Measured and Calculated Gear Tooth Temperatures [11.12]

Calculation by Eq. 11.12 [°C]			Measurement [°C]	
T_{Base}	T_{Flank}	T_{IR}	$T_{\text{TV Base}}$	$T_{\text{TV max}}$
33	113	—	40	46
60	380	85	—	—
33	109	—	43	47
43	117	54	—	—
30	70	—	36	40
48	233	70	63	63
47	235	53	53	66
33	110	44	41	46
46	219	62	64	—
46	230	65	60	74
45	232	62	63	70
35	127	—	63	63

T_{IR} = temperature measured by infrared thermometry

$T_{\text{TV max}}$ = maximum temperature measured by thermovision camera

$T_{\text{TV Base}}$ = temperature measured at base of tooth by thermovision camera

**Figure 11.6** Flank temperature calculated using Eq. 11.12 versus the difference between the calculated and measured temperatures [11.12]

11.1.5.3 Relative Contact Time

The relative contact time CT is defined as:

$$CT = \frac{t}{\tau} \cdot 100 \quad (11.13)$$

where

t = sum of time under load in min occurring with the cycle time,

τ = cycle time in min.

In order to determine the cycle time of significance for the mated pair in a gear wheel system, the time to reach a steady thermal state was measured by analogy with the sliding bearing calculation [11.33]. It was further determined what percentage of the steady final temperature a gear wheel reached after t min loading time. From this, a factor was derived that takes into account the relative contact time in the temperature calculation. For this purpose, gears were placed stepwise under load for t_i min and their increase in temperature and final temperature were recorded. When analyzing this experiment, the quotient of the temperatures at t and τ min is used. It is not critical that the measured temperatures coincide exactly with those occurring experimentally.

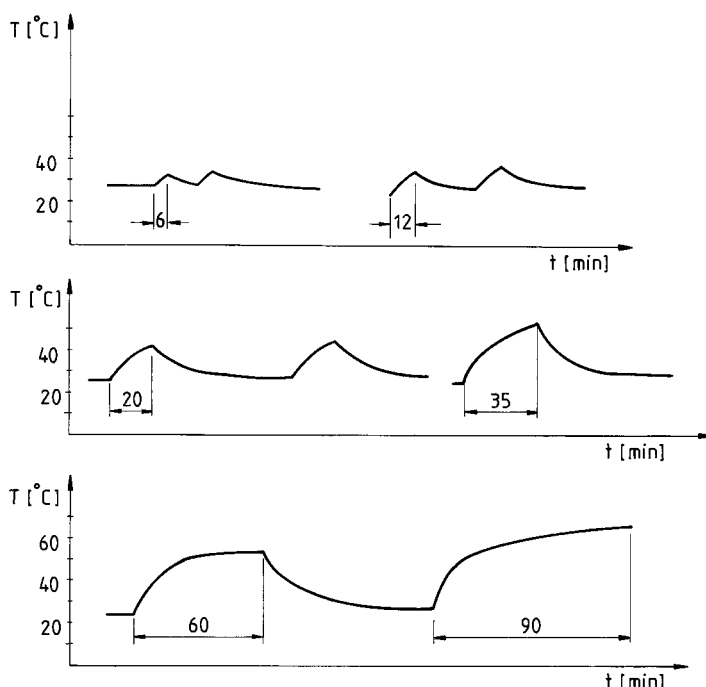


Figure 11.7 Temperature curves as a function of contact time [11.12]

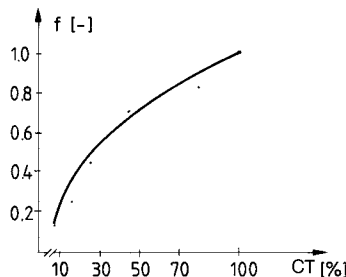


Figure 11.8 Correction factor as a function of the relative contact time for determining the base and flank temperature in intermittent operation [11.12]

The time to reach an approximately steady thermal operating state was established at approx. 90 min. To be on the safe side, this time was reduced. Therefore, it seems justified to set the cycle time $\tau = 75$ min. Any load lasting longer than 75 min should, therefore, be regarded as continuous operation. Figure 11.7 shows some characteristic temperature curves under constant load but with different contact times. From the difference between the final temperature reached in each case and the final temperature in steady state operation (after 75 min), a correction factor f_{CT} can be formulated, which takes the relative contact time into account in the calculation of the temperature (see Figure 11.8).

11.1.5.4 Optimized Numerical Value Equation

Taking account of the reducing effect of the factor f_{CT} in Figure 11.8 on the final gear temperature occurring during intermittent operation and of the optimized correction factors, the following equation is obtained for estimating temperatures in spur gears made from polymeric materials:

$$T_{t_1, t_2 \text{ CT}} = T_E + f_{CT} \cdot P \cdot f \cdot 136 \frac{i+1}{t_1 + 5i} \left[\frac{k_2 \cdot 17100}{w \cdot t_{1,2} \cdot (\nu m)^4} + 7.33 \cdot \frac{k_3}{A} \right] \quad (11.14)$$

where

T_E = temperature of surroundings in °C

P = power in kW

f = coefficient of friction

w = tooth width in mm

i = transmission ratio, $i = t_1/t_2$ with t_1 the number of teeth in the small wheel

ν = sliding velocity in m/s

m = module in mm

A = surface area of gear housing in m^2

Using Eq. 11.14, depending on the choice of value for k_2 , the temperature at the base of the tooth or the tooth flank temperature can be calculated.

- $k_2 = 7$ for flank temperature with steel/PA
- $k_2 = 10$ for flank temperature with PA/PA
- $k_2 = 1.0$ for base temperature with steel/PA
- $k_2 = 2.4$ for base temperature with PA/PA
- $k_2 = 0$ when oil lubrication is provided
- $k_2 = 0$ if $v \leq 1$ m/s

The factor k_3 represents the effect of the gear housing.

- $k_3 = 0$ for unenclosed gear in $\text{m}^2 \text{ K/W}$
- $k_3 = 0.043 - 0.129$ for partly enclosed gear in $\text{m}^2 \text{ K/W}$
- $k_3 = 0.172$ for enclosed gear in $\text{m}^2 \text{ K/W}$

Coefficients of friction f :

- $f = 0.04$ for gear with long-term lubrication
- $f = 0.07$ for gear lubricated by oil mist
- $f = 0.09$ for one-off greasing on assembly
- $f = 0.2$ PA/steel
- $f = 0.4$ PA/PA
- $f = 0.25$ PA/POM
- $f = 0.35$ PA/PBT
- $f = 0.18$ POM/steel
- $f = 0.2$ POM/POM
- $f = 0.18$ POM/PBT
- $f = 0.18$ PBT/steel
- $f = 0.3$ PBT/PBT

Equation 11.14 is not restricted to polyamide gear wheels. It can also be applied without modification to other thermoplastics with similar thermal conductivity.

11.2 Calculation of Load-Bearing Capacity

The standard literature covering the design of gear wheels made of polymeric materials generally refers to DIN 3990 [11.8], which applies to the design of metal gear wheels. This does provide a uniform basis for design. The design calculations are applicable to internally and externally geared straight and helical gears.

The numerous effects that can act on a toothed gear are described and taken into account in this standard by a series of factors, which can be determined by different methods identified as A, B, C, etc. Of these methods, A is the most appropriate, but also the most demanding because it involves extensive mathematical analyses and experimental measurements. However, *the neatly differentiated division into individual factors suggests a degree of accuracy that is not attainable for gear wheels made from polymeric materials.* There are no adequate studies for determining permissible stress levels for polymeric gears. Therefore, gear design calculations here will be done using method C, which is best suited to the unique behavior of polymeric materials.

11.2.1 Tooth Damage

Figure 11.1 distinguishes between the calculation of volume damage (breaking failure) and surface damage (fatigue, wear). These different types of damage arise from different stresses acting on the teeth.

Volume damage includes fracture at the base of the tooth (see Figure 11.10), breaking off of corners of teeth, and excessive deformation of the teeth. The latter form of damage is typical when gears are produced from ductile polymeric materials. The most common form of surface fatigue is pitting and chipping on the flank (see Figure 11.11), wear, partly fused flanks, formation of thermally induced brittle areas, and cracking close to the pitch diameter with subsequent fracture (see Figure 11.12). While the types of damage first mentioned are also found in metallic gear wheels, the other forms of damage are observed only in gear wheels made from polymeric materials.

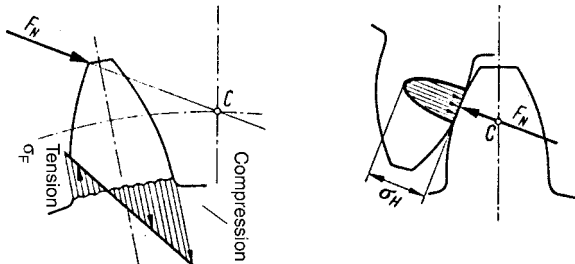


Figure 11.9 Bending stress acting on the tooth base (left) and pressure on the tooth flanks (right)

Figure 11.10 Fracture at the base of the tooth

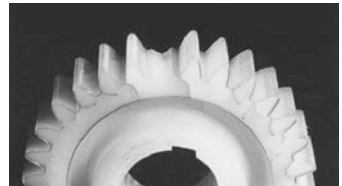


Figure 11.11 Pitting shortly before failure of the gear wheel [11.20]

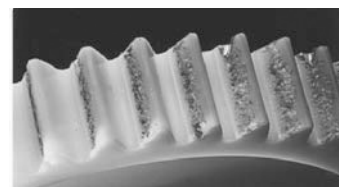


Figure 11.12 Cracks emanating from the tooth flank close to the pitch diameter

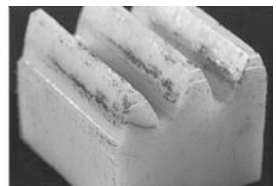


Table 11.3 Failure Matrix for Different Polymeric Materials and Types of Lubrication when Paired with Steel Gear Wheels

Material	Unlubricated	Grease	Oil
PA	Flank, base at high speeds [11.33]	Flank	Flank
$F/w = 20 \text{ N/mm}$ $v = 7.5 \text{ m/s}$	Initial fusion of tooth flanks [11.34]		
$F/w = 15 \text{ N/mm}$ $v = 7.5 \text{ m/s}$	Fracture close to pitch circle [11.34]		
POM	Flank [11.33]	Base [11.28]	Base [11.19]
PBT	Flank [11.33]	Flank	Flank
PEEK	Base, flank, wear at high ambient temperatures		
$F/w = 30 \text{ N/mm}$ $v = 7.5 \text{ m/s}$	Initial fusion of tooth flanks [11.34]	Flank	
$F/w = 15 \text{ N/mm}$ $v = 5 \text{ m/s}$ $T_E = 140^\circ\text{C}$	Wear [11.34]	Flank	

The type of damage actually occurring depends on the operating conditions and on the nature of the polymer from which the gear is made. Table 11.3 provides an overview of the types of damage to which PA, POM, PBT, and PEEK are susceptible under different forms of lubrication.

11.2.2 General Parameters

The *torque* M_t in Nm is given by:

$$M_t = 9550 \cdot \frac{P}{n} \quad (11.15)$$

where

P = power in kW

n = speed of rotation in min^{-1}

The *circumferential force* is given by:

$$F_C = 2 \cdot 10^3 \cdot \frac{M_t}{d_0} \quad (11.16)$$

where

d_0 = diameter of reference circle in mm

The *circumferential velocity* is given by:

$$\nu = \frac{d_0 \cdot \pi \cdot n}{60 \cdot 10^3} \quad (11.17)$$

The *application factor* K_A encompasses loads that vary over time, act on the gear from the outside, and represent an increase in the nominal torque. Reference [11.8] contains recommended values and instructions for these calculations when loads are known. When $K_A = 1.0$, calculation is done on the basis of a constant rated load.

The *dynamic factor* K_V covers internal dynamic forces generated by vibrations of the gear wheels themselves. However, in the case of gear wheels made from polymeric materials, inertia effects (due to the low specific gravity of polymers) and elastic rigidity are lower, so the force transferred relative to the tooth width is at least an order of magnitude smaller than for steel gears. In addition, damping by the material is high so that there is no need for an additional vibrational load term in the calculation. Accordingly, it is generally the case that $K_V = 1.0$.

The *width factor* $K_{F\beta}$ and the *face factor* $K_{F\alpha}$ are usually set to 1.0 for gear wheels made of polymeric materials.

11.2.3 Calculation of the Load-Bearing Capacity of the Tooth Base

Breaking of a tooth is avoided if the maximum stress σ_F occurring at the base of the tooth is kept lower than the permissible stress at the base of the tooth σ_{FP} (see Eq. 11.22). The maximum stress σ_F is determined separately for the pinion and the gear wheel when both are made of polymeric materials. The relationship for both gears is:

$$\sigma_F = Y_{Fa} \cdot Y_{Sa} \cdot Y_\epsilon \cdot Y_\beta \cdot K_A \cdot K_V \cdot K_{F\alpha} \cdot K_{F\beta} \cdot \frac{F_C}{w \cdot m_n} \quad (11.18)$$

Because of the length of the mathematical formulae and the related derivation, this will not be covered in full here. For further details the reader is referred to [11.8]. Only some brief explanations required to carry out design calculations common in practice are provided below (symbols used are those in the original publication; z_1, z_2 , etc. corresponds to t_1, t_2 , etc., F_U to F_C and b to w in previous equations).

Y_{Fa} = *Form factor*, which takes the shape of the tooth into account (see Figure 11.13).

Y_{Sa} = *Stress correction factor*, which takes the stress associated with the radius at the base of the tooth into account. This factor is not used because there is no data for gear wheels made from polymeric materials or because the results of any notch effect are already included in the values for the permissible stress. See also stress correction factor Y_{Sz} (permissible stresses).

Y_ϵ = *Overlap factor*, which covers the distribution of the load over several pairs of teeth.

$Y_\epsilon = 1/\epsilon_\alpha$, where $\epsilon_\alpha = \epsilon_{\alpha1} + \epsilon_{\alpha2}$ can be obtained from Table 11.4 for gears without profile adjustments.

Table 11.4 Partial overlap of teeth without profile adjustment [11.8]

z	14	25	36	47	58	69	80	91
ε_α	0.731	0.805	0.846	0.872	0.889	0.903	0.913	0.920
z	15	26	37	48	59	70	81	92
ε_α	0.740	0.810	0.849	0.873	0.891	0.903	0.913	0.921
z	16	27	38	49	60	71	82	93
ε_α	0.749	0.815	.851	0.875	0.892	0.904	0.914	0.922
z	17	28	39	50	61	72	83	94
ε_α	0.757	0.819	0.854	0.877	0.893	0.906	0.915	0.922
z	18	29	40	51	62	73	84	95
ε_α	0.765	0.822	0.857	0.879	0.895	0.906	0.916	0.923
z	19	30	41	52	63	74	85	96
ε_α	0.771	0.827	0.859	0.880	0.896	0.907	0.917	0.924
z	20	31	42	53	64	75	86	97
ε_α	0.778	0.830	0.861	0.882	0.897	0.909	0.917	0.924
z	21	32	43	54	65	76	87	98
ε_α	0.784	0.833	0.863	0.883	0.898	0.909	0.918	0.925
z	22	33	44	55	66	77	88	99
ε_α	0.790	0.837	0.866	0.885	0.899	0.910	0.919	0.925
z	23	34	45	56	67	78	89	100
ε_α	0.796	0.840	0.868	0.887	0.900	0.911	0.919	0.926
z	24	35	46	57	68	79	90	101
ε_α	0.801	0.843	0.870	0.888	0.901	0.912	0.920	0.927

For toothed structures having profile adjustment the following relationships apply:

$$\varepsilon_\alpha = z_1/2 \pi (\tan \alpha_{E1} - \tan \alpha_{A1}) \text{ and}$$

$$\tan \alpha_{A1} = \tan \alpha_{tw} (1 + z_2/z_1) - z_2/z_1 \tan \alpha_{A2}.$$

The value of $\tan \alpha_{E1}$ as a function of the auxiliary value $D_1 = d_{K1}/d_{G2}$, and that of $\tan \alpha_{A2}$ as a function of $D_2 = d_{K2}/d_{G1}$ may be found in Figure 11.14 (d_K = tip diameter, d_G = base diameter).

The pitch angle α_{tw} in the leading face is plotted for straight gears in Figure 11.15.

Y_β = *Helical factor*, which takes account of the ratios in helical gearing. In the case of helical gear wheels made of polymeric materials $Y_\beta = 1$ due to lack of data.

K_A = *Application factor*, see Section 11.2.2.

$K_v, K_{F\omega}$

$K_{F\beta} = 1.0$, see Section 11.2.2.

b = *Tooth width*. When there are different tooth widths in a mated pair the maximum value of b is given by $b = b_{min} + m_n$.

m_n = *Module* in normal section.

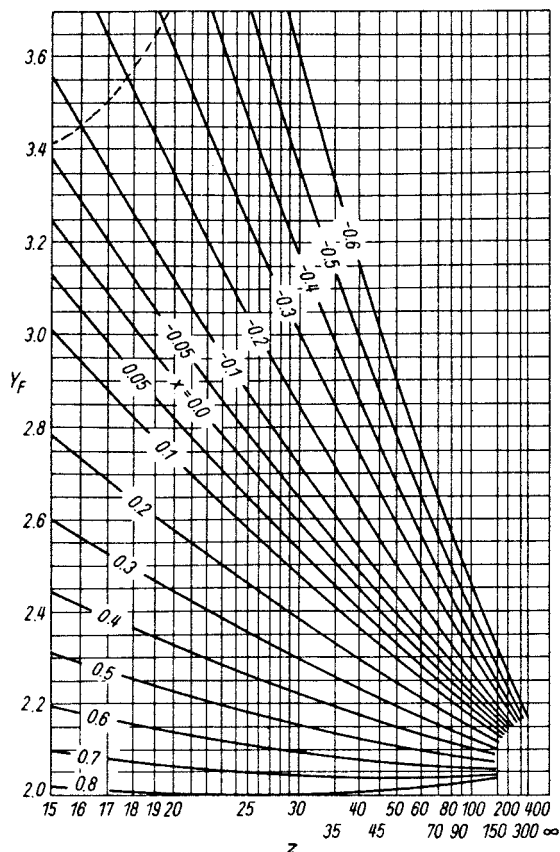


Figure 11.13 Tooth form factor for external gearing [11.8]

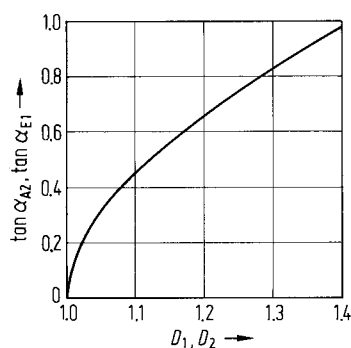


Figure 11.14 Auxiliary diagram for calculating ϵ_α

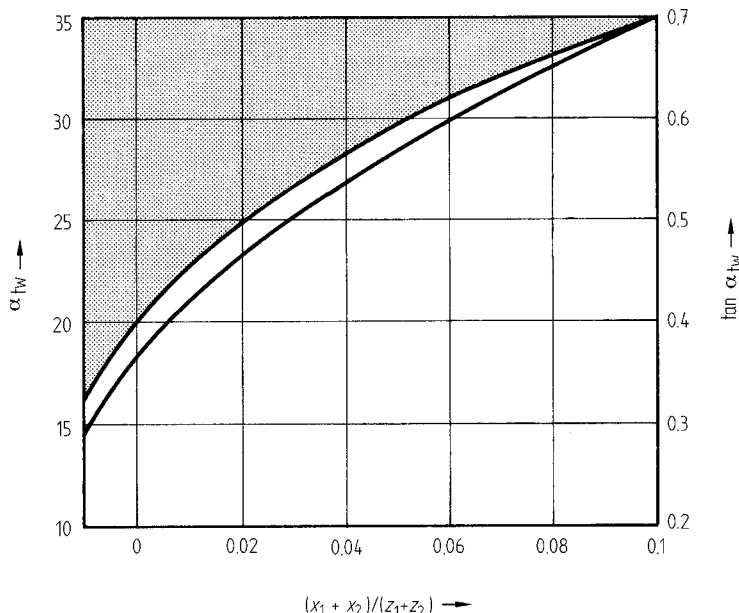


Figure 11.15 Pitch angles α_{tw} and $\tan \alpha_{tw}$

Thus, the equation for the maximum stress occurring at the gear tooth base for gears made from polymeric materials can be simplified from that given in Eq. 11.18 to:

$$\sigma_F = K_A \cdot Y_{Fa} \cdot \gamma_\varepsilon \cdot \frac{F_u}{b \cdot m_n} \quad (11.19)$$

The permissible gear tooth base stress is calculated separately for the pinion and gear from the following equation:

$$\sigma_{FP} = \frac{\sigma_{F\lim} \cdot Y_{ST} \cdot Y_{NT}}{S_{F\min}} \cdot Y_{\delta\text{ rel T}} \cdot Y_{R\text{ rel T}} \cdot Y_X \quad (11.20)$$

$\sigma_{F\lim}$ = *Tooth base flexural fatigue strength*, determined from running trials on test gears or from material vibration experiments after $3 \cdot 10^6$ load cycles. After this number of load cycles, an endurance limit has not yet been reached for gear wheels made of polymeric material. The strength value is, therefore, taken as a function of the number of load cycles from the diagrams $\sigma_{FN} = f(L_w)$ in Figures 11.16 to 11.19 for the tooth base temperature calculated by Eq. 11.14. In this way, the factor Y_{NT} is not required. The extent to which there is a relationship between the tooth base flexural fatigue strength determined on gear wheels and vibrational fatigue strengths measured on test pieces has not yet been investigated systematically. It is obvious that comparison is inappropriate as the stresses are not comparable.

Y_{NT} = Service life factor = 1.0 (see above)

Y_{ST} = Stress correction factor. Y_{ST} like Y_{Sa} (qv) is not required. If $Y_{ST} = 2.0$, as specified in DIN 3990, the ordinate values in the $\sigma_{FN} = f(L_w)$ diagrams would have to be doubled. While this would be formally correct, it would give rise to tooth base strengths which are higher than the tensile strength of the polymeric material in question. This procedure was used in [11.11]. It follows that: $Y_{Sa} > 1.0$.

$S_{F \min}$ = Minimum safety factor against fracture at the tooth base

$Y_{\delta \text{ rel T}}$ = Relative support number = 1.0 (due to lack of data)

$Y_{R \text{ rel T}}$ = Relative surface factor = 1.0 (due to lack of data)

Y_X = Size factor = 1.0 (due to lack of data)

Accordingly, the permissible stress at the base of the gear teeth for gears made of a polymeric material is given by:

$$\sigma_{FP} = \frac{\sigma_{FN}}{\sigma_{F \min}} \quad (11.21)$$

and, reverting to the symbols in Eq. 11.18, the condition to prevent failure is:

$$\sigma_F = \frac{F_C}{w \cdot m_n} \cdot K_A \cdot Y_{Fa} \cdot Y_\varepsilon \leq \frac{\sigma_{FN}}{\sigma_{F \min}} \quad (11.22)$$

The tooth base strength σ_{FN} based on the number of load cycles for the tooth base temperature $T_{t1, t2}$ calculated from Eq. 11.14 and for the type of lubrication in use is taken from Figures 11.16 to 11.19.

In Figure 11.16, sample single measured values are plotted and from these, the Wöhler curves in Figures 11.17 to 11.19 are constructed. The extensive scatter shows that these curves represent lower limits with a high degree of confidence.

With reference to the type of lubrication, there is no need to demonstrate adequate tooth base strength because, as shown in Table 11.3, this does not determine service life.

Reference [11.21] provides experimental curves of $\sigma_{FN} = f(L_w)$ for PA 6 and PA 6 GF lubricated by oil. They differ by $\pm 5\%$ from those in Figure 11.17 for PA 66 so that the latter can also be used with a sufficient degree of accuracy for PA 6 and even for glass fiber reinforced PA lubricated with oil. It is noteworthy in this case that the superior strength of glass fiber reinforced PA under static load is lost when it is used for a lubricated gear wheel.

The high-temperature thermoplastic PEEK is distinctly superior to standard thermoplastics, particularly at high ambient temperatures. At 140 °C, PEEK withstands a load about 10 times higher than POM [11.34].

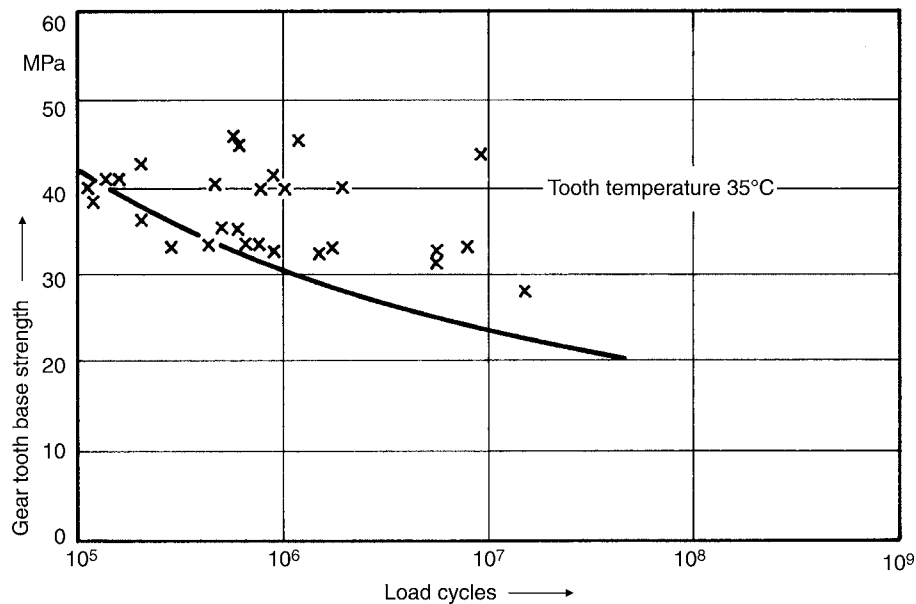


Figure 11.16 Tooth base strength σ_{FN} for POM lubricated with grease at a tooth base temperature of 35 °C. Note the extreme scattering of the individual measured values [11.18].

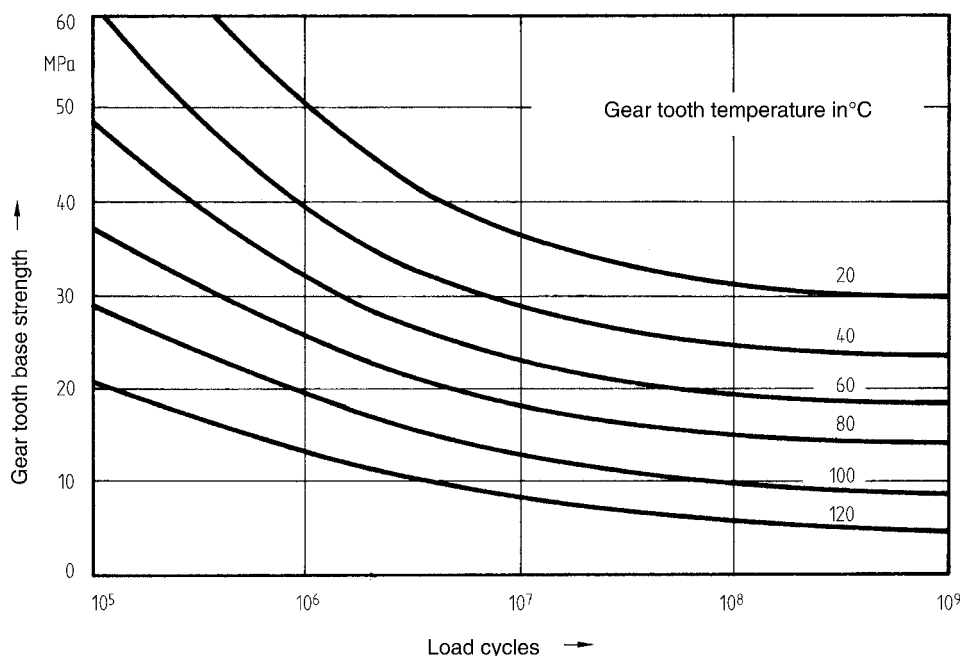


Figure 11.17 Tooth base strength σ_{FN} for unlubricated PA 66 gear wheels produced by machining [11.10]

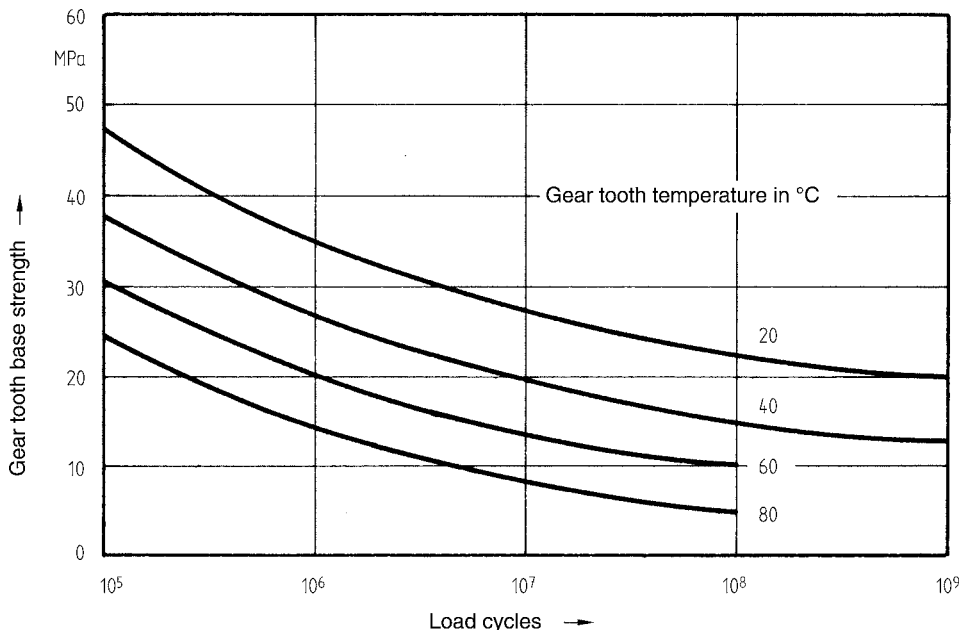


Figure 11.18 Tooth base strength σ_{FN} for POM gear wheels produced by machining and lubricated with grease

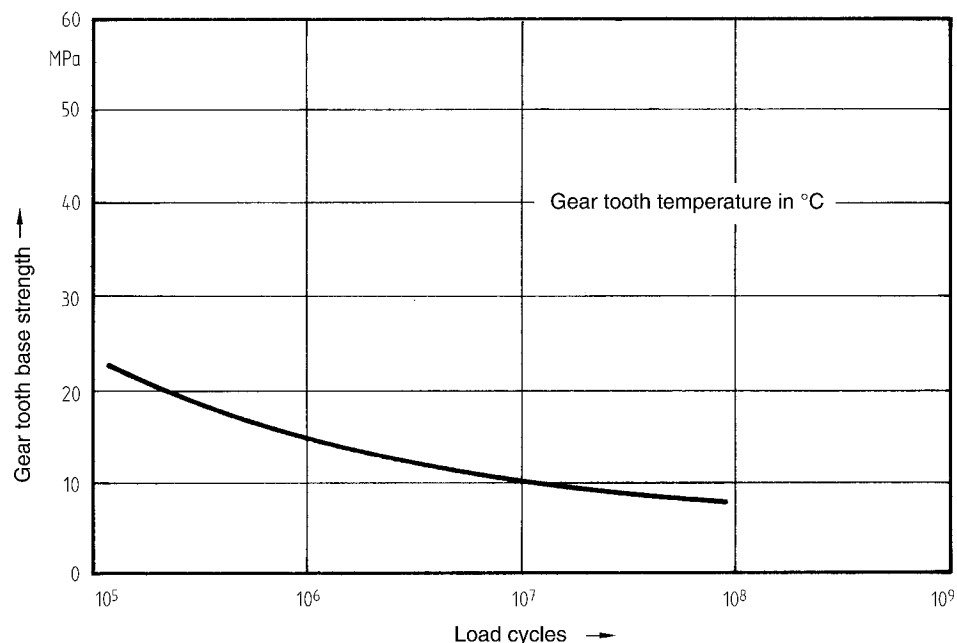


Figure 11.19 Tooth base strength σ_{FN} for HDPE gear wheels produced by machining and lubricated with an oil-in-water emulsion [11.33]

11.2.4 Calculation of the Load-Bearing Capacity of the Tooth Flank

Strictly speaking, the Hertzian relationships for stress in arched surfaces do not apply to polymeric materials because the assumption of elastic behavior is not fulfilled. Nevertheless, the load-bearing capacity of the flanks for polymeric gears is commonly calculated on the basis of the Hertzian stress σ_H , which must not be greater than the permitted flank stress σ_{HP} . Since this permitted flank stress is determined in the same way on gear wheels, the application of the Hertzian relationships is justified as a working hypothesis. It would be more appropriate though, to refer to a stress parameter. The effective flank stress is given by:

$$\sigma_H = Z_H \cdot Z_E \cdot Z_\epsilon \cdot Z_\beta \cdot \sqrt{K_A \cdot K_V \cdot K_{H\alpha} \cdot K_{H\beta} \cdot \frac{t_1 + t_2}{t_2} \cdot \frac{F_C}{d_0 \cdot w}} \quad (11.23)$$

The factors K_A , K_V , $K_{H\alpha}$, and $K_{H\beta}$ have already been explained in Section 11.2.2. The Z factors are defined below.

Z_H = *Zone factor*, which takes account of the curvature of the tooth flanks.

$$Z_H = \frac{1}{\cos \alpha} \cdot \sqrt{\frac{1}{\tan \alpha_{tw}}}$$

$\tan \alpha_{tw}$ is taken from Figure 11.15.

Z_E = *Elasticity factor*, which takes account of the elasticity of the paired materials. This factor can be estimated with sufficient accuracy as:

$$Z_E = \sqrt{0.38 \cdot E'}$$

where $E' = 2 E_1 \cdot E_2 / E_1 + E_2$ takes account of the differences in modulus values of the materials involved. The value of the modulus of elasticity is inserted for the flank temperature calculated by Eq. 11.14 (see Figure 11.20). In the case of a polymeric material mated with steel, $E' \approx 2 E_{\text{polymeric material}}$.

Z_ϵ = *Overlap factor*. This takes overlap into account and in the case of polymeric materials is assumed to be the same for straight and helical gearing. $\epsilon_{\alpha t}$ is taken from Table 11.4.

$$Z_\epsilon = \sqrt{\frac{4 - (\epsilon_{\alpha t_1} + \epsilon_{\alpha t_2})}{3}}$$

Z_β = *Helical factor*, which takes account of the nonuniform distribution of force.

$$Z_\beta = 1.0$$

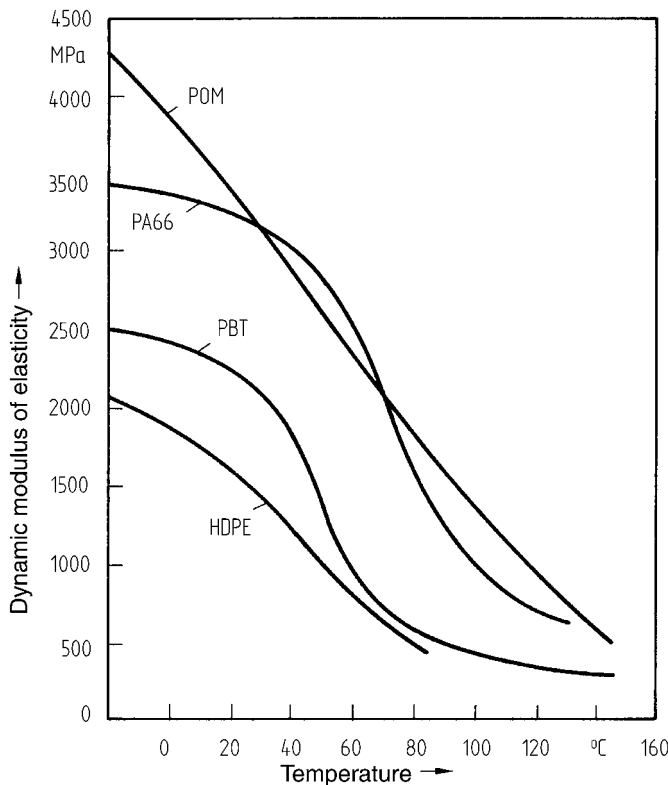


Figure 11.20 Dynamic modulus of elasticity as a function of temperature [11.17]

With these simplifications, Eq. 11.23 for polymeric materials is generated:

$$\sigma_H = Z_H \cdot Z_E \cdot Z_\varepsilon \cdot \sqrt{K_A \cdot \frac{t_1 + t_2}{t_2} \cdot \frac{F_C}{d_0 \cdot w}} \quad (11.24)$$

The permissible tooth flank stress is determined separately for the drive gear and the driven gear from the following equation:

$$\sigma_{HP} = \frac{\sigma_{H\lim}}{S_{H\min}} \cdot Z_N \cdot Z_L \cdot Z_R \cdot Z_V \cdot Z_W \cdot Z_X \quad (11.25)$$

$\sigma_{H\lim}$ = Pitch strength. $\sigma_{H\lim}$ is read off (like $\sigma_{F\lim}$ in the tooth base strength calculation) from the $\sigma_{HN} = f(L_w)$ diagrams (Figures 11.21 to 11.25) as a function of the number of load cycles for the tooth flank temperature calculated by Eq. 11.14.

Thus, the factors Z_N , Z_L , and Z_W are not required.

Z_N = Service life factor = 1.0

Z_L = Lubricant factor = 1.0

Z_V = Velocity factor = 1.0

Z_W = Paired materials factor = 1.0

Z_X = Size factor = 1.0

The permissible tooth flank stress for gear wheels made from polymeric materials, therefore, assumes the form:

$$\sigma_{HP} = \frac{\sigma_{HN}}{S_{H\ lim}} \quad (11.26)$$

The condition for avoiding failure is:

$$\sigma_H = Z_H \cdot Z_E \cdot Z_\epsilon \cdot \sqrt{K_A \cdot \frac{t_1 + t_2}{t_2} \cdot \frac{F_C}{d_0 \cdot w}} \leq \frac{\sigma_{HN}}{S_{H\ lim}} \quad (11.27)$$

The limiting flank stress for gear wheels made from PA 6 [11.20] suggests that

$$\sigma_{HN\ PA\ 6} = 0.8 \sigma_{HN\ PA\ 66}$$

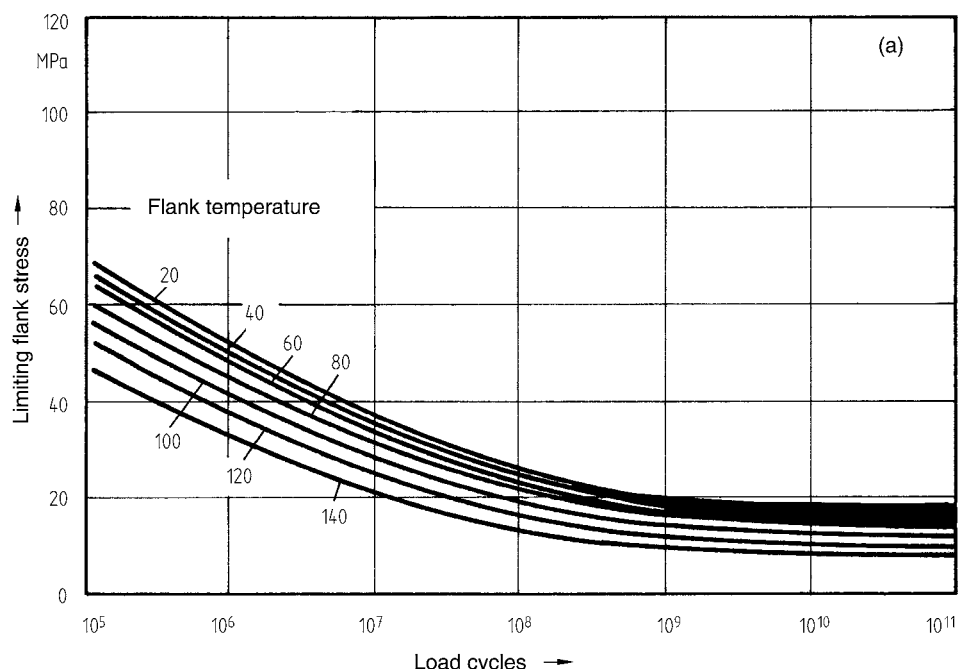


Figure 11.21 Limiting flank stress σ_{HN} for PA 66 gear wheels produced by machining

- a) Unlubricated
- b) Lubricated with grease
- c) Lubricated with oil [11.20]

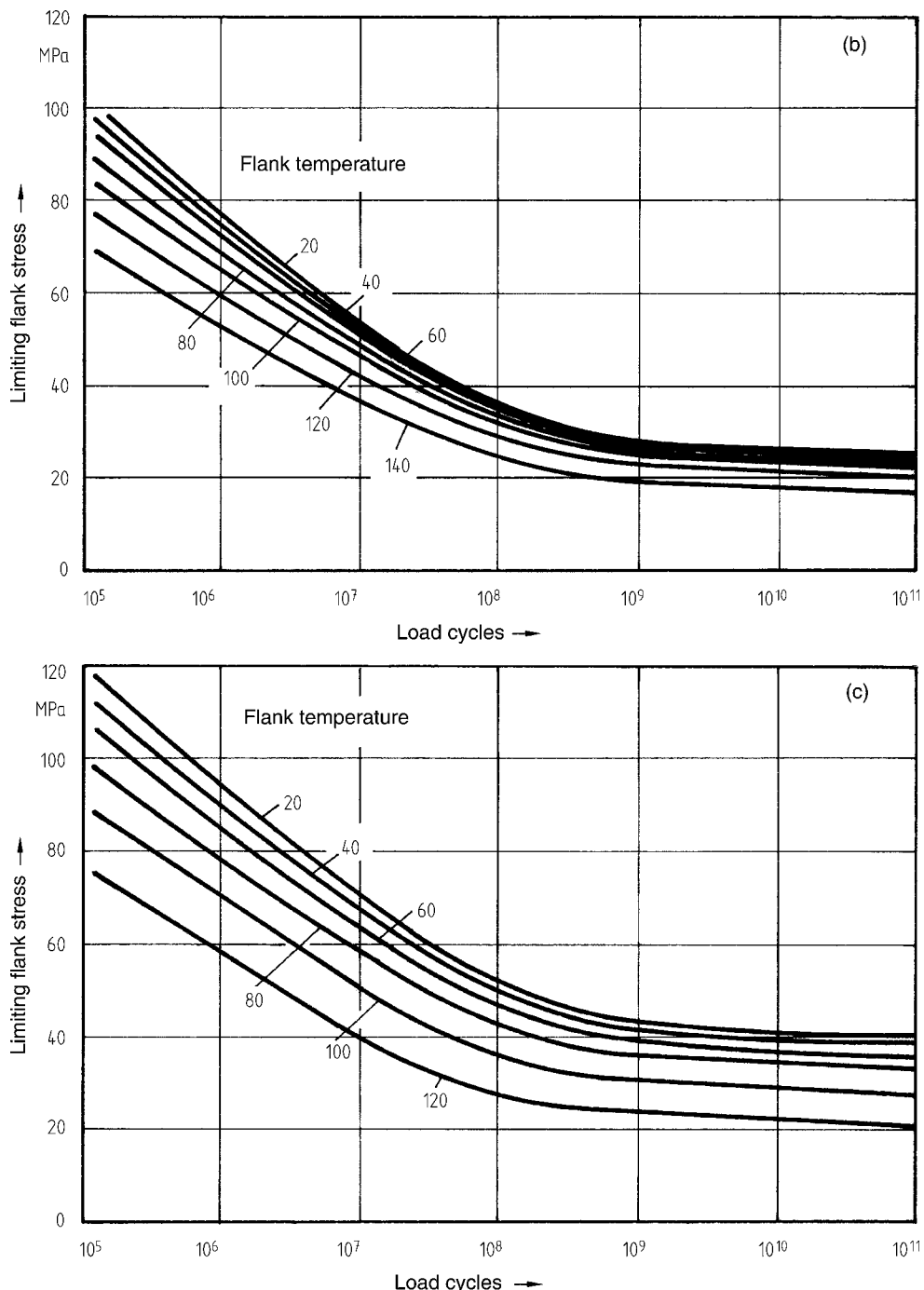


Figure 11.21 (continued)

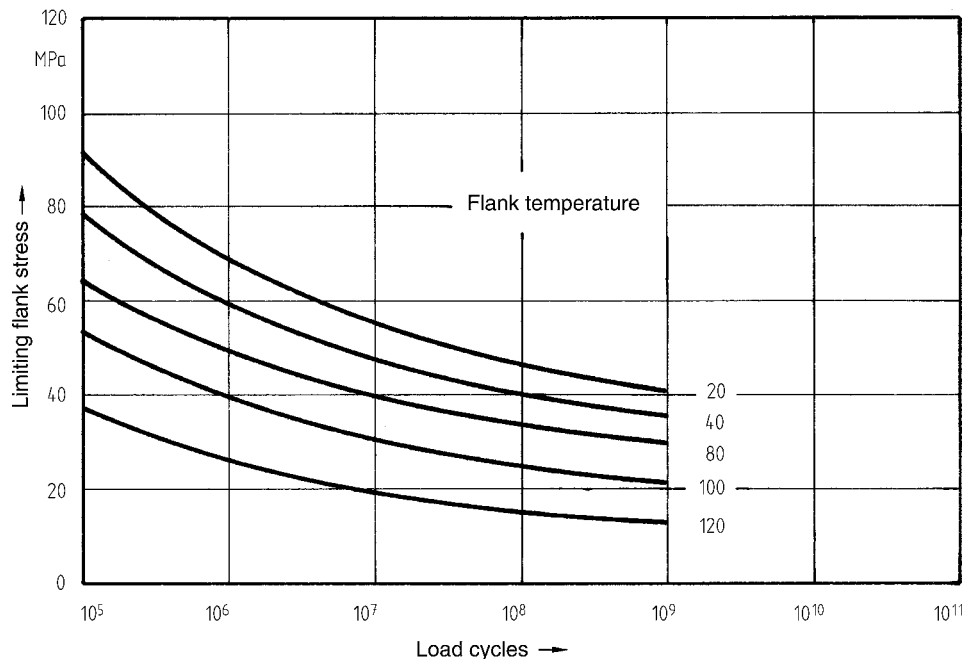


Figure 11.22 Limiting flank stress σ_{HN} for unlubricated POM gear wheels produced by machining [11.18]

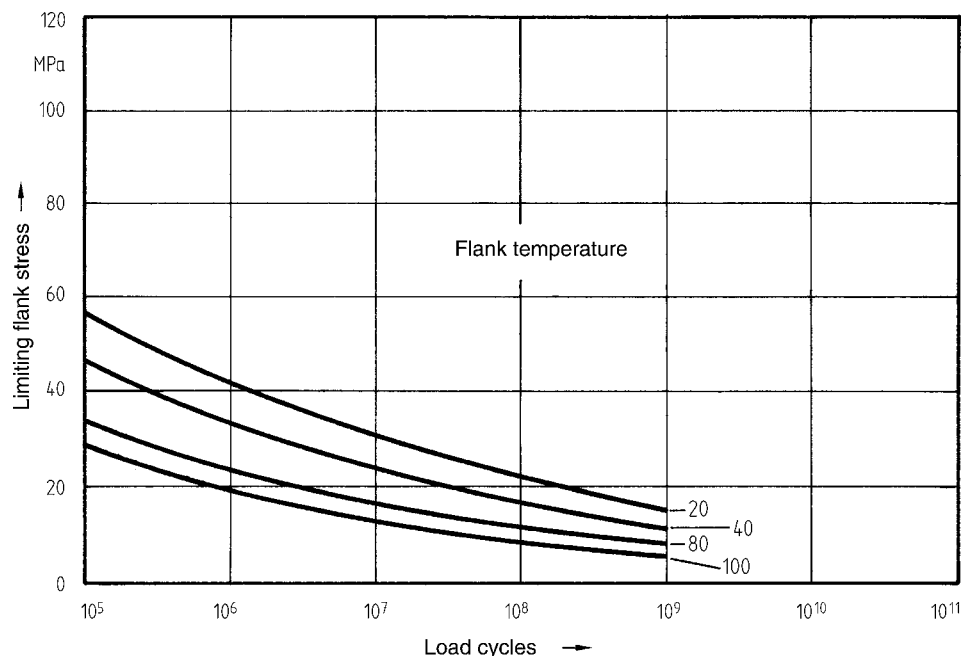


Figure 11.23 Limiting flank stress σ_{HN} for unlubricated PBT gear wheels produced by machining [11.18]

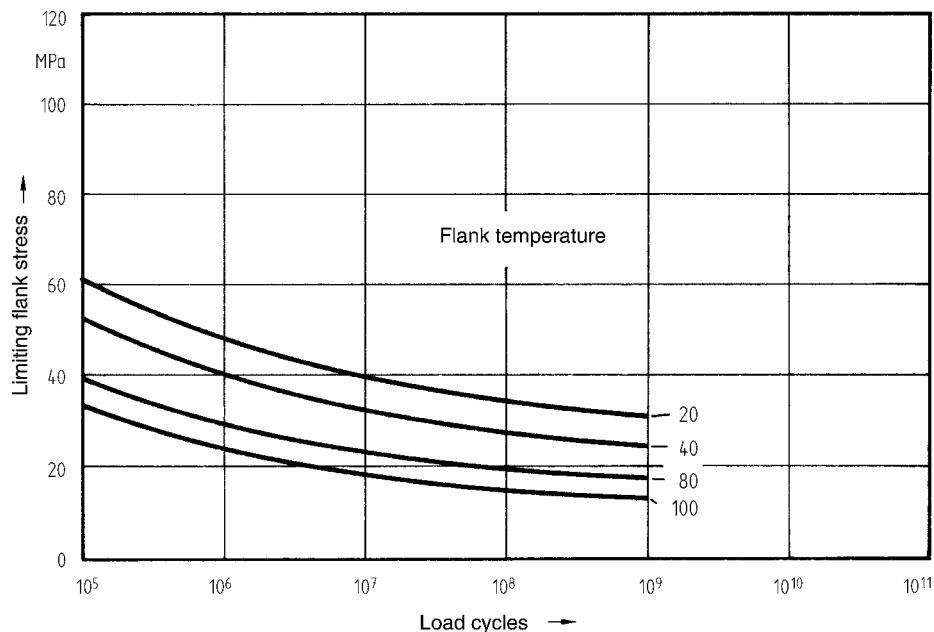


Figure 11.24 Limiting flank stress σ_{HN} for PBT gear wheels produced by machining and lubricated with grease [11.18]

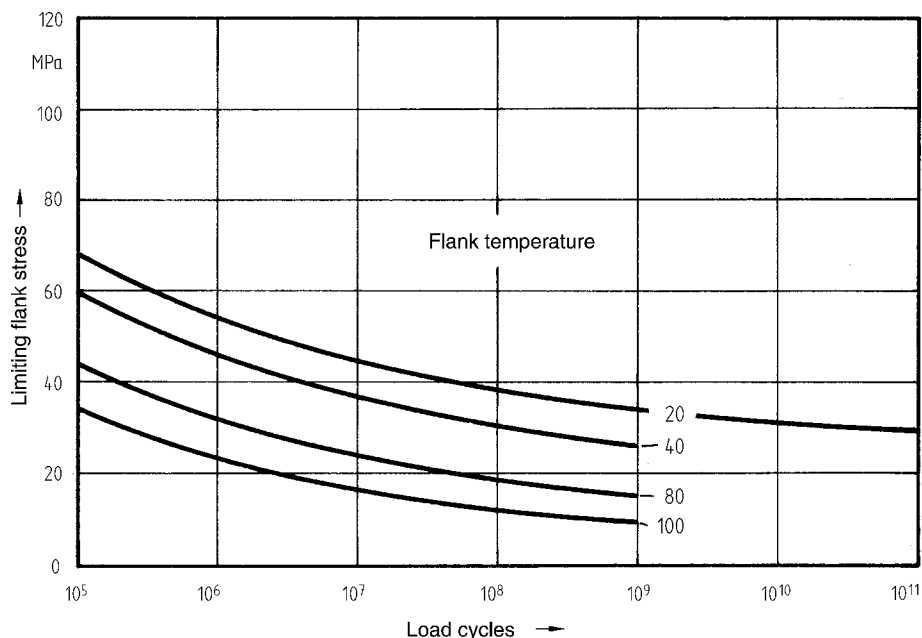


Figure 11.25 Limiting flank stress σ_{HN} for PBT gear wheels produced by machining and lubricated with oil [11.18]

11.2.5 Calculation of Tooth Deformation

As a supplement to the DIN specifications, tooth deformation should be calculated as a possible form of damage in gear wheels made from polymeric material. Deformation of the gear teeth occurs during the transition from the unloaded to the loaded state resulting in a condition much like a pitch error. Deformation can also occur when the tooth is under a static load. The deformation f_K may be considered to be a shift of the tip of the gear tooth in the circumferential direction and is expressed as:

$$f_K = \frac{3 \cdot F_C}{2 \cdot w \cdot \cos \alpha_0} \varphi \left(\frac{\Psi_1}{E_1} \right) \quad (11.28)$$

where

φ = coefficient from Figure 11.26

$\Psi_{1,2}$ = coefficients from Figure 11.27

$E_{1,2}$ = modulus of elasticity (in dynamic operation from Figure 11.20; creep modulus when under long-term load)

When a polymeric material is mated with steel, $\Psi_{\text{steel}}/E_{\text{steel}} = 0$.

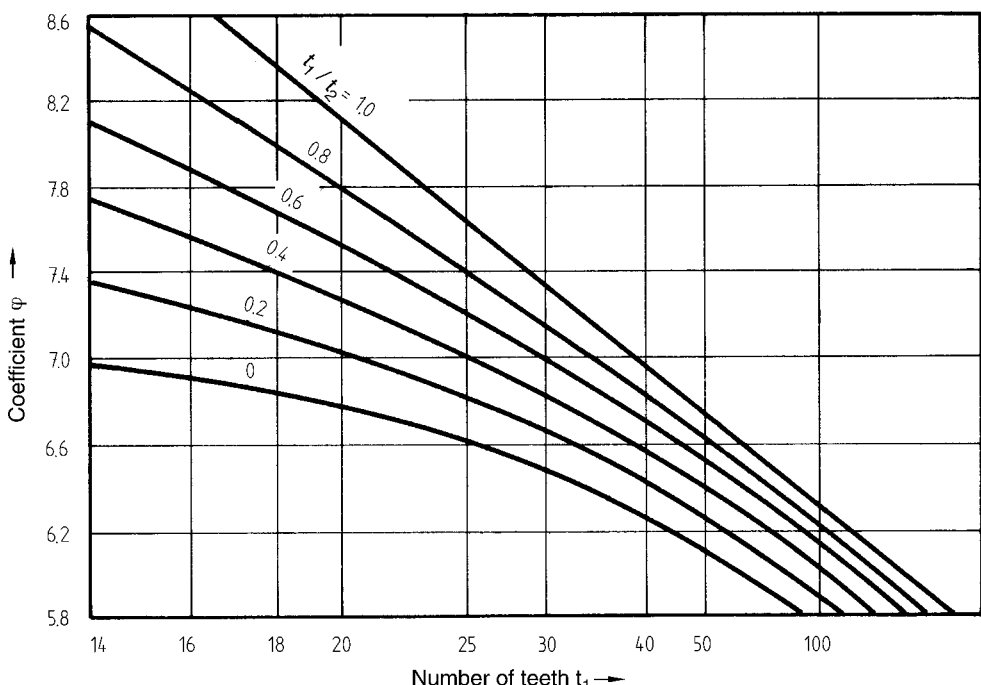


Figure 11.26 Coefficient φ for calculating tooth deformation [11.10]

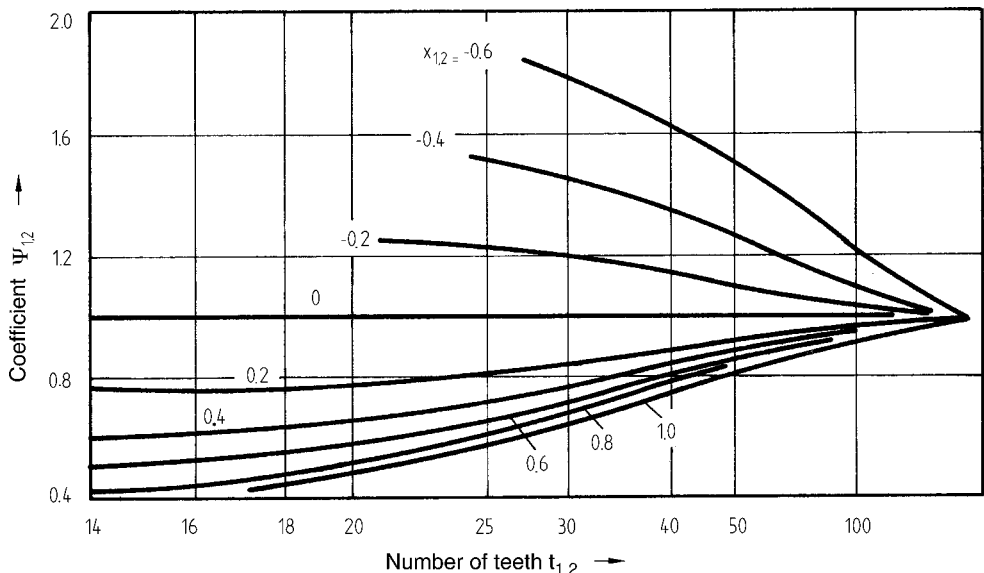


Figure 11.27 Coefficients $\psi_{1,2}$ for calculating tooth deformation [11.10]

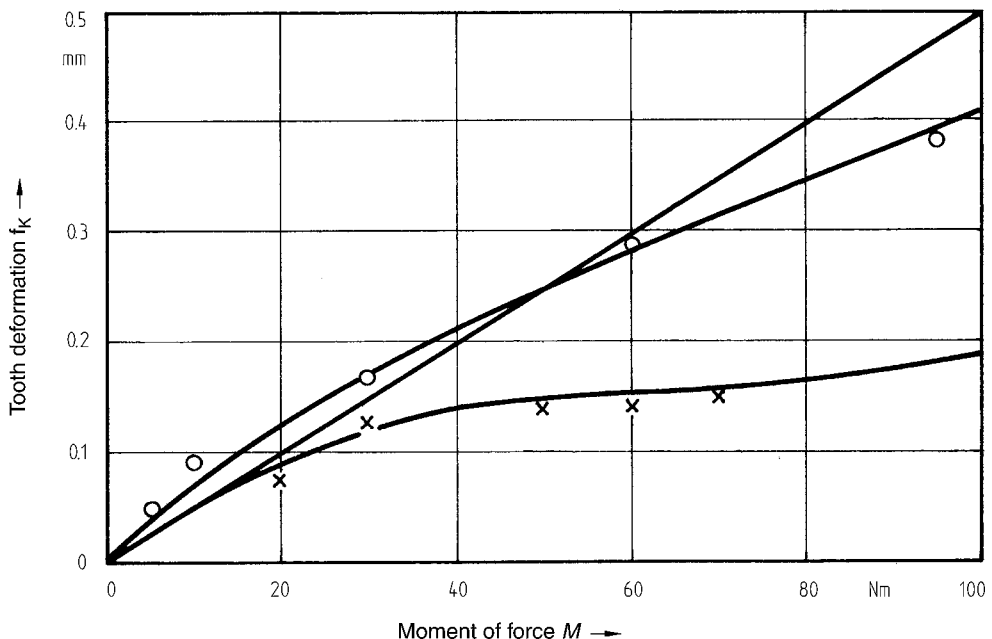


Figure 11.28 Tooth deformation on a gear wheel made of PA 66 with $m = 4.5 \text{ mm}$, $t = 24$, and $x = 0.18$ [11.10]; — calculated, —○— measured on a single tooth —×— measured on the gear wheel

The permissible tooth deformation is determined by the requirements with regard to running noise and service life. Experimental studies have shown [11.10] that running noise begins to increase appreciably from $f_K = 0.4$ mm. Another threshold is specified as $f_K \leq 0.1$ multiplied by the modulus. Thus, we have

$$f_{K \text{ perm}} \leq 0.4 \text{ mm} \quad (11.29)$$

or

$$f_{K \text{ perm}} \leq 0.1 \cdot m \quad (11.30)$$

In Figure 11.28, the deformation calculated from Eq. 11.28 is compared with values measured in static experiments. As expected, measurements on single teeth yield higher values than those determined for the entire gear wheel.

11.3 Design

11.3.1 Injection Molding

Gear wheels are rotationally symmetrical parts on which high demands for accuracy are imposed. Forming them from a molten polymeric material by injection molding, therefore, requires symmetrical filling of the mold to help ensure uniform dimensions. The highest precision, truest running gears can be expected when a gear wheel is filled using an internal disc (or diaphragm) gate (see Figure 11.29). The sprue and disc must be removed at a later stage if it cannot be used as part of the gear wheel (see Figure 7.39).

In smaller gear wheels, a triple pin gate in the wheel hub (see Figure 11.30) has proved to be an effective gating scheme. A pin gate arranged off-center on the front end of the hub is particularly easy to separate.

Figures 11.29 and 11.30 show that the wall thickness distribution in gears is important. Thick wall sections should be avoided.

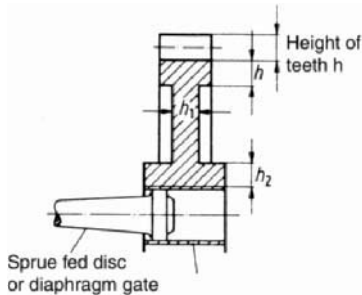


Figure 11.29 Disc gate and wall thickness ratio: $h < h_1 < h_2$ for an injection molded gear

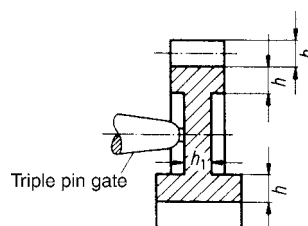


Figure 11.30 Triple pin gate and wall thickness ratio: $h_1 > 1.1 h$ for an injection molded gear

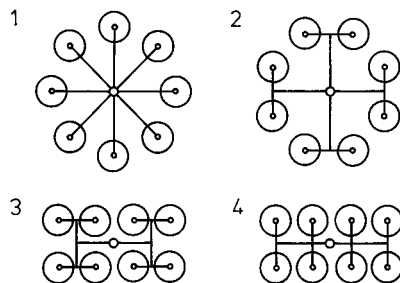


Figure 11.31 Examples of naturally balanced runner systems (1, 2, and 3) and an unbalanced runner system (4) [11.32]

Small gear wheels are usually produced in multi-cavity molds. If this is the case, care should be taken that the gating system, *i.e.*, the runners to the individual mold cavities, are matched in length and diameter so that each cavity is filled at the same time and has the same pressure history. This is essential for uniform molding quality. If naturally matched runners are used (see Figure 11.31, 1, 2, and 3) this requirement is met from the outset, otherwise (Figure 11.31, 4) balancing must be done artificially by other means (*e.g.*, using a computer simulation to determine runner dimensions for each cavity) [11.22].

Reinforcement of the body of the gear wheel using ribs is often required, especially in the case of larger gear wheels. This may then result in the loss of balance. The ribs should radiate outwards on both sides so that symmetry is retained as much as possible. If ribs are used on only one side, there is an added risk of warpage (see also Section 7.2.3).

Figure 11.32 shows that designing for production can sometimes be misunderstood. In order to produce teeth with good dimensional accuracy, without voids, and without sink marks, the gear teeth are cored out on both sides. The result, however, in this case is that the loss of load-bearing capacity is more serious than the potential void-related problems. This design may be adequate for non-critical applications.

Metal/polymer composite gears as shown in Figure 11.33 make little sense. As a result of tooth flank stress such gear wheels fail after just a short service life [11.33], because the polymer layer is too thin.

One of the advantageous design freedoms in the injection molding process is the ability to combine a number of functional elements to form a single component. Figure 11.34 shows such a multifunctional design for a drive wheel in a lawn mower. The gear wheel drive, bearing, and drive wheel are integrated in one part. The running track is snapped on over ribs on the outer edge.

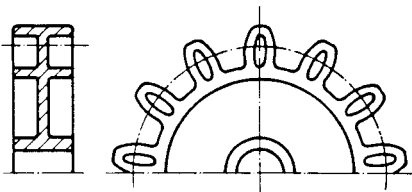


Figure 11.32 Gear wheel with cored out sections to avoid accumulation of material and related shrinkage problems [11.23]



Figure 11.33 Metal base element encased by polymeric material. Example of a design unsuitable for withstand stress [11.33].

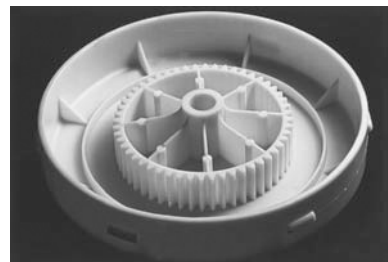
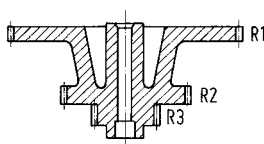


Figure 11.34 Drive wheel made from PA 6 as a multi-functional component of a lawn mower [11.33]



Wheel number	W1	W2	W3
Number of teeth	72	42	21
Modulus m	0.5	0.5	0.5
Reference diameter d_0	36	21	10.5
Profile adjustment factor x	- 0.3	-	-
Tolerance zone (wheel)	10 fd S"	10 fds"	10 fds"
Pitch zones	0.071	0.063	0.056
Pitch increasement	0.025	0.022	0.020

Figure 11.35 Set of stepped gears designed for the injection molding process [11.24]

Figure 11.35 shows a design for a set of gear wheels optimized for injection molding. The three wheels are produced in one operation as a single component. The illustration also provides data on production accuracy.

With injection-molded gear wheels, there is no need for an exit location for the gear cutting tool (as with ground or milled gears), so the teeth can be engaged on only one side (see Figure 11.34 and Figure 11.35, R_3). This gives rise to a certain increase in rigidity but also results in a nonuniform contact pattern over the width of the teeth. The upswept shoulder of the spur gear in a worm drive in Figure 11.36 is intended to increase the transmittable power and the service life. This measure, which is readily implemented in the injection mold, provides a greater contact surface between the screw and the worm gear and as a result, stress is reduced [11.17].

An improvement would be a worm gear that can intermesh with a larger segment of the screw. As a single part, however, this would not be demoldable. Such a worm gear can be manufactured in two identical halves, each of which are easily demoldable (see Section 7.3.3). The two halves are then joined together by snap-fit joints, screws, or rivets and centered by means of pins and corresponding bosses (see Figure 11.37).

A worm gear is easier to demold if it is flattened on two sides. This should only be done if the resultant loss in load-bearing capacity is acceptable in the application (see Figure 11.38).

Toothed racks can be rendered flexible up to a point by providing notches on the reverse side so that articulated joints are produced between the teeth (Figure 11.39; see also Sections 6.1 and 6.2).

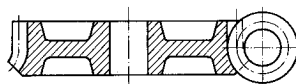


Figure 11.36 Spur gear with upswept shoulder for a worm gear [11.17]

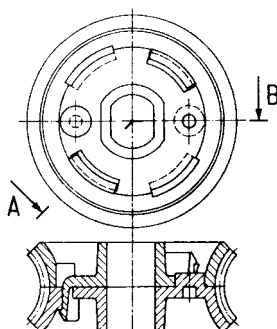


Figure 11.37 Two-part worm gear, designed for production by injection molding [11.25]



Figure 11.38 Flattening one side of the surfaces allows demolding without undercuts
(Manufacturer: IMS Morath, Donaueschingen)



Figure 11.39 Flexible rack produced by notching the back side of the rack [11.39]

11.3.2 Production of Gears by Machining

Compared with injection molding, design freedom for machined gears produced from semifinished products (*e.g.*, extruding polymeric materials, profiles, or rods) is very limited. This method, however, is useful for producing rotationally symmetrical parts, parts that have very tight tolerances, gears that are difficult to demold, and for prototypes or small production runs.

- For gear wheels with a large module ($m > 3$ mm), production accuracy by machining is always higher. Even in high volume production of gear wheels with high precision requirements, the gearing is sometimes reworked by machining after injection molding.
- Machined gear wheels with solid wheels exhibit higher strength compared to injection molded gear wheels, which must be designed with relatively thin walls and ribbing to accommodate process requirements. The wheel faces are planar without protruding hubs. Cored-out sections for reducing mass and avoiding shrinkage problems are not needed.
- Polymeric materials of high molecular weight are employed for extruding the semifinished products. This means that the gears produced from these materials will have good mechanical properties and significantly higher resistance to wear (see also Figure 4.37).
- Compared with the machining of metals, gear wheels of high module (*i.e.*, high volume of material to be removed) can be produced with a cost savings of up to 40% due to the higher rates of machining possible with plastics. The gear wheel in Figure 11.40 is an example of this [11.26].
- The cutter advancement speed is critical and can cause differences in operating characteristics of the gear. The tooth faces become steadily more undulatory as the rate of cutter advancement increases [see Figure 11.41].

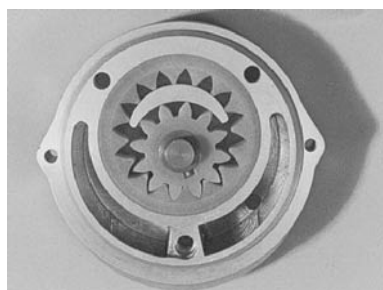


Figure 11.40 Damping member for hydraulic equipment in ski lifts. The wheels in the gear wheel are manufactured from POM and PBT, in conformity with tolerance grade IT 7 [4.18].

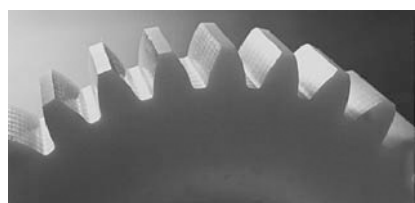


Figure 11.41 Tooth flanks cut at a rate of 0.2 mm (top) and 6.0 mm (bottom) [11.33]

The highly undulatory tooth flanks in a POM gear wheel operating *without lubrication* are soon smoothed (or worn) after a short start-up phase. After this, the torsional face backlash is, as expected, a few μm higher. In the case of *lubricated* POM tooth flanks, pitting occurs due to the high local stresses at the tips of the undulations. Nevertheless, the lubricated POM gear wheel has a longer service life than the unlubricated one. Therefore, POM gear wheels can be manufactured at higher cutter advancement speeds without significant loss in quality. This reduces costs considerably.

In the case of PA gear wheels, there is less initial smoothing of the flanks due to the higher resistance of PA to wear. Whether *lubricated* or *unlubricated*, the load-bearing capacity of wheels cut at higher cutter advancement speeds is slightly lower due to the gradual increase in pitting [11.33].

11.3.3 Shaft-Hub Joints

The best method of fastening a gear wheel to a metal shaft depends on the magnitude of the torque to be transmitted, the temperature, and production efficiency considerations. Simple frictional joints (*i.e.*, press fits) suffice for transmitting very small torques (see also Section 1.1.2). At any rate, a higher torque can be transmitted via the toothed structure than via a frictional joint. If temperatures higher than about 60°C occur, a more costly type of joint must be chosen, *e.g.*, a pretensioned form-fitting joint.

11.3.3.1 Press-Fit Joints

A distinction is made between longitudinal and transverse press-fit joints. In a *longitudinal press-fit joint*, the gear wheel is pushed axially onto the shaft. The prerequisite for a sound joint is to provide the shaft with a chamfer of 1.5 to 2 mm at a 30° angle. In the case of rough metal shafts, there is a danger that the polymeric material will be shaved off by surface irregularities on joining, thus reducing the effectiveness of the deliberate undersizing of the gear. *Transverse press-fitting joints* are obtained by hot-shrinking. They are useful particularly in the case of larger dimensions for keeping the assembly force within reasonable limits. In the case of *clamp joints*, pressure is applied by tightening a cone (see Figures 11.50 and 11.51).

Calculation of the Transmittable Torque

It may be assumed that, when a hub made of polymeric material is pressed onto a metal shaft, all deformations will be absorbed by the hub. The state of stress may be regarded as equivalent to that in an infinitely long, thick-walled pipe under internal pressure. The radial stresses are pressure stresses, which tend to zero at the outer perimeter. In the joint they are determined by the pressing forces. The tangential stress likewise attains its highest value at the contact surface and decreases with increasing outward distance. At the outer circumference, however, it does not assume the value zero.

This biaxial state of stress can be simplified using the HMH criterion (see Section 5.2.3.1) to a uniaxial reference stress. The maximum strain in the material at the joining surface (assuming elastic behavior) is given by:

$$\sigma_v = p \cdot \frac{\sqrt{3 \cdot a^4 + 1}}{a^2 - 1} \quad (11.31)$$

where

$$a = \frac{r_o}{r_i}$$

$$p = \frac{\Delta d_{\text{eff}} \cdot E}{2 r_i \cdot \left(\frac{a^2 + 1}{a^2 - 1} + \mu \right)} \quad (11.32)$$

Δd_{eff} = effective decrement in size (Eqs. 11.32 to 11.36)

An empirical relationship is given in [11.33] for calculating the appropriate interference Δd for joining.

$$\Delta d = K \cdot \sqrt{d}$$

where K is a physical constant of the material as specified in Table 11.5.

The most effective interference to be used when operating under varying temperature conditions is given by:

$$\Delta d_{\text{eff}} = \Delta d - \Delta d_T \quad (11.33)$$

where Δd_T represents the change in hub bore size due to changes in temperature relative to room temperature.

In order to cover temperatures fluctuating about room temperature, ΔT should be set to both ($T_{\max} - 20^\circ\text{C}$) as well as ($T_{\min} - 20^\circ\text{C}$). If temperatures are less than 20°C , it should be determined that the boundary condition:

$$\Delta d_{\text{lim}} = K \cdot d^{0.7} \quad (11.35)$$

is not exceeded.

Table 11.5 Physical Constant K for Various Polymeric Materials to Be Used in Estimating the Interference for a Press-Fit Assembly [11.33]

Material	K
PA 6	0.045
PA 66	0.04
PBT, POM	0.03
PA GF, PBT GF	0.02
HDPE, PA 11	0.06

The criteria that:

$$0 < \Delta d_{\text{eff}} \leq \Delta d_{\text{lim}} \quad (11.36)$$

should be met. Using the effective interference, it is now possible to estimate the torque transmittable by a press-fit joint. This is given by:

$$M_t = \frac{\Delta d_{\text{eff}} \cdot d \cdot p \cdot w \cdot f \cdot E}{2 \left(\frac{a^2 + 1}{a^2 - 1} \right)} \quad (11.37)$$

where

f = coefficient of static friction as shown in Table 11.6

μ = Poisson's ratio of the gear material

This calculation is done using only the hub dimensions. The support provided by the remainder of the face of the wheel is taken into account using a weighting factor. A wheel disk having a thickness which is 0.7 to 0.8 times that of the hub increases the torque by approximately 10 and at most by 25%. A solid disk is treated as though $r_o/r_i = 2.5$, even if it has a greater diametric ratio.

The objective of covering stress relaxation in the calculation can be achieved by introducing a creep modulus into Eq. 11.37. However, this produces results that do not correlate well with practical experience.

It is not advisable to use press-fit joints made of PA for underwater applications, because PA absorbs moisture and as a result, its specific volume and other properties change. This is demonstrated by test results showing the loss (over time) of shrinkage tension in PA rings injection molded onto smooth metal shafts when they are stored under various conditions (see Figure 11.42).

Table 11.6 Measured Values for Coefficient of Friction of Polymeric Gear Materials with Steel Having a Surface Roughness $R_z = 1.5 \mu\text{m}$; Direction of Slip Perpendicular to Machining Stria; Unlubricated; Contact Time 1 min; Room Temperature [11.33]

Polymeric material mated with steel	Surface pressure		
	20 MPa	30 MPa	40 MPa
PA 6, PA 66	0.20	0.18	0.17
PBT	0.16	0.16	0.15
PBT GF	0.13	0.12	0.10
POM	0.10	0.10	0.10
HDPE	0.11	0.09	0.07

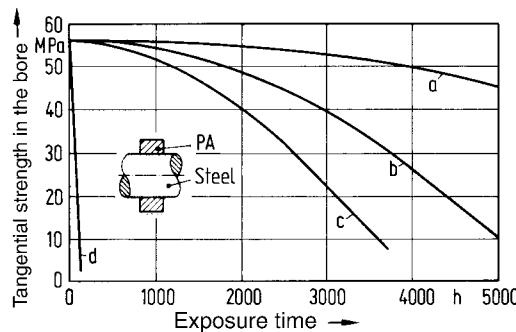


Figure 11.42 Loss of shrinkage tension in overmolded polyamide hubs under different ambient conditions

- a $T = 20^\circ\text{C}$ stored in air
- b $T = 80^\circ\text{C}$ stored in air
- c $T = 120^\circ\text{C}$ immersed in oil
- d $T = 100^\circ\text{C}$ immersed in water

11.3.3.2 Form-Grip Joints

The method of joining parts using a groove and a keyway has the disadvantage of limiting the load range of gear wheels made of polymeric materials. When the keyway is in an unfavorable position with respect to the point of action of the circumferential force, the hub can lift away from the shaft as may be seen in Figure 11.43.

It is better, but more costly, to create a joint using a multi-groove profile. Figure 11.44 shows the effect of the number of grooves on the transmittable circumferential force.

The flank pressure is given by:

$$p_m = \frac{M_t}{i \cdot r_m \cdot h \cdot w} \cdot 10^3 \quad (11.38)$$

where

- M_t = torque in Nm,
- i = number of grooves (it may be assumed that all grooves in polymeric materials provide the same support) and for r_m , h , and w in mm (see Figure 11.46).

Permissible values of p_m are presented in Figure 11.45.

Figure 11.46 provides design tips for the groove in a hub made of polymeric material.

In secondary drives, the keyway, which may also be made of polymeric material, can be integrated into the hub (see Figure 11.47). As a result of this the transmittable moment is reduced by about 50% with respect to Eq. 11.38.

The keyway thus molded into position can be reinforced by hot-embedding of suitably profiled stamped sheet metal parts (see Figure 11.48).

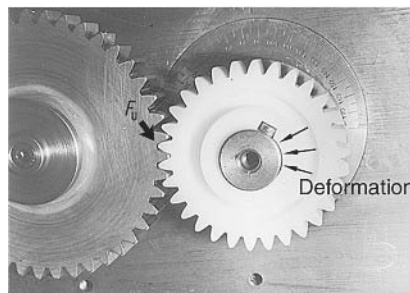


Figure 11.43 In spur gears under high load, the polymeric hub deforms when the moment is transferred to the shaft only via keyway [11.29]

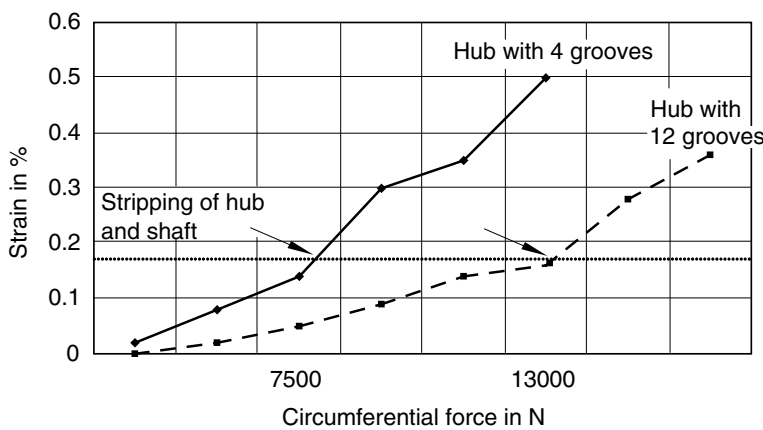


Figure 11.44 Deformation of a PA hub with different numbers of grooves according to Keim and Strickle

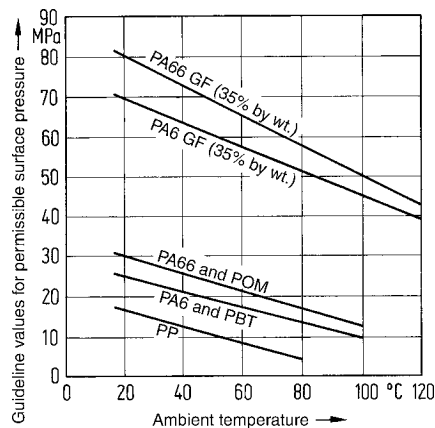


Figure 11.45 Guideline values for the permissible surface pressure on the flanks of keyways [11.33]

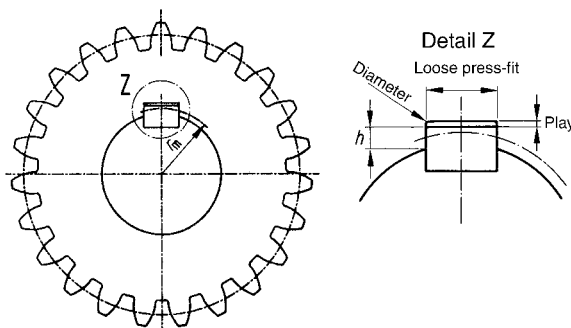


Figure 11.46 Construction of groove for keyway joints

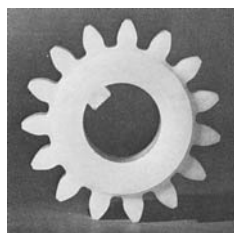


Figure 11.47 Keyway molded *in situ*

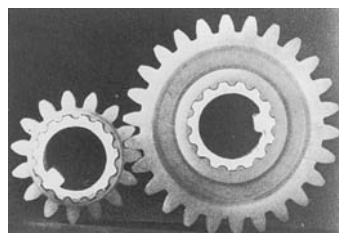


Figure 11.48 Hot-embedded stamped parts for hub reinforcement

11.3.3.3 Pretensioned Form-Grip Joints

A reliable connection to knurled metal shafts (*e.g.*, longitudinal knurls as specified in DIN 82) can be obtained with ductile thermoplastics by simply using mechanical force to push the part into position [11.30]. The optimum hub diameter d_H is given by:

$$d_H \approx d_K - t \quad (11.39)$$

where

- d_K = outer knurled diameter in mm
- t = knurl spacing in mm

The transmittable torque can be determined with surprisingly good agreement using the relationship:

$$M_t = \frac{d_K^2 \cdot \pi \cdot l}{2} \cdot \tau_s \quad (11.40)$$

where

- τ_s = failure shear stress ($\tau \approx 0.5 \sigma$) (see also Section 5.2.3.2 and Figure 5.8).

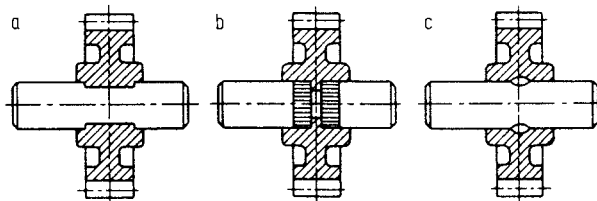


Figure 11.49 Form-grip elements

- a Partly ground level surfaces
- b Longitudinal knurling with groove for axial fixing
- c Partly compressed lugs

The pretensioning in a form-grip joint can be applied much more effectively by the shrinkage of the polymeric material during injection molding when the appropriately profiled metal element is inserted in the injection mold and encapsulated.

Figure 11.49 shows gear wheels of quite small dimensions with proven form-fitting elements which are injected directly onto an axis.

Larger gear wheels under high load are reinforced with metal in the hub. These metal hub parts are encapsulated during injection molding. This is a costly measure but it affords the highest level of operational reliability. Particular attention is paid in the design of form-grip geometry to a symmetrical arrangement, *i.e.*, uniform distribution of the polymeric material. The following guidelines also apply.

- Only *one* axial anchor point is provided and no impediment to shrinkage to this fixed point is allowed.
- If possible, the axial anchor should be positioned close to the gate.
- The flanks of the form-grip profile transmitting force should be perpendicular to the circumferential direction and be uniformly distributed about the circumference.
- The wall thickness for a hub made of polymeric material is governed by the relationship: $r_o/r_i \approx 1.3$ to 2.0.

A particularly low-cost and technically sound solution can be achieved, for example, by using drawn aluminum profiles as shown in Figure 11.50. The hub pieces cut from the bar are provided only with a circular groove for absorbing axial forces.

Thermal expansion, particularly in the case of large gear wheels, can give rise to malfunctions. This can be counteracted by making the entire body of the wheel from metal and injecting only the toothed structure on top (see also Figure 1.13). Alternatively, the toothed ring can be bolted to a central wheel core composed of sheet metal and the hub (see Figure 11.51).

A solution for this problem is available for small gear wheels, as shown in Figure 11.52. Two gear wheels in a precision instrument are each mounted in a fork composed of the same polymeric material. Fastened only centrally by a clamping cone, this can largely compensate for the thermal expansion of the gear wheels [11.31].

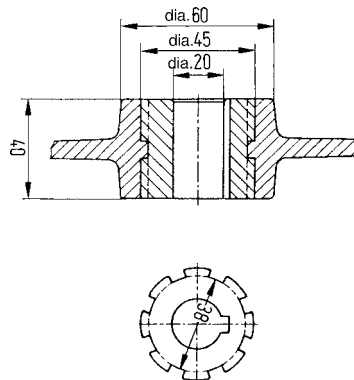


Figure 11.50 Hub composed of drawn aluminum profile

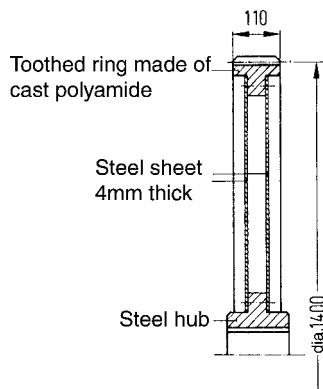


Figure 11.51 In large gear wheels the toothed ring is bolted to the hub [11.33]

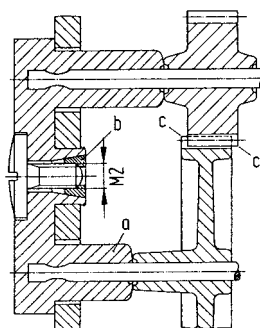


Figure 11.52 Mounting of gear wheels in precision instruments to provide compensation for thermal expansion. The wheels are offset relative to one another so that any flash due to the parting surface of the mold does not impede free running [11.31].

- a Fork
- b Terminal cone
- c Floating membrane

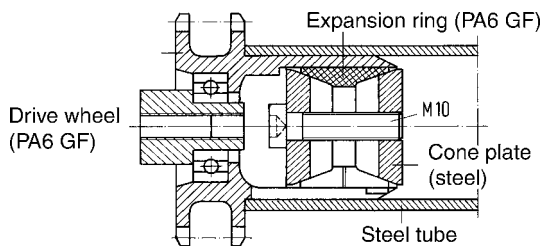
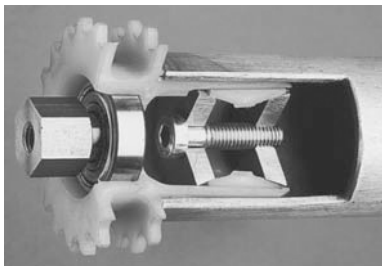


Figure 11.53 Fastening of a drive wheel made from glass reinforced PA 6 (B3WG5) in the end of a transport roller. The roller is a commercially available galvanized 2 in. tube with production tolerances in internal diameter of up to 2 mm. The tripod expansion part in the drive wheel is pressed against the inner wall of the tube by two steel cone plates. This provides a frictional joint, which is able to transmit reliably an alternating torque of ± 25 Nm in the temperature range of -15 to $+50$ °C.

(Photograph: Technical Development Dr. Becker, Wetter/Mannesmann-Demag)

References

- [11.1] ROTH, K.-H.: Untersuchungen über die Eignung der Evolventen-Zahnform für eine allgemein verwendbare feinwerktechnische Normverzahnung (Studies of the suitability of the Evolventen tooth shape for a generally usable standard toothed structure in precision engineering), Dissertation, Technische Hochschule Munich 1963
- [11.2] KERN, E.: Kreisbogenzahnprofile zur konstanten Momentenübertragung bei Übersetzungen ins Schnelle, insbesondere für Uhrenverzahnungen (Circular arc tooth profiles for constant torque transmission in transitions to fast speed, in particular for clock movements), Dissertation, University of Stuttgart 1969
- [11.3] WILLMANN, N.: Computerunterstütztes Optimieren von Verzahnungen (Computer-aided optimization of gear systems), *dima* (1984) 4, pp 21/22
- [11.4] NILL, E.: Übertragungsverhalten extrem kleiner Kunststoffzahnräder Konstruktion, Fertigung und Anwendung feinwerktechnischer Kunststoffteile (Transmission properties of extremely small plastic gear wheels. Design, production and application of plastic parts in precision engineering), VDI-Verlag, Düsseldorf 1976
- [11.5] CORNELIUS, E. A.: Tragfähigkeit und Lebensdauer geradverzahnter Stirnräder aus thermoplastischen Kunststoffen bei einer Paarung Stahl/Kunststoff (Load-bearing capacity and service life of spur-toothed gears made of thermoplastics when mated with steel), *ASÜG-Mitt.* 5 (1968) 1, pp. 30/32
- [11.6] BLOK, H.: Measurement of Temperature Flashes on Gear Teeth under E. P. Conditions, Proc. Gen. Disc. on Lubrication and Wear 1937
- [11.7] SIEDKE, E.: Tragfähigkeitsuntersuchungen an ungeschmierten Zahnrädern aus thermoplastischen Kunststoffen (Studies on the load-bearing capacity of unlubricated gear wheels made of thermoplastics), Dissertation, Technical University Berlin 1977
- [11.8] DIN 3990 Grundlagen der Tragfähigkeitsberechnung von Gerad- und Schrägstirnräder (Fundamentals of the load-bearing capacity of spur and helical gears), Parts 1 to 4, Draft 1980, Beuth-Verlag, Berlin
- [11.9] TAKANASHI, S. and A. SHOJI: On the Temperature Risk in the Teeth of Plastic Gears, Internat. Power Transmission & Gearing Conference, San Francisco 1980

- [11.10] HACHMANN, H. and E. STRICKLE: Polyamide als Zahnradwerkstoffe (Polyamides as materials for gear wheels), *Konstruktion* **18** (1966) 3, pp. 81/94
- [11.11] NIEMANN, G. and H. WINTER: Maschinenelemente (Machine elements), Vol. 2, Springer-Verlag, Berlin, Göttingen Heidelberg 1980
- [11.12] ERHARD, G. and CH. WEIS: Zur Berechnung der Zahn- und Flankentemperatur von Zahnrädern aus Polymerwerkstoffen (On the calculation of tooth and tooth flank temperatures in gear wheels made of polymeric materials), *Konstruktion* **39** (1987) 11, pp. 423/430
- [11.13] TILWICH, M., W. STEHR, W. DRESEL and M. STUBENVOLL: Schmierstoffe in der Feinwerktechnik (Lubricants in precision engineering), *Schmiertechnik und Tribologie* **29** (1982) 5, pp. 200/205
- [11.14] STEHR, W.: "Etsyntha" – Spezialuhrenöl für Kunsststofflager ("Etsyntha" – Special clock oil for plastic bearings), *Uhren, Juwelen, Schmuck* (1976) 7, pp. 106/108
- [11.15] ERHARD, G.: Erfahrungen mit Gleitlagern aus Polyamid (Experience with sliding bearings made from polyamide), *TZ für prakt. Metallbearbeitung* **59** (1965) 7, pp. 449/453
- [11.16] KOGLER, H.-G.: Örtliche und mittlere Betriebstemperaturen an kleinen Kunststoffzahnrädern Konstruktion, Fertigung und Anwendung feinwerktechnischer Kunststoffteile (Local and average operating temperatures in small plastic gear wheels. Design, production and application of plastic parts in precision engineering), VDI-Verlag, Düsseldorf 1976
- [11.17] VDI-Richtlinie 2545 Zahnräder aus thermoplastischen Kunststoffen (Gear wheels made from thermoplastics), Beuth-Verlag, Berlin 1981
- [11.18] WEIS, CH.: Optimierung des Berechnungsverfahrens zur Abschätzung der Belastbarkeit und Lebensdauer von Zahnrädern aus Polymerwerkstoffen (Optimization procedure for estimating the load-bearing capacity and service life of gear wheels made from polymeric materials), Thesis, University of Karlsruhe 1986
- [11.19] BUDICH, W.: Beitrag zur Untersuchung öl- und fettgeschmierter geradverzahnter Stirnräder aus Acetalpolymerisat (Contribution to the study of oil- and grease-lubricated spur gears made from acetal polymer), Dissertation, TU Berlin 1969
- [11.20] BECK, K. and H. BRÜNINGS: Grenzflankenpressung bei Stirnrädern aus PA 66 und PA 6 (Limiting tooth flank stress in spur gears made from PA 66 and PA 6), *Konstruktion* **25** (1973) 11, pp. 451/454
- [11.21] BOGDANZALIEW, K. and V. DRECHSLER: Betriebsverhalten und Berechnung von Polyamidzahnrädern (Operational properties and calculation of polyamide gear wheels), *Maschinenbautechnik* **29** (1980) 5, pp. 226/233
- [11.22] BOES, D.: Abstimmung von Verteilersystemen und Beeinflussung des Füllvorgangs durch rheologische Werkzeugauslegung (Matching runner systems and controlling the filling operation by rheological design of molds), *Kunststoffe* **74** (1983) 10, pp. 568/572
- [11.23] HORVARTH, L. S.: Zahnräder aus Delrin-Polyacetal und Zytel-66-Polyamid (Gear wheels made from Delrin polyacetal and Zytel 66 polyamide), Du Pont Techn. Mitteilung D/Z 2010-7009
- [11.24] Prefocon, Deutsche Star brochure, Schweinfurt
- [11.25] N. N.: Erstes zusammengesetztes Schneckenrad aus Kunststoff (First worm gear constructed of plastic), *Technica* (1971) 21, p. 2106
- [11.26] ENSINGER, W.: Verbal communication
- [11.27] ERHARD, G.: Die Preßverbindung von Kunststoffring und Metallwelle (Press-fitting of a plastic ring and metal shaft), *Kunststoffe* **58** (1968) 4, pp. 315/317
- [11.28] MARTINI, J.: Lebensdaueruntersuchungen an fettgeschmierten Kunststoffzahnrädern (Service life studies on plastic gear wheels lubricated with grease), *Konstruktion* **38** (1986) 3, pp. 91/96
- [11.29] ERHARD G. and E. STRICKLE: Maschinenelemente aus thermoplastischen Kunststoffen Bd. 1 Grundlagen und Verbindungselemente (Thermoplastic machine elements, Vol. 1 Fundamentals and connecting elements), VDI-Verlag, Düsseldorf 1974

- [11.30] ERHARD, G. and E. STRICKLE: Die Preßverbindung von gerändelten Bolzen mit Kunststoffbauteilen (Press-fitting knurled bolts to plastic parts), *Konstruktion Elemente Methoden* (1976) 9, pp. 58/60
- [11.31] HERZIG, K.: Konstruktionsbeispiele aus der Feinwerktechnik (Examples of design in precision engineering), *Kunststoff-Berater* **18** (1973) 4, pp. 231/38
- [11.32] GEYER, H., H. GEMMER and H. STRELOW: Qualitätsformteile aus thermoplastischen Kunststoffen (Quality thermoplastic moldings), VDI-Verlag, Düsseldorf 1974
- [11.33] ERHARD G. and E. STRICKLE: Maschinenelemente aus thermoplastischen Kunststoffen (Thermoplastic machine elements), VDI-Verlag, Düsseldorf 1985
- [11.34] HEYM, B. and W. BEITZ: Zur Belastbarkeit von Stirnrädern aus dem Hochtemperatur-Thermoplast PEEK (On the load-bearing capacity of spur gears made from the high-temperature thermoplastic PEEK), *Konstruktion* **47** (1995) 11, pp. 351/357
- [11.35] WOLF, W.: Oechsler AG, Ansbach, Personal communication 2002

12 Friction Bearings

The generic term “bearing” encompasses the mounting of moving machine parts. A friction bearing is a special type of bearing in which this movement takes the form of sliding, thus causing sliding friction. Accordingly, the contact surfaces move relative to one another.

The main characteristics of polymeric materials that make them suitable for this form of mechanical loading include:

- Acting as bearings without lubrication due to low coefficient of friction;
- Small dimensions (low weight); and
- Direct mounting (bearing point can be integrated within a part).

Materials

The polymeric materials most commonly employed for friction bearings are thermoplastics with a semi-crystalline structure (see Table 12.1). These materials can be further modified by numerous additives for special purposes, such as lowering sliding friction, improving resistance to wear, and increasing compressive strength. The most important additives and their intended effects are presented in Table 12.2.

Table 12.1 Common Thermoplastic Base Materials for Friction Bearings [12.1]

Friction bearing materials	Bearing production	Typical applications
PA 66	Injection molding ($s_L = 0.5$ to 8 mm) or machining semifinished products	General purpose friction bearings for mechanical engineering applications
PA 6		
PA casting grade	Casting, centrifugal casting; thick-walled ($s_L > 10$ mm) and large parts	Precision engineering, bearings having higher dimensional stability than PA 66 and PA 6
PA 11 PA 12		
POM	Injection molding or from semifinished products	Linings, friction strips, joint endoprostheses
PBT		
HDPE	Predominantly by machining semifinished products	
PTFE	Compression molding and from semi-finished products	Resistance to chemicals and heat
Polyimide PEEK	and injection molding for polyether ketones	Resistance to high thermal loads

Table 12.2 Additives, Fillers and Desired Effects

Additives	Desired effect	Disadvantages
Glass fibers, carbon fibers	Increase in compressive strength, reduction of creep, hence higher static loading. Reduction of thermal expansion. Better resistance to wear	Increased wear, especially in paired material due to glass fibers in polar matrices. Anisotropic shrinkage
Graphite, molybdenum disulfide	Like glass fibers. Slight improvement in thermal conductivity, improved wear resistance	Reduced toughness. No significant improvement in sliding friction
Chalk, glass beads, particulate fillers	Increased compressive strength, isotropic shrinkage, improved wear, especially in nonpolar matrices	Reduced toughness
PTFE, HDPE	“Solid lubricant” in polar (glass fiber reinforced) polymeric materials, prevention of stick-slip	Acts only under adhesive friction conditions
Low molecular weight lubricants	Reduction of friction in polar matrices, prevention of stick-slip	Acts only under adhesive friction conditions

It should also be noted that sometimes, composite materials supplied as semifinished products or as bearings ready for installation are used. They are designed in different ways, but usually have a steel support overmolded with sintered porous layers, whose pores are filled mainly with PTFE or on which a PTFE-filled resin (e.g., epoxy resin) is applied.

In a special variant, PTFE fibers are interwoven with glass or metal fibers in such a way that the PTFE fibers come to lie almost exclusively on the sliding surface. The entire fabric is impregnated with a thermosetting resin and mounted on steel supports.

Lubrication

As a general rule, friction bearings made of polymeric materials are employed in the unlubricated state. Lubricated bearings, however, may have a longer service life depending on the nature of the lubricant because wear and thermal effects are reduced. Nonpolar lubricants can reduce the coefficient of sliding friction only for polar polymeric materials (e.g., PA), but not for nonpolar ones (e.g., PTFE, HDPE). Nevertheless, initial lubrication is always useful (for further information on lubrication see Chapter 11).

Paired Materials

An unlubricated friction bearing exhibits its best sliding properties and highest load-bearing capacity when it is paired with hardened steel.

Steel ensures good heat dissipation and its surface hardness prevents abrasion, which in the case of softer metals, can only be precluded by adequate lubrication. When steel is mated with

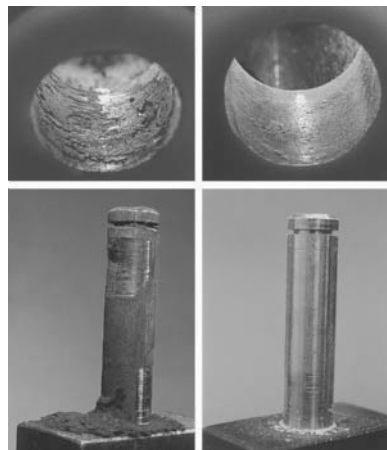


Figure 12.1 Bearing under dynamic load ($p_{\min} = 0.1 \text{ MPa}$, $p_{\max} = 2.0 \text{ MPa}$, pivot angle $\pm 30^\circ$) with 15 load cycles/min after 600,000 load cycles. Bearing bushing (top): glass fiber reinforced PA 66 (50% by weight); Bearing journal: 200 HV 10 steel (left), 800 HV 10 steel (right).

glass-fiber reinforced materials or polar bearing materials, it is essential that it be hardened (see Figure 12.1).

The surface roughness of the steel has to be matched to the desired tribological properties of the polymeric material (see Figure 4.34 to 4.38). In addition, it should be determined whether there is any directionality in the roughness relative to the direction of the sliding movement. For example, the machining marks on a finished shaft run more or less tangentially so that roughness is distinctly higher in the axial direction than transverse to it.

If polymeric materials are mated with one another, greater wear is to be expected on the polymeric material whose intermolecular binding energy is lower (see Section 4.7.2 and Figure 4.48). When glass-fiber reinforced, polar polymeric materials (e.g., glass-fiber reinforced PA and glass-fiber reinforced PBT) are used without lubrication, they must be paired with a nonpolar polymeric material (e.g., PTFE, HDPE) or with a bearing material containing these substances as an additive (e.g., PA/PE). These nonpolar materials generally act as “solid lubricants” to reduce friction and wear.

12.1 Friction Bearing Damage

Damage in friction bearings can be classified according to the cause of the damage as follows [12.2]:

- Product damage (stress in normal operation)
- Damage due to extraneous effects (stress in abnormal operation)
- Damage due to operating faults (operational errors).

Bearing damage and its causes can be important because of liability-related issues. Only the first type of bearing damage, that is to say damage occurring in use according to normal operating specifications at more or less predictable loads, is of interest here. Damage of this type provides the failure criteria for the design of such parts.

Under excessively high mechanical load, the bearing bushing is *deformed* to an extent, rising with the temperature of the bearing and the length of time the load acts on the part. This deformation results in greater clearance (play) and in changes in contact conditions resulting in a greater frictional moment.

Excessively high stress in combination with a high sliding speed or faulty supply of lubricant usually brings about *fusion of the bearing material* within a short time. This catastrophic damage can also occur directly due to an unexpected increase in the temperature of the surroundings or a reduction in play due to differential thermal expansion.

If a plastic bearing is run at a high bearing temperature, the polymeric material can suffer *thermal damage* in the course of time and this in turn causes a serious increase in wear, even if the temperatures are not high enough to cause melting.

Wear generally becomes apparent as increased play which finally results in failure of the bearing. The material abraded by highly polar polymeric materials (e.g., PA) may also cause an increase in the coefficient of friction unless it can be removed from the bearing point (see also Figure 12.18). The consequence of excessive friction is that the bearing finally fails due to melting.

Wear may be caused by:

- Excessive roughness of the mating metal,
- Abrasive foreign bodies,
- Corrosive media in the immediate surroundings (including moisture),
- High surface pressure,
- High sliding interface temperature, and
- Processing-related defects.

The paired metallic material can also wear due, for example, to:

- Rust or corrosion,
- Abrasive particles (glass fibers, abraded metal, foreign bodies especially in the case of unhardened metals), and
- Frictional corrosion.

The well known phenomenon of *frictional corrosion (fretting corrosion)* can also be observed in plastic bearings paired with steel shafts, when under normal low-amplitude forces, the surfaces rub or knock against one another.

It has been found that non-polar polymeric materials, or those containing non-polar polymeric additives (e.g., PTFE, HDPE, POM/PTFE, PA/PE, etc.), cause less fretting corrosion than polar polymeric materials, especially those reinforced with glass fibers. If a friction element is supplied with a free-flowing lubricant, wear due to fretting corrosion can be further reduced.

The term “stick-slip” is used to describe the variation in coefficient of friction and, depending on the ability of the system to resonate, the noise (squeaking, screeching) associated with this (see also Section 4.7.6). Although a bearing can still function under stick-slip conditions, this effect must be regarded as bearing damage because disturbing noises can be produced. As a result of the noise, it may not be possible to continue operating the bearing. Stick-slip movements can also contribute to increased wear and elevated bearing temperatures. Apart from choosing the right material (non-polar polymeric materials) and providing enough play, factors that help counteract stick-slip include:

- Lubrication,
- Minimizing loading, and
- Pairing with a rough material having the highest possible surface hardness (higher wear).

12.2 Calculation of Load-Bearing Capacity for Bearings

The theoretical load-bearing capacity of a friction bearing is estimated in the same way as for a gear (see Chapter 11, Figure 11.1).

12.2.1 Calculation of Mean Bearing Temperature

The temperature of a friction bearing has a decisive effect on its load-bearing capacity and service life. The operating temperature of a friction bearing is the result of the heat of friction. It can be estimated by calculation on the basis of a heat balance. Such a calculation can be done only as an approximation using empirically determined values specific to the design of the bearing [12.2]. The determination of the coefficient of friction is, moreover, subject to great uncertainties.

Radial Bearings (Journal Bearings)

This calculation assumes that the friction work converted to heat in the bearing is dissipated only via the surface of the bearing bushing (B) and the shaft (S). Any cooling due to a lubricant is not taken into consideration.

$$Q_F = Q_B + Q_S \quad (12.1)$$

The friction work converted to heat per second is given by:

$$Q_F = d_S \cdot w \cdot p_m \cdot v \cdot f \quad (12.2)$$

where

d_S = diameter of shaft in mm

w = width of bearing in mm

p_m = mean surface pressure in MPa (Equation 12.10)

v = sliding velocity in m/s

f = coefficient of sliding friction

The quantity of heat transported through the surface of the bearing bushing per second is:

$$Q_B = \frac{d_S \cdot w \cdot \pi}{s_L \cdot 10^3} \cdot \lambda_P \cdot K_1 \cdot \Delta T \quad (12.3)$$

and the quantity transported through the shaft per second is:

$$Q_S = \frac{d_S \cdot \pi}{2 \cdot 10^3} \cdot \lambda_M \cdot K_2 \cdot \Delta T \quad (12.4)$$

where

s_L = bearing wall thickness in mm

λ_P = thermal conductivity of the polymeric material in W/m K

λ_M = thermal conductivity of the metal in W/m K

K_1, K_2 are factors specifying how heat dissipation is affected by the design of the bearing.

Equations 12.2 to 12.4 lead to Eq. 12.1 in the form:

$$\Delta T = \frac{p_m \cdot v \cdot f}{\pi \cdot \left(\frac{\lambda_P \cdot K_1}{s_L} + \frac{\lambda_M \cdot K_2}{2 \cdot w} \right)} \cdot 10^3 \quad (12.5)$$

Experiments on bearings [12.2], shown in Figure 12.2, revealed that the sliding velocity has an exponential effect on operating temperature. In the case of PA/PE and HDPE, the coefficient of sliding friction is markedly dependent on temperature. This is taken into account by an exponent κ and by a factor a . The constants were determined as $K_1 = 3/4$ and $K_2 = 7/120$. In this way, the relationship for estimating the mean bearing temperature in a radial bearing can be formulated as follows:

$$T_{Lr} = \frac{T_E + \frac{318.3 \cdot p_m \cdot v^\kappa}{\left(\frac{0.18}{s_L} + \frac{1.36}{w} \right)} \cdot f}{1 + \frac{318.3 \cdot p_m \cdot v^\kappa}{\left(\frac{0.18}{s_L} + \frac{1.36}{w} \right)} \cdot a} \quad (12.6)$$

This expression is valid only for radial bearings as shown in Figure 12.2 and for environmental temperatures ≤ 80 °C.

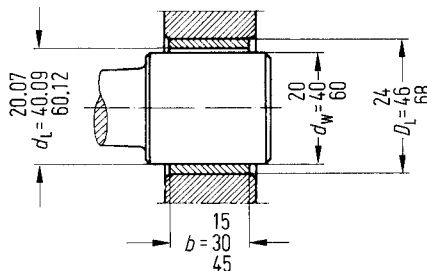


Figure 12.2 Geometry and dimensions of the radial bearings used in the experiments.
Eq. 12.6 applies only to similar bearings.

The values for κ to be inserted in Eq. 12.6 are as follows.

- $\kappa = 1.4$ for radial bearings having a rotary motion
- $\kappa = 1.3$ for radial bearings having an oscillating motion (pivot angle $\alpha \geq 45^\circ$)
- $\kappa = 1.2$ for radial bearings having an oscillating motion (pivot angle $25^\circ < \alpha < 45^\circ$)
- $\kappa = 1.0$ for radial bearings having an oscillating motion (pivot angle $\alpha \leq 25^\circ$) and for axial bearings.

The coefficient of sliding friction f for unlubricated operation under the corresponding boundary conditions is taken from Figures 4.34 to 4.38.

Under lubricated conditions f can assume the following values.

- $f = 0.12$ for bearings lubricated with grease once during installation
- $f = 0.09$ for friction bearings with a grease reservoir or for bearings employed in oil spray
- $f = 0.04$ for oil-lubricated or water-lubricated bearings with mixed friction.

The dependence of the coefficient of sliding friction on temperature in the range of validity of Eq. 12.6 is important only for HDPE and blends of PA/PE.

- $a = 0$ for PA, POM, and PBT
- $a = 7 \cdot 10^{-4}$ for HDPE
- $a = 33 \cdot 10^{-4}$ for PA/PE.

It may be assumed that the values for polymeric materials containing PE or PTFE additives are similar to that of PA/PE.

Axial Bearings (Thrust Bearings)

In the case of axial bearings involving steel paired with a polymeric material, given a geometry such as the one shown in Figure 12.3, the mean bearing temperature can be determined by a similar relationship*.

* The equations for the bearing temperature in axial bearings are less often supported by practical applications than those for radial bearings.

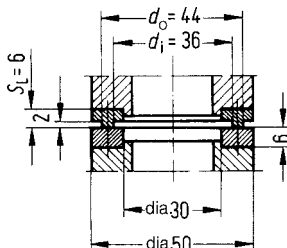


Figure 12.3 Geometry and dimensions of the axial bearings used in the experiments.
Equations 12.7 and 12.8 apply only to similar bearings.

$$T_{La} = T_E + \left(\frac{p_m \cdot v \cdot f}{\frac{2}{S_L} + \frac{d_a^2}{d_o^2 - d_i^2}} \right) \cdot 10^4 \quad (12.7)$$

If polymeric materials having the same thermal conductivity and the same wall thickness are mated, the following equation applies.

$$T_{LaP} = T_E + (p_m \cdot v \cdot f \cdot S_L) \cdot 10^3 \quad (12.8)$$

12.2.2 Calculation of Temperature of Sliding Surface

The temperature of the bearing surface is considerably higher than the mean bearing temperature. Surface temperature can be a critical variable in terms of bearing performance. On the basis of Eq. 12.6, a mean sliding surface temperature can be estimated using the empirical expression in Eq. 12.9.

$$T_S = T_E + (1.15) \cdot (T_L - T_E) \quad (12.9)$$

With this calculation, a judgment can be made whether a sliding bearing under a specified load will fail due to melting. Moreover, the sliding surface temperature provides a basis for evaluating wear.

12.2.3 Static Load-Bearing Capacity

When designing sliding bearings under a load F_L , either stationary or moving at an extremely low sliding velocity, the designer must ensure that the bearing is not overloaded and that the deformation is still within permissible limits [12.3].

12.2.3.1 Load on the Bearing Material

Mean Surface Pressure

The contact surface, and hence the contact pressure between the bearing bushing and the shaft, are determined from the load on the bearing, the built-in play, wear, temperature, and the elasticity of the polymeric material. Thus, the mean surface pressure p_m can be estimated only very imprecisely and be used only for preliminary designs. In most cases, the pressure acting on the bearing is not uniformly distributed over the circumference or width. As a result, the mean surface pressure is always less than the actual load on the material.

$$p_m = \frac{F_L}{d_S \cdot w} \quad (12.10)$$

Pressure in the Case of Small Contact Widths

The theoretical solutions by Hertz and Föppel for calculating the width of actual load-bearing surfaces and the load on the material, when bodies with arched surfaces are in contact, are strictly speaking not applicable to polymeric materials exhibiting viscoelastic deformation behavior (see also Chapters 11 and 13). In addition, the geometric requirements are far from being fulfilled in most thin-walled bearing bushings. However, the condition specified in Eq. 12.11 can be used as an approximation. The Hertzian equations apply only for a certain ratio of the projected surface area of the compressed body to the actual contact surface area.

$$2B \leq \frac{d_S}{6} \quad (12.11)$$

where $2B$ is the breadth of the projected contact surface area.

In design terms, this means:

- Low load acting on the bearing,
- High bearing play, and
- Low deformability of the bearing bushing.

Converted into more common variables, Eq. 12.11 becomes:

$$F_L \leq 0.012 \cdot E_{PR} \cdot w \cdot h_0 \quad (12.12)$$

where

E_{PR} = modulus from Figure 12.9 in MPa

h_0 = bearing play in mm ($h_0 = d_L - d_S$)

d_L = diameter of bearing (in the operating state) in mm

When the condition in Eq. 12.12 is met, the projected breadth $2B$ of the pressure surface formed is determined by Eq. 12.13 (see also Eq. 13.4):

$$2B = 4 \sqrt{\frac{F_L \cdot r}{w} \cdot \frac{2(1 - \mu^2)}{\pi \cdot E_S}} \quad (12.13)$$

The maximum Hertzian pressure in the center line of this contact surface for $\mu = 0.4$ is given by:

$$\max p_H = \sqrt{0.19 \cdot \frac{F_L \cdot E_S}{w \cdot r_S}} \quad (12.14)$$

where

E_S = substitute modulus for different shaft and bearing materials in MPa

$$E_S = 2 \cdot \frac{E_M \cdot E_L}{E_M + E_L} \quad (12.15)$$

(when $E_M = E_{\text{Steel}} \gg E_L = E_P$ (polymeric material), $E_S = 2 E_P$)

r_S = substitute radius in mm

$$r_S = \frac{(-r_L) \cdot r_M}{r_M + (-r_L)} \quad (12.16)$$

(because the curvature is in the same direction r_L has a negative sign).

Equation 12.25 can be used to determine if the value of p_H is permissible.

Pressure in the Case of Large Contact Widths

In the event that the Hertzian equations are not applicable because the contact surface width is greater than that allowed by Eq. 12.11, a design calculation proposed by Detter [12.4] can be used.

Proceeding from a structurally permissible displacement of the shaft Δh , the width $2B$ of the contact surface can be derived from the geometric relationships (see Figure 12.4) arising as a result of static loading.

$$2B = d_S \sqrt{\left[1 - \frac{1}{\left(\frac{2 \cdot \Delta h}{h_0} + 1 \right)^2} \right] \cdot \left(1 + \frac{h_0}{d_L} \right)} \quad (12.17)$$

According to Detter, there is an approximately sinusoidal (cosine function) pressure distribution in the contact surface and the highest pressure ($\max p_C$) occurring under a bearing load F_L is given by:

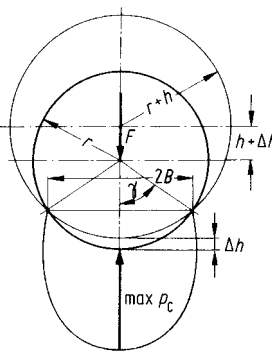


Figure 12.4 Geometric relationships and distribution of pressure in radial bearings with a large contact width [12.4]

$$\max p_C = \frac{F_L \cdot (n^2 - 1)}{d_S \cdot w \cdot n \cdot \cos \gamma} \quad (12.18)$$

where

$$n = \frac{90}{\gamma} \quad (12.19)$$

and

$$\gamma = \arcsin \frac{2B}{d_S} \quad (12.20)$$

These geometric relationships are linked to the properties of the material by Hooke's law:

$$\max p = E_p \cdot \frac{\Delta h}{s_L} \quad (12.21)$$

Equation 12.25 can be used to determine if this pressure is still permissible.

Equating Eqs. 12.18 and 12.21 and resolving for F_L , the bearing load resulting in the displacement Δh originally assumed is obtained.

$$F_L = \Delta h \cdot E_p \cdot d_S \cdot w \cdot \frac{n \cdot \cos \gamma}{(n^2 - 1) \cdot s_L} \quad (12.22)$$

Approximate Solution for Large Contact Widths

Frequently, the conditions under which a friction bearing is operating are not known with sufficient precision to justify investing major effort in a design calculation having high demands on accuracy. In such cases, a simplified approximation is proposed for estimating the load

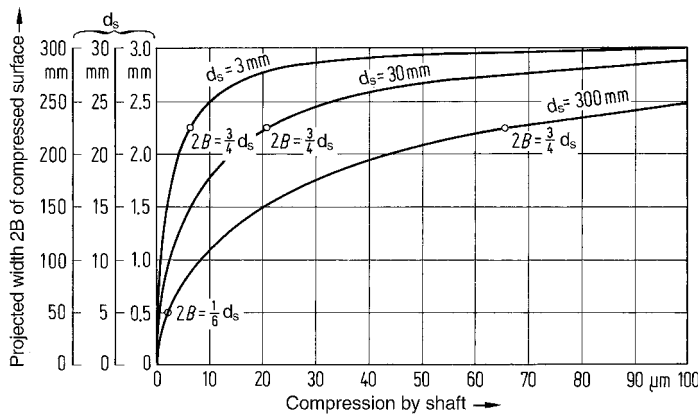


Figure 12.5 Dependence of the projected contact surface width on compression by the shaft for three bearing diameters [12.2]

acting on the material. The difference with respect to p_m is that the contact surface breadth $2 B$ is taken to be approximately equal to 0.7 to 0.8 d_s . The justification for this assumption is provided in Figure 12.5. This shows that after even the slightest compression by the shaft, the contact surface width extends to $3/4$ of the diameter of the shaft.

The distribution of pressure is assumed to be sinusoidal.

The pressure is then obtained as follows:

$$\max p_{\text{approx}} = \frac{16}{3 \cdot \pi} \cdot \frac{F_L}{d_s \cdot w} \quad (12.23)$$

It should be determined if $\max p_{\text{approx}}$ is still permissible using Eq. 12.25. This determination may also be performed as a function of wall thickness using Figures 12.5 and 12.6. Alternatively, the maximum bearing load may be estimated as follows:

$$F_{L \text{ approx max}} = \frac{3 \cdot \pi}{16} \cdot \sigma_Y \cdot d_s \cdot w \quad (12.24)$$

As an alternative to σ_Y , the wall-thickness-dependent maximum pressure from Figures 12.6 and 12.7 may be inserted in Eq. 12.24.

This maximum bearing load should be reduced using an appropriate safety factor (see Section 5.2.1.2) to arrive at the permissible bearing load.

Permissible Pressure

The design Eq. 12.25 for permissible pressure may be regarded as a very conservative condition [12.2].

$$\max p \leq (0.8 \text{ to } 1) \cdot \sigma_Y \quad (12.25)$$

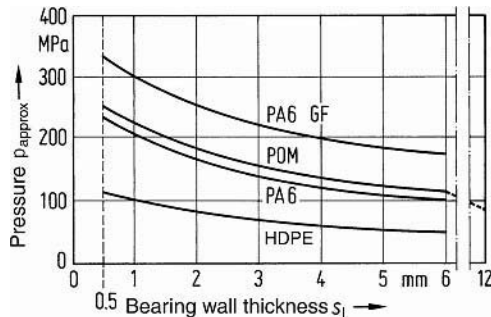


Figure 12.6 Limiting pressure, $\max p_{\text{approx}}$ as a function of bearing wall thickness; $T = 23^\circ\text{C}$

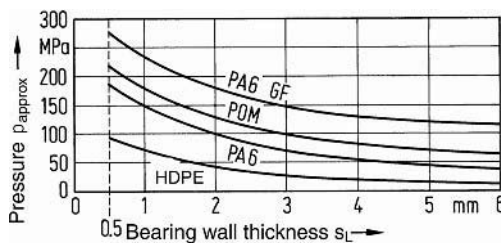


Figure 12.7 Limiting pressure, $\max p_{\text{approx}}$ as a function of bearing wall thickness; $T = 80^\circ\text{C}$ for PA 6, glass fiber reinforced PA 6, POM; $T = 50^\circ\text{C}$ for HDPE

This is based on the assumption that – apart from locally bounded flow processes at surface protuberances – for a material under Hertzian contact conditions, the yield point at the point of greatest shear stress under the vertex of the contact surface corresponds approximately to the yield stress σ_y . The lower value in Eq. 12.25 should be used for dynamic loads.

Test results on the effect of the wall thickness of the bearing and the bracing effect associated with metal support on the limiting load-bearing capacity of bearing bushings made of polymeric materials can assist with the design of precision bearings [12.5]. Figures 12.6 and 12.7 show the maximum pressure ($\max p_{\text{approx}}$ in Eq. 12.23) as a function of bearing wall thickness. The maximum pressure increases markedly as the bearing wall thickness decreases. The end of the linear stress/strain region (see Figure 12.8) is defined as the limiting value for these graphs.

12.2.3.2 Deformation of the Bearing Bushing

If the serviceability of a bearing bushing under quasi static load is determined by its deformation (shaft displacement), the maximum bearing load is restricted by this criterion. In this case, small contact surface widths do not arise (see Figure 12.5)*.

* If bearing deformation is of interest, $2B$ for small contact widths can be calculated from Eq. 12.13 and Δh from Eq. 12.26.

Bearing Deformation in the Case of Large Contact Widths

The method used for calculating pressure can also be used in principle for determining the bearing bushing deformation Δh . To do this, Eq. 12.22 must be used iteratively for different values for Δh (already included in Eq. 12.17), until the calculated value for F_L at some point is equal to its previous value in the iterative process.

Approximate Solution in the Case of Large Contact Widths

Reference [12.3] proposes a readily implemented method for calculation of deformation using various simplifying assumptions. On this basis:

$$\Delta h = \frac{F_L}{\left(\frac{2B}{s_L} + \sin 45 \right) \cdot w} \cdot \frac{4}{\pi \cdot E_p} \quad (12.26)$$

Depending on the load, $2B = 0.7 d_S$ as shown in Figure 12.5 and the modulus of elasticity is taken as $E_{P\text{ theor}}$ from Figure 12.9.

$$\Delta h = \frac{1.8 \cdot F_L}{\left(\frac{d_S}{s_L} + 1 \right) \cdot w \cdot E_{P\text{ theor}}} \quad (12.27)$$

The modulus values $E_{P\text{ theor}}$ ("theoretical moduli") are calculated from stress-strain experiments on bearing bushings having diameters in the range of 10 to 30 mm, bearing widths of 7 to 21 mm, and wall thicknesses of 0.5 to 6 mm, using Eq. 12.27. Bearing play relative to the shaft diameter is $(h_0/d_S) \cdot 100 = 0.6\%$ [12.5].

The stress-strain curves assume the characteristic shape shown in Figure 12.8. If the force and deformation at the end of the linear (primary) region of the curve are inserted in Eq. 12.27, the part-specific modulus values $E_{P\text{ theor}}$ are obtained (Figure 12.9).

The end of the linear region in Figure 12.8 determines the limits of validity of Eq. 12.27 and of the permissible load-bearing capacity of the bearing (see Figures 12.6 and 12.7).

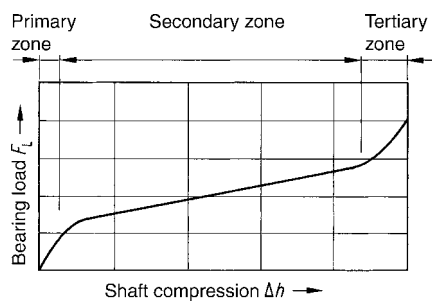
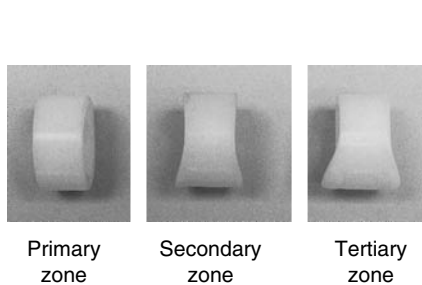


Figure 12.8 Pattern of load-dependent bearing deformation (shaft compression)

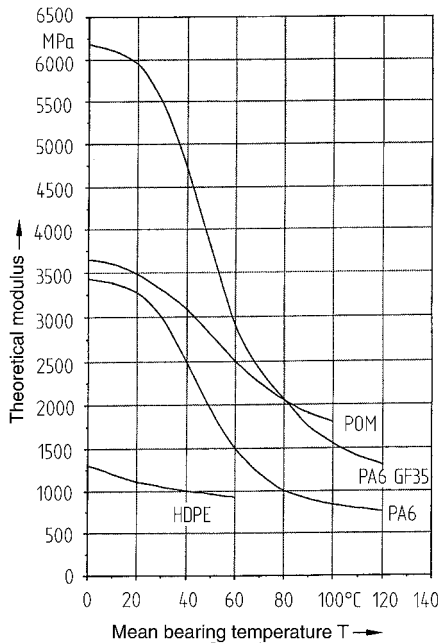


Figure 12.9 Part-specific theoretical moduli for short-term loading as a function of the mean bearing temperature

Effect of Bearing Play

Bearing play is not taken into consideration in Eq. 12.27. A small number of experiments [12.5], however, confirm the expectation that the deformation of a bearing bushing having relatively large play will likewise be relatively large due to the higher stresses on the material. Thus, when bearing play is increased from 0.6% to 2%, deformation nearly doubles. Even though there are no conclusive results quantifying this effect, this trend should be taken into account when using Eq. 12.27.

Effect of Time under Load

The results of calculations done using Eq. 12.27 together with the theoretical moduli in Figure 12.9, reflect the deformation of bearing bushings after approximately 1 minute under load. As a result of the time-dependence of the deformation behavior, however, compression by the shaft will also increase over time. In fact, under the same load, this deformation will increase as the wall thickness of the bearing increases. This relationship clearly emerges from the shape of the part-specific creep curves in Figure 12.10, which correlates with the characteristic creep behavior determined using test specimens.

Due to the high cost of conducting such experiments, there are relatively few part-specific modulus values presented as a function of time, temperature, and wall thickness as in Figure 12.9. Accordingly, it is not possible to make statements with general validity.

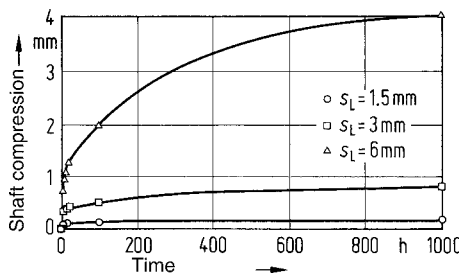


Figure 12.10 Bearing deformation (shaft compression) as a function of time for three different wall thicknesses; Material: POM, $d_L = 30 \text{ mm}$, $w = 21 \text{ mm}$, $F_L = 80 \text{ kN}$, $T = 23^\circ\text{C}$

Example

A radial bearing made of PA 6 is subjected to a short-term static load $F_L = 25 \text{ kN}$.

Shaft diameter $d_S = 25 \text{ mm}$

Bearing width $w = 15 \text{ mm}$

Temperature $T = 23^\circ\text{C}$

- Compression by the shaft shortly after application of the load has been applied is to be determined.

The pressure is determined according to Eq. 12.23:

$$\max p_{\text{approx}} = \frac{16}{3 \cdot \pi} \cdot \frac{25,000}{25 \cdot 15} = 113 \text{ MPa}$$

In Figure 12.6, $p_{\text{approx}} = 113 \text{ MPa}$ corresponds to $s_{L \text{ max}} = 4 \text{ mm}$.

Taking $s_L = 3 \text{ mm}$ and substituting this value in Eq. 12.27, we obtain:

$$\Delta h = \frac{1.8 \cdot 25,000}{\left(\frac{25}{3} + 1\right) \cdot 15 \cdot 3,100} = 0.1 \text{ mm}$$

Shortly after application of the load, the compression by the shaft $\Delta h = 0.1 \text{ mm}$.

- Considering creep, what will the Δh be after 10,000 h under load?

Using $E_C = 1,000 \text{ MPa}$ from Table 12.3:

$$\Delta h = \frac{1.8 \cdot 25,000}{\left(\frac{25}{3} + 1\right) \cdot 15 \cdot 1,000} = 0.32 \text{ mm}$$

After 10^4 hours, compression by the shaft increases to approximately 0.3 mm.

Table 12.3 Creep Moduli of Materials for 1% Strain According to CAMPUS (BASF)

Time under load [h]	Creep modulus [MPa]		
	10^2	10^3	10^4
POM (H 2320)	1430	1230	1000
PA 6 (B 4, air-moistened)	710	670	620
PA 6-glass fiber reinforced 25 (B3WG5)	2800	2620	2450
HDPE (5261 Z)	300	270	230

However, a comparison of the limited experimental data with calculated values shows that an estimate of the order of magnitude of time-dependent bearing bushing deformation may be obtained when the creep modulus of the material is used in Eq. 12.27 and the pressure is reduced to at least half the value shown in Figures 12.6 and 12.7.

Table 12.3 presents creep modulus values of some typical bearing materials for 1% strain.

12.2.4 Dynamic Load-Bearing Capacity

Under dynamic load conditions by a pressure p and at a sliding velocity v , different causes of failure occur than those found under static contact. These include:

- Increase in temperature,
- Wear (in different forms),
- Stick-slip.

A friction bearing must be designed to withstand these causes of failure.

12.2.4.1 Continuous Operation

The product of mean surface pressure and the mean sliding velocity provides a very rough basis for dynamic bearing design. The use of such a pv value as a permissible limiting value largely depends on structural factors and the exact operating conditions. It can be used to obtain a rough estimate of bearing performance. Table 12.4 is a guide to permissible pv values for unlubricated radial bearings as shown in Figure 12.2.

A substantially more reliable basis for evaluation is provided by equation (12.9) for the sliding surface temperature in association with the permissible pv value data shown in Table 12.4.

Table 12.4 Guide to Permissible pv Values for Unlubricated Radial Bearings and Limiting Values for the Sliding Surface Temperature

Sliding bearing material	Abbreviation	pv guide value [MPa · m/s]	Coefficient of friction	Limiting value for sliding surface temperature in °C
Polyamide 66	PA 66	0.05	0.38	100
Polyamide 6	PA 6	0.04	0.4	95
Polyamide/polyethylene	PA/PE	0.25	0.21	150
Polyoxymethylene	POM	0.07 (wear!)	0.35	120
Polyoxymethylene, slip-modified (N2310 P)	POM	0.1	0.24	130
Polybutylene terephthalate	PBT	0.07	0.33	120
Polyethylene	HDPE	0.1	0.2	90
Polyaryl ether ketone, modified	PEEK CF 15 + 15 PTFE	1.0	0.25	approx. 200

12.2.4.2 Intermittent Operation

Since dynamic load-bearing capacity is determined primarily by the level of heating which the material can withstand, friction bearings made of thermoplastics are better employed in applications where the dynamic load is intermittent. The higher the load they are subjected to, the shorter their operating time can be. The relative operating time OT is defined as the ratio of the load time t to the total cycle time τ in percent.

$$OT = \frac{t}{\tau} \cdot 100 \quad (12.28)$$

In contrast with electrical engineering applications, where, for example, the cycle time τ for electric motors is generally set at 10 min, in the case of thermoplastic friction bearings, a longer cycle time must be used. The state of thermal equilibrium in friction bearings is reached only after times as long as 100 to 120 min. A cycle time of 60 min is a reliable guideline for thermoplastic bearings. The load time is defined as the duration of time that the bearing is under load within this period of 60 min.

The maximum sliding surface temperature which occurs during intermittent operation is calculated with the aid of Figure 12.11 and Eq. 12.29. This value can be compared with the permissible limiting temperature given in Table 12.4.

$$T_{S,OT} = f \cdot (T_S - T_E) + T_E \quad (12.29)$$

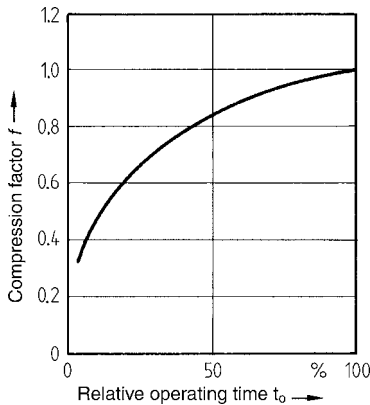


Figure 12.11 Correction factor f as a function of the relative operating time for determining the sliding surface temperature in intermittent operation for bearings

12.2.4.3 Wear

It is not always possible to calculate wear reliably in advance or to predict the expected service life for plastic bearings. In a comparison [12.6] of pin-on-disk experiment test results (see Section 4.7.2) with those obtained from bearing bushing tests carried out under approximately the same conditions of temperature, roughness, and sliding velocity, it was found that the coefficient of wear* is largely identical in both tribological systems (see Table 12.5). The coefficient of friction of HDPE in the bearing bushing system, however, is significantly lower than that determined for the pin-on-disk system. This is explained by the considerable amount of material abraded from HDPE whose “lubricating effect” is well known. It should not be expected that there will always be such good agreement between these two systems, but the trends observed using the pin-on-disk apparatus can at least be extrapolated.

The principal causes of wear identified in Section 12.1 should be given appropriate consideration in establishing the boundary conditions of a bearing structure.

Table 12.5 Comparison of Measurements of Friction and Wear Obtained in a Pin-on-Disk System and in a Radial Bearing System [12.6]

	HDPE		PA 66	
	Coefficient of wear	Coefficient of friction	Coefficient of wear	Coefficient of friction
Pin-on-disk ¹	71	0.3	9	0.54
Radial bearing ²	65	0.21	7	0.55

¹⁾ $R_Z = 3 \mu\text{m}$, $T_E = 23^\circ\text{C}$, $v = 0.3 \text{ m/s}$, $p_m = 4 \text{ MPa}$

²⁾ $R_Z = 3 \mu\text{m}$, $T_E = 23^\circ\text{C}$, $v = 0.2 \text{ m/s}$, $p_m = 0.5 \text{ MPa}$

* The coefficient of wear is the ratio of volumetric wear to travel with reference to a force applied normally.

12.3 Bearing Design

12.3.1 Bearing Clearance

A distinction must be made between operating clearance h_0 , installed clearance h_i , and production clearance h_p (see Figure 12.12).

- The *operating clearance (basic clearance or minimum clearance)* h_0 is the clearance or play which, under the most unfavorable conditions, must still be available so the bearing can function and does not seize.

This play is plotted as a function of the bearing diameter in Figure 12.13. In addition, according to [12.4], a play of 3% for bearings with inner diameters of approx. 0.5 mm is recommended.

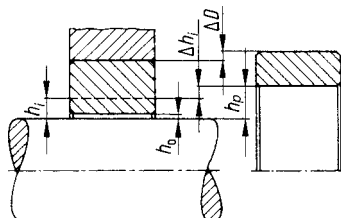


Figure 12.12 Schematic illustration of the various dimensions associated with bearing clearance

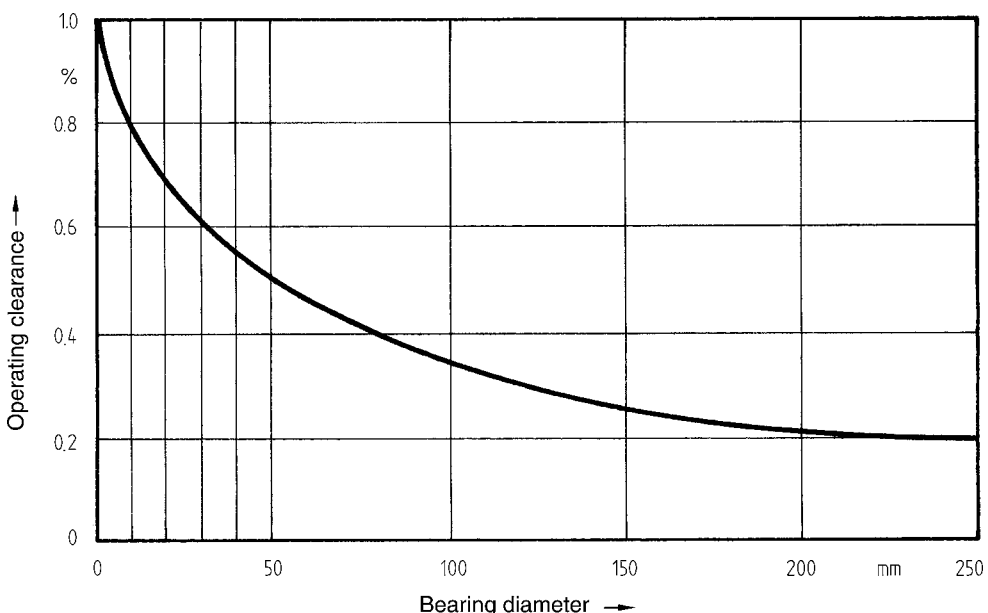


Figure 12.13 Operating clearance of bearing bushings composed of thermoplastic polymeric materials as a function of the inner diameter of the bearing [12.1]

When precision running requirements are imposed on a bearing and the operating conditions – especially the effect of temperature – are known with sufficient accuracy, the operating clearance can be set on the basis of the empirical equation (12.30).

$$h_0 = 0.008 \text{ to } 0.015 \cdot \sqrt{d_s} \quad (12.30)$$

- The *installed clearance* h_i is the play in the assembled state but not in the hot operating state.

Equation 12.31 provides an estimate of the reduction in diameter after pressing the bearing into the metal housing.

$$\Delta h_i = \frac{\Delta D}{D_L} \cdot (d_L + 3 \cdot s_L) \quad (12.31)$$

where

ΔD = as defined in Figure 12.12

D_L = bearing outer diameter in mm

d_L = bearing inner diameter in mm $\approx d_s$

s_L = wall thickness in mm

- The *production clearance* h_p is the amount by which the inner diameter of the bearing must exceed the diameter of the shaft in order to ensure the correct operating clearance under operating conditions.

In addition to the reduction in play after pressing the bearing into the metal housing, the following equation also takes into account the expected changes in dimensions as a result of thermal expansion and absorption of moisture.

$$h_p = h_0 + 3 s_L \cdot (\varepsilon_m + \alpha \cdot \Delta T) + \Delta h_i \quad (12.32)$$

In the equation, ΔT is set equal to $T_L - 20$ K, where T_L is the maximum mean bearing temperature to be expected. The moisture factor ε_m can be used to take moisture absorption into account if the bearing is installed in the dry state. This is particularly important for PA bearings.

The values for ε_m given in Table 12.6 are used to calculate the changes in dimensions that occur from the freshly molded state (*i.e.*, dry) through saturation under the specified conditions of exposure to moisture. The data are based on measurements carried out on test specimens and agree well with experience in practice to date.

While there is no significant difference in ε_m for injection-molded bearing bushings having wall thicknesses between 3 and 6 mm, the moisture factor decreases markedly for cast PA bearings having thicker wall sections (see Figure 12.14).

In the case of glass-fiber reinforced polyamides, the lower values given in Table 12.6 apply to changes in dimensions in the direction of fiber alignment and the higher values to such changes

Table 12.6 Moisture Factor ε_m for Calculating Bearing Clearance for Unconditioned Friction Bearings Having Wall Thicknesses Between 3 and 6 mm

	PA 66 PA/PE Cast PA	PA 6	Glass fiber reinforced PA (30 to 35% by weight)	POM	PBT
Bearing in typical ambient humidity	0.006	0.0065	0.001 to 0.003	—	—
Saturation in 23/50 atmosphere	0.011	0.012	0.0015 to 0.005	—	—
Water-lubrication	0.028	0.03	0.005 to 0.015	0.0035	0.001

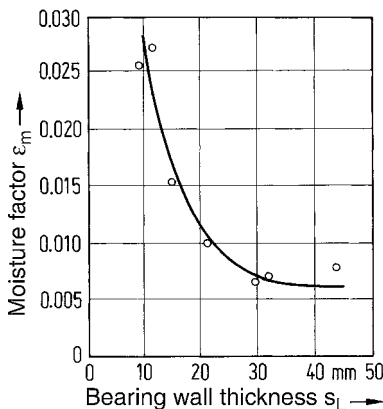


Figure 12.14 Moisture factor ε_m for calculating bearing clearance for underwater bearings made of cast PA. Measurements were carried out on depressed bushings having diameters in the range of 150 to 270 mm after immersion in water at approx. 20 °C for 26 months.

transverse to the direction of fiber alignment. The effect of varying moisture levels and temperatures on bearing clearance is negligible for very thin-walled, slotted bearing bushings (see Figure 12.16).

12.3.2 Bearing Wall Thickness

Ideally, the wall thickness of bearings should be small in order to achieve good heat dissipation and dimensional stability. A reliable wall thickness value is given by the empirical relation 12.33.

$$s_L = 0.4 \cdot \sqrt{d_S} \quad (12.33)$$

Example

The production clearance for a radial bearing made of PBT is to be calculated.

$$d_S = 10 \text{ mm}$$

$$s_L = 1.2 \text{ mm}$$

$$T_E = 50^\circ\text{C}$$

$$\Delta D/D_L = 0.5\%$$

According to Eq. 12.32:

$$h_p = h_0 + 3 s_L \cdot \alpha \cdot \Delta T + \Delta h_i$$

- Operating clearance according to Eq. 12.30:
 $h_0 = 0.008 \text{ to } 0.015 \sqrt{10} = 0.025 \text{ to } 0.047 \text{ mm}$
- Operating clearance according to Figure 12.13:
 $h_0 = 0.08 \text{ mm}$

h_0 taken to be 0.06 mm

- Thermal expansion (α in Figure 4.23):
 $h_\alpha = 3 \cdot 1.2 \cdot 100 \cdot 10^{-6} \cdot 27 = 0.01 \text{ mm}$
- Dimensional loss caused by the pressing-in:
 $\Delta h_i = 0.005 (10 + 3 \cdot 1.2) = 0.07 \text{ mm}$

$$h_p = 0.06 + 0.01 + 0.07 = 0.14 \text{ mm}$$

The production clearance should be about 0.14 mm.

12.3.3 Bearing Production

Rotationally symmetrical plastic bearing bushings are also conveniently produced in large numbers by machining semifinished products on a lathe. The key advantages of bearing bushings produced by machining include good dimensional features (true running and no demolding related draft angle required, even in wide bearings) as well as the use of superior quality polymer materials. The high molecular weight of the extrusion grade materials exhibit improved resistance to wear, especially in the case of highly crystalline materials (see also Figure 4.37). On the other hand, the injection molding process affords the advantages of design freedom and the production of integral bearings.

12.3.4 Design Examples of Bearings

Figures 12.15 to 12.18 show examples of some of the principles involved in bearing design. Some incorporate unique features; other good examples are provided in Figures 1.8 to 1.10, 1.27, 6.21, 7.20, 7.32, 8.40, 8.58, 9.2, 11.34, and 11.51.

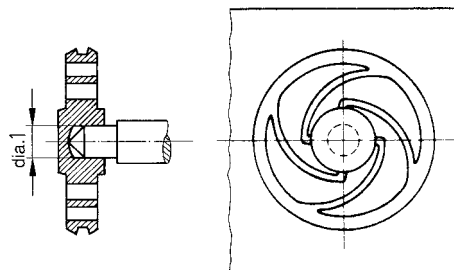


Figure 12.15 Spring-mounted, self-adjusting small bearing

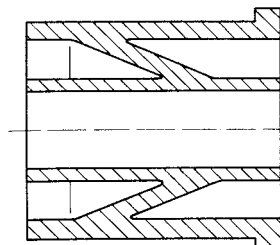


Figure 12.16

This bearing can compensate for tolerances in the housing bore to a certain degree. Due to the conical shape between the inner and outer bushing, a high ratio of housing bore to shaft diameter can be achieved. In addition, the hollow bearing has better damping properties than a solid bearing. These advantages are, however, gained at the expense of load-bearing capacity.

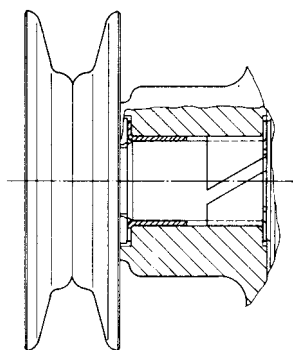


Figure 12.17

Dimensional changes due to temperature fluctuations or equilibration of moisture levels can be counteracted without an appreciable change in play



Figure 12.18 Slip plate fitted with grooves running at an angle to the direction of sliding. The grooves are intended to pick up dirt, foreign bodies, and abraded material and carry them away from the sliding surface. Grooves of this type have proved to be effective in other bearing geometries as well.

(Photograph: TKG Ensinger, Nufringen)

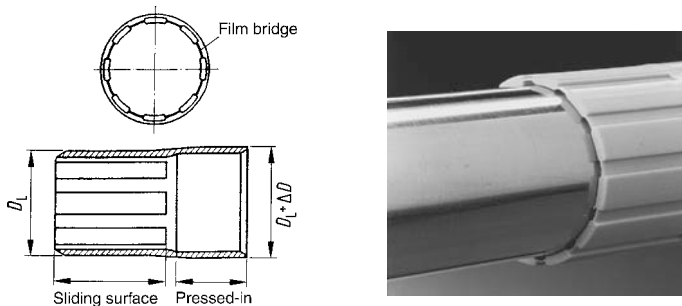


Figure 12.19 Low-play friction bearing for linear motion. The actual sliding surface area is divided into segments connected by film bridges 0.2 mm thick that compensate for differential thermal expansion. In this region, the fit with the receiving bore is sized for a close sliding fit ($D_L \approx D_B$), while the outer diameter of the pressed-in bushing is oversized so that $\Delta D \approx 1.5\%$. (Photograph: igus GmbH, Bergisch Gladbach, patent pending)

References

- [12.1] VDI-Richtlinie 2541 Gleitlager aus thermoplastischen Kunststoffen (Friction bearings made from thermoplastics), VDI-Verlag, Düsseldorf 1975
- [12.2] ERHARD, G. and E. STRICKLE: Maschinenelemente aus thermoplastischen Kunststoffen (Machine elements made from thermoplastics), VDI-Verlag, Düsseldorf 1984
- [12.3] ERHARD, G. and E. STRICKLE: Berechnung der statischen Tragfähigkeit von Querlagern aus thermoplastischen Kunststoffen (Calculation of the static load-bearing capacity of radial bearings made from thermoplastics), *Konstruktion* **29** (1977) 6, pp. 237/241
- [12.4] DETTER, H. and K. HOLECEK: Der Reibungswiderstand und die Beanspruchung von feinmechanischen Lagern im Trockenlauf bei kleinen Gleitgeschwindigkeiten (Frictional resistance and loads on unlubricated precision engineering bearings at low sliding velocities), *Feinwerktechnik* **74** (1970) 11, pp. 461/465
- [12.5] BUTZ, S.: Untersuchung der statischen Belastbarkeit von Radiallagern aus Polymerwerkstoffen (Study of the static load-bearing capacity of radial bearings made from polymeric materials), Diploma thesis, Fachhochschule Darmstadt 1992
- [12.6] SONG, J.: Reibung und Verschleiß eigenverstärkter Polymerwerkstoffe (Friction and wear in independently reinforced polymeric materials), Dissertation, University (GH) Kassel, 1990

13 Wheels and Rollers

Polymeric materials are suitable for making wheels and rollers subjected to relatively low loads. Due to their unique properties, plastics extend the range of performance possible with more traditional materials for wheels and rollers, particularly when the following properties are demanded:

- Silent running (damping)
- Conservation of tread (low pressure)
- Resistance to wear
- Low weight
- Efficient production (multifunctionality)
- Widely variable coefficient of friction.

Materials

Polyamide 6 is one of the most widely used materials for rollers. Injection-molded or flow-molded webbed rollers made of PA 6 measuring up to 250 mm in diameter are available in industry. For higher technical demands, materials with higher relative molecular weights (see Section 2.1.1) or PA 66 must be used. Very large, thick-walled roller blanks and even finished rollers can be made from *cast polyamide** using a special casting process. The high crystallinity of cast PA 6 gives rise to a comparatively high modulus of elasticity, a lower tendency to creep, and greater hardness.

Polyoxymethylene exhibits similar properties to PA 6. The running surface of a POM roller tends to be rougher than that of a PA roller, but its resistance to wear is much lower.

Other relatively important materials for wheels and rollers are *polyurethanes*. Both the physically cross-linked (TPU) and the chemically cross-linked (PU) forms are used in these applications. The former are thermoplastics while the latter are elastomers having very pronounced rubber-elastic properties.

Basic Forms

According to [13.1], rollers are classified into four basic forms, as shown in Figure 13.1.

* Cast polyamide type 6 is a form of PA 6 produced by activated anionic lactam polymerization (ALP). In this process, monomeric lactam can be rapidly polymerized using special catalysts. The reaction mixture is poured at atmospheric pressure into heated molds where it solidifies after a short time. Since polymerization proceeds at a temperature below the melting point of the crystallites, parts and semifinished products can be cast that have thicker walls than is possible by the usual injection molding process. The modulus of elasticity of cast polyamide can be varied over a range of 1,500 to 4,000 MPa.

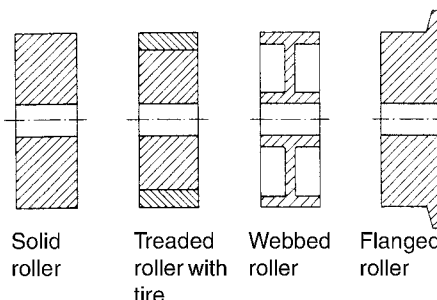


Figure 13.1 Basic forms of rollers

13.1 Roller Damage

Rollers made of thermoplastic polymeric materials subjected to excessive *static* loads will eventually become unusable because of flattening of the running surface. In the case of rollers subjected to excessive *dynamic* loads, failure is usually directly or indirectly due to high temperatures caused by internal friction or viscous heating. Direct thermally induced failure occurs when the melting point of the roller material is reached and molten material escapes at the faces of the roller (see Figure 13.2). Voids or other defects in the region of the running surface or tread accelerate the fusion process.

It is noteworthy that in the case of PA rollers, the melting point is very rapidly reached as soon as the temperature in the interior of the wheel rises to 42 °C [13.2]. This is explained by the fact that internal friction starts to increase steeply at 40 °C (see Figure 13.20). In the case of POM rollers, this effect occurs only at higher roller temperatures, as described by a curve of internal friction versus temperature for this material. In the case of rollers made of materials whose internal friction vs. temperature curves show a degressive trend (e.g., TPU), this rise in temperature should not be a concern as long as the load is not increased.

Indirect failure can occur when a roller heats up during a load cycle and then, while at rest under load and high temperatures, flattens out to an unacceptable degree.

Overmolded or press-molded rollers or tires can work themselves loose when their wall thickness is not sufficient.

Overloaded webbed rollers usually fail due to fatigue cracks and subsequent fracture at the transition from the web to the running surface or in the reinforcing spokes (see Figure 13.3).

Fatigue phenomena can lead to pitting and cracks on the running surface of the roller or wheel. As in the case of gear wheels, this occurs primarily in the presence of liquids, oil, and grease on the tread or roller surface (see Figure 13.4).

Greater wear can be expected when there is both a rolling motion and a sliding component due to slip, or when the roller or wheel must absorb high side forces (see also Figure 1.18).

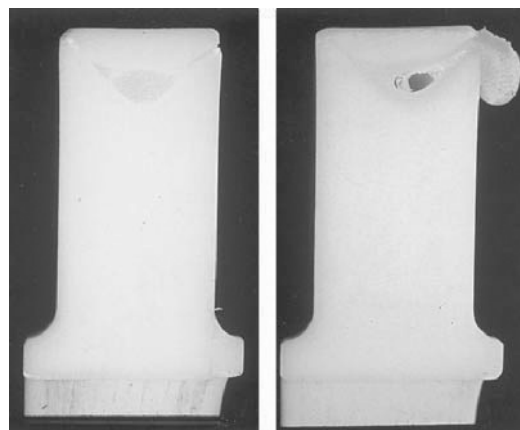


Figure 13.2 Fused roller due to excessive dynamic load in the interior (left); melt exudes from the side of the roller (right)



Figure 13.3 Pattern of cracking on an overloaded webbed roller
($d = 125$ mm, $w = 22$ mm, $F_N = 7,500$ N, $V_R = 1.5$ m/s) [13.3]

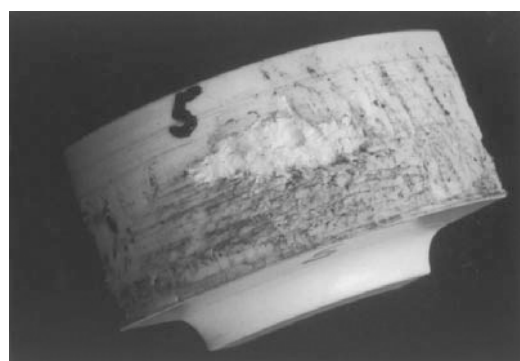


Figure 13.4 Typical fatigue damage on an overloaded PBT roller

13.2 Calculation of Load-Bearing Capacity

13.2.1 Pressure Parameter as an Approximate Design Limit

Hertzian equations have been used to determine quantitative estimates of loading on rollers made of polymeric materials. A material-specific pressure parameter based on the Hertzian equations has already been specified for this purpose [13.3]. Its usefulness in practice has been confirmed [13.4, 13.5]. This pressure parameter applies to PA as a roller material and to materials having a much higher modulus of elasticity as track materials (*e.g.*, steel, concrete). A further requirement is that the radii of curvature in the second principal plane must be infinite (*i.e.*, cylindrical roller and track, not spherical).

$$p'_{PA} = 25.4 \sqrt{\frac{F_N}{w \cdot r}} \leq p'_{\max} \quad (13.1)$$

where

F_N = roller loading in N

w = load-bearing width of roller in mm

r = roller radius in mm

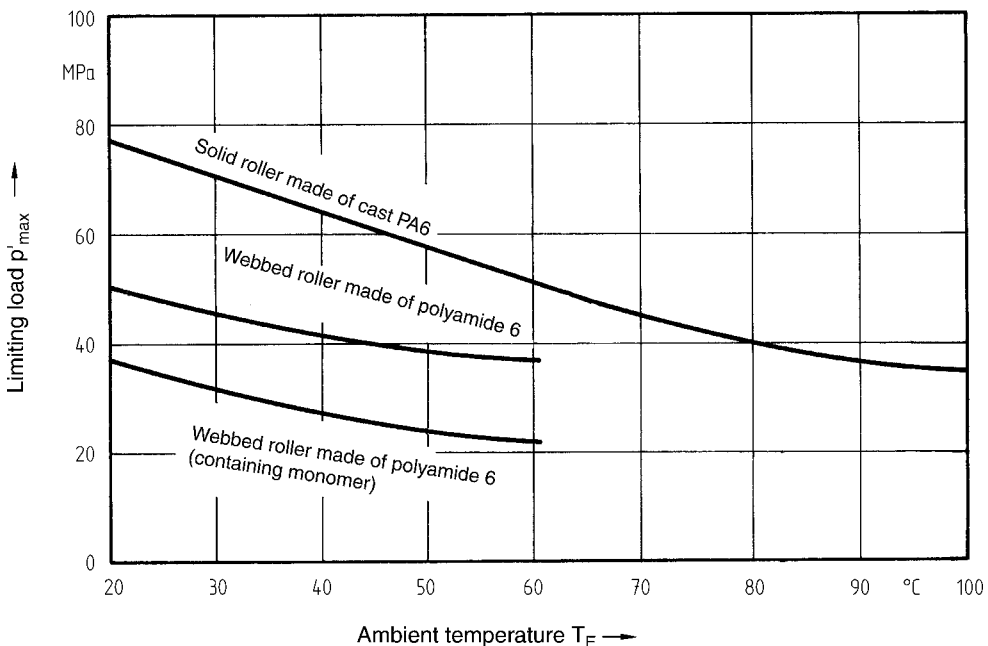


Figure 13.5 Limiting load on rollers made of PA rolling on a steel track as a function of ambient temperature under static load [13.3]

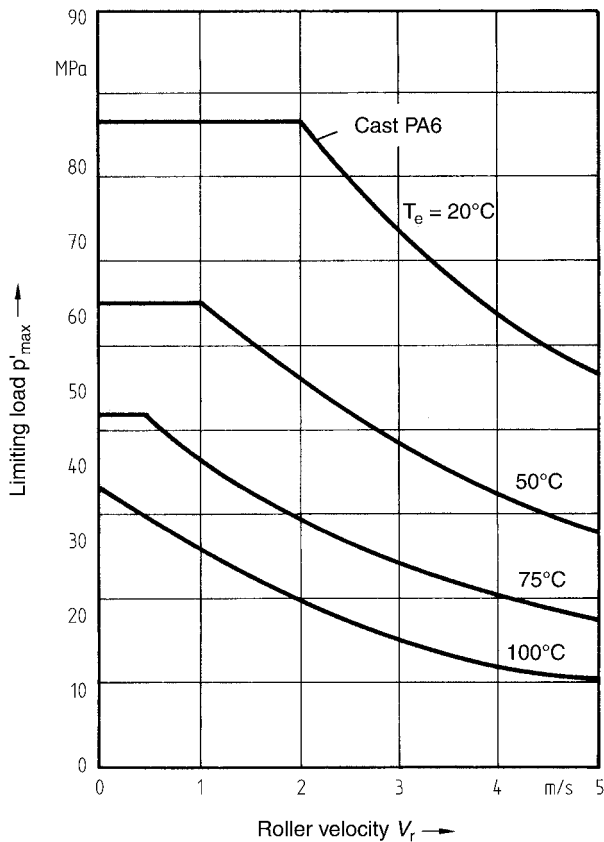


Figure 13.6 Limiting load on bearing-mounted solid rollers made of cast PA on a steel track as a function of roller velocity at various ambient temperatures (continuous operation) [13.3]

When the track is curved, the substitute radius r_s has to be used.

$$r_s = \frac{r_1 \cdot r_2}{r_1 + r_2} \quad (13.2)$$

where

- r_1 = roller radius
- r_2 = track radius

The constant in Eq. 13.1 includes the numerical value of the modulus of elasticity of PA at room temperature. Therefore, p' is not the actual load but is used as a pressure parameter only in comparison with the limiting loads p'_{\max} determined for rollers made from PA as given in Figures 13.5 to 13.7.

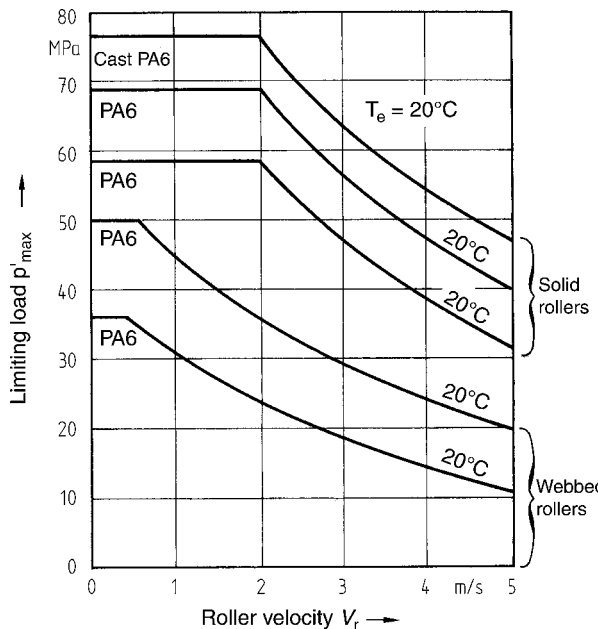


Figure 13.7 Limiting load on bearing-mounted rollers produced using different forms of polyamide rolling on a steel track as a function of roller velocity (continuous operation) [13.3]

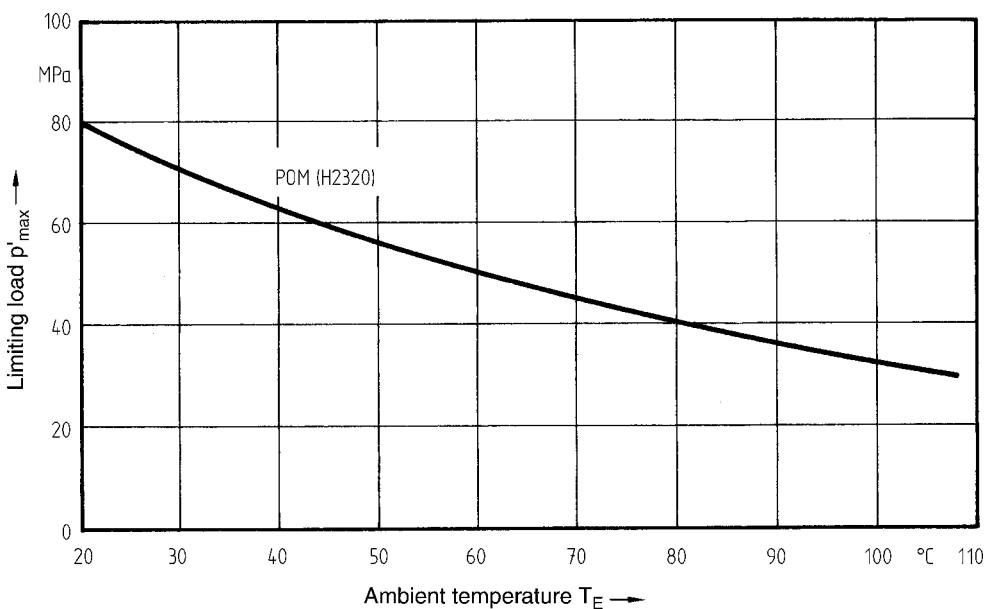


Figure 13.8 Limiting load on rollers made of POM copolymer rolling on a steel track as a function of ambient temperature under static load [13.5]

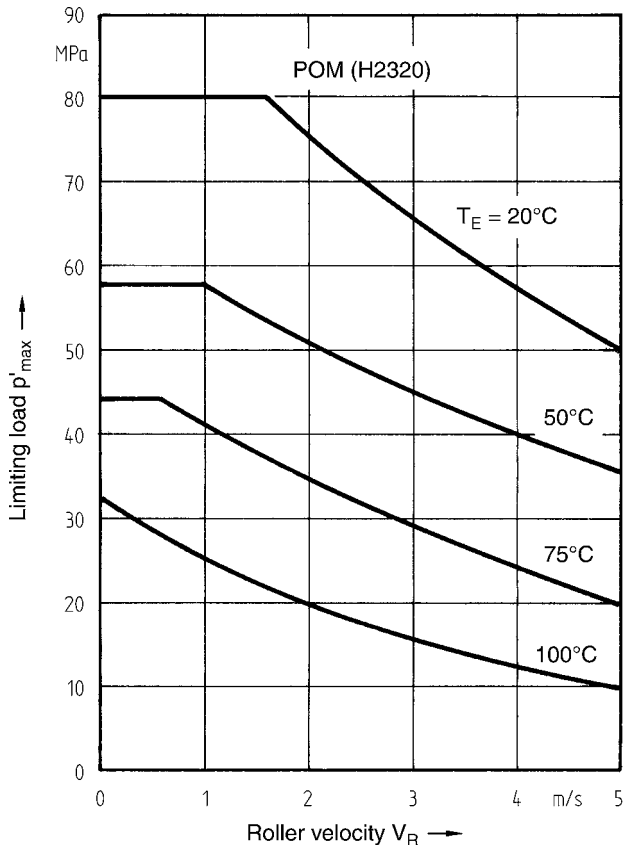


Figure 13.9 Limiting load on bearing-mounted solid rollers made of POM copolymer rolling on a steel track as a function of roller velocity at various ambient temperatures (continuous operation) [13.5]

The pressure parameter for rollers made of POM copolymer is given by an analogous relationship:

$$p'_{\text{POM}} = 33.7 \sqrt{\frac{F_N}{w \cdot r}} \leq p_{\max} \quad (13.3)$$

p'_{\max} for static loading is taken from Figure 13.8 and for dynamic continuous loading it is taken from Figure 13.9.

The load-bearing capacity of rollers made of PU can be estimated using Figure 13.10.

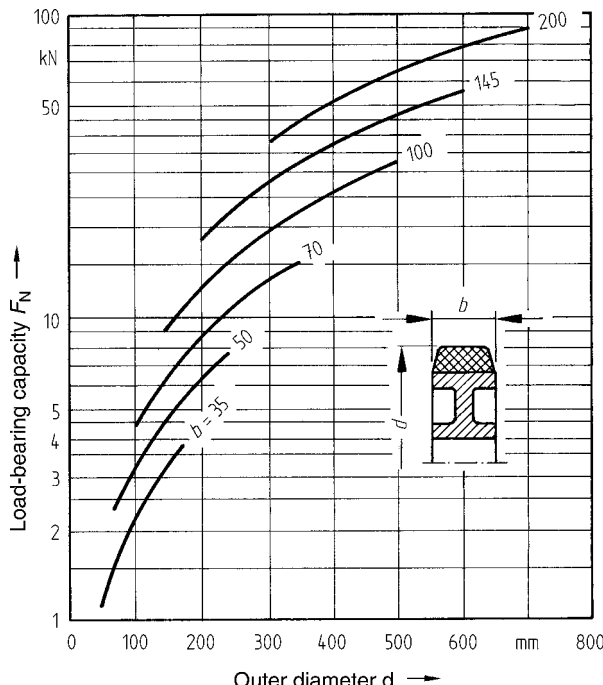


Figure 13.10 Load-bearing capacity of rollers (or tire treads) made of PU as a function of the outer diameter of the roller $v_R < 1.6 \text{ m/s}$ [13.6]

13.2.2 Deformation of Rollers under Static Load

There are a number of theories or models addressing the deformation of bodies in contact with one another. These theories are based on different sets of boundary conditions. A brief review of the analytical solutions for these models is presented in [13.24].

The theory proposed by Hertz in 1881 for the contact of solid elastic bodies determines the normal stress and deformation in the contact plane between two bodies having principal radii of curvature r_{11}, r_{12} and r_{21}, r_{22} which are pressed against one another by a normal force F_N . The Hertzian theory assumes homogeneous isotropic materials exhibiting elastic deformation. The contact area must be small in comparison with the surface areas of the bodies, and the coefficient of friction $f = 0$. When $E_1 = E_2$, the theory can also be extended to the case of a constant coefficient of friction in the contact plane.

Although these conditions generally do not apply or only partially apply for polymeric materials, the Hertzian equations are useful when the required physical properties of the material can be determined under similar conditions to those prevailing in the part. Reference [13.8] provides a practicable method for calculating the flattening of rollers subjected to static loads using such characteristic values for the polymeric materials and idealized geometric relationships.

Breadth of Contact Surface and Surface Pressure

According to Hertz, the breadth $2B$ of the contact surface is given by:

$$2B = 4 \sqrt{\frac{F_N \cdot r}{w} \cdot \frac{2(1 - \mu^2)}{\pi \cdot E_S}} \quad (13.4)$$

where

μ = Poisson's ratio ≈ 0.4

and the pressure is determined by

$$p_H = \sqrt{\frac{F_N}{r \cdot w} \cdot \frac{E_S}{2 \cdot \pi \cdot (1 - \mu^2)}} \quad (13.5)$$

The substitute modulus E_S is used when the roller and track are made of different materials.

$$E_S = 2 \cdot \frac{E_1 \cdot E_2}{E_1 + E_2} \quad (13.6)$$

If the modulus of elasticity of the roller material is used for E_1 in Eq. 13.6, Eq. 13.5 yields the pressure occurring spontaneously. According to the experimental findings in [13.8], this initial value decreases more rapidly at higher loads (see Figure 13.11). In the experiments conducted to generate these curves, the contact surface area $A = 2B \cdot h$ was measured using interposed pressure-sensitive paper.

Time-Dependent Flattening

Equations for the flattening δ can be derived from the geometric relationships between contact force and flattening (see Figure 13.12). The equation for the combination of a roller and a flat plate is:

$$\delta = r_1 - \sqrt{r_1^2 - 0.405 \cdot \left(\frac{F_N}{w \cdot p}\right)^2} \quad (13.7)$$

and that for a roller/roller combination is:

$$\delta = r_1 + r_2 - \sqrt{r_1^2 - 0.405 \cdot \left(\frac{F_N}{w \cdot p}\right)^2} - \sqrt{r_2^2 - 0.405 \cdot \left(\frac{F_N}{w \cdot p}\right)^2} \quad (13.8)$$

The pressure p is determined using Figure 13.11.

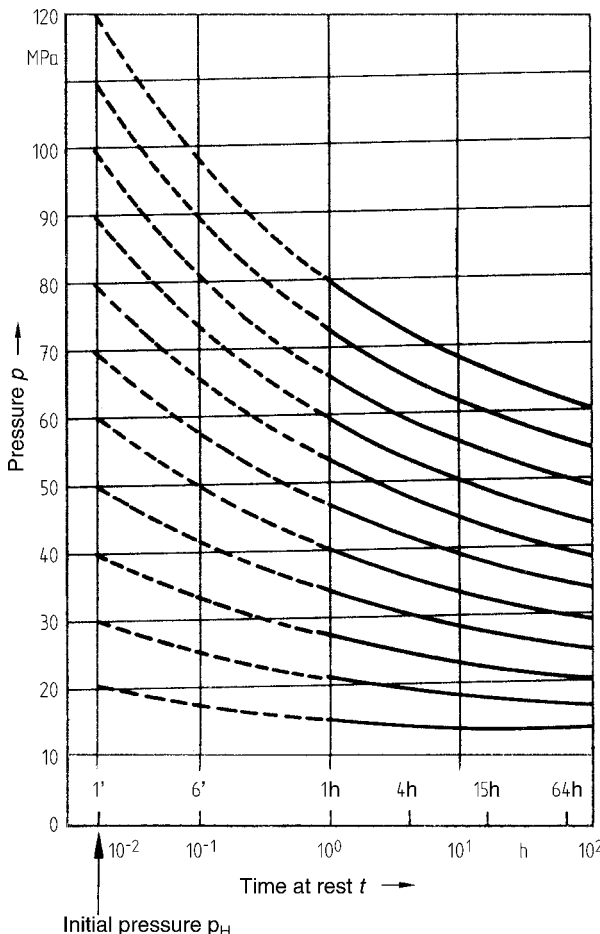


Figure 13.11 Decrease in surface pressure of POM rollers under static load.
The curves are independent of roller temperature [13.8].

Experiments [13.9], however, show that the measured flattening is greater than the values calculated on the basis of the idealized geometric relationships given in Eqs. 13.7 and 13.8 by as much as a factor of three.

An empirical relationship for estimating roller deformation that is based on laboratory experiments conducted using rollers made of POM is given in [13.3].

$$\Delta_{\text{tot}} = 2.45 \cdot \frac{F_N}{w \cdot E_C} \quad (13.9)$$

where

E_c = creep modulus as shown in Figure 13.13

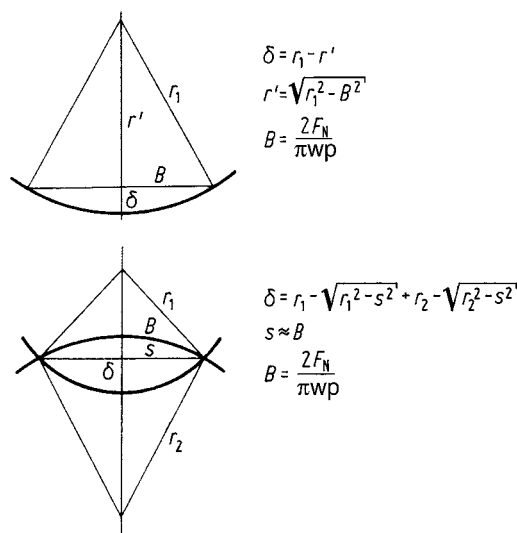


Figure 13.12 Geometric relationships for flattening of a roller on a flat plate (top); roller/roller combination (bottom)

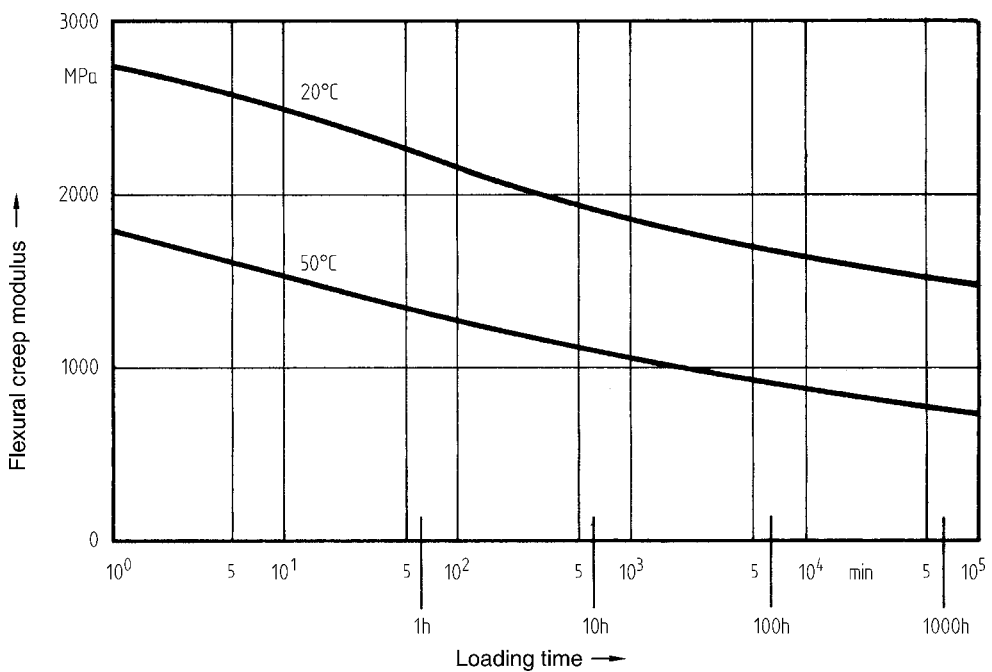


Figure 13.13 Flexural creep modulus E_c of POM copolymer [13.3]

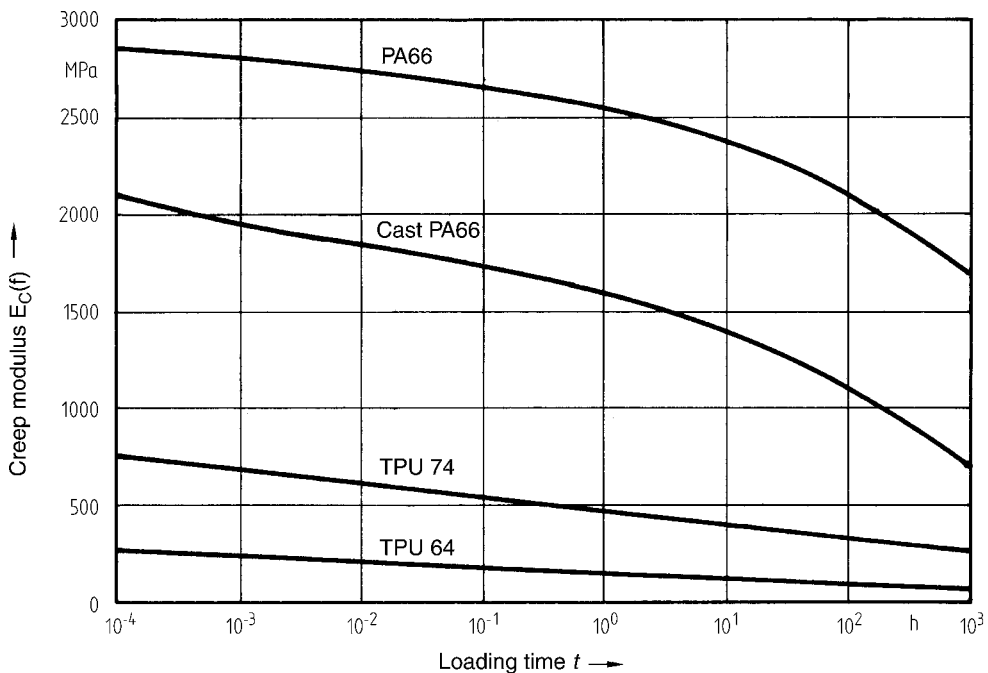


Figure 13.14 Creep moduli for selected materials. Approximated from measured values in accordance with the Findley power function for PA and in accordance with a logarithmic time function for TPU [13.2].

Δ_{tot} in Eq. 13.9 is the total deformation of the roller, that is to say, the offset of the axis of the shaft or axle. This variable is determined by the deformation δ of the running surface and the journal depression Δh (see Section 12.3). Therefore, Eq. 13.9 always yields higher values than Eq. 13.7.

Another method of calculating time-dependent flattening of rollers is given in [13.2], in which the roller height h is taken into consideration. According to this:

$$\Delta_{\text{tot}}(h) = \frac{2 F_N \cdot (1 - \mu^2)}{E \cdot w \cdot \pi} \cdot \left[\ln \left(\frac{h + \sqrt{h^2 + B^2}}{B^2} \right) - \frac{\mu \cdot h}{(1 - \mu) \cdot B^2} \cdot \left(\sqrt{B^2 + h^2} - h \right) \right] \quad (13.10)$$

Deformation at the start of loading is calculated using the modulus of elasticity, while the time-dependent increase in flattening is calculated using a creep modulus $E_c(t)$ specific to the part. These modulus values are determined in creep experiments on rollers. In that way, the modulus values obtained correspond to the state of stress of the loaded roller (see also Figure 11.1).

Relaxation of Flattening and Permissible Residual Flattening

The flattening δ during a stationary period will tend to reduce or even out during a subsequent rolling phase. The magnitude of the change is a function of the load on the roller and the roller velocity, having an essentially exponential relationship.

$$t = a \cdot e^{q\delta} \quad (13.11)$$

where

t = recovery time in h

δ = flattening in μm in accordance with Eqs. 13.7 and 13.8

a = experimentally determined factor (Figure 13.15)

$q \approx 1.4 \cdot 10^{-3} (\nu_R - 10)$

ν_R = roller surface velocity in m/s

The values for a and q apply for $T_E = 23^\circ\text{C}$. Various experiments indicate that flattening relaxes faster at higher ambient temperatures.

The time t_{rel} needed for flattening δ to recover to a residual flattening δ_{rel} is formulated as follows:

$$t_{\text{rel}} = a \cdot (e^{q\delta_{\text{rel}}} - e^{q\delta}) \quad (13.12)$$

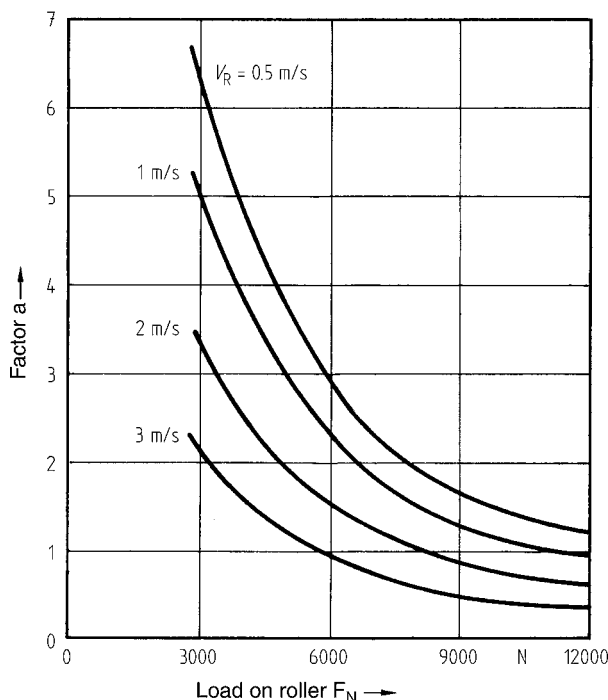


Figure 13.15 Factor a as a function of load on the roller and roller surface velocity at $T_E = 23^\circ\text{C}$ [13.8]

The residual flattening δ_{rel} (applicable in calculations based on Eqs. 13.7 to 13.9 and 13.12) is defined as the deformation of the roller still remaining after a reasonable relaxation period under conditions of smooth operation. According to observations in [13.8] for rollers having a diameter > 30 mm moving at a velocity $v_R = 0.5$ to 3 m/s, the residual flattening $\delta_{\text{rel}} = 30$ to 50 μm . The irregularity in rolling in this case differs only slightly from normal operating conditions of a roller that has not been deformed.

If the total deformation Δ_{tot} is calculated using Eq. 13.10, a limiting upper value of 0.3% with respect to the roller diameter d ($\Delta_{\text{tot}}/d \approx 0.003$) is thought to be permissible in most applications.

13.2.3 Rollers under Dynamic Load

The behavior of rolling contact between two rotating bodies composed of elastic materials is fairly well understood. In-depth studies of these solutions are presented in references [13.10] to [13.13].

In the case of viscoelastic materials, however, the circumstances of rolling contact are substantially more complex. Some theoretical approaches to solutions may be found in references [13.14] to [13.16]. Some of the methods of computation require considerable resources, especially when the contact problem is solved using a finite element method [13.17]*.

In the following section, some limited, semiempirical, but easy-to-use design calculations for dynamic roller performance are considered. They are primarily based on theoretical approaches, which have been adapted to the results of laboratory tests on rollers.

13.2.3.1 Free-Wheeling Rollers (without Drive)

Permissible Load on Rollers

One of the most common cases of roller failure is due to the lost work of deformation that leads to softening or fusing (see Figure 13.2). In the absence of a theoretical method for estimating the stationary temperature distribution when a roller is rotated at high frequency, the lost work has been determined experimentally in a series of tests using rollers made of POM. The lost work is determined by the deformed volume V , the frequency f and the stress amplitude p , described by a characteristic value (C factor). These C factors (see Figure 13.16) depend on the ambient temperature, the roller velocity, and the mode of operation (involving skips or largely skip-free). On the basis of these values, and with another empirical factor k (see Figure 13.17), a permissible load on the roller can then be determined using Eq. 13.13.

$$F_{\text{perm}} = \sqrt{\frac{C \cdot w}{k \cdot f}} \quad (13.13)$$

where

f = frequency

* An example of a model and computer program for solving the rolling contact problem for linearly viscoelastic, isotropic materials under conditions of constant rolling temperature is presented in [13.18].

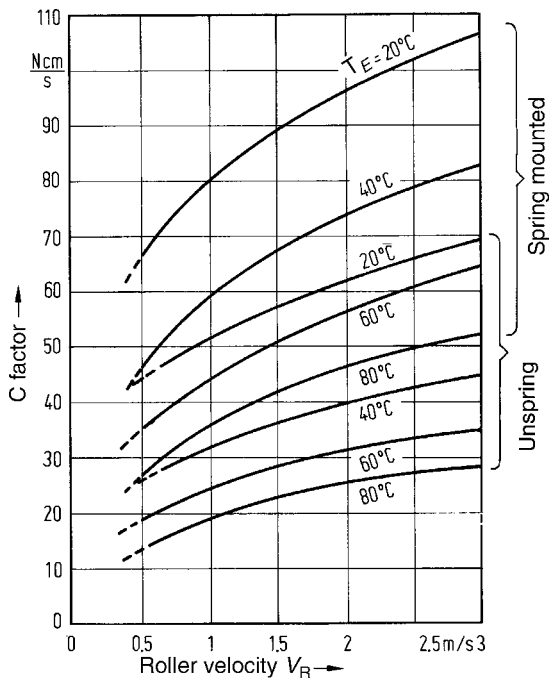


Figure 13.16 C factors for rollers made of POM, which are either spring-loaded or not spring-loaded [13.8]

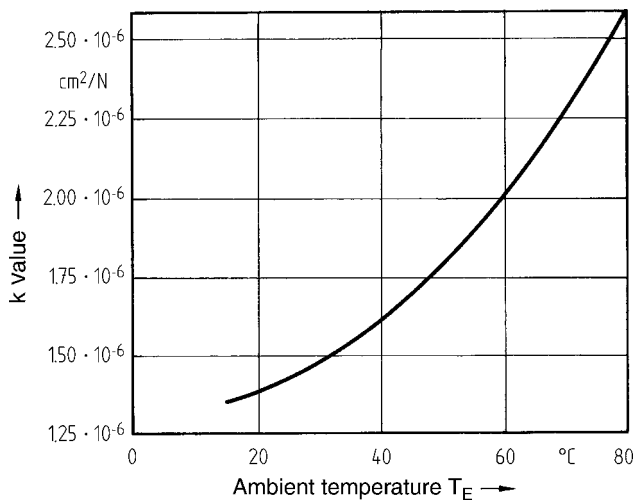


Figure 13.17 k value as a function of ambient temperature [13.8]

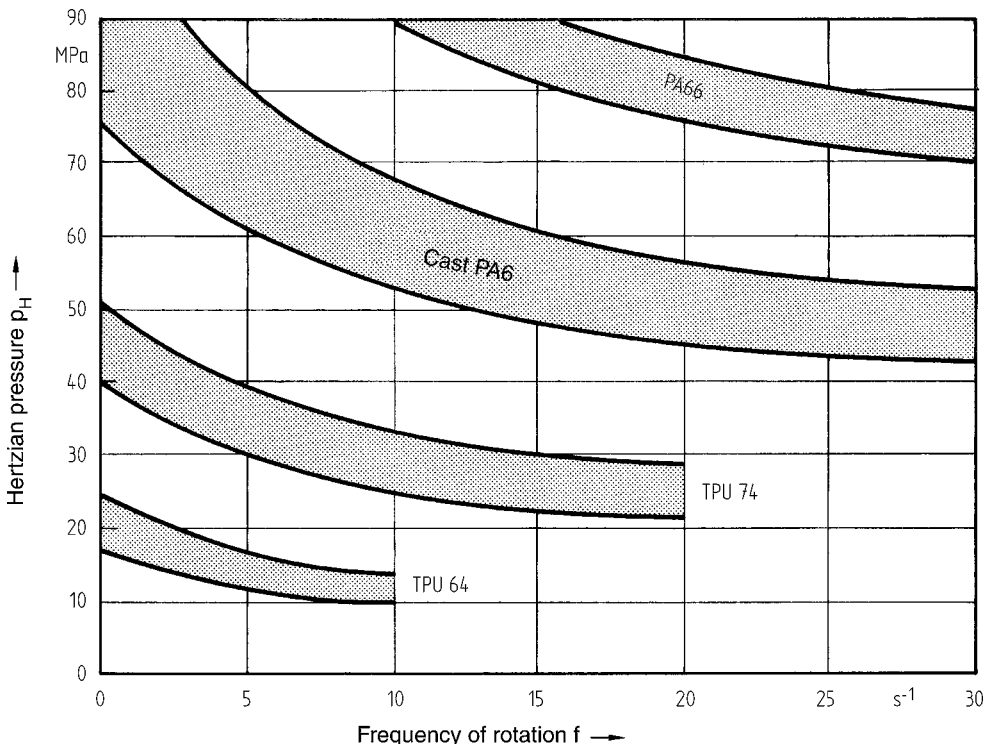


Figure 13.18 Hertzian pressures calculated from empirically determined limiting loads for rollers or wheels of different geometries ($d = 63$ to 125 mm; $w = 16$ to 32 mm) as a function of the frequency of rotation at room temperature [13.2]

From test results on rollers made of polyamides and polyurethanes [13.2], a relationship can be established between Hertzian pressure and frequency of rotation, which identifies the limiting load above which an unacceptable rise in roller temperature may be expected (see also Section 13.1). In Figure 13.18, the upper pressure values in the scattered data fields apply to small roller (or wheel) diameters and/or low roller widths, because of their better heat dissipation characteristics. The lower values apply to rollers (or wheels) having a large diameter and/or high width.

Calculations of the Hertzian pressure are based on the following moduli of elasticity for the wheel materials:

$E = 2,900$ MPa for PA 66; $E = 2,200$ MPa for cast PA;

$E = 790$ MPa for TPU 74; $E = 250$ MPa for TPU 64.

Following suitable rearrangement of Eq. 13.5 and using p_H from Figure 13.18, the maximum load on a roller is given by:

$$F_{N \max} = 2 \cdot \pi \cdot (1 - \mu^2) \cdot p_H^2 \cdot \frac{r \cdot w}{E_S} \quad (13.14)$$

where

$$\mu = \text{Poisson's ratio} \approx 0.4$$

A comparison of the methods for calculating $F_{N\max}$ shows that the estimates obtained from Eqs. 13.1 and 13.2 tend to underestimate $F_{N\max}$. Equation 13.13 in contrast yields values for the permissible load on the roller that are rather too high. Therefore, for realistic results Eq. 13.14 is generally used.

Rolling Friction

To maintain a steady rolling motion, the friction losses of the bearing and any other opposing forces have to be overcome along with the rolling friction force F_R . By analogy with the coefficient of sliding friction, the coefficient of rolling friction f_R is defined as:

$$f_R = \frac{F_R}{F_N} \quad (13.15)$$

The imperfect elasticity of the material is primarily responsible for the rolling friction force. Therefore, it has to be expected that in the case of rollers made of polymeric materials, relatively high rolling friction losses will have to be overcome. This has to be taken into account when drive systems for rollers are specified.

Figure 13.19 presents a schematic diagram of the hysteresis in the distribution of stress and strain when a viscoelastic material makes rolling contact. The asymmetry of the force distribution is also shown.

In Figure 13.19, the following equilibrium condition applies:

$$F_R \cdot r = F_N \cdot e \quad (13.16)$$

In references [13.9] and [13.19] the unknown e is calculated for linear viscoelastic materials on the basis of a sinusoidal strain function using a Maxwell model (see Section 4.2.1). This finally yields the following expression for the rolling friction force:

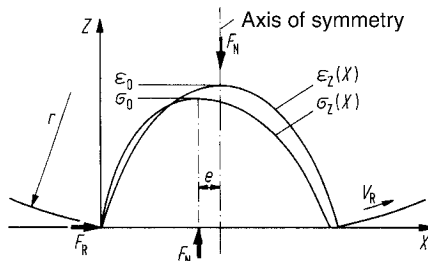


Figure 13.19 Schematic curves of normal stress and normal strain when a viscoelastic material makes rolling contact [13.9]

e = lever arm of rolling friction force

ε_0 = amplitude of strain function $\varepsilon_z(x)$

σ_0 = amplitude of stress function $\sigma_z(x)$

$$F_R = \frac{2 \cdot F_N}{r_1 \cdot \pi} \cdot d_{(T)} \cdot \sqrt{\frac{F_N \cdot r_s \cdot \pi}{w \cdot E_{(T)} \cdot 2 \cdot (1 - \mu)}} \quad (13.17)$$

where

r_1 = roller radius in mm

r_s = substitute radius in mm (see Eq. 13.2)

μ = Poisson's ratio ≈ 0.4

$E_{(T)}$ = temperature-dependent modulus of elasticity in MPa (see Figure 13.20)

$d_{(T)}$ = temperature-dependent loss factor (see Figure 13.20)

Reference [13.2] specifies a practical approximation for rolling friction force. The starting point of this approach is the temperature difference prevailing between the wheel as a whole and its surroundings at the limiting stress prior to failure. This is approx. 4 K for polyamide wheels and about 6 K for polyurethane wheels.

The result of this approach is that the rolling friction force is given by:

$$F_R \leq \Delta T \cdot \sqrt{\frac{8 \cdot B}{\pi \cdot v_R}} \cdot w \cdot \beta + 0.02725 \cdot \sqrt{\frac{r^3}{v_R}} \quad (13.18)$$

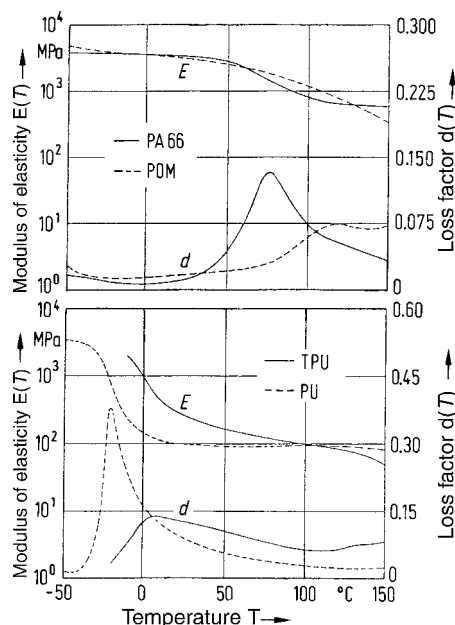


Figure 13.20 Modulus of elasticity and loss factor for some typical roller materials for estimating the rolling friction force using Eq. 13.17

where

$$\Delta T = 4 \text{ K for PA; } 6 \text{ K for TPU}$$

B = half the breadth of the contact surface area (see Eq. 13.4)

and

$$\begin{aligned}\beta &= \text{heat penetration factor} \approx \sqrt{\lambda \cdot c \cdot \rho} \\ &= 0.793 \text{ N/mm K s}^{1/2} \text{ for PA} \\ &= 0.810 \text{ N/mm K s}^{1/2} \text{ for POM} \\ &= 0.630 \text{ N/mm K s}^{1/2} \text{ for TPU}\end{aligned}$$

Figures 13.21 and 13.22 present a comparison of the values of the rolling friction force based on actual measurements and as calculated by Eq. 13.17. These figures also reveal the effects of rolling velocity and roller or wheel diameter.

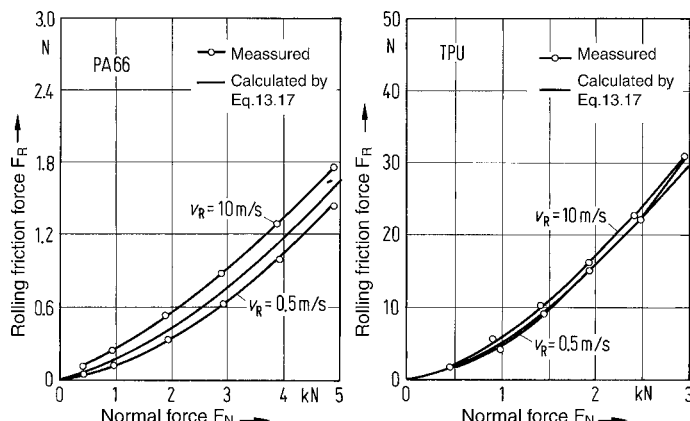


Figure 13.21 Rolling friction forces for different rolling velocities as measured and calculated according to Eq. 13.17; wheel diameter: 150 mm [13.19]

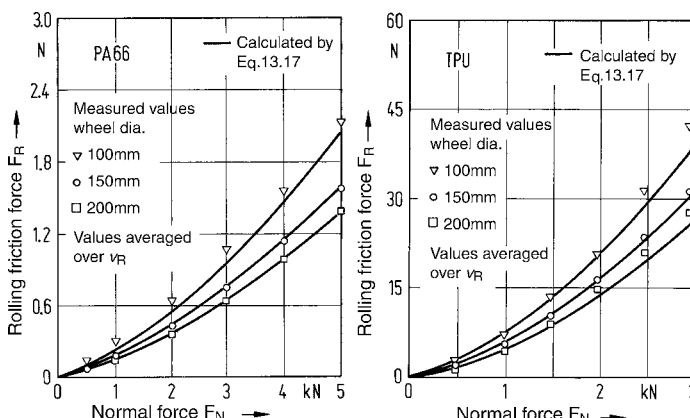


Figure 13.22 Rolling friction forces for different roller diameters as measured experimentally and calculated according to Eq. 13.17 [13.19]

13.2.3.2 Driven Rollers

If a roller under a normal load is additionally driven by a rotary force, a tangential force must be transmitted between the roller and the track on which it runs. The ratio of the rolling friction force (tangential force) and the load on the roller (force acting in the normal direction) is known as the tangential adhesion coefficient f_t .

$$f_t = \frac{F_T}{F_N} \quad (13.19)$$

In this case, a tangential slipping motion (sliding friction) is superimposed on the rolling motion. This means that the contact zone is divided into an area of gripping contact at the leading edge and of sliding contact at the trailing edge. Therefore, the tangential slip s_t is made up of a shape-changing component and a sliding component.

On reaching the limiting slip s_{t0} , sliding takes over completely and the rolling friction force then rises to its maximum level.

$$F_{R\max} = f_{t\max} \cdot F_N$$

where

$$f_{t\max} = \text{adhesion coefficient}$$

On this basis, the maximum transmissible rolling friction force can be roughly estimated by setting $f_{t\max} = f(R_Z)$ (see Section 4.7.2.1). In reference [13.20], values for $f_{t\max}$ measured on actual roller systems are given. These tend to be in good agreement (see Table 13.1) with friction values measured using the pin-on-disk system (see Figures 4.35 and 4.36 for a mean pressure of 8.8 MPa and a peak-to-valley height of surface roughness of 1.7 μm).

In order to accurately determine the transmissible torque in a driven roller, the dependence of the tangential adhesion on the tangential slip is important. Existing theories for determining the tangential stress over the flattened length [13.10], [13.21]–[13.23] finally lead to a numerical treatment [13.12] of the problem.

A practical treatment and solution is the adhesion-slip relationship between normalized tangential adhesion f_t/f and normalized tangential slip s_t/s_{t0} provided by Carter and Fromm [13.10], [13.20].

Table 13.1 Adhesion Coefficients

Roller material	$f_{t\max}$
PA 66 (A4K)	0.31
POM (H 2320)	0.34
TPU (598 U)	0.7
PU (30)	1.2

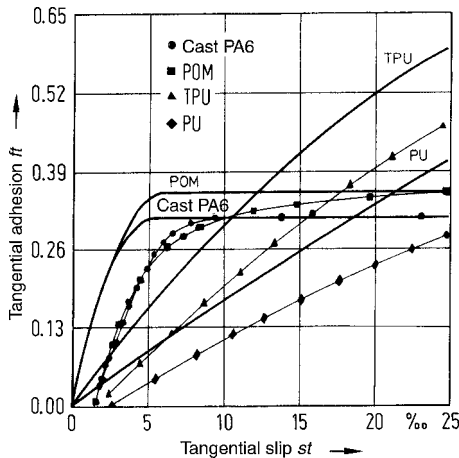


Figure 13.23 Comparison of experimentally determined adhesion/slip relationships (symbols) with those calculated on the basis of the theory of Carter and Fromm
($r_1 = 100 \text{ mm}$, $F_N = 2,000 \text{ N}$, $v_R = 1 \text{ m/s}$) [13.7]

$$\frac{f_t}{f} = 1 - \left(1 - \frac{s_t}{s_{to}} \right)^2 \quad (13.21)$$

where

$$s_{to} = f \cdot \sqrt{\frac{8 \cdot F_N}{\pi \cdot w \cdot r_s} \cdot \frac{1 - \mu^2}{E}} \quad (13.22)$$

f = coefficient of friction

μ = Poisson's ratio ≈ 0.4

As before, however, there is still a major source of error in the very limited data available for the material and system parameters E , μ , and f . This is made clear in [13.7], for example, where differences between adhesion/slip curves calculated in this way can be interpreted by dependencies of these parameters which were not taken into account. There is, however, relatively good agreement in trends. Figure 13.23 presents an example of this with comparisons of calculated and experimentally determined values.

Wear, Surface Fatigue

Sliding processes in the area of contact inevitably result in increased wear compared with simple rolling. Few, if any studies have been specifically conducted to evaluate driven roller wear or surface fatigue, but the following observations may be noted.

1. Measured values of wear from the pin-on-disk system (see Section 4.7) have proved to be very satisfactory for qualitative comparisons of materials.
2. If steel tracks are repeatedly or constantly rolled over, the surface of the steel becomes significantly smoother. This results in reduced roller wear. Even an originally coarse rolled steel profile will become smooth and shiny in the course of time.
3. Flanged wheels exposed to wear should be replaced by more costly guide rollers (see Figure 1.18).

With regard to tread fatigue resulting in cracks, pitting, or serious erosion, test results on PA rollers provide guidance on the attainable service life. In Figures 13.24 and 13.25, the permissible loads per unit width $F_{N/w}$ are plotted for different roller diameters as a function of the number of roller passes. These results apply for conditions where heating of the roller remains below 4 K (see Section 13.2.3.1 – Rolling Friction).

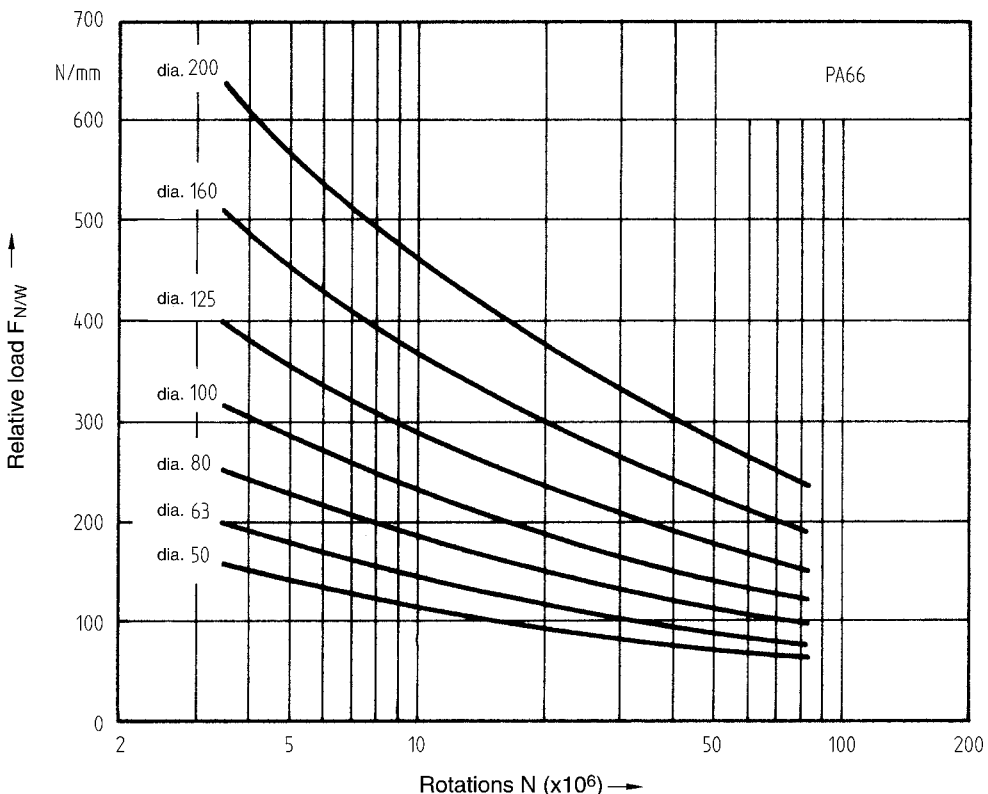


Figure 13.24 Wöhler curves for characterizing initial surface damage on rollers made of PA 66 ($E = 2,900 \text{ MPa}$) [13.2]

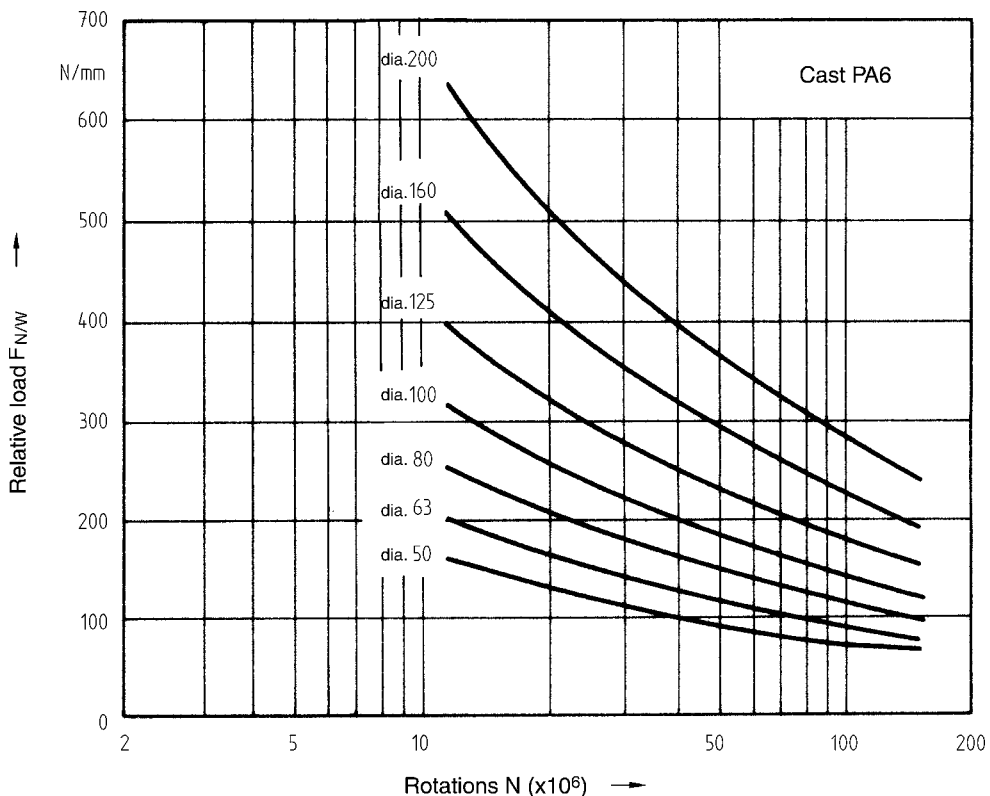


Figure 13.25 Wöhler curves for characterizing initial surface damage on rollers made of cast PA 6 ($E = 2,200 \text{ MPa}$) [13.24]

References

- [13.1] KUNZ, J., W. MICHAELI, N. HERRLICH and W. LAND: Kunststoffpraxis: Konstruktion. Band 2, Teil 8A (Plastics practice: Design), WEKA-Fachverlag für techn. Führungskräfte, Augsburg 1999 et seq.
- [13.2] SEVERIN, D. and B. KÜHLKEN: Tragfähigkeit von Kunststoffräder unter Berücksichtigung der Eigenwärmung (Load-bearing capacity of plastic wheels with self-heating being taken into account), Part 1, *Konstruktion* 43 (1991) 2, pp. 65/71, Part 2, *Konstruktion* 43 (1991) 4, pp. 153/160
- [13.3] ERHARD, G. and E. STRICKLE: Laufrollen aus Polyamid Werkstoffblatt 541 Gruppe K (Rollers made of polyamide, Material data sheet 541, Group K), Hanser Verlag, München 1971
- [13.4] ALICKE, G.: Erfahrungen mit Laufrollen und Seilrollen aus Polyamid (Experience with rollers and pulley wheels made of polyamide), *Fördern und Heben* 24 (1974) 7, pp. 709/714
- [13.5] TIETZ, J.: Belastbarkeit von Maschinenelementen aus thermoplastischen Kunststoffen (Load-bearing capacity of machine elements made of thermoplastics), *Maschinenmarkt* 80 (1974) 33, pp. 1362/1366

- [13.6] REUFELS, F. J.: Räder, Rollen und Reifen mit Laufbelägen aus Polyurethan-Elastomeren Werkstattblatt 557 Gruppe K (Wheels, rollers and tires with tread layers made of polyurethane, Material data sheet 557, Group K), Hanser Verlag, München 1972
- [13.7] SEVERIN, D. and W. HAMMELE: Zur Kraftübertragung zwischen Kunststoffrad und Stahllaufbahn (Transmission of force between a plastic wheel and steel track) Part 1 and Part 2, *Konstruktion* **41** (1989), pp. 123/129 and 163/171
- [13.8] BECK, K. and W.-D. BRÜNINGS: Belastungsgrenzen von Laufrollen aus ®Ultraform (Loading limits of rollers made from ®Ultraform), *Industrie-Anzeiger* **97** (1975) 79, pp. 1716/1720
- [13.9] LÜTKEBOHLE, H.: Roll- und Wälzreibung zylindrischer Räder aus thermoplastischen Kunststoffen (Rolling and sliding friction of cylindrical thermoplastic wheels), Dissertation, TU Berlin 1984
- [13.10] CARTER, F. W.: On the action of locomotive driving wheels, *Proc. Roy. Soc. A* **112** (1926) A760, pp. 151/157
- [13.11] BENTALL, R. H. and K. L. JOHNSON: Slip in the rolling contact of two dissimilar elastic rollers, *Int. J. Mech. Sci.* **9** (1967) 6, pp. 389/404
- [13.12] KALKER, J. J.: On the rolling contact of two elastic bodies in the presence of dry friction, Thesis, Delft Univ. of Technol. 1967
- [13.13] BUTLER, H.: Beanspruchung und Schlupf beim Rollen elastischer Walzen (Stress and slip when elastic rollers roll), *Forsch. Ing.wes.* **27** (1961) 4, pp. 121/126
- [13.14] HUNTER, S. C.: The rolling contact of a rigid cylinder with a viscoelastic half space, *J. Appl. Mech.* **28** (1961) 4, pp. 611/617
- [13.15] SCHMIDT, H.: Rollen aus Hostaform Verformungsverhalten und Versagenskriterien (Deformation behavior in and failure criteria for rollers made of Hostaform), *Konstruktion* **25** (1973), pp. 211/219
- [13.16] GORIOCHEVA, I. G.: Contact problem of rolling of a viscoelastic cylinder on a base of the same material, *PMM* **37** (1973) 5, pp. 925/933
- [13.17] ODEN, J. T. and T. L. LIU: On the general rolling contact problem for finite deformations of a viscoelastic cylinder, *Comput. Meth. Appl. Mech. Eng.* **57** (1986) 3, pp. 297/367
- [13.18] KNOTHE, K. and G. WANG: Zur Theorie der Rollreibung zylindrischer Kunststofflaufräder (On the theory of rolling friction for cylindrical plastic rollers), *Konstruktion* **41** (1989), pp. 193/200
- [13.19] SEVERIN, D. and H. LÜTKEBOHLE: Rollreibung zylindrischer Laufräder aus Kunststoff (Rolling friction of cylindrical plastic rollers), *Konstruktion* **37** (1985) 5, pp. 177/184
- [13.20] SEVERIN, D. and H. LÜTKEBOHLE: Wälzreibung zylindrischer Räder aus Kunststoff (Combined sliding and rolling friction of cylindrical plastic wheels), *Konstruktion* **38** (1986) 5, pp. 173/179
- [13.21] FROMM, H.: Berechnung des Schlupfes beim Rollen deformierbarer Scheiben (Calculation of slip when deformable disks are rolled), *Z. f. angew. Math. u. Mech.* **7** (1927) 1, pp. 27/58
- [13.22] VERMEULEN, P. J. and K. L. JOHNSON: Contact of nonspherical bodies transmitting tangential forces, *J. Appl. Mech.* **31** (1964) 6, pp. 338/340
- [13.23] HAINES, D. J. and E. OLLERTON: Contact stress distributions on elliptical contact surfaces subjected to radial and tangential forces, *Proc. Inst. Mech. Eng.* **177** (1963) 4, pp. 95/114
- [13.24] MORLAND, L. W.: Exact solutions for rolling contact between viscoelastic cylinders, *Q. J. Mech. Appl. Math.* **20** (1967) Part I, pp. 73/106

Index

Index Terms

A

absorption of water	109
acoustic emission	122
acrylonitrile -butadiene -styrene (ABS)	75
adaptor rib	228
adhesion	138
adhesive friction	139
adhesive joint	311
adhesive sliding	145
aging effects	182
air pocket	252
air traps	208
amorphous	54
	56
	57
	64
angle	71
angular deflection	321
angular warpage	197
anisotropic materials	276
anisotropy	126
	60
	61
	176
factors	243
	246
	271
application factor	244
applications	247
aerospace	428
automotive engineering	4
construction industry	9
	18

Links

Index Terms

applications (*Cont.*)

general mechanical engineering	14
new	25
precision engineering	7
technical equipment	15
under the hood	10
aramid fibers	97
Arrhenius plot	133
assembly force	314
atactic	48
automotive engineering	25
average degree of polymerization	34

B

bearing

axial	465
clearance	478
design	478
design examples	481
installed clearance	479
journal	463
load-bearing capacity	463
mean sliding surface temperature	466
operating clearance	478
production	481
production clearance	479
radial	463
thrust	465
wall thickness	480
bearing bushing	
deformation	471

Links

Index Terms

bearing bushing (<i>Cont.</i>)	
large contact widths	472
wear	477
bearing damage	462
deformation	462
fretting corrosion	462
frictional corrosion	462
fusion of the bearing material	462
thermal damage	462
wear	462
bearing play	473
bending loads	226
bending moment	196 197
bending support	199
biaxial deformation	196
biaxial stress	186 191
biaxial tensile stress	187
biodegradable polymers	86 87
blends	50
block copolymer	38
Blok's hypothesis	414
Boltzmann's law	176
boron fibers	98
boss	
outer diameter	379
pilot hole diameter	378
relief bore	379
boundary element method	207
branching	48
breaking of chains	133
bridge bearings	227

Links

Index Terms

brittle	57	170
failure	178	
built-in tension	275	
Burger's model	113	
burst stress	183	

C

CAMPUS	71	129		
carbon black	85			
carbon fibers	97			
cascade injection molding	257			
ceramic fibers	97			
chain scission	153			
characteristic strength	178			
Charpy notched impact test	116			
chemical composition	31			
chemical cross-linking	50			
chopped fiber glass	96			
co-injection molding	289			
coefficient of friction	148	149	150	151
	152	166	167	
coefficient of linear expansion	127	128		
coefficient of thermal expansion	127			
collapsible core	281	282		
complex modulus	123			
compression spring	227	228	337	
compression-resistant	227			
compressive rigidity	227			
computer-aided design (CAD)	207			
conductive additives	84			
conductive layers	86			

Index Terms

Links

conductive paints	84			
conductive properties	84			
conductivity	85			
configuration	47			
contact pressure	168			
continuous fibers	200			
continuum theory	205			
cooling	261	275		
rate	261			
copolymerization	38			
copper	275			
alloys	275			
corrugations	219	389		
blow-molded	403			
crack	178			
growth	122			
initiation	138			
propagation	138			
craze limit stress	178			
craze zones	178			
creep curves				
mathematical description	113			
creep modulus	129	198		
crimps	389			
cross-linking	49	153		
crystalline	55	56	57	71
regions	37			
crystallite	57			
crystallization	64			
cyclic loads	120			

Index Terms

Links

D

damping behavior	123	
dart drop impact test	119	120
deflection force	322	
deflection temperature	130	
deformation	138	144
behavior	101	103
craze	103	
energy-elastic	103	
entropy-elastic	103	
reversible	101	
shear	103	
spontaneous elastic	101	
time-dependent viscoelastic	101	
time-dependent viscous	101	
deformative component	146	
deformative conditions	144	
deformative friction	139	
deformative sliding	145	153
demolding	277	
forced	281	
of undercuts	280	
temperature	281	
depolymerization	133	
design stress limit	115	
diagonal ribbing	222	
diaphragm gate	273	
differential calorimetry	64	
dimensional stability	129	

<u>Index Terms</u>	<u>Links</u>		
dipole	140		
interactions	40		
direct melt process	95		
direction of flow	247		
direction of orientation	248		
disk spring	338	339	
dispersion energy	140		
doping	86		
draft	280		
angle	280		
ductile	170		
ductility	57	115	
dynamic failure	179		
dynamic load	178	182	
dynamic load-bearing capacity	475		
continuous operation	475		
intermittent operation	476		
dynamic tensile stress	175		
 E			
ejector bushes	277		
ejector pins	277		
elastic ejectors	282		
elastic elements	335		
elasticity factor	434		
elasticity variables	202		
elastomer	49	67	88
application	89		
chemically cross-linked	60	88	
comparison of properties	90		
physically cross-linked	60	88	

<u>Index Terms</u>	<u>Links</u>
electrical engineering	27
electrically conducting polymers	84
electromagnetic compatibility	86
elongation at break	105
embossing	349
energy storage devices	323
energy-absorbing capacity	105
entropy-elastic	57
state	66
ethylene	31
expansion compensation	232
expansion joints	232
external gas pressure technology	303
 F	
fabric reinforcement	200
failure criteria	184
FEM	266
fiber	201
alignment	62
orientation	159
composite structures	199
filament	95
filler	51
film	52
biaxially oriented	61
uniaxially	61
Findley's power function	114
finite beam element	196
finite difference	207
finite element	207

Index Terms

		<u>Links</u>
flank temperature		421
flash		283
flexing elements		311
flexing springs		335 343
flexural fatigue tests		120 121
flexural impact test		116 117
flexural loading		218
flexural loads		196
flexural stiffness		218
flexural stress		197
flexurally and torsionally rigid		224
flexurally flexible		220
flexurally rigid		221
flow hesitation		241
flow inhibitor		251 255 260
flow lines		241
flow promoter		255
flow promotion		250
flow resistance		37 246
form factor		427
form-fitting joint		311
form-grip joints		450
pretensioned		452
fracture mechanisms		101
freeze-off		241
friction		145 150 151 155
		158
bearing		459
damage		461
due to cracking and crack propagation		139
lubrication		460

Index Terms

friction (<i>Cont.</i>)	
materials	459
paired materials	460
frictional form-fitting joint	311
frictional joint	311
functional polymers	83
fused deposition modeling	209
fusible cores	283
fusion	64

G

gas injection technology	299
gate position	248
gear tooth temperatures	421
gear wheel	14 411
contact time	422
flank temperature	420
injection molding	442
lubrication	412
machining	446
materials	411
mating materials	412
speed of rotation	420
temperature	414
geometry factor	317
glass fiber	95 96
fabric	95
mat	95
short strands	96
glass transition	64
temperature	57 66 103 243

Index Terms

graft copolymer

Links

39

H

Hachmann and Strickle method

416

419

halving interval

135

heat aging

132

heat flux

274

heat transfer

274

helical factor

428

434

heterogeneous

50

high-density polyethylene (HDPE)

72

high-energy radiation

153

hinge joints

 bi-stable

355

 lid/container

355

HMH criterion

185

holding pressure

245

homogeneous

50

homopolymerization

38

Hooke's law

65

125

190

200

hub

447

450

 bore

448

hydrogen bonding

40

71

140

hysteresis behavior

124

hysteresis loop

123

hysteresis loss

144

hysteresis measurements

122

I

impact factor

198

impact load

198

impact resistance

115

<u>Index Terms</u>	<u>Links</u>
impact stress	198
impact-resistant polystyrene	75
incorporated lubrication	163
index plate method	294
inorganic additives	163
inserts	
expansion	370
screw-in	370
integral hinge	345
assembly aid	346
calculation	352
captive binding	353
design	361
dynamically loaded	361
example applications	361
gate position	361
materials	361
simplified production	361
integral joint	345
internal pressure	271
internal stress	176
intrinsically electrically conducting polymers	177
investment casting	86
ionic forces	284
ISO 10 350	40
ISO 11 403	104
ISO 527	104
isochronous stress-strain curves	105
isotactic	111
isotropy	48

Index Terms

Links

J

jet erosion	168
-------------	-----

K

Kevlar	97
keyway	450
knurled joint	187

L

lamella	55
lamellar structure	102
laminate	199
mechanical properties	200
laminated object manufacturing	210
laser etching	290
suitability	292
leaf spring	342
lightweight stabilizer	12
limiting flank stress	436
linear elastic behavior	190
linear visco-elastic range	111
linear viscoelastic behavior	123
liquid crystal polymer (LCP GF30)	78
load-bearing capacity	424
roller	488
tooth base	427
tooth flank	434
locking ring	314
long-term aging	179
long-term loads	178
loss modulus	123

Index Terms

low-density polyethylene (LDPE)

Links

72

M

market	1
mat laminates	202
mat reinforcement	200
materials testing protocols	135
matrix	201
Maxwell model	113
mechanical fasteners	365
mechanical loads	213
mechanical loss factor	123
mechanical properties	175
medical technology	28
melt flow	243
melt temperature	274
metal fibers	97
metallocene catalysts	23
micelle formation	55
microcircuitry	27
minimum safety factor	431
modulus of elasticity	32
	105
	129
	175
	190
	213
	219
	247
of UP mat laminates	203
modulus of rigidity	129
mold filling	239
time	244
molecular alignment	60
molecular deformation	101
molecular orientation	243

Index Terms

molecular weight	36		
molten state	65		
moment of inertia	197	214	
monomers	31		
morphology	31	54	58
multi-groove profile	450		
multiaxial state of stress	184		
multipart designs	287		

N

network theory	205	
nominal elongation at break	105	
non-Newtonian flow	247	
nonlinear elastic behavior	191	
nonlinear viscoelastic behavior	123	
nonlinear viscoelastic deformation	190	
nonpolar	140	
notched tensile impact test	118	

O

offset yield stress	105	
opening aids	323	
optical purposes	83	
orientation	241	246
flow-induced	243	
longitudinal	245	
transverse	245	
overflow channel	252	
overlap factor	427	434
overstrain safeguards	322	
Owens and Wendt relationship	141	
oxidation	133	

Index Terms

Links

P

percolation	84
peripheral reinforcements	304
phase adhesion	81
physical cross-linking	50
piercing cores	285
pitch strength	435
plasticization	51
plasticized poly(vinyl chloride) (pPVC)	76
Poisson's ratio	125
for UP mat laminates	204
polar	140
components	140
polymeric materials	41
poly(methyl methacrylate) (PMMA)	76
poly(vinyl chloride) (PVC)	76
polyaddition	31
polyamide 6 (PA 6)	73
polyamide 66 (PA 66)	73
polyaryl ether ketone (PAEK)	78
polybutylene terephthalate (PBT)	74
polycarbonate (PC)	77
polycondensation	31
polyether sulfone	33
polyether sulfone (PES), 0.7% moisture	77
polyethylene (HDPE)	31
polymer blend	80
ABS + PC	82
ASA + PC	82
PA + PPE	82

Index Terms

Links

polymer blend (<i>Cont.</i>)	
PBT + ABS	82
PBT + ASA	82
PC + LCP	82
PMMA + PBS	83
PPE + SB	82
polymeric additives	163
polymeric material	
consumption	2
production	1
polymerization	31
polyoxymethylene (POM)	74
polyphenylene	
not fusible	34
polyphenylene sulfide (PPS GF40)	77
polypropylene (PP)	47
highly crystalline	24
talc-reinforced	24
polypyrone	
not fusible	34
polystyrene (PS)	47
melting behavior	24
morphology	24
tacticity	24
polysulfone (PSU)	33
polytetrafluoroethylene (PTFE)	33
polyvinyl chloride (PVC)	47
post molding shrinkage	267
press-fit joints	447
pressure	
large contact widths	468

Index Terms

pressure (<i>Cont.</i>)	
mean surface	467
permissible	470
small contact widths	467
pressure bars	216
pressure profile	274
pressure-yielding	227
properties	71
pvT diagrams	264

R

railcar	26
random copolymer	38
rapid prototyping	208
rapid tooling	210
rate of wear	146
	148
	149
	150
	151
	152
reducing factors	181
reinforcement	51
reinforcing fibers	94
properties	96
relative molecular weight	34
	36
	37
relative support number	431
relative surface factor	431
release force	314
residual strain	316
retaining force	321
loss of	316
retaining guard	314
	323
	330
	334
rheological simulations	208

Links

Index Terms

rib		219	245	246	273
		387	392		
blow-molded		403	405		
compression-molded		406			
cooling time		397			
gas-assist molding		401			
injection direction		398			
injection-molded		396			
intersection points		400			
mounting condition		395			
number of		393			
thickness		396			
rib height		390			
rib position		391			
rigid		57			
rigid-flexible combinations		293			
roller		14	216	216	485
breadth of contact surface		493			
damage		486			
driven		504			
free-wheeling		498			
permissible load		498			
permissible residual flattening		497			
relaxation of flattening		497			
surface pressure		493			
time-dependent flattening		493			
under dynamic load		498			
under static load		492			
rotating element		198			
roving		95			
reinforcement		200			

Links

Index Terms

S

safety factor	135
bending and buckling	180
fracture	181
fracture stresses	181
screw	374
assembly conditions	385
extraction (pull-out) force	383
stripping torque	383
tensioning force	384
tightening moment	384
screw boss	
design of	377
screw drive torque	381
screw engagement depth	378
screw thread	187
self-locking	377
seals	334
secant modulus	105 107 129 191
secondary valence bonds	40
selective laser sintering	210
self-threading screw	374 381
assembly process	375
geometries	375
shapes	375
semi-crystalline	55 57 66
sequential injection molding	257
service life factor	431

Links

Index Terms

shaft-hub joints	447			
press-fit joints	447			
shear flow	61			
shear loads	187	226		
shear stress	226			
short-term stress peaks	198			
shrinkage	176	208	231	247
	264	265	266	280
shutoffs	285			
single-phase	50			
sink marks	263	272		
size factor	431			
slide members	14			
sliding elements	331			
sliding friction	156			
slip velocity	166			
slit bushings	234			
Smith diagrams	120	121		
snap-fit	287	288	312	316
	317			
assembly	314			
beam	317			
demolding	319			
connection	182			
height	317			
hook	313	321		
joint	216	311	323	
annular	327			
assembly force	328			
retaining force	328			
size of undercut	328			

Links

Index Terms

	<u>Links</u>
snap-fit (<i>Cont.</i>)	
assembly force	326
cylindrical annular	313
segmented	287
size of the undercut	326
slotted annular	332
assembly force	332
retaining force	332
size of the undercut	332
spherical annular	313
torsion	326
torsional	313 325
length	317
solid ground curing	209
solidification	261
spherulite	57 102
spiral spring	340
split	286
cavity	281
molds	283
technique	294
spur gears	413
standard	135
standard polystyrene (PS)	74
stereolithography	208
stick-slip	165 166 167
storage modulus	123
strain rate	108
strength	37
stress correction factor	427 431

Index Terms

Links

stress craze	
normal	102
shear	102
stress for uniaxial tensile loads	182
stress-strain curves	103
	104
	107
	110
mathematical description	109
stress-strain diagrams	71
stripper plates	277
stripping torque	383
structure	31
	58
styrene-acrylonitrile (SAN)	75
surface energy	140
	141
	142
	143
surface roughness	145
	147
syndiotactic	48

T

tacticity	48
Takanashi	419
method	414
taper	280
temperature index	135
tensil creep testing	111
	112
tensile creep strength	32
tensile impact test	116
tensile strength	32
at break	105
of various UP mat laminates	203
test	104
	106
UD layer	201
tensile stress	101
	105

<u>Index Terms</u>	<u>Links</u>
tension springs	337
tensionally rigid and torsionally flexible	225
thermal degradation	133
thermal expansion	127 230 232 233
	234 235
thermal stress	230
thermo-mechanical behavior	64
thermoplastic	31
fusible	33
linear amorphous	60
linear semicrystalline	60
thermoset	67 90
applications	92
chemically cross-linked	60
properties	91
thermotropic	83
thin-wall technology	263
thread	
blow-molded	368
injection-molded	366 368
machined	366 368
thread angle	377
threaded inserts	
embedded by ultrasound	368
encapsulated	368
evaluation	372 373
press-in	369
tolerance	267 269
tooth base flexural fatigue strength	430
tooth base strength	432 433
tooth damage	425

Index Terms

tooth deformation	
calculation of	440
tooth width	428
torque	188
torsion springs	341
torsion-resistant	221
torsional loads	187
torsional modulus	64
torsional stiffness	222
torsionally flexible	221
torsionally rigid	220
toughness	221
temperature dependence	115
transfer method	116
transition temperature	294
tribological properties	65
tribology	136
turntable method	138
two-color injection molding	294
two-phase	289

U

undercut	280	281	283
internal	286		
uniaxial state of stress	182	183	
universal joints	235		
unscrewing molds	283		

V

van der Waals forces	40	71	
Vicat softening point	131		
Vicat softening temperature	131		

Links

Index Terms

visco-elastic behavior	123
viscosity	263
voids	263
Voigt model	415
Voigt-Kelvin element	166
Voigt-Kelvin model	113
volume shrinkage	265

W

wall thickness	261	263	388	
uniform	262			
warpage	208	263	271	273
angular	274			
thermally induced	272	274	275	
water absorption	41			
water injection technology	303			
wear	145	150	151	155
characteristics	147			
weight reduction	11			
weld line	178	208	241	245
252				
254	255			
factor	254			
wheels	216	485		
withdrawal force	188			
Wöhler curves	120	121		

Y

yield point	178	
yield strain	105	179

Links

Index Terms

yield stress
Young's equation

Links

105	179	181
141		